

*Polymer Solutions: An Introduction to Physical Properties.* Iwao Teraoka  
Copyright © 2002 John Wiley & Sons, Inc.  
ISBNs: 0-471-38929-3 (Hardback); 0-471-22451-0 (Electronic)

## **POLYMER SOLUTIONS**

# **POLYMER SOLUTIONS**

---

## **An Introduction to Physical Properties**

**IWAO TERAOKA**

Polytechnic University  
Brooklyn, New York

 **WILEY-  
INTERSCIENCE**

A JOHN WILEY & SONS, INC., PUBLICATION

Designations used by companies to distinguish their products are often claimed as trademarks. In all instances where John Wiley & Sons, Inc., is aware of a claim, the product names appear in initial capital or ALL CAPITAL LETTERS. Readers, however, should contact the appropriate companies for more complete information regarding trademarks and registration.

Copyright © 2002 by John Wiley & Sons, Inc., New York. All rights reserved.

No part of this publication may be reproduced, stored in a retrieval system or transmitted in any form or by any means, electronic or mechanical, including uploading, downloading, printing, decompiling, recording or otherwise, except as permitted under Sections 107 or 108 of the 1976 United States Copyright Act, without the prior written permission of the Publisher. Requests to the Publisher for permission should be addressed to the Permissions Department, John Wiley & Sons, Inc., 605 Third Avenue, New York, NY 10158-0012, (212) 850-6011, fax (212) 850-6008, E-Mail: PERMREQ @ WILEY.COM.

This publication is designed to provide accurate and authoritative information in regard to the subject matter covered. It is sold with the understanding that the publisher is not engaged in rendering professional services. If professional advice or other expert assistance is required, the services of a competent professional person should be sought.

**ISBN 0-471-22451-0**

This title is also available in print as ISBN 0-471-38929-3.

For more information about Wiley products, visit our web site at [www.Wiley.com](http://www.Wiley.com).

*To my wife, Sadae*

# CONTENTS

<b>Preface</b>	xv
<b>1 Models of Polymer Chains</b>	1
1.1 Introduction	1
1.1.1 Chain Architecture	1
1.1.2 Models of a Linear Polymer Chain	2
1.1.2.1 Models in a Continuous Space	2
1.1.2.2 Models in a Discrete Space	4
1.1.3 Real Chains and Ideal Chains	5
1.2 Ideal Chains	7
1.2.1 Random Walk in One Dimension	7
1.2.1.1 Random Walk	7
1.2.1.2 Mean Square Displacement	9
1.2.1.3 Step Motion	10
1.2.1.4 Normal Distribution	10
1.2.2 Random Walks in Two and Three Dimensions	12
1.2.2.1 Square Lattice	12
1.2.2.2 Lattice in Three Dimensions	13
1.2.2.3 Continuous Space	14
1.2.3 Dimensions of Random-Walk Chains	15
1.2.3.1 End-to-End Distance and Radius of Gyration	15
1.2.3.2 Dimensions of Ideal Chains	18
1.2.3.2 Dimensions of Chains with Short-Range Interactions	19
1.2.4 Problems	20
1.3 Gaussian Chain	23
1.3.1 What is a Gaussian Chain?	23
1.3.1.1 Gaussian Distribution	23
1.3.1.2 Contour Length	25
1.3.2 Dimension of a Gaussian Chain	25
1.3.2.1 Isotropic Dimension	25
1.3.2.2 Anisotropy	26
	vii

1.3.3 Entropy Elasticity	28
1.3.3.1 Boltzmann Factor	28
1.3.3.2 Elasticity	30
1.3.4 Problems	31
1.4 Real Chains	33
1.4.1 Excluded Volume	33
1.4.1.1 Excluded Volume of a Sphere	33
1.4.1.2 Excluded Volume in a Chain Molecule	34
1.4.2 Dimension of a Real Chain	36
1.4.2.1 Flory Exponent	36
1.4.2.2 Experimental Results	37
1.4.3 Self-Avoiding Walk	39
1.4.4 Problems	40
1.5 Semirigid Chains	41
1.5.1 Examples of Semirigid Chains	41
1.5.2 Wormlike Chain	43
1.5.2.1 Model	43
1.5.2.2 End-to-End Distance	44
1.5.2.3 Radius of Gyration	45
1.5.2.4 Estimation of Persistence Length	46
1.5.3 Problems	47
1.6 Branched Chains	49
1.6.1 Architecture of Branched Chains	49
1.6.2 Dimension of Branched Chains	50
1.6.3 Problems	52
1.7 Molecular Weight Distribution	55
1.7.1 Average Molecular Weights	55
1.7.1.1 Definitions of the Average Molecular Weights	55
1.7.1.2 Estimation of the Averages and the Distribution	57
1.7.2 Typical Distributions	58
1.7.2.1 Poisson Distribution	58
1.7.2.2 Exponential Distribution	59
1.7.2.3 Log-Normal Distribution	60
1.7.3 Problems	62
1.8 Concentration Regimes	63
1.8.1 Concentration Regimes for Linear Flexible Polymers	63
1.8.2 Concentration Regimes for Rodlike Molecules	65
1.8.3 Problems	66

<b>2 Thermodynamics of Dilute Polymer Solutions</b>	<b>69</b>
2.1 Polymer Solutions and Thermodynamics	69
2.2 Flory-Huggins Mean-Field Theory	70
2.2.1 Model	70
2.2.1.1 Lattice Chain Model	70
2.2.1.2 Entropy of Mixing	72
2.2.1.3 $\chi$ Parameter	72
2.2.1.4 Interaction Change Upon Mixing	74
2.2.2 Free Energy, Chemical Potentials, and Osmotic Pressure	75
2.2.2.1 General Formulas	75
2.2.2.2 Chemical Potential of a Polymer Chain in Solution	77
2.2.3 Dilute Solutions	77
2.2.3.1 Mean-Field Theory	77
2.2.3.2 Virial Expansion	78
2.2.4 Coexistence Curve and Stability	80
2.2.4.1 Replacement Chemical Potential	80
2.2.4.2 Critical Point and Spinodal Line	81
2.2.4.3 Phase Separation	82
2.2.4.4 Phase Diagram	84
2.2.5 Polydisperse Polymer	87
2.2.6 Problems	89
2.3 Phase Diagram and Theta Solutions	99
2.3.1 Phase Diagram	99
2.3.1.1 Upper and Lower Critical Solution Temperatures	99
2.3.1.2 Experimental Methods	100
2.3.2 Theta Solutions	101
2.3.2.1 Theta Temperature	101
2.3.2.2 Properties of Theta Solutions	103
2.3.3 Coil-Globule Transition	105
2.3.4 Solubility Parameter	107
2.3.5 Problems	108
2.4 Static Light Scattering	108
2.4.1 Sample Geometry in Light-Scattering Measurements	108
2.4.2 Scattering by a Small Particle	110
2.4.3 Scattering by a Polymer Chain	112
2.4.4 Scattering by Many Polymer Chains	115
2.4.5 Correlation Function and Structure Factor	117
2.4.5.1 Correlation Function	117
2.4.5.2 Relationship Between the Correlation Function and Structure Factor	117

2.4.5.3	Examples in One Dimension	119
2.4.6	Structure Factor of a Polymer Chain	120
2.4.6.1	Low-Angle Scattering	120
2.4.6.2	Scattering by a Gaussian Chain	121
2.4.6.3	Scattering by a Real Chain	124
2.4.6.4	Form Factors	125
2.4.7	Light Scattering of a Polymer Solution	128
2.4.7.1	Scattering in a Solvent	128
2.4.7.2	Scattering by a Polymer Solution	129
2.4.7.3	Concentration Fluctuations	131
2.4.7.4	Light-Scattering Experiments	132
2.4.7.5	Zimm Plot	133
2.4.7.6	Measurement of $dn/dc$	135
2.4.8	Other Scattering Techniques	136
2.4.8.1	Small-Angle Neutron Scattering (SANS)	136
2.4.8.2	Small-Angle X-Ray Scattering (SAXS)	139
2.4.9	Problems	139
2.5	Size Exclusion Chromatography and Confinement	148
2.5.1	Separation System	148
2.5.2	Plate Theory	150
2.5.3	Partitioning of Polymer with a Pore	151
2.5.3.1	Partition Coefficient	151
2.5.3.2	Confinement of a Gaussian Chain	153
2.5.3.3	Confinement of a Real Chain	156
2.5.4	Calibration of SEC	158
2.5.5	SEC With an On-Line Light-Scattering Detector	160
2.5.6	Problems	162
<b>APPENDIXES</b>		
2.A:	Review of Thermodynamics for Colligative Properties in Nonideal Solutions	164
2.A.1	Osmotic Pressure	164
2.A.2	Vapor Pressure Osmometry	164
2.B:	Another Approach to Thermodynamics of Polymer Solutions	165
2.C:	Correlation Function of a Gaussian Chain	166
<b>3</b>	<b>Dynamics of Dilute Polymer Solutions</b>	<b>167</b>
3.1	Dynamics of Polymer Solutions	167
3.2	Dynamic Light Scattering and Diffusion of Polymers	168
3.2.1	Measurement System and Autocorrelation Function	168
3.2.1.1	Measurement System	168
3.2.1.2	Autocorrelation Function	169
3.2.1.3	Photon Counting	170



3.2.2	Autocorrelation Function	170
3.2.2.1	Baseline Subtraction and Normalization	170
3.2.2.2	Electric-Field Autocorrelation Function	172
3.2.3	Dynamic Structure Factor of Suspended Particles	172
3.2.3.1	Autocorrelation of Scattered Field	172
3.2.3.2	Dynamic Structure Factor	174
3.2.3.3	Transition Probability	174
3.2.4	Diffusion of Particles	176
3.2.4.1	Brownian Motion	176
3.2.4.2	Diffusion Coefficient	177
3.2.4.3	Gaussian Transition Probability	178
3.2.4.4	Diffusion Equation	179
3.2.4.5	Concentration	179
3.2.4.6	Long-Time Diffusion Coefficient	180
3.2.5	Diffusion and DLS	180
3.2.5.1	Dynamic Structure Factor and Mean Square Displacement	180
3.2.5.2	Dynamic Structure Factor of a Diffusing Particle	181
3.2.6	Dynamic Structure Factor of a Polymer Solution	182
3.2.6.1	Dynamic Structure Factor	182
3.2.6.2	Long-Time Behavior	183
3.2.7	Hydrodynamic Radius	184
3.2.7.1	Stokes-Einstein Equation	184
3.2.7.2	Hydrodynamic Radius of a Polymer Chain	185
3.2.8	Particle Sizing	188
3.2.8.1	Distribution of Particle Size	188
3.2.8.2	Inverse-Laplace Transform	188
3.2.8.3	Cumulant Expansion	189
3.2.8.4	Example	190
3.2.9	Diffusion From Equation of Motion	191
3.2.10	Diffusion as Kinetics	193
3.2.10.1	Fick's Law	193
3.2.10.2	Diffusion Equation	195
3.2.10.3	Chemical Potential Gradient	196
3.2.11	Concentration Effect on Diffusion	196
3.2.11.1	Self-Diffusion and Mutual Diffusion	196
3.2.11.2	Measurement of Self-Diffusion Coefficient	
3.2.11.3	Concentration Dependence of the Diffusion Coefficients	198
3.2.12	Diffusion in a Nonuniform System	200
3.2.13	Problems	201
3.3	Viscosity	209
3.3.1	Viscosity of Solutions	209

3.3.1.1	Viscosity of a Fluid	209
3.3.1.2	Viscosity of a Solution	211
3.3.2	Measurement of Viscosity	213
3.3.3	Intrinsic Viscosity	215
3.3.4	Flow Field	217
3.3.5	Problems	219
3.4	Normal Modes	221
3.4.1	Rouse Model	221
3.4.1.1	Model for Chain Dynamics	221
3.4.1.2	Equation of Motion	222
3.4.2	Normal Coordinates	223
3.4.2.1	Definition	223
3.4.2.2	Inverse Transformation	226
3.4.3	Equation of Motion for the Normal Coordinates in the Rouse Model	226
3.4.3.1	Equation of Motion	226
3.4.3.2	Correlation of Random Force	228
3.4.3.3	Formal Solution	229
3.4.4	Results of the Normal-Coordinates	229
3.4.4.1	Correlation of $\mathbf{q}_i(t)$	229
3.4.4.2	End-to-End Vector	230
3.4.4.3	Center-of-Mass Motion	231
3.4.4.4	Evolution of $\mathbf{q}_i(t)$	231
3.4.5	Results for the Rouse Model	232
3.4.5.1	Correlation of the Normal Modes	232
3.4.5.2	Correlation of the End-to-End Vector	234
3.4.5.3	Diffusion Coefficient	234
3.4.5.4	Molecular Weight Dependence	234
3.4.6	Zimm Model	234
3.4.6.1	Hydrodynamic Interactions	234
3.4.6.2	Zimm Model in the Theta Solvent	236
3.4.6.3	Hydrodynamic Radius	238
3.4.6.4	Zimm Model in the Good Solvent	238
3.4.7	Intrinsic Viscosity	239
3.4.7.1	Extra Stress by Polymers	239
3.4.7.2	Intrinsic Viscosity of Polymers	241
3.4.7.3	Universal Calibration Curve in SEC	243
3.4.8	Dynamic Structure Factor	243
3.4.8.1	General Formula	243
3.4.8.2	Initial Slope in the Rouse Model	247
3.4.8.3	Initial Slope in the Zimm Model, Theta Solvent	247
3.4.8.4	Initial Slope in the Zimm Model, Good Solvent	248
3.4.8.5	Initial Slope: Experiments	249
3.4.9	Motion of Monomers	250

CONTENTS	xiii
3.4.9.1 General Formula	250
3.4.9.2 Mean Square Displacement: Short-Time Behavior Between a Pair of Monomers	251
3.4.9.3 Mean Square Displacement of Monomers	252
3.4.10 Problems	257
 3.5 Dynamics of Rodlike Molecules	 262
3.5.1 Diffusion Coefficients	262
3.5.2 Rotational Diffusion	263
3.5.2.1 Pure Rotational Diffusion	263
3.5.2.2 Translation-Rotational Diffusion	266
3.5.3 Dynamic Structure Factor	266
3.5.4 Intrinsic Viscosity	269
3.5.5 Dynamics of Wormlike Chains	269
3.5.6 Problems	270
 <b>APPENDICES</b>	
3.A: Evaluation of $\langle \mathbf{q}_i^2 \rangle_{\text{eq}}$	271
3.B: Evaluation of $\langle \exp[i\mathbf{k} \cdot (A\mathbf{q} - B\mathbf{p})] \rangle$	273
3.C: Initial Slope of $S_1(\mathbf{k}, t)$	274
 <b>4 Thermodynamics and Dynamics of Semidilute Solutions</b>	 277
4.1 Semidilute Polymer Solutions	277
4.2 Thermodynamics of Semidilute Polymer Solutions	278
4.2.1 Blob Model	278
4.2.1.1 Blobs in Semidilute Solutions	278
4.2.1.2 Size of the Blob	279
4.2.1.3 Osmotic Pressure	282
4.2.1.4 Chemical Potential	285
4.2.2 Scaling Theory and Semidilute Solutions	286
4.2.2.1 Scaling Theory	286
4.2.2.2 Osmotic Compressibility	289
4.2.2.3 Correlation Length and Monomer Density Correlation Function	289
4.2.2.4 Chemical Potential	294
4.2.2.5 Chain Contraction	295
4.2.2.6 Theta Condition	296
4.2.3 Partitioning with a Pore	298
4.2.3.1 General Formula	298
4.2.3.2 Partitioning at Low Concentrations	299
4.2.3.3 Partitioning at High Concentrations	300
4.2.4 Problems	301

4.3 Dynamics of Semidilute Solutions	307
4.3.1 Cooperative Diffusion	307
4.3.2 Tube Model and Reptation Theory	310
4.3.2.1 Tube and Primitive Chain	310
4.3.2.2 Tube Renewal	312
4.3.2.3 Disengagement	313
4.3.2.4 Center-of-Mass Motion of the Primitive Chain	315
4.3.2.5 Estimation of the Tube Diameter	318
4.3.2.6 Measurement of the Center-of-Mass Diffusion Coefficient	319
4.3.2.7 Constraint Release	320
4.3.2.8 Diffusion of Polymer Chains in a Fixed Network	321
4.3.2.9 Motion of the Monomers	322
4.3.3 Problems	324
References	325
Further Readings	326
Appendices	328
A1 Delta Function	328
A2 Fourier Transform	329
A3 Integrals	331
A4 Series	332
Index	333

## PREFACE

The purpose of this textbook is twofold. One is to familiarize senior undergraduate and entry-level graduate students in polymer science and chemistry programs with various concepts, theories, models, and experimental techniques for polymer solutions. The other is to serve as a reference material for academic and industrial researchers working in the area of polymer solutions as well as those in charge of chromatographic characterization of polymers. Recent progress in instrumentation of size exclusion chromatography has paved the way for comprehensive one-stop characterization of polymer without the need for time-consuming fractionation. Size-exclusion columns and on-line light scattering detectors are the key components in the instrumentation. The principles of size exclusion by small pores will be explained, as will be principles of light-scattering measurement, both static and dynamic.

This textbook emphasizes fundamental concepts and was not rewritten as a research monograph. The author has avoided still-controversial topics such as polyelectrolytes. Each section contains many problems with solutions, some offered to add topics not discussed in the main text but useful in real polymer solution systems.

The author is deeply indebted to pioneering works described in the famed textbooks of de Gennes and Doi/Edwards as well as the graduate courses the author took at the University of Tokyo. The author also would like to thank his advisors and colleagues he has met since coming to the U.S. for their guidance.

This book uses three symbols to denote equality between two quantities A and B.

- 1) ' $A = B$ ' means A and B are exactly equal.
- 2) ' $A \cong B$ ' means A is nearly equal to B. It is either that the numerical coefficient is approximated or that A and B are equal except for the numerical coefficient.
- 3) ' $A \sim B$ ' and ' $A \propto B$ ' mean A is proportional to B. The dimension (unit) may be different between A and B.

Appendices for some mathematics formulas have been included at the end of the book. The middle two chapters have their own appendices. Equations in the book-end appendices are cited as Eq. Ax.y; equations in the chapter-end appendices are cited as Eq. x.A.y; all the other equations are cited as Eq. x.y. Important equations have been boxed.

# INDEX

- amorphous 69
- athermal 37
- athermal solution 75
- autocorrelation function 117
  - concentration fluctuations 131
  - decay rate 188
  - electric field 172, 173, 174, 188
  - Gaussian chain 122
  - intensity 169, 171
  - real chain 124
- autocorrelator 168
  
- backflow correction 200
- baseline 169
- bead-spring model 3, 4, 15, 221
- bead-stick model 3
- binodal line 85
- blob 279, 308
  - model 279
  - number of monomers 281
  - size 279, 301
- Boltzmann distribution 29
- bond angle 19
- branched chain 2, 49
  - radius of gyration 52
- branching parameter 50
- Brownian motion 176
- $\chi$  parameter 73
  
- center-of-mass motion 183, 223
- chain contraction 295
- chemical potential 77, 196, 285, 294, 298, 304
- chromatogram 149
- Clausius-Mossotti equation 129, 143
- cloud point 101
- coexistence curve 85, 99
- coherence factor 171
- coherent 113
- coil-globule transition 105
- column 148
- comb polymer 49
  - radius of gyration 54
- concentrated solution 6, 65, 278
- concentration gradient 194
- confinement
  - enthalpy 152
  - entropy 152
  - Gaussian chain 153
  - real chain 156
- conformation 3
- constraint release 321
- CONTIN 189
- contour length 3
- contrast matching 138
- copolymer 2
  - differential refractive index 144

- copolymer (*continued*)
  - enthalpy of mixing 90
  - excess scattering 145
  - static structure factor 139
- correlation function 117
  - examples 119
  - Ornstein-Zernike 291
- correlation length 120
  - dynamic 308
- could-point method 100
- critical phenomena 286
  - point 82, 99
  - temperature 99
- cross-linked chain 2
- crystalline 69
- cubic lattice 5, 13
- cumulant expansion 189
  
- de Gennes 286, 310
- Debye function 122
- degree of polymerization 1
- delay time 169
- delta function 24, 328
- dendrimer 50
- diamond lattice 5
- diblock copolymer 2
  - hydrodynamic radius 204
  - radius of gyration 21
- differential refractive index 130
- diffusion 176, 178
  - concentration effect 196
  - cooperative 308
  - mutual 197
  - in nonuniform system 200
  - self 197
- diffusion coefficient 177, 181, 184, 195
  - center-of-mass 184, 319
  - concentration dependence 199
  - cooperative 308
  - curvilinear 314
  - long-time 180
  - mutual 197, 199, 307
  - reptation theory 318
  - rotational 262
  - self 197, 199, 319
  - sphere 184
  - tracer 198, 320, 322
  - translational 262
- diffusion equation 25, 179, 180, 196
  - rotational 263
- dilute solution 64
- disengagement time 314
- DLS 168
- $dn/dc$  130, 135
- DNA 43, 48
- Doi 310
- dynamic light scattering
  - 168, 307, 320
- dynamic structure factor 174, 180, 181
  - bead-spring model 244, 246
  - long-time 183
  - particles 174
  - polymer solution 182
  - rodlike molecule 266
  - single chain 182
  - single particle 174, 175
  
- Edwards 310
- efflux time 215
- electric permittivity 112, 128
- eluent 148
- end-to-end distance 16, 180
- end-to-end vector 15
- ensemble average 169
- entanglement 279, 310
- entropy elasticity 30, 31
- equation of motion 191, 207
- equipartition law 193, 207
- ergodicity 169, 221
- excess chemical potential 285
  - polarizability 128
  - scattering 129
- excluded volume 5, 6, 33
  - chain 6
  - shielding 295
- exclusion limit 159
- exponential distribution 58, 59
  
- Fick's law 195
- Fickian diffusion 195
- Flory 36, 70
- Flory exponent 36
- Flory's  $\chi$  parameter 73
- Flory's method
  - confinement 158, 162
  - good solvent 36
  - semidilute solution 305
  - theta solvent 104, 108

- Flory-Huggins
  - mean-field theory 71
  - $\chi$  parameter 73
- flow
  - capillary 214
  - elongational 218
  - field 217
  - laminar 209
- fluctuation-dissipation theorem 184
- fluorescence recovery after photobleaching 197, 319
- flux 193
- forced Rayleigh scattering 197, 319
- form factor 125
  - Gaussian chain 125
  - rodlike molecule 126, 141
  - sphere 126, 141
  - star polymer 126, 142
- forward-scattered beam 109
- Fourier transform 118, 329
- FRAP 197
- FRS 197
- freely rotating chain 3, 19, 22
- freely-jointed chain 3
- friction coefficient 184
  
- Gaussian chain 23, 121
  - anisotropy 26
  - contour length 25
  - end-to-end distance 25
  - radius of gyration 26
- Gaussian distribution 23
- gel 321
- gel filtration chromatography 150
- gel permeation chromatography 150
- GFC 150
- Gibbs-Duhem theorem 94, 95, 143
- good solvent 69, 87
- GPC 150
- Green's theorem 195
  
- homopolymer 2
- hydrodynamic interaction 185, 234
- hydrodynamic radius 185
  - Gaussian chain 186
  - polymer chain 186, 238
  - rodlike molecule 263, 270
- hydrodynamic volume 243
- hyperbranched chain 50
  
- ideal chain 6, 7
  - end-to-end distance 18
  - radius of gyration 18
- index matching 108, 130
- instability 81, 95
- interference 113, 114
- intrinsic viscosity 64, 211, 216
  - bead-spring model 240, 241
- inverse-Fourier transform 118, 330
- inverse-Laplace transform 189
- isorefractive 130, 198
  
- Kratky-Porod model 43
- Kuhn segment length 45
  
- Laplacian 179
- lattice 5
- lattice chain theory 70
- lattice coordinate 5, 73
- LCST 100
- Legendre polynomials 264
- lever rule 84, 96
- light scattering 108
  - Gaussian chain 121
  - many polymer chains 115
  - polymer chain 112
  - polymer solution 129
  - real chain 124
  - sample geometry 108
  - small particle 110
  - solvent 128
- linear chain 2
  - concentration regime 63
- log-normal distribution 58, 60
- long-range interaction 35
- long-time average 169
- low-angle scattering 120
- lower critical solution temperature 100, 103
  
- MALDI-TOF 57
- Mark-Houwink-Sakurada equation 216
- Mark-Houwink-Sakurada exponent 216
- Markoffian 8, 14, 177
- mass conservation 195
- master curve 287
- matrix 198, 320
- Maxwell construction 83
- mean square displacement 10, 177, 178, 180, 192



- mean-field theory  
   chemical potential 77  
   enthalpy of mixing 70  
   entropy of mixing 70, 72  
   Helmholtz free energy 75, 88  
   osmotic compressibility 78  
   osmotic pressure 76, 77, 88  
   replacement chemical potential 80  
 membrane osmometry 70, 77  
 metastable 84  
 miscibility gap 85  
 mobile phase 148  
 molecular weight distribution 55, 148  
 monodisperse 55  
 mutual diffusion 197  
  
 Nernst-Einstein equation 184  
 Newtonian fluid 210  
 nonreverse random walk 48  
 nonsolvent 69, 87  
 normal coordinate 223  
   autocorrelation 229, 230  
   center-of-mass diffusion coefficient 231  
   cross correlation 229, 230  
   end-to-end vector 230  
   equation of motion 228  
   fluctuations 230  
   transition probability 232  
 normal distribution 11  
 normal mode 223  
 number-average molecular weight 55  
  
 Oseen tensor 185, 235  
 osmotic compressibility 144  
 osmotic pressure 76, 164, 282  
 overlap concentration 64, 80, 277  
  
 pair distribution function 117  
 particle sizing 168, 188  
 partition coefficient 150, 152  
   Gaussian chain 154, 155  
   real chain 157  
   rodlike molecule 155  
 partition ratio 151  
 PCS 168  
 pearl-necklace model 3, 4, 34  
 persistence length 44, 46  
 PFG-NMR 197  
 phase diagram 84, 99  
 phase separation 82  
  
 photon correlation spectroscopy 168  
 photon counting 170  
 plate 150  
 plate theory 150  
 poise 211  
 Poiseuille law 214  
 Poisson distribution 58, 62  
 polarizability 112  
 poly( $\alpha$ -methylstyrene)  
   hydrodynamic radius 188  
   mutual diffusion coefficient 200  
   osmotic pressure 284  
 poly(ethylene glycol) 75  
   mass spectrum 57  
   solvent/nonsolvent 69  
   universal calibration curve 244  
 poly( $\gamma$ -benzyl-L-glutamate) 43  
   persistence length 48  
 poly(methyl methacrylate)  
   solvent/nonsolvent 69  
   theta temperature 102  
   universal calibration curve 244  
 poly(*n*-hexyl isocyanate) 42  
   intrinsic viscosity 270  
   persistence length 47  
   radius of gyration 48  
 poly(*N*-isopropyl acrylamide)  
   radius of gyration 106  
   theta temperature 102  
 poly(*p*-phenylene) 42, 48  
 poly(vinyl *neo*-decanoate)  
   intrinsic viscosity 216  
 polydiacetylene 42  
 polydisperse 55, 87, 97, 133  
   diffusion coefficient 205  
   intrinsic viscosity 220  
 polydispersity index 57  
 polyelectrolyte 43  
 polyethylene  
   branched 52  
   radius of gyration 38  
 polystyrene  
   autocorrelation function 190  
   correlation length 293, 309  
   hydrodynamic radius 188, 191  
   osmotic compressibility 289  
   phase diagram 101  
   radius of gyration 38, 104, 296  
   second virial coefficient 103  
   self-diffusion coefficient 319

- solvent/nonsolvent 69
- theta temperature 102
- tracer diffusion coefficient 320, 322
- universal calibration curve 244
- poor solvent 87
- pore 148
- primitive chain 311
  - center-of-mass motion 315
- probe 198, 320
- pulsed-field gradient nuclear magnetic resonance 197, 319
  
- QELS 168
- quasi-elastic light scattering 168
  
- radius of gyration 16, 120, 132
- random coil 3
- random copolymer 2
- random force 191, 222, 228
- random walk 7, 311
  - continuous space 14
  - cubic lattice 13
  - square lattice 12
- random-branched chain 49
- Rayleigh scattering 111
- real chain 5, 6, 7
  - end-to-end distance 33, 36
  - free energy 36
  - radius of gyration 36
- reduced viscosity 212
- refractive index 108, 109, 129
- relative viscosity 211
- renormalization group theory 36, 239, 287
- reptation 312
  - monomer diffusion 324
  - theory 310
- retention
  - curve 149
  - time 149
  - volume 149
- ring polymer 52
  - radius of gyration 53
- rodlike molecule 43
  - concentration regime 65
  - dynamics 262
  - overlap concentration 65
  - rotational correlation 265
- rotational isometric state model 3
- Rouse model 221, 314, 323
  - center-of-mass diffusion coefficient 234
  - end-to-end vector 234
  - equation of motion 222, 226, 227
  - fluctuations 233
  - initial slope 247
  - intrinsic viscosity 243
  - monomer displacement 252, 253, 254
  - relaxation time 228
  - spring constant 227
- SANS 136
- SAXS 139
- scaling
  - function 287
  - plot 287
  - theory 286
- scatterer 110
- scattering
  - angle 109
  - cross section 137
  - function 116
  - intensity 168, 169
  - length 137
  - vector 109
  - volume 110
- SEC 148
- second virial coefficient 79, 93, 98, 131, 132
- segment 4
  - density 117
  - length 15, 23
- self-avoiding walk 39
  - chain contraction 296
  - chemical potential 294
  - radius of gyration 40, 296
- self-diffusion 197
- semidilute regime
  - upper limit 278
- semidilute solution 65, 277
  - chemical potential 285, 294, 298, 304
  - correlation length 282, 290
  - excess scattering 289, 305
  - Flory's method 305
  - osmotic compressibility 289
  - osmotic pressure 282, 286, 297, 303, 306
  - partition coefficient 299, 301, 306
  - radius of gyration 295
  - self-diffusion coefficient 319
  - theta condition 296, 305, 306
- semiflexible polymer 41
- semirigid chain 41

- shear flow 217
- shear rate 218
- shear stress 210
- short-range interaction 19, 35, 72
- single-phase regime 85
- site 5, 71
- size exclusion chromatography 38, 148, 300
  - calibration curve 159
  - light scattering detector 160
  - universal calibration curve 243
  - viscosity detector 216
- SLS 109
- small-angle neutron scattering 136, 296
- small-angle X-ray scattering 139
- solubility parameter 107
- specific refractive index increment 130
- specific viscosity 212
- spinodal line 82
- square lattice 5, 12
- star polymer 49
  - hydrodynamic radius 203
  - polydispersity index 62
- star-branched chain 49
- static light scattering 109
- static structure factor 116
  - copolymer 139
  - Gaussian chain 122, 166
  - real chain 125
  - semidilute solution 292
- stationary phase 148
- Stirling's formula 11
- Stokes radius 184
- Stokes-Einstein equation 184
  
- telechelic molecule 146, 147
- test chain 310
- theta condition 86
  - radius of gyration 104
  - self-avoiding walk 105
- theta solvent 6
- theta temperature 86, 200, 102
- third virial coefficient 79, 93, 98
- tracer 198
- transition probability 23
  - concentration 179
  - Gaussian 178
  - particles 175
- triangular lattice 5
  
- tube 310
  - diameter 318, 324
  - disengagement 313
  - length 312
  - model 310
  - renewal 312
- two-phase regime 85
  
- UCST 99
- unstable 81
- upper critical solution temperature 99, 103
  
- vapor pressure osmometry 77, 164
- velocity gradient 210
- virial expansion 79, 93, 98
- viscometer 213
  - Ubbelohde 213
- viscosity 211
  - kinematic 214
  - zero-shear 218
  
- wave vector 109
- weak-to-strong penetration transition 301
- weight-average molecular weight 55
- Wiener process 178
- wormlike chain 43
  - dynamics 269
  - end-to-end distance 45
  - overlap concentration 66
  - radius of gyration 45
  
- z-average molecular weight 56
- Zimm model 234
- Zimm model (good solvent) 238
  - center-of-mass diffusion coefficient 239
  - fluctuations 271
  - initial slope 249
  - intrinsic viscosity 243
  - monomer displacement 252, 256
  - relaxation time 239
  - spring constant 239
- Zimm model (theta solvent) 236
  - center-of-mass diffusion coefficient 237
  - equation of motion 237
  - initial slope 248
  - intrinsic viscosity 243
  - monomer displacement 252, 255
  - relaxation time 238
  - spring constant 237
- Zimm plot 133, 147

---

# 1

---

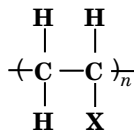
## Models of Polymer Chains

### 1.1 INTRODUCTION

#### 1.1.1 Chain Architecture

A polymer molecule consists of the same repeating units, called monomers, or of different but resembling units. Figure 1.1 shows an example of a vinyl polymer, an industrially important class of polymer. In the repeating unit, X is one of the monofunctional units such as H, CH<sub>3</sub>, Cl, and C<sub>6</sub>H<sub>5</sub> (phenyl). The respective polymers would be called polyethylene, polypropylene, poly(vinyl chloride), and polystyrene. A double bond in a vinyl monomer CH<sub>2</sub>=CHX opens to form a covalent bond to the adjacent monomer. Repeating this polymerization step, a polymer molecule is formed that consists of  $n$  repeating units. We call  $n$  the **degree of polymerization** (DP). Usually,  $n$  is very large. It is not uncommon to find polymers with  $n$  in the range of  $10^4$ – $10^5$ .

In the solid state, polymer molecules pack the space with little voids either in a regular array (crystalline) or at random (amorphous). The molecules are in close contact with other polymer molecules. In solutions, in contrast, each polymer molecule is surrounded by solvent molecules. We will learn in this book about properties of the polymer molecules in this dispersed state. The large  $n$  makes many of the properties common to all polymer molecules but not shared by small molecules. A difference in the chemical structure of the repeating unit plays a secondary role. The difference is usually represented by parameters in the expression of each physical property, as we will see throughout this book.



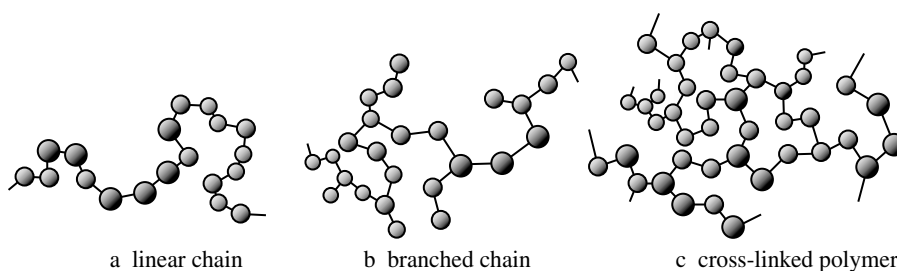
**Figure 1.1.** Vinyl polymer.

Figure 1.2 shows three architectures of a polymer molecule: a **linear chain** (a), a **branched chain** (b), and a **cross-linked polymer** (c). A bead represents a monomer here. A vinyl polymer is a typical linear polymer. A branched chain has branches, long and short. A cross-linked polymer forms a network encompassing the entire system. In fact, there can be just one supermolecule in a container. In the branched chain, in contrast, the branching does not lead to a supermolecule. A cross-linked polymer can only be swollen in a solvent. It cannot be dissolved. We will learn linear chain polymers in detail and about branched polymers to a lesser extent.

Some polymer molecules consist of more than one kind of monomers. An **A–B copolymer** has two constituent monomers, A and B. When the monomer sequence is random, i.e., the probability of a given monomer to be A does not depend on its neighbor, then the copolymer is called a **random copolymer**. There is a different class of linear copolymers (Fig. 1.3). In an **A–B diblock copolymer**, a whole chain consists of an A block, a B block, and a joint between them. In a triblock copolymer, the chain has three blocks, A, B, and C. The C block can be another A block. A polymer consisting of a single type of monomers is distinguished from the copolymers and is called a **homopolymer**.

### 1.1.2 Models of a Linear Polymer Chain

**1.1.2.1 Models in a Continuous Space** A polymer chain in the solution is changing its shape incessantly. An instantaneous shape of a polymer chain in



**Figure 1.2.** Architecture of polymer chain: a linear chain (a), a branched chain (b), and a cross-linked polymer (c).

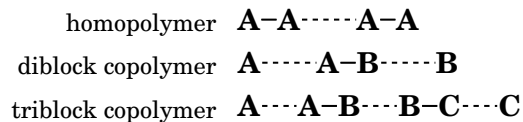


**Figure 1.3.** Homopolymer and block copolymers.

solution (Fig. 1.4a) is called a **conformation**. To represent the overall chain conformation, we strip all of the atoms except for those on the backbone (Fig. 1.4b). Then, we remove the atoms and represent the chain by connected bonds (Fig. 1.4c). In linear polyethylene, for instance, the chain is now represented by a link of carbon–carbon bonds only. We can further convert the conformation to a smoothed line of thread (Fig. 1.4d). In the last model, a polymer chain is a geometrical object of a thin flexible thread.

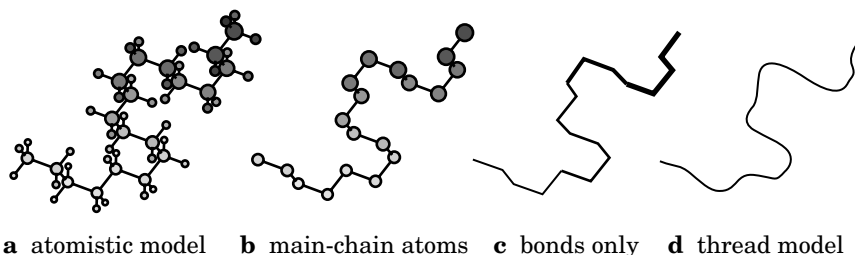
We now pull the two ends of the skeletal linear chain to its full extension (Fig. 1.5). In a vinyl polymer, the chain is in all-*trans* conformation. The distance between the ends is called the **contour length**. The contour length ( $L_c$ ) is proportional to DP or the molecular weight of the polymer. In solution, this fully stretched conformation is highly unlikely. The chain is rather crumpled and takes a conformation of a **random coil**.

Several coarse-grained geometrical models other than the skeletal chain model are being used to predict how various physical quantities depend on the chain length, the polymer concentration, and so forth, and to perform computer simulations. Figure 1.6 illustrates a **bead-stick model** (a), a **bead-spring model** (b), and a **pearl-necklace model** (c).

In the bead-stick model, the chain consists of beads and sticks that connect adjacent beads. Many variations are possible: (1) the bead diameter and the stick thickness can be any nonnegative value, (2) we can restrict the angle between two adjacent sticks or let it free, or (3) we can restrict the torsional angle (dihedral angle) of a stick relative to the second next stick. Table 1.1 compares two typical variations of the model: a **freely jointed chain** and a **freely rotating chain**. When the bond angle is fixed to the tetrahedral angle in the  $sp^3$  orbitals of a carbon atom and the dihedral angle is fixed to the one of the three angles corresponding to *trans*, *gauche* +, and *gauche* –, the model mimics the backbone of an actual linear vinyl polymer. The latter is given a special name, **rotational isometric state model** (RIMS). A more sophisticated model would allow the stick length and the bond

**TABLE 1.1** Bead-Stick Models

Model	Bond Length	Bond Angle	Dihedral Angle
Freely jointed chain	fixed	free	free
Freely rotating chain	fixed	fixed	free



**a** atomistic model   **b** main-chain atoms   **c** bonds only   **d** thread model

**Figure 1.4.** Simplification of chain conformation from an atomistic model (a) to main-chain atoms only (b), and then to bonds on the main chain only (c), and finally to a flexible thread model (d).

angle to vary according to harmonic potentials and the dihedral angle following its own potential function with local minima at the three angles. In the bead-stick model, we can also regard each bead as representing the center of a monomer unit (consisting of several or more atoms) and the sticks as representing just the connectivity between the beads. Then, the model is a **coarse-grained** version of a more atomistic model. A bead-stick pair is called a **segment**. The segment is the smallest unit of the chain. When the bead diameter is zero, the segment is just a stick.

In the bead-spring model, the whole chain is represented by a series of beads connected by springs. The equilibrium length of each spring is zero. The bead-spring model conveniently describes the motion of different parts of the chain. The segment of this model is a spring and a bead on its end.

In the pearl-necklace model, the beads (pearls) are always in contact with the two adjacent beads. This model is essentially a bead-stick model with the stick length equal to the bead diameter. The bead always has a positive diameter. As in the bead-stick model, we can restrict the bond angle and the dihedral angle.

There are other models as well. This textbook will use one of the models that allows us to calculate most easily the quantity we need.

**1.1.2.2 Models in a Discrete Space** The models described in the preceding section are in a continuous space. In the bead-stick model, for instance, the bead centers can be anywhere in the three-dimensional space, as long as the arrangement satisfies the requirement of the model. We can construct a linear chain on a discrete

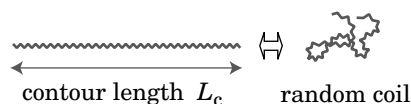


**Figure 1.5.** A random-coil conformation is pulled to its full length  $L_c$ .

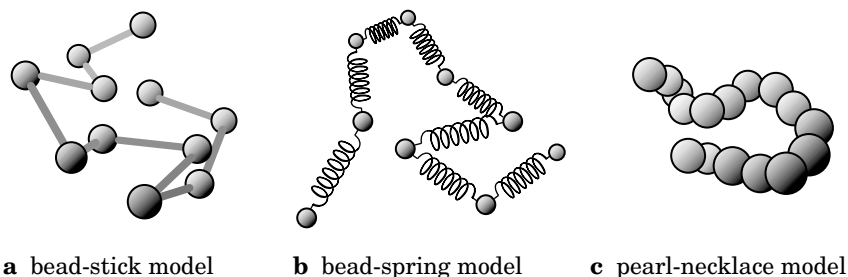


**Figure 1.6.** Various models for a linear chain polymer in a continuous space: a bead-stick model (a), a bead-spring model (b), and a pearl-necklace model (c).

space as well. The models on a discrete space are widely used in computer simulations and theories.

The discrete space is called a **lattice**. In the lattice model, a polymer chain consists of monomers sitting on the grids and bonds connecting them. The grid point is called a **site**; Figure 1.7 illustrates a linear polymer chain on a square lattice (a) and a triangular lattice (b), both in two dimensions. The segment consists of a bond and a point on a site. In three dimensions, a cubic lattice is frequently used and also a diamond lattice to a lesser extent. Figure 1.8 shows a chain on the cubic lattice. The diamond (tetrahedral) lattice is constructed from the cubic lattice and the body centers of the cubes, as shown in Figure 1.9. The chain on the diamond lattice is identical to the bead-stick model, with a bond angle fixed to the tetrahedral angle and a dihedral angle at one of the three angles separated by  $120^\circ$ . There are other lattice spaces as well.

The **lattice coordinate**  $Z$  refers to the number of nearest neighbors for a lattice point. Table 1.2 lists  $Z$  for the four discrete models.

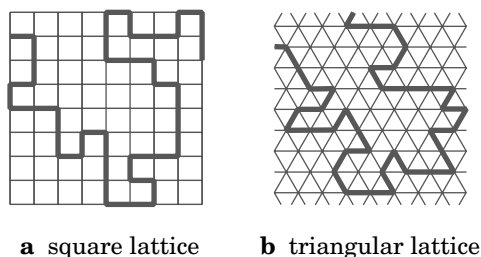
### 1.1.3 Real Chains and Ideal Chains

In any real polymer chain, two monomers cannot occupy the same space. Even a part of a monomer cannot overlap with a part of the other monomer. This effect is called an **excluded volume** and plays a far more important role in polymer solutions than it does in solutions of small molecules. We will examine its ramifications in Section 1.4.

**TABLE 1.2** Coordination Number

Dimensions	Geometry	$Z$
2	square	4
2	triangular	6
3	cubic	6
3	diamond	4





**a** square lattice      **b** triangular lattice

**Figure 1.7.** Linear chains on a square lattice (a) and a triangular lattice (b).

We often idealize the chain to allow overlap of monomers. In the lattice model, two or more monomers of this **ideal chain** can occupy the same site. To distinguish a regular chain with an excluded volume from the ideal chain, we call the regular chain with an excluded volume a **real chain** or an **excluded-volume chain**. Figure 1.10 illustrates the difference between the real chain (right) and the ideal chain (left) for a thread model in two dimensions. The chain conformation is nearly the same, except for a small part where two parts of the chain come close, as indicated by dashed-line circles. Crossing is allowed in the ideal chain but not in the real chain. The ideal chain does not exist in reality, but we use the ideal-chain model extensively because it allows us to solve various problems in polymer solutions in a mathematically rigorous way. We can treat the effect of the excluded effect as a small difference from the ideal chains. More importantly, though, the real chain behaves like an ideal chain in some situations. One situation is concentrated solutions, melts, and glasses. The other situation is a dilute solution in a special solvent called a theta solvent. We

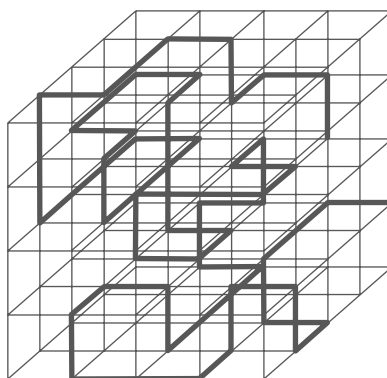


**Figure 1.8.** Linear chain on a cubic lattice.

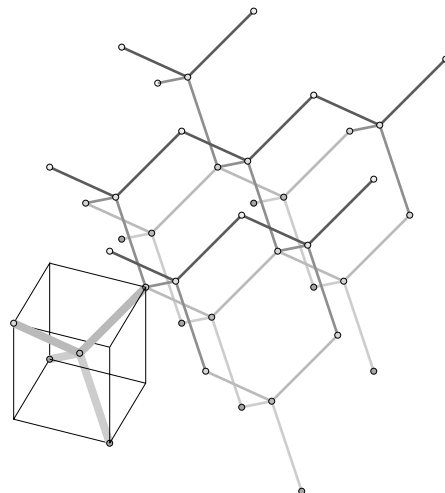


**Figure 1.9.** Diamond lattice.

will learn about the theta solvent in Section 2.3 and the concentrated solution in Chapter 4.

## 1.2 IDEAL CHAINS

### 1.2.1 Random Walk in One Dimension

**1.2.1.1 Random Walk** A linear flexible polymer chain can be modeled as a **random walk**. The concept of the random walk gives a fundamental frame for the conformation of a polymer chain. If visiting the same site is allowed, the trajectory of the random walker is a model for an ideal chain. If not allowed, the trajectory resembles a real chain. In this section, we learn about the ideal chains in three dimensions. To familiarize ourselves with the concept, we first look at an ideal random walker in one dimension.

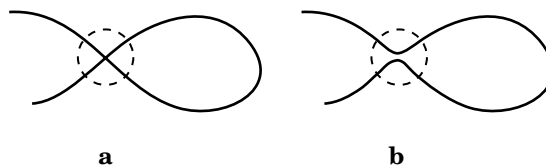


**Figure 1.10.** Conformations of an ideal chain (a) and a real chain (b) in two dimensions.

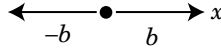


**Figure 1.11.** Step motion in one-dimensional random walk.

The random walker moves in each step by  $b$  either to the right or to the left, each with a probability of one-half (Fig. 1.11). Each time it decides where to move next independently of its preceding moves. The walker does not have a memory regarding where it has come from. The latter property is called **Markoffian** in stochastic process theory. The walker can come back to the sites previously visited (ideal). The  $N$ -step trajectory of the random walker is a chain of length  $Nb$  folded one-dimensionally, as illustrated in Figure 1.12. The movement of the random walker is specified by a sequence of “+” and “-,” with + being the motion to the right and - being that to the left. In this example the sequence is ++----+-----+----+--. Thus one arrangement of the chain folding corresponds to an event of having a specific sequence of + and -. Another way to look at this sequence is to relate + to the head and - to the tail in a series of coin tosses.

Suppose there are  $n$  “+” out of a total  $N$  trials ( $n = 0, 1, \dots, N$ ). Then the random walker that started at  $x = 0$  on the  $x$ -axis has reached a final position of  $x = nb + (N - n)(-b) = b(2n - N)$ . How these  $n+$  are arranged is irrelevant to the final position. What matters is how many + there are. If all are +,  $x = Nb$ ; if all are -,  $x = -Nb$ . The probability  $P_n$  to have  $n+$  is given by

$$P_n = 2^{-N} {}_N C_n = 2^{-N} \frac{N!}{n!(N-n)!} \quad (1.1)$$

The probability distribution is called a binomial distribution, because  $P_n$  is equal to the  $n$ th term in the expansion of

$$(p + q)^N = \sum_{n=0}^N p^n q^{N-n} {}_N C_n \quad (1.2)$$

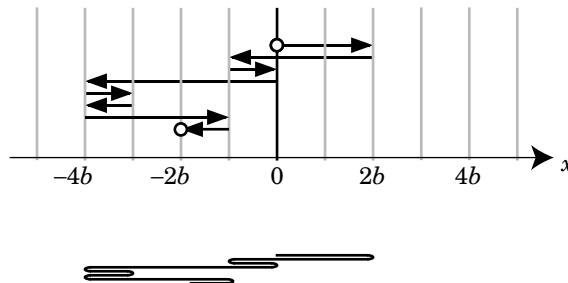


**Figure 1.12.** One-dimensional random walk of 16 steps. The trajectory is a folded chain.

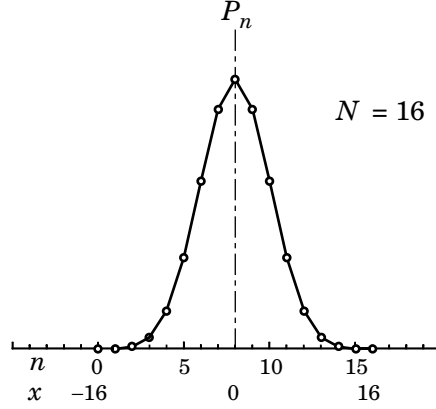


**Figure 1.13.** Probability distribution for the number  $n$  of positive moves. The corresponding final position  $x$  is also indicated.

with  $p = q = 1/2$ . Thus we find that  $P_n$  given by Eq. 1.1 is normalized. An example of  $P_n$  is shown in Figure 1.13 for  $N = 16$ . The range of  $n$  is between 0 and  $N$ , which translates into the range of  $x$  between  $-N$  and  $N$ . Only every other integral values of  $x$  can be the final position of the random walker for any  $N$ .

**1.2.1.2 Mean Square Displacement** If we set  $p = q = 1$  in Eq. 1.2, we have the identity

$$2^N = \sum_{n=0}^N \frac{N!}{n!(N-n)!} \quad (1.3)$$

Using the identity, the mean (expectation) of  $n$  is calculated as follows:

$$\langle n \rangle = \sum_{n=0}^N n P_n = 2^{-N} \sum_{n=0}^N \frac{n N!}{n!(N-n)!} = 2^{-N} N \sum_{n=1}^N \frac{(N-1)!}{(n-1)!(N-n)!} = 2^{-N} N 2^{N-1} = N/2 \quad (1.4)$$

On the average, the random walker moves half of the steps to the right. Likewise, the average of  $n^2$  is calculated as

$$\begin{aligned} \langle n^2 \rangle &= \sum_{n=0}^N n^2 P_n = 2^{-N} \sum_{n=0}^N \frac{n^2 N!}{n!(N-n)!} \\ &= 2^{-N} \left[ N(N-1) \sum_{n=2}^N \frac{(N-2)!}{(n-2)!(N-n)!} + N \sum_{n=1}^N \frac{(N-1)!}{(n-1)!(N-n)!} \right] \quad (1.5) \\ &= N(N+1)/4 \end{aligned}$$

Then the variance, the mean square of  $\Delta n \equiv n - \langle n \rangle$ , is

$$\langle \Delta n^2 \rangle = \langle (n - \langle n \rangle)^2 \rangle = \langle n^2 \rangle - \langle n \rangle^2 = N/4 \quad (1.6)$$

Its square root,  $\langle \Delta n^2 \rangle^{1/2}$ , called the standard deviation, is a measure for the broadness of the distribution. Note that both  $\langle n \rangle$  and  $\langle \Delta n^2 \rangle$  increase linearly with  $N$ . Therefore, the relative broadness,  $\langle \Delta n^2 \rangle^{1/2} / \langle n \rangle$ , decreases with increasing  $N$ .

Let us translate these statistical averages of  $n$  into those of  $x$ . Because  $x = b(2n - N)$ , the mean and the variance of  $x$  are

$$\boxed{\langle x \rangle = 0, \quad \langle \Delta x^2 \rangle = \langle x^2 \rangle = Nb^2 \quad \text{1D random walk}} \quad (1.7)$$

where  $\Delta x = x - \langle x \rangle$  is the displacement of the random walker in  $N$  steps. Because  $x = 0$  before the random walk,  $\Delta x = x$ . The average of its square,  $\langle \Delta x^2 \rangle$ , is called the **mean square displacement**.

**1.2.1.3 Step Motion** Now we look at the  $N$ -step process from another perspective. Let  $\Delta x_n$  be the displacement in the  $n$ th step. Then,  $\Delta x_n$  is either  $b$  or  $-b$  with an equal probability. Therefore,  $\langle \Delta x_n \rangle = 0$  and  $\langle \Delta x_n^2 \rangle = b^2$ . Different steps are not correlated. Mathematically, it is described by  $\langle \Delta x_n \Delta x_m \rangle = 0$  if  $n \neq m$ . Combining  $n = m$  and  $n \neq m$ , we write

$$\langle \Delta x_n \Delta x_m \rangle = b^2 \delta_{nm} \quad (1.8)$$

where  $\delta_{nm}$  is the Kronecker's delta ( $\delta_{nm} = 1$  if  $n = m$ ;  $\delta_{nm} = 0$  otherwise). In  $N$  steps, the random walker arrives at  $x$ , starting at  $x = 0$ . The total displacement  $\Delta x = x - 0$  of the  $N$  steps is given as

$$\Delta x = \sum_{n=1}^N \Delta x_n \quad (1.9)$$

The mean and the variance of  $\Delta x$  are calculated as

$$\langle \Delta x \rangle = \left\langle \sum_{n=1}^N \Delta x_n \right\rangle = \sum_{n=1}^N \langle \Delta x_n \rangle = 0 \quad (1.10)$$

$$\langle \Delta x^2 \rangle = \left\langle \sum_{n=1}^N \Delta x_n \sum_{m=1}^N \Delta x_m \right\rangle = \left\langle \sum_{n,m=1}^N \Delta x_n \Delta x_m \right\rangle = \sum_{n,m=1}^N \langle \Delta x_n \Delta x_m \rangle = \sum_{n=1}^N \langle \Delta x_n^2 \rangle = Nb^2 \quad (1.11)$$

As required, the results are identical to those in Eq. 1.7.

**1.2.1.4 Normal Distribution** Let us see how  $P_n$  or  $P(x)$  changes when  $N$  increases to a large number. Figure 1.14 compares  $P_n$  for  $N = 4, 16, \text{ and } 64$ . As  $N$

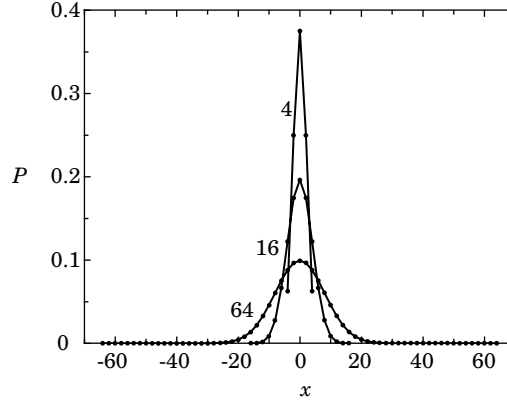


**Figure 1.14.** Distribution of the final position  $x$  for 4-, 16-, and 64-step random walks.

increases, the plot approaches a continuously curved line. To predict the large  $N$  asymptote of  $P_n$ , we use Stirling's formula  $\ln N! \cong N(\ln N - 1)$ . Equation 1.1 is rewritten to

$$\begin{aligned} \ln P_n &= -N \ln 2 + N(\ln N - 1) - n(\ln n - 1) - (N - n)[\ln(N - n) - 1] \\ &= -N \ln 2 + N \ln N - n \ln n - (N - n) \ln(N - n) \end{aligned} \quad (1.12)$$

With  $n = (N + x/b)/2$ , this equation is converted to a function of  $x$ :

$$\begin{aligned} \ln P &\cong -N \ln 2 + N \ln N - \frac{1}{2}(N - x/b) \ln[(N - x/b)/2] \\ &\quad - \frac{1}{2}(N + x/b) \ln[(N + x/b)/2] \\ &= N \ln N - \frac{1}{2}(N - x/b) \ln(N - x/b) - \frac{1}{2}(N + x/b) \ln(N + x/b) \\ &= -\frac{1}{2}N \left[ \left(1 - \frac{x}{Nb}\right) \ln \left(1 - \frac{x}{Nb}\right) + \left(1 + \frac{x}{Nb}\right) \ln \left(1 + \frac{x}{Nb}\right) \right] \\ &\cong -\frac{1}{2}N \left(\frac{x}{Nb}\right)^2 = -\frac{x^2}{2Nb^2} \end{aligned} \quad (1.13)$$

where the Taylor expansion was taken up to the second order of  $x/(Nb)$  in the last part, because  $P(x)$  is almost zero except at small  $|x/(Nb)|$ . This equation does not satisfy the normalization condition because we used a crude version of Stirling's formula. Normalization leads Eq. 1.13 to

$$\boxed{P(x) = (2\pi Nb^2)^{-1/2} \exp\left(-\frac{x^2}{2Nb^2}\right) \quad \text{1D random walk}} \quad (1.14)$$

This probability distribution, shown in Figure 1.15, is a **normal distribution** with a zero mean and a variance of  $Nb^2$ . Note that the mean and the variance are the same

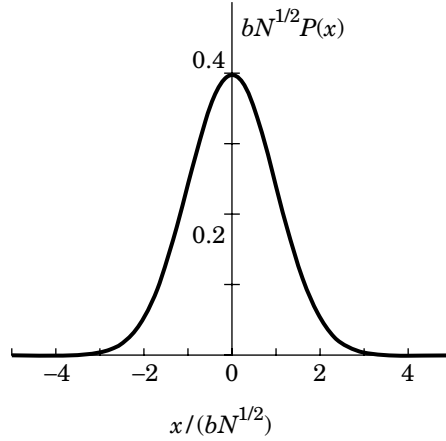


**Figure 1.15.** Distribution of the final position  $x$  for a random walk of infinite number of steps.

as those we calculated for its discrete version  $P_n$ . Now  $x$  is continuously distributed. The probability to find the walker between  $x$  and  $x + dx$  is given by  $P(x)dx$ .

For a large  $N$ , the binomial distribution approaches a normal distribution. This rule applies to other discrete distributions as well and, in general, is called the **law of large numbers** or the **central limit theorem**. When  $N \gg 1$ , the final position  $x$  of the random walker is virtually continuously distributed along  $x$ .

## 1.2.2 Random Walks in Two and Three Dimensions

**1.2.2.1 Square Lattice** We consider a random walk on a square lattice extending in  $x$  and  $y$  directions with a lattice spacing  $b$ , as shown in Figure 1.7a. The random walker at a grid point chooses one of the four directions with an equal probability of  $1/4$  (Fig. 1.16). Each step is independent. Again, the random walker can visit the same site more than once (ideal). The move in one step can be expressed by a displacement  $\Delta \mathbf{r}_1 = [\Delta x_1, \Delta y_1]$ . Similarly to the random walker in one dimension,  $\langle \Delta x_1 \rangle = \langle \Delta y_1 \rangle = 0$  and hence  $\langle \Delta \mathbf{r}_1 \rangle = 0$ . The variances are  $\langle \Delta x_1^2 \rangle = \langle \Delta y_1^2 \rangle = b^2/2$ ; therefore, the mean square displacement is  $\langle \Delta \mathbf{r}_1^2 \rangle = b^2$ . In a total  $N$  steps starting at  $\mathbf{r} = 0$ , the statistics for the final position  $\mathbf{r}$  and the displacement  $\Delta \mathbf{r}$  are:  $\langle x \rangle = \langle \Delta x \rangle = 0$ ,  $\langle y \rangle = \langle \Delta y \rangle = 0$  and hence  $\langle \mathbf{r} \rangle = \langle \Delta \mathbf{r} \rangle = 0$ ;  $\langle x^2 \rangle = \langle \Delta x^2 \rangle = Nb^2/2$ ,  $\langle y^2 \rangle = \langle \Delta y^2 \rangle = Nb^2/2$  and hence  $\langle \mathbf{r}^2 \rangle = \langle \Delta \mathbf{r}^2 \rangle = Nb^2$ .

The  $x$  component of the position after the  $N$ -step random walk on the two-dimensional (2D) square lattice has a zero mean and a variance of  $Nb^2/2$ . When  $N \gg 1$ , the probability density  $P_x(\mathbf{r})$  for the  $x$  component approaches a normal distribution with the same mean and variance. Thus,

$$P_x(\mathbf{r}) = (\pi Nb^2)^{-1/2} \exp[-x^2/(Nb^2)] \quad (1.15)$$

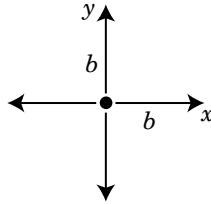


**Figure 1.16.** Step motion in a two-dimensional random walk on a square lattice.

The  $y$ -component  $P_y(\mathbf{r})$  has a similar expression. When the two components are combined, we have the joint probability density  $P(\mathbf{r}) = P_x(\mathbf{r})P_y(\mathbf{r})$  as

$$P(\mathbf{r}) = (\pi Nb^2)^{-1} \exp\left(-\frac{\mathbf{r}^2}{Nb^2}\right) \quad \text{2D random walk} \quad (1.16)$$

Again, the mean and the variance are held unchanged in the limiting procedure.

**1.2.2.2 Lattice in Three Dimensions** We place the random walker on a cubic lattice with a lattice spacing  $b$  in three dimensions, as shown in Figure 1.8. In each step, the random walker chooses one of the six directions with an equal probability of  $1/6$  (Fig. 1.17). The displacement in one step is expressed by  $\Delta\mathbf{r}_1 = [\Delta x_1, \Delta y_1, \Delta z_1]$ . Statistical properties of  $\Delta\mathbf{r}_1$  and their components are  $\langle\Delta\mathbf{r}_1\rangle = 0$ ,  $\langle\Delta x_1^2\rangle = \langle\Delta y_1^2\rangle = \langle\Delta z_1^2\rangle = b^2/3$ ; therefore,  $\langle\Delta\mathbf{r}_1^2\rangle = b^2$ . In a total  $N$  steps starting at  $\mathbf{r} = 0$ , the statistics for the final position  $\mathbf{r}$  and the displacement  $\Delta\mathbf{r}$  are  $\langle\mathbf{r}\rangle = \langle\Delta\mathbf{r}\rangle = 0$ ;  $\langle\Delta x^2\rangle = \langle\Delta y^2\rangle = \langle\Delta z^2\rangle = Nb^2/3$  and  $\langle\mathbf{r}^2\rangle = \langle\Delta\mathbf{r}^2\rangle = Nb^2$ .

The  $x$  component of the position after the  $N$ -step random walk on the three-dimensional (3D) cubic lattice has a zero mean and a variance of  $Nb^2/3$ . When  $N \gg 1$ , the probability density  $P_x(\mathbf{r})$  for the  $x$  component approaches that of a normal distribution with the same mean and variance. Thus,

$$P_x(\mathbf{r}) = (2\pi Nb^2/3)^{-1/2} \exp[-3x^2/(2Nb^2)] \quad (1.17)$$

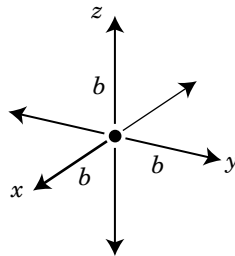


**Figure 1.17.** Step motion in a three-dimensional random walk on a cubic lattice.



The other components have a similar expression. When the three components are combined, we have the joint probability density  $P(\mathbf{r}) = P_x(\mathbf{r})P_y(\mathbf{r})P_z(\mathbf{r})$  as

$$P(\mathbf{r}) = (2\pi Nb^2/3)^{-3/2} \exp\left(-\frac{3\mathbf{r}^2}{2Nb^2}\right) \quad \text{3D random walk} \quad (1.18)$$

Note that  $P(\mathbf{r})$  depends only on  $|\mathbf{r}|$ ; i.e., the distribution of  $\mathbf{r}$  is isotropic.

The random walk is not limited to rectangular lattices. In the nonrectangular lattices such as a triangular lattice and a diamond lattice with lattice unit  $= b$ , we let the random walker choose one of the  $Z$  nearest-neighbor sites with an equal probability irrespective of its past (Markoffian). Then, the same statistics holds for  $\Delta\mathbf{r}_i$  as the one in the rectangular lattices:

$$\langle \Delta\mathbf{r}_i \rangle = 0, \quad \langle \Delta\mathbf{r}_i \cdot \Delta\mathbf{r}_j \rangle = b^2 \delta_{ij} \quad (1.19)$$

In a total  $N$  steps,  $\langle \Delta\mathbf{r} \rangle = 0$  and  $\langle \Delta\mathbf{r}^2 \rangle = Nb^2$ . Then, for  $N \gg 1$ , the probability density for  $\mathbf{r}$  is given by the same equations (Eqs. 1.16 and 1.18 for the 2D and 3D lattices, respectively). The type of the lattice is irrelevant. When  $N$  is not sufficiently large, however,  $P(\mathbf{r})$  is different from lattice to lattice, reflecting its detailed structure. Note that  $b$  is the lattice unit, not its projection onto the  $x$ ,  $y$ , or  $z$  axis.

**1.2.2.3 Continuous Space** The random walks are not limited to those on a lattice. Here, we consider a random walker who jumps by a fixed distance  $b$ . The trajectory is shown in Figure 1.18 for a two-dimensional version of the continuous-space random walk. Starting at  $\mathbf{r}_0$ , the walker moves by  $\Delta\mathbf{r}_1, \Delta\mathbf{r}_2, \dots, \Delta\mathbf{r}_N$  to arrive at  $\mathbf{r}_N$  in a total  $N$  steps. When the direction is random in three dimensions, the trajectory represents a freely jointed chain (Table 1.1). Like a random walk on the lattice, the  $i$ th jump  $\Delta\mathbf{r}_i$  is not correlated with the  $j$ th jump  $\Delta\mathbf{r}_j$  if  $i \neq j$ . As long as  $\Delta\mathbf{r}_i$  satisfies Eq. 1.19, the displacement in a total  $N$  steps has the same statistical

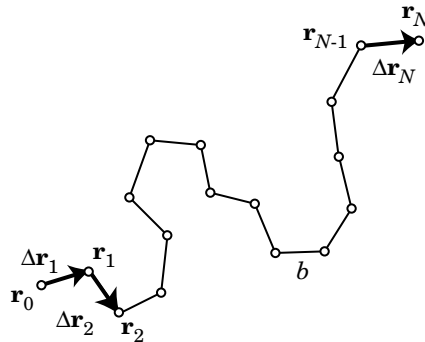


**Figure 1.18.** Trajectory of a two-dimensional random walk of  $N$  steps with a fixed step displacement length  $b$ .

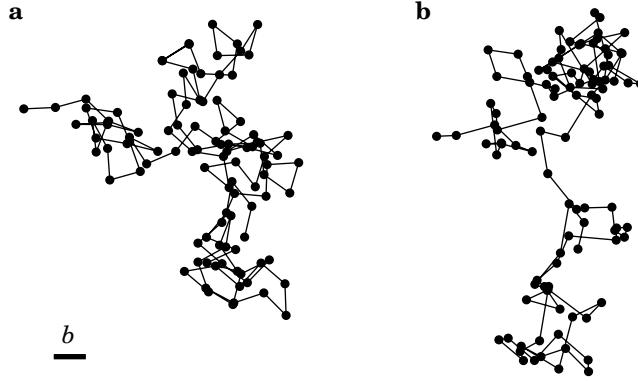


**Figure 1.19.** Example of a freely jointed chain (a) and a bead-spring model (b) of 100 steps with the same orientation of each pair of jumps in two dimensions. The bar shows the bond length  $b$ .

properties as a random walk on the cubic lattice:  $\langle \Delta \mathbf{r} \rangle = 0$  and  $\langle \Delta \mathbf{r}^2 \rangle = Nb^2$ . When  $N \gg 1$ , the probability density of the final position  $\mathbf{r}_N$  is given by

$$P(\mathbf{r}_N) = (2\pi Nb^2/3)^{-3/2} \exp\left(-\frac{3(\mathbf{r}_N - \mathbf{r}_0)^2}{2Nb^2}\right) \quad \text{3D random walk} \quad (1.20)$$

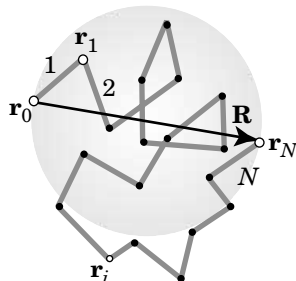
The step length does not have to be fixed to  $b$  either. Suppose the step length has some distribution, but each step follows the same distribution to yield  $\langle \Delta \mathbf{r}_i^2 \rangle = b^2$ . A typical trajectory of this type of random walk is seen in a bead-spring model. With a randomness in the orientation of  $\Delta \mathbf{r}_i$  and a common distribution for all of  $\Delta \mathbf{r}_i$ ,  $\Delta \mathbf{r}_i$  will satisfy Eq. 1.19. If  $\Delta \mathbf{r}_i$  and  $\Delta \mathbf{r}_j$  ( $i \neq j$ ) are not correlated, the final position  $\mathbf{r}_N$  follows the distribution given by Eq. 1.20.

Figure 1.19 compares a freely jointed chain with a fixed bond length  $b$  (also called a **segment length**) and a bead-spring model with  $\langle \Delta \mathbf{r}_i^2 \rangle = b^2$ , both in two dimensions. Examples of a 100-step random walk are shown. The bead-spring model can have greater density fluctuations for the same  $Nb^2$ .

## 1.2.3 Dimensions of Random-Walk Chains

**1.2.3.1 End-to-End Distance and Radius of Gyration** Here, we learn how to assess the dimension or the size of a polymer molecule. We consider a linear chain consisting of  $N$  bonds of length  $b$  (Fig. 1.20). The positions of the joints are denoted by  $\mathbf{r}_i$  ( $i = 0, 1, \dots, N$ ). The two ends of the  $i$ th bond are at  $\mathbf{r}_{i-1}$  and  $\mathbf{r}_i$ . It is convenient to define the **end-to-end vector**  $\mathbf{R}$  by

$$\mathbf{R} \equiv \mathbf{r}_N - \mathbf{r}_0 \quad (1.21)$$



**Figure 1.20.** End-to-end vector  $\mathbf{R}$  is defined by  $\mathbf{R} = \mathbf{r}_N - \mathbf{r}_0$  in the bead-stick model. The sphere with  $\mathbf{R}$  as its diameter contains most of the segments.

$\mathbf{R}$  is different for each configuration of the chain. Although the chain ends are not necessarily faced outward and therefore  $\mathbf{R}$  does not always span the largest dimension of the chain, its average length is a good measure for the overall chain dimension. The **root-mean-square end-to-end distance**  $R_F$  (or simply **end-to-end distance**) of the chain is the root mean square of  $\mathbf{R}$ :

$$R_F^2 = \langle \mathbf{R}^2 \rangle \equiv \langle (\mathbf{r}_N - \mathbf{r}_0)^2 \rangle \quad (1.22)$$

We can regard the whole chain as roughly being contained in a sphere of diameter  $R_F$ .

Another often used measure of the chain dimension is the **root-mean-square radius of gyration**  $R_g$  (or simply **radius of gyration**). Its square,  $R_g^2$ , is the second moment around the center of mass of the chain. The latter is defined as the mean square of the distance between the beads and the center of mass (Fig. 1.21). Roughly, the chain occupies a space of a sphere of radius  $R_g$ . The center of mass  $\mathbf{r}_G$  of the chain is given as

$$\mathbf{r}_G = \frac{1}{N+1} \sum_{i=0}^N \mathbf{r}_i \quad (1.23)$$

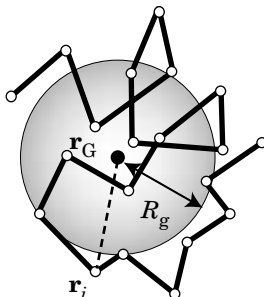


**Figure 1.21.** Center of mass  $\mathbf{r}_G$  and the radius of gyration  $R_g$  in the bead-stick model.

where we assume that beads have the same mass and are connected by massless bonds. Then,  $R_g$  is given by

$$R_g^2 = \left\langle \frac{1}{N+1} \sum_{i=0}^N (\mathbf{r}_i - \mathbf{r}_G)^2 \right\rangle = \frac{1}{N+1} \sum_{i=0}^N \langle (\mathbf{r}_i - \mathbf{r}_G)^2 \rangle \quad (1.24)$$

where the summation and averaging can be interchanged. As the name suggests,  $mR_g^2$  is the moment of inertia ( $m$  represents mass of the molecule) for rotational motion of this molecule around its center of mass.

The following formula is useful:

$$R_g^2 = \frac{1}{2} \left\langle \frac{1}{(N+1)^2} \sum_{i,j=0}^N (\mathbf{r}_i - \mathbf{r}_j)^2 \right\rangle = \frac{1}{2(N+1)^2} \sum_{i,j=0}^N \langle (\mathbf{r}_i - \mathbf{r}_j)^2 \rangle \text{ any conformation} \quad (1.25)$$

This formula indicates that we can use the mean square distance between two monomers to obtain  $R_g$  in place of first calculating  $\mathbf{r}_G$  and then the mean square distance between  $\mathbf{r}_G$  and each monomer. Because summation with respect to  $i$  and  $j$  is another averaging, we can say that  $R_g^2$  is half of the average square distance between two monomers on the chain (Fig. 1.22).

We can prove the formula by using the following identity:

$$\begin{aligned} \sum_{i,j=0}^N (\mathbf{r}_i - \mathbf{r}_j)^2 &= \sum_{i,j=0}^N [(\mathbf{r}_i - \mathbf{r}_G) - (\mathbf{r}_j - \mathbf{r}_G)]^2 \\ &= \sum_{i,j=0}^N (\mathbf{r}_i - \mathbf{r}_G)^2 - 2 \sum_{i,j=0}^N (\mathbf{r}_i - \mathbf{r}_G) \cdot (\mathbf{r}_j - \mathbf{r}_G) + \sum_{i,j=0}^N (\mathbf{r}_j - \mathbf{r}_G)^2 \quad (1.26) \\ &= 2(N+1) \sum_{i=0}^N (\mathbf{r}_i - \mathbf{r}_G)^2 - 2 \sum_{i=0}^N (\mathbf{r}_i - \mathbf{r}_G) \cdot \sum_{j=0}^N (\mathbf{r}_j - \mathbf{r}_G) \\ &= 2(N+1) \sum_{i=0}^N (\mathbf{r}_i - \mathbf{r}_G)^2 \end{aligned}$$

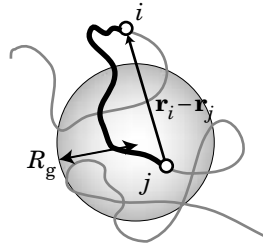


**Figure 1.22.** The mean square distance between two monomers  $i$  and  $j$  is twice as large as  $R_g^2$ .

where Eq. 1.23 was used. This transformation does not assume any specific chain model. Equation 1.25 applies therefore to any chain conformation.

Note that  $R_F$  is defined for linear chains only, but  $R_g$  can be defined for any chain architecture including nonlinear chains such as branched chains. In this sense,  $R_g$  gives a more universal measure for the chain dimension.

**1.2.3.2 Dimensions of Ideal Chains** Now we obtain  $R_F$  and  $R_g$  for ideal chains whose conformations are given as trajectories of random walkers. They include a random walk on a lattice, a freely jointed chain, a bead-spring model, and any other model that satisfies the requirement of Markoffian property (Eq. 1.19). The bond vector  $\mathbf{r}_i - \mathbf{r}_{i-1}$  of the  $i$ th bond is then the displacement vector  $\Delta\mathbf{r}_i$  of the  $i$ th step. We assume Eq. 1.19 only. Then the end-to-end distance is  $Nb^2$ . To calculate  $R_g$ , we note that a part of the ideal chain is also ideal. The formula of the mean square end-to-end distance we obtained for a random walk applies to the mean square distance between the  $i$ th and  $j$ th monomers on the chain just by replacing  $N$  with  $|i - j|$ :

$$\boxed{\langle(\mathbf{r}_i - \mathbf{r}_j)^2\rangle = b^2|i - j| \quad \text{ideal chain}} \quad (1.27)$$

From Eqs. 1.25 and 1.27, we can calculate the radius of gyration of the chain as

$$\begin{aligned} 2R_g^2 &= \frac{1}{(N+1)^2} \sum_{i,j=0}^N b^2|i - j| = \frac{2b^2}{(N+1)^2} \sum_{i=0}^N \sum_{j=0}^i (i - j) \\ &= \frac{2b^2}{(N+1)^2} \sum_{i=0}^N \frac{1}{2}i(i+1) = b^2 \frac{N(N+2)}{3(N+1)} \end{aligned} \quad (1.28)$$

Thus, we find for large  $N$  ideal chains with no correlations between bonds have the dimensions of

$$\boxed{R_F^2 = b^2N, \quad R_g^2 = \frac{1}{6}b^2N \quad \text{ideal chain, } N \gg 1} \quad (1.29)$$

The ratio of  $R_F$  to  $R_g$  is  $6^{1/2} \cong 2.45$  for the ideal chain, close to the diameter to radius ratio.

Both  $R_F^2$  and  $R_g^2$  consist of  $x$ ,  $y$ , and  $z$  components. In Section 1.2.2, we have seen this property for  $R_F^2$  already. The  $x$  component of  $R_g^2$  is defined by

$$R_{gx}^2 = \left\langle \frac{1}{N+1} \sum_{i=0}^N (x_i - x_G)^2 \right\rangle = \frac{1}{N+1} \sum_{i=0}^N \langle (x_i - x_G)^2 \rangle \quad (1.30)$$

where  $x_i$  and  $x_G$  are the  $x$  components of  $\mathbf{r}_i$  and  $\mathbf{r}_G$ , respectively. If there is no preferred orientation of the chain,  $\langle (x_i - x_G)^2 \rangle = \langle (\mathbf{r}_i - \mathbf{r}_G)^2 \rangle / 3$ . Then,  $R_{gx}^2 = R_g^2 / 3$ .

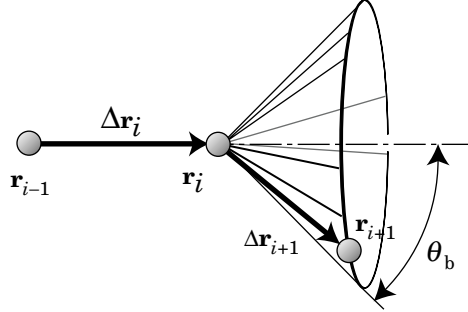


**Figure 1.23.** Bond vectors in the bead-stick model with a fixed bond angle.

**1.2.3.2 Dimensions of Chains with Short-Range Interactions** Now we lift the condition of  $\langle \Delta \mathbf{r}_i \cdot \Delta \mathbf{r}_j \rangle = b^2 \delta_{ij}$  and consider a bead-stick model with a restriction on the choice of the bond angle. In Figure 1.23, the angle  $\theta$  between two adjacent bond vectors (bond angle =  $\pi - \theta$ ) is fixed to  $\theta_b (>0)$ , but there is no restriction on the dihedral angle (freely rotating chain; see Table 1.1). The next bead ( $\mathbf{r}_{i+1}$ ) can be anywhere on the circular base of a cone. Then,  $\langle \Delta \mathbf{r}_i \cdot \Delta \mathbf{r}_{i+1} \rangle = b^2 \cos \theta_b$ .

To calculate  $\langle \Delta \mathbf{r}_{i-1} \cdot \Delta \mathbf{r}_{i+1} \rangle$ , we first obtain  $\langle \Delta \mathbf{r}_{i+1} \rangle_{\Delta \mathbf{r}_i}$ , the average of  $\Delta \mathbf{r}_{i+1}$  for a given  $\Delta \mathbf{r}_i$ .<sup>1</sup> We decompose  $\Delta \mathbf{r}_{i+1}$  into a component parallel to  $\Delta \mathbf{r}_i$  and a component perpendicular to  $\Delta \mathbf{r}_i$  (see Fig. 1.24). The parallel component is  $(\cos \theta_b) \Delta \mathbf{r}_i$ , common to all dihedral angles. The perpendicular component is different from one orientation to another orientation of  $\Delta \mathbf{r}_{i+1}$ , but the randomness in the dihedral angle makes the perpendicular component uniformly distributed on a plane perpendicular to  $\Delta \mathbf{r}_i$ . Thus,  $\langle \Delta \mathbf{r}_{i+1} \rangle_{\Delta \mathbf{r}_i} = (\cos \theta_b) \Delta \mathbf{r}_i$ . Next, we calculate  $\langle \Delta \mathbf{r}_{i-1} \cdot \Delta \mathbf{r}_{i+1} \rangle$  in two steps:  $\langle \Delta \mathbf{r}_{i-1} \cdot \Delta \mathbf{r}_{i+1} \rangle = \langle \Delta \mathbf{r}_{i-1} \cdot \langle \Delta \mathbf{r}_{i+1} \rangle_{\Delta \mathbf{r}_i} \rangle$ , where the interior bracket of the right-hand side refers to the average for a given  $\Delta \mathbf{r}_i$  and the exterior bracket refers to that

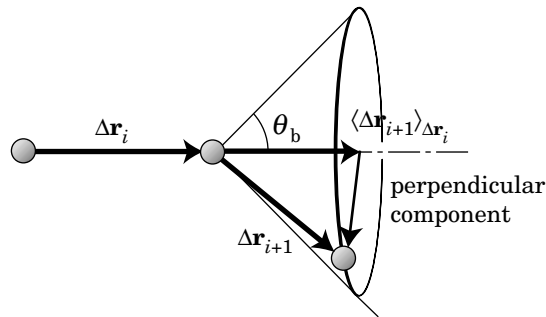


**Figure 1.24.** Average of  $\Delta \mathbf{r}_{i+1}$  for a given  $\Delta \mathbf{r}_i$ . The perpendicular component averages to zero.

for a given  $\Delta\mathbf{r}_{i-1}$  (or without any condition). Then,  $\langle\Delta\mathbf{r}_{i-1}\cdot\Delta\mathbf{r}_{i+1}\rangle = b^2\cos^2\theta_b$ . Repeating the same procedure, we obtain

$$\langle\Delta\mathbf{r}_i\cdot\Delta\mathbf{r}_j\rangle = b^2\cos^{|i-j|}\theta_b \quad (1.31)$$

The correlation diminishes exponentially with an increasing distance between the two bonds along the chain contour. The displacement in a total  $N$  steps is

$$\begin{aligned} R_F^2 = \langle\Delta\mathbf{r}^2\rangle &= \sum_{i,j=1}^N \langle\Delta\mathbf{r}_i\cdot\Delta\mathbf{r}_j\rangle = \sum_{i,j=1}^N b^2\cos^{|i-j|}\theta_b = b^2\left[N + 2\sum_{i=1}^{N-1}\sum_{j=i+1}^N \cos^{j-i}\theta_b\right] \\ &= b^2N\frac{1+\cos\theta_b}{1-\cos\theta_b} - 2b^2\cos\theta_b\frac{1-\cos^N\theta_b}{(1-\cos\theta_b)^2} \end{aligned} \quad (1.32)$$

When  $N \gg 1$ ,

$$\boxed{R_F^2 = b^2N\frac{1+\cos\theta_b}{1-\cos\theta_b} \quad \text{bond angle} = \pi - \theta_b} \quad (1.33)$$

When  $\theta_b$  is the tetrahedral angle,  $\cos\theta_b = 1/3$ . Then,  $R_F^2 = 2Nb^2$ .

A smaller  $\theta_b$  denotes that the bond vector changes its orientation by a smaller angle, effectively making the chain stiffer. Equation 1.33 demonstrates that a stiffer chain has a longer end-to-end distance, a reasonable result. A restriction on the local correlation of the bond direction does not change the proportionality between  $R_F$  and  $N^{1/2}$ . Thus we can regard the chain as consisting of freely jointed bonds of an effective bond length of  $b_{\text{eff}} = b[(1+\cos\theta_b)/(1-\cos\theta_b)]^{1/2}$ . This equivalence allows us to estimate  $R_g$  in a simple way: From Eq. 1.29,  $R_g^2$  is 1/6 of the value of  $R_F^2$  given by Eq. 1.33. It is possible to obtain an exact formula for  $R_g^2$  that applies to any  $N$ .

As seen in this example, short-range interactions such as the restriction on the bond angle do not deprive the chain of the characteristics of the ideal chain. Other examples of the short-range interactions include a restriction on the dihedral angle. The short-range interactions are only between monomers that are close to each other along the chain backbone. The correlation between the bond orientations decreases with an increasing distance along the backbone, as we saw in Eq. 1.31.

#### 1.2.4 PROBLEMS

**Problem 1.1:** When we obtained Eq. 1.16, we implicitly assumed that  $\Delta x$  and  $\Delta y$  were uncorrelated. This assumption is, however, correct only when  $N \gg 1$ . In each step,  $\Delta x_1$  and  $\Delta y_1$  are correlated; When the random walker moves in the  $y$  direction,  $\Delta x_1 = 0$ . Then,  $\langle\Delta x_1^2\Delta y_1^2\rangle = 0$  is not equal to  $\langle\Delta x_1^2\rangle\langle\Delta y_1^2\rangle = (b^2/2)^2$ . Show that  $\langle\Delta x^2\Delta y^2\rangle = \langle\Delta x^2\rangle\langle\Delta y^2\rangle$  when  $N \gg 1$ .

**Solution 1.1:**

$$\begin{aligned}
\langle \Delta x^2 \Delta y^2 \rangle &= \sum_i \sum_j \sum_k \sum_l \langle \Delta x_i \Delta x_j \Delta y_k \Delta y_l \rangle = \sum_{i=j=k=l} \langle \Delta x_i \Delta x_j \Delta y_k \Delta y_l \rangle \\
&= \sum_{i=j=k=l} \langle \Delta x_i \Delta x_j \Delta y_k \Delta y_l \rangle + \sum_{i=j \neq k=l} \langle \Delta x_i \Delta x_j \Delta y_k \Delta y_l \rangle \\
&= 0 + N(N-1) \langle \Delta x_1^2 \rangle \langle \Delta y_2^2 \rangle = N(N-1)(b^2/2)^2
\end{aligned}$$

$\langle \Delta x^2 \Delta y^2 \rangle$  approaches  $(Nb^2/2)^2 = \langle \Delta x^2 \rangle \langle \Delta y^2 \rangle$  as  $N \rightarrow \infty$ .

**Problem 1.2:** Find a formula similar to Eq. 1.25 that allows us to calculate  $R_g^2$  without explicitly obtaining  $\mathbf{r}_G$  for a linear polymer chain in which mass  $m_i$  of the  $i$ th monomer may be different from monomer to monomer. Here,  $R_g^2$  is the average of the second moment around  $\mathbf{r}_G$ , weighted by the mass of each monomer.

**Solution 1.2:** Let  $M = \sum_{i=0}^N m_i$ , then  $\mathbf{r}_G = \frac{1}{M} \sum_{i=0}^N m_i \mathbf{r}_i$

$R_g^2$  for this polymer chain is defined as

$$R_g^2 = \left\langle \frac{1}{M} \sum_{i=0}^N m_i (\mathbf{r}_i - \mathbf{r}_G)^2 \right\rangle$$

By definition, it is rewritten to

$$R_g^2 = \left\langle \frac{1}{M} \sum_{i=0}^N m_i \mathbf{r}_i^2 - \mathbf{r}_G^2 \right\rangle$$

Since

$$\frac{1}{2} \sum_{i,j=0}^N m_i m_j (\mathbf{r}_i - \mathbf{r}_j)^2 = M \sum_{i=0}^N m_i \mathbf{r}_i^2 - (M \mathbf{r}_G)^2$$

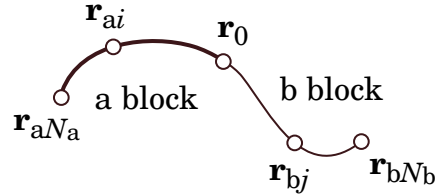
we obtain

$$R_g^2 = \frac{1}{2} \left\langle \frac{1}{M^2} \sum_{i,j=0}^N m_i m_j (\mathbf{r}_i - \mathbf{r}_j)^2 \right\rangle$$

**Problem 1.3:** In an a–b diblock copolymer, the monomer molecular weights in the two blocks are  $M_{1a}$  and  $M_{1b}$  and the degrees of polymerization are  $N_a$  and  $N_b$  ( $N_a, N_b \gg 1$ ), respectively. The two blocks are ideal chains with a segment



length  $b_a$  and  $b_b$ , respectively. Calculate  $R_g^2$  of the whole chain. Neglect the joint.



**Solution 1.3:**

The molecular weight  $M$  of the whole chain is given by  $M = M_{1a}N_a + M_{1b}N_b$ . Now we use the formula we obtained in Problem 1.2:

$$2M^2R_g^2 = \sum_{i=1}^{N_a} \sum_{j=1}^{N_a} M_{1a}^2 \langle (\mathbf{r}_{ai} - \mathbf{r}_{aj})^2 \rangle + 2 \sum_{i=1}^{N_a} \sum_{j=1}^{N_b} M_{1a}M_{1b} \langle (\mathbf{r}_{ai} - \mathbf{r}_{bj})^2 \rangle + \sum_{i=1}^{N_b} \sum_{j=1}^{N_b} M_{1b}^2 \langle (\mathbf{r}_{bi} - \mathbf{r}_{bj})^2 \rangle$$

where  $\mathbf{r}_{ai}$  and  $\mathbf{r}_{bj}$  are the positions of monomers  $i$  and  $j$  on a block and b block, respectively, with  $\mathbf{r}_{a0} = \mathbf{r}_{b0} = \mathbf{r}_0$  being the joint. In the second term, the mean square distance between monomers on different blocks is

$$\langle (\mathbf{r}_{ai} - \mathbf{r}_{bj})^2 \rangle = \langle (\mathbf{r}_{ai} - \mathbf{r}_0)^2 \rangle + \langle (\mathbf{r}_0 - \mathbf{r}_{bj})^2 \rangle = b_a^2 i + b_b^2 j$$

Thus,

$$2M^2R_g^2 = M_{1a}^2 \sum_{i=1}^{N_a} \sum_{j=1}^{N_a} b_a^2 |i-j| + 2M_{1a}M_{1b} \sum_{i=1}^{N_a} \sum_{j=1}^{N_b} (b_a^2 i + b_b^2 j) + M_{1b}^2 \sum_{i=1}^{N_b} \sum_{j=1}^{N_b} b_b^2 |i-j|$$

$$\cong M_{1a}^2 b_a^2 \frac{1}{3} N_a^3 + M_{1a}M_{1b} N_a N_b (b_a^2 N_a + b_b^2 N_b) + M_{1b}^2 b_b^2 \frac{1}{3} N_b^3$$

**Problem 1.4:** In the freely rotating chain with bond length  $b$  and bond angle  $\pi - \theta_b$ , the dihedral angle is unrestricted. How do  $\langle \Delta \mathbf{r}_i \cdot \Delta \mathbf{r}_{i+1} \rangle$ ,  $\langle \Delta \mathbf{r}_{i-1} \cdot \Delta \mathbf{r}_{i+1} \rangle$ , and  $\langle \Delta \mathbf{r}_i \cdot \Delta \mathbf{r}_j \rangle$  change from those for the freely rotating chain when the dihedral angles are restricted to *trans*, *gauche* +, and *gauche* -, but the three angles are chosen with equal probabilities?

**Solution 1.4:**

$$\langle \Delta \mathbf{r}_i \cdot \Delta \mathbf{r}_{i+1} \rangle = b^2 \cos \theta_b$$

For a given  $\Delta \mathbf{r}_i$ ,  $\langle \Delta \mathbf{r}_{i+1} \rangle_{\Delta \mathbf{r}_i} = (\cos \theta_b) \Delta \mathbf{r}_i$  because the average of the components perpendicular to  $\Delta \mathbf{r}_i$  is zero. Then,  $\langle \Delta \mathbf{r}_{i-1} \cdot \Delta \mathbf{r}_{i+1} \rangle = \langle \Delta \mathbf{r}_{i-1} \cdot \Delta \mathbf{r}_i \rangle \cos \theta_b = b^2 \cos^2 \theta_b$ . Likewise,  $\langle \Delta \mathbf{r}_i \cdot \Delta \mathbf{r}_j \rangle = b^2 \cos^{|i-j|} \theta_b$ . There are no changes.

### 1.3 GAUSSIAN CHAIN

#### 1.3.1 What is a Gaussian Chain?

**1.3.1.1 Gaussian Distribution** We have learned that, in the limit of  $N \rightarrow \infty$ , all ideal chains become identical and follow the normal distribution as long as each step satisfies the same statistics given by Eq. 1.19. We define a **Gaussian chain** by extending the ideality to short parts of the chain. In the Gaussian chain, any two points  $\mathbf{r}_1$  and  $\mathbf{r}_2$  on the chain follow a **Gaussian distribution**  $G(\mathbf{r}_1, \mathbf{r}_2; n)$ . For a given  $\mathbf{r}_2$ , the probability density for  $\mathbf{r}_1$  is given as

$$G(\mathbf{r}_1, \mathbf{r}_2; n) = (2\pi n b^2/3)^{-3/2} \exp\left(-\frac{3(\mathbf{r}_1 - \mathbf{r}_2)^2}{2n b^2}\right) \quad (1.34)$$

where the partial chain between the two points consists of  $n$  ( $n \leq N$ ) segments of segment length  $b$ . We do not limit  $n$  to integers but allow it to change continuously.

Essentially  $G(\mathbf{r}_1, \mathbf{r}_2; n)d\mathbf{r}_1$  is a **transition probability** for a point  $\mathbf{r}_2$  to move into a small volume  $d\mathbf{r}_1$  around  $\mathbf{r}_1$  in  $n$  steps. Likewise,  $G(\mathbf{r}_1, \mathbf{r}_2; n)d\mathbf{r}_2$  gives a probability for the chain of  $n$  segments with one end at  $\mathbf{r}_1$  to have the other end in a small volume  $d\mathbf{r}_2$  around  $\mathbf{r}_2$ . We can show that  $G(\mathbf{r}_1, \mathbf{r}_2; n)$  satisfies the following multiplication law:

$$\int G(\mathbf{r}_1, \mathbf{r}'; n_1)G(\mathbf{r}', \mathbf{r}_2; n_2) d\mathbf{r}' = G(\mathbf{r}_1, \mathbf{r}_2; n_1 + n_2) \quad (1.35)$$

This law states that a Gaussian chain of  $n_1$  segments and another Gaussian chain of  $n_2$  segments can be joined into a single Gaussian chain of  $n_1 + n_2$  segments, as illustrated in Figure 1.25. Alternatively, a Gaussian chain of  $N$  segments can be divided into two parts of  $n$  segments and  $N - n$  segments.

Just as in  $P(\mathbf{r})$  for the three-dimensional random walk on a discrete lattice (Eq. 1.18),  $G(\mathbf{r}_1, \mathbf{r}_2; n)$  consists of three independent factors:

$$G(\mathbf{r}_1, \mathbf{r}_2; n) = G_x(x_1, x_2; n)G_y(y_1, y_2; n)G_z(z_1, z_2; n) \quad (1.36)$$

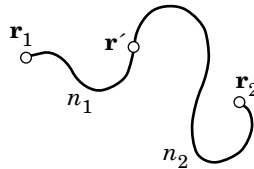


**Figure 1.25.** Two jointed Gaussian chains with  $n_1$  and  $n_2$  segments are equivalent to a single Gaussian chain with  $n_1 + n_2$  segments.

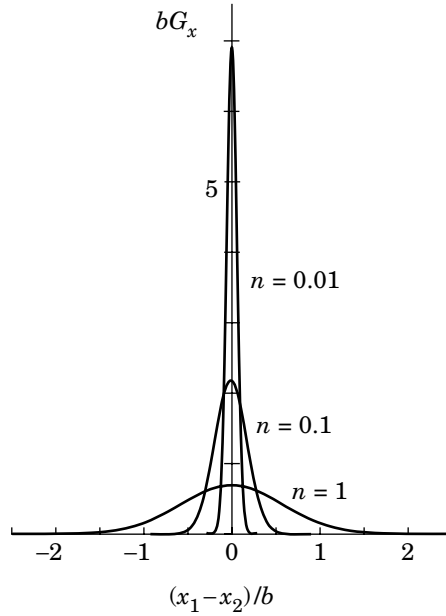


**Figure 1.26.** As  $n$  decreases to 0,  $G_x$  approaches the delta function at  $x_1 - x_2 = 0$ .

where, for example, the  $x$  component

$$G_x(x_1, x_2; n) = (2\pi nb^2/3)^{-1/2} \exp\left(-\frac{3(x_1 - x_2)^2}{2nb^2}\right) \quad (1.37)$$

is the one-dimensional transition probability from  $x_2$  to  $x_1$  in  $n$  steps. When the Gaussian chain is projected onto  $x, y$  plane, the projection forms a two-dimensional Gaussian chain with  $n$  and  $(2/3)^{1/2}b$ . We can find the segment length,  $(2/3)^{1/2}b$ , by comparing  $G_x G_y$  with Eq. 1.16.

Unlike the ideal random walk, the Gaussian chain is defined also in the limit of  $n \rightarrow 0$ . As shown in Figure 1.26,  $G_x(x_1, x_2; n)$  narrows at around  $x_1 - x_2 = 0$  as  $n$  approaches 0 without changing the area under the curve (normalization). Then,  $G_x(x_1, x_2; 0)$  must be a delta function of  $x_1$  centered at  $x_2$ :

$$G_x(x_1, x_2; 0) = \delta(x_1 - x_2) \quad (1.38)$$

See Appendix A1 for the delta function. The same limiting procedure is applied to  $G_y$  and  $G_z$ . Combining the three factors,

$$G(\mathbf{r}_1, \mathbf{r}_2; 0) = \delta(\mathbf{r}_1 - \mathbf{r}_2) \quad (1.39)$$

The Gaussian distribution is of the same functional form as the solution of a

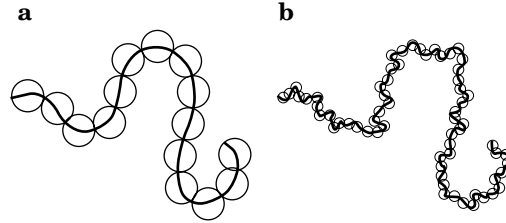


**Figure 1.27.** The contour length of a Gaussian chain depends on the number of segments. Compared with panel **a**, panel **b** has a more detailed contour and therefore has a longer contour. The end-to-end distance is common to both.

diffusion equation, which we will learn in Section 3.2. Thus,  $G(\mathbf{r}, \mathbf{r}'; n)$  satisfies

$$\left[ \frac{\partial}{\partial n} - (b^2/6)\nabla^2 \right] G(\mathbf{r}, \mathbf{r}'; n) = \delta(n) \delta(\mathbf{r} - \mathbf{r}') \quad (1.40)$$

where  $\nabla^2 = \partial^2/\partial x^2 + \partial^2/\partial y^2 + \partial^2/\partial z^2$  is the Laplacian. The right-hand side is zero except for  $n = 0$ .

**1.3.1.2 Contour Length** Each segment of the Gaussian chain has a root-mean-square length of  $b$ . It may appear that the whole chain of  $N$  segments has a contour length of  $Nb$ , but this is wrong. The contour length is not defined in the Gaussian chain because the choice of  $N$  is arbitrary and the apparent contour length  $Nb$  depends on  $N$ . This situation is illustrated in Figure 1.27. As  $N$  increases and the trajectory becomes more detailed, the path length increases, resulting in an increase of  $Nb$ . What is held unchanged in the Gaussian chain between different choices of  $N$  is  $Nb^2$ . A Gaussian chain should rather be viewed as a hypothetical chain with the end-to-end distance  $R_F$  that, when coarse-grained into  $N$  segments, each segment follows a Gaussian distribution with the mean square end-to-end length of  $R_F^2/N$ .

The Gaussian chain has another unrealistic property. In Eq. 1.34,  $\mathbf{r}_1$  and  $\mathbf{r}_2$  can be separated by more than  $nb$ , although its probability is low when  $n$  is large (see Problem 1.7). Despite this shortcoming, the Gaussian chain is the most preferred model in calculating various physical quantities in theories. It often happens that we can obtain an explicit analytical expression for the quantity in question only in the Gaussian chain model. It is the only model that gives an exact yet simple expression for the density of the chain ends, for instance.

### 1.3.2 Dimension of a Gaussian Chain

**1.3.2.1 Isotropic Dimension** Because a Gaussian chain is ideal, the end-to-end distance and the radius of gyration are given by Eq. 1.29. Here, we use Eq. 1.34 to confirm these dimensions for a Gaussian chain consisting of  $N$  segments of length  $b$ .

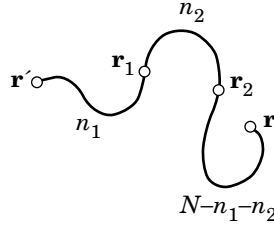


**Figure 1.28.** Two points,  $\mathbf{r}_1$  and  $\mathbf{r}_2$ , on the Gaussian chain of  $N$  segments.

A partial chain of a Gaussian chain is also a Gaussian. The mean square distance between two monomers separated by  $n$  segments is calculated as follows:

$$\begin{aligned} \langle (\mathbf{r}_1 - \mathbf{r}_2)^2 \rangle &= \int (\mathbf{r}_1 - \mathbf{r}_2)^2 G(\mathbf{r}_1, \mathbf{r}_2; n) d(\mathbf{r}_1 - \mathbf{r}_2) \\ &= (2\pi n b^2/3)^{-3/2} \int_0^\infty r^2 \exp\left(-\frac{3r^2}{2nb^2}\right) 4\pi r^2 dr = nb^2 \end{aligned} \quad (1.41)$$

The three components of  $\langle (\mathbf{r}_1 - \mathbf{r}_2)^2 \rangle$  are equal:

$$\langle (x_1 - x_2)^2 \rangle = \langle (y_1 - y_2)^2 \rangle = \langle (z_1 - z_2)^2 \rangle = nb^2/3 \quad (1.42)$$

These relationships apply to the whole chain ( $n = N$ ) as well.

We calculate  $R_g^2$  of the whole chain by first placing  $\mathbf{r}_1$  and  $\mathbf{r}_2$  on the chain, as shown in Figure 1.28, and then taking average of  $\langle (\mathbf{r}_1 - \mathbf{r}_2)^2 \rangle = n_2 b^2$  with respect to  $n_1$  and  $n_2$  (also shown in Fig. 1.28). The random variables  $n_1$  and  $n_2$  are uniformly distributed in  $[0, N]$  and  $[0, N - n_1]$ , respectively. Using a formula similar to Eq. 1.25, we obtain  $R_g^2$  as

$$R_g^2 = \frac{1}{2} \frac{2}{N^2} \int_0^N dn_1 \int_0^{N-n_1} dn_2 \langle (\mathbf{r}_1 - \mathbf{r}_2)^2 \rangle = \frac{1}{N^2} \int_0^N dn_1 \int_0^{N-n_1} n_2 b^2 dn_2 = \frac{1}{6} b^2 N \quad (1.43)$$

The above results are identical to those in Eq. 1.29, as required. Again,  $x$ ,  $y$ , and  $z$  components of  $R_g^2$  are equal.

**1.3.2.2 Anisotropy** The Gaussian chain is isotropic when averaged over many conformations and orientations. In the crudest approximation, we can regard it as a sphere of radius  $R_g$ . The instantaneous shape of the chain, however, does not look like a sphere. We will examine its anisotropic shape here.

In Figure 1.29, a Gaussian chain shown as a dark line is placed with its end-to-end vector on the  $z$  axis. We estimate how much the segments are away from the  $z$  axis. The distance from the  $z$  axis is better represented by the projection of the chain onto the  $x,y$ -plane, which is shown as a gray line. To evaluate the distance,

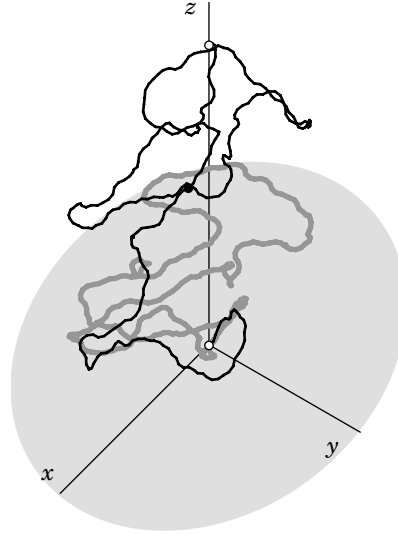


**Figure 1.29.** Gaussian chain with its end-to-end vector on the  $z$  axis is shown as a dark line. Its projection onto the  $x,y$ -plane is shown as a gray line. The small filled circle on the  $y,z$ -plane is the midpoint of the chain.

we consider the conditional distribution  $G_{0\mathbf{R}}(\mathbf{r}; n)$  for the position  $\mathbf{r}$  of the  $n$ th segment ( $0 \leq n \leq N$ ), when one of the ends is at the origin and the other at  $\mathbf{R} = [0, 0, R_F]$  on the  $z$  axis. It is given by

$$G_{0\mathbf{R}}(\mathbf{r}; n) = \frac{G(\mathbf{r}, 0; n) G(\mathbf{R}, \mathbf{r}; N - n)}{G(\mathbf{R}, 0; N)} \quad (1.44)$$

Note that this probability distribution is already normalized. Using Eq. 1.34, we can rearrange the right-hand side into (Problem 1.8)

$$G_{0\mathbf{R}}(\mathbf{r}; n) = G\left(\mathbf{r}, \frac{n}{N} \mathbf{R}; \frac{n(N - n)}{N}\right) \quad (1.45)$$

We take the segment at the midpoint of the two chain ends,  $n = N/2$ . Its distribution

$$G_{0\mathbf{R}}(\mathbf{r}; N/2) = G(\mathbf{r}, \mathbf{R}/2; N/4) \quad (1.46)$$

is identical to the distribution for the end of the  $N/4$ -segment Gaussian chain with the one end at  $\mathbf{R}/2$ . Because  $\mathbf{R}/2 = [0, 0, R_F/2]$  in our arrangement, the average of  $x^2 + y^2$  is equal to  $2/3$  of the mean square end-to-end distance. It is calculated as

$$\langle x^2 + y^2 \rangle = \frac{N}{4} b^2 \times \frac{2}{3} = \frac{1}{6} N b^2 \quad (1.47)$$

The excursion into  $x$  and  $y$  directions is much shorter than  $R_F = bN^{1/2}$ , the principal extension of the chain in the  $z$  direction. It is premature to say that the Gaussian chain resembles a football, however. The cross section of the Gaussian chain is not circular, as shown below.

Now we rotate the chain around the  $z$  axis until the midpoint  $\mathbf{r}$  sits on the  $y,z$ -plane. We consider how much the midpoint of the half chain, i.e., the quarterpoint of the original chain, extends in the  $x$  direction. As in Eq. 1.46, the probability density of the quarterpoint  $\mathbf{r}_1$  is given by

$$\frac{G(\mathbf{r}_1, 0; N/4)G(\mathbf{r}, \mathbf{r}_1; N/4)}{G(\mathbf{r}, 0; N/2)} = G(\mathbf{r}_1; \mathbf{r}/2; N/8) \quad (1.48)$$

This distribution is equivalent to the one for the end of a Gaussian chain that consists of  $N/8$  segments and has the other end at  $\mathbf{r}/2$ . Because  $\mathbf{r}/2 = [0, y/2, z/2]$ , the mean square of  $x_1$  is calculated as

$$\langle x_1^2 \rangle = \frac{N}{8} b^2 \times \frac{1}{3} = \frac{1}{24} Nb^2 \quad (1.49)$$

The overall shape of the Gaussian chain is thus approximated by an ellipsoidal body with the lengths of its principal axes in the ratio of

$$R_F: \langle x^2 + y^2 \rangle^{1/2}: \langle x_1^2 \rangle^{1/2} = 1: \frac{1}{\sqrt{6}}: \frac{1}{2\sqrt{6}} \cong 1: 0.4: 0.2 \quad (1.50)$$

Figure 1.30 depicts the ellipsoid. However, the Gaussian chain in solution does not behave like a solid ellipsoid. The overall shape is constantly changing. At a given time, the shape is different from chain to chain. The overall shape can be either more spherical or more elongated than the one shown in the figure.

### 1.3.3 Entropy Elasticity

**1.3.3.1 Boltzmann Factor** The Gaussian chain of  $N$  segments is physically realized by a bead-spring model consisting of  $N$  independent springs of a force constant

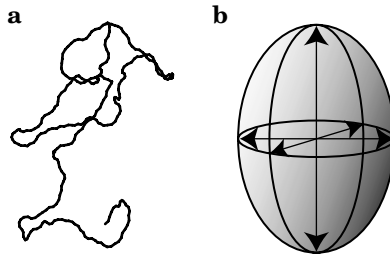


**Figure 1.30.** An instantaneous shape of the Gaussian chain (a) is approximated by an ellipsoid (b).

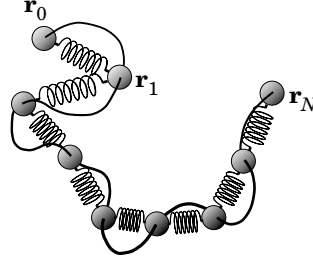


**Figure 1.31.** Gaussian chain of  $N$  segments is realized by a bead-spring model in which  $N$  springs are connected in series.

$k_{\text{sp}}$  (Fig. 1.31). Let the beads be at  $\mathbf{r}_0, \mathbf{r}_1, \dots, \mathbf{r}_N$ . The potential energy  $U$  of the chain resides in the elastic energy of the springs:

$$U(\mathbf{r}_0, \dots, \mathbf{r}_N) = \frac{1}{2} k_{\text{sp}} \sum_{n=1}^N (\mathbf{r}_n - \mathbf{r}_{n-1})^2 \quad (1.51)$$

The kinetic energy is negligible in a viscous solvent where the motion is overdamped. Then, the Boltzmann distribution with Eq. 1.51 gives the probability (unnormalized) for a specific arrangement of  $\mathbf{r}_0, \dots, \mathbf{r}_N$ :

$$\exp[-U(\mathbf{r}_0, \dots, \mathbf{r}_N)/k_{\text{B}}T] = \prod_{n=1}^N \exp\left[-\frac{k_{\text{sp}}}{2k_{\text{B}}T}(\mathbf{r}_n - \mathbf{r}_{n-1})^2\right] \quad (1.52)$$

where  $k_{\text{B}}$  is the Boltzmann constant and  $T$  the temperature. Each factor,  $\exp[-(k_{\text{sp}}/2k_{\text{B}}T)(\mathbf{r}_n - \mathbf{r}_{n-1})^2]$ , is identical to the Gaussian distribution of a single segment given by Eq. 1.34 with  $n = 1$ , when

$$b^2 = \frac{3k_{\text{B}}T}{k_{\text{sp}}} \quad (1.53)$$

The force constant is equal to  $3k_{\text{B}}T/b^2$ , where  $b^2$  is the mean square length of the spring.

With Eq. 1.53, the Boltzmann factor given by Eq. 1.52 can be rewritten to an expression that does not involve  $k_{\text{sp}}$ :

$$\exp[-U(\mathbf{r}_0, \dots, \mathbf{r}_N)/k_{\text{B}}T] = \exp\left[-\frac{3}{2b^2} \sum_{n=1}^N (\mathbf{r}_n - \mathbf{r}_{n-1})^2\right] \quad (1.54)$$

We can take  $i$  to be continuous and write

$$\exp[-U(\mathbf{r}_0, \dots, \mathbf{r}_N)/k_{\text{B}}T] = \exp\left[-\frac{3}{2b^2} \int_0^N \left(\frac{\partial \mathbf{r}}{\partial n}\right)^2 dn\right] \quad (1.55)$$



This factor gives a statistical weight for each conformation given as a continuous line,  $\mathbf{r}(n)$ .

**1.3.3.2 Elasticity** We model the whole chain by a single spring. Its force constant is given by

$$k_{\text{sp}} = \frac{3k_{\text{B}}T}{R_{\text{F}}^2} = \frac{3k_{\text{B}}T}{Nb^2} \quad (1.56)$$

The two ends of the Gaussian chain behave like two points connected by a spring with a force constant of  $3k_{\text{B}}T/R_{\text{F}}^2$ . Another way to look at this elastic property is described below.

Equation 1.34 allows us to express the entropy  $S$  of the Gaussian chain as a function of the two ends at  $\mathbf{r}$  and  $\mathbf{r}'$ :

$$S = \text{const.} + k_{\text{B}} \ln G = \text{const.} - \frac{3k_{\text{B}}}{2R_{\text{F}}^2} (\mathbf{r} - \mathbf{r}')^2 \quad (1.57)$$

Then, the Helmholtz free energy  $A$  of the chain is calculated as

$$A = \text{const.} + \frac{3k_{\text{B}}T}{2R_{\text{F}}^2} (\mathbf{r} - \mathbf{r}')^2 \quad (1.58)$$

The chain tries to decrease the magnitude of  $\mathbf{r} - \mathbf{r}'$  to minimize  $A$  and thus approach the equilibrium. To hold the end-to-end vector at a nonzero  $\mathbf{r} - \mathbf{r}'$  in Figure 1.32 requires a force of

$$\frac{\partial A}{\partial \mathbf{r}} = \frac{3k_{\text{B}}T}{R_{\text{F}}^2} (\mathbf{r} - \mathbf{r}') \quad (1.59)$$

which is nothing more than the spring force of a force constant  $3k_{\text{B}}T/R_{\text{F}}^2$ .

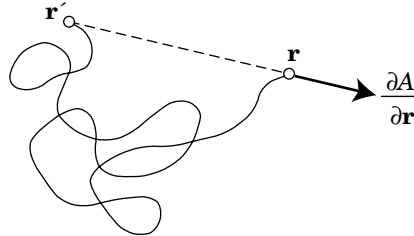


**Figure 1.32.** Entropy elasticity. To hold the end-to-end vector at  $\mathbf{r} - \mathbf{r}'$ , the Gaussian chain needs to be pulled with a force of  $\partial A / \partial \mathbf{r} = (3k_{\text{B}}T/R_{\text{F}}^2)(\mathbf{r} - \mathbf{r}')$ .

Because of the entropic origin, the above property is called the **entropy elasticity**. It is not limited to Gaussian chains. Any chain that has a finite size, including ideal chains and real chains, has this elasticity. By the same reason, a rubber is elastic. A rubber is a cross-linked polymer. A partial chain between two cross-links behaves elastically, giving rise to the elasticity of the material as a whole.

### 1.3.4 PROBLEMS

**Problem 1.5:** What is the most probable end-to-end distance  $R_{mp}$  of a Gaussian chain? At  $R = R_{mp}$ ,  $R^2 G(R; N)$  maximizes, where  $G(R; N) = G(\mathbf{r}, \mathbf{r}'; N)$  with  $R = |\mathbf{r} - \mathbf{r}'|$ .

**Solution 1.5:** At  $R = R_{mp}$ ,

$$\begin{aligned} 0 &= \frac{\partial}{\partial R} R^2 G(R; N) = \frac{\partial}{\partial R} R^2 (2\pi N b^2/3)^{-3/2} \exp\left(-\frac{3R^2}{2Nb^2}\right) \\ &= (2\pi N b^2/3)^{-3/2} \left(2R - \frac{3R^3}{Nb^2}\right) \exp\left(-\frac{3R^2}{2Nb^2}\right) \end{aligned}$$

Then,  $R_{mp} = b(2N/3)^{1/2} = 2R_g$ .

**Problem 1.6:** What is the second moment of the segments from one of the chain ends in the Gaussian chain? The square root of this second moment gives the “size” of the molecule tethered to a point in space.

**Solution 1.6:** Let  $\mathbf{r}$  be the position of the  $n$ th segment. Then, the second moment around the end at 0 is

$$\frac{1}{N} \int_0^N dn \langle (\mathbf{r} - 0)^2 \rangle = \frac{1}{N} \int_0^N n b^2 dn = \frac{1}{2} N b^2$$

**Problem 1.7:** Calculate the probability for the two ends of a Gaussian chain with the mean square end-to-end distance  $Nb^2$  to be longer than its “fully stretched length”  $Nb$ . How large is the probability when  $N = 5$ ? When  $N = 10$ ?

**Solution 1.7:** The probability  $P$  is given as

$$P = \int_{Nb}^{\infty} 4\pi r^2 (2\pi N b^2/3)^{-3/2} \exp\left(-\frac{3r^2}{2Nb^2}\right) dr$$

With  $t = (3/2N)^{1/2} r/b$ ,

$$P = 4\pi^{-1/2} \int_{(3N/2)^{1/2}}^{\infty} t^2 \exp(-t^2) dt = 2\pi^{-1/2} \left[ (3N/2)^{1/2} \exp(-3N/2) + \text{Erfc}\left((3N/2)^{1/2}\right) \right] (*)$$

Where

$$\operatorname{Erfc}(z) \equiv \int_z^{\infty} \exp(-t^2) dt$$

When  $Z \gg 1$ ,

$$\operatorname{Erfc}(z) \cong (2z)^{-1} \exp(-z^2)$$

Therefore, the first term is dominant in (\*):

$$P \cong (6N/\pi)^{1/2} \exp(-3N/2)$$

At  $N = 5$ ,  $P = 1.7 \times 10^{-3}$ . At  $N = 10$ ,  $P = 1.3 \times 10^{-6}$ .

**Problem 1.8:** Verify Eq. 1.45.

**Solution 1.8:** From Eq. 1.44,

$$\begin{aligned} G_{0\mathbf{R}}(\mathbf{r}; n) &= \frac{(2\pi n b^2/3)^{-3/2} \exp\left(-\frac{3\mathbf{r}^2}{2n b^2}\right) (2\pi(N-n)b^2/3)^{-3/2} \exp\left(-\frac{3(\mathbf{R}-\mathbf{r})^2}{2(N-n)b^2}\right)}{(2\pi N b^2/3)^{-3/2} \exp\left(-\frac{3\mathbf{R}^2}{2N b^2}\right)} \\ &= \left(2\pi \frac{n(N-n)}{N} b^2/3\right)^{-3/2} \exp\left[-\frac{3}{2b^2} \left(\frac{\mathbf{r}^2}{n} + \frac{(\mathbf{R}-\mathbf{r})^2}{N-n} - \frac{\mathbf{R}^2}{N}\right)\right] \\ &= \left(2\pi \frac{n(N-n)}{N} b^2/3\right)^{-3/2} \exp\left[-\frac{3(\mathbf{r} - (n/N)\mathbf{R})^2}{2b^2 n(N-n)/N}\right] = G\left(\mathbf{r}, \frac{n}{N} \mathbf{R}; \frac{n(N-n)}{N}\right) \end{aligned}$$

**Problem 1.9:** Equation 1.45 gives the distribution of an arbitrary point on the Gaussian chain when its ends are at 0 and  $\mathbf{R}$ . Place  $\mathbf{R}$  on the  $z$  axis and calculate the average of  $\langle x^2 + y^2 \rangle$  when  $n$  is swept from 0 to  $N$ .

**Solution 1.9:**

$$\begin{aligned} \langle x^2 + y^2 \rangle &= \frac{1}{N} \int_0^N dn \iint (x^2 + y^2) G_{0\mathbf{R}}(x, y; n) dx dy \\ &= \frac{1}{N} \int_0^N dn \iint (x^2 + y^2) \left(2\pi \frac{n(N-n)}{N} b^2/3\right)^{-1} \\ &\quad \times \exp\left(-\frac{3(x^2 + y^2)}{2[n(N-n)/N]b^2}\right) dx dy \end{aligned}$$

$$\begin{aligned}
&= \frac{1}{N} \int_0^N dn \int_0^{\infty} dx \left( 2\pi \frac{n(N-n)}{N} b^2/3 \right)^{-1/2} \\
&\quad \times \exp\left(-\frac{3x^2}{2[n(N-n)/N]b^2}\right) dx \\
&= \frac{1}{N} \int_0^N dn \int_0^{\infty} dx \left( 2\pi \frac{n(N-n)}{N} b^2/3 \right)^{-1/2} \\
&= \frac{1}{N} \int_0^N dn \int_0^{\infty} dx \left( 2\pi \frac{n(N-n)}{N} b^2/3 \right)^{-1/2} = \frac{1}{9} Nb^2
\end{aligned}$$

**Problem 1.10:** A Gaussian chain with fluorescent tag on one end and its quencher on the other end is dissolved in a non-quenching solvent. If there is no specific interaction between the two ends other than the fluorescence quenching, how does the fluorescence intensity change with the chain length? The fluorescence is quenched when the quencher is in close proximity.

**Solution 1.10:** The probability  $P$  for the two chain ends to come close is proportional to  $(2\pi Nb^2)^{-3/2}$ . Thus,  $P \propto N^{-3/2}$ . The intensity per molecule increases as  $\text{const.} \cdot N^{-3/2}$ .

## 1.4 REAL CHAINS

### 1.4.1 Excluded Volume

**1.4.1.1 Excluded Volume of a Sphere** The excluded volume makes the real chains nonideal. The dimension of the real chain is different from that of the ideal chain of the same contour length, for instance. Before considering the excluded volume effect in a chain molecule, we look at the effect in a suspension of hard spheres of diameter  $d_s$ . In Figure 1.33, the center-to-center distance between spheres A and B cannot be less than  $d_s$ . In effect, sphere B is excluded by sphere A. The space not available to the center of sphere B is a sphere of radius  $d_s$  indicated by a dashed line. Thus the excluded volume ( $v_e$ ) is eight times the volume of the sphere.

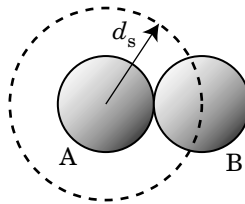


**Figure 1.33.** Excluded volume in a suspension of spheres. The center of sphere B is excluded from the spherical region (dashed line) by sphere A.

Consider a hypothetical process in which the volume excluded by each of the two spheres increases from 0 to  $v_e$ . The space available to the other sphere decreases from the volume  $V$  of the system to  $V - v_e$ . Therefore, the configurational entropy of the sphere changes by

$$\Delta S = k_B \ln \frac{V - v_e}{V} \cong -k_B \frac{v_e}{V} \quad (1.60)$$

where  $v_e \ll V$  is assumed. The change in the Helmholtz free energy is then  $\Delta A/k_B T = -\Delta S/k_B = v_e/V$ .

When the system has  $N$  identical spheres in the volume of  $V$ , there are  $N^2/2$  pairs of excluded-volume interaction. Then, the change in the total free energy due to the excluded volume is  $\Delta A/k_B T = (N^2/2)v_e/V$ . The change per sphere,  $(\Delta A/k_B T)/N$ , is proportional to the density  $N/V$ . At low concentrations, the excluded volume is negligible. As the concentration increases and  $Nv_e$  approaches  $V$ , the effect becomes stronger. The same effect appears in the van der Waals equation of state for a real gas; The correction to the volume is equal to the excluded volume.

**1.4.1.2 Excluded Volume in a Chain Molecule** In the polymer solution, the excluded volume does not disappear even in the low concentration limit. Connectivity of monomers makes the situation different from that in the suspension of spheres.

Suppose a polymer chain consisting of  $N$  spheres of diameter  $b$  (pearl-necklace model; see Fig. 1.34). We consider the dilute solution limit in which each chain is isolated from the other chains in the solution. When the chain dimension is  $R$ , these  $N$  spheres are contained in a cube of volume close to  $R^3$ , but no other spheres

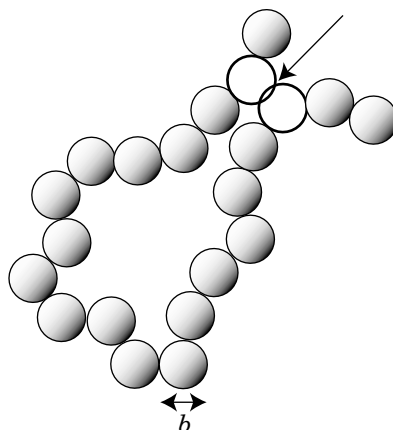


**Figure 1.34.** Excluded volume in a chain molecule. The two white beads cannot overlap each other.

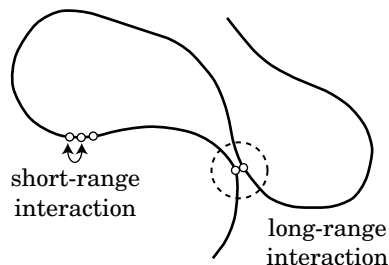


**Figure 1.35.** Short-range interaction and long-range interaction on a polymer chain.

will be found there. The free-energy change per chain due to the excluded volume is then  $\Delta A_{\text{ch}}/k_{\text{B}}T = (N^2/2)v_e/R^3$ . Although entropic in origin, we regard the excluded volume as an interaction and we write  $\Delta U_{\text{ch}}/k_{\text{B}}T = (N^2/2)v_e/R^3$ . Because  $v_e \cong b^3$ ,

$$\Delta U_{\text{ch}}/k_{\text{B}}T \cong b^3 N^2/R^3 \quad (1.61)$$

where the numerical coefficient is dropped. Note that  $N^2/R^3$  is equal to the volume  $R^3$  multiplied by the square of the monomer density ( $= N/R^3$ ). Other types of direct interactions between monomers such as van der Waals interactions are included in this expression of  $\Delta U_{\text{ch}}$  because the magnitude of any direct interaction in a given small volume is proportional to the square of the monomer density. Therefore, Eq. 1.61 can be written as  $v_{\text{eff}}(N^2/R^3)$ , in general. Note that the effective excluded volume ( $v_{\text{eff}}$ ) is negative when the attractive interaction dominates, which occurs when the monomers prefer other monomers to solvent molecules. In the following, we take  $v_{\text{eff}} = b^3 > 0$  for simplicity unless otherwise specified.

The interactions we are considering here are between monomers that may be widely apart along the chain contour. To distinguish these interactions from the short-range interactions such as the restriction on the bond angle and the dihedral angle we considered in Section 1.2.3, we call them long-range interactions (Fig. 1.35). The “long” and “short” do not refer to the distance between the monomers in space. They refer to the distance along the backbone of the polymer chain. Unlike the short-range interactions that are always present, the long-range interactions do not manifest themselves unless another monomer happens to come close. It is rather the large probability of this event that makes the long-range interactions dominant in the statistical properties of the polymer chain. The presence of many other monomers in a small volume of  $R^3$ , due to the chain connectivity, gives rise to the dominance of the long-range interactions even in the dilute solution limit.

The excluded volume is not limited to a pair of monomers on the same chain (intra-chain interaction). It exists equally for a pair of monomers on different chains (interchain interaction). At higher concentrations, the interchain interaction is the dominant part of the excluded volume effect.

## 1.4.2 Dimension of a Real Chain

**1.4.2.1 Flory Exponent** It is easy to expect that the excluded volume effect “swells” the chain compared with the dimension it would take were it not for the excluded volume effect. The swelling becomes more serious with an increasing contour length. We can see  $\Delta U_{\text{ch}}/k_{\text{B}}T$  to increase with  $N$  in Eq. 1.61. With  $R \cong bN^{1/2}$ , the dimension of the ideal chain, we have  $\Delta U_{\text{ch}}/k_{\text{B}}T \cong N^{1/2}$ .

When we write the radius of gyration of the real chain consisting of  $N$  monomers as  $R_{\text{g}} = bN^{\nu}$ , the exponent  $\nu$  is greater than 0.5, the exponent for the ideal chain. In fact,  $\nu$  was found to be around 0.59. Using the approximate value,  $0.6 = 3/5$ , is more common:

$$\boxed{R_{\text{g}} \cong bN^{\nu} \quad \nu = 0.59 \text{ or } 3/5 \quad \text{real chains}} \quad (1.62)$$

The numerical coefficient is dropped again. Within this level of approximation, the same formula applies to the end-to-end distance  $R_{\text{F}}$  of the real chain.

The exact exponent was estimated in the **renormalization group theory**.<sup>2</sup> The proof is difficult. Fortunately, however, Flory correctly obtained the approximate  $\nu$  in a simple method.<sup>3</sup> The exponent  $\nu$  is called the **Flory exponent**. Below we briefly review his method.

Flory expressed the free energy of the real chain as a function of the overall dimension of  $R$ . Here,  $R$  is not the average dimension but is allowed to change as the shape of the chain changes. The free energy consists of two terms—one is the entropy due to the freedom for different chain conformations and the other is the interaction mostly due to the excluded volume. In Section 1.3.3, we obtained the entropy term as  $S \cong -k_{\text{B}}R^2/(Nb^2)$  [Eq. 1.57 with  $(\mathbf{r} - \mathbf{r}')^2 = R^2$  and  $R_{\text{F}}^2 = Nb^2$ ; the numerical coefficient is dropped here]. The interaction term is given by Eq. 1.61. Then the free energy of the chain ( $A_{\text{ch}}$ ) is given as

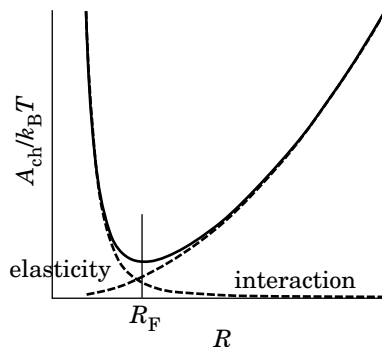
$$\frac{A_{\text{ch}}}{k_{\text{B}}T} \cong \frac{R^2}{Nb^2} + b^3 \frac{N^2}{R^3} \quad (1.63)$$

Figure 1.36 is a sketch of  $A_{\text{ch}}/k_{\text{B}}T$ . The two terms on the right-hand side have the opposite  $R$  dependence. The interaction becomes weaker as the monomer density becomes lower with an increasing  $R$ , but the entropy term gains. As a result, there is a minimum in  $A_{\text{ch}}$ . The  $R$  that minimizes  $A_{\text{ch}}$  is the most probable value of  $R$  for a given  $N$ . The excluded volume chain will have that dimension. Thus  $R_{\text{F}}$  can be obtained from  $\partial(A_{\text{ch}}/k_{\text{B}}T)/\partial R|_{R=R_{\text{F}}} = 0$  as  $R_{\text{F}} \cong bN^{3/5}$ , reproducing Eq. 1.62.

The ratio of  $R_{\text{g}}^2$  to  $R_{\text{F}}^2$  is insensitive to the excluded volume effect. The renormalization group theory gives<sup>2</sup>

$$\frac{6R_{\text{g}}^2}{R_{\text{F}}^2} = 0.952 \quad (1.64)$$

In the ideal chain, the ratio is 1 (Eq. 1.29).



**Figure 1.36.** Free energy of a chain,  $A_{\text{ch}}$ , as a function of the chain dimension  $R$ . The free energy consists of the elastic energy and the interaction.

Note that the chain dimension thus obtained is independent of the temperature. For this reason, the real chains are often called **athermal** chains. The independence results from the fact that both the elasticity and the excluded volume are entropic in origin. The two terms on the right-hand side of Eq. 1.63 are independent of  $T$ . In some polymer solutions, however, the interaction is enthalpic. Dividing the interaction by  $k_B T$  makes the interaction term in Eq. 1.63 reciprocally proportional to  $T$ . Consequently, the polymer chain dimension depends on the temperature. In Section 2.3, we will see this effect.

**1.4.2.2 Experimental Results** Experiments conducted on dilute polymer solutions verified that the chain dimension follows Eq. 1.62. Figure 1.37 shows a

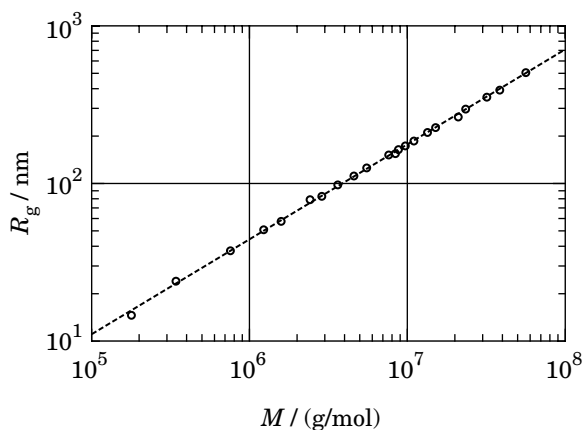


**Figure 1.37.** Radius of gyration  $R_g$  of polystyrene in toluene and benzene, plotted as a function of molecular weight  $M$ . The dashed line is the optimal fit by a power relationship. (From Ref. 2.)



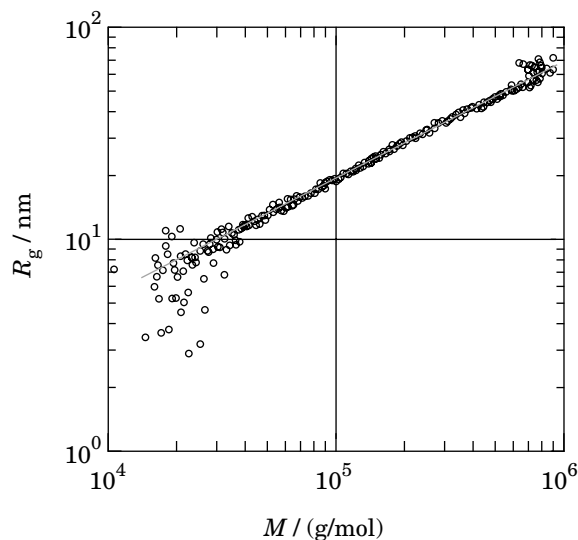


**Figure 1.38.** Radius of gyration  $R_g$  of linear high-density polyethylene in trichlorobenzene, plotted as a function of molecular weight  $M$ . The gray line is the optimal fit by a power relationship. (From Ref. 4.)

typical result for polystyrene in toluene and benzene at around room temperature.<sup>2</sup> The latter is a typical athermal chain. The data were obtained in lightscattering experiments that can measure  $R_g$  and the average molecular weight ( $M$ ) of a polymer chain in a dilute solution, as we will see in Section 2.4. All the data fall on a straight line in the double logarithmic scale. Curve fitting yields

$$R_g/\text{nm} = 0.01234 \times (M/(\text{g/mol}))^{0.5936} \quad \text{polystyrene in toluene and benzene} \quad (1.65)$$

The exponent is in agreement with the theoretically predicted value. At lower molecular weights ( $M < 10^4$  g/mol),  $R_g$  is smaller than the one given by this equation. There is a slight difference in the coefficient and the exponent from solvent to solvent, but the difference is small in a wide range of solvents that dissolve the polymer easily.

The coefficient and the exponent are quite different for other polymers. For instance, linear high-density polyethylene in trichlorobenzene at 135°C has the following  $R_g$ :<sup>4</sup>

$$R_g/\text{nm} = 0.0335 \times (M/(\text{g/mol}))^{0.553} \quad \text{polyethylene in trichlorobenzene} \quad (1.66)$$

Figure 1.38 shows the dependence. The data were obtained by using an on-line lightscattering detector in size exclusion chromatography. In the study,  $R_g$  and  $M$  were measured simultaneously and instantaneously as the polymer was separated in

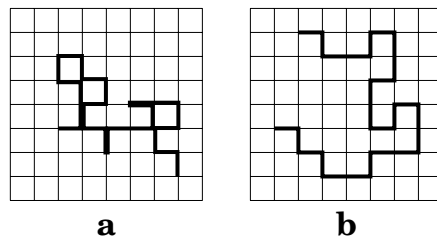


**Figure 1.39.** Polymer chain on a square lattice. a: Random walk for an ideal chain. b: Self-avoiding walk for a real chain.

column chromatography (Section 2.5). Compared with polystyrene of the same  $M$ , polyethylene has a greater  $R_g$  primarily because its monomer molecular weight is lower.

### 1.4.3 Self-Avoiding Walk

A polymer chain with an excluded volume can be modeled by a **self-avoiding walk** (SAW) on the lattice. Unlike the random walker we have seen in Section 1.2 for the ideal chain, this walker is not allowed to visit the sites it has already visited. Its trajectory is close to the conformation of a real chain with excluded volume on the lattice. For the SAW to represent a real chain, the SAW must be equilibrated by moving the chain around on the lattice. Figure 1.39 illustrates a difference between the random walk and the SAW on a square lattice. Apparently, the dimension of the latter is greater; The excluded volume swells the chain. SAW is widely used in computer simulations to calculate properties of the polymer chain that are difficult to obtain in experiments.

Figure 1.40 shows a typical result of the simulation.<sup>5</sup> An  $N$ -step SAW was generated on a cubic lattice of lattice unit  $b$ . After equilibration, the root-mean-square

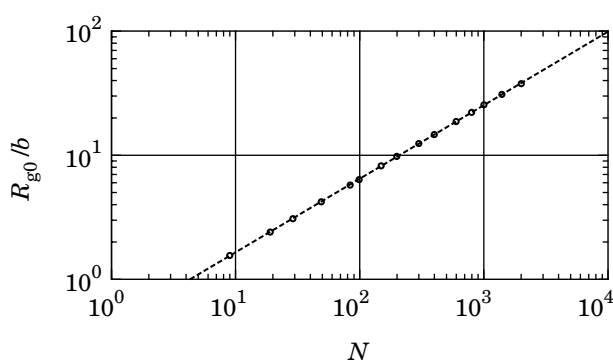


**Figure 1.40.** Radius of gyration  $R_g$  of a self-avoiding walk on a cubic lattice of lattice unit  $b$ , plotted as a function of the number  $N$  of the steps. The solid line is the optimal fit by a power relationship. (From Ref. 5.)

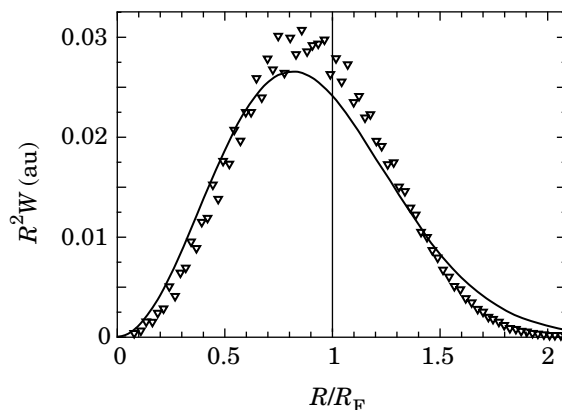


**Figure 1.41.** Distribution of the end-to-end distance.  $R^2W(\mathbf{R})$  is plotted as a function of  $R/R_F$ . Symbols were obtained in computer simulation; the solid line represents the distribution for the Gaussian chain. (From Ref. 6.)

radius of gyration,  $R_g$ , was calculated over many different arrangements of the chain. Again, the data are on a straight line in the double logarithmic scale. Curve fitting gives

$$\boxed{R_g/b = 0.4205 \times N^{0.5934} \quad \text{SAW on a cubic lattice}} \quad (1.67)$$

Unlike in Figure 1.36, a good fitting persists to  $N$  as small as 9.

A difference between SAW and the Gaussian chain is also evident in the distribution of the end-to-end distance  $R$ . Figure 1.41 compares  $R^2W(\mathbf{R})$ , where  $W(\mathbf{R})$  is the distribution function for  $\mathbf{R}$ . Note that  $4\pi R^2W(\mathbf{R}) dR$  gives the probability to find the end-to-end distance between  $R$  and  $R + dR$ . In the Gaussian chain,  $W(\mathbf{R}) = G(\mathbf{R}, 0; N)$ , where  $G$  is given by Eq. 1.34. The SAW of  $N = 199$  steps was generated on a tetrahedral lattice.<sup>6</sup> In the figure, the Gaussian chain has a broader distribution, especially at large  $R$ . It is one of the shortcomings of the Gaussian chain model to describe the conformation of the real chain.

#### 1.4.4 PROBLEMS

**Problem 1.11:** A self-avoiding walk (SAW) generated on a lattice is slightly different from the trace of a real chain on the same lattice. Explain why.

**Solution 1.11:** The environment for a growing chain end of SAW changes as more monomers are added to the chain and more sites become unavailable to the next monomer.

**Problem 1.12:** Assume that we can use the expression for the mean square distance between the two ends of a real chain ( $R_F^2 = b^2 N^{2\nu}$ ) also for the mean square distance between two monomers, i.e.,  $\langle (\mathbf{r}_i - \mathbf{r}_j)^2 \rangle = b^2 |i - j|^{2\nu}$ . Calculate  $R_g^2$  of the real chain. In Eq. 1.25, replace the sum with a double integral. What is  $6R_g^2/R_F^2$  for  $\nu = 0.59$ ? Why do you think it is different from the one calculated in a more rigorous theory (renormalization theory)?

**Solution 1.12:**

$$\begin{aligned} R_g^2 &= \frac{1}{2N^2} \int_0^N di \int_0^N dj b^2 |i - j|^{2\nu} = \frac{b^2}{N^2} \int_0^N di \int_0^i dj (i - j)^{2\nu} \\ &= \frac{b^2 N^{2\nu}}{(2\nu + 1)(2\nu + 2)} \\ \frac{6R_g^2}{R_F^2} &= \frac{6}{(2\nu + 1)(2\nu + 2)} \cong 0.87 \end{aligned}$$

The real chain is more rigid over a short distance, which makes a contribution of close pairs of  $i$  and  $j$  greater than it is in the above calculation.

**Problem 1.13:** We can apply Flory's method to find the Flory exponent for the dimension of a two-dimensional excluded-volume chain. In two dimensions, the entropy term is the same as that of the three-dimensional chain, but the interaction term changes to  $\Delta U_{\text{ch}}/k_B T = b^2 R^2 (N/R^2)^2 = b^2 N^2/R^2$ .

**Solution 1.13:**

$$\frac{A_{\text{ch}}}{k_B T} \cong \frac{R^2}{Nb^2} + b^2 \frac{N^2}{R^2}$$

The derivative is zero at the free energy minimum:

$$0 = \frac{\partial}{\partial R} \frac{A_{\text{ch}}}{k_B T} \cong \frac{2R}{Nb^2} - 2b^2 \frac{N^2}{R^3}$$

From which we obtain  $R = bN^{3/4}$ .

## 1.5 SEMIRIGID CHAINS

### 1.5.1 Examples of Semirigid Chains

In the preceding sections, we assumed that the polymer chain is flexible and coil-shaped. However, some linear chains have an inherent backbone rigidity. In contrast to flexible chains that look like a cotton thread, the inherently rigid chains resemble a fishing thread. These polymers are called **semirigid** polymers or **semiflexible** polymers. There are several mechanisms that support the backbone rigidity (Fig. 1.42):

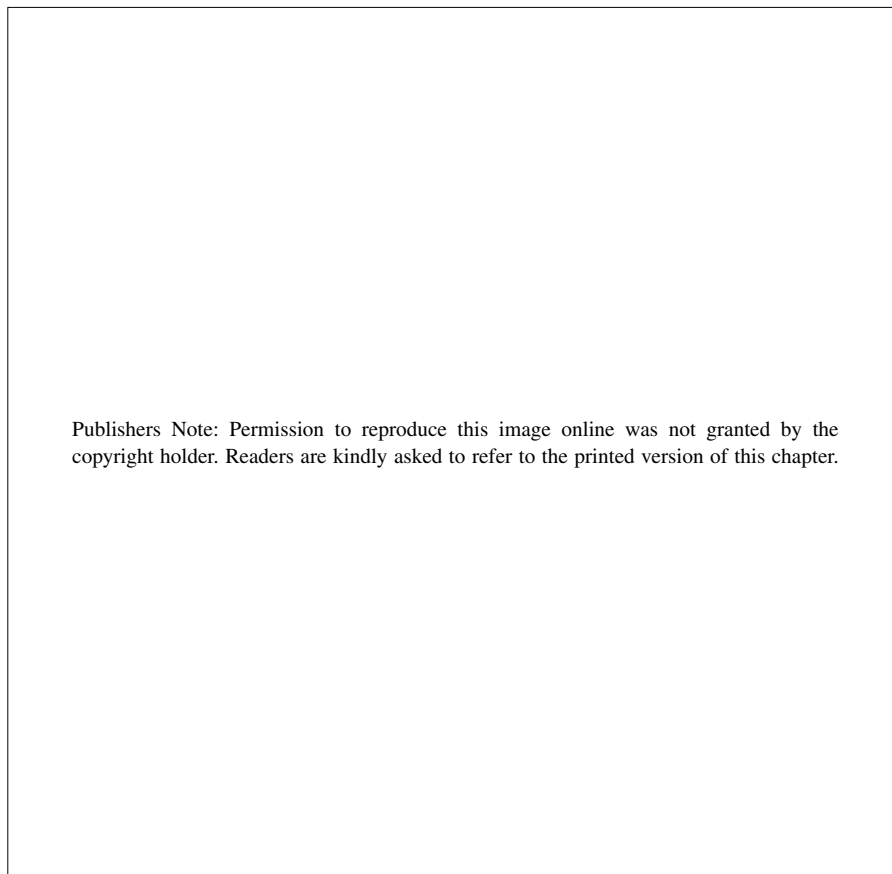


**Figure 1.42.** Examples of a wormlike chain. a: Chain with a  $\pi$ -conjugated backbone [poly(*p*-phenylene) and polydiacetylene]. b: Chain with a bulky side chain [poly(*n*-hexyl isocyanate); also helical]. c: Helical chain (double-stranded DNA). d: Polyelectrolyte [poly(styrene sulfonate); ionized in neutral water]. The rigidity is supported by the high density of negative charges on the backbone. (b is from Ref. 7.)

- (a)  $\pi$ -Conjugation in the valence electrons of the main chain. The delocalized electrons prefer a straight backbone. Polyacetylene, poly(*p*-phenylene), and polydiacetylene are typical of these polymers. Side groups ( $\mathbf{R}, \mathbf{R}'$ ) are attached to make these polymers soluble in solvents without compromising the rigidity.
- (b) Bulky side groups. Bulky pendant groups grafted at high density to the main chain force the chain to adopt an extended conformation. Poly(*n*-hexyl isocyanate) belongs to this group.<sup>7</sup>
- (c) Hydrogen bonding. Hydrogen bonding between hydrogen donors and acceptors on the main chain or side groups locks the chain into a specific

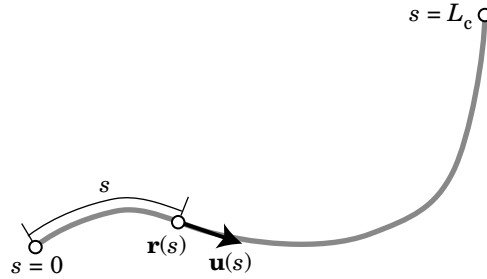


**Figure 1.43.** Conformation of a wormlike chain is specified by  $\mathbf{r}(s)$ . Its unit tangential vector is  $\mathbf{u}(s)$ .

arrangement, mostly into a straight conformation. The bonding can be between immediate neighbors or between monomers a few units apart.  $\alpha$ -Helix forming synthetic polypeptides such as poly( $\gamma$ -benzyl-L-glutamate) and double-stranded DNA fragments belong to this category. These polymers may change into flexible coils at high temperatures (helix-coil transition).

- (d) Coulomb repulsions. Same charges distributed along the chain at high density repel each other to extend the otherwise flexible chain. Strong **polyelectrolytes** such as poly(styrene sulfonate) in a neutral, salt-free solution at low concentrations belong to this category.

The rigidity depends on the solvent, temperature, and additives. When the chain is straight, the polymer is called a **rodlike molecule**.

## 1.5.2 Wormlike Chain

**1.5.2.1 Model** In Section 1.2.3, we looked at a freely rotating chain with a fixed bond angle  $\pi - \theta_b$  but an unrestricted dihedral angle. When the bond angle is close to  $\pi$  and the bond length  $b$  is short, this model can represent a semirigid chain, as shown below. The orientation correlation of the  $i$ th stick and the  $j$ th stick was obtained as  $\langle \mathbf{u}_i \cdot \mathbf{u}_j \rangle = \cos^{|i-j|} \theta_b$ , where  $\mathbf{u}_i$  is the unit vector parallel to the  $i$ th stick (Eq. 1.31). We now decrease  $\theta_b$ . When  $\theta_b \ll 1$ , the correlation between  $\mathbf{u}$  and  $\mathbf{u}'$  at two points separated by  $l = b|i-j|$  along the contour is  $\langle \mathbf{u} \cdot \mathbf{u}' \rangle = (1 - \theta_b^2/2)^{l/b}$ . We take the limit of  $b \rightarrow 0$  while holding  $2b/\theta_b^2$  unchanged. Then,

$$\langle \mathbf{u} \cdot \mathbf{u}' \rangle = [(1 - b/L)^{1/b}]^l \rightarrow \exp(-l/L) \quad (1.68)$$

where  $L \equiv 2b/\theta_b^2$ , and  $(1 + bx)^{1/b} \rightarrow e^x$  ( $b \rightarrow 0$ ) with  $x = -1/L$  was used.

In the limit, the conformation of the chain is not zigzag but rather a smooth curve in a three-dimensional space, as illustrated in Figure 1.43. This model is called a **wormlike chain** or a **Kratky-Porod model**. A continuous

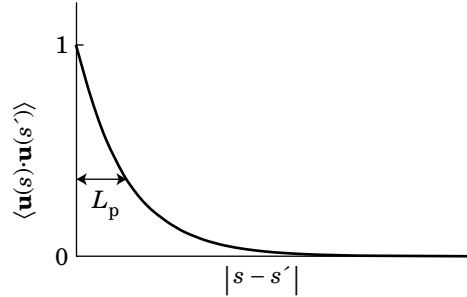


**Figure 1.44.** Correlation of the tangential vector is lost with an increasing segment distance.

variable  $\mathbf{r}(s)$  describes the conformation, where  $s$  is measured along the contour from one of the chain ends ( $0 < s < L_c$ ). The tangential vector  $\mathbf{u}(s)$  of unit length at  $s$  is given by

$$\mathbf{u}(s) = \frac{d\mathbf{r}(s)}{ds} \quad (1.69)$$

and represents the local orientation of the segment in the semirigid chain. As in the bead-stick model, the correlation between  $\mathbf{u}(s)$  and  $\mathbf{u}(s')$  of two segments at  $s$  and  $s'$  decreases to zero with a growing distance between the two segments along the contour:

$$\langle \mathbf{u}(s) \cdot \mathbf{u}(s') \rangle = \exp(-|s - s'|/L_p) \quad (1.70)$$

where  $L_p$  is called the **persistence length**. The correlation is lost exponentially as shown in Figure 1.44. The wormlike chain is described by two parameters,  $L_p$  and  $L_c$  (the contour length). The chain can be realized in a computer modeling by a bead-stick model of  $L_c/b$  sticks of length  $b$  ( $L_c/b \gg 1$ ) with a bond angle of  $\pi - \theta_b = \pi - (2b/L_p)^{1/2}$ .

**1.5.2.2 End-to-End Distance** We now calculate the end-to-end distance  $R_F$ . The end-to-end vector  $\mathbf{R}$  is related to  $\mathbf{u}(s)$  by

$$\mathbf{R} = \mathbf{r}(L_c) - \mathbf{r}(0) = \int_0^{L_c} \mathbf{u}(s) ds \quad (1.71)$$

Therefore,

$$\langle \mathbf{R}^2 \rangle = \int_0^{L_c} \int_0^{L_c} \langle \mathbf{u}(s) \mathbf{u}(s') \rangle ds ds' = 2 \int_0^{L_c} ds \int_0^s ds' \langle \mathbf{u}(s) \cdot \mathbf{u}(s') \rangle \quad (1.72)$$

With Eq. 1.70, we obtain

$$\boxed{R_F^2 = 2L_p[L_c + L_p(\exp(-L_c/L_p) - 1)] \quad \text{wormlike chain}} \quad (1.73)$$

Two limiting cases are interesting. When  $L_p \gg L_c$ , i.e., the chain is either sufficiently rigid or short,

$$R_F^2 = L_c^2 \left( 1 - \frac{L_c}{3L_p} + \dots \right) \quad (1.74)$$

In the limit of  $L_c/L_p \rightarrow 0$ , the wormlike chain is a rod ( $L_c = R_F$ ). When  $L_c \gg L_p$ , i.e., the chain is sufficiently flexible or long,

$$R_F^2 = 2L_cL_p \left( 1 - \frac{L_p}{L_c} + \dots \right) \quad (1.75)$$

In the limit of  $L_c \rightarrow \infty$ ,  $R_F \propto L_c^{1/2}$ , the same as the ideal chain. Comparison with Eq. 1.29 ( $L_c = bN$ ) gives an effective segment length of  $2L_p$ . The wormlike chain behaves like an ideal chain of a bond length of  $2L_p$  when  $L_c \gg L_p$ . The segment length defined in this way is called the **Kuhn segment length**.

**1.5.2.3 Radius of Gyration** To calculate the radius of gyration of the wormlike chain, we use a slightly different version of Eq. 1.25:

$$R_g^2 = \frac{1}{2L_c^2} \int_0^{L_c} \int_0^{L_c} [\mathbf{r}(s) - \mathbf{r}(s')]^2 ds ds' = \frac{1}{L_c^2} \int_0^{L_c} ds \int_0^s ds' [\mathbf{r}(s) - \mathbf{r}(s')]^2 \quad (1.76)$$

Since  $[\mathbf{r}(s) - \mathbf{r}(s')]^2 = 2L_p[|s - s'| + L_p(\exp(-|s - s'|/L_p) - 1)]$  has been already obtained in Eq. 1.73, it is easy to calculate  $R_g$ . The result is

$$\boxed{R_g^2 = \frac{1}{3} L_p L_c - L_p^2 + 2 \frac{L_p^3}{L_c} \left( 1 - \frac{L_p}{L_c} [1 - \exp(-L_c/L_p)] \right) \quad \text{wormlike chain}} \quad (1.77)$$

In the short-chain or the rigid-chain limit ( $L_c/L_p \ll 1$ ),

$$R_g^2 = \frac{1}{12} L_c^2 \left( 1 - \frac{L_c}{5L_p} + \dots \right) \quad (1.78)$$

In the long-chain limit or the flexible-chain limit ( $L_c/L_p \gg 1$ ),

$$R_g^2 = \frac{1}{3} L_p L_c \left( 1 - \frac{3L_p}{L_c} + \dots \right) \quad (1.79)$$



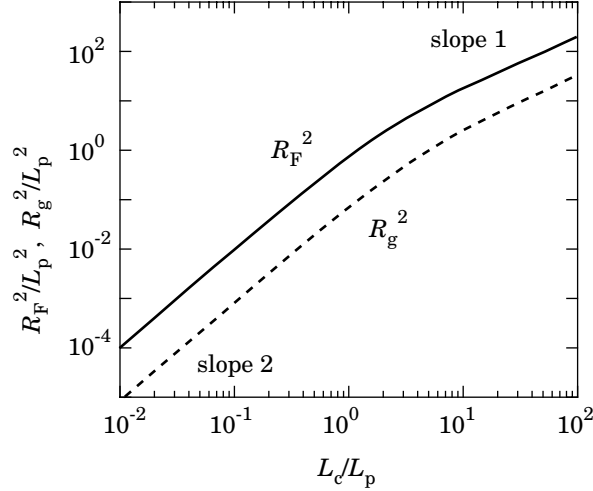


**Figure 1.45.** Mean square end-to-end distance  $R_F^2$  (solid line) and mean square radius of gyration  $R_g^2$  (dashed line) reduced by  $L_p^2$ , plotted as a function of  $L_c/L_p$ .

As in  $R_F^2$ ,  $2L_p = b$  makes the wormlike chain in the asymptote of  $L_c/L_p \gg 1$  have the same  $R_g$  as the ideal chain of the same  $L_c$ .

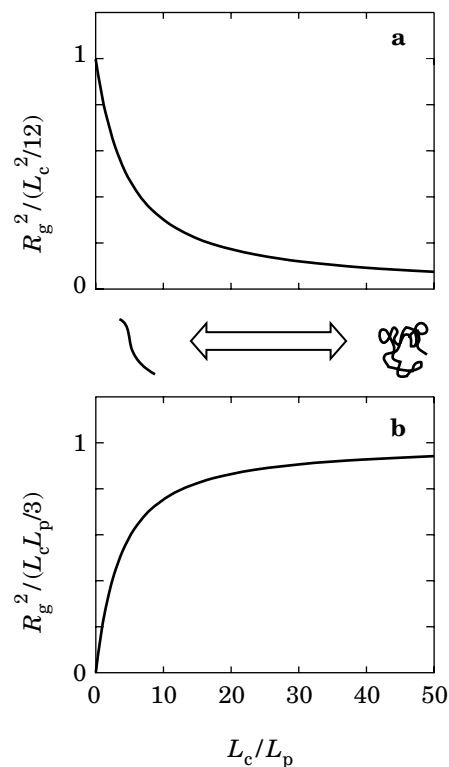
Figure 1.45 shows how  $R_F^2$  and  $R_g^2$  change with  $L_c/L_p$ . The slope shows a crossover from that of a rigid rod (slope = 2) to that of a flexible chain (slope = 1) for both  $R_F^2$  and  $R_g^2$ . The value of  $6R_g^2/R_F^2$  increases from 1/2 to 1 with an increasing  $L_c/L_p$ . The crossover occurs at around  $L_c/L_p \cong 1$ .

Figure 1.46 shows how  $R_g$  changes with  $L_c/L_p$ . Parts a and b are the plots of  $R_g^2/(L_c^2/12)$  and  $R_g^2/(L_p L_c/3)$  as a function of  $L_c/L_p$ , respectively. Figure 1.46a indicates how the chain dimension decreases from that of the rigid rod conformation of the same  $L_c$  as the chain becomes longer or more flexible. Figure 1.46b shows how the chain approaches an ideal chain as  $L_c/L_p$  increases. Because  $L_c \propto M$ , the two plots are essentially the plots of  $R_g^2/M^2$  and  $R_g^2/M$ , respectively, as a function of  $M$ .

**1.5.2.4 Estimation of Persistence Length** As we will learn in Section 2.4, the lightscattering experiments for different molecular weights of a semirigid polymer give the estimates of  $R_g$  and  $M$  for each fraction of the polymer. From the dependence of  $R_g$  on  $M$ , we can estimate  $L_p$ . For this purpose, we rewrite Eq. 1.77 into

$$\frac{R_g^2}{M} = \frac{L_p}{3m_L} - \frac{L_p^2}{M} + \frac{2L_p^3 m_L}{M^2} \left( 1 - \frac{L_p m_L}{M} [1 - \exp(-M/(L_p m_L))] \right) \quad (1.80)$$

where  $m_L = M/L_c$  is the molecular weight per unit length of the chain contour.



**Figure 1.46.** Mean square radius of gyration, reduced by (a)  $L_c^2/12$  and (b)  $L_p L_c/3$ , is plotted as a function of  $L_c/L_p$ . When  $L_c/L_p \ll 1$ , the wormlike chain is rodlike. When  $L_c/L_p \gg 1$ , the wormlike chain is a linear flexible chain.

An example of the lightscattering studies is shown in Figure 1.47 for poly(*n*-hexyl isocyanate) in hexane.<sup>8</sup> The data are on the curve shown in Figure 1.46b. Curve-fitting of the data by Eq. 1.80 gives the estimate of the two parameters as  $L_p = 42$  nm and  $m_L = 715$  g/(mol·nm). In Figure 1.47,  $R_g$  of poly(*n*-hexyl isocyanate) for  $M = 10^5$  g/mol is 31 nm. This value is much greater than those of polystyrene and polyethylene of the same  $M$  (compare Fig. 1.47 with Figs. 1.37 and 1.38).

Examples of  $L_p$  thus estimated are listed in Table 1.3 for some semirigid polymers. The persistence length depends on the solvent, the temperature, the concentration, and, for polyelectrolytes, on the ionic strength and pH.

### 1.5.3 PROBLEMS

**Problem 1.14:** What is  $L_p$  in the freely rotating chain with bond length  $b$  and bond angle  $\pi - \theta_b$ ?

**TABLE 1.3 Persistence Length of Some Semirigid Polymers**

Polymer	Solvent	$L_p$ /nm
poly( <i>p</i> -phenylene) <sup>a</sup>	toluene	13
poly( <i>n</i> -hexyl isocyanate) <sup>b</sup>	hexane	42
DNA <sup>c</sup>	aqueous	~50
poly( $\gamma$ -benzyl-L-glutamate) <sup>d</sup>	DMF	~200

<sup>a</sup>S. Vanhee et al. *Macromolecules* **29**, 5136 (1996).

<sup>b</sup>H. Murakami et al. *Macromolecules* **13**, 345 (1980).

<sup>c</sup>B. Zimm, *Macromolecules* **31**, 6089 (1998).

<sup>d</sup>E. Temyanko et al. *Macromolecules* **34**, 582 (2001).

**Solution 1.14:** For two bonds  $\mathbf{u}_i$  and  $\mathbf{u}_j$  separated by  $s$ ,  $|i - j| = s/b$ . Then,

$$\langle \mathbf{u}(s) \cdot \mathbf{u}(0) \rangle = (\cos \theta_b)^{s/b} = \exp[(s/b) \ln(\cos \theta_b)]$$

Comparison with Eq. 1.70 gives

$$L_p = \frac{b}{-\ln(\cos \theta_b)}$$

**Problem 1.15:** What is the expectation of the projection of the end-to-end vector  $\mathbf{R}$  onto the tangential vector  $\mathbf{u}_0 = \mathbf{u}(0)$  at the end of a wormlike chain?

**Solution 1.15:** The projection is given by

$$\begin{aligned} \langle \mathbf{R} \cdot \mathbf{u}_0 \rangle &= \left\langle \int_0^{L_c} \mathbf{u}(s) \, ds \cdot \mathbf{u}_0 \right\rangle = \int_0^{L_c} \langle \mathbf{u}(s) \cdot \mathbf{u}(0) \rangle \, ds \\ &= \int_0^{L_c} \exp(-s/L_p) \, ds = L_p [1 - \exp(-L_c/L_p)] \end{aligned}$$

**Problem 1.16:** Nonreverse random walk (NRRW) is often used in lattice simulations. The random walker can choose any direction except for returning to the preceding site. Otherwise, the walker can return to the site it visited earlier. We can expect that the trajectory is between that of an ideal chain and that of an excluded volume chain. For a cubic lattice of lattice unit  $b$ , assume that the random walker chooses one out of the five directions at random and answer the following questions.

- (1) What is  $\langle \Delta \mathbf{r}_i \cdot \Delta \mathbf{r}_{i+1} \rangle$ ? How about  $\langle \Delta \mathbf{r}_i \cdot \Delta \mathbf{r}_j \rangle$ ?
- (2) What is the mean square displacement of  $N$  steps when  $N \gg 1$ ?
- (3) The nonreverse condition makes NRRW somewhat rigid. What is the persistence length?

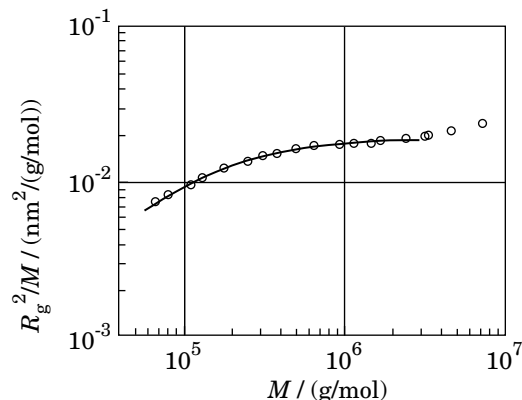


**Figure 1.47.** Mean square radius of gyration reduced by molecular weight  $M$  for different fractions of poly(*n*-hexyl isocyanate) in hexane. The optimal curve fitting by the wormlike chain model is shown as a solid line. (From Ref. 8.)

**Solution 1.16:**

- (1)  $\langle \Delta \mathbf{r}_i \cdot \Delta \mathbf{r}_{i+1} \rangle = b^2/5$ .  $\langle \Delta \mathbf{r}_i \cdot \Delta \mathbf{r}_j \rangle = b^2/5^{|i-j|}$ .
- (2)  $\langle \Delta \mathbf{r}^2 \rangle = \sum_{i,j=1}^N \langle \Delta \mathbf{r}_i \cdot \Delta \mathbf{r}_j \rangle = \sum_{i,j=1}^N b^2 5^{-|i-j|} = b^2 \left[ N + 2 \sum_{i=1}^{N-1} \sum_{j=i+1}^N 5^{i-j} \right] \cong \frac{3}{2} b^2 N$
- (3) Equate  $\langle \mathbf{u}_i \cdot \mathbf{u}_j \rangle = (1/5)^{|i-j|}$  with  $\langle \mathbf{u}_i \cdot \mathbf{u}_j \rangle = \exp(-b|i-j|/L_p)$ . Then, we get  $L_p = b/\ln 5$ . It is close to  $(3/4)b$  estimated from (2).

## 1.6 BRANCHED CHAINS

### 1.6.1 Architecture of Branched Chains

There are different architectures in branched chains as shown in Figure 1.48. A **star-branched chain** or **star polymer** (a) consists of a core and arms of a more or less similar length. A two-arm star polymer is essentially a linear polymer. A **comb polymer** (b) consists of a linear-chain backbone and many small combs stemming from trifunctional units distributed along the backbone. The joints may be uniformly spaced. The comb length is more or less uniform. The comb polymer with a uniform distribution of branching points and a uniform distribution of branching length can be prepared by polymerizing monomers that have a long side chain.

Copolymerization of monomers having a side chain with side chain-free monomers is one of the methods to introduce randomness in the branching points. In the **random-branched chain** (Figure 1.48, c and d), branching points are distributed randomly. The branches may have further branches, although its probability is usually low. The branching density can be controlled by changing the mixing ratio of the two types of monomers. It is difficult to pick up the main chain or the

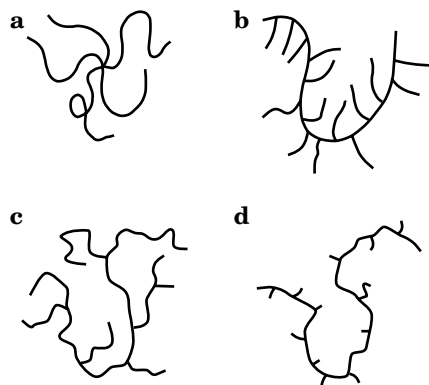


**Figure 1.48.** Architectures of branched polymers: star polymer (a), comb copolymer (b), short-chain branching (c), and long-chain branching (d).

backbone in the random-branched chain. The length of the branches distinguishes long-chain branching (c) from short-chain branching (d). Long-chain branching is sometimes naturally introduced in the chain-reaction polymerization. When the frequency of branching is high, then the chain is called a highly branched chain or **hyperbranched chain**.

There is a different class of branched polymer. In a **dendrimer** shown in Figure 1.49, every repeating unit is trifunctional. Starting at the center, the number of monomers in a layer (generation) increases twofold every generation.

### 1.6.2 Dimension of Branched Chains

The best quantity to characterize the overall dimension of the branched chain is the radius of gyration,  $R_g$ ; The end-to-end distance cannot be well defined for nonlinear chains. The **branching parameter**  $g_g$  is defined as

$$g_g \equiv \frac{R_{gb}^2}{R_{gl}^2} \quad \text{branching parameter} \quad (1.81)$$

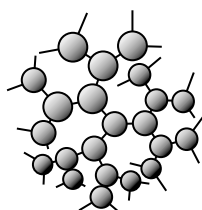


**Figure 1.49.** Dendrimer.

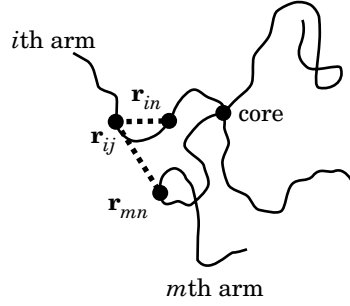


**Figure 1.50.** Two monomers can be on the same arm or on different arms.

where  $R_{\text{gb}}^2$  is the mean square radius of gyration for the branched chain, and  $R_{\text{gl}}^2$  is the mean square radius of gyration for the linear chain. The ratio is calculated for the two polymers of the same molecular weight. Branching makes the monomers more congested around the center of mass. Therefore  $g_g \leq 1$ .

For demonstration, we calculate here  $g_g$  for an  $n_A$ -arm star polymer. We assume that each arm is an ideal chain and has the same number of monomers,  $N_1$  ( $N_1 \gg 1$ ). Let  $\mathbf{r}_{ij}$  be the position of the  $j$ th monomer ( $j = 0, 1, \dots, N_1$ ) on the  $i$ th arm ( $i = 1, 2, \dots, n_A$ ), as illustrated in Figure 1.50. The core is at  $\mathbf{r}_{i0}$ . With the use of Eq. 1.25, the mean-square radius of gyration  $R_{\text{gb}}^2$  is expressed as

$$R_{\text{gb}}^2 = \frac{1}{2n_A^2 N_1^2} \sum_{i,m=1}^{n_A} \sum_{j,n=1}^{N_1} \langle (\mathbf{r}_{ij} - \mathbf{r}_{mn})^2 \rangle \quad (1.82)$$

where the core is not included in the sum. The mean square of the monomer distance is calculated for monomers on the same arm and those on difference arms separately (see Figure 1.50):

$$\begin{aligned} \sum_{i,m=1}^{n_A} \sum_{j,n=1}^{N_1} \langle (\mathbf{r}_{ij} - \mathbf{r}_{mn})^2 \rangle &= \sum_{i=1}^{n_A} \sum_{j,n=1}^{N_1} \langle (\mathbf{r}_{ij} - \mathbf{r}_{in})^2 \rangle + \sum_{i \neq m}^{n_A} \sum_{j,n=1}^{N_1} \langle (\mathbf{r}_{ij} - \mathbf{r}_{mn})^2 \rangle \\ &= \sum_{i=1}^{n_A} \sum_{j,n=1}^{N_1} |j - n| b^2 + \sum_{i \neq m}^{n_A} \sum_{j,n=1}^{N_1} (j + n) b^2 \\ &= b^2 \left[ n_A \sum_{j,n=1}^{N_1} |j - n| + n_A(n_A - 1) \sum_{j,n=1}^{N_1} (j + n) \right] \\ &= \frac{1}{3} b^2 n_A N_1 (N_1 + 1) (3n_A N_1 - 2N_1 - 1) \end{aligned} \quad (1.83)$$

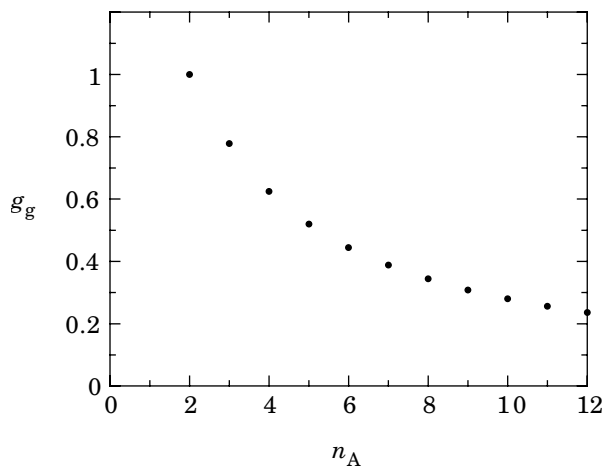


**Figure 1.51.** The branching parameter of a star polymer, plotted as a function of the number of arms,  $n_A$ .

From Eqs. 1.82 and 1.83, we have

$$R_{gb}^2 = \frac{b^2(N_1 + 1)}{6n_A N_1} (3n_A N_1 - 2N_1 - 1) \cong b^2 \frac{N}{n_A} \left( \frac{1}{2} - \frac{1}{3n_A} \right) \quad (1.84)$$

where  $N_1 \gg 1$  was used, and  $N = n_A N_1$  is the total chain length. For linear polymer ( $n_A = 2$ ), the mean-square radius of gyration is  $R_{gl}^2 = b^2 N/6$ . Thus,

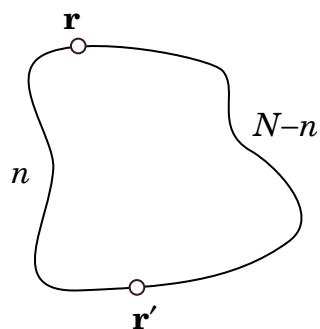
$$g_g = \frac{1}{n_A} \left( 3 - \frac{2}{n_A} \right) \quad \begin{array}{l} \text{branching parameter} \\ n_A\text{-arm star} \end{array} \quad (1.85)$$

Figure 1.51 shows a plot of  $g_g$  as a function of  $n_A$ . As the number of arms increases, the chain becomes more compact and therefore  $g_g$  decreases.

Branching is widely observed in polyolefins. Figure 1.52 shows  $R_g$  of branched polyethylene as a function of molecular weight  $M$  of the polymer.<sup>9</sup> As in Figure 1.38, size-exclusion chromatography with an on-line light-scattering detector was employed to measure  $R_g$  and  $M$  simultaneously for every fraction separated in the chromatography. Different sets of data (distinguished by different symbols in the plot) were obtained by changing the reaction pressure. Each set follows approximately a power law of  $R_g \sim M^{0.59}$ . We can estimate the branching parameter  $g_g$  for each sample by comparing  $R_g$  at some value of  $M$ .

### 1.6.3 PROBLEMS

**Problem 1.17:** Calculate  $R_g$  of a ring polymer (also called a cyclic polymer) consisting of  $N$  segments of length  $b$ . Assume Gaussian statistics for any part of the chain.

**Solution 1.17:**

Two segments at  $\mathbf{r}$  and  $\mathbf{r}'$  separated by  $n$  segments on one side and  $N - n$  segments on the other side are distributed with a probability proportional to

$$\exp\left(-\frac{3(\mathbf{r} - \mathbf{r}')^2}{2nb^2}\right) \exp\left(-\frac{3(\mathbf{r} - \mathbf{r}')^2}{2(N-n)b^2}\right) = \exp\left(-\frac{3(\mathbf{r} - \mathbf{r}')^2}{2n'b^2}\right)$$

where  $1/n' = 1/n + 1/(N - n) = N/[n(N - n)]$ . When normalized, the probability is given by  $G(\mathbf{r}, \mathbf{r}'; n')$ . The average of  $(\mathbf{r} - \mathbf{r}')^2$  is

$$\begin{aligned} \langle (\mathbf{r} - \mathbf{r}')^2 \rangle &= N^{-1} \int_0^N dn \int d\mathbf{r} (\mathbf{r} - \mathbf{r}')^2 G(\mathbf{r}, \mathbf{r}'; n') \\ &= N^{-1} \int_0^N dn n' b^2 = N^{-1} b^2 \int_0^N dn \frac{n(N-n)}{N} = \frac{1}{6} N b^2 \end{aligned}$$

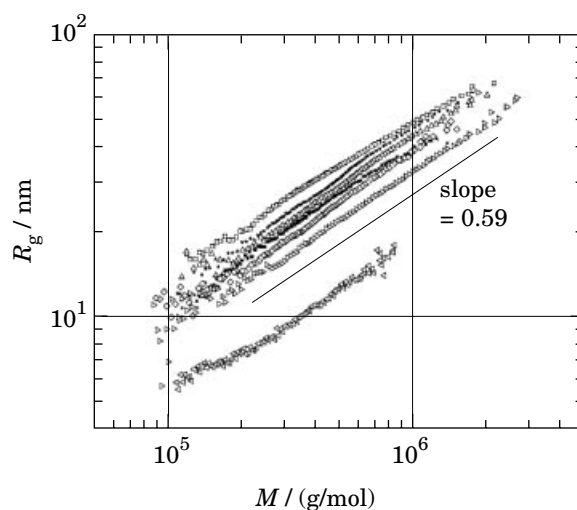


**Figure 1.52.** Radius of gyration  $R_g$  of branched polyethylene prepared at different reaction pressures, plotted as a function of the molecular weight  $M$ . (From Ref. 9.)

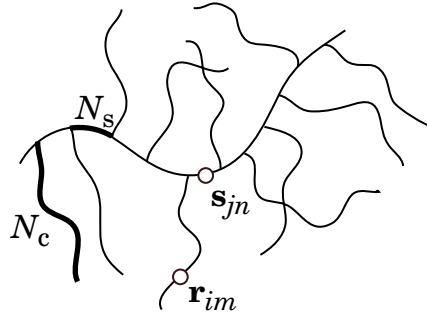


Thus,

$$R_{\text{g,ring}}^2 = \frac{1}{2} \langle (\mathbf{r} - \mathbf{r}')^2 \rangle = \frac{1}{12} N b^2$$

**Problem 1.18:** A comb polymer has  $n_A$  anchors along its backbone, interspaced by  $N_s$  monomers. Each comb consists of  $N_c$  monomers. What is  $R_g$  of this comb polymer, when all monomers have an equal mass? Assume that all parts of the comb polymer are ideal, each monomer has a size of  $b$ , and  $N_s, N_c, n_A \gg 1$ .

**Solution 1.18:**



Let  $\mathbf{r}_{im}$  be the position of the  $m$ th monomer on the  $i$ th comb and  $\mathbf{s}_{jn}$  be the position of the  $n$ th monomer on the  $j$ th block on the main chain.  $1 \leq m \leq N_c$ ,  $1 \leq n \leq N_s$ ,  $1 \leq i, j \leq n_A$ . There are a total  $n_A(N_c + N_s)$  monomers in the chain. The mean square distance between the two monomers has four parts:  $S_A$  (two monomers on the same comb),  $S_B$  (two monomers on different combs),  $S_C$  (two monomers on the main chain), and  $S_D$  (one monomer on the comb, the other on the main chain):

$$\begin{aligned} S_A &= \sum_{i=1}^{n_A} \sum_{m,n=1}^{N_c} \langle (\mathbf{r}_{im} - \mathbf{r}_{in})^2 \rangle \cong n_A b^2 \frac{1}{3} N_c^3 \\ S_B &= \sum_{i \neq j}^{n_A} \sum_{m,n=1}^{N_c} \langle (\mathbf{r}_{im} - \mathbf{r}_{jn})^2 \rangle = \sum_{i \neq j}^{n_A} \sum_{m,n=1}^{N_c} b^2 (|i - j| N_s + m + n) \\ &= b^2 \sum_{i \neq j}^{n_A} \left( N_s |i - j| N_c^2 + 2 \sum_{m,n=1}^{N_c} m \right) \cong n_A^2 b^2 N_c^2 \left( \frac{1}{3} N_s n_A + N_c \right) \\ S_C &= \sum_{i,j=1}^{n_A} \sum_{m,n=1}^{N_s} \langle (\mathbf{s}_{im} - \mathbf{s}_{jn})^2 \rangle \cong \frac{1}{3} b^2 (n_A N_s)^3 \\ S_D &= \sum_{i,j=1}^{n_A} \sum_{m=1}^{N_c} \sum_{n=1}^{N_s} \langle (\mathbf{r}_{im} - \mathbf{s}_{jn})^2 \rangle = \sum_{i,j=1}^{n_A} \sum_{m=1}^{N_c} \sum_{n=1}^{N_s} b^2 (|i - j| N_s + m + n) \end{aligned}$$

$$\cong b^2 \left( \frac{1}{3} n_A^3 N_s^2 N_c + \frac{1}{2} n_A^2 N_s N_c (N_s + N_c) \right)$$

We find that  $S_A \ll S_B$ . The means square distance between two monomers is

$$\frac{S_B + S_C + 2S_D}{n_A^2 (N_s + N_c)^2} = b^2 \left[ \frac{1}{3} n_A N_s + \frac{N_c (N_c^2 + N_s N_c + N_s^2)}{(N_s + N_c)^2} \right]$$

Thus,  $R_g^2$  is given by

$$R_g^2 = \frac{1}{2} b^2 \left[ \frac{1}{3} n_A N_s + \frac{N_c (N_c^2 + N_s N_c + N_s^2)}{(N_s + N_c)^2} \right]$$

Note that the second term in the square bracket is negligible when  $n_A N_s \gg N_c$ . The chain dimension is determined by the main chain only.

## 1.7 MOLECULAR WEIGHT DISTRIBUTION

### 1.7.1. Average Molecular Weights

**1.7.1.1 Definitions of the Average Molecular Weights** Nearly all of polymer is a mixture of molecules with a different degree of polymerization. This **polydispersity** is absent in some synthetic oligomers and some polymers of biological origin such as proteins. **Monodisperse** polymers refer to those with a single molecular weight. They are exceptions. Polymers are usually polydisperse and have a molecular weight distribution. A few representative values are used as a typical molecular weight of the polymer. We learn here about average molecular weights.

Let the sample of the polymer consist of  $n_i$  chains of exact molecular weight  $M_i$ , where the  $i$ th component has a degree of polymerization  $i$ . The difference between  $M_i$  and  $M_{i+1}$  is the mass of the repeating unit. The **number-average molecular weight**  $M_n$  is defined as

$$M_n = \frac{\sum_i n_i M_i}{\sum_i n_i} \quad \text{number-average molecular weight} \quad (1.86)$$

The weight-average molecular weight  $M_w$  is defined as

$$M_w = \frac{\sum_i n_i M_i^2}{\sum_i n_i M_i} \quad \text{weight-average molecular weight} \quad (1.87)$$

Note that  $n_i / \sum n_i$  gives the number fraction of the  $i$ th component and  $n_i M_i / \sum n_i M_i$  is its weight fraction. For  $i \gg 1$ ,  $M_i \propto i$  because the chain ends are only a small part of the long chain; therefore, the weight fraction is given by  $i n_i / \sum i n_i$  as well. It is not necessary that  $n_i$  be the actual number of polymer molecules, but  $n_i$

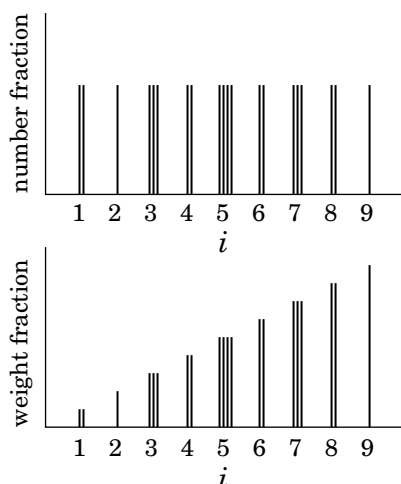


**Figure 1.53.** Distribution of chain length in a polymer sample. a: Number fraction. b: Weight fraction. The total height of the bars at each  $i$  gives the weight factor to calculate the number average and the weight average, respectively.

must be proportional to the number. Figure 1.53 illustrates the difference between the number fraction and the weight fraction. The total height of the bars at each  $i$  gives the weight factor in calculating the average. In the number average, each polymer chain is counted equally regardless of its length. In the weight average, a longer chain is counted with a greater proportion.

Also used is the z-average molecular weight  $M_z$  further weighted with  $M_i$ :

$$M_z = \frac{\sum_i n_i M_i^3}{\sum_i n_i M_i^2} \quad \text{z-average molecular weight} \quad (1.88)$$

For a perfectly monodisperse polymer,  $M_n = M_w = M_z$ . Otherwise,  $M_n < M_w < M_z$ . The ratio of  $M_w$  to  $M_n$  is often used to express how polydisperse the polymer sample is. The ratio is called **polydispersity index**, often abbreviated as PDI:

$$\text{PDI} = \frac{M_w}{M_n} = \frac{\sum_i n_i \sum_i n_i M_i^2}{\left(\sum_i n_i M_i\right)^2} \quad \text{polydispersity index} \quad (1.89)$$

Unless the polymer is monodisperse,  $\text{PDI} > 1$ . A sample with a greater PDI has a broader molecular weight distribution.

A continuous version of the molecular weight distribution is also used in the definition of the average molecular weights. The discrete variable  $M_i$  is now replaced by a continuous variable  $M$ , and  $n_i$  is replaced by  $f(M)$ , where  $f(M)dM$  is proportional to the number of polymer molecules with molecular weights between  $M$  and



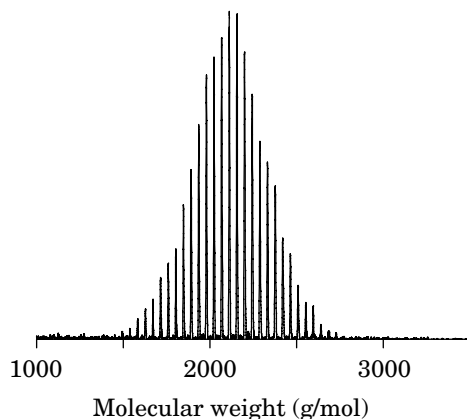


**Figure 1.54.** Example of a mass spectrum of a polymer obtained in MALDI-TOF mass spectrometry. Poly(ethylene glycol) of a nominal molecular weight of 2,000 g/mol is shown. (From Ref. 10.)

$M + dM$ . Now the three definitions of the average molecular weight are

$$M_n = \frac{\int Mf(M) dM}{\int f(M) dM} \quad (1.90)$$

$$M_w = \frac{\int M^2f(M) dM}{\int Mf(M) dM} \quad (1.91)$$

$$M_z = \frac{\int M^3f(M) dM}{\int M^2f(M) dM} \quad (1.92)$$

**1.7.1.2 Estimation of the Averages and the Distribution** Osmometry (membrane or vapor pressure) counts the number of independently moving units (polymer chains) per volume and therefore can be used to estimate  $M_n$ . A proton NMR spectrum can also give  $M_n$ . If the polymer is end-functionalized, titration can give an estimate of  $M_n$ . In Section 2.4, we will learn that light scattering gives an estimate of  $M_w$ .

Recently, mass spectroscopy has been increasingly applied to the analysis of the molecular weight distribution of polymers. Development of a soft ionization method that allows a whole polymer chain to be ionized without fragmentation has facilitated the application. The method is called matrix-assisted laser desorption ionization (MALDI) and usually coupled with time-of-flight (TOF) mass analyzer. Figure 1.54 shows an example of the mass spectrum.<sup>10</sup> The sample is poly(ethylene glycol) of a nominal molecular weight of 2,000 g/mol. The peaks are interspaced by the monomer molecular weight of 44 g/mol. The width of each peak is due to the presence of isotopes (mostly  $^{13}\text{C}$ ). The application has been limited, however, to

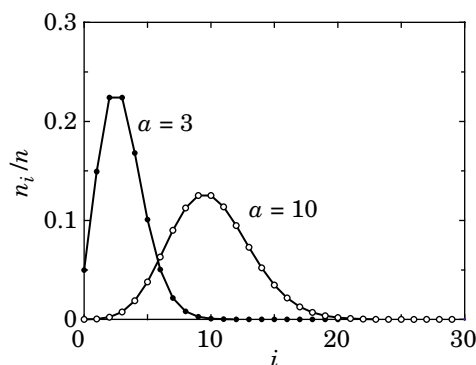


**Figure 1.55.** Poisson distribution. The number fraction  $n_i/n$  is shown for  $a = 3$  and 10.

polymers with a narrow molecular weight distribution or with molecular weights less than a few tens of thousand g/mol. Ions consisting of a single molecule but with multiple charges and ions consisting of more than one polymer molecules cause significant ghost peaks at twice as large  $m/z$ , half as large  $m/z$ , and so forth. A sample with a broad molecular weight distribution makes these ghost peaks overlap. Furthermore, there is a question of the molecular weight-dependent ionization efficiency.

Size exclusion chromatography has been the mainstay in the analysis of the molecular weight distribution. Although the resolution is poorer than that of mass spectrometry by orders of magnitude, the chromatographic separation gives an unbiased molecular weight distribution. We will learn about the chromatographic method in Section 2.5.

## 1.7.2 Typical Distributions

**1.7.2.1 Poisson Distribution** We now calculate the average molecular weights for some typical distributions of a linear polymer. The examples are a **Poisson distribution** and an **exponential distribution** in a discrete space and a **log-normal distribution** in a continuous space.

In the Poisson distribution, the number fraction of the  $i$ th component is given by

$$n_i/n = e^{-a} a^i / i! \quad (i = 0, 1, 2, \dots) \quad (1.93)$$

where  $n$  is the total number of chains and  $a$  is a constant. A greater  $a$  makes the distribution heavier at larger values of  $i$ . Figure 1.55 shows the Poisson distributions with  $a = 3$  and 10. For simplicity, we assume that  $M_i = iM_1$ , where  $M_1$  is the monomer molecular weight. Then,  $M_n$  is calculated as

$$M_n = \sum_{i=0}^{\infty} M_i n_i/n = M_1 e^{-a} \sum_{i=0}^{\infty} i a^i / i! = M_1 e^{-a} a \sum_{i=1}^{\infty} a^{i-1} / (i-1)! = M_1 a \quad (1.94)$$

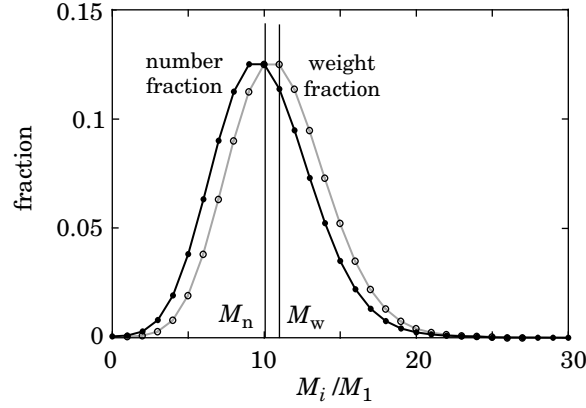


**Figure 1.56.** Number fraction and weight fraction of the Poisson distribution.  $M_n$  and  $M_w$  are also indicated.

The constant  $a$  is the number-average degree of polymerization. Likewise,

$$\sum_{i=0}^{\infty} M_i^2 n_i/n = M_1^2 e^{-a} \left[ a^2 \sum_{i=2}^{\infty} a^{i-2}/(i-2)! + a \sum_{i=1}^{\infty} a^{i-1}/(i-1)! \right] = M_1^2 (a^2 + a) \quad (1.95)$$

Thus  $M_w = (1 + a)M_1$ . Note that  $M_n$  and  $M_w$  differ only by  $M_1$ . Therefore,

$$\text{PDI} = 1 + \frac{1}{a} = 1 + \frac{M_1}{M_n} \quad (1.96)$$

PDI decreases toward 1 as  $M_n$  increases. Figure 1.56 shows  $M_n$  and  $M_w$  together with its parent Poisson distribution with  $a = 10$ . If  $a = 1,000$ , then  $\text{PDI} = 1.001$ . Polymers prepared in living polymerization are known to have a distribution close to the Poisson distribution.

**1.7.2.2 Exponential Distribution** In the exponential distribution, the number fraction of the  $i$ th component is given by

$$n_i/n = (1 - a)a^{i-1} \quad (i = 1, 2, \dots) \quad (1.97)$$

where  $a$  is a constant ( $a < 1$ ).  $n_i$  decreases with an increasing  $i$ . With  $M_i = iM_1$ ,  $M_n$  is calculated as

$$M_n = \sum_{i=1}^{\infty} M_i n_i/n = M_1 (1 - a) \sum_{i=0}^{\infty} i a^{i-1} = \frac{M_1}{1 - a} \quad (1.98)$$

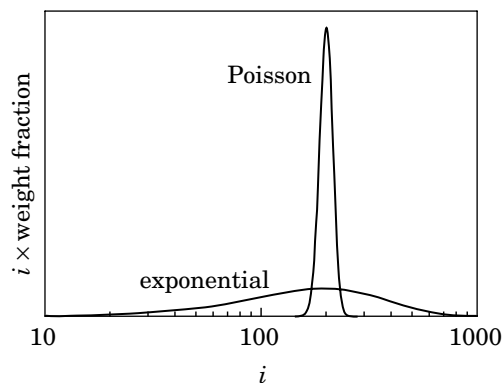


Figure 1.57. Poisson distribution and exponential distribution with the same  $M_w$ .

To have a high molecular weight,  $a$  must be close to 1. Likewise,

$$\sum_{i=1}^{\infty} M_i^2 n_i / n = M_1^2 (1 - a) \sum_{i=0}^{\infty} i^2 a^{i-1} = M_1^2 \frac{1 + a}{(1 - a)^2} \quad (1.99)$$

which gives  $M_w = M_1(1 + a)/(1 - a)$ . Thus the polydispersity is

$$\text{PDI} = 1 + a = 2 - \frac{M_1}{M_n} \quad (1.100)$$

As  $M_n$  increases, PDI increases to 2. Polymers prepared in condensation polymerization follows this distribution. In the latter,  $a$  is the probability for the reactive end to add another monomeric unit, not the terminator.

Figure 1.57 compares the weight fraction distribution of the Poisson distribution and the exponential distribution with the same  $M_w$ . The abscissa is on a logarithmic scale; therefore, the ordinate is the weight fraction  $\times i$ . The difference in the width between the two distributions is large.

**1.7.2.3 Log-Normal Distribution** Size-exclusion chromatography (Section 2.5) is widely used to obtain a continuous distribution of the molecular weight. The direct signal from the detector is proportional to the mass of the polymer in the relevant fraction, and the signal plotted as a function of time is close to the weight fraction on a logarithmic scale of  $M$ . Therefore, we usually display  $d\Sigma/d \ln M$  as a function of  $\ln M$ , where  $\Sigma$  is the cumulative weight fraction defined as

$$\Sigma(M) \equiv \int_0^M Mf(M) dM \quad (1.101)$$

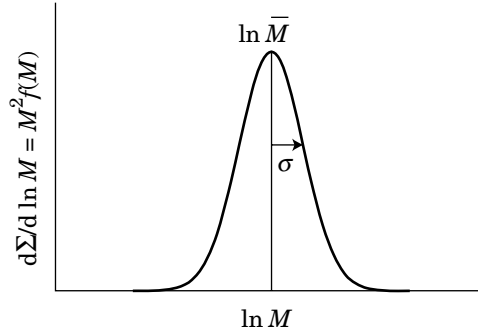


Figure 1.58. Log-normal distribution.

Then, what is displayed is  $M^2f(M)$ . The log-normal distribution is a normal distribution for  $M^2f(M)$  with a random variable of  $\ln M$ :

$$M^2f(M) = (2\pi\sigma^2)^{-1/2} \exp\left[-(\ln M - \ln \bar{M})^2/2\sigma^2\right] \quad (1.102)$$

where  $\bar{M}$  is the peak molecular weight on the log scale and  $\sigma^2$  is the variance. The weight distribution function is normalized:

$$\int Mf(M)dM = \int M^2f(M)d \ln M = 1 \quad (1.103)$$

The distribution is shown in Figure 1.58. We notice that the log-normal distribution has almost the same shape as that of the Poisson distribution or the exponential distribution. The similarity is due to the law of large numbers.

Other relevant integrals are calculated as follows:

$$\begin{aligned} \int f(M) dM &= (2\pi\sigma^2)^{-1/2} \int \exp\left[-(\ln M - \ln \bar{M} + \sigma^2)^2/2\sigma^2 - \ln \bar{M} + \sigma^2/2\right] d \ln M \\ &= (1/\bar{M})\exp(\sigma^2/2) \end{aligned} \quad (1.104)$$

$$\begin{aligned} \int M^2f(M) dM &= (2\pi\sigma^2)^{-1/2} \int \exp\left[-(\ln M - \ln \bar{M} - \sigma^2)^2/2\sigma^2 + \ln \bar{M} + \sigma^2/2\right] d \ln M \\ &= \bar{M} \exp(\sigma^2/2) \end{aligned} \quad (1.105)$$

Thus,

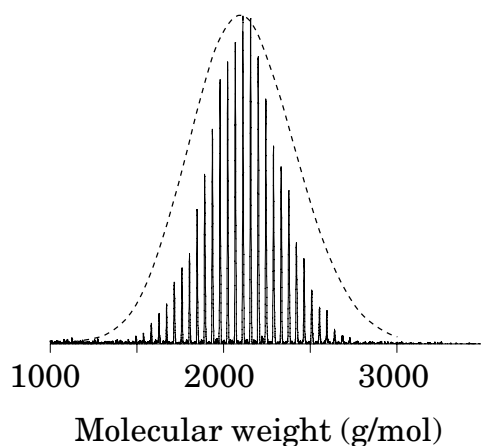
$$M_n = \bar{M} \exp(-\sigma^2/2), \quad M_w = \bar{M} \exp(\sigma^2/2), \quad \text{PDI} = \exp(\sigma^2) \quad (1.106)$$



### 1.7.3 PROBLEMS

**Problem 1.19:** The peak of the molecular weight distribution in Fig. 1.54 is around 2,100 g/mol. Compare the plot in the figure with the Poisson distribution with this peak molecular weight.

**Solution 1.19:** The dashed line was calculated for  $DP = 48$ .



**Problem 1.20:** Find the molecular weight of the polymer that maximizes the number fraction in the Poisson distribution (Eq. 1.93). Assume that  $i \gg 1$ .

**Solution 1.20:**

$$\ln(n_i/n) = -a + i \ln a - \ln i! \cong -a + i \ln a - i(\ln i - 1)$$

At the peak,

$$0 = \frac{\partial}{\partial i} \ln(n_i/n) = \ln a - (\ln i - 1) - 1 = \ln(a/i)$$

The value of  $i$  that gives the peak is  $a$ . The peak molecular weight is  $aM_1$ .

**Problem 1.21:** Show that the polydispersity of an  $n_A$ -arm star polymer,  $PDI_{\text{star}}$ , is related to the polydispersity of the arm,  $PDI_{\text{arm}}$ , as

$$PDI_{\text{star}} = 1 + \frac{PDI_{\text{arm}} - 1}{n_A}$$

**Solution 1.21:** Let  $f(M)$  be the normalized number distribution of the molecular weight of each arm. The molecular weight  $M_{\text{star}}$  of the star polymer is the sum

of the molecular weights  $M_j$  of the arm ( $j = 1, \dots, n_A$ ):

$$M_{\text{star}} = \sum_{j=1}^{n_A} M_j$$

From definition,

$$\text{PDI}_{\text{star}} = \frac{\int f(M_1) dM_1 \dots \int f(M_{n_A}) dM_{n_A} \left( \sum_{j=1}^{n_A} M_j \right)^2}{\left( \int f(M_1) dM_1 \dots \int f(M_{n_A}) dM_{n_A} \sum_{j=1}^{n_A} M_j \right)^2}$$

The denominator and the numerator are calculated respectively as

$$\begin{aligned} \int f(M_1) dM_1 \dots \int f(M_{n_A}) dM_{n_A} \sum_{j=1}^{n_A} M_j &= \sum_{j=1}^{n_A} \int f(M_1) dM_1 \dots \int f(M_{n_A}) dM_{n_A} M_j \\ &= \sum_{j=1}^{n_A} \int M_j f(M_j) dM_j = n_A \int M_1 f(M_1) dM_1 \\ \int f(M_1) dM_1 \dots \int f(M_{n_A}) dM_{n_A} \left( \sum_{j=1}^{n_A} M_j \right)^2 &= \sum_{i,j=1}^{n_A} \int f(M_1) dM_1 \dots \int f(M_{n_A}) dM_{n_A} M_i M_j \\ &= n_A \int M_1^2 f(M_1) dM_1 + n_A(n_A - 1) \left( \int M_1 f(M_1) dM_1 \right)^2 \end{aligned}$$

Then,

$$\begin{aligned} \text{PDI}_{\text{star}} &= \frac{n_A \int M_1^2 f(M_1) dM_1 + n_A(n_A - 1) \left( \int M_1 f(M_1) dM_1 \right)^2}{\left( n_A \int M_1 f(M_1) dM_1 \right)^2} \\ &= \frac{1}{n_A} \frac{\int M_1^2 f(M_1) dM_1}{\left( \int M_1 f(M_1) dM_1 \right)^2} + 1 - \frac{1}{n_A} = 1 + \frac{1}{n_A} (\text{PDI}_{\text{arm}} - 1) \end{aligned}$$

## 1.8 CONCENTRATION REGIMES

### 1.8.1 Concentration Regimes for Linear Flexible Polymers

In a crude approximation, each linear polymer chain occupies a space of a sphere or a cube of a linear dimension of  $R_g$ , as illustrated in Figure 1.59. Each

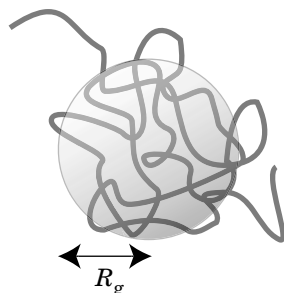


**Figure 1.59.** A polymer chain has a volume approximately of a sphere of radius  $R_g$ .

monomer occupies a volume of  $\sim b^3$ . The volume fraction of the monomers in this volume is

$$\frac{Nb^3}{R_g^3} \cong \frac{Nb^3}{(bN^\nu)^3} = N^{1-3\nu} \quad (1.107)$$

The exponent  $1 - 3\nu$  is  $-1/2$  for an ideal chain and  $-4/5$  (or  $-0.77$  for  $\nu = 0.59$ ) for a real chain. The monomer volume fraction decreases as the chain becomes longer. The real chain is expanded; therefore, the decrease is steeper than that of the ideal chain. The monomer volume fraction is low in the sphere. It is 0.029 at  $N = 100$  and 0.0049 at  $N = 1,000$  for the real chain.

At low concentrations, these spheres or cubes are separated from each other. As the concentration  $c$  (mass concentration; expressed in g/mL, for instance) increases, they become congested and eventually touch each other. At the so-called **overlap concentration** ( $c^*$ ), the whole volume of the solution is packed with these spheres. The overall concentration of the solution is equal to the concentration in the sphere given by Eq. 1.107 at the chain overlap. Thus  $c^* \sim N^{1-3\nu}$ . More quantitative definitions of  $c^*$  are usually used:

$$c^* \left( \frac{4\pi}{3} R_g^3 \right) = \frac{M}{N_A} \quad (1.108)$$

$$c^* (\sqrt{2} R_g)^3 = \frac{M}{N_A} \quad (1.109)$$

$$c^* [\eta] = 1 \quad (1.110)$$

where  $M/N_A$  is the mass of each chain, with  $N_A$  being the Avogadro's number. The last equation relies on the intrinsic viscosity  $[\eta]$  of the polymer, which we will further discuss in Section 3.3.

Figure 1.60 depicts three ranges of concentration  $c$ :  $c \ll c^*$ ,  $c \cong c^*$ , and  $c \gg c^*$ . When  $c$  is below  $c^*$ , the solution is called **dilute**. At  $c \ll c^*$ , the chains are separated

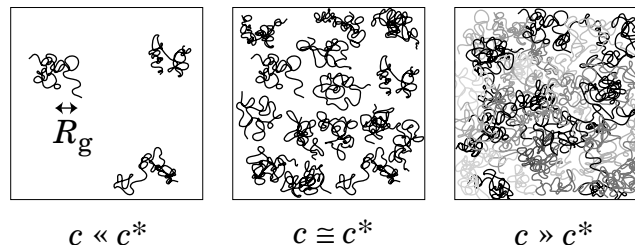


**Figure 1.60.** Concentration regimes for solutions of linear flexible polymers: dilute solution,  $c \ll c^*$ ; solution at the overlap concentration  $c \cong c^*$ ; semidilute solution,  $c \gg c^*$ .

from each other and behave more or less independently. The polymer chain interacts primarily with the solvent molecules. The solution is close to an ideal solution. The situation is different at concentrations above  $c^*$ . The solution in this regime is called **semidilute**. At  $c \gg c^*$ , chains are overlapped and entangled. Their mobility is greatly reduced compared with the chains in dilute solutions. The thermodynamic properties of the semidilute solutions are greatly different from those of an ideal solution extrapolated to the same concentration. In polymer solutions, deviation from the ideal solution takes place at a low concentration in terms of the volume fraction or the mass concentration. The existence of the semidilute regime is characteristic of the polymer solutions. At a higher concentration  $c^{**}$ , the solution enters a so-called **concentrated** regime in which each segment of the polymer chain does not have a sufficient space available. Typically, the volume fraction of the polymer at  $c^{**}$  is between 0.2 and 0.3. For a polymer of a sufficiently high molecular weight, there is a broad range of concentrations between  $c^*$  and  $c^{**}$ . For polystyrene of  $M = 3 \times 10^5$  g/mol that has  $R_g = 21$  nm, for instance, Eq. 1.108 gives  $c^* = 0.013$  g/mL, and  $c^{**}$  is 0.2 to 0.3 g/mL.

We rely on  $R_g$  to define  $c^*$ . This provision allows us to apply the same definition to solutions of nonlinear polymers such as star polymer, a branched polymer, and a spherical polymer. As chains become more spherical,  $R_g$  decreases compared at the same molecular weight. Then, the overlap occurs at a higher concentration.

### 1.8.2 Concentration Regimes for Rodlike Molecules

The concentration regimes are different for rigid-chain polymers. Here we consider solutions of rodlike molecules (the contour length  $L \gg L_p$ ). A thin rodlike molecule of length  $L$  occupies a volume of  $L^3$  to allow tumbling of the molecule without colliding with other molecules. The overlap concentration  $c^*$  is then given by

$$c^* L^3 = \frac{M}{N_A} \quad (1.111)$$

The dilute solution, the solution at  $c^*$ , and the semidilute solution are illustrated in Figure 1.61. Compared with a linear flexible chain,  $c^*$  is much lower. Because

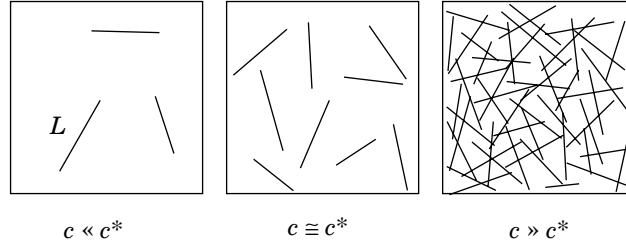


**Figure 1.61.** Concentration regimes for solutions of rodlike polymers: dilute solution,  $c \ll c^*$ ; solution at the overlap concentration  $c \cong c^*$ ; semidilute solution,  $c \gg c^*$ .

$L \sim M$ ,  $c^* \sim M^{-2}$ . As expected, the effect of neighboring polymer molecules is more evident in its motion, rather than it is in the thermodynamic properties.

At higher concentrations, the solution loses isotropy and turns into a nematic liquid crystal. In the nematic phase, the molecules are more or less aligned along one axis, but their centers are still randomly distributed.

### 1.8.3 PROBLEMS

**Problem 1.22:** How does  $c^*$  of a wormlike chain with  $L_p$  and  $L_c$  depend on the molecular weight  $M$ ?

**Solution 1.22:**

$$c^* \cong \frac{M}{N_A} R_g^{-3} = \frac{m_L}{N_A} R_g^{-3} L_c$$

where  $m_L = M/L_c$  is the molecular weight per length along the chain contour and therefore independent of  $M$ . When  $L_c \ll L_p$ ,  $R_g \cong L_c$ . Therefore,  $c^* \sim L_c/L_c^3 \sim L_c^{-2} \sim M^{-2}$ . When  $L_c \gg L_p$ ,  $R_g \cong (L_c L_p)^{1/2}$ . Therefore,  $c^* \sim L_c/(L_c L_p)^{3/2} \sim (L_p^3 L_c)^{-1/2} \sim M^{-1/2}$ .

**Problem 1.23:** The overlap concentration can also be defined for a solution of a polydisperse polymer. We impose the condition that the whole volume of the solution be filled with cubes of volume equal to (radius of gyration)<sup>3</sup> for each chain. Find the concentration  $c_i$  of component  $i$  at the chain overlap.

**Solution 1.23:** Let  $n_i$  chains of component  $i$  be present in the solution of volume  $V$ . At the chain overlap,

$$a \sum_i n_i R_{g,i}^3 = V$$

where  $a$  is a constant and  $R_{g,i}$  is the radius of gyration for component  $i$ . In the solution of a single component  $i$ , the condition is given by

$$an_i^* R_{g,i}^3 = V$$

where  $n_i^*$  is the number of chains at the overlap in the monodisperse solution. Thus,

$$\sum_i \frac{n_i}{n_i^*} = 1$$

which is identical to

$$\sum_i \frac{c_i}{c_i^*} = 1$$

where  $c_i^*$  is the overlap concentration for the solution of monodisperse polymer  $i$ , and  $c_i$  is the concentration of component  $i$  in the solution.

---

# 2

---

## Thermodynamics of Dilute Polymer Solutions

### 2.1 POLYMER SOLUTIONS AND THERMODYNAMICS

For a given polymer, there are solvents that dissolve the polymer well and solvents that do not dissolve the polymer. The former solvents are called “good solvents” and the latter “nonsolvents”. Table 2.1 lists a typical good solvent and a nonsolvent for polystyrene, poly(methyl methacrylate), and poly(ethylene glycol). *Polymer Handbook*<sup>11</sup> has a long list of solvents and nonsolvents for many polymers. The concentration of the polymer in the good solvent can be as high as 100%, yet the solution remains clear and uniform. Adding a nonsolvent to the solution causes the polymer to precipitate, if the nonsolvent mixes with the good solvent. A solvent with an intermediate quality dissolves the polymer to some extent.

Like low-molecular-weight solutes, a polymer dissolves in a solvent when solvation lowers the free energy. A good solvent lowers the free energy substantially. A nonsolvent increases the free energy.

Amorphous polymers (transparent in the solid state; to be precise, it is not a solid but rather a supercooled liquid) are usually easy to dissolve in the good solvent. In contrast, crystalline and semicrystalline polymers (opaque in the solid state) are sometimes not easy to dissolve. Within a crystallite, polymer chains are folded into a regular, thermodynamically stable arrangement. It is not easy to unfold the chain from the self-locked state into a disordered state in solution even if the latter state is thermodynamically more stable. Heating may help the dissolution because it facilitates the unfolding. Once dissolved, polymer chains take a random-coil conformation unless the chain is rigid.

**TABLE 2.1 Good Solvents and Nonsolvents for Some Polymers**

Polymer	Crystallinity	Good Solvent	Nonsolvent
Polystyrene	Amorphous	Toluene	Methanol
Poly(methyl methacrylate)	Amorphous	Tetrahydrofuran	Methanol
Poly(ethylene glycol)	Crystalline	Water (cold)	Ether

Thermodynamic properties of the polymer solution depend on how “good” the solvent is for the polymer as well as on the polymer itself. The interaction between the solvent and the polymer and the degree of polymerization dictate the properties, as we will see in the following sections of this chapter. We will examine the mean-field theory to understand the features of polymer solutions that are distinctly different from those of the other solutions. We will then examine static light scattering and size exclusion chromatography. These techniques belong to the most often used experimental methods to study dilute polymer solutions and to characterize the polymer in a state isolated from other polymer molecules. Our attention will be directed to understanding the measurement principles.

As we have learned in Section 1.8, there are a few concentration regimes in the polymer solution. Chapter 2 will primarily focus on the thermodynamics of dilute solutions, that is, below the overlap concentration, although we will also look at how the thermodynamics of the solution deviates from that of the ideal solution with an increasing concentration. Properties characteristic of nondilute solutions will be examined in detail in Chapter 4.

## 2.2 FLORY–HUGGINS MEAN-FIELD THEORY

### 2.2.1 Model

**2.2.1.1 Lattice Chain Model** Dissolution of a polymer into a solvent lowers the free energy of the polymer–solvent system when the enthalpy decreases by dissolution or, if it does not, when the product of the temperature and the entropy of mixing is greater than the enthalpy of mixing. Miscibility is much lower in polymer–solvent systems because adding solvent molecules to the polymer does not increase the entropy as much as it does to the low-molecular-weight solutes. Solvents that dissolve a given polymer are often limited to those that preferentially surround the polymer chain. We will learn in this section how small the entropy gain is in the polymer–solvent mixture. We will also learn what phenomena characteristic of polymer solutions are expected.

Miscibility of the polymer with a given solvent is well explained in the **mean-field theory**.<sup>3</sup> The theory is an extension of the lattice fluid theory originally developed to explain the miscibility of two low-molecular-weight liquids. Flory pioneered the application of the mean-field lattice fluid theory to polymer solutions. The simplest version of this **lattice chain theory** is generally referred to as



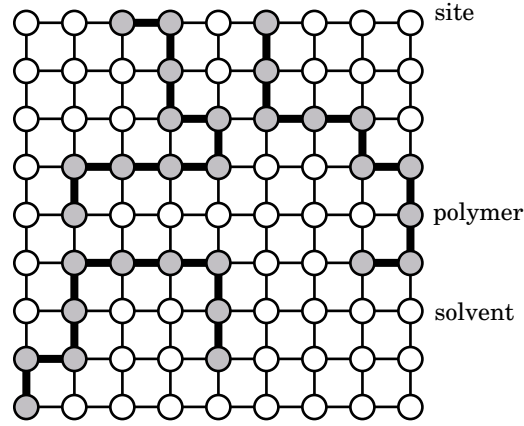


**Figure 2.1.** Lattice model for polymer solution. Gray sites are occupied by polymer chains, and white sites are occupied by solvent molecules.

**Flory–Huggins mean-field theory.** A similar mean-field theory successfully describes thermodynamics of polymer blends and, with some modifications, diblock copolymers and their blends with homopolymers.

The mean-field theory for the polymer solution compares the free energy of the polymer–solvent system before mixing and the free energy after mixing. We consider a simple situation: the polymer is a monodisperse homopolymer and is in an amorphous state or in a liquid state (melt) before mixing.

The Flory–Huggins theory uses the lattice model to arrange the polymer chains and solvents. We have looked at the lattice chain model in Section 1.4 for an excluded-volume chain. Figure 2.1 shows a two-dimensional version of the lattice model. The system consists of  $n_{\text{site}}$  sites. Each site can be occupied by either a monomer of the polymer or a solvent molecule (the monomer and the solvent molecule occupies the same volume). Double occupancy and vacancy are not allowed. A linear polymer chain occupies  $N$  sites on a string of  $N-1$  bonds. There is no preference in the direction the next bond takes when a polymer chain is laid onto the lattice sites (flexible). Polymer chains consisting of  $N$  monomers are laid onto empty sites one by one until there are a total  $n_p$  chains. Then, the unoccupied sites are filled with solvent molecules. The volume fraction  $\phi$  of the polymer is related to  $n_p$  by

$$n_p = n_{\text{site}}\phi/N \quad (2.1)$$

and the number of the solvent molecules  $n_s$  is given by

$$n_s = n_{\text{site}}(1 - \phi) \quad (2.2)$$

See Table 2.2 for summary.

**TABLE 2.2 Lattice Chain Model**

	Volume Fraction	Number of Molecules
Polymer	$\phi$	$n_P = n_{\text{site}}\phi/N$
Solvent	$1 - \phi$	$n_S = n_{\text{site}}(1 - \phi)$

Before mixing, the polymer occupies the volume of  $n_P N v_{\text{site}}$  and the solvent occupies the volume of  $n_S v_{\text{site}}$ , where  $v_{\text{site}}$  is the volume per site. The total volume  $n_{\text{site}} v_{\text{site}}$  does not change upon mixing (incompressible). Thus, the enthalpy of mixing  $\Delta H_{\text{mix}}$  in the constant-pressure process is equal to the change in the internal energy,  $\Delta U_{\text{mix}}$ , and the Gibbs free energy change  $\Delta G_{\text{mix}}$  is equal to the Helmholtz free energy change  $\Delta A_{\text{mix}}$ .

**2.2.1.2 Entropy of Mixing** Flory counted the number of possible arrangements of  $n_P$  chains on  $n_{\text{site}}$  sites and compared it with the number of arrangements on  $n_P N$  sites before mixing, that is, in the melt. Thus, he obtained the entropy of mixing  $\Delta S_{\text{mix}}$  per site as

$$-\Delta S_{\text{mix}}/(k_B n_{\text{site}}) = \frac{\phi}{N} \ln \phi + (1 - \phi) \ln(1 - \phi) \quad \text{Flory-Huggins} \quad (2.3)$$

This expression is similar to the entropy of mixing for two gaseous substances. The difference is that the volume fraction appears in the argument of logarithm, in place of the mole fraction. Note that the first term is divided by the chain length. The division by a large  $N$  makes  $\Delta S_{\text{mix}}$  small, especially at low concentrations ( $\phi \ll 1$ ; the second term is near zero) compared with  $\Delta S_{\text{mix}}$  for  $N = 1$  (mixture of two solvents). The division also makes  $\Delta S_{\text{mix}}$  asymmetric with respect to  $\phi = 1/2$ . As shown in Figure 2.2, longer chains decrease  $\Delta S_{\text{mix}}$  at low  $\phi$  and shift the maximum to the right. At  $N = 100$ , the plot is already close to the one for  $N = \infty$  in which the entropy of mixing is determined by solvent molecules only.

We can show that  $\Delta S_{\text{mix}}$  given by Eq. 2.3 is greater than the entropy of mixing for an ideal solution of  $n_P$  solute molecules and  $n_S$  solvent molecules (Problem 2.1). The difference is due to a greater number of conformations a polymer chain can take when the requirement that all the sites be occupied by the monomers is lifted.

**2.2.1.3  $\chi$  Parameter** The entropy of mixing is small for polymer-solvent systems, especially at low concentrations. Therefore, the change in the interactions upon mixing (= enthalpy of mixing) governs the miscibility. The interactions we are considering here are short-ranged ones only, typically van der Waals interactions (also known as dispersions), hydrogen-bonding, and dipole-dipole interactions.

The lattice fluid model considers interactions between nearest neighbors only. The interactions reside in the contacts. We denote by  $\epsilon_{SS}$ ,  $\epsilon_{PP}$ , and  $\epsilon_{PS}$  the interactions for a solvent-solvent (S-S) contact, a polymer-polymer (P-P) contact, and a polymer-solvent (P-S) contact, respectively. Mixing the solvent and polymer changes the overall interaction energy through rearrangement of contacts. Figure 2.3 illustrates the change in the two-dimensional rendering of the lattice.

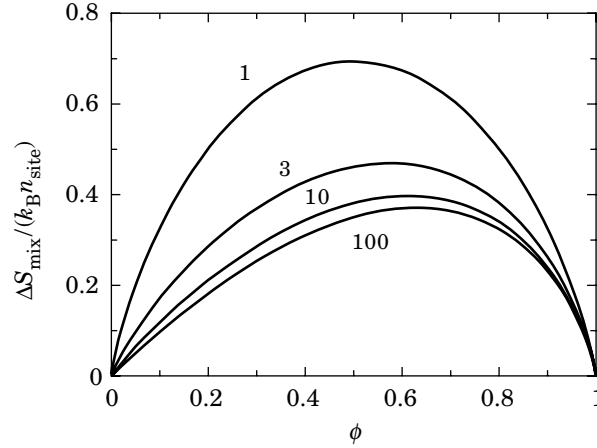


**Figure 2.2.** Entropy of mixing per site,  $\Delta S_{\text{mix}}/(k_B n_{\text{site}})$ , plotted as a function of polymer volume fraction  $\phi$ . The number adjacent to each curve denotes  $N$ .

Before mixing, there are four P–P contacts and four S–S contacts between a total of eight sites. Mixing replaces two P–P contacts and two S–S contacts with four P–S contacts. The interaction energy on these eight bonds changes from  $4\epsilon_{SS} + 4\epsilon_{PP}$  to  $4\epsilon_{PS} + 2\epsilon_{SS} + 2\epsilon_{PP}$ . The difference is  $4\epsilon_{PS} - 2(\epsilon_{SS} + \epsilon_{PP})$ . Per newly created P–S contact, the change is  $\epsilon_{PS} - (\epsilon_{SS} + \epsilon_{PP})/2$ . The  $\chi$  (**chi**) **parameter**, also called **Flory’s  $\chi$  parameter** or **Flory–Huggins  $\chi$  parameter**, is defined as the product of the lattice coordinate  $Z$  and the energy change reduced by  $k_B T$ :

$$\chi = Z[\epsilon_{PS} - (\epsilon_{PP} + \epsilon_{SS})/2]/k_B T \quad (2.4)$$

A positive  $\chi$  denotes that the polymer–solvent contacts are less favored compared with the polymer–polymer and solvent–solvent contacts (see Fig. 2.4). A negative  $\chi$  means that polymer–solvent contacts are preferred, promoting solvation of the polymer. In general,  $\chi$  decreases its magnitude with an increasing temperature because of  $k_B T$  in the denominator, but the pair interactions also depend on the temperature in a manner characteristic of each polymer–solvent system. In a hydrogen bonding pair, for instance,  $\chi$  usually changes from negative to positive with increasing temperature.

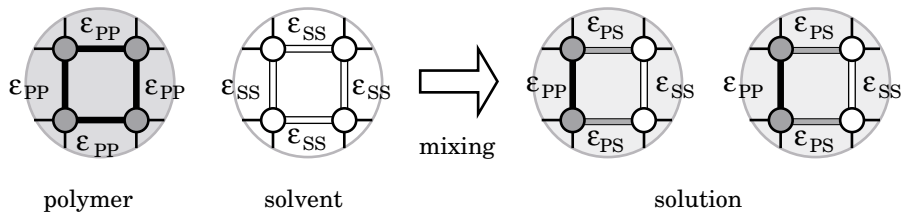


**Figure 2.3.** Change in the contacts between nearest neighbors when a polymer chain mixes with solvent molecules.

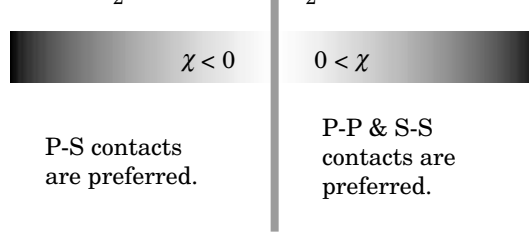


**Figure 2.4.** Negative  $\chi$  promotes mixing of polymer with the solvent, whereas positive  $\chi$  prefers polymer–polymer and solvent–solvent contacts to polymer–solvent contacts.

There are  $n_{\text{site}}$  sites, each with  $Z$  bonds. The product  $Zn_{\text{site}}$  is twice as large as the total number of bonds in the mixture because  $Zn_{\text{site}}$  counts each bond twice. Thus,  $Z/2$  is the number of bonds per site. In the two-dimensional square lattice, the number is 2. In the three-dimensional cubic lattice, it is 3.

**2.2.1.4 Interaction Change Upon Mixing** For a site occupied by a monomer, two of its  $Z$  neighbors are always adjacent monomers on the same chain, except for the chain ends. Other monomers on the same chain are also likely to occupy some of the other neighbors. The mean-field theory neglects this fact and calculates the change in the interaction,  $\Delta U_{\text{mix}}$ , by mixing  $Nn_{\text{P}} = n_{\text{site}}\phi$  unconnected monomers and  $n_{\text{S}} = n_{\text{site}}(1 - \phi)$  solvent molecules at random. The probability for a given bond to be a P–P contact is  $\phi^2$ , the probability for the S–S contact is  $(1 - \phi)^2$ , and the probability for the P–S contact is  $2\phi(1 - \phi)$ . Thus, the change  $\Delta U_{\text{mix}}$  in the internal energy is

$$\Delta U_{\text{mix}} = \frac{Zn_{\text{site}}}{2} [\varepsilon_{\text{PS}} - (\varepsilon_{\text{PP}} + \varepsilon_{\text{SS}})/2] \cdot 2\phi(1 - \phi) \quad (2.5)$$

The change per site is

$$\boxed{\Delta U_{\text{mix}}/(n_{\text{site}}k_{\text{B}}T) = \chi\phi(1 - \phi) \quad \text{Flory–Huggins}} \quad (2.6)$$

As shown in Figure 2.5,  $\Delta U_{\text{mix}}$  maximizes at  $\phi = 1/2$ . The sign of  $\Delta U_{\text{mix}}$  is the same as that of  $\chi$ .

$\Delta U_{\text{mix}}$  depends on the interaction through  $\chi$ . A system with the same  $\chi$  has the same  $\Delta U_{\text{mix}}$ . For instance, a mixture with  $\varepsilon_{\text{PP}} = \varepsilon_1$  and  $\varepsilon_{\text{PS}} = \varepsilon_{\text{SS}} = 0$  is thermodynamically equivalent to a mixture with  $\varepsilon_{\text{PP}} = \varepsilon_{\text{SS}} = 0$  and  $\varepsilon_{\text{PS}} = -\varepsilon_1/2$ .

Another way to arrive at Eq. 2.5 in the mean-field approximation is to tally all the contacts before and after the mixing. Table 2.3 lists the probability for a bond in the polymer–solvent system to be a P–P, P–S, or S–S contact before and after the mixing. The average contact energy is  $\phi\varepsilon_{\text{PP}} + (1 - \phi)\varepsilon_{\text{SS}}$  before the mixing. After the mixing, it changes to  $\phi^2\varepsilon_{\text{PP}} + 2\phi(1 - \phi)\varepsilon_{\text{PS}} + (1 - \phi)^2\varepsilon_{\text{SS}}$ . The difference is  $\phi(1 - \phi)(2\varepsilon_{\text{PS}} - \varepsilon_{\text{PP}} - \varepsilon_{\text{SS}})$ . For a total  $Zn_{\text{site}}/2$  bonds, we obtain Eq. 2.5.

**TABLE 2.3** Probability of Nearest-Neighbor Contacts

Contact	Energy	Probability Before Mixing	Probability After Mixing
P-P	$\varepsilon_{PP}$	$\phi$	$\phi^2$
P-S	$\varepsilon_{PS}$	0	$2\phi(1 - \phi)$
S-S	$\varepsilon_{SS}$	$1 - \phi$	$(1 - \phi)^2$

A solution with  $\chi = 0$  is called an **athermal solution**. There is no difference between the P-S contact energy and the average energy for the P-P and S-S contacts. In the athermal solution,  $\Delta U_{\text{mix}} = \Delta H_{\text{mix}} = 0$  regardless of  $\phi$ . We can regard that the polymer chain is dissolved in a sea of monomer molecules. Note however that, in an actual polymer-solvent system, the monomer before polymerization is chemically different from the repeating unit in the polymer. For instance, an oxyethylene repeating unit ( $-\text{CH}_2-\text{CH}_2-\text{O}-$ ) in poly(ethylene glycol) is different from ethylene oxide or ethylene glycol.

## 2.2.2 Free Energy, Chemical Potentials, and Osmotic Pressure

**2.2.2.1 General Formulas** From Eqs. 2.3 and 2.6, the Helmholtz free energy of mixing,  $\Delta A_{\text{mix}} = \Delta U_{\text{mix}} - T\Delta S_{\text{mix}}$ , per site is given as

$$\frac{\Delta A_{\text{mix}}}{n_{\text{site}}k_{\text{B}}T} = \frac{\phi}{N} \ln \phi + (1 - \phi) \ln(1 - \phi) + \chi \phi(1 - \phi) \quad \text{Flory-Huggins} \quad (2.7)$$

For a total  $n_{\text{site}}$  sites,

$$\Delta A_{\text{mix}}/(k_{\text{B}}T) = n_{\text{p}} \ln \phi + n_{\text{s}} \ln(1 - \phi) + \chi N n_{\text{p}}(1 - \phi) \quad (2.8)$$

or

$$\Delta A_{\text{mix}}/(k_{\text{B}}T) = n_{\text{p}} \ln \phi + n_{\text{s}} \ln(1 - \phi) + \chi n_{\text{s}} \phi \quad (2.9)$$

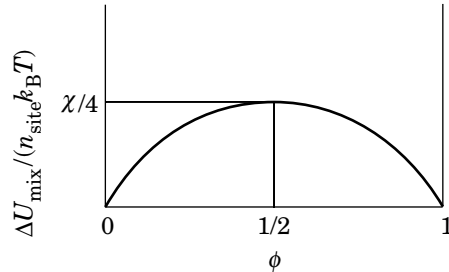


**Figure 2.5.** Change in the interaction by mixing,  $\Delta U_{\text{mix}}/(k_{\text{B}}T n_{\text{site}})$ , plotted as a function of polymer volume fraction  $\phi$ . The plot is shown for a positive  $\chi$ .

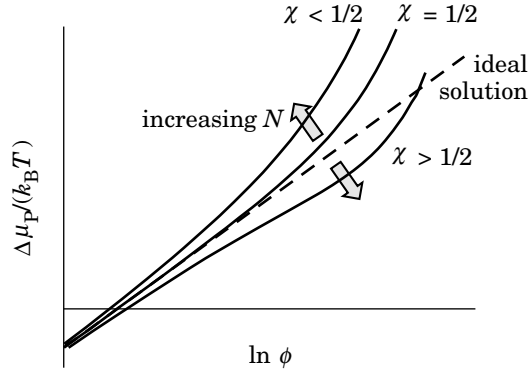


**Figure 2.6.** Chemical potential  $\Delta\mu_P$  of the polymer chain plotted as a function of  $\ln\phi$  for the ideal solution (dashed line) and for nonideal solutions of  $\chi > 1/2$ ,  $\chi = 1/2$ , and  $\chi < 1/2$ . An increase in  $N$  inflates the deviation of the solid lines from the dashed line.

The following identities are useful:

$$\begin{aligned} \left(\frac{\partial\phi}{\partial n_P}\right)_{n_S} &= -\frac{\partial}{\partial n_P}(1-\phi) = -\frac{\partial}{\partial n_P}\frac{n_S}{Nn_P+n_S} = \frac{Nn_S}{(Nn_P+n_S)^2} \\ &= \frac{1}{n_P}\phi(1-\phi) = \frac{N}{n_S}(1-\phi)^2 \end{aligned} \quad (2.10)$$

$$\begin{aligned} \left(\frac{\partial\phi}{\partial n_S}\right)_{n_P} &= \frac{\partial}{\partial n_S}\frac{Nn_P}{Nn_P+n_S} = -\frac{Nn_P}{(Nn_P+n_S)^2} = -\frac{\phi}{n_{\text{site}}} \\ &= -\frac{1}{n_S}\phi(1-\phi) = -\frac{1}{Nn_P}\phi^2 \end{aligned} \quad (2.11)$$

The chemical potential difference  $\Delta\mu_P$  of the polymer chain between the solution and the polymer melt is calculated from Eqs. 2.9 and 2.10 as

$$\frac{\Delta\mu_P}{k_B T} = \left(\frac{\partial}{\partial n_P}\frac{\Delta G_{\text{mix}}}{k_B T}\right)_{T,p,n_S} = \ln\phi - (N-1)(1-\phi) + \chi N(1-\phi)^2 \quad (2.12)$$

where  $\Delta G_{\text{mix}} = \Delta A_{\text{mix}}$  was used. Likewise, the chemical potential difference  $\Delta\mu_S$  of the solvent molecule between the solution and the pure solvent is calculated from Eqs. 2.8 and 2.11 as

$$\frac{\Delta\mu_S}{k_B T} = \left(\frac{\partial}{\partial n_S}\frac{\Delta G_{\text{mix}}}{k_B T}\right)_{T,p,n_P} = \ln(1-\phi) + \left(1 - \frac{1}{N}\right)\phi + \chi\phi^2 \quad (2.13)$$

Then, with Eq. 2.A.4 ( $v^* = v_{\text{site}}$  in the lattice chain model), the osmotic pressure  $\Pi$  is given as

$$\boxed{\frac{\Pi v_{\text{site}}}{k_B T} = \frac{\Pi V}{n_{\text{site}} k_B T} = \frac{\phi}{N} - \ln(1-\phi) - \phi - \chi\phi^2 \quad \text{Flory-Huggins}} \quad (2.14)$$

where  $V = v_{\text{site}} n_{\text{site}}$  is the volume of the solution. **Membrane osmometry** and **vapor pressure osmometry** measure the osmotic pressure (Appendix 2.A).

**2.2.2.2 Chemical Potential of a Polymer Chain in Solution** When  $N \gg 1$ , Eq. 2.12 is rearranged to

$$\Delta\mu_p/(k_B T) = \ln \phi + N[\chi - 1 + (1 - 2\chi)\phi + \chi\phi^2] \quad \text{Flory–Huggins} \quad (2.15)$$

The first term is the chemical potential of the ideal solution.  $N(\chi - 1)$  is just a constant and therefore irrelevant to the further discussion.  $N[(1 - 2\chi)\phi + \chi\phi^2]$  represents the nonideal part. Figure 2.6 illustrates how  $\Delta\mu_p$  changes with  $\phi$ . At low concentrations,  $\Delta\mu_p/k_B T \cong \ln \phi$ , and the solution is nearly ideal. As  $\phi$  increases, the nonideal term increases its magnitude. The shape of the plot depends primarily on whether  $\chi < 1/2$ . When  $\chi < 1/2$  on the one hand, the nonideal terms are positive and the plot deviates upward compared with the ideal solution. When  $\chi > 1/2$  on the other hand, the leading term in the nonideal part is negative and therefore the plot deviates downward. At higher concentrations, the positive second-order term lets the plot eventually cross the line for the ideal solution. The nonideality minimizes at  $\chi = 1/2$ .

The deviation from the ideal solution is magnified by  $N$ . A small difference of  $\chi$  from  $1/2$  shows up as a large nonideality when  $N$  is large. Thus the polymer solutions, especially those of high-molecular-weight polymers, can be easily nonideal. When  $\chi > 1/2$ , in particular,  $N(1 - 2\chi)$  can be easily as large as to cause a dip in the plot of  $\Delta\mu_p$ .

Equations 2.7, 2.14, and 2.15 serve as a starting point for further discussion of thermodynamics of the polymer solution in the lattice fluid model. Another approach to the thermodynamics based on these equations is given in Appendix 2.B.

The Flory–Huggins theory neglects the chain connectivity, the chain rigidity, and the shape of the monomer. Modifications to the Flory–Huggins theory are possible by taking into account these effects.<sup>12,13</sup> The chain rigidity can be incorporated by giving preference to straight bonds over angled ones, for instance.

## 2.2.3 Dilute Solutions

**2.2.3.1 Mean-Field Theory** In this subsection, we consider dilute solutions. When  $\phi \ll 1$ ,  $\ln(1 - \phi) = -\phi - (1/2)\phi^2 - (1/3)\phi^3 - \dots$ . Then, Eq. 2.14 is rewritten to

$$\frac{\Pi V}{n_{\text{site}} k_B T} = \frac{\phi}{N} + \left(\frac{1}{2} - \chi\right)\phi^2 + \frac{1}{3}\phi^3 + \dots \quad \text{Flory–Huggins, dilute solution} \quad (2.16)$$

In the low concentration limit, Eq. 2.16 gives the osmotic pressure  $\Pi_{\text{ideal}}$  of the ideal solution:

$$\Pi_{\text{ideal}} = \frac{n_{\text{site}}\phi}{NV} k_B T \quad (2.17)$$

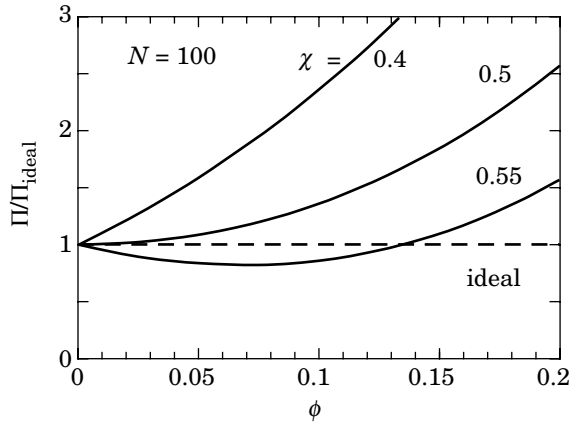


**Figure 2.7.** Osmotic compressibility ( $\Pi/\Pi_{\text{ideal}}$ ) plotted as a function of  $\phi$  for the ideal solution (dashed line) and nonideal solutions with  $N = 100$  and  $\chi = 0.4, 0.5,$  and  $0.55$  (solid lines).

Thus the ratio of  $\Pi$  to  $\Pi_{\text{ideal}}$  compared at the same concentration is

$$\frac{\Pi}{\Pi_{\text{ideal}}} = 1 + N \left[ \left( \frac{1}{2} - \chi \right) \phi + \frac{1}{3} \phi^2 + \dots \right] \quad (2.18)$$

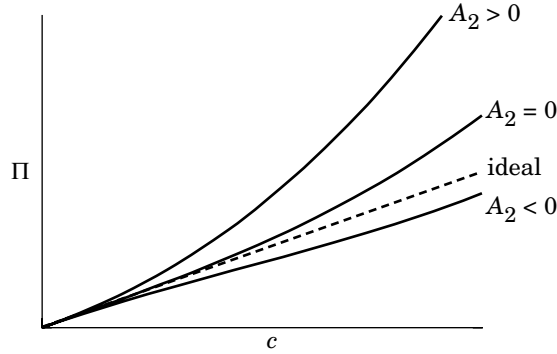
The ratio is often called the **(osmotic) compressibility**.

Figure 2.7 shows  $\Pi/\Pi_{\text{ideal}}$  as a function of  $\phi$ . Three curves with  $\chi = 0.4, 0.5,$  and  $0.55$  are plotted for chains of  $N = 100$ . The upward or downward deviation of  $\Pi$  from  $\Pi_{\text{ideal}}$  depends on whether  $\chi < 1/2$ . When  $\chi = 1/2$ , the solution is close to ideal. A small enthalpic penalty ( $\chi = 1/2 > 0$ ; P-S contacts are disfavored) of mixing is compensated by the entropy of mixing, which gives rise to the coefficient  $1/2$  in the linear term of Eq. 2.18. When  $\chi > 1/2$ , the entropy of mixing is not sufficient to offset the increase in the interaction due to unfavorable polymer-solvent contacts. Then, the polymer-polymer contacts are promoted, effectively lowering the osmotic pressure. At higher concentrations, the positive  $(N/3)\phi^2$  drives  $\Pi$  above  $\Pi_{\text{ideal}}$ . When  $\chi < 1/2$ , in contrast, the entropy dominates, and  $\Pi > \Pi_{\text{ideal}}$  in the entire range of  $\phi$  (Problem 2.6). As  $\chi$  decreases and turns negative, the polymer-solvent contacts are favored also in terms of the interaction. Then,  $\Pi$  is even greater. It is apparent in Eq. 2.18 that the deviation from  $\Pi_{\text{ideal}}$  is magnified by  $N$ . The nonideality is large in polymer solutions.

**2.2.3.2 Virial Expansion** To compare the theory with experiments,  $\Pi$  needs to be expressed in terms of mass concentration  $c$ , typically in g/L or mg/L. Using the identity

$$c = \frac{M}{N_A N} \frac{\phi}{v_{\text{site}}} \quad (2.19)$$





**Figure 2.8.** Osmotic pressure  $\Pi$  plotted as a function of polymer concentration  $c$  for the ideal solution (dashed line) and nonideal solutions with  $A_2 > 0$ ,  $= 0$ , and  $< 0$  (solid lines).

where  $M/(N_A N)$  is the mass of the monomer (not molar mass),  $\Pi/(N_A k_B T)$  is, in general, expanded in a power series of  $c$ :

$$\boxed{\frac{\Pi}{N_A k_B T} = \frac{c}{M} + A_2 c^2 + A_3 c^3 + \cdots \quad \text{virial expansion}} \quad (2.20)$$

In this **virial expansion**,  $A_2$  is the (osmotic) **second virial coefficient**, and  $A_3$  is the **third virial coefficient**. A positive  $A_2$  deviates  $\Pi$  upward compared with that of the ideal solution ( $\Pi_{\text{ideal}}/(N_A k_B T) = c/M$ ). When  $A_2 = 0$ , the solution is close to the ideal solution in a wide range of concentrations. Figure 2.8 illustrates how  $\Pi$  deviates from that of the ideal solution, depending on the sign of  $A_2$ . The meanings of  $A_2$  and  $A_3$  will become clearer when we express them in the lattice model by comparing Eqs. 2.18 and 2.20:

$$\boxed{A_2 = \left(\frac{1}{2} - \chi\right) N_A v_{\text{site}} (N/M)^2} \quad (2.21)$$

$$A_3 = \frac{1}{3} (N_A v_{\text{site}})^2 (N/M)^3 \quad (2.22)$$

Table 2.4 summarizes the relationship between  $A_2$  and  $\chi$ .  $A_2$  is a measure of the nonideality of the solution.  $A_2 = 0$  when the entropy of mixing compensates repulsive polymer–solvent interactions or attractive polymer–polymer interactions.

As seen in the expansion of  $\Pi/(N_A k_B T) = (c/M)[1 + A_2 M c + A_3 M c^2 + \cdots]$ , the magnitude of  $A_2 M c$  tells how much thermodynamics of the solution deviates from that of the ideal solution. A solution with a greater  $A_2 M$  will develop a

**TABLE 2.4 Relationship Between  $A_2$  and  $\chi$**

$A_2$	$\Pi$	$\chi$
+	$> \Pi_{\text{ideal}}$	$< 1/2$
0	$\cong \Pi_{\text{ideal}}$	$= 1/2$
–	$< \Pi_{\text{ideal}}$	$> 1/2$

nonideality at a lower mass concentration. Separately in Section 1.8, we defined the overlap concentration  $c^*$ . We expect that  $c/c^*$  gives another measure of the nonideality. It is then natural to expect

$$A_2M \cong \frac{1}{c^*} \quad (2.23)$$

This equality applies to a sufficiently good solvent only in which  $A_2M$  dominates over the third term. Because  $c^* \cong (M/N_A)/R_g^3$  (Eq. 1.108) and  $R_g \cong b(M/M_b)^{\nu}$  with  $M_b$  being the molecular weight of the segment,  $c^* \cong M_b^{3\nu}/(N_A b^3 M^{3\nu-1})$ . With Eq. 2.23, we obtain

$$A_2 \cong \frac{N_A b^3 M^{3\nu-2}}{M_b^{3\nu}} \propto M^{3\nu-2} \quad (2.24)$$

The exponent on  $M$  is  $-1/5$  or  $-0.23$ . We thus find that  $A_2$  decreases with  $M$ , but its dependence is weak. This dependence was verified in experiments.<sup>14</sup>

Likewise the virial expansion of  $\Pi/\Pi_{\text{ideal}}$  in terms of  $\phi$  allows us to find the overlap volume fraction  $\phi^*$  as  $\phi^* \cong [N(1/2 - \chi)]^{-1}$ . This result is, however, wrong. We know that  $\phi^*$  should rather be  $\sim N^{-4/5}$  or  $\sim N^{-0.77}$  for real chains in a good solvent. Here, we see a shortcoming of the mean-field theory.

## 2.2.4 Coexistence Curve and Stability

**2.2.4.1 Replacement Chemical Potential** As  $\chi$  exceeds  $1/2$  and increases further,  $A_2$  becomes negative and its absolute value increases. The unfavorable polymer-solvent interaction can be sufficiently strong to cause the solution to separate into two phases. We will examine the phase diagram of the solution in the mean-field theory for a system of a fixed volume.

In the lattice model, we cannot change  $n_p$  and  $n_s$  independently. A polymer chain, when added to the system, replaces  $N$  solvent molecules, thereby holding the total volume unchanged. It is convenient to introduce a replacement chemical potential  $\Delta\mu_{\text{rep}} \equiv \Delta\mu_p - N\Delta\mu_s$ . It is the change in the free energy of the solution when the polymer increases its concentration by removing  $N$  solvent molecules and placing a polymer chain. From Eqs. 2.12 and 2.13,  $\Delta\mu_{\text{rep}}$  is expressed as

$$\frac{\Delta\mu_{\text{rep}}}{k_B T} = \ln\phi + 1 - N - N\ln(1 - \phi) + \chi N(1 - 2\phi) \quad (2.25)$$

This  $\Delta\mu_{\text{rep}}$  is also calculated directly from  $\Delta A_{\text{mix}}$  (Eq. 2.7) using

$$\frac{\Delta\mu_{\text{rep}}}{k_B T} = \left( \frac{\partial}{\partial n_p} \frac{\Delta A_{\text{mix}}}{k_B T} \right)_{T,V} = \frac{N}{n_{\text{site}}} \frac{\partial}{\partial \phi} \frac{\Delta A_{\text{mix}}}{k_B T} \quad (2.26)$$

because an increase in  $n_p$  (increase in  $\phi$ ) implies a decrease in  $n_s$  at constant  $V$ .

The plot of  $\Delta\mu_{\text{rep}}/(k_B T)$  is shown in Figure 2.9 for  $N = 100$ . The three lines are for  $\chi = 0.595$ ,  $0.605$ , and  $0.615$ . When the plot has a dip as for  $\chi = 0.615$ , the solution can be unstable. In the range of  $\phi$  where the tangent to the plot of  $\Delta\mu_{\text{rep}}$  has

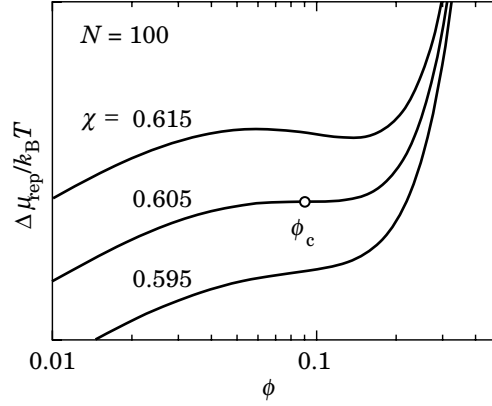


**Figure 2.9.** Replacement chemical potential  $\Delta\mu_{\text{rep}}/(k_B T)$ , plotted as a function of  $\phi$  for  $N = 100$  and  $\chi = 0.595, 0.605,$  and  $0.615$ . At  $\chi = 0.595$ , the plot is an increasing function of  $\phi$ . At  $\chi = \chi_c = 0.605$ , the plot has a stagnant point at  $\phi = \phi_c$ . At  $\chi = 0.615$ , the tangent to the plot is negative in  $0.060 < \phi < 0.135$ .

a negative slope, the solution is unstable; As a polymer chain is brought into the system, its chemical potential drops, thereby promoting further influx of the polymer. This situation is not physical, and, therefore, a negative slope in  $\Delta\mu_{\text{rep}}$  indicates instability. In Figure 2.10, the system is stable in the range of a positive slope ( $\phi < \phi_A$  or  $\phi_B < \phi$  in the figure) and unstable in the other range ( $\phi_A < \phi < \phi_B$ ).

**2.2.4.2 Critical Point and Spinodal Line** The boundaries to the instability,  $\phi_A$  and  $\phi_B$ , can be found from  $\partial\Delta\mu_{\text{rep}}/\partial\phi = 0$ . They are the two roots of the quadratic equation in the lattice model:

$$\frac{1}{\phi} + \frac{N}{1-\phi} = 2\chi N \quad (2.27)$$

The instability condition is given as

$$\frac{1}{\phi} + \frac{N}{1-\phi} < 2\chi N \quad (2.28)$$

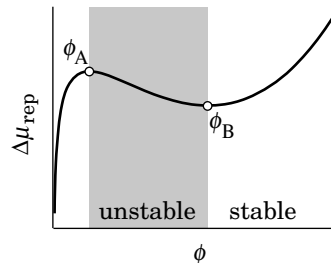


**Figure 2.10.** The solution is unstable between  $\phi_A$  and  $\phi_B$ , where  $\Delta\mu_{\text{rep}}$  decreases on increasing  $\phi$ .

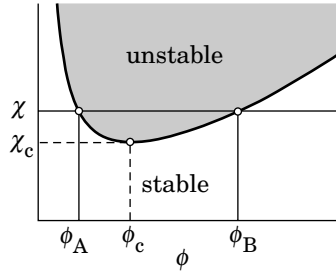


**Figure 2.11.** Plot of  $\chi$  at  $\partial\Delta\mu_{\text{rep}}/\partial\phi = 0$  as a function of  $\phi$ . The curve minimizes to  $\chi_c$  at  $\phi_c$ . When  $\chi > \chi_c$ , the derivative is zero at  $\phi_A$  and  $\phi_B$ . The solution is unstable in the shaded region above the curve and stable in the other region.

The same condition can be obtained from the stability of an open system that allows  $n_p$  and  $n_s$  to change independently (Problem 2.10).

We can regard Eq. 2.27 as expressing  $\chi$  at the stability–instability boundary as a function of  $\phi$ . The dependence is indicated by a curve in Figure 2.11. The curve is asymmetric because  $N \gg 1$ . The unstable region (Inequality 2.28) is indicated by the shaded area. The curve that separates the stable region from the unstable region minimizes to  $\chi_c$  at  $\phi = \phi_c$ . This point is called the **critical point**. When  $\chi > \chi_c$ , Eq. 2.27 has two roots,  $\phi_A$  and  $\phi_B$ , given as the intersections of the curve with the horizontal line at  $\chi$ , and the plot of  $\Delta\mu_{\text{rep}}(\phi)$  has a dip, as seen in the curve of  $\chi = 0.615$  in Figure 2.9. When  $\chi = \chi_c$ , there is only one root:  $\phi = \phi_c$ . The horizontal is tangential to the curve at  $\phi = \phi_c$ . The plot of  $\Delta\mu_{\text{rep}}(\phi)$  has a stagnant point at  $\phi = \phi_c$  indicated by a circle on the curve of  $\chi = 0.605$  in Figure 2.9 and has a positive slope everywhere else. When  $\chi < \chi_c$ , Eq. 2.27 does not have real roots, and  $\Delta\mu_{\text{rep}}$  is an increasing function of  $\phi$  in the entire range, as for the curve of  $\chi = 0.595$  in Figure 2.9. The solution is stable in the whole range of  $\phi$ . The line that separates the stable region from the unstable region is called the **spinodal line**. It is represented by Eq. 2.27. Table 2.5 summarizes the behavior of  $\Delta\mu_{\text{rep}}(\phi)$  and stability of the solution.

**2.2.4.3 Phase Separation** When  $\chi > \chi_c$  and  $\phi_A < \phi < \phi_B$ , the instability separates the solution spontaneously into two phases with different polymer volume fractions  $\phi_1$  and  $\phi_2$  ( $\phi_1 < \phi_2$ ). The latter are determined from the condition that  $\Delta\mu_p$  and  $\Delta\mu_s$  be the same between the two phases. Both the polymer chain and the solvent molecule are free to leave one of the phases and enter the other phase (dynamic equilibrium). Figure 2.12 shows  $\Delta\mu_{\text{rep}}$ ,  $\Delta\mu_p$ , and  $\Delta\mu_s$  on a common  $\phi$  axis. As proved in Problem 2.10, the region of the negative slope in  $\Delta\mu_p$  and the region of the positive slope in  $\Delta\mu_s$  (i.e.,  $(\partial\Delta\mu_s/\partial n_s)_{n_p} < 0$ ) coincide. Because

**TABLE 2.5**  $\chi$  parameter and stability

$\chi$	$\Delta\mu_{\text{rep}}(\phi)$	Stable	Unstable
$\chi < \chi_c$	always increasing	everywhere	—
$\chi = \chi_c$	stagnant at $\phi = \phi_c$	$\phi \neq \phi_c$	$\phi = \phi_c$
$\chi > \chi_c$	having a dip	$\phi < \phi_A, \phi_B < \phi$	$\phi_A < \phi < \phi_B$

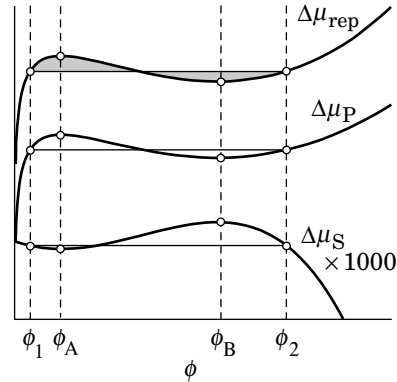


**Figure 2.12.** Plot of  $\Delta\mu_{\text{rep}}$ ,  $\Delta\mu_{\text{p}}$ , and  $\Delta\mu_{\text{s}} \times 1000$ , vertically displaced for easy comparison, when  $\Delta\mu_{\text{rep}}$  has a dip. The three curves share  $\phi_{\text{A}}$  and  $\phi_{\text{B}}$ , which give the local maximum and local minimum of each curve. The two parts in the shaded area have an equal area. The chemical potential is equal between  $\phi_1$  and  $\phi_2$  for each of  $\Delta\mu_{\text{rep}}$ ,  $\Delta\mu_{\text{p}}$ , and  $\Delta\mu_{\text{s}}$ .

$\Delta\mu_{\text{p}}(\phi_1) = \Delta\mu_{\text{p}}(\phi_2)$  and  $\Delta\mu_{\text{s}}(\phi_1) = \Delta\mu_{\text{s}}(\phi_2)$ , the two phases have the same  $\Delta\mu_{\text{rep}}$ . At  $\phi_1$  and  $\phi_2$ , replacing  $N$  solvent molecules with a polymer chain or the other way around does not change the overall free energy. It can be shown that the average of  $\Delta\mu_{\text{rep}}(\phi)$  for  $\phi$  between  $\phi_1$  and  $\phi_2$  is equal to  $\Delta\mu_{\text{rep}}(\phi_1) = \Delta\mu_{\text{rep}}(\phi_2)$  (Problem 2.11). Therefore, the two shaded parts in Figure 2.12 have an equal area. This situation is the same as the constant-pressure line for the vapor-liquid coexistence in the isothermal process of a single-component system (Maxwell construction). We can find  $\phi_1$  and  $\phi_2$  from this equality of the areas. It is, however, easier to find  $\phi_1$  and  $\phi_2$  from  $\Delta\mu_{\text{p}}(\phi_1) = \Delta\mu_{\text{p}}(\phi_2)$  and  $\Delta\mu_{\text{s}}(\phi_1) = \Delta\mu_{\text{s}}(\phi_2)$ , although solving these two equations simultaneously requires numerical computation.

When  $\chi > \chi_{\text{c}}$  and  $\phi$  is either between  $\phi_1$  and  $\phi_{\text{A}}$  or between  $\phi_{\text{B}}$  and  $\phi_2$ , the solution is still stable ( $\partial\Delta\mu_{\text{rep}}/\partial\phi > 0$ ). The chemical potential of either the polymer chain or the solvent molecule is, however, higher than the counterpart at  $\phi_1$  and  $\phi_2$ : In  $\phi_1 < \phi < \phi_{\text{A}}$ ,  $\Delta\mu_{\text{p}}(\phi) > \Delta\mu_{\text{p}}(\phi_1) = \Delta\mu_{\text{p}}(\phi_2)$ , as seen in Figure 2.12. The polymer chain is ready to move into one of the two phases with  $\phi_1$  and  $\phi_2$ , if they exist, to lower its chemical potential. In  $\phi_{\text{B}} < \phi < \phi_2$ ,  $\Delta\mu_{\text{s}}(\phi) > \Delta\mu_{\text{s}}(\phi_1) = \Delta\mu_{\text{s}}(\phi_2)$ . The solvent molecule is ready to move into one of the two phases. The solution will separate into two phases with  $\phi_1$  and  $\phi_2$  if the separation lowers the overall free energy of the system.

Now we examine whether the free energy decreases by the phase separation. For this purpose, we plot in Figure 2.13 the free energy  $\Delta G_{\text{mix}}$  given by Eq. 2.7 with  $\Delta G_{\text{mix}} = \Delta A_{\text{mix}}$  as a function of  $\phi$ . We compare  $\Delta G_{\text{mix}}$  for the single-phase solution at  $\phi$  and a two-phase solution with  $\phi_1$  and  $\phi_2$ . Equation 2.26 tells that the slope of the curve is essentially  $\Delta\mu_{\text{rep}}$ . Together with the result of Problem 2.11, we find that the curve has a cotangent line at  $\phi_1$  and  $\phi_2$  (Problem 2.12). The inflexion points of the curve are at  $\phi_{\text{A}}$  and  $\phi_{\text{B}}$  where  $\partial\Delta\mu_{\text{rep}}/\partial\phi = 0$  or  $\partial^2\Delta G_{\text{mix}}/\partial\phi^2 = 0$ . Between  $\phi_1$  and  $\phi_2$ , the curve is located higher than the cotangent line.

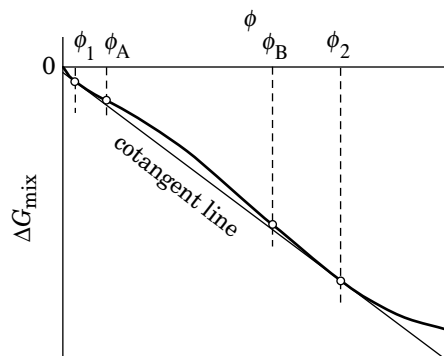


**Figure 2.13.** Free energy of mixing  $\Delta G_{\text{mix}}$ , plotted as a function of  $\phi$  when  $\Delta\mu_{\text{rep}}$  has a dip. The difference between  $\Delta G_{\text{mix}}$  and the cotangent at  $\phi_1$  and  $\phi_2$  is magnified.

In the two-phase solution, the volumes  $V_1$  and  $V_2$  of the two phases are determined by the distance of  $\phi$  to  $\phi_1$  and  $\phi_2$  (lever rule):

$$\frac{V_1}{V_2} = \frac{\phi_2 - \phi}{\phi - \phi_1} \quad (2.29)$$

When  $\phi = \phi_2$ ,  $V_1$  is zero and the whole solution is in phase 2; When  $\phi = \phi_1$ ,  $V_2 = 0$ . Adding the polymer to a single-phase solution of  $\phi_1$  creates a new phase with  $\phi_2$ . The lever rule requires that the two-phase solution with  $\phi$  in the range of  $\phi_1 < \phi < \phi_2$  have  $\Delta G_{\text{mix}}$  on the cotangent line in Figure 2.13 (Problem 2.13). Therefore, the solution in that range, even if it is in the stable region of  $\phi$ , can lower the total free energy by separating into two phases.

The phase separation in the stable region does not occur spontaneously, however. Therefore, we say that the solution with  $\phi_1 < \phi < \phi_A$  or  $\phi_B < \phi < \phi_2$  is **metastable**. The separation requires an external perturbation, such as stirring or the presence of dust particles. Fortunately, these perturbations are usually present in the solution. Therefore, a solution in the range of  $\phi_1 < \phi < \phi_2$  separates into two phases spontaneously or not, as illustrated in Figure 2.14. Many domains in the two-phase solution coalesce into two macroscopic domains.

**2.2.4.4 Phase Diagram** Figure 2.15 shows the curve for  $\phi_1$  and  $\phi_2$  and the curve for  $\phi_A$  and  $\phi_B$ . The figure is essentially the **phase diagram** of the solution in

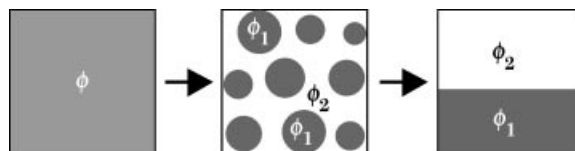


**Figure 2.14.** Polymer solution with  $\phi$  between  $\phi_1$  and  $\phi_2$  separates into two phases with  $\phi_1$  and  $\phi_2$ . The multiple domains coalesce into two macroscopic phases.

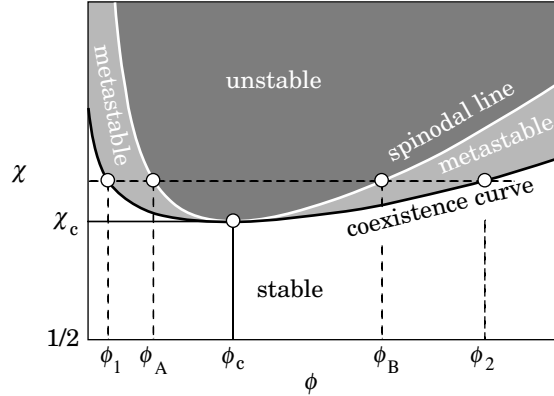


**Figure 2.15.** Spinodal line and the coexistence curve in the mean-field theory. The solution is unstable in the darkly shaded region, metastable in lightly shaded region, and stable in the other region.

the Flory–Huggins mean–field theory. The two curves share the apex at  $\phi_c$  and  $\chi_c$ . The lower curve for  $\phi_1$  and  $\phi_2$  demarcates the **single-phase regime** from the **two-phase regime** and therefore is called the **coexistence curve** (or a **binodal line**). The upper curve (spinodal line) is for  $\phi_A$  and  $\phi_B$ . Above the spinodal line, the system is unstable and spontaneously separates into two phases. Above the coexistence curve, the phase-separated state is thermodynamically more stable than the single-phase state is. Solutions in the two regions between the two curves are metastable.

A solution with  $\chi < \chi_c$  is in a single phase in the entire range of concentrations. When  $\chi > \chi_c$ , the solution has a **miscibility gap**. Usually we cannot prepare a single-phase solution with  $\phi$  between  $\phi_1$  and  $\phi_2$ . The phase with  $\phi_1$  is a solution saturated with the polymer (the concentration of polymer cannot be higher), and the phase with  $\phi_2$  is a solution saturated with the solvent (the concentration of solvent cannot be higher).

Now we look at how  $\chi_c$  and  $\phi_c$  change with  $N$ . From Eq. 2.27 and  $\partial\chi/\partial\phi = 0$ , we obtain

$$\chi_c = \frac{(1 + N^{1/2})^2}{2N} \cong \frac{1}{2} + N^{-1/2} \quad (2.30)$$

at

$$\phi_c = \frac{1}{1 + N^{1/2}} \cong N^{-1/2} \quad (2.31)$$

Figure 2.16 shows how  $\chi_c$  approaches  $1/2$  with an increasing  $N$  and how  $\phi_c$  approaches zero. Both of them decrease in  $N^{-1/2}$ .

Solid lines in Figure 2.17a are the spinodal lines for  $N = 32, 100, 316,$  and  $1,000$ . The critical point on each spinodal line is on the curve given by  $\chi_c = 1/[2(1 - \phi_c)^2]$

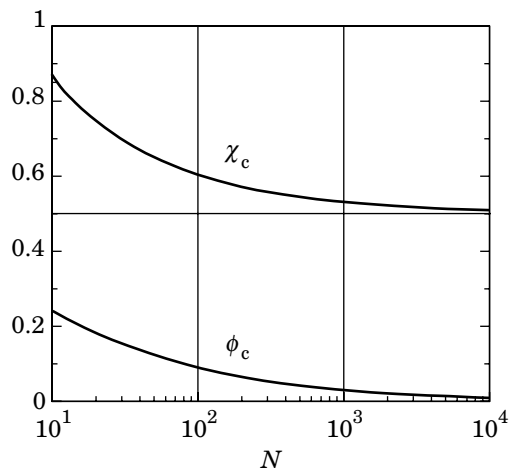


**Figure 2.16.** As  $N$  increases,  $\chi_c$  approaches  $1/2$ , and  $\phi_c$  decreases to zero.

(dashed line). As  $N$  increases, the spinodal line approaches the ordinate and the horizontal at  $\chi = 1/2$ . Figure 2.17b shows corresponding coexistence curves. Both the spinodal lines and the coexistence curves are skewed toward  $\phi_c \ll 1$  because  $N \gg 1$ . For  $N = 1$  (mixture of two small-molecule liquids),  $\phi_c = 1/2$  and  $\chi_c = 2$ . The spinodal line and the coexistence curve are symmetric with respect to  $\phi_c = 1/2$ .

The **theta condition** refers to the critical condition in the long-chain limit,  $N \rightarrow \infty$ . A solvent that gives the theta condition to a given polymer is called a **theta solvent**. In the mean-field theory, a solvent that provides the polymer with  $\chi = 1/2$  is the theta solvent. In general, theta condition is determined from  $A_2 = 0$  (see

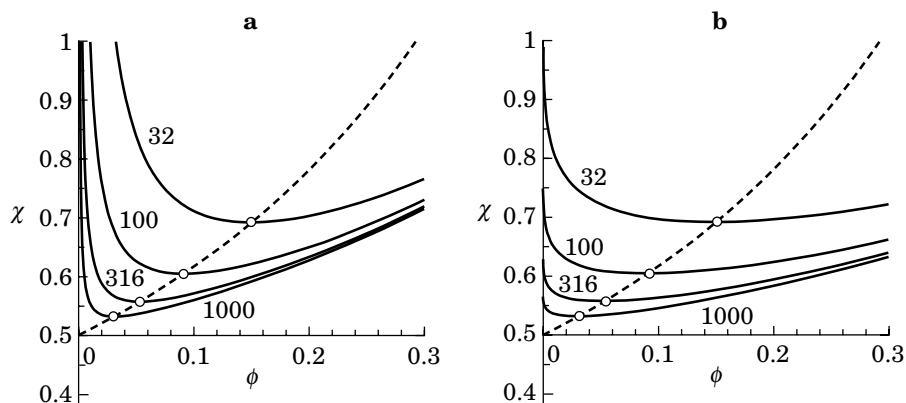


**Figure 2.17.** Spinodal lines (a) and coexistence curves (b) for  $N = 32, 100, 316,$  and  $1,000$ . The open circles indicate the critical point for each  $N$ . It approaches  $\chi = 1/2$  and  $\phi = 0$  along the dashed line as  $N$  increases.



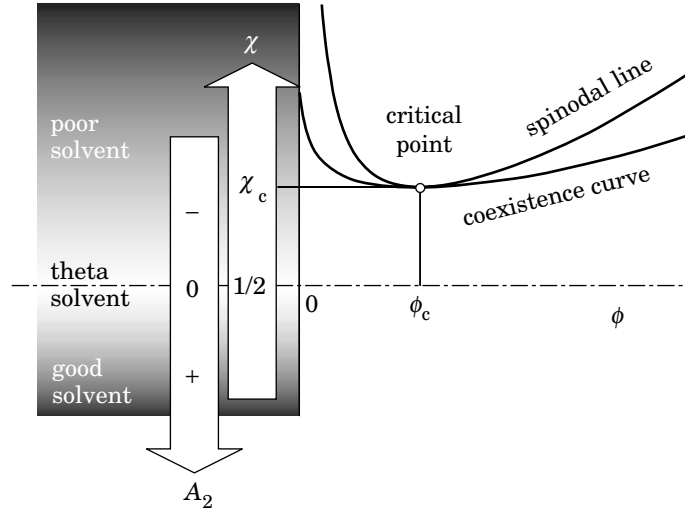


**Figure 2.18.** Good solvent ( $A_2 > 0$ ,  $\chi < 1/2$ ), theta solvent ( $A_2 = 0$ ,  $\chi = 1/2$ ), and poor solvent ( $A_2 < 0$ ,  $\chi > 1/2$ ).

Eq. 2.21). When it has a molecular weight dependence, its high molecular weight limit gives the theta condition. In the mean-field theory, the condition is independent of the molecular weight.

A solvent with  $\chi$  sufficiently smaller than  $1/2$  ( $A_2$  is positive and sufficiently large), including negative  $\chi$ , is called a **good solvent**. A solvent with  $\chi > 1/2$  ( $A_2 < 0$ ) is called a **poor solvent**. As  $\chi$  increases, the solvent becomes unable to dissolve the polymer. Then, it is called a **nonsolvent**. Figure 2.18 illustrates the ranges of these solvents together with the phase diagram. Along the horizontal line of  $\chi = 1/2$ ,  $A_2 = 0$ . Note that, in the theta solvent, polymer chains with a finite length (all polymers have a finite length) are still dissolved in the solvent in the entire range of concentrations. For a polymer solution to separate into two phases,  $A_2$  has to be sufficiently negative, especially when its molecular weight is low.

### 2.2.5 Polydisperse Polymer

Almost all the polymer is polydisperse. We consider here the osmotic pressure of the solution of a polydisperse polymer.

Before mixing the polymer with the solvent, the polymer is already a mixture consisting of  $n_i$  chains of  $N_i$  beads for component  $i$ . This mixture is further mixed with  $n_s$  solvent molecules. The entropy of mixing of the polydisperse polymer with  $n_s$  solvent molecules is obtained as

$$-\Delta S_{\text{mix}}/(k_B n_{\text{site}}) = \sum_i \frac{\phi_i}{N_i} \ln \phi_i + (1 - \phi) \ln(1 - \phi) \quad (2.32)$$

where  $\phi_i = n_i N_i / n_{\text{site}}$ ,  $\phi = \sum_i \phi_i$  (the sum is with respect to  $i$ ), and  $n_{\text{site}} = n_s + \sum_i (n_i N_i)$ . The energy of mixing is the same; we can naturally assume that P–P interactions are the same between chains of different lengths. Then, the free energy of mixing per site is

$$\Delta A_{\text{mix}} / (n_{\text{site}} k_B T) = \sum_i \frac{\phi_i}{N_i} \ln \phi_i + (1 - \phi) \ln(1 - \phi) + \chi \phi (1 - \phi) \text{ polydisperse} \quad (2.33)$$

Following the method we used in Section 2.2.2, the chemical potential of the solvent molecule,  $\Delta \mu_s$ , is calculated, from which we obtain the osmotic pressure (Problem 2.14):

$$\frac{\Pi V}{n_{\text{site}} k_B T} = \sum_i \frac{\phi_i}{N_i} - \ln(1 - \phi) - \phi - \chi \phi^2 \text{ polydisperse} \quad (2.34)$$

In the dilute solution limit, the solution is ideal:

$$\frac{\Pi_{\text{ideal}} V}{n_{\text{site}} k_B T} = \sum_i \frac{\phi_i}{N_i} \quad (2.35)$$

It is now apparent that the osmotic pressure counts the total number of polymer chains. Colligative properties such as the osmotic pressure give, in general, a measure for the number of independently moving species per unit volume of the solution.

If we force the ideal solution of the polydisperse polymer to have the osmotic pressure of a solution of a monodisperse polymer consisting of  $\langle N \rangle$  beads dissolved at volume fraction  $\phi$ , then

$$\sum_i \frac{\phi_i}{N_i} = \frac{\phi}{\langle N \rangle} \quad (2.36)$$

which leads to

$$\langle N \rangle = \frac{\sum_i \phi_i}{\sum_i \phi_i / N_i} = \frac{\sum_i N_i n_i}{\sum_i n_i} \quad (2.37)$$

Thus we find that  $\langle N \rangle$  is the number average of  $N_i$ . The molecular weight estimated from the measurement of the osmotic pressure and Eq. 2.20 in the dilute solution limit is therefore the number-average molecular weight.

In Eq. 2.35, the nonideal terms depend on  $\phi$  only. Then polydispersity affects the ideal solution part, but not the nonideal part, in the Flory–Huggins mean–field theory.

## 2.2.6 PROBLEMS

**Problem 2.1:** Calculate the entropy of mixing  $\Delta S_{\text{mix,id}}$  for an ideal solution that consists of  $n_p = n_{\text{site}}\phi/N$  solute molecules and  $n_s = n_{\text{site}}(1 - \phi)$  solvent molecules. Compare it with  $\Delta S_{\text{mix}}$  given by Eq. 2.3. [Note: the entropy of mixing for a rigid-chain polymer and a solvent is given approximately by  $\Delta S_{\text{mix,id}}$ , because dissolution does not provide the polymer molecule with an additional freedom in the conformation compared with the state without solvent, except for the orientational freedom. The latter is negligible compared with the freedom a flexible chain would acquire when mixed with solvent molecules.]

**Solution 2.1:** The entropy of mixing is given as

$$-\Delta S_{\text{mix,id}}/k_B = n_p \ln x_p + n_s \ln x_s = (n_{\text{site}}\phi/N) \ln x_p + n_{\text{site}}(1 - \phi) \ln x_s$$

where  $x_p = (\phi/N)/(1 - \phi + \phi/N)$  and  $x_s = (1 - \phi)/(1 - \phi + \phi/N)$  are the mole fractions of the polymer and solvent, respectively. Then,

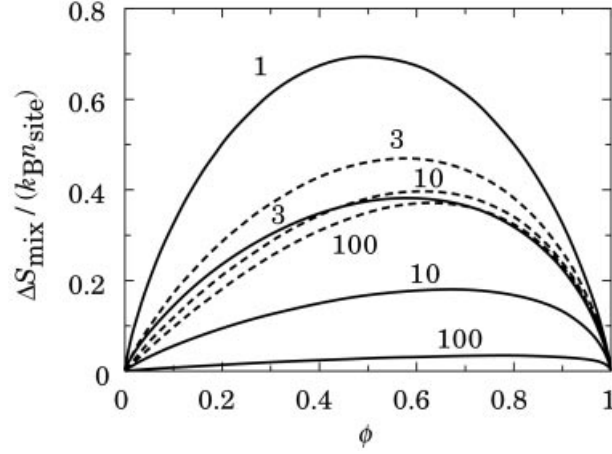
$$\begin{aligned} -\Delta S_{\text{mix,id}}/(k_B n_{\text{site}}) &= \frac{\phi}{N} \ln \frac{\phi/N}{1 - \phi + \phi/N} \\ &\quad + (1 - \phi) \ln \frac{1 - \phi}{1 - \phi + \phi/N} \\ &= (\phi/N) \ln(\phi/N) + (1 - \phi) \ln(1 - \phi) \\ &\quad - (1 - \phi + \phi/N) \ln(1 - \phi + \phi/N) \\ &= (\phi/N) \ln \phi + (1 - \phi) \ln(1 - \phi) - (\phi/N) \ln N \\ &\quad - (1 - \phi + \phi/N) \ln(1 - \phi + \phi/N) \end{aligned}$$

With Eq. 2.3,

$$\begin{aligned} \Delta S_{\text{mix,id}}/(k_B n_{\text{site}}) &= \Delta S_{\text{mix}}/(k_B n_{\text{site}}) + (\phi/N) \ln N \\ &\quad + (1 - \phi + \phi/N) \ln(1 - \phi + \phi/N) \end{aligned}$$

Let  $F(x) \equiv x \ln(\phi/x) + (1 - \phi + x) \ln(1 - \phi + x)$ , where  $x \equiv \phi/N$  ranges between 0 ( $N = \infty$ ) and  $\phi$  ( $N = 1$ ). Simple algebra shows that  $dF/dx = \ln[\phi/(x(1 - \phi + x))]$  is always positive. Then, with  $F(\phi) = 0$ ,  $F(x) < 0$  for all  $0 < x < \phi$ . Therefore,  $\Delta S_{\text{mix,id}} < \Delta S_{\text{mix}}$ .

Solid lines in the figure below show the plot of  $\Delta S_{\text{mix,id}}$  for  $N = 1, 3, 10$ , and 100. Dashed lines are  $\Delta S_{\text{mix}}$  for  $N = 1, 3, 10$ , and 100. For  $N = 1$ ,  $\Delta S_{\text{mix,id}} = \Delta S_{\text{mix}}$ . For the other values of  $N$ ,  $\Delta S_{\text{mix,id}}$  is smaller compared with  $\Delta S_{\text{mix}}$ . As  $N$  increases, the plot of  $\Delta S_{\text{mix,id}}$  approaches zero in the entire range of  $\phi$ . In contrast,  $\Delta S_{\text{mix}}$  for flexible chains remains finite in the limit of  $N \rightarrow \infty$ . For the rodlike molecule with a large  $N$  to dissolve (to make  $\Delta A_{\text{mix}}$  negative),  $\Delta H_{\text{mix}}$  must be negative.



**Problem 2.2:** We used Table 2.3 to calculate  $\Delta U_{\text{mix}}$  of a homopolymer with a solvent. Use the same method to show that Eq. 2.6 holds for a binary solution of an A–B copolymer (its volume fraction is  $\phi$ ) and a solvent S in the mean-field approximation with the effective  $\chi$  parameter given as  $x_a\chi_{as} + x_b\chi_{bs} - x_ax_b\chi_{ab}$ . Here  $x_a$  and  $x_b$  are the mole fractions of monomers A and B in the copolymer ( $x_a + x_b = 1$ ), respectively,  $\chi_{js}$  is the  $\chi$  parameter for a binary solution of a homopolymer of  $j$  and solvent S, and  $\chi_{ab}$  is the  $\chi$  parameter for a binary mixture of the two homopolymers.

**Solution 2.2:**

#### Probability of Nearest-Neighbor Contacts

Contact	Energy	Probability before mixing	Probability after mixing
A–A	$\varepsilon_{aa}$	$\phi x_a^2$	$\phi^2 x_a^2$
A–B	$\varepsilon_{ab}$	$2\phi x_a x_b$	$2\phi^2 x_a x_b$
B–B	$\varepsilon_{bb}$	$\phi x_b^2$	$\phi^2 x_b^2$
A–S	$\varepsilon_{as}$	0	$2\phi(1 - \phi)x_a$
B–S	$\varepsilon_{bs}$	0	$2\phi(1 - \phi)x_b$
S–S	$\varepsilon_{ss}$	$1 - \phi$	$(1 - \phi)^2$

The change in the average energy per bond is

$$\begin{aligned}
 & \varepsilon_{aa}(\phi^2 - \phi)x_a^2 + \varepsilon_{ab}(\phi^2 - \phi)2x_ax_b + \varepsilon_{bb}(\phi^2 - \phi)x_b^2 \\
 & + \varepsilon_{as}2\phi(1 - \phi)x_a + \varepsilon_{bs}2\phi(1 - \phi)x_b + \varepsilon_{ss}[(1 - \phi)^2 - (1 - \phi)] \\
 & = \phi(1 - \phi)[x_a(2\varepsilon_{as} - \varepsilon_{aa} - \varepsilon_{ss}) + x_b(2\varepsilon_{bs} - \varepsilon_{bb} - \varepsilon_{ss}) \\
 & - x_ax_b(2\varepsilon_{ab} - \varepsilon_{aa} - \varepsilon_{bb})]
 \end{aligned}$$

Then,

$$\begin{aligned}\Delta U_{\text{mix}} = & \frac{Zn_{\text{site}}}{2}\phi(1-\phi)[x_a(2\varepsilon_{\text{as}} - \varepsilon_{\text{aa}} - \varepsilon_{\text{ss}}) \\ & + x_b(2\varepsilon_{\text{bs}} - \varepsilon_{\text{bb}} - \varepsilon_{\text{ss}}) - x_ax_b(2\varepsilon_{\text{ab}} - \varepsilon_{\text{aa}} - \varepsilon_{\text{bb}})]\end{aligned}$$

In terms of  $\chi$  parameter,

$$\frac{\Delta U_{\text{mix}}}{n_{\text{site}}k_{\text{B}}T} = \phi(1-\phi)(x_a\chi_{\text{as}} + x_b\chi_{\text{bs}} - x_ax_b\chi_{\text{ab}})$$

Comparison with Eq. 2.6 leads to  $\chi = x_a\chi_{\text{as}} + x_b\chi_{\text{bs}} - x_ax_b\chi_{\text{ab}}$ .

**Problem 2.3:** Verify that Eq. 2.7 with  $\Delta A_{\text{mix}} = \Delta G_{\text{mix}}$  and Eqs. 2.12 and 2.13 satisfy  $\Delta G_{\text{mix}} = n_{\text{p}}\Delta\mu_{\text{p}} + n_{\text{s}}\Delta\mu_{\text{s}}$ .

**Solution 2.3:**

$$\begin{aligned}\frac{n_{\text{p}}\Delta\mu_{\text{p}} + n_{\text{s}}\Delta\mu_{\text{s}}}{k_{\text{B}}T} &= n_{\text{p}}[\ln\phi - (N-1)(1-\phi) + \chi N(1-\phi)^2] \\ &+ n_{\text{s}}[\ln(1-\phi) + (1-1/N)\phi + \chi\phi^2] \\ &= n_{\text{site}}\left[\frac{\phi}{N}(\ln\phi - (N-1)(1-\phi) + \chi N(1-\phi)^2) \right. \\ &\quad \left. + (1-\phi)(\ln(1-\phi) + (1-1/N)\phi + \chi\phi^2)\right] \\ &= n_{\text{site}}\left[\frac{\phi}{N}\ln\phi + (1-\phi)\ln(1-\phi) + \chi\phi(1-\phi)\right]\end{aligned}$$

**Problem 2.4:** The osmotic pressure of the polymer solution can also be obtained by using the formula (see Appendix 2.B):

$$\frac{\Pi}{k_{\text{B}}T} = -\left(\frac{\partial}{\partial V}\frac{\Delta A_{\text{mix}}}{k_{\text{B}}T}\right)_{T,n_{\text{p}}} = -\frac{1}{v_{\text{site}}}\left(\frac{\partial}{\partial n_{\text{site}}}\frac{\Delta A_{\text{mix}}}{k_{\text{B}}T}\right)_{T,n_{\text{p}}}$$

Use the identity  $\partial/\partial n_{\text{site}} = -(\phi/n_{\text{site}})\partial/\partial\phi$  that applies to changes at a fixed number of solute molecules to derive Eq. 2.14.

**Solution 2.4:** Use Eq. 2.7. At a fixed  $n_{\text{p}}$ ,

$$\frac{\Pi}{k_{\text{B}}T} = -\frac{1}{v_{\text{site}}}\left(-\frac{\phi}{n_{\text{site}}}\right)\frac{\partial}{\partial\phi}\frac{n_{\text{p}}N}{\phi}\frac{\Delta A_{\text{mix}}}{n_{\text{site}}k_{\text{B}}T} = \frac{\phi^2}{v_{\text{site}}}\frac{\partial}{\partial\phi}\frac{1}{\phi}\frac{\Delta A_{\text{mix}}}{n_{\text{site}}k_{\text{B}}T}$$

$$\begin{aligned}
&= \frac{\phi^2}{v_{\text{site}}} \frac{\partial}{\partial \phi} \left[ \frac{1}{N} \ln \phi + (\phi^{-1} - 1) \ln(1 - \phi) + \chi(1 - \phi) \right] \\
&= \frac{1}{v_{\text{site}}} \left[ \frac{\phi}{N} - \ln(1 - \phi) - \phi - \chi\phi^2 \right]
\end{aligned}$$

**Problem 2.5:** Show that  $\Delta A_{\text{mix}} + \Pi V(1 - \phi) = n_{\text{p}} \Delta \mu_{\text{p}}$ . The left-hand side is the Gibbs free energy change in the process that “vaporizes” the polymer in the condensed amorphous state into a total volume of  $V$  ( $\Delta V_{\text{mix}} = V(1 - \phi)$ ).

**Solution 2.5:** From Eqs. 2.7 and 2.14,

$$\begin{aligned}
\frac{\Delta A_{\text{mix}} + \Pi V(1 - \phi)}{n_{\text{site}} k_{\text{B}} T} &= \frac{\phi}{N} \ln \phi + (1 - \phi) \ln(1 - \phi) + \chi \phi(1 - \phi) \\
&\quad + (1 - \phi) \left[ \frac{\phi}{N} - \ln(1 - \phi) - \phi - \chi\phi^2 \right] \\
&= \frac{\phi}{N} \left[ \ln \phi - (N - 1)(1 - \phi) \right. \\
&\quad \left. + \chi N(1 - \phi)^2 \right] = \frac{n_{\text{p}} \Delta \mu_{\text{p}}}{n_{\text{site}} k_{\text{B}} T}
\end{aligned}$$

In the last equality, Eq. 2.12 was used.

**Problem 2.6:** Equation 2.18 tells that  $\Pi > \Pi_{\text{ideal}}$  when  $\chi < 1/2$  in the dilute solution ( $\phi \ll 1$ ). Use Eq. 2.14 to verify that it is also the case in the whole range of  $\phi$ .

**Solution 2.6:** From Eq. 2.14,

$$\frac{(\Pi - \Pi_{\text{ideal}})V}{n_{\text{site}} k_{\text{B}} T} = -\ln(1 - \phi) - \phi - \chi\phi^2 \equiv f(\phi)$$

Since  $f(0) = 0$  and

$$\frac{df}{d\phi} = \frac{1}{1 - \phi} - 1 - 2\chi\phi = \frac{\phi[1 - 2\chi(1 - \phi)]}{1 - \phi} > 0$$

in the whole range of  $\phi$  when  $\chi < 1/2$ , we find that  $f(\phi) > 0$  for  $0 \leq \phi < 1$ .

**Problem 2.7:** What is the free energy of mixing that corresponds to the virial expansion of the osmotic pressure given by Eq. 2.20? Also show that the  $\Delta A_{\text{mix}}$  you obtained reproduces Eq. 2.7 with  $A_2$  and  $A_3$  given by Eqs. 2.21 and 2.22.

**Solution 2.7:** At a constant  $cV$ , that is, at a constant  $n_p$ ,

$$\frac{\Pi}{k_B T} = - \left( \frac{\partial}{\partial V} \frac{\Delta A_{\text{mix}}}{k_B T} \right)_{T,cV} = \frac{c}{V} \left( \frac{\partial}{\partial c} \frac{\Delta A_{\text{mix}}}{k_B T} \right)_{T,cV}$$

With Eq. 2.20,

$$\left( \frac{\partial}{\partial c} \frac{\Delta A_{\text{mix}}}{k_B T} \right)_{T,cV} = \frac{V}{c} \frac{\Pi}{k_B T} = N_A c V \left( \frac{1}{cM} + A_2 + A_3 c + \dots \right)$$

Integration with respect to  $c$  at constant  $cV$  yields

$$\frac{\Delta A_{\text{mix}}}{k_B T} = N_A c V \left( \text{const.} + \frac{1}{M} \ln c + A_2 c + \frac{1}{2} A_3 c^2 + \dots \right)$$

With Eqs. 2.19, 2.21, and 2.22, and neglecting the constant terms,

$$\frac{\Delta A_{\text{mix}}}{n_{\text{site}} k_B T} = \frac{\phi}{N} \ln \phi + \left( \frac{1}{2} - \chi \right) \phi^2 + \frac{1}{6} \phi^3 + \dots$$

Equation 2.7 is expanded with respect to  $\phi$  as

$$\begin{aligned} \frac{\Delta A_{\text{mix}}}{n_{\text{site}} k_B T} &= \frac{\phi}{N} \ln \phi + (1 - \phi) \left( -\phi - \frac{1}{2} \phi^2 - \frac{1}{3} \phi^3 - \dots \right) + \chi \phi (1 - \phi) \\ &= \frac{\phi}{N} \ln \phi + (\chi - 1) \phi + \left( \frac{1}{2} - \chi \right) \phi^2 + \frac{1}{6} \phi^3 + \dots \end{aligned}$$

The above two equations are identical except for the linear term that becomes a constant term upon differentiation.

**Problem 2.8:** Show that  $A_2 M = \left( \frac{1}{2} - \chi \right) N v_{\text{sp}}$  and  $A_3 M = \frac{1}{3} N v_{\text{sp}}^2$  in the lattice chain model, where  $v_{\text{sp}}$  is the specific volume of the polymer in solution.

**Solution 2.8:** From Eq. 2.21,

$$A_2 M = \left( \frac{1}{2} - \chi \right) \frac{N_A v_{\text{site}} N}{M} N$$

where  $N_A v_{\text{site}} N$  is the molar volume of the polymer chain, and  $M$  is the molar mass of the polymer. The ratio,  $N_A v_{\text{site}} N / M$ , is the reciprocal of the density of the polymer. In the solution, it is the specific volume ( $v_{\text{sp}}$ ), that is, the increment in the solution volume when a unit mass of the polymer is added.

Likewise,

$$A_3M = \frac{1}{3} \frac{(N_A v_{\text{site}} N)^2}{M^2} N = \frac{1}{3} N v_{\text{sp}}^2$$

**Problem 2.9:** Use the Gibbs-Duhem theorem

$$n_p d\Delta\mu_p + n_s d\Delta\mu_s = 0$$

to find  $\Delta\mu_p$  for the virial expansion of  $\Pi$  given by Eq. 2.20.

**Solution 2.9:** The Gibbs-Duhem theorem is rewritten to

$$n_p \frac{d\Delta\mu_p}{dc} + n_s \frac{d\Delta\mu_s}{dc} = 0$$

From Eq. 2.A.4,

$$\frac{\Delta\mu_s}{k_B T} = -N_A v^* \left( \frac{c}{M} + A_2 c^2 + A_3 c^3 + \dots \right)$$

Combining the two equations yields

$$\frac{d}{dc} \frac{\Delta\mu_p}{k_B T} = \frac{n_s v^*}{n_p M / N_A} (1 + 2A_2 M c + 3A_3 M c^2 + \dots)$$

Here,  $n_s v^* / (n_p M / N_A)$  is the ratio of the total volume of the solvent to the total mass of the polymer. Assuming that the volume  $V$  of the solution is given by

$$V = n_s v^* + (n_p M / N_A) v_{\text{sp}}$$

with  $v_{\text{sp}}$  being the specific volume of the polymer in solution (see Problem 2.8), we find

$$\frac{n_s v^*}{n_p M / N_A} = \frac{1}{c} - v_{\text{sp}}$$

where  $c = (n_p M / N_A) / V$  is the mass concentration of the polymer. Thus,

$$\frac{d}{dc} \frac{\Delta\mu_p}{k_B T} = \frac{1}{c} + (2A_2 M - v_{\text{sp}}) + (3A_3 M - 2A_2 M v_{\text{sp}})c + \dots$$

Upon integration,

$$\frac{\Delta\mu_p}{k_B T} = \ln c + (2A_2 M - v_{\text{sp}})c + (3A_3 M / 2 - A_2 M v_{\text{sp}})c^2 + \dots$$



**Problem 2.10:** For a lattice fluid system that allows  $n_p$  and  $n_s$  to change independently (total volume is not fixed),

$$\frac{\partial \Delta \mu_p}{\partial n_p} = 0 \quad \text{and} \quad \frac{\partial \Delta \mu_p}{\partial n_p} \frac{\partial \Delta \mu_s}{\partial n_s} = \frac{\partial \Delta \mu_p}{\partial n_s} \frac{\partial \Delta \mu_s}{\partial n_p}$$

gives the boundary of the stable state. Show that this condition is equivalent to Eq. 2.27. Show also that  $\partial \Delta \mu_p / \partial n_p$  and  $\partial \Delta \mu_s / \partial n_s$  share the sign.

**Solution 2.10:** Because

$$\frac{\partial \Delta \mu_p}{\partial n_p} = \frac{\partial \Delta \mu_p}{\partial \phi} \frac{\partial \phi}{\partial n_p}, \text{ etc.}$$

the second part of the condition always holds when the first part holds. From Eq. 2.12, the first part is calculated as

$$\frac{\partial(\Delta \mu_p / k_B T)}{\partial n_p} = \frac{\partial \phi}{\partial n_p} \left[ \frac{1}{\phi} + (N - 1) - 2\chi N(1 - \phi) \right] = 0$$

Rearrangement gives Eq. 2.27. Likewise,

$$\frac{\partial(\Delta \mu_s / k_B T)}{\partial n_s} = \frac{\partial \phi}{\partial n_s} \left[ -\frac{1}{1 - \phi} + 1 - \frac{1}{N} + 2\chi \phi \right] = 0$$

is equivalent to Eq. 2.27.

Comparison of the above two equations yields

$$\frac{\partial(\Delta \mu_p / k_B T)}{\partial n_p} \bigg/ \frac{\partial \phi}{\partial n_p} = -\frac{N(1 - \phi)}{\phi} \frac{\partial(\Delta \mu_s / k_B T)}{\partial n_s} \bigg/ \frac{\partial \phi}{\partial n_s}$$

Because  $\partial \phi / \partial n_p$  and  $\partial \phi / \partial n_s$  have the opposite sign,  $\partial \Delta \mu_p / \partial n_p$  and  $\partial \Delta \mu_s / \partial n_s$  have the same sign.

**Problem 2.11:** Use Gibbs-Duhem equation (in Problem 2.9) to show that

$$\int_{\phi_1}^{\phi_2} \Delta \mu_{\text{rep}}(\phi) d\phi = (\phi_2 - \phi_1) \Delta \mu_{\text{rep}}(\phi_1)$$

where  $\Delta \mu_p(\phi_1) = \Delta \mu_p(\phi_2)$  and  $\Delta \mu_s(\phi_1) = \Delta \mu_s(\phi_2)$ .

**Solution 2.11:** The Gibbs-Duhem equation

$$\frac{\phi}{N} \frac{\partial \Delta \mu_p}{\partial \phi} + (1 - \phi) \frac{\partial \Delta \mu_s}{\partial \phi} = 0$$

leads to

$$\phi \frac{\partial \Delta \mu_{\text{rep}}}{\partial \phi} = -N \frac{\partial \Delta \mu_{\text{S}}}{\partial \phi}$$

Using integral by parts,

$$\begin{aligned} \int_{\phi_1}^{\phi_2} \Delta \mu_{\text{rep}} d\phi &= \left[ \phi \Delta \mu_{\text{rep}} \right]_{\phi_1}^{\phi_2} - \int_{\phi_1}^{\phi_2} \phi \frac{\partial \Delta \mu_{\text{rep}}}{\partial \phi} d\phi \\ &= (\phi_2 - \phi_1) \Delta \mu_{\text{rep}}(\phi_1) + N \int_{\phi_1}^{\phi_2} \frac{\partial \Delta \mu_{\text{S}}}{\partial \phi} d\phi = (\phi_2 - \phi_1) \Delta \mu_{\text{rep}}(\phi_1) \end{aligned}$$

**Problem 2.12:** Use the result of Problem 2.11 to show that the plot of  $\Delta G_{\text{mix}}$  has a cotangent line at  $\phi_1$  and  $\phi_2$  (see Fig. 2.13).

**Solution 2.12:** The slope of the line that connects the two points on  $\Delta G_{\text{mix}}/(n_{\text{site}} k_{\text{B}} T)$  at  $\phi_1$  and  $\phi_2$  is

$$\begin{aligned} \frac{[\Delta G_{\text{mix}}(\phi_2) - \Delta G_{\text{mix}}(\phi_1)]/(n_{\text{site}} k_{\text{B}} T)}{\phi_2 - \phi_1} &= \frac{1}{\phi_2 - \phi_1} \frac{1}{N} \int_{\phi_1}^{\phi_2} \frac{\Delta \mu_{\text{rep}}(\phi)}{k_{\text{B}} T} d\phi \\ &= \frac{1}{N} \frac{\Delta \mu_{\text{rep}}(\phi_1)}{k_{\text{B}} T} = \frac{1}{N} \frac{\Delta \mu_{\text{rep}}(\phi_2)}{k_{\text{B}} T} \end{aligned}$$

where Eq. 2.26 and the result of Problem 2.11 were used. The last part of the above equation is the slope of the  $\Delta G_{\text{mix}}/(n_{\text{site}} k_{\text{B}} T)$  at  $\phi_1$  and  $\phi_2$  according to Eq. 2.26.

**Problem 2.13:** Use the lever rule to show that the two-phase solution has its  $\Delta G_{\text{mix}}$  on the cotangent line (see Fig. 2.13).

**Solution 2.13:** From Eq. 2.29, the total free energy of the two-phase solution is given as

$$\begin{aligned} \frac{V_1}{v_{\text{site}}} \frac{\Delta G_{\text{mix}}(\phi_1)}{n_{\text{site}}} + \frac{V_2}{v_{\text{site}}} \frac{\Delta G_{\text{mix}}(\phi_2)}{n_{\text{site}}} &= \frac{V_1 + V_2}{v_{\text{site}} n_{\text{site}}} \\ &\left( \frac{\phi_2 - \phi}{\phi_2 - \phi_1} \Delta G_{\text{mix}}(\phi_1) + \frac{\phi - \phi_1}{\phi_2 - \phi_1} \Delta G_{\text{mix}}(\phi_2) \right) \end{aligned}$$

which represents a straight line through the two points  $[\phi_1, \Delta G_{\text{mix}}(\phi_1)]$  and  $[\phi_2, \Delta G_{\text{mix}}(\phi_2)]$  in the figure.

**Problem 2.14:** Derive Eq. 2.34 from Eq. 2.33.

**Solution 2.14:** For a total  $n_{\text{site}}$  sites,

$$\Delta A_{\text{mix}}/(k_{\text{B}}T) = \sum_i n_i \ln \phi_i + n_{\text{S}} \ln(1 - \phi) + \chi(1 - \phi) \sum_i N_i n_i$$

Using the identities

$$\left( \frac{\partial \phi}{\partial n_{\text{S}}} \right)_{n_i} = -\frac{\phi}{n_{\text{site}}}, \quad \left( \frac{\partial \phi_j}{\partial n_{\text{S}}} \right)_{n_i \neq j} = -\frac{\phi_j}{n_{\text{site}}}$$

the chemical potential of the solvent molecule is calculated as

$$\begin{aligned} \frac{\Delta \mu_{\text{S}}}{k_{\text{B}}T} &= \left( \frac{\partial}{\partial n_{\text{S}}} \frac{\Delta G_{\text{mix}}}{k_{\text{B}}T} \right)_{T,p,n_i} = \sum_i n_i \frac{1}{\phi_i} \frac{\partial \phi_i}{\partial n_{\text{S}}} + \ln(1 - \phi) \\ &\quad - n_{\text{S}} \frac{\partial \phi}{\partial n_{\text{S}}} \frac{1}{1 - \phi} - \chi \frac{\partial \phi}{\partial n_{\text{S}}} \sum_i N_i n_i \\ &= \ln(1 - \phi) + \phi - \sum_i \frac{\phi_i}{N_i} + \chi \phi^2 \end{aligned}$$

Then, with Eq. 2.A.4, the osmotic pressure is obtained as

$$\frac{\Pi V}{n_{\text{site}} k_{\text{B}}T} = \sum_i \frac{\phi_i}{N_i} - \ln(1 - \phi) - \phi - \chi \phi^2$$

**Problem 2.15:** Show that the chemical potential of component  $i$  of the poly-disperse polymer in the solution is given as

$$\frac{\Delta \mu_i}{k_{\text{B}}T} = \ln \phi_i + 1 + N_i \left[ -1 + \phi - \sum_k \frac{\phi_k}{N_k} + \chi(1 - \phi)^2 \right]$$

**Solution 2.15:** First, we rewrite Eq. 2.33 into

$$\frac{\Delta A_{\text{mix}}}{k_{\text{B}}T} = \sum_k n_k \ln \phi_k + n_{\text{S}} \ln(1 - \phi) + \chi n_{\text{S}} \phi$$

Using the identities

$$\left( \frac{\partial \phi_k}{\partial n_i} \right)_{n_{\text{S}}, n_{j \neq i}} = \frac{\partial}{\partial n_i} \frac{N_k n_k}{n_{\text{S}} + \sum_k N_k n_k} = \frac{\phi_i}{n_i} \delta_{ik} - \frac{\phi_i \phi_k}{n_i}$$

and

$$\left(\frac{\partial \phi}{\partial n_i}\right)_{n_s, n_j \neq i} = \sum_k \left( \frac{\phi_i}{n_i} \delta_{ik} - \frac{\phi_i \phi_k}{n_i} \right) = \frac{\phi_i}{n_i} (1 - \phi)$$

$\Delta \mu_i$  is calculated as

$$\begin{aligned} \frac{\Delta \mu_i}{k_B T} &= \left( \frac{\partial}{\partial n_i} \frac{\Delta G_{\text{mix}}}{k_B T} \right)_{n_s, n_j \neq i} = \frac{\partial}{\partial n_i} \left( \sum_k n_k \ln \phi_k + n_s \ln(1 - \phi) + \chi n_s \phi \right) \\ &= \ln \phi_i + \sum_k \frac{n_k}{\phi_k} \left( \frac{\phi_i}{n_i} \delta_{ik} - \frac{\phi_i}{n_i} \phi_k \right) + \left( \chi - \frac{1}{1 - \phi} \right) n_s \frac{\phi_i}{n_i} (1 - \phi) \\ &= \ln \phi_i + 1 + N_i \left[ -1 + \phi - \sum_k \frac{\phi_k}{N_k} + \chi(1 - \phi)^2 \right] \end{aligned}$$

**Problem 2.16:** The osmotic pressure of the lattice polymer solution is, in general, given in the virial expansion with respect to  $\phi$ :

$$\frac{\Pi V}{n_{\text{site}} k_B T} = \frac{\phi}{N} + B_2 \phi^2 + B_3 \phi^3 + B_4 \phi^4 + \dots$$

Assume that the second virial coefficient  $B_2$  is susceptible to the environmental change but its effect on the higher-order coefficients ( $B_3, B_4, \dots$ ) is weak. What are the values of  $B_2$  and  $\phi$  at the critical condition?

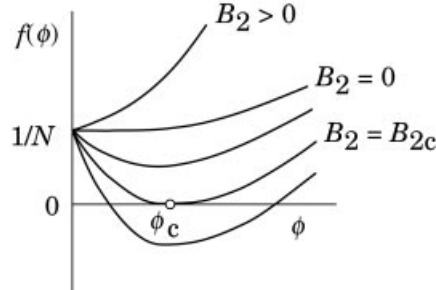
**Solution 2.16:** From Eq. 2.A.4,

$$\frac{\Delta \mu_s}{k_B T} = -\frac{\Pi V}{n_{\text{site}} k_B T} = -\left( \frac{\phi}{N} + B_2 \phi^2 + B_3 \phi^3 + B_4 \phi^4 + \dots \right)$$

As we have seen in Problem 2.10, the spinodal line is given by

$$\frac{\partial}{\partial \phi} \frac{\Delta \mu_s}{k_B T} = -\left( \frac{1}{N} + 2B_2 \phi + 3B_3 \phi^2 + 4B_4 \phi^3 + \dots \right) = 0$$

Let  $f(\phi) \equiv 1/N + 2B_2 \phi + 3B_3 \phi^2 + 4B_4 \phi^3 + \dots$ . The plot of  $f(\phi)$  depends on  $B_2$ . The system is stable if  $f(\phi) > 0$  for all  $\phi > 0$ . At  $B_2 = B_{2c}$ , the plot of  $f(\phi)$  is tangent on the  $\phi$  axis at  $\phi = \phi_c$ . The critical condition is therefore



given as

$$f(\phi_c) = 1/N + 2B_{2c}\phi_c + 3B_3\phi_c^2 + 4B_4\phi_c^3 + \dots = 0$$

$$f'(\phi_c) = 2B_{2c} + 6B_3\phi_c + 12B_4\phi_c^2 + \dots = 0$$

which leads to

$$\phi_c = (3B_3N)^{-1/2} - \frac{4}{9} \frac{B_4}{B_3^2N} + \dots, B_{2c} = -(3B_3/N)^{1/2} - \frac{2}{3} \frac{B_4}{B_3N} + \dots$$

## 2.3 PHASE DIAGRAM AND THETA SOLUTIONS

### 2.3.1 Phase Diagram

**2.3.1.1 Upper and Lower Critical Solution Temperatures** The quality of the solvent for a given polymer can be changed either by changing the temperature or by changing the mixing ratio of a good solvent to a poor solvent. When the temperature is changed, it is customary to draw a coexistence curve on a temperature–composition plane. We use the temperature for the ordinate in place of  $\chi$ , because of convenience. Any scale can be used to represent the composition: mass concentration, volume fraction, molar fraction, mass fraction, and so forth.

There are different types of phase diagram. Figure 2.19a shows the most commonly observed diagram. The parabolic coexistence curve is inverted from the one on the  $\chi - \phi$  plane in the figures in Section 2.2 because increasing  $T$  decreases  $\chi$  in general. The temperature at the critical condition is called the **critical temperature**. The phase diagram has the critical temperature ( $T_c$ ) at the highest point on the coexistence curve. Therefore, the critical temperature is referred to as the **upper critical solution temperature (UCST)**. The phase diagram shown in Figure 2.19a is called a UCST-type phase diagram. At high temperatures, the solution is uniform and therefore transparent. At  $T < T_c$  the system has a miscibility gap. When cooled to temperatures below the coexistence curve, the solution separates into two phases. Each of the two phases is uniform, but they have different compositions. A polymer–solvent system with a near-constant and positive  $\Delta\varepsilon = \varepsilon_{PS} - (\varepsilon_{PP} + \varepsilon_{SS})/2$  will yield a UCST. Note  $\chi = Z\Delta\varepsilon/k_B T$  in Eq. 2.4.

An inverted phase diagram shown in Figure 2.19b is observed in some polymer–solvent systems. Because  $T_c$  is at the lowest point on the coexistence

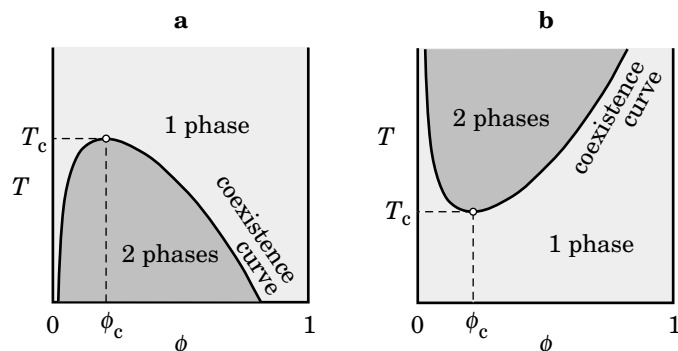


**Figure 2.19.** Phase diagram of polymer solution on temperature–composition plane. a: UCST-type phase diagram. b: LCST-type phase diagram. The critical point is at the apex of the coexistence curve and is specified by the critical temperature  $T_c$  and the critical composition  $\phi_c$ .

curve, this  $T_c$  is called the **lower critical solution temperature (LCST)**. The phase diagram shown in Figure 2.19b is called a LCST-type phase diagram. A polymer soluble in water due to hydrogen bonding usually has an LCST-type phase diagram because the hydrogen bonding disrupts at higher temperatures.

It can happen that the coexistence curve is closed and has both UCST and LCST, as shown in Figure 2.20. The solution is in a single phase exterior to the loop but in two phases within the loop.

It is common to all three types of the phase diagram that the system is in a single phase at compositions close to the vertical line at  $\phi = 0$  or the other vertical line at  $\phi = 1$ . The majority component can always accommodate a small amount of the minority component with a help from the entropy of mixing.

**2.3.1.2 Experimental Methods** The **cloud-point method** is commonly used to determine the phase diagram. Let us consider a solution that has a UCST-type phase diagram. We prepare solutions at different concentrations and bring them into a single phase by heating. The solutions are then cooled slowly. In Figure 2.21, the

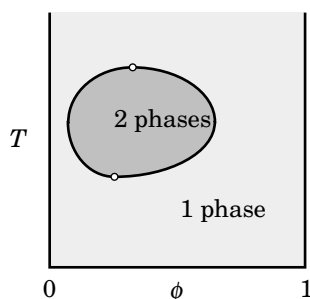


**Figure 2.20.** A phase diagram can show both upper and lower critical solution temperatures.

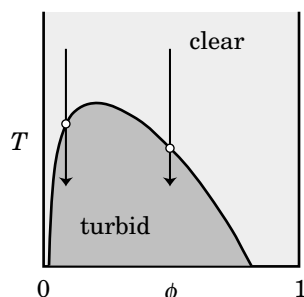


**Figure 2.21.** Cloud point is defined as the temperature at which the solution becomes turbid as the solution in a single phase is brought into the two-phase regime. Illustration is given for the UCST-type phase diagram.

polymer–solvent system changes its state along a vertical line. As the temperature crosses the coexistence curve, the solution becomes turbid, indicating microscopic heterogeneity. The point is called the **cloud point**. The turbidity is due to scattering of light by a difference in the refractive index between the two phases. When left for a sufficiently long time, the polymer–solvent system separates into two macroscopic phases, each of which is uniform and therefore transparent. The lighter phase is now on top of the heavier phase. In some solutions, crystallization of the polymer occurs simultaneously as the polymer-rich phase separates. The crystallite that has grown from a solution may be clear. By connecting the cloud points measured for solutions of different concentrations, we can obtain the coexistence curve and construct the phase diagram.

Naked eyes can easily detect the cloudiness. A more sophisticated method will use a photodetector. A polymer solution in a single phase is prepared in a cuvette. The intensity of the light transmitted through the solution, or the intensity of light scattered, typically at  $90^\circ$ , is continuously monitored as the temperature is lowered across the coexistence curve. The scattering intensity shoots up and the transmission drops as the solution becomes turbid.

Atactic polystyrene in cyclohexane is the most famous example of polymer solutions that exhibit a UCST-type phase diagram. Figure 2.22 shows the phase diagrams for different molecular weights of polystyrene.<sup>15</sup> For each molecular weight, the critical point is at the highest point of the curve. As the molecular weight increases, the critical temperature ( $T_c$ ) becomes higher and the critical volume fraction  $\phi_c$  decreases. The extrapolate of  $T_c$  to infinite molecular weight is about  $35.4^\circ\text{C}$ .

## 2.3.2 Theta Solutions

**2.3.2.1 Theta Temperature** For a given polymer–solvent system, the light-scattering experiment at different concentrations gives an estimate of  $A_2$  at the temperature of the measurement, as we will learn in the following section. In a system that has a UCST-type phase diagram (Fig. 2.23a), the sign of  $A_2$  changes from

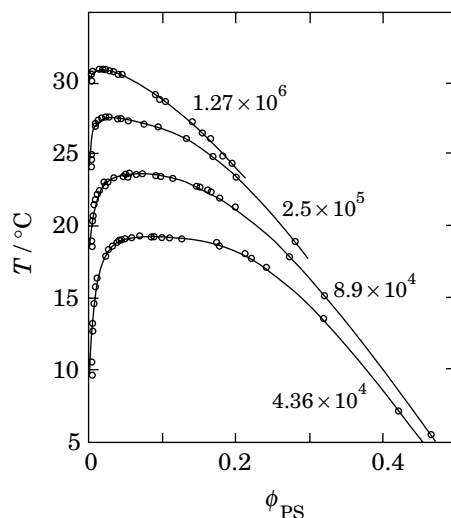


**Figure 2.22.** Coexistence curves determined from the cloud-point method (circles) for solutions of polystyrene of different molecular weights in cyclohexane. The abscissa is the volume fraction of polystyrene. The molecular weight of the polymer in g/mol is indicated adjacent to each curve. (From Ref. 15.)

positive to negative as the temperature drops below a certain level. The temperature at which  $A_2 = 0$  is called the **theta temperature** and expressed by  $T_\theta$  or  $\Theta$ . The solvent at  $T_\theta$  is a theta solvent for the polymer. The theta temperature thus defined is identical to the extrapolate of  $T_c$  to infinite molecular weight of the polymer. The latter is another definition of  $T_\theta$ . In a solution of a polymer in g/mol of a finite molecular weight with UCST,  $T_c < T_\theta$ .

In polymer solutions with LCST, the critical temperature  $T_c$  is higher than  $T_\theta$  (Fig. 2.23b). The sign of  $A_2$  changes from positive to negative as the temperature exceeds  $T_\theta$ .

The theta temperature is different for each combination of polymer and solvent. Table 2.6 lists  $T_\theta$  for some polymer solutions.<sup>11</sup> Each system has its own theta temperature, although it may not be reached in the liquid phase of the solvent or below the decomposition temperature of the polymer.

There is a slight molecular weight dependence of the temperature that renders  $A_2 = 0$  when the molecular weight is not sufficiently high. The dependence is much

**TABLE 2.6 Theta Conditions**

Polymer	Solvent	Temperature	Type
polystyrene	cyclohexane	~35°C	UCST
polystyrene	<i>trans</i> -decahydronaphthalene	~21°C	UCST
poly(methyl methacrylate)	acetonitrile	~44°C	UCST
poly( <i>N</i> -isopropyl acrylamide)	water	~30°C	LCST



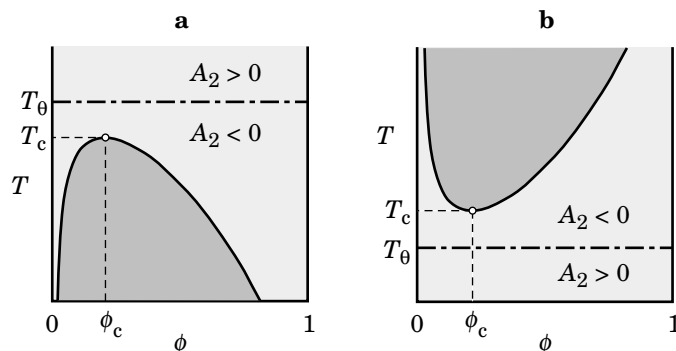
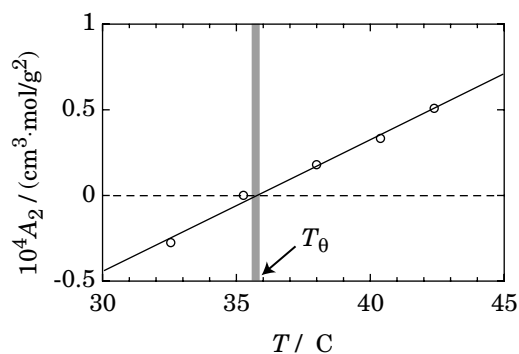


**Figure 2.23.** Relationship between the theta temperature  $T_\theta$  with the critical temperature  $T_c$ . a: UCST-type phase diagram. b: LCST-type phase diagram. The second virial coefficient  $A_2$  changes its sign at  $T = T_\theta$ .

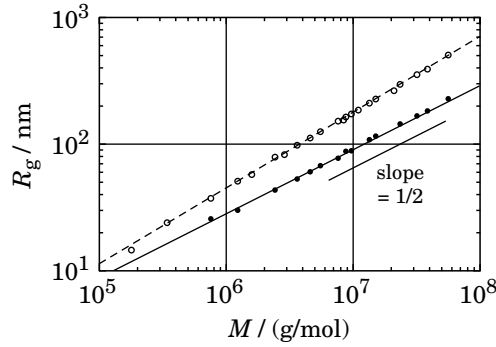
smaller compared with the dependence of  $T_c$  on the molecular weight. Therefore, the light-scattering experiments do not need to be repeated on polymer fractions of different molecular weights to find  $T_\theta$ . Measurement of  $A_2$  on a single fraction of the polymer should suffice.

Figure 2.24 shows an example of  $A_2$  obtained in the light-scattering experiments at several different temperatures near  $T_\theta$  for a solution of polystyrene in cyclohexane.<sup>16</sup> Apparently,  $A_2 \cong 0$  at around 35.7°C for the solution. The temperature agrees with the extrapolate of  $T_c$  within experimental errors.

**2.3.2.2 Properties of Theta Solutions** Solutions in the theta condition have  $A_2 = 0$ . When  $A_2 = 0$ , the second-order term in  $\Pi/\Pi_{\text{ideal}} = 1 + A_2Mc + A_3Mc^2 + \dots$  (Eq. 2.20) is absent. The nonideality of the solution does not become apparent until the third-order term  $A_3Mc^2$  becomes sufficiently large. The osmotic pressure is



**Figure 2.24.** Second virial coefficient  $A_2$  for polystyrene in cyclohexane at different temperatures near the theta temperature. (From Ref. 16.)



**Figure 2.25.** Radius of gyration  $R_g$  of polystyrene in cyclohexane at the theta temperature (35.4°C), plotted as filled circles as a function of molecular weight. Open symbols indicate  $R_g$  of polystyrene in toluene and benzene (good solvents) and are the same as those in Figure 1.37. A slope of 1/2 is indicated in the figure. (From Ref. 2.)

close to that of the ideal solution in a wide range of concentrations. The near ideality of the theta solution is not limited to the osmotic pressure.

The chain dimension such as  $R_g$  and  $R_F$  in theta solution increases with the molecular weight  $M$  just as the ideal chains do. Figure 2.25 shows an example obtained for polystyrene in cyclohexane at 35.4°C.<sup>2</sup> The data for  $R_g$  are plotted as solid circles. For reference,  $R_g$  in the good solvent is plotted as open circles (same as Fig. 1.37). The polymer chain in the theta solvent is shrunk compared with the good solvent. The curve fitting (for  $M < 10^7$  g/mol) gives

$$R_g/\text{nm} = 0.02675 \times (M/(\text{g/mol}))^{0.5040} \quad \text{polystyrene in cyclohexane, } 35.4^\circ\text{C} \quad (2.28)$$

close to the predicted  $R_g \propto M^{1/2}$ .

In Section 1.4.2, we derived  $R_F \cong bN^{3/5}$  for an excluded-volume chain using Flory's method. Here, we use a similar method to derive  $R_F \cong bN^{1/2}$  for theta chains. The difference in the free energy  $A_{\text{ch}}$  of the chain is in the second term of Eq. 1.63. For the theta chains, binary interaction is effectively absent ( $A_2 = 0$ ) and therefore the leading term in the polymer-polymer interaction is  $b^6 R^3 (N/R^3)^3 = b^6 N^3 / R^6$ , which is due to the ternary interactions. Then,  $A_{\text{ch}}$  is given as

$$\frac{A_{\text{ch}}}{k_B T} \cong \frac{R^2}{Nb^2} + b^6 \frac{N^3}{R^6} \quad (2.39)$$

$A_{\text{ch}}$  minimizes when  $\partial(A_{\text{ch}}/k_B T)/\partial R|_{R=R_F} = 0$ , that is,  $R_F \cong bN^{1/2}$ , reproducing the experimental results. The relationship becomes questionable when  $N$  is large, however. See Problem 2.17.

The nature of the theta solvent can be better understood in the lattice chain model. We choose the interaction with a solvent to be zero:  $\varepsilon_{\text{PS}} = \varepsilon_{\text{PP}} = 0$ . Then  $\chi = -(Z/2)\varepsilon_{\text{PP}}/k_B T$ . The theta condition,  $\chi = 1/2$ , is realized by  $\varepsilon_{\text{PP}}/k_B T = -1/Z$ .

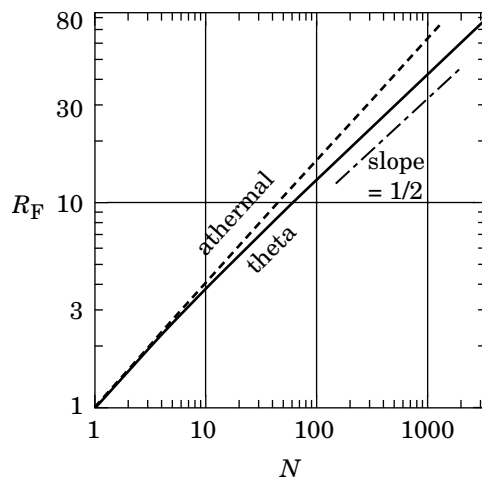


**Figure 2.26.** End-to-end distance  $R_F$  of self-avoiding walks on the cubic lattice, plotted as a function of the number of bonds,  $N$ , of the chain. The solid line and the dashed line represent the theta chains and athermal chains, respectively. The dash-dotted line has a slope of  $1/2$ . (From Ref. 18.)

This negative interaction in the monomer–monomer contact promotes association between monomers and contracts the polymer chain. The repulsive interaction due to the excluded volume is compensated by the attractive  $\varepsilon_{pp}$ .

However, the Flory–Huggins theory is an approximate theory based on random mixing of monomers. The interaction for the theta condition is slightly different in the computer simulation on the cubic lattice:<sup>17</sup>

$$\boxed{\varepsilon_{pp}/k_B T = -0.2693 \quad \text{theta condition, cubic lattice simulation}} \quad (2.40)$$

Figure 2.26 compares a plot of the root mean square end-to-end distance  $R_F$  for polymer chains on the cubic lattice for the theta chains with a plot for athermal chains.<sup>18</sup> The chain contraction in the theta condition is evident. The data for the theta solution follow a power law of  $R_F \sim N^{1/2}$  when  $N \gg 1$ .

### 2.3.3 Coil-Globule Transition

As the solvent quality turns poorer to the polymer from the theta condition, polymer–solvent contacts become more unfavorable, and the chain contracts even more. Eventually, the random-coil conformation changes to a globular shape to minimize the polymer–solvent contacts and maximize the contacts between monomers. The chain dimension should be now proportional to  $N^{1/3}$ , as expected for a packed sphere. When  $N$  is sufficiently large, the change from  $R_g \cong bN^{1/2}$  to  $bN^{1/3}$  is rather abrupt; therefore, it is called **coil-globule transition**. Figure 2.27 summarizes how

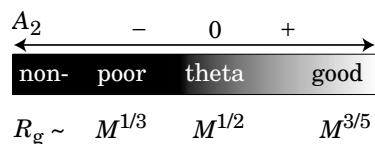
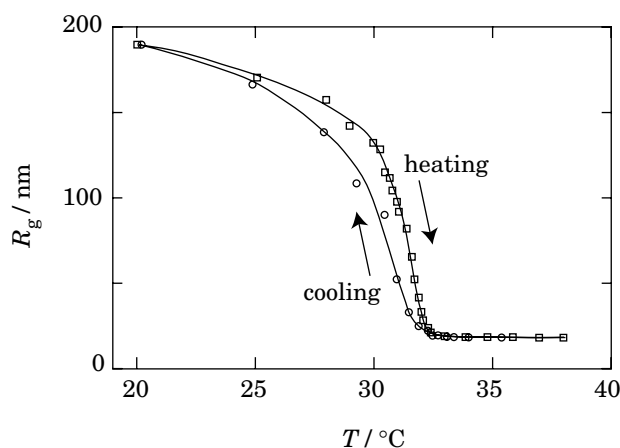


**Figure 2.27.** Molecular-weight ( $M$ ) dependence of the radius of gyration  $R_g$  changes as the solvent quality, and therefore the second virial coefficient  $A_2$ , change.

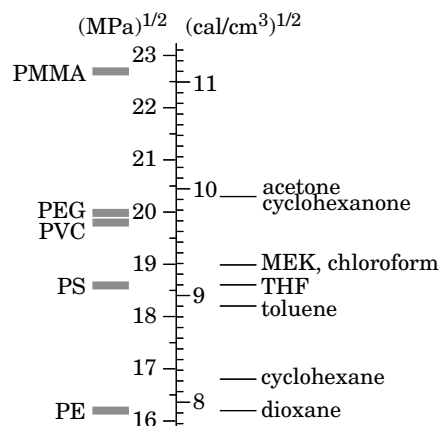
the chain dimension changes with  $A_2$ . It is not easy to observe the transition in experiments because, as the intrachain attraction becomes stronger, the interchain attraction becomes stronger as well, leading to formation of aggregates. Then, the light-scattering measurements give the size of the aggregate, not a single chain dimension.

Figure 2.28 is a rare example of a successful observation.<sup>19</sup> It shows how  $R_g$  of poly(*N*-isopropyl acrylamide) in water changes with the solvent quality. The solution exhibits an LCST-type phase diagram with  $T_\theta \cong 30.5^\circ\text{C}$ . At  $T \ll T_\theta$ , the solvent is good to the polymer and the chains are swollen. As  $T$  rises, the solvent quality becomes poorer and  $R_g$  decreases. At  $T > T_c \cong 32^\circ\text{C}$ ,  $R_g$  is nearly independent of temperature. A slight hysteresis was observed.

Most protein molecules are globular. Strong interactions due to hydrogen bonding and S–S linkage force the protein to take a specific structure close to a globule.



**Figure 2.28.** Contraction and swelling of linear poly(*N*-isopropyl acrylamide) chains in water by cooling and heating. The radius of gyration  $R_g$  is plotted as a function of temperature  $T$ . (From Ref. 19.)



**Figure 2.29.** Solubility parameters of some solvents and polymers, given in (MPa)<sup>1/2</sup> and (cal/cm<sup>3</sup>)<sup>1/2</sup>.

### 2.3.4 Solubility Parameter

The interaction between a polymer and a solvent is often expressed by a **solubility parameter**. The solubility parameter  $\delta_i$  of substance  $i$  is defined as

$$\delta_i \equiv (\Delta E_i^{\text{vap}}/V_i)^{1/2} \quad (2.41)$$

where  $\Delta E_i^{\text{vap}}$  is the molar energy of vaporization and  $V_i$  is the molar volume of substance  $i$ . Figure 2.29 shows a partial list of the solubility parameter expressed in (MPa)<sup>1/2</sup> and (cal/cm<sup>3</sup>)<sup>1/2</sup>.<sup>11</sup> Simple thermodynamics on the binary mixture gives the  $\chi$  parameter expressed by the solubility parameters:

$$\chi = \frac{V_s}{N_A k_B T} (\delta_s - \delta_p)^2 + 0.34 \quad (2.42)$$

where subscripts S and P stand for solvent and polymer, respectively.

Equation 2.42 illustrates that the polymer and the solvent mix when their solubility parameters are close and do not when they differ a lot. However, this is not always the case. For instance, polyethylene and 1,4-dioxane have similar solubility parameters but do not mix partly because of crystallinity of polyethylene. Poly(methyl methacrylate) dissolves well in tetrahydrofuran, although the solubility parameters are greatly different. Furthermore, Eq. 2.42 is always positive. It fails to describe specific interactions that may make  $\chi$  negative such as the hydrogen bonding. We should regard Eq. 2.42 as one of the possible ways to describe  $\chi$  for some polymer–solvent systems.

### 2.3.5 PROBLEMS

**Problem 2.17:** We apply Flory's method (Section 1.4) to find how much a small deviation from the theta condition changes the end-to-end distance. For this purpose, we express the free energy per chain that has an end-to-end distance  $R$  by

$$\frac{A_{\text{ch}}}{k_{\text{B}}T} \cong \frac{R^2}{Nb^2} + b^6 \frac{N^3}{R^6} + \beta b^3 \frac{N^2}{R^3}$$

where  $\beta = 0$  at theta. Treat the last term as a perturbation and evaluate its effect on  $R_{\text{F}}$ .

**Solution 2.17:** At  $R = R_{\text{F}}$ ,

$$\frac{\partial}{\partial R} \frac{A_{\text{ch}}}{k_{\text{B}}T} = \frac{2R}{Nb^2} - 6b^6 \frac{N^3}{R^7} - 3\beta b^3 \frac{N^2}{R^4} = 0$$

which leads to

$$R_{\text{F}}^8 = 3b^8 N^4 + \frac{3}{2} \beta b^5 N^3 R^3$$

Treat the second term as a perturbation:

$$R_{\text{F}} \cong bN^{1/2} \left( 1 + \beta \frac{R^3}{Nb^3} \right)^{1/8} \cong bN^{1/2} \left( 1 + \frac{1}{8} \frac{\beta}{N} \frac{R^3}{b^3} \right) \cong bN^{1/2} \left( 1 + \frac{\beta}{8} N^{1/2} \right)$$

where  $R$  was replaced by the unperturbed dimension,  $bN^{1/2}$ . Even when  $\beta$  is close to zero,  $R_{\text{F}}$  may deviate from  $bN^{1/2}$  as  $N$  increases. The deviation is more serious for high-molecular-weight fractions.

## 2.4 STATIC LIGHT SCATTERING

### 2.4.1 Sample Geometry in Light-Scattering Measurements

**Light scattering** has been widely used to characterize polymer chains in a solution. We can find the weight-average molecular weight ( $M_w$ ), the radius of gyration ( $R_g$ ), and the second virial coefficient ( $A_2$ ). We can also learn about the shape of the polymer molecule—whether it is spherical, random-coiled, or rodlike. These quantities are difficult to obtain with other methods. Commercial instruments are available.

Figure 2.30 shows a sample geometry. A cylindrical test tube containing a clear polymer solution is immersed in a glass vat filled with a fluid that has a refractive index close to that of the glass. The fluid is called an index-matching liquid and is thermostatted. A coherent, collimated laser beam enters the index-matching liquid through the vat and then into the test tube. Nearly all of the incoming photons travel

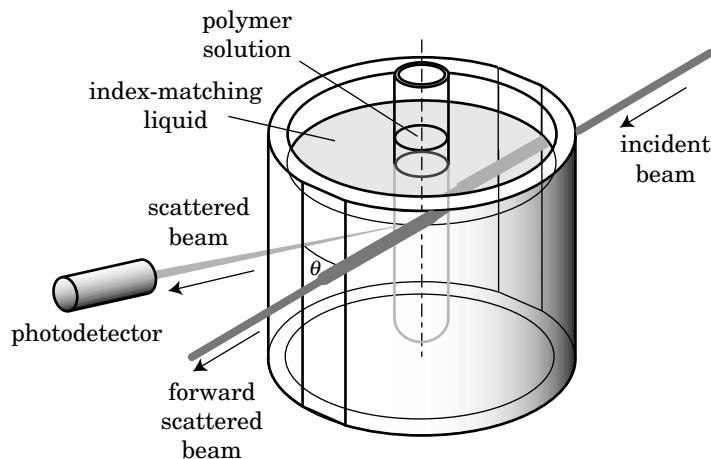


**Figure 2.30.** Schematic of the geometry around a sample cell in a light-scattering measurement system. A photodetector detects the light scattered by a polymer solution in the beam path into a direction at angle  $\theta$  from the forward direction. The vat is filled with an index-matching liquid.

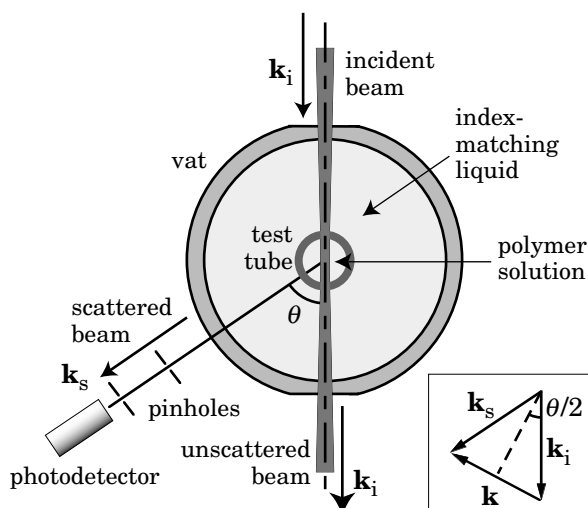
straight through the index-matching liquid and the polymer solution, forming a strong, unscattered (or forward-scattered) beam. The molecules in the beam path scatter a tiny fraction of the photons in all directions. The intensity of the scattered beam is detected by a photodetector, typically a photomultiplier, placed horizontally at an angle  $\theta$  (**scattering angle**) from the forward-scattering direction. To prevent streak scattering at the air-glass interface, the glass vat has a planar cut at each side of the path of the direct beam.

Figure 2.31 is a top view of the sample geometry. The incident beam has a wave vector  $\mathbf{k}_i$ . The **wave vector** is parallel to the propagation direction of the beam and has a magnitude of  $2\pi/(\lambda/n_{\text{sol}})$ , where  $\lambda/n_{\text{sol}}$  is the wavelength of light in the solvent of refractive index  $n_{\text{sol}}$ , with  $\lambda$  being the wavelength of light in vacuum. The wave vector  $\mathbf{k}_s$  of the scattered beam has nearly the same magnitude as that of  $\mathbf{k}_i$ . In the **static light scattering** (often abbreviated as **SLS**) in which the molecules are assumed to be motionless, the two magnitudes are exactly equal. In reality, motions of the molecules make  $\mathbf{k}_s$  different from  $\mathbf{k}_i$ , but the change is so small (typically less than 0.01 ppm) that we can regard  $|\mathbf{k}_i| = |\mathbf{k}_s|$ . The change in the wave vector upon scattering is called the **scattering vector**. The scattering vector  $\mathbf{k}$  is defined as

$$\mathbf{k} \equiv \mathbf{k}_s - \mathbf{k}_i \quad (2.43)$$

The inset of Figure 2.31 allows the magnitude of  $|\mathbf{k}| = k$  to be conveniently calculated as

$$k = \frac{4\pi n_{\text{sol}}}{\lambda} \sin \frac{\theta}{2} \quad \text{scattering wave vector} \quad (2.44)$$



**Figure 2.31.** Top view of the geometry around the sample cell. The wave vector  $\mathbf{k}_i$  of the incident beam changes to  $\mathbf{k}_s$  when scattered. Two pinholes or two slits specify the scattering angle. The inset defines the scattering wave vector  $\mathbf{k}$ .

For the forward-scattered beam,  $k = 0$ . With an increasing  $\theta$ ,  $k$  increases. Figure 2.32 shows how  $k$  changes with  $\theta$  for water ( $n_{\text{sol}} = 1.331$ ) at  $25^\circ\text{C}$  and He-Ne laser ( $\lambda = 632.8$  nm) as a light source and for toluene ( $n_{\text{sol}} = 1.499$ ) at  $25^\circ\text{C}$  and  $\text{Ar}^+$  laser ( $\lambda = 488.0$  nm; there is another strong beam at  $514.5$  nm). For the first system,  $k$  spans from  $3.46 \times 10^6 \text{ m}^{-1}$  at  $\theta = 15^\circ$  to  $2.56 \times 10^7 \text{ m}^{-1}$  at  $\theta = 150^\circ$ .

Two pinholes or two vertical slits are placed along the path of the scattered beam to restrict the photons reaching the detector to those scattered by the molecules in a small part of the solution called the **scattering volume**. The scattering volume is an intersection of the laser beam with the solid angle subtended by the two pinholes (Fig. 2.33).

Polymer molecules, especially those with a high molecular weight, scatter the light strongly. In the following subsections, we will first learn the scattering by small particles and then find why it is strong for the polymer molecules. We will also learn what characteristics of the polymer molecules can be obtained from the scattering pattern.

#### 2.4.2 Scattering by a Small Particle

Small particles (solvent molecules and monomers constituting the polymer) suspended in vacuum can scatter the light. They are called **scatterers**. An electromagnetic wave, also called radiation, enters the isotropic particle to cause polarization in the direction of the electric field of the incident wave (Fig. 2.34). The polarization is a displacement of the spatial average of the positively charged nuclei with



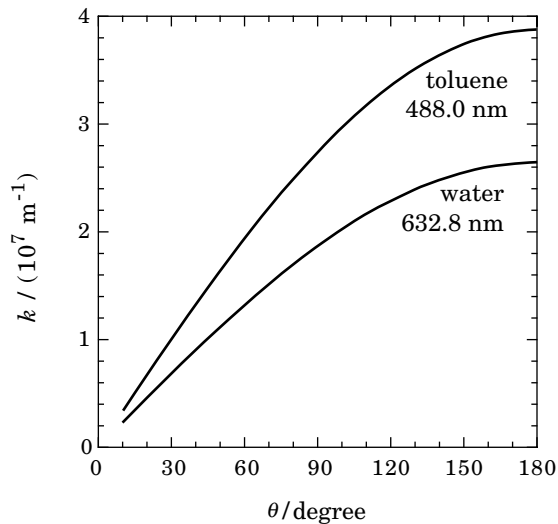


**Figure 2.32.** The magnitude  $k$  of the scattering wave vector plotted as a function of the scattering angle  $\theta$  for water at  $25^\circ\text{C}$  and  $\lambda = 632.8 \text{ nm}$  and for toluene at  $25^\circ\text{C}$  and  $\lambda = 488.0 \text{ nm}$ .

respect to the negatively charged electrons. The polarization, oscillating with the frequency of the radiation, serves as a broadcasting station that emits a weak radiation in all directions. The scattered radiation has the same frequency as that of the incident radiation. This mechanism of scattering is called **Rayleigh scattering**.

Figure 2.34 shows the relationship between the vertically polarized incident beam of intensity  $I_0$  and the radiation scattered by the vertically polarized particle.

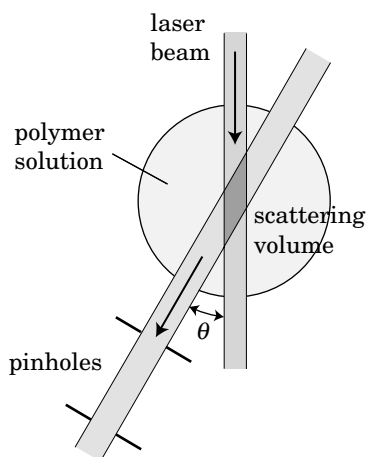


**Figure 2.33.** Scattering volume is an intersection of the laser beam with the solid angle subtended by the two pinholes.

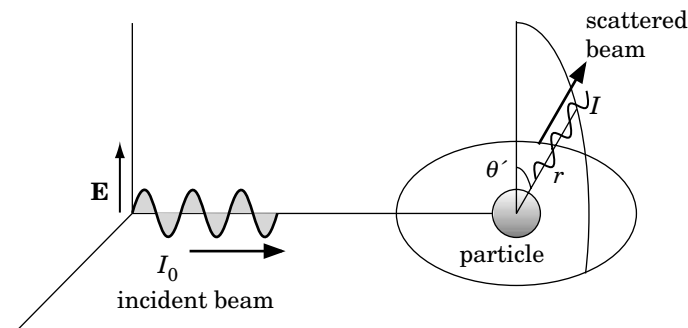


**Figure 2.34.** Vertically polarized beam causes polarization in the particle, which radiates into different directions. Angle  $\theta'$  is defined as the angle between the electric field of the incident beam and the scattering direction. The particle size is drawn much larger than it is relative to the wavelength of light.

At a distance  $r$  from the particle and at angle  $\theta'$  from the vertical, the intensity  $I$  of the scattered light is given by

$$\frac{I}{I_0} = \frac{\pi^2}{\lambda^4} \frac{\alpha^2}{\epsilon_0^2} \frac{\sin^2 \theta'}{r^2} \quad \text{Rayleigh scattering, vacuum} \quad (2.45)$$

where  $\alpha$  is the polarizability of the particle in SI unit and  $\epsilon_0 = 8.854 \times 10^{-12}$  F/m is the electric permittivity of vacuum. Most measurement systems detect the light scattered horizontally and therefore  $\theta' = \pi/2$ .

The polarizability  $\alpha$  is proportional to the volume of the particle. The light scattered by a single atom or a small molecule is too weak to be detected in the visible range of light, even if the volume has many of these particles. A strong scattering by these small particles can occur in the X-ray range, where  $\lambda$  is sufficiently small. To have a strong scattering in the visible range, the volume of the scatterer must be sufficiently large. Then, it is necessary to take into account the interference between the beams scattered by different parts of the scatterer. We will see this effect first for a single polymer chain. The scatterer does not have to be filled like a solid sphere to cause the strong scattering. A string of monomers can also scatter the light strongly.

In Eq. 2.45,  $I/I_0 \propto \lambda^{-4}$ . The Rayleigh scattering is a lot stronger for light of a shorter wavelength. The sky is blue because the scattering is stronger toward the short-wavelength end of the visible spectrum. Each molecule of the atmosphere is too small to scatter the visible light effectively. What we see as the blue sky is due to density fluctuations in the atmosphere.

### 2.4.3 Scattering by a Polymer Chain

Scattering by a larger molecule is stronger, because beams scattered by different parts of the molecule can interfere constructively. We consider here how the

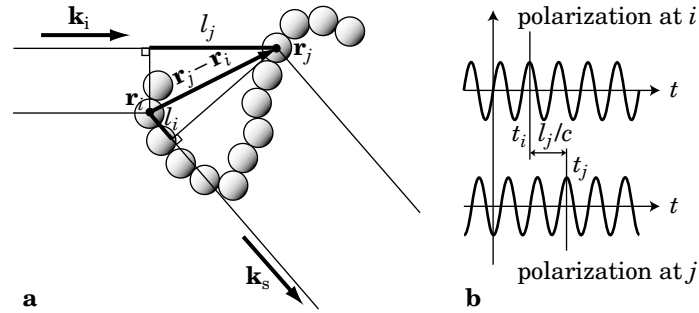


**Figure 2.35.** A polymer chain, on exposure to an incoming plane wave of radiation, scatters light. (a) A beam path for the incoming light and a beam path for the scattered light are drawn for two monomers  $i$  and  $j$  at  $\mathbf{r}_i$  and  $\mathbf{r}_j$  on the chain. The difference in the path length is  $l_j - l_i$ . b: Polarizations at monomers  $i$  and  $j$  as a function of time  $t$ . The phase difference is  $k_i l_j$  in the geometry in a.

**interference** affects the overall scattering intensity for a single polymer chain. We model the chain as a sequence of  $N$  motionless monomers each of which scatters the radiation. Figure 2.35a is a two-dimensional rendering of the polymer chain. The incident light is a plane wave with a wave vector  $\mathbf{k}_i$  and an electric field  $\mathbf{E}_i$  oscillating with an angular frequency  $\omega$  in the direction perpendicular to  $\mathbf{k}_i$  (any direction in the plane perpendicular to  $\mathbf{k}_i$ ). At position  $\mathbf{r}$  and time  $t$ ,  $\mathbf{E}_i$  is given by

$$\mathbf{E}_i = \mathbf{E}_{i0} \exp [i(\mathbf{k}_i \cdot \mathbf{r} - \omega t)] \quad (2.46)$$

where  $\mathbf{E}_{i0}$  is the complex amplitude of the field. The intensity of the light is calculated as the product of  $\mathbf{E}_{i0}$  and its complex conjugate. The photons on a plane perpendicular to  $\mathbf{k}_i$  are assumed to be all in phase (**coherent**). It means that their electric fields oscillate without a delay to each other. A laser beam has a large area of coherence.

These photons enter the monomers to cause polarization on each of them. Because monomers are located at different positions along the beam path, the  $\mathbf{E}_i$  that causes the polarization at a given time is different from monomer to monomer. Therefore, compared at the same time, the phase of the oscillating polarization is different for each monomer. The scattered radiation  $\mathbf{E}_{si}$  caused by the polarization on the  $i$ th monomer at  $\mathbf{r}_i$  at time  $t_i$  and traveling with a wave vector  $\mathbf{k}_s$  is given by

$$\mathbf{E}_{si} = \mathbf{E}_{sm} \exp [i(\mathbf{k}_s \cdot (\mathbf{r} - \mathbf{r}_i) - \omega(t - t_i))] \quad (2.47)$$

where  $\mathbf{E}_{sm}$  is the complex amplitude of the beam scattered by a single monomer and propagating in the direction of  $\mathbf{k}_s$ . Note that  $\mathbf{E}_{si}$  is one of many radiations emanating from the  $i$ th monomer. The same phase of the plane wave that has caused  $\mathbf{E}_{si}$  travels further and causes  $\mathbf{E}_{sj}$  in the same propagation direction as  $\mathbf{E}_{si}$  by polarization of the

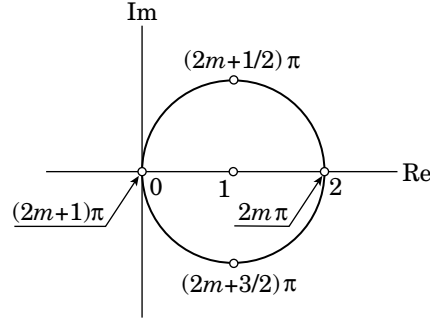


**Figure 2.36.** Real and imaginary parts of  $1 + \exp(i\phi_{ij})$  are shown for  $\phi_{ij}$  as a parameter. When  $\phi_{ij} = 2m\pi$  ( $m = 0, \pm 1, \pm 2, \dots$ ),  $1 + \exp(i\phi_{ij}) = 2$ , and the interference is constructive.

$j$ th monomer at  $\mathbf{r}_j$  at time  $t_j$ :

$$\mathbf{E}_{sj} = \mathbf{E}_{sm} \exp[i(\mathbf{k}_s \cdot (\mathbf{r} - \mathbf{r}_j) - \omega(t - t_j))] \quad (2.48)$$

Figure 2.35b compares the change of the polarizations with time on monomers  $i$  and  $j$ .

The photodetector detects the total amplitude of the radiation scattered by different monomers. The total electric field of the scattered light is  $\mathbf{E}_{s1} + \mathbf{E}_{s2} + \dots + \mathbf{E}_{sN}$ . Before adding all of them, we first consider the sum of  $\mathbf{E}_{si}$  and  $\mathbf{E}_{sj}$ :

$$\mathbf{E}_{si} + \mathbf{E}_{sj} = \mathbf{E}_{sm}[1 + \exp(i\phi_{ij})] \exp[i(\mathbf{k}_s \cdot (\mathbf{r} - \mathbf{r}_i) - \omega(t - t_i))] \quad (2.49)$$

where  $\phi_{ij}$  is the phase difference between the two beams and given as

$$\phi_{ij} \equiv \mathbf{k}_s \cdot (\mathbf{r}_i - \mathbf{r}_j) - \omega(t_i - t_j) \quad (2.50)$$

Now  $\mathbf{E}_{sm}[1 + \exp(i\phi_{ij})]$  is the complex amplitude for  $\mathbf{E}_{si} + \mathbf{E}_{sj}$ . Depending on  $\phi_{ij}$ ,  $1 + \exp(i\phi_{ij})$  can vary widely. This phenomenon is called interference. Figure 2.36 shows how the real and imaginary parts of  $1 + \exp(i\phi_{ij})$  change with  $\phi_{ij}$ . When  $\phi_{ij} = 0, \pm 2\pi, \pm 4\pi, \dots$ , we have  $1 + \exp(i\phi_{ij}) = 2$ , and the amplitude maximizes (constructive interference). When  $\phi_{ij} = \pm\pi, \pm 3\pi, \dots$ , in contrast,  $1 + \exp(i\phi_{ij}) = 0$ , and the amplitude is zero (destructive interference). The interference is in-between at other angles of  $\phi_{ij}$ .

For the chain configuration in Figure 2.35a,

$$\omega(t_j - t_i) = \omega l_j / c = k l_j = k \hat{\mathbf{k}}_i \cdot (\mathbf{r}_j - \mathbf{r}_i) = -\mathbf{k}_i \cdot (\mathbf{r}_i - \mathbf{r}_j) \quad (2.51)$$

where  $c$  is the velocity of light,  $l_j$  is defined in the figure, and  $\hat{\mathbf{k}}_i$  is the unit vector parallel to  $\mathbf{k}_i$ . Thus,

$$\phi_{ij} \equiv (\mathbf{k}_s - \mathbf{k}_i) \cdot (\mathbf{r}_i - \mathbf{r}_j) = \mathbf{k} \cdot (\mathbf{r}_i - \mathbf{r}_j) \quad (2.52)$$

The  $\phi_{ij}$  can also be calculated from the difference in the path length between the two beams reaching the detector. The difference is  $l_j - l_i$  as seen in Figure 2.35a. The corresponding phase difference is  $\phi_{ij} = (\omega/c)(l_j - l_i)$ , which is equal to Eq. 2.52.

For 1 through  $N$  monomers,

$$\sum_{i=1}^N \mathbf{E}_{si} = \mathbf{E}_{sm} \exp[i(\mathbf{k}_s \cdot (\mathbf{r} - \mathbf{r}_1) - \omega(t - t_1))] \sum_{i=1}^N \exp(i\phi_{1i}) \quad (2.53)$$

Thus we find that the complex amplitude of the light scattered by the whole chain is modified by a factor of  $\sum_{i=1}^N \exp(i\phi_{1i})$ . The square of the magnitude of the factor determines how the beams scattered by the  $N$  monomers interfere. Thus the intensity of the light scattered by the whole chain is proportional to

$$\begin{aligned} \left| \sum_{i=1}^N \exp(i\phi_{1i}) \right|^2 &= \sum_{i=1}^N \exp[-i\mathbf{k} \cdot (\mathbf{r}_1 - \mathbf{r}_i)] \sum_{j=1}^N \exp[i\mathbf{k} \cdot (\mathbf{r}_1 - \mathbf{r}_j)] \\ &= \sum_{i,j=1}^N \exp[i\mathbf{k} \cdot (\mathbf{r}_i - \mathbf{r}_j)] \end{aligned} \quad (2.54)$$

If the monomers are isotropic particles with the same polarizability  $\alpha$ , the intensity  $I$  of horizontally scattered light ( $\theta' = \pi/2$  in Eq. 2.45) is

$$\frac{I}{I_0} = \frac{\pi^2}{\lambda^4} \frac{\alpha^2}{\epsilon_0^2} \frac{1}{r^2} \sum_{i,j=1}^N \exp[i\mathbf{k} \cdot (\mathbf{r}_i - \mathbf{r}_j)] \quad (2.55)$$

At low angles,  $\exp[i\mathbf{k} \cdot (\mathbf{r}_i - \mathbf{r}_j)] \cong 1$  and  $I/I_0$  is increased by a factor of  $N^2$  compared with a single monomer. The constructive interference between photons scattered by different parts of the polymer chain causes this  $N^2$  dependence. If each part scatters the light independently, then  $I/I_0$  would increase only by a factor of  $N$ .

#### 2.4.4 Scattering by Many Polymer Chains

The scattering volume contains many polymer chains. We consider here how these chains collectively contribute to the total scattering intensity. We forget for now the presence of solvent molecules as we did in the preceding section and assume that the polymer chains are suspended in vacuum to scatter the light. To obtain the formula for the scattering intensity by a single polymer chain, we did not invoke connectivity of monomers. The formula, Eq. 2.55, can easily be extended to a system of  $n_p$  chains ( $n_p \gg 1$ ), each consisting of  $N$  monomers. We denote by  $\mathbf{r}_{mi}$  the position of the  $i$ th monomer of the  $m$ th chain. Equation 2.54 now reads

$$\begin{aligned} &\sum_{m,n=1}^{n_p} \sum_{i,j=1}^N \exp[i\mathbf{k} \cdot (\mathbf{r}_{mi} - \mathbf{r}_{nj})] \\ &= \sum_{m=1}^{n_p} \sum_{i,j=1}^N \exp[i\mathbf{k} \cdot (\mathbf{r}_{mi} - \mathbf{r}_{mj})] + \sum_{m \neq n=1}^{n_p} \sum_{i,j=1}^N \exp[i\mathbf{k} \cdot (\mathbf{r}_{mi} - \mathbf{r}_{nj})] \end{aligned} \quad (2.56)$$

The first term is a contribution from two monomers on the same chain, and the second term is a contribution from two monomers on different chains. There are various chain configurations occurring simultaneously on different chains. The summations in Eq. 2.56 can therefore be replaced by statistical averages:

$$\begin{aligned} & \sum_{m,n=1}^{n_p} \sum_{i,j=1}^N \exp[i\mathbf{k} \cdot (\mathbf{r}_{mi} - \mathbf{r}_{nj})] \\ &= n_p \sum_{i,j=1}^N \langle \exp[i\mathbf{k} \cdot (\mathbf{r}_{1i} - \mathbf{r}_{1j})] \rangle + n_p^2 \sum_{i,j=1}^N \langle \exp[i\mathbf{k} \cdot (\mathbf{r}_{1i} - \mathbf{r}_{2j})] \rangle \end{aligned} \quad (2.57)$$

where  $n_p(n_p - 1)$  was approximated by  $n_p^2$  in the second term. The average in the first term is taken with a statistical weight of a configuration for a single chain. The average in the second term is taken with a weight of configurations for the two chains. The latter configurations refer to the relative position of the two chains and the monomer arrangement of each chain.

At low concentrations, polymer chains are sufficiently separated from each other. Interference by monomers on different chains are cancelled out on the average; therefore, the second term is negligible compared with the first term. Thus, the scattering intensity  $I(\mathbf{k})$  is given by

$$\frac{I(\mathbf{k})}{I_0} = \frac{\pi^2}{\lambda^4} \frac{\alpha^2}{\varepsilon_0^2} \frac{1}{r^2} n_p \sum_{i,j=1}^N \langle \exp[i\mathbf{k} \cdot (\mathbf{r}_i - \mathbf{r}_j)] \rangle \quad (2.58)$$

where the index “1” was dropped in  $\mathbf{r}_{1i}$ . The summation factor in Eq. 2.58 divided by  $N$  is called the (single-chain) **static structure factor**  $S_1(\mathbf{k})$ :

$$S_1(\mathbf{k}) = \frac{1}{N} \sum_{i,j=1}^N \langle \exp[i\mathbf{k} \cdot (\mathbf{r}_i - \mathbf{r}_j)] \rangle \quad \text{single-chain static structure factor} \quad (2.59)$$

In the absence of constructive interference between different monomers, only terms with  $i = j$  would survive and therefore  $S_1(\mathbf{k})$  would be equal to 1. The interference makes  $S_1(\mathbf{k})$  and  $I(\mathbf{k})$  depend on  $\mathbf{k}$ . With  $S_1(\mathbf{k})$ , Eq. 2.58 becomes to  $I(\mathbf{k})/I_0 = (\pi^2/\lambda^4)(\alpha/\varepsilon_0)^2 r^{-2} n_p N S_1(\mathbf{k})$ . Note that uncorrelated  $n_p N$  monomers in solution have  $I(\mathbf{k})/I_0 = (\pi^2/\lambda^4)(\alpha/\varepsilon_0)^2 r^{-2} n_p N$ . Thus we find that  $S_1(\mathbf{k})$  indicates how much the interference from different parts of the chain increases  $I(\mathbf{k})$ .

The static structure factor (also called **scattering function**) that applies also to finite concentrations is obtained from Eq. 2.57 as

$$\begin{aligned} S(\mathbf{k}) &= \frac{1}{n_p N} \sum_{m,n=1}^{n_p} \sum_{i,j=1}^N \langle \exp[i\mathbf{k} \cdot (\mathbf{r}_{mi} - \mathbf{r}_{nj})] \rangle \\ &= S_1(\mathbf{k}) + \frac{n_p}{N} \sum_{i,j=1}^N \langle \exp[i\mathbf{k} \cdot (\mathbf{r}_{1i} - \mathbf{r}_{2j})] \rangle \end{aligned} \quad (2.60)$$

The second term is due to correlations between different chains. Note that chains 1 and 2 have to be nearby to scatter beams that interfere constructively. At low

concentrations, the statistical average for different chains is mostly zero, and  $S(\mathbf{k})$  becomes identical to  $S_1(\mathbf{k})$ . The interference between different chains becomes more significant with an increasing concentration.

## 2.4.5 Correlation Function and Structure Factor

**2.4.5.1 Correlation Function** We now find how the structure factor is related to the local **segment density**  $\rho(\mathbf{r})$  defined by

$$\rho(\mathbf{r}) = \sum_{m,i} \delta(\mathbf{r} - \mathbf{r}_{mi}) \quad (2.61)$$

The segment density (monomer density) counts the number of monomers per unit volume locally. Integration of the right-hand side over the entire volume gives  $n_p N$ , which is the total number of monomers in volume  $V$ , as it should be. Thus  $\rho = \langle \rho(\mathbf{r}) \rangle = n_p N / V$  is the global segment density. Mathematically,  $\rho(\mathbf{r})$  itself can be a continuous distribution, although the definition given here is for a discrete distribution of the monomers.

The **pair distribution function** is the statistical average of the product of the densities at  $\mathbf{r}_1$  and  $\mathbf{r}_2$ :

$$\langle \rho(\mathbf{r}_1) \rho(\mathbf{r}_2) \rangle = \sum_{m,n=1}^{n_p} \sum_{i,j=1}^N \left\langle \sum_{m,i} \delta(\mathbf{r}_1 - \mathbf{r}_{mi}) \sum_{n,j} \delta(\mathbf{r}_2 - \mathbf{r}_{nj}) \right\rangle = \langle \rho(\mathbf{r}_1 - \mathbf{r}_2) \rho(0) \rangle \quad (2.62)$$

where the last equality holds for a macroscopically homogeneous solution (the system can be microscopically heterogeneous, but after taking statistical average, the system gains a translational symmetry). The pair distribution function depends on  $\mathbf{r}_1 - \mathbf{r}_2$ . Then,  $\langle \rho(\mathbf{r}) \rho(0) \rangle$  is called the **autocorrelation function** (or **correlation function**) of the segment density.

When the solution is isotropic in addition,  $\langle \rho(\mathbf{r}) \rho(0) \rangle = \langle \rho(r) \rho(0) \rangle$  is a function of the distance  $r = |\mathbf{r}|$  only.

### 2.4.5.2 Relationship Between the Correlation Function and Structure Factor

The statistical average in the definition of the structure factor  $S(\mathbf{k})$  in Eq. 2.60 is taken with respect to the pair distribution. With Eq. 2.62, Eq. 2.60 is rewritten to

$$\begin{aligned} S(\mathbf{k}) &= \frac{1}{n_p N} \int_V d\mathbf{r}_1 \int_V d\mathbf{r}_2 \sum_{m,n=1}^{n_p} \sum_{i,j=1}^N \left\langle \sum_{m,i} \delta(\mathbf{r}_1 - \mathbf{r}_{mi}) \sum_{n,j} \delta(\mathbf{r}_2 - \mathbf{r}_{nj}) \right\rangle \exp[i\mathbf{k} \cdot (\mathbf{r}_1 - \mathbf{r}_2)] \\ &= \frac{1}{n_p N} \int_V d\mathbf{r}_1 \int_V d\mathbf{r}_2 \langle \rho(\mathbf{r}_1) \rho(\mathbf{r}_2) \rangle \exp[i\mathbf{k} \cdot (\mathbf{r}_1 - \mathbf{r}_2)] \\ &= \frac{V}{n_p N} \int_V \langle \rho(\mathbf{r}) \rho(0) \rangle \exp(i\mathbf{k} \cdot \mathbf{r}) d\mathbf{r} \end{aligned} \quad (2.63)$$

With the average density  $\rho = n_p N/V$ , Eq. 2.63 leads to

$$S(\mathbf{k}) = \frac{1}{\rho} \int_V \langle \rho(\mathbf{r})\rho(0) \rangle \exp(i\mathbf{k} \cdot \mathbf{r}) d\mathbf{r} \quad \begin{array}{l} \text{static structure factor} \\ \text{by segment correlation} \end{array} \quad (2.64)$$

Note that  $\rho(0)/\rho$  is the segment density at  $\mathbf{r} = 0$  normalized by the average. We can therefore interpret  $\langle \rho(\mathbf{r})\rho(0) \rangle/\rho$  as measuring the average number of monomers per volume at  $\mathbf{r}$  when there is already a monomer at  $\mathbf{r} = 0$ .

Equation 2.64 illustrates that the static structure factor, and hence the scattering pattern obtained in the light-scattering experiments, is the **Fourier transform** (see Appendix A2) of the autocorrelation function of the local segment density.  $S(\mathbf{k})$  indicates which wave vector components are present in the correlation function.

If the local segment density were continuously distributed at a uniform density  $\rho$ , then  $\langle \rho(\mathbf{r})\rho(0) \rangle/\rho = \rho$  and  $S(\mathbf{k}) = (2\pi)^3 \rho \delta(\mathbf{k})$ . A uniform medium does not scatter the light at all (or forward scattering only). Another view is that  $S(\mathbf{k})$  is essentially the average of  $\exp[i\mathbf{k} \cdot (\mathbf{r}_1 - \mathbf{r}_2)]$  weighted with the pair distribution function  $\langle \rho(\mathbf{r}_1)\rho(\mathbf{r}_2) \rangle$ .

If  $N = 1$  (only nonbonded small particles are present) and correlation between scatterers is absent, that is,  $\langle \rho(\mathbf{r})\rho(0) \rangle/\rho = \delta(\mathbf{r})$ , then  $S(\mathbf{k}) = 1$ . The scattering is uniform at all angles. This pattern is observed in the scattering by a solvent. The wavelength  $\lambda$  of visible light is too long to detect any correlations among small particles. On the length scale of  $\lambda$ ,  $\langle \rho(\mathbf{r})\rho(0) \rangle/\rho = \delta(\mathbf{r})$ .

From Eq. A2.7, we find that the inverse-Fourier transform of  $S(\mathbf{k})$  gives the correlation function of the segment density:

$$\langle \rho(\mathbf{r})\rho(0) \rangle = \frac{\rho}{(2\pi)^3} \int S(\mathbf{k}) \exp(-i\mathbf{k} \cdot \mathbf{r}) d\mathbf{k} \quad \text{segment density correlation} \quad (2.65)$$

In the isotropic solution, the above Fourier transform and inverse-Fourier transform are

$$S(\mathbf{k}) = \frac{4\pi}{\rho} \int_0^\infty \langle \rho(r)\rho(0) \rangle \frac{\sin kr}{kr} r^2 dr \quad \text{isotropic} \quad (2.66)$$

$$\langle \rho(r)\rho(0) \rangle = \frac{\rho}{2\pi^2} \int_0^\infty S(k) \frac{\sin kr}{kr} k^2 dk \quad \text{isotropic} \quad (2.67)$$

In practice, the relationships between the structure factor and the local monomer concentration  $c(\mathbf{r})$  are more useful. The local concentration is related to  $\rho(\mathbf{r})$  by

$$c(\mathbf{r}) = \frac{M}{N_A N} \sum_{m,i} \delta(\mathbf{r} - \mathbf{r}_{mi}) = \frac{M}{N_A N} \rho(\mathbf{r}) \quad (2.68)$$



where  $M$  is the molecular weight of the polymer chain. The relationships between  $S(\mathbf{k})$  and  $c(\mathbf{r})$  are

$$S(\mathbf{k}) = \frac{N_A N}{cM} \int_V \langle c(\mathbf{r})c(0) \rangle \exp(i\mathbf{k} \cdot \mathbf{r}) d\mathbf{r} \quad (2.69)$$

where  $c = \langle c \rangle = Mn_p/(N_A V)$  is the average concentration, and

$$\langle c(\mathbf{r})c(0) \rangle = \frac{cM}{(2\pi)^3 N_A N} \int S(\mathbf{k}) \exp(-i\mathbf{k} \cdot \mathbf{r}) d\mathbf{k} \quad (2.70)$$

**2.4.5.3 Examples in One Dimension** Before leaving this subsection, we look at the relationship between the density autocorrelation function and the structure factor for some examples in one-dimensional isotropic systems. Figure 2.37 shows four pairs of  $\langle \rho(x)\rho(0) \rangle$  and  $S(k)$ . Isotropy makes the autocorrelation function an even function of  $x$ .

In panel a,  $\langle \rho(x)\rho(0) \rangle$  is a constant plus a cosine function with a period of  $a$ . This correlation function is observed when  $\rho(x)$  changes sinusoidally. The Fourier transform converts the constant into  $\delta(k)$  and  $\cos(2\pi x/a)$  into  $\delta(k - 2\pi/a)$ . In part b,  $\langle \rho(x)\rho(0) \rangle$  has a harmonic at  $k = 4\pi/a$ . The density correlation is slightly distorted from the cosine function.

Panel c shows  $\langle \rho(x)\rho(0) \rangle$  that consists of more harmonics with a fundamental wave vector being 1/4 of that shown in panels a and b.  $\langle \rho(x)\rho(0) \rangle$  has a period equal to the window of  $x$  shown, but, within the period, it looks like a decaying

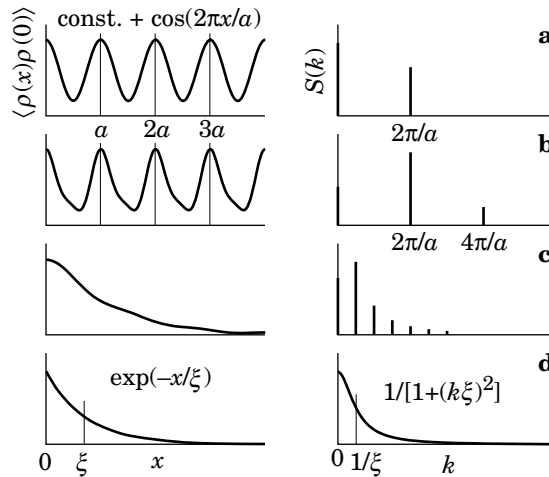


**Figure 2.37.** Segment density autocorrelation function  $\langle \rho(x)\rho(0) \rangle$  and structure factor  $S(k)$  for four examples of distribution in one dimension. The autocorrelation functions are cosine + constant (a), with a harmonic (b), with more harmonics (c), and exponential decay (d).

function. Panel d is for an exponentially decaying autocorrelation function with a **correlation length**  $\xi$  for all  $x \geq 0$ . Its Fourier transform is a Lorentzian:  $1/[1 + (k\xi)^2]$ . We notice that  $\langle \rho(x)\rho(0) \rangle$  and  $S(k)$  in panel c resemble the counterparts in panel d. In fact, we can construct  $\exp(-x/\xi)$  by overlapping many cosine functions as in panel c.  $S(k) \propto 1/[1 + (k\xi)^2]$  tells how to overlap these cosine functions of different  $k$ .

In the following subsections, we will examine the scattering from polymer chains in three dimensions. Chain connectivity gives rise to a specific pattern in the correlation and the scattering, depending on the conformation.

## 2.4.6 Structure Factor of a Polymer Chain

**2.4.6.1 Low-Angle Scattering** At low scattering angles, that is, when  $k$  is small,

$$\exp[i\mathbf{k} \cdot (\mathbf{r}_i - \mathbf{r}_j)] \cong 1 + i\mathbf{k} \cdot (\mathbf{r}_i - \mathbf{r}_j) - \frac{1}{2}[\mathbf{k} \cdot (\mathbf{r}_i - \mathbf{r}_j)]^2 + \cdots \quad (2.71)$$

Then, Eq. 2.59 is rewritten to

$$S_1(\mathbf{k}) = N - \frac{1}{2N} \sum_{i,j=1}^N \langle [\mathbf{k} \cdot (\mathbf{r}_i - \mathbf{r}_j)]^2 \rangle + \cdots \quad (2.72)$$

where  $\langle \mathbf{r}_i - \mathbf{r}_j \rangle = 0$  was used. In this equation,

$$\langle [\mathbf{k} \cdot (\mathbf{r}_i - \mathbf{r}_j)]^2 \rangle = k^2 \langle [\hat{\mathbf{k}} \cdot (\mathbf{r}_i - \mathbf{r}_j)]^2 \rangle = k^2 \langle (x_i - x_j)^2 \rangle = \frac{1}{3} k^2 \langle (\mathbf{r}_i - \mathbf{r}_j)^2 \rangle \quad (2.73)$$

where  $\hat{\mathbf{k}} = \mathbf{k}/k$ , and the  $x$  direction is taken to be parallel to  $\mathbf{k}$ . The isotropy of the chain configuration [ $\langle (x_i - x_j)^2 \rangle = \langle (y_i - y_j)^2 \rangle = \langle (z_i - z_j)^2 \rangle$ ] was used in the last equality. Thus  $S_1(\mathbf{k})$  is further converted to

$$S_1(\mathbf{k}) = N - k^2 \frac{1}{6N} \sum_{i,j=1}^N \langle (\mathbf{r}_i - \mathbf{r}_j)^2 \rangle + \cdots = N(1 - k^2 R_g^2/3 + \cdots) \quad (2.74)$$

where Eq. 1.25 ( $N \gg 1$ ) was used. It is usually rewritten to

$$S_1(\mathbf{k}) \cong \frac{N}{1 + k^2 R_g^2/3} \quad kR_g < 1, \text{ any conformation} \quad (2.75)$$

The last expression compensates the neglect of the higher-order terms in Eq. 2.72 to some extent.

We did not assume any specific chain conformation or a chain model to derive Eqs. 2.74 and 2.75. The formulas apply to any chain conformation. When the reciprocal of the light-scattering intensity is plotted as a function of  $k^2$ , the slope in the small  $k$  limit is equal to  $R_g^2/3$ , as illustrated in Figure 2.38.

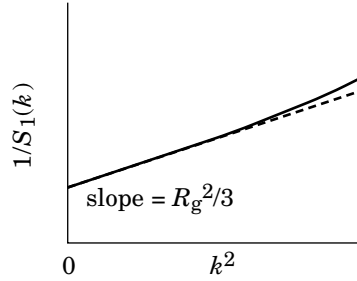


**Figure 2.38.** Reciprocal of the single-chain structure factor  $S_1(k)$  plotted as a function of the square of the scattering vector  $k$  has a slope equal to  $R_g^2/3$  at low angles.

**2.4.6.2 Scattering by a Gaussian Chain** It is possible to calculate  $S_1(\mathbf{k})$  in the whole range of  $k$  for a Gaussian chain without approximations. A continuous version of Eq. 2.59 is needed for the definition of  $S_1(\mathbf{k})$ .

$$S_1(\mathbf{k}) = \frac{1}{N} \int_0^N dn \int_0^N dn' \langle \exp[i\mathbf{k} \cdot (\mathbf{r} - \mathbf{r}')] \rangle \quad (2.76)$$

where the statistical average in the integrand is taken with respect to  $\mathbf{r}$  and  $\mathbf{r}'$ , the spatial positions of the segments at distance  $n$  and  $n'$ , respectively, from the chain end (Fig. 2.39). Because a partial chain between the two segments is also a Gaussian chain (see Section 1.3 and Eq. 1.34),

$$\begin{aligned} \langle \exp[i\mathbf{k} \cdot (\mathbf{r} - \mathbf{r}')] \rangle &= \int d(\mathbf{r} - \mathbf{r}') \exp[i\mathbf{k} \cdot (\mathbf{r} - \mathbf{r}')] (2\pi|n - n'|b^2/3)^{-3/2} \\ &\quad \times \exp\left(-\frac{3(\mathbf{r} - \mathbf{r}')^2}{2|n - n'|b^2}\right) \\ &= \exp(-\frac{1}{6}\mathbf{k}^2|n - n'|b^2) \end{aligned} \quad (2.77)$$

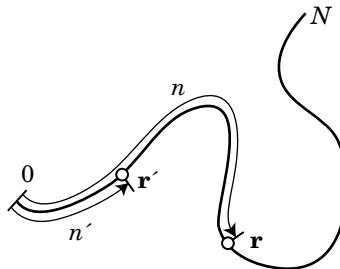


**Figure 2.39.** Scattering by two monomers at  $\mathbf{r}'$  and  $\mathbf{r}$  at distances  $n'$  and  $n$  along the chain from its end interferes.

which is essentially the Fourier-transform of the Gaussian probability density. Because the probability density is isotropic, its Fourier transform is also isotropic. The double integral with respect to  $n$  and  $n'$  leads to

$$S_1(\mathbf{k}) = \frac{1}{N} \int_0^N dn \int_0^N dn' \exp\left(-\frac{1}{6} \mathbf{k}^2 |n - n'| b^2\right) = N f_D(kR_g) \quad (2.78)$$

where  $f_D(x)$  is called a Debye function and defined as

$$f_D(x) = 2x^{-2} \left[ 1 - x^{-2} \left( 1 - \exp(-x^2) \right) \right] \quad \text{Debye function, Gaussian} \quad (2.79)$$

At  $x \gg 1$ ,  $f_D(x) \cong 2x^{-2}$ . At  $x \ll 1$ ,  $f_D(x) \cong 1 - x^2/3$ , in agreement with Eq. 2.74. Figure 2.40 shows  $N/S_1(\mathbf{k}) = N/S_1(k) = [f_D(kR_g)]^{-1}$  as a function of  $kR_g$ . The slope is  $1/3$  at low scattering angles and  $1/2$  at high angles.

The density autocorrelation function for two segments on the Gaussian chain is given as

$$\frac{1}{\rho} \langle \rho(\mathbf{r}) \rho(\mathbf{r}') \rangle = \frac{1}{N} \int_0^N dn \int_0^N dn' (2\pi |n - n'| b^2/3)^{-3/2} \exp\left(-\frac{3(\mathbf{r} - \mathbf{r}')^2}{2|n - n'| b^2}\right) \quad (2.80)$$

After some calculations (see Appendix 2.C), Eq. 2.80 with  $\mathbf{r}' = 0$  simplifies to

$$\frac{1}{\rho} \langle \rho(\mathbf{r}) \rho(0) \rangle = \frac{N}{\pi^{3/2}} \frac{1}{rR_g^2} \left[ (1 + 2u) \text{Erfc}(u^{1/2}) - u^{1/2} \exp(-u) \right] \quad (2.81)$$

where  $u = (r/2R_g)^2$  and the error function  $\text{Erfc}(x)$  is defined by

$$\text{Erfc}(x) \equiv \int_x^\infty \exp(-t^2) dt \quad (2.82)$$

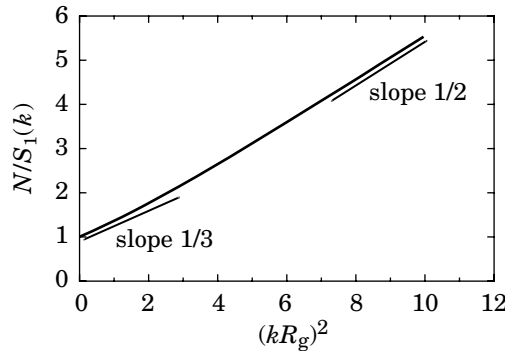


**Figure 2.40.** Reciprocal of the static structure factor  $S_1(k)$  of a Gaussian chain.  $N/S_1(k)$  is a linear function of  $k^2$  at both  $kR_g \ll 1$  and  $kR_g \gg 1$  but with different slopes.

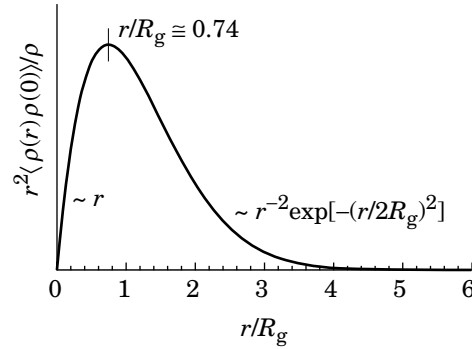


**Figure 2.41.** Probability distribution for the distance  $r$  of other segments from a given segment in a Gaussian chain. The segment density autocorrelation function  $\langle\rho(r)\rho(0)\rangle/\rho$  multiplied by  $r^2$  is plotted as a function of  $r/R_g$ . Short-distance and long-distance asymptotes are indicated.

Now we examine  $\langle\rho(r)\rho(0)\rangle/\rho$  in the small  $r$  and large  $r$  asymptotes. When  $x \ll 1$ ,  $\text{Erfc}(x) \cong \pi^{1/2}/2 - x$ . Then, at short distances,

$$\frac{1}{\rho} \langle\rho(r)\rho(0)\rangle = \frac{N}{2\pi} \frac{1}{rR_g^2} \quad (2.83)$$

This relationship can also be intuitively obtained in the following discussion. When  $r < R_g$ , a partial chain of  $n$  segments is contained in the sphere of a radius  $r = bn^{1/2}/2$ . The average segment density within the sphere is

$$\frac{1}{\rho} \langle\rho(r)\rho(0)\rangle = \frac{n}{(4\pi/3)r^3} = \frac{3}{\pi r b^2} = \frac{N}{2\pi} \frac{1}{rR_g^2} \quad (2.84)$$

When  $x \gg 1$ ,  $\text{Erfc}(x) \cong \exp(-x^2)[1/(2x) - 1/(4x^3) + 3/(8x^5)]$ . Thus, over long distances, the correlation is lost exponentially:

$$\frac{1}{\rho} \langle\rho(r)\rho(0)\rangle = \frac{4N}{\pi^{3/2}} \frac{R_g}{r^4} \exp[-(r/2R_g)^2] \quad (2.85)$$

Figure 2.41 is a plot of  $r^2\langle\rho(r)\rho(0)\rangle/\rho$ . The prefactor  $r^2$  is for the surface area of the sphere of radius  $r$ . Note that  $4\pi r^2\langle\rho(r)\rho(0)\rangle/\rho dr$  is the probability of finding another segment at distance between  $r$  and  $r + dr$  from a given segment for this isotropic autocorrelation function. When  $r \ll R_g$ ,  $r^2\langle\rho(r)\rho(0)\rangle/\rho$  is proportional to  $r$ . When  $r \gg R_g$ ,  $r^2\langle\rho(r)\rho(0)\rangle/\rho \sim r^{-2} \exp[-(r/2R_g)^2]$ . The probability peaks at  $r/R_g \cong 0.74$ . The other segments can be most probably found at a distance of  $r \cong 0.74 \times R_g$ .

**2.4.6.3 Scattering by a Real Chain** At low-scattering angles,  $S_1(\mathbf{k})$  of a real chain is essentially the same as that of the Gaussian chain when plotted as a function of  $R_g$ , as we have seen in Section 2.4.6.1. At high angles, however,  $S_1(\mathbf{k})$  of the real chain does not follow  $k^{-2}$  dependence. Intuitively,  $S_1(\mathbf{k})$  at large  $\mathbf{k}$  can be obtained from the pair distribution function of two segments within a sphere of radius  $R_g$ . For the real chain with  $r \cong bn^\nu$ , Eq. 2.84 changes to

$$\frac{1}{\rho} \langle \rho(\mathbf{r})\rho(0) \rangle \cong \frac{n}{r^3} = r^{1/\nu-3} b^{-1/\nu} \quad (r < R_g) \quad (2.86)$$

The correlation decays as  $r^{-4/3}$  (or  $r^{-1.31}$ ) with an increasing  $r$  at short distances in a real chain, as opposed to  $r^{-1}$  in the Gaussian chain. Figure 2.42 compares  $r^2 \langle \rho(r)\rho(0) \rangle$  for the real chain obtained in the computer simulation<sup>20</sup> and the Gaussian chain. What is plotted here is  $r^2 \langle \rho(r)\rho(0) \rangle$ , which is proportional to the probability of finding a segment at  $r$  from another segment at  $\mathbf{r} = 0$ . At  $r \ll R_g$ , the real chain has a slightly higher value ( $r^{0.69}$  vs.  $r^1$ ). The peak position relative to  $R_g$  is greater for the real chain. The monomers are more spread in the real chain. However, the difference is small.

The Fourier transform of Eq. 2.86 by Eq. 2.66 gives

$$S_1(k) \cong \frac{4\pi}{k} b^{-1/\nu} \int r^{1/\nu-2} \sin kr \, dr \quad (2.87)$$

The integrand is valid only for  $r < R_g$ , but, at large  $k$  ( $kR_g \gg 1$ ),  $\sin kr$  is a rapidly varying function, especially for large  $r$  ( $r > R_g$ ). Therefore, the contribution of the integral from  $r > R_g$  is negligible, and we can use the same integrand from

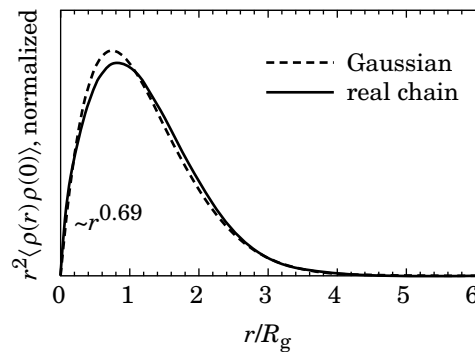


**Figure 2.42.** Comparison of  $r^2 \langle \rho(r)\rho(0) \rangle$  for a real chain and a Gaussian chain. At short distance, the real chain follows a power law of  $r^{0.69}$ , as opposed to  $r^1$  for the Gaussian chain.

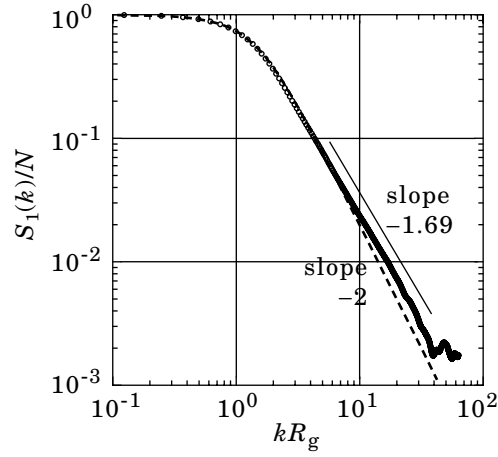


**Figure 2.43.** Comparison of  $S_1(k)$  of a self-avoiding walk on a cubic lattice obtained in computer simulation with a Debye function. When  $S_1(k)/N$  is plotted as a function of  $kR_g$ , the Debye function describes  $S_1(k)$  of a self-avoiding walk at low angles, but they have different dependences at high angles. The self-avoiding walk follows the power law of  $S_1 \sim k^{-1.69}$  as predicted by the theory. (From Ref. 5.)

$r = 0$  to  $\infty$ :

$$\begin{aligned} S_1(k) &= \frac{4\pi}{k} b^{-1/\nu} \int_0^\infty r^{1/\nu-2} \sin kr dr \\ &= \frac{4\pi}{k} b^{-1/\nu} \frac{\Gamma(1/\nu-1)}{k^{1/\nu-1}} \sin \frac{(1/\nu-1)\pi}{2} \cong \frac{1}{(kb)^{1/\nu}} \end{aligned} \quad (2.88)$$

See Appendix A3. At high angles,  $S_1(\mathbf{k}) \sim k^{-1/\nu} \cong k^{-5/3}$ .

Figure 2.43 compares  $S_1(\mathbf{k})/N = S_1(k)/N$  obtained in the cubic lattice Monte Carlo simulations for a real chain and the Debye function.<sup>5</sup> At  $kR_g < 1$ ,  $S_1(k)/N$  of the real chain follows the Debye function, but, at large  $kR_g$ ,  $S_1(k)/N$  deviates from the Debye function (slope  $-2$ ) and follows  $\sim k^{-1.69}$  as predicted.

**2.4.6.4 Form Factors** The plot of  $S_1(\mathbf{k})$  as a function of  $k^2$  at small  $k$  gives the radius of gyration for any conformation, but, beyond that range,  $S_1(\mathbf{k})$  depends on the conformation. For a Gaussian chain,  $S_1(\mathbf{k})$  follows the Debye function. Equations 2.59 and 2.76 allow us to calculate  $S_1(\mathbf{k})$  for other conformations. Let us first define a **form factor**  $P(\mathbf{k})$  by

$$P(\mathbf{k}) \equiv \frac{S_1(\mathbf{k})}{S(0)} = \frac{1}{N} S_1(\mathbf{k}) \quad \text{form factor} \quad (2.89)$$

It is also called a shape factor or an internal structure factor. For a Gaussian chain, it is

$$P_{\text{Gaussian}}(\mathbf{k}) = f_D(kR_g) \quad (2.90)$$

Let us calculate  $P(\mathbf{k})$  for a spherical molecule of radius  $R_s$  stuffed uniformly with monomers that scatter light with the same intensity. Now we use Eq. 2.76 to directly integrate with respect to  $\mathbf{r}$  and  $\mathbf{r}'$  in the sphere:

$$P_{\text{sphere}}(\mathbf{k}) = \frac{1}{V_{\text{sp}}^2} \int_{V_{\text{sp}}} \mathbf{dr} \int_{V_{\text{sp}}} \mathbf{dr}' \exp[i\mathbf{k} \cdot (\mathbf{r} - \mathbf{r}')] = \left| \frac{1}{V_{\text{sp}}^2} \int_{V_{\text{sp}}} \mathbf{dr} \exp(i\mathbf{k} \cdot \mathbf{r}) \right|^2 \quad (2.91)$$

where the integral is carried out over the volume  $V_{\text{sp}} = (4\pi/3)R_s^3$  of the sphere. After some calculations (Problem 2.19), we find that

$$P_{\text{sphere}}(\mathbf{k}) = [3x^{-3}(\sin x - x \cos x)]^2 \quad \text{with } x = kR_s \quad (2.92)$$

For a rodlike molecule with length  $L$ , it can be shown that (Problem 2.20)

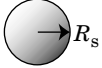
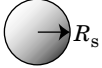
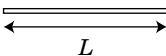
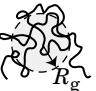
$$P_{\text{rod}}(\mathbf{k}) = x^{-1} \int_0^{2x} \frac{\sin z}{z} dz - \left( \frac{\sin x}{x} \right)^2 \quad \text{with } x = kL/2 \quad (2.93)$$

Figure 2.44 summarizes  $P(\mathbf{k}) = P(k)$  for three polymer conformations of a simple geometry. Figure 2.45 compares  $P_{\text{Gaussian}}(k)$ ,  $P_{\text{sphere}}(k)$ , and  $P_{\text{rod}}(k)$  plotted as a function of  $kR_g$ . The three factors are identical for  $kR_g \ll 1$  as required. At higher  $kR_g$ , the three curves are different.

We now calculate the form factor  $P_{\text{star}}(k)$  for an  $n_A$ -arm star polymer with a uniform arm length  $N_1$ . When calculating the average of  $\exp[i\mathbf{k} \cdot (\mathbf{r} - \mathbf{r}')]$ , it is necessary to distinguish two cases for  $\mathbf{r}$  and  $\mathbf{r}'$ : (1) being on the same arm and (2) being on different arms. The former takes place with a probability of  $1/n_A$ . Then,

$$P_{\text{star}}(\mathbf{k}) = \frac{1}{n_A} \langle\langle \exp[i\mathbf{k} \cdot (\mathbf{r} - \mathbf{r}')] \rangle\rangle_1 + \left( 1 - \frac{1}{n_A} \right) \langle\langle \exp[i\mathbf{k} \cdot (\mathbf{r} - \mathbf{r}')] \rangle\rangle_2 \quad (2.94)$$

where the subscripts 1 and 2 correspond to the two cases, and  $\langle\langle \exp[i\mathbf{k} \cdot (\mathbf{r} - \mathbf{r}')] \rangle\rangle$  stands for the average of  $\langle \exp[i\mathbf{k} \cdot (\mathbf{r} - \mathbf{r}')] \rangle$  with respect to the two monomers over

shape		$R_g^2$	$x$	$P(\mathbf{k})$
spherical		$(3/5)R_s^2$	$kR_s$	$[3x^{-3}(\sin x - x \cos x)]^2$
rodlike		$L^2/12$	$kL/2$	$x^{-1} \int_0^{2x} z^{-1} \sin z dz - (x^{-1} \sin x)^2$
Gaussian		$b^2 N/6$	$kR_g$	$2x^{-2}[1 - x^{-2}(1 - \exp(-x^2))]$

**Figure 2.44.** Polymers with a simple geometry and their form factors.



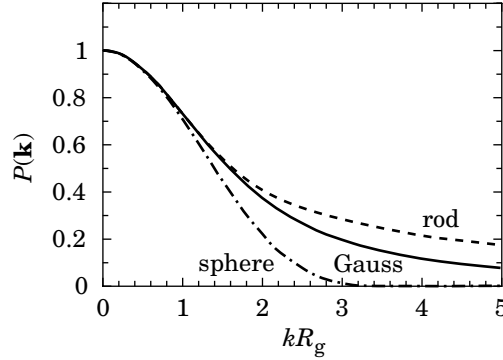


**Figure 2.45.** Form factor  $P(k)$  for a spherical molecule, a rodlike molecule, and a Gaussian chain, plotted as a function of  $kR_g$ .

the length of the arm(s). Using, Eq. 2.78, we have

$$\langle\langle \exp[i\mathbf{k} \cdot (\mathbf{r} - \mathbf{r}')] ] \rangle\rangle_1 = f_D(kR_{g1}) \quad (2.95)$$

where  $R_{g1}^2 = N_1 b^2 / 6 = R_g^2 / (3 - 2/n_A)$  is the mean square radius of gyration of the arm, with  $R_g$  being the radius of gyration of the whole star polymer (see Eq. 1.84). In the second average,

$$\begin{aligned} \langle\langle \exp[i\mathbf{k} \cdot (\mathbf{r} - \mathbf{r}')] ] \rangle\rangle_2 &= \langle\langle \exp[i\mathbf{k} \cdot (\mathbf{r} - \mathbf{r}_0) + i\mathbf{k} \cdot (\mathbf{r}_0 - \mathbf{r}')] ] \rangle\rangle \\ &= \langle\langle \exp[i\mathbf{k} \cdot (\mathbf{r} - \mathbf{r}_0)] \rangle\rangle \langle\langle \exp[i\mathbf{k} \cdot (\mathbf{r}_0 - \mathbf{r}')] ] \rangle\rangle = |\langle\langle \exp[i\mathbf{k} \cdot (\mathbf{r} - \mathbf{r}_0)] \rangle\rangle|^2 \end{aligned} \quad (2.96)$$

where  $\mathbf{r}_0$  is the position of the core of the star polymer, and the average in the last equation is calculated for a single arm as

$$\begin{aligned} \langle\langle \exp[i\mathbf{k} \cdot (\mathbf{r} - \mathbf{r}_0)] \rangle\rangle &= \frac{1}{N_1} \int_0^{N_1} dn \langle \exp[i\mathbf{k} \cdot (\mathbf{r} - \mathbf{r}_0)] \rangle \\ &= \frac{1}{N_1} \int_0^{N_1} dn \exp(-\frac{1}{6} k^2 n b^2) = (kR_{g1})^{-2} [1 - \exp(-(kR_{g1})^2)] \end{aligned} \quad (2.97)$$

Thus,

$$P_{\text{star}}(k) = \frac{1}{n_A} f_D(kR_{g1}) + \left(1 - \frac{1}{n_A}\right) \left( (kR_{g1})^{-2} [1 - \exp(-(kR_{g1})^2)] \right)^2 \quad (2.98)$$

The difference in  $P_{\text{star}}(k)$  between a 2-arm star (= linear chain) and a 6-arm star is not as striking as the difference between a Gaussian chain and a rodlike molecule. At low  $kR_g$ , all the curves overlap (not shown), as required. At  $kR_{g1} \gg 1$ , the second term becomes negligible, and the scattering comes mostly from two nearby monomers on the same arm. The difference in  $P_{\text{star}}(k)$  is, however, clearly seen in the plot of  $(kR_g)^2 P_{\text{star}}(k)$  as a function of  $kR_g$ . Figure 2.46 compares the form factor

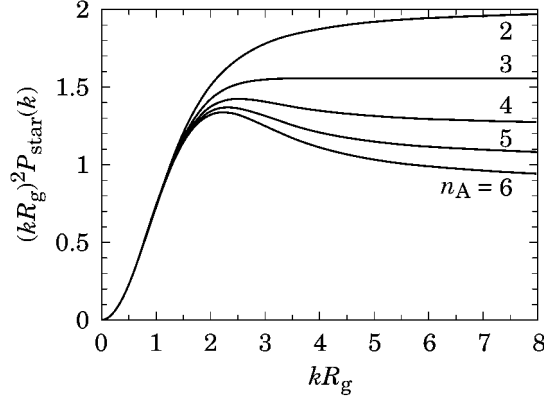


**Figure 2.46.** Plot of  $(kR_g)^2 P_{\text{star}}(k)$  of an  $n_A$ -arm star polymer as a function of  $kR_g$ . The number adjacent to each curve indicates  $n_A$ .

for star polymers with  $n_A = 2, 3, 4, 5,$  and  $6$ . For  $n_A = 3$ ,  $(kR_g)^2 P_{\text{star}}(k)$  approaches the asymptote of  $14/9$  at high  $kR_g$ . For  $n_A \geq 4$ , there is a peaking at around  $kR_g \cong 2$ . The peaking, also observed in a spherical molecule, indicates the compactness of the polymer molecule.

## 2.4.7 Light Scattering of a Polymer Solution

**2.4.7.1 Scattering in a Solvent** We have assumed so far that polymer chains and particles are suspended in vacuum. Now we consider the light scattered by a fluid or, in general, a continuous dielectric medium of scattering volume  $V$ . Scattering by particles suspended in a solvent is obtained from the Rayleigh scattering formula for particles in vacuum. In a medium with a refractive index  $n$ , the wavelength is  $\lambda/n$  and the electric permittivity is  $\epsilon_0 n^2$ . In Eq. 2.45, we change  $\lambda$  to  $\lambda/n$ ,  $\epsilon_0$  to  $\epsilon = \epsilon_0 n^2$ , and  $\alpha$  to  $\alpha_{\text{ex}}$ , where  $\alpha_{\text{ex}}$  is the excess polarizability of the suspended particle relative to the surrounding medium. The result is

$$\frac{I}{I_0} = \frac{\pi^2}{(\lambda/n)^4} \frac{\alpha_{\text{ex}}^2}{(\epsilon_0 n^2)^2} \frac{\sin^2 \theta'}{r^2} = \frac{\pi^2}{\lambda^4} \frac{\alpha_{\text{ex}}^2}{\epsilon_0^2} \frac{\sin^2 \theta'}{r^2} \quad (2.99)$$

In effect,  $\alpha$  is replaced by  $\alpha_{\text{ex}}$ , but no other changes. The wavelength  $\lambda$  refers to the one in vacuum. The other equations (Eqs. 2.55 and 2.58) are rewritten in the same way.

It is more convenient to extend Eq. 2.99 to include spatial fluctuations in  $\alpha_{\text{ex}}$ . Every part of the scattering volume has naturally occurring fluctuations in the density and, for solutions, also in the concentration, as illustrated in Figure 2.47. The density and concentration are slightly different from place to place. The density fluctuations and concentration fluctuations cause fluctuations in  $\alpha_{\text{ex}}$  through fluctuations  $\Delta \epsilon_r$  in the relative electric permittivity  $\epsilon_r = \epsilon/\epsilon_0$  (also called dielectric

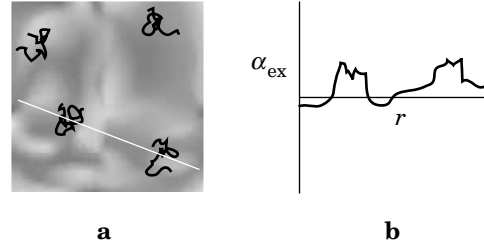


**Figure 2.47.** Spatial variations of the local solvent density and the polymer concentration lead to fluctuation in the excess polarizability  $\alpha_{\text{ex}}$ . The plot in b shows  $\alpha_{\text{ex}}$  along the white line in a.

constant) because the latter is determined by the number of charges (electrons and protons) in a unit volume. The Clausius-Mossotti equation gives the extra polarizability  $d\alpha_{\text{ex}}$  due to  $\Delta\epsilon_r$  of a small volume  $d\mathbf{r}$  at  $\mathbf{r}$  as  $d\alpha_{\text{ex}} = \epsilon_0\Delta\epsilon_r d\mathbf{r}$ , when  $\epsilon_r$  is not too large (which is the case in water and most organic solvents; Problem 2.24). Note that  $d\alpha_{\text{ex}}$  can be either positive or negative depending on the sign of  $\Delta\epsilon_r$ . Because  $\epsilon_r = n^2$  in the visible range of the spectrum,  $d\alpha_{\text{ex}}(\mathbf{r}) = 2\epsilon_0 n \Delta n(\mathbf{r}) d\mathbf{r}$ . As the refractive index fluctuation  $\Delta n$  is different from place to place in the volume,  $d\alpha$  also depends on  $\mathbf{r}$ . Similar to the calculation of interference of light scattered by different parts of a polymer chain in Section 2.4.3, we can calculate contributions from different parts of the volume. The extension of Eq. 2.55 gives the total scattering intensity  $I$  as

$$\begin{aligned} \frac{I}{I_0} &= \frac{\pi^2}{\lambda^4 r^2} \int \frac{d\alpha_{\text{ex}}(\mathbf{r}_1)}{\epsilon_0} \int \frac{d\alpha_{\text{ex}}(\mathbf{r}_2)}{\epsilon_0} \exp[i\mathbf{k} \cdot (\mathbf{r}_1 - \mathbf{r}_2)] \\ &= \frac{4\pi^2 n^2}{\lambda^4 r^2} \int_V d\mathbf{r}_1 \int_V d\mathbf{r}_2 \Delta n(\mathbf{r}_1) \Delta n(\mathbf{r}_2) \exp[i\mathbf{k} \cdot (\mathbf{r}_1 - \mathbf{r}_2)] \end{aligned} \quad (2.100)$$

where the integrals are calculated over the scattering volume  $V$  (Fig. 2.33).

**2.4.7.2 Scattering by a Polymer Solution** Light-scattering study of a polymer is usually carried out by first measuring the scattering intensity  $I_S$  of the pure solvent at different angles  $\theta$  and then repeating the procedure on polymer solutions to obtain the scattering intensity  $I$  at different angles. The excess scattering ( $I_{\text{ex}}$ ) is defined by  $I_{\text{ex}} \equiv I - I_S$  (Fig. 2.48). Usually  $I_S$  is flat, if  $V$  is constant, by the reason explained in Section 2.4.5.

In Eq. 2.100,  $\Delta n(\mathbf{r})$  has two components:  $\Delta_d n(\mathbf{r})$  and  $\Delta_c n(\mathbf{r})$ . The former is due to density fluctuations of the fluid that appears also in  $I_S$ . The latter is caused by concentration fluctuations of the polymer and is unique to the solutions. The excess scattering  $I_{\text{ex}}$  is due to  $\Delta_c n(\mathbf{r})$ :

$$\frac{I_{\text{ex}}}{I_0} = \frac{4\pi^2 n^2}{\lambda^4 r^2} \int_V d\mathbf{r}_1 \int_V d\mathbf{r}_2 \langle \Delta_c n(\mathbf{r}_1) \Delta_c n(\mathbf{r}_2) \rangle \exp[i\mathbf{k} \cdot (\mathbf{r}_1 - \mathbf{r}_2)] \quad (2.101)$$

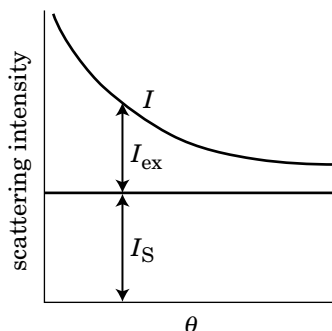


**Figure 2.48.** The excess scattering  $I_{\text{ex}}$  is the increment in the scattering intensity of the polymer solution,  $I$ , over that of the pure solvent,  $I_S$ .

where the statistical average is taken with respect to the concentration fluctuations. We set the reference for  $n$  to the refractive index of the solvent. The refractive index fluctuation  $\Delta_c n(\mathbf{r})$  is related to the concentration fluctuation  $\Delta c(\mathbf{r})$  by

$$\Delta_c n(\mathbf{r}) = \frac{dn}{dc} \Delta c(\mathbf{r}) \quad (2.102)$$

where  $dn/dc$  is called the **differential refractive index** (or **specific refractive index increment**). It expresses how much the refractive index of the polymer solution increases as the concentration  $c$  of the polymer increases. Each polymer–solvent pair has its own value of  $dn/dc$ . It also depends on the temperature and the wavelength. Roughly,  $dn/dc$  is approximated by

$$\frac{dn}{dc} \cong (n_{\text{polymer}} - n_{\text{solvent}})v_{\text{sp}} \quad (2.103)$$

where  $n_{\text{polymer}}$  and  $n_{\text{solvent}}$  are the refractive indices of the bulk polymer in the amorphous state and of the solvent, respectively, and  $v_{\text{sp}}$  is the specific volume of the polymer in the solution. If the volumes of the polymer and the solvent are additive,  $v_{\text{sp}}$  is the reciprocal of the density of the polymer.

Note that  $dn/dc$  can be positive or negative, depending on whether the polymer has a higher refractive index than the solvent does. As we will see below, the scattering intensity is proportional to  $(dn/dc)^2$ . A greater contrast in the refractive index between the polymer and the solvent gives a stronger scattering. In some polymer–solvent systems,  $dn/dc$  is near zero, making the excess scattering near zero. Then, the polymer is optically indistinguishable from the solvent. This condition is called **index matching**. A solvent **isorefractive** with the polymer makes the polymer invisible.

**2.4.7.3 Concentration Fluctuations** With Eq. 2.102, Eq. 2.101 is rewritten to

$$\frac{I_{\text{ex}}(\mathbf{k})}{I_0} = \frac{4\pi^2 n^2}{\lambda^4 r^2} \left( \frac{dn}{dc} \right)^2 \psi_{\text{cc}}(\mathbf{k}) \quad (2.104)$$

with  $\psi_{\text{cc}}(\mathbf{k})$  being the Fourier transform for the correlation function of the concentration fluctuations:

$$\psi_{\text{cc}}(\mathbf{k}) \equiv \int_V d\mathbf{r}_1 \int_V d\mathbf{r}_2 \langle \Delta c(\mathbf{r}_1) \Delta c(\mathbf{r}_2) \rangle \exp[i\mathbf{k} \cdot (\mathbf{r}_1 - \mathbf{r}_2)] \quad (2.105)$$

We consider  $\psi_{\text{cc}}(\mathbf{k})$  in the limit of  $\mathbf{k} = 0$  and in the low concentration limit separately. First, at  $\mathbf{k} = 0$ ,

$$\psi_{\text{cc}}(0) = \left\langle \left[ \int_V d\mathbf{r}_1 \Delta c(\mathbf{r}_1) \right]^2 \right\rangle = V^2 \langle \Delta c_{\text{tot}}^2 \rangle \quad (2.106)$$

where  $\Delta c_{\text{tot}}$  is the fluctuation in the overall concentration in the scattering volume. It is not the local concentration fluctuation  $\Delta c(\mathbf{r}) = c(\mathbf{r}) - \langle c \rangle$  with  $\langle c \rangle = Mn_p/(N_A V)$  defined in Eq. 2.68. The scattering volume is not in any container, and the solvent and solid molecules are free to leave the volume and enter the volume from the surroundings. The system is open to exchange of matter. Now we use the osmotic compressibility requirement for an open system in general:

$$\boxed{\langle \Delta c_{\text{tot}}^2 \rangle = \frac{ck_B T}{V} \frac{\partial c}{\partial \Pi} \quad \text{osmotic compressibility requirement}} \quad (2.107)$$

The relationship can be obtained from the statistical mechanics for the open system (Problem 2.25). From the virial expansion of  $\Pi$  given in Eq. 2.20,

$$\frac{\partial \Pi}{\partial c} = N_A k_B T \left[ \frac{1}{M} + 2A_2 c + \dots \right] \quad (2.108)$$

From Eqs. 2.106–2.108, we find

$$\psi_{\text{cc}}(0) = \frac{cV}{N_A} \left[ \frac{1}{M} + 2A_2 c + \dots \right]^{-1} \quad (2.109)$$

Next, we consider  $\psi_{\text{cc}}(\mathbf{k})$  for a small  $\mathbf{k}$  in the low-concentration limit. Because  $\langle \Delta c(\mathbf{r}_1) \Delta c(\mathbf{r}_2) \rangle = \langle c(\mathbf{r}_1) c(\mathbf{r}_2) \rangle - c^2$ , Eq. 2.70 leads to

$$\langle \Delta c(\mathbf{r}_1) \Delta c(\mathbf{r}_2) \rangle = \frac{cM}{(2\pi)^3 N_A N} \int S(\mathbf{k}') \exp[-i\mathbf{k}' \cdot (\mathbf{r}_1 - \mathbf{r}_2)] d\mathbf{k}' - c^2 \quad (2.110)$$

Then, Eq. 2.105 leads to

$$\begin{aligned}\psi_{cc}(\mathbf{k}) &= \frac{cM}{(2\pi)^3 N_A N} \int S(\mathbf{k}') d\mathbf{k}' \int_V d\mathbf{r}_1 \int_V d\mathbf{r}_2 \exp[i(\mathbf{k} - \mathbf{k}') \cdot (\mathbf{r}_1 - \mathbf{r}_2)] \\ &\quad - c^2 \int_V d\mathbf{r}_1 \int_V d\mathbf{r}_2 \exp[i\mathbf{k} \cdot (\mathbf{r}_1 - \mathbf{r}_2)] \\ &= \frac{cMV}{N_A N} S(\mathbf{k}) - (2\pi)^3 c^2 V \delta(\mathbf{k})\end{aligned}\quad (2.111)$$

where Eq. A1.8 was used. The second term is nonzero only at  $\mathbf{k} = 0$  (forward scattering). Because  $I_{ex}(\mathbf{k})/I_0 \propto \psi_{cc}(\mathbf{k})$ , the negative sign for this term indicates how the concentration fluctuations decrease the intensity of unscattered light. We neglect this second term because it is not what is detected by the photodetector in the static light scattering experiments. We thus find from Eq. 2.75 that, at small  $\mathbf{k}$ ,

$$\psi_{cc}(k) = \frac{cMV}{N_A N} \frac{N}{1 + k^2 R_g^2/3} = \frac{cV}{N_A} M(1 + k^2 R_g^2/3)^{-1} \quad (2.112)$$

Combining Eqs. 2.109 and 2.112, we obtain  $\psi_{cc}(k)$  as

$$\psi_{cc}(k) = \frac{cV}{N_A} (1 + k^2 R_g^2/3)^{-1} \left[ \frac{1}{M} + 2A_2c + \dots \right]^{-1} \quad (2.113)$$

This expression applies to small scattering angles and low concentrations.

**2.4.7.4 Light-Scattering Experiments** From Eqs. (2.104) and (2.113), we finally obtain

$$\boxed{\frac{I_{ex}(k)}{I_0} = \frac{1}{N_A} \frac{4\pi^2 n^2}{\lambda^4} \left( \frac{dn}{dc} \right)^2 \frac{cV}{r^2} (1 + k^2 R_g^2/3)^{-1} \left[ \frac{1}{M} + 2A_2c + \dots \right]^{-1}} \quad (2.114)$$

Here we introduce the **Rayleigh ratio**  $R_\theta$  according to

$$\frac{I_{ex}}{I_0} \equiv \frac{R_\theta V}{r^2} \quad (2.115)$$

The Rayleigh ratio eliminates the geometry-dependent factors in  $I_{ex}(k)/I_0$  such as the scattering volume  $V(\theta)$  and the detector-sample distance  $r$  and retains the factors related to the solution only. In the actual measurement system,  $I_0$  and  $V(\theta)$  cannot be measured correctly. Therefore, a pure solvent such as benzene and toluene is used as a calibration standard. See Refs. 21 and 22 for details. With  $R_\theta$ , Eq. 2.114 is rewritten to

$$\boxed{\frac{Hc}{R_\theta} = \frac{1}{M} \left( 1 + \frac{1}{3} k^2 R_g^2 + 2A_2Mc + \dots \right)} \quad \text{static light scattering, monodisperse} \quad (2.116)$$

where

$$H \equiv \frac{1}{N_A} \left( \frac{2\pi n}{\lambda^2} \frac{dn}{dc} \right)^2 \quad (2.117)$$

The equations we derived in the above assume that the polymer in solution is monodisperse. Usually, the polymer is polydisperse.  $M$  and  $R_g$  that we obtain in the static light-scattering experiments are then averages of  $M$  and  $R_g$ . Below we find what kind of averages they are.

For a monodisperse polymer,  $I_{\text{ex}}/I_0 \propto cM - (1/3)k^2cMR_g^2$  in the low concentration limit. When the solution contains components of molecular weight  $M_i$  and radius of gyration  $R_{gi}$  at concentration  $c_i$  ( $c = \sum c_i$ ), the total excess scattering intensity from all the components is

$$I_{\text{ex}}/I_0 \propto \sum_i c_i M_i - \frac{k^2}{3} \sum_i c_i M_i R_{gi}^2 = c \sum_i \frac{c_i}{c} M_i \left[ 1 - \frac{k^2}{3} \frac{\sum_i c_i M_i R_{gi}^2}{\sum_i c_i M_i} \right] \quad (2.118)$$

Because  $c_i/c$  is the weight fraction of component  $i$ ,  $\sum_i (c_i/c)M_i = M_w$  by definition. For  $R_g^2$ ,  $c_i M_i$  is proportional to the product of the weight fraction and  $M_i$ . Thus, the average for  $R_g^2$  is the  $z$ -average.

$\frac{Hc}{R_\theta} = \frac{1}{M_w} \left( 1 + \frac{1}{3}k^2 \langle R_g^2 \rangle_z \tau 2A_2 M_w c + \dots \right) \quad \text{static light scattering, polydisperse}$
--

(2.119)

There is also an effect of the polydispersity on  $A_2$ , but the effect is usually weak, as we have seen in Section 2.2.3.

**2.4.7.5 Zimm Plot** Here we learn how  $M_w$ ,  $\langle R_g^2 \rangle_z$ , and  $A_2$  are evaluated in the light-scattering experiments conducted on solutions of finite concentrations and at finite scattering angles. The excess scattering intensity is recorded at different scattering angles. The measurement is repeated for several concentrations of the polymer at the same set of angles for a given polymer solution. The intensity data are converted into  $Hc/R_\theta$  and plotted as a function of  $\sin^2(\theta/2) + \text{const.} \times c$ . The constant is arbitrary. The plot is called a **Zimm plot**. Open circles in Figure 2.49 illustrate the ideal data. Each dashed line represents a series of measurements at a constant angle. Each solid gray line is for those at a constant concentration. The plot looks like a lattice deformed by a shear. The data obtained at nonzero angles and nonzero concentrations are extrapolated to  $\theta = 0$  and  $c = 0$ , represented by two solid dark lines with a common intercept. The intercept gives  $M_w^{-1}$ . The slope of the  $c = 0$  line is equal to  $(1/3)(4\pi n/\lambda)^2 R_g^2/M_w$ , where we write  $R_g^2$  for  $\langle R_g^2 \rangle_z$  here. The slope of the  $\theta = 0$  line is equal to  $2A_2/\text{const.}$  Thus, the Zimm plot gives estimates of  $M_w$ ,  $R_g$ , and  $A_2$  with no need of other references. If the constant coefficient on  $c$  is large, the sheared lattice can be inverted with the  $\theta = 0$  line lying below the  $c = 0$  line. A negative  $A_2$  inverts the plot vertically (Problem 2.32).

An example of the actual data is shown in Figure 2.50. The data were obtained for polyguanidine in tetrahydrofuran.<sup>23</sup> The intercept gives  $M_w = 6.73 \times 10^5$  g/mol.

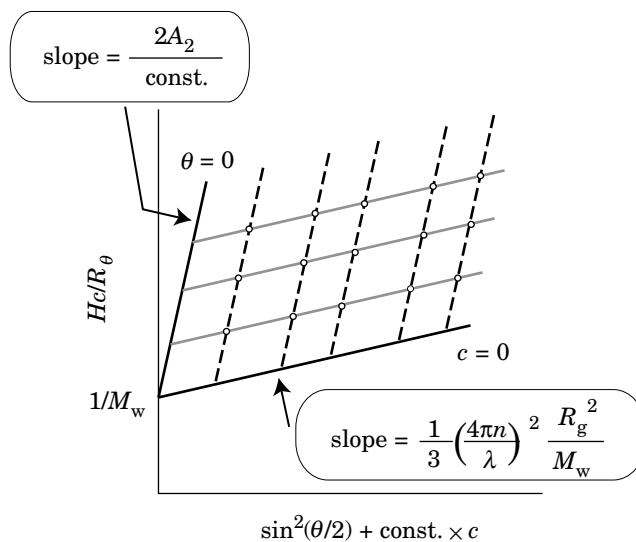


**Figure 2.49.** Schematic of the Zimm plot. Results obtained for solutions of different concentrations  $c$  at different scattering angles  $\theta$  are converted to  $Hc/R_\theta$  and plotted as a function of  $\sin^2(\theta/2) + \text{const.} \times c$ . The extrapolate to  $c = 0$  has a slope of  $(1/3)(4\pi n/\lambda)^2 R_g^2/M_w$ . The extrapolate to  $\theta = 0$  has a slope of  $2A_2/\text{const.}$  The two extrapolates have a common intercept of  $1/M_w$ .

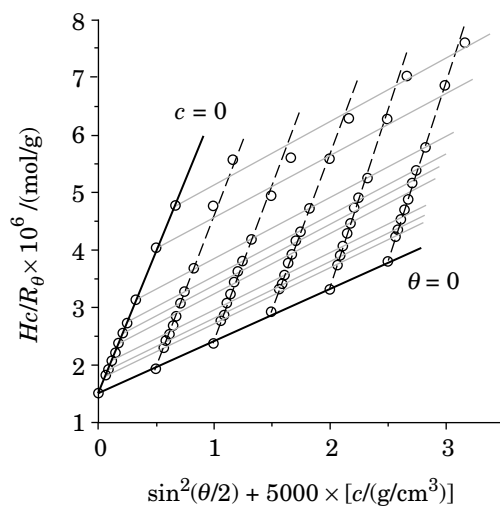


**Figure 2.50.** Example of the Zimm plot. Data were obtained for polyguanidine in tetrahydrofuran. (From Ref. 23.)



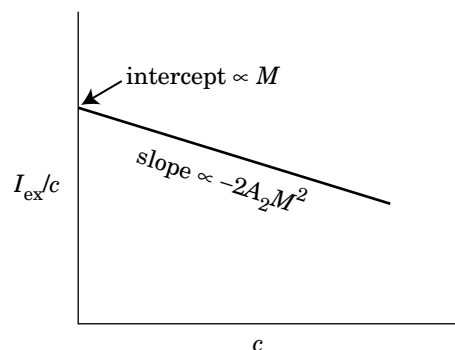


**Figure 2.51.** A plot of  $I_{\text{ex}}/c$  as a function of  $c$  at sufficiently low scattering angles has an intercept proportional to  $M$  and a slope proportional to  $-2A_2M^2$ . The ratio gives an estimate of  $A_2M$ .

The slope of the  $c = 0$  line gives  $R_g = 99$  nm, and the slope of the  $\theta = 0$  lines gives  $A_2 = 2.59 \times 10^{-3}$  (mol·cm<sup>3</sup>)/g<sup>2</sup>.

When the light-scattering data are available only for one concentration, but the concentration is sufficiently low, we can regard that the line connecting the measured data as the  $c = 0$  line in the Zimm plot. The intercept of the line gives  $M_w$  and the slope gives  $R_g$ .

A simpler alternative to estimate  $A_2M$  is to measure  $I_{\text{ex}}$  at a sufficiently low angle ( $kR_g \leq 1$ ) for solutions of different concentrations and plot  $I_{\text{ex}}/c$  as a function of  $c$ . The plot is schematically explained in Figure 2.51. The data for low concentrations ( $c < c^*$ ) will lie on a straight line. The ratio of the slope to the intercept is equal to  $-2A_2M$ .

**2.4.7.6 Measurement of  $dn/dc$**  To have a good accuracy in the estimates of  $M_w$ ,  $\langle R_g^2 \rangle_z$ , and  $A_2$ ,  $dn/dc$  must be evaluated with a high accuracy because the relative error in  $dn/dc$  is doubled in the errors in  $M_w$ ,  $\langle R_g^2 \rangle_z$ , and  $A_2$ . The  $dn/dc$  is usually measured by using a differential refractometer for solutions of the polymer at different concentrations in the dilute regime. Fitting the plot of  $\Delta n$  as a function of  $c$  by a straight line through the origin gives the estimate of  $dn/dc$ . The measurement of  $dn/dc$  must be done at the same temperature and wavelength as those in the light-scattering measurements.

Commercial instruments based on two different principles are available. One uses a vertically divided cell.<sup>24</sup> The top view is shown in Figure 2.52a. One of the chambers contains a reference fluid, typically the pure solvent, and the other chamber contains the sample solution. A laser beam passes the divided cell twice before reaching a two-part photodetector. The detector is placed so that the beam hits the two parts equally when the two chambers of the cell have the same refractive index. A difference in the refractive index in the chambers deflects the beam, resulting in unequal intensities on the two parts of the detector. Thus the imbalance of the two intensities gives the refractive index difference  $\Delta n$ .

A variant of this scheme is also used. A mirror is on a rotation stage. The mirror is rotated so that the beam hits the two parts of the detector with the same intensity. The angle of rotation gives the refractive index difference  $\Delta n$ .

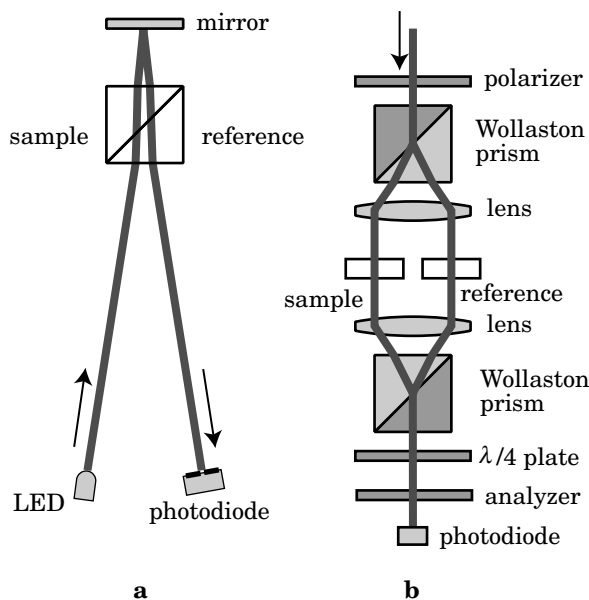


**Figure 2.52.** Differential refractive index  $dn/dc$  is measured usually in one of two methods: refraction (a) and interferometer (b).

The other method uses an interferometer.<sup>25</sup> In Figure 2.52b, a beam linearly polarized at  $45^\circ$  from vertical is split into two beams by a Wollaston prism. One of the two beams passes a sample cell, and the other beam passes a reference cell. When there is a difference in the refractive index between the two fluids, one of the beams is delayed compared with the other, resulting in a phase shift. When the two beams are coupled by another prism, they form a circularly polarized light. A quarterwave plate converts it into a linearly polarized beam. With the analyzer (another polarizer) adjusted to be extinct when there is no phase shift, the intensity of light though the analyzer is proportional to the phase shift. The latter is proportional to  $\Delta n$ .

As an alternative, we can use a regular Abbe refractometer that reads the refractive index of a liquid for a typical light source of a sodium lamp (D line;  $\lambda = 589.3$  nm) at a given temperature. Unlike the differential refractometer, the fluid is exposed to the atmosphere; therefore, this method is not suitable for a solution dissolved in a volatile solvent.

## 2.4.8 Other Scattering Techniques

**2.4.8.1 Small-Angle Neutron Scattering (SANS)** Small-angle neutron scattering (SANS) has become a preferred tool of research for a variety of polymer systems, including pure and blend bulk polymers, phase-separated systems, micellar suspensions, and solutions, especially concentrated ones. Unlike light scattering, it is

available only in a limited number of facilities around the globe. Labeling of polymer by deuterium, that is, straight synthesis of the polymer using deuterated compounds, is often required. SANS is therefore best suited where light-scattering measurements fail, for instance, for opaque systems such as micellar suspensions in which multiple light-scattering complicates the scattering pattern.

As in light scattering, SANS provides information on static structures of the system, but the length scale is smaller. The range of the scattering vector is typically from 0.02 to 3 nm<sup>-1</sup>, overlapping with the high end of the scattering vectors in the light scattering (see Fig. 2.32). It is customary to use symbol  $\mathbf{q}$  to denote the scattering vector whose magnitude  $q$  is given by

$$q = \frac{4\pi}{\lambda} \sin \frac{\theta}{2} \quad (2.120)$$

where  $\lambda$  is the de Broglie wavelength of neutrons and  $\theta$  is the scattering angle. The particles that scatter neutrons are nuclei. The scattering intensity by each nucleus is proportional to a **scattering length**  $b$ , which is different from nucleus to nucleus. For a proton <sup>1</sup>H,  $b < 0$  and there is no change in phase upon scattering. With a deuterium D = <sup>2</sup>H and most other nuclei that constitute polymers,  $b > 0$  and the phase shifts by  $\pi$  upon scattering.

We can imagine that each atom has a shield of area  $4\pi b^2$  to block the incident neutrons and scatter them in all directions. This area is called a **scattering cross section**. The cross section of the entire sample is denoted by  $\Sigma$ . The coherent part of the scattering intensity  $I_{\text{coh}}$  per unit solid angle  $d\Omega$  at  $\mathbf{q}$  is related to the position  $\mathbf{r}_i$  and the scattering length  $b_i$  of the  $i$ th nucleus by

$$I_{\text{coh}}(\mathbf{q}) = \frac{d\Sigma^{\text{coh}}(\mathbf{q})}{d\Omega} = \left\langle \sum_{i,j} b_i b_j \exp[i\mathbf{q} \cdot (\mathbf{r}_i - \mathbf{r}_j)] \right\rangle \quad (2.121)$$

where  $\Sigma^{\text{coh}}$  is the coherent component of the scattering cross section. Incoherent component does not interfere to take part in the structure factor. Equation 2.121 is similar to the structure factor we obtained in the static light scattering. The contrast factor  $dn/dc$  is now replaced by  $b_i$ .

Now we apply the general formula to a solution of polymer. We consider that the polymer consists of hydrogenated chains (regular chains) and deuterated chains, both having the same distribution in the chain length. The coherent scattering by the solution of total concentration  $c$  is given as

$$\frac{d\Sigma^{\text{coh}}(\mathbf{q})}{d\Omega} = \frac{M_w c N_A}{m_0^2} [(a_H - a_D)^2 x_H x_D S_1(\mathbf{q}) + (a_p - a_s)^2 S(\mathbf{q})] \quad (2.122)$$

where  $m_0$  is the mass of a monomer,  $a_H$  and  $a_D$  are the scattering lengths per monomer for hydrogenated and deuterated polymers, respectively,  $x_H$  and  $x_D$  are their mole fractions in the polymer sample (without solvent), and  $S_1(\mathbf{q})$  and  $S(\mathbf{q})$  are the single-chain and total structure factors, respectively, as we defined earlier in

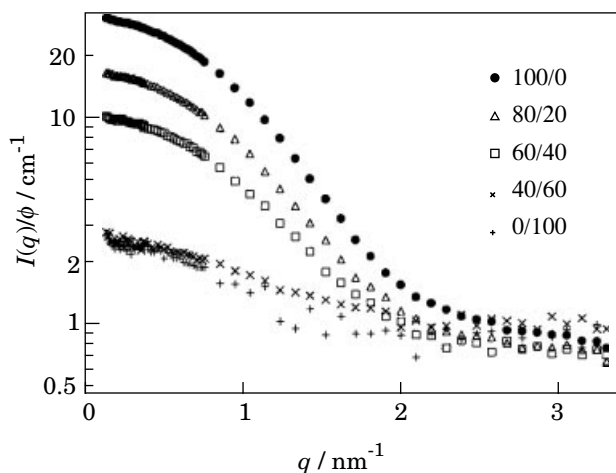


**Figure 2.53.** Scattering intensity  $I$  in SANS divided by the polymer volume fraction  $\phi$ , plotted as a function of the scattering vector  $q$ . The sample was a hydrogenated dendrimer in a mixture of deuterated (D) and hydrogenated (H) solvents. The D-to-H mixing ratio is indicated in the legend. (From Ref. 26.)

the sections on light scattering. The  $a_p$  and  $a_s$  are defined as

$$a_p = x_H a_H + x_D a_D, \quad a_s = x_{sH} a_{sH} + x_{sD} a_{sD} \quad (2.123)$$

where  $a_{sH}$  and  $a_{sD}$  are the scattering lengths of hydrogenated and deuterated solvent molecules, respectively, and  $x_{sH}$  and  $x_{sD}$  are their mole fractions in the solvent mixture (without polymer). Note that  $M_w c / m_0^2$  in Eq. 2.122 is the same between hydrogenated and deuterated chains, as long as the molar concentration is common.

Extraction of  $S_1(\mathbf{q})$  from  $I(\mathbf{q})$  is facilitated by contrast matching in which  $a_p$  and  $a_s$  are brought to be equal by choosing an appropriate isotopic mixture of the solvents for a given isotopic mixture of the polymer samples. Because of the factor  $x_H x_D$ , the scattering intensity maximizes for a 50:50 mixture of the isotopes. Once we obtain  $S_1(\mathbf{q})$ , the methods used in the analysis of SLS data can be applied, including the Zimm plot.

Example of SANS experiments is shown in Figure 2.53.<sup>26</sup> The scattering intensity from a hydrogenated dendrimer ( $x_H = 1$ ,  $x_D = 0$ ) normalized by its volume fraction  $\phi$  is plotted as a function of the scattering vector. At high  $q$ ,  $I(q)$  levels off to a constant due to incoherent scattering. Mixtures of deuterated (D) and hydrogenated (H) solvents with different mixing ratios were used as a solvent. Apparently, the contrast matching is reached at around 20% of the hydrogenated solvent in this example. The concentration was sufficiently low for this compact molecule; thus  $S_1(\mathbf{q}) \cong S(\mathbf{q})$ . The coherent part of the scattering is close to  $1/(1 + q^2 R_g^2/3)$  dependence.

**2.4.8.2 Small-Angle X-Ray Scattering (SAXS)** Small-angle X-ray scattering (SAXS) is, in principle, the same as wide-angle X-ray diffraction (WAXD), broadly used in crystallography. In SAXS, the scattering angles are low to allow investigation of structures over the length much longer than 1 Å. The mechanism of scattering discussed in Section 2.4.2 applies as it is. Unlike WAXD, the intensity of scattered X-ray is weak. Therefore, a synchrotron radiation source that provides a strong monochromatic beam is usually used. The scattering vector is given by the same formula as the one used for SANS, with  $\lambda$  being the wavelength of the X-ray. Note that the relative electric permittivity is nearly equal to unity in the relevant range of wavelength (to be precise, it is slightly smaller than 1). The magnitude of the scattering vector is typically 0.2 to 4 nm<sup>-1</sup>, much greater than the range available in static light scattering. Therefore, SAXS is suitable to study local structures of polymer molecules. The form factor studied at a high  $q$  range gives, for instance, an estimate for the diameter of a rodlike molecule.

## 2.4.9 PROBLEMS

**Problem 2.18:** A copolymer chain consisting of  $N_a$  beads of monomer a and  $N_b$  beads of monomer b has three single-chain structure factors:  $S_{aa}(\mathbf{k})$ ,  $S_{ab}(\mathbf{k})$ , and  $S_{bb}(\mathbf{k})$ . They are defined as

$$S_{ll'}(\mathbf{k}) = \frac{1}{N} \sum_{i,j=1}^N \langle \exp[i\mathbf{k} \cdot (\mathbf{r}_i - \mathbf{r}_j)] \delta_i^l \delta_j^{l'} \rangle \quad (l, l' = a, b)$$

where  $N = N_a + N_b$  is the total number of beads in the chain and  $\delta_i^l$  specifies the monomer type:

$$\delta_i^l = \begin{cases} 1 & \text{(the } i\text{th bead is } l) \\ 0 & \text{(otherwise)} \end{cases}$$

By definition,  $\delta_i^a + \delta_i^b = 1$ . Assume that the copolymer chain follows the Gaussian statistics and has a common segment length  $b$ . Find  $S_{aa}(\mathbf{k})$ ,  $S_{ab}(\mathbf{k})$ , and  $S_{bb}(\mathbf{k})$  for (1) a diblock copolymer and (2) a random copolymer in which the two monomers are placed without correlation to the neighboring monomers. Also evaluate each of  $S_{aa}(\mathbf{k})$ ,  $S_{ab}(\mathbf{k})$ , and  $S_{bb}(\mathbf{k})$  in the small  $\mathbf{k}$  limit up to the order of  $\mathbf{k}^2$ .

**Solution 2.18 (1):**

$$\delta_i^a = 1 \text{ for } i = 1, \dots, N_a \quad \text{and} \quad \delta_i^b = 1 \text{ for } i = N_a + 1, \dots, N_a + N_b$$

$$S_{aa}(\mathbf{k}) = \frac{1}{N} \sum_{i,j=1}^N \langle \exp[i\mathbf{k} \cdot (\mathbf{r}_i - \mathbf{r}_j)] \delta_i^a \delta_j^a \rangle = \frac{1}{N} \sum_{i,j=1}^{N_a} \langle \exp[i\mathbf{k} \cdot (\mathbf{r}_i - \mathbf{r}_j)] \rangle = \frac{N_a^2}{N} f_D(kR_{ga})$$

$$\begin{aligned}
S_{bb}(\mathbf{k}) &= \frac{1}{N} \sum_{i,j=1}^N \langle \exp[i\mathbf{k} \cdot (\mathbf{r}_i - \mathbf{r}_j)] \delta_i^b \delta_j^b \rangle = \frac{1}{N} \sum_{i,j=N_a+1}^{N_a+N_b} \langle \exp[i\mathbf{k} \cdot (\mathbf{r}_i - \mathbf{r}_j)] \rangle \\
&= \frac{N_b^2}{N} f_D(kR_{gb})
\end{aligned}$$

where  $R_{gl}^2 = b^2 N_l / 6$  ( $l = a, b$ ) is the mean square radius of gyration of block  $l$ .

$$\begin{aligned}
S_{ab}(\mathbf{k}) &= \frac{1}{N} \sum_{i,j=1}^N \langle \exp[i\mathbf{k} \cdot (\mathbf{r}_i - \mathbf{r}_j)] \delta_i^a \delta_j^b \rangle = \frac{1}{N} \sum_{i=1}^{N_a} \sum_{j=N_a+1}^{N_a+N_b} \langle \exp[i\mathbf{k} \cdot (\mathbf{r}_i - \mathbf{r}_j)] \rangle \\
&= \frac{1}{N} \int_0^{N_a} dn \int_{N_a}^{N_a+N_b} dn' \exp\left(-\frac{1}{6}k^2(n' - n)b^2\right) \\
&= \frac{1}{N} \int_0^{N_a} dn \exp\left(\frac{1}{6}k^2 nb^2\right) \int_{N_a}^{N_a+N_b} dn' \exp\left(-\frac{1}{6}k^2 n' b^2\right) \\
&= \frac{N_a N_b}{N} \left( \frac{1 - \exp(-k^2 R_{ga}^2)}{k^2 R_{ga}^2} \right) \left( \frac{1 - \exp(-k^2 R_{gb}^2)}{k^2 R_{gb}^2} \right)
\end{aligned}$$

In the small  $\mathbf{k}$  limit,

$$\begin{aligned}
S_{aa}(\mathbf{k}) &= \frac{N_a^2}{N} \left( 1 - \frac{1}{3}k^2 R_{ga}^2 \right), \quad S_{bb}(\mathbf{k}) = \frac{N_b^2}{N} \left( 1 - \frac{1}{3}k^2 R_{gb}^2 \right), \\
S_{ab}(\mathbf{k}) &= \frac{N_a N_b}{N} \left( 1 - \frac{1}{2}k^2 (R_{ga}^2 + R_{gb}^2) \right)
\end{aligned}$$

**Solution 2.18 (2):**  $\delta_i^a = 1$  with a probability of  $N_a/N$  for any  $i$ . Whether the bead  $i$  is monomer a or b is independent of other factors and  $\langle \delta_i^a \rangle = N_a/N$ . Therefore,

$$\begin{aligned}
S_{aa}(\mathbf{k}) &= \frac{1}{N} \sum_{i,j=1}^N \langle \exp[i\mathbf{k} \cdot (\mathbf{r}_i - \mathbf{r}_j)] \rangle \langle \delta_i^a \rangle \langle \delta_j^a \rangle \\
&= \frac{N_a^2}{N^3} \sum_{i,j=1}^N \langle \exp[i\mathbf{k} \cdot (\mathbf{r}_i - \mathbf{r}_j)] \rangle = \frac{N_a^2}{N} f_D(kR_g)
\end{aligned}$$

where  $R_g$  is the radius of gyration of the whole chain. Likewise,

$$S_{bb}(\mathbf{k}) = \frac{N_b^2}{N} f_D(kR_g), \quad S_{ab}(\mathbf{k}) = \frac{N_a N_b}{N} f_D(kR_g)$$

In the small  $\mathbf{K}$  limit,

$$S_{aa}(\mathbf{k}) = \frac{N_a^2}{N} \left(1 - \frac{1}{3}k^2 R_g^2\right), \quad S_{bb}(\mathbf{k}) = \frac{N_b^2}{N} \left(1 - \frac{1}{3}k^2 R_g^2\right),$$

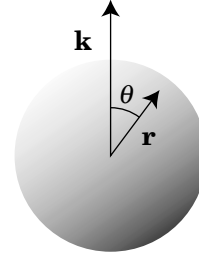
$$S_{ab}(\mathbf{k}) = \frac{N_a N_b}{N} \left(1 - \frac{1}{3}k^2 R_g^2\right)$$

Real random copolymers may have a correlation between  $\delta_i'$  of different  $i$ .

**Problem 2.19:** Calculate the form factor for a spherical molecule.

**Solution 2.19:** Choose the polar axis along  $\mathbf{k}$ . Then,

$$\begin{aligned} \int_V \mathbf{dr} \exp(i\mathbf{k} \cdot \mathbf{r}) &= \int_0^{R_s} r^2 dr \int_0^\pi \sin\theta d\theta \int_0^{2\pi} d\phi \exp(ikr \cos\theta) \\ &= 2\pi \int_0^{R_s} r^2 dr \frac{2 \sin kr}{kr} \\ &= \frac{4\pi}{k} \text{Im} \int_0^{R_s} r dr \exp(ikr) \\ &= \frac{4\pi}{k} \text{Im} \left[ \frac{R_s}{ik} \exp(ikR_s) + \frac{1}{k^2} (\exp(ikR_s) - 1) \right] \\ &= 4\pi k^{-3} (\sin kR_s - kR_s \cos kR_s) \end{aligned}$$



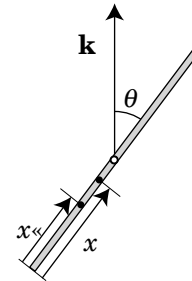
Then,

$$P_{\text{sphere}}(\mathbf{k}) = \left| V^{-1} \int_V \mathbf{dr} \exp(i\mathbf{k} \cdot \mathbf{r}) \right|^2 = [3(kR_s)^{-3} (\sin kR_s - kR_s \cos kR_s)]^2$$

**Problem 2.20:** Calculate the form factor for a rodlike molecule.

**Solution 2.20:** Let  $\theta$  be the angle between  $\mathbf{k}$  and the molecule.

$$\begin{aligned} P_{\text{rod}} &= \frac{1}{2L^2} \int_0^L dx \int_0^L dx' \int_0^\pi \sin\theta d\theta \exp[ik(x-x')\cos\theta] \\ &= \frac{1}{L^2} \int_0^L dx \int_0^L dx' \frac{\sin k(x-x')}{k(x-x')} \\ &= \frac{2}{L^2} \int_0^L dx \int_0^x dx' \frac{\sin k(x-x')}{k(x-x')} \\ & \quad [k(x-x') \equiv z, kx = y] \end{aligned}$$



$$\begin{aligned}
&= \frac{2}{k^2 L^2} \int_0^{kL} dy \int_0^y dz \frac{\sin z}{z} = \frac{2}{k^2 L^2} \int_0^{kL} dz \frac{\sin z}{z} (kL - z) \\
&= (kL/2)^{-1} \int_0^{kL} \frac{\sin z}{z} dz - \left( \frac{\sin(kL/2)}{kL/2} \right)^2
\end{aligned}$$

**Problem 2.21:** Verify that the form factor of a two-arm star polymer ( $n_A = 2$  in Eq. 2.98) reproduces the form factor of a Gaussian chain.

**Solution 2.21:** When  $n_A = 2$ , with  $x = kR_{g1}$ ,

$$\begin{aligned}
P_{\text{star}} &= \frac{1}{2} f_D(x) + \frac{1}{2} \left( x^{-2} [1 - \exp(-x^2)] \right)^2 \\
&= \frac{1}{2} \cdot 2x^{-2} \left[ 1 - x^{-2} (1 - \exp(-x^2)) \right] + \frac{1}{2} x^{-4} [1 - \exp(-x^2)]^2 \\
&= x^{-2} \left[ 1 - \frac{1}{2} x^{-2} (1 - \exp(-2x^2)) \right] \\
&= 2(2^{1/2}x)^{-2} \left[ 1 - (2^{1/2}x)^{-2} (1 - \exp(-(2^{1/2}x)^2)) \right] = f_D(2^{1/2}kR_{g1})
\end{aligned}$$

$2^{1/2}R_{g1}$  is the radius of gyration of the two-arm star polymer.

**Problem 2.22:** Show that Eq. 2.98 reduces to Eq. 2.74 when  $kR_g \ll 1$ .

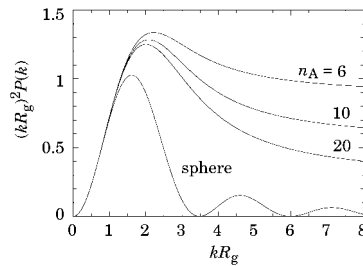
**Solution 2.22:** In Eq. 2.98, when  $k$  is small,

$$\begin{aligned}
P_{\text{star}}(k) &\cong \frac{1}{n_A} \left( 1 - \frac{1}{3} (kR_{g1})^2 \right) + \left( 1 - \frac{1}{n_A} \right) \left( 1 - \frac{1}{2} (kR_{g1})^2 \right)^2 \\
&= 1 - \left( 1 - \frac{2}{3n_A} \right) (kR_{g1})^2 = 1 - \frac{1}{3} (kR_g)^2
\end{aligned}$$

where Eq. 1.84 or Eq. 1.85 was used.

**Problem 2.23:** Compare the form factor of a sphere and that of a star polymer by plotting  $(kR_g)^2 P_{\text{sphere}}(k)$  and  $(kR_g)^2 P_{\text{star}}(k)$  as a function of  $kR_g$ . Consider  $n_A = 6, 10,$  and  $20$  for the number of arms of the star polymer.

**Solution 2.23:**





**Problem 2.24:** Clausius-Mossotti formula is given as

$$\frac{\epsilon_r - 1}{\epsilon_r + 2} \nu = \frac{\alpha}{3\epsilon_0}$$

where  $\nu$  is the volume per molecule. Use this formula to derive  $d\alpha_{\text{ex}} = \epsilon_0 \Delta\epsilon_r d\mathbf{r}$ .

**Solution 2.24:** The contribution to  $\alpha$  from a small volume  $d\mathbf{r}$  is given as

$$d\alpha = 3\epsilon_0 \frac{\epsilon_r - 1}{\epsilon_r + 2} d\mathbf{r}$$

When a fluctuation  $\Delta\epsilon_r$  in  $\epsilon_r$  causes  $d\alpha$  to fluctuate by  $d\alpha_{\text{ex}}$ ,

$$d\alpha + d\alpha_{\text{ex}} = 3\epsilon_0 \frac{\epsilon_r + \Delta\epsilon_r - 1}{\epsilon_r + \Delta\epsilon_r + 2} d\mathbf{r}$$

Comparison of the above two equations leads to

$$d\alpha_{\text{ex}} \cong 3\epsilon_0 \frac{\Delta\epsilon_r}{\epsilon_r + 2} d\mathbf{r} \cong \epsilon_0 \Delta\epsilon_r d\mathbf{r}$$

when  $\epsilon_r$  is close to unity.

**Problem 2.25:** Statistical mechanics for an open system gives the following relationship between the mean square fluctuation in  $n_p$ , the number of polymer chains in volume  $V$ , and the mean of  $n_p$ :

$$\langle \Delta n_p^2 \rangle = k_B T \left( \frac{\partial n_p}{\partial \mu_p} \right)_{T,p}$$

Derive Eq. (2.107) using this relationship and the Gibbs-Duhem theorem,  $n_p d\mu_p + n_s d\mu_s = 0$ .

**Solution 2.25:** From the Gibbs-Duhem theorem,

$$\frac{\partial \mu_p}{\partial n_p} = - \frac{n_s}{n_p} \frac{\partial \mu_s}{\partial n_p}$$

Because

$$-\Delta\mu_s = \Pi \frac{V_m}{N_A}$$

where  $V_m$  is the molar volume of the solvent,

$$\langle \Delta n_P^2 \rangle = -k_B T \frac{n_P}{n_S} \frac{\partial n_P}{\partial \mu_S} = k_B T \frac{n_P}{n_S} \frac{N_A}{V_m} \frac{\partial n_P}{\partial \Pi}$$

Thus we obtain

$$\langle \Delta c_{\text{tot}}^2 \rangle = \frac{ck_B T}{V} \frac{\partial c}{\partial \Pi}$$

where  $n_S V_m / N_A \cong V$  was used.

**Problem 2.26:** Show that

$$\int_V \frac{1}{c} \langle \Delta c(\mathbf{r}) \Delta c(0) \rangle d\mathbf{r} = k_B T \frac{\partial c}{\partial \Pi}$$

(another expression for Eq. 2.107).

**Solution 2.26:** From Eq. 2.105,

$$\psi_{cc}(0) \equiv \int_V d\mathbf{r}_1 \int_V d\mathbf{r}_2 \langle \Delta c(\mathbf{r}_1) \Delta c(\mathbf{r}_2) \rangle = V \int_V \langle \Delta c(\mathbf{r}) \Delta c(0) \rangle d\mathbf{r}$$

Then, with Eqs. (2.106) and (2.107),

$$\int_V \frac{1}{c} \langle \Delta c(\mathbf{r}) \Delta c(0) \rangle d\mathbf{r} = \frac{1}{cV} \psi_{cc}(0) = \frac{V}{c} \langle \Delta c_{\text{tot}}^2 \rangle = k_B T \frac{\partial c}{\partial \Pi}$$

**Problem 2.27:** For a diblock copolymer or a random copolymer consisting of monomers a and b that have different contrasts to the solvent, the refractive index fluctuation  $\Delta_c n(\mathbf{r})$  due to concentration fluctuation has two parts:

$$\Delta_c n(\mathbf{r}) = \left( \frac{dn}{dc} \right)_a \Delta c_a(\mathbf{r}) + \left( \frac{dn}{dc} \right)_b \Delta c_b(\mathbf{r})$$

where  $(dn/dc)_l$  is the differential refractive index of homopolymer  $l$  ( $l = a, b$ ), and  $\Delta c_l(\mathbf{r}) = c_l(\mathbf{r}) - c_l$  with  $c_l = \langle c_l(\mathbf{r}) \rangle$  denotes the concentration fluctuation of monomer  $l$ . Following the procedure in Section 2.4.7.4, we find the excess scattering intensity from the solution of the copolymer in the low

concentration limit as

$$\frac{I_{\text{ex}}(\mathbf{k})}{I_0} = \frac{4\pi^2 n^2}{\lambda^4 r^2} \left[ \left( \frac{dn}{dc} \right)_a^2 \psi_{\text{aa}}(\mathbf{k}) + 2 \left( \frac{dn}{dc} \right)_a \left( \frac{dn}{dc} \right)_b \psi_{\text{ab}}(\mathbf{k}) + \left( \frac{dn}{dc} \right)_b^2 \psi_{\text{bb}}(\mathbf{k}) \right]$$

where

$$\psi_{ll'}(\mathbf{k}) \equiv \int_V d\mathbf{r}_1 \int_V d\mathbf{r}_2 \langle \Delta c_l(\mathbf{r}_1) \Delta c_{l'}(\mathbf{r}_2) \rangle \exp[i\mathbf{k} \cdot (\mathbf{r}_1 - \mathbf{r}_2)] \quad (l, l' = a, b)$$

with  $\psi_{\text{ab}}(\mathbf{k}) = \psi_{\text{ba}}(\mathbf{k})$ . Because  $\langle \Delta c_l(\mathbf{r}_1) \Delta c_{l'}(\mathbf{r}_2) \rangle = \langle c_l(\mathbf{r}_1) c_{l'}(\mathbf{r}_2) \rangle - c_l c_{l'}$ ,

$$\psi_{ll'}(\mathbf{k}) = \frac{MVN}{cN_A} \frac{c_l c_{l'}}{N_l N_{l'}} S_{ll'}(\mathbf{k}) - (2\pi)^3 V c_l c_{l'} \delta(\mathbf{k})$$

where  $c = c_a + c_b$  is the total concentration,  $M$  and  $N$  refer to the whole chain,  $N_l$  is the number of  $l$  monomers in the polymer chain, and  $S_{ll'}(\mathbf{k})$  is defined in Problem 2.18. After eliminating the unscattered beam,

$$\begin{aligned} \frac{I_{\text{ex}}(\mathbf{k})}{I_0} &= \frac{4\pi^2 n^2}{\lambda^4 r^2} \frac{MVN}{cN_A} \left[ \frac{C_a^2}{N_a^2} \left( \frac{dn}{dc} \right)_a^2 S_{\text{aa}}(\mathbf{k}) + 2 \frac{c_a c_b}{N_a N_b} \left( \frac{dn}{dc} \right)_a \left( \frac{dn}{dc} \right)_b S_{\text{ab}}(\mathbf{k}) \right. \\ &\quad \left. + \frac{C_b^2}{N_b^2} \left( \frac{dn}{dc} \right)_b^2 S_{\text{bb}}(\mathbf{k}) \right] \end{aligned}$$

Answer the following questions assuming the whole chain follows the Gaussian statistics.

- (1) Show that, for the random copolymer, Eq. 2.114 (in the low concentration limit) holds with  $dn/dc$  replaced by the effective differential refractive index of the copolymer as a whole,  $(c_a/c)(dn/dc)_a + (c_b/c)(dn/dc)_b$ .
- (2) What is the radius of gyration  $R_{g,\text{eff}}$  estimated from the linear relationship between  $\mathbf{k}^2$  and the reciprocal of the scattering intensity in the small  $\mathbf{k}$  limit for the diblock copolymer?

**Solution 2.27 (1):**

$$\begin{aligned} \frac{I_{\text{ex}}(\mathbf{k})}{I_0} &= \frac{4\pi^2 n^2}{\lambda^4 r^2} \frac{MV}{cN_A} \left[ c_a^2 \left( \frac{dn}{dc} \right)_a^2 + 2c_a c_b \left( \frac{dn}{dc} \right)_a \left( \frac{dn}{dc} \right)_b \right. \\ &\quad \left. + c_b^2 \left( \frac{dn}{dc} \right)_b^2 \right] f_D(kR_g) \\ &= \frac{4\pi^2 n^2}{\lambda^4 r^2} \frac{cMV}{N_A} \left[ \frac{c_a}{c} \left( \frac{dn}{dc} \right)_a + \frac{c_b}{c} \left( \frac{dn}{dc} \right)_b \right]^2 f_D(kR_g) \end{aligned}$$

**Solution 2.27 (2):** In the small  $\mathbf{k}$  limit,

$$\begin{aligned} \frac{I_{\text{ex}}(\mathbf{k})}{I_0} &= \frac{4\pi^2 n^2}{\lambda^4 r^2} \frac{MV}{cN_A} \left[ \left( \frac{dn}{dc} \right)_a^2 c_a^2 \left( 1 - \frac{1}{3} k^2 R_{\text{ga}}^2 \right) \right. \\ &\quad + 2 \left( \frac{dn}{dc} \right)_a \left( \frac{dn}{dc} \right)_b c_a c_b \left( 1 - \frac{1}{2} k^2 (R_{\text{ga}}^2 + R_{\text{gb}}^2) \right) \\ &\quad \left. + \left( \frac{dn}{dc} \right)_b^2 c_b^2 \left( 1 - \frac{1}{3} k^2 R_{\text{gb}}^2 \right) \right] \\ &\cong \frac{4\pi^2 n^2}{\lambda^4 r^2} \frac{cMV}{N_A} \left[ \frac{c_a}{c} \left( \frac{dn}{dc} \right)_a + \frac{c_b}{c} \left( \frac{dn}{dc} \right)_b \right]^2 \frac{1}{1 + \frac{1}{3} k^2 R_{\text{g,eff}}^2} \end{aligned}$$

with

$$R_{\text{g,eff}}^2 = \frac{\frac{c_a^2}{c^2} \left( \frac{dn}{dc} \right)_a^2 R_{\text{ga}}^2 + \frac{c_b^2}{c^2} \left( \frac{dn}{dc} \right)_b^2 R_{\text{gb}}^2 + 3 \frac{c_a c_b}{c^2} \left( \frac{dn}{dc} \right)_a \left( \frac{dn}{dc} \right)_b (R_{\text{ga}}^2 + R_{\text{gb}}^2)}{\left[ \frac{c_a}{c} \left( \frac{dn}{dc} \right)_a + \frac{c_b}{c} \left( \frac{dn}{dc} \right)_b \right]^2}$$

**Problem 2.28:** In the preceding question, what happens to the light scattering of the diblock copolymer solution if the solvent is selected so that (1)  $(dn/dc)_a = 0$ , (2)  $(dn/dc)_b = 0$ , (3)  $(c_a/c)(dn/dc)_a + (c_b/c)(dn/dc)_b = 0$ ?

**Solution 2.28 (1):**  $R_{\text{g,eff}} = R_{\text{gb}}$  (a is invisible).

**Solution 2.28 (2):**  $R_{\text{g,eff}} = R_{\text{ga}}$ .

**Solution 2.28 (3):**

$$\frac{I_{\text{ex}}(\mathbf{k})}{I_0} \cong \frac{4\pi^2 n^2}{\lambda^4 r^2} \frac{cMV}{N_A} \left( \frac{dn}{dc} \right)_a^2 \frac{c_a^2}{c^2} \frac{2}{3} k^2 (R_{\text{ga}}^2 + R_{\text{gb}}^2)$$

Note that  $I_{\text{ex}}(0) = 0$ . The condition of the zero average differential refractive index is sometimes called *optical theta*.

**Problem 2.29:** What is the scattering from a telechelic molecule in which two identical small spheres are attached to the ends of a flexible chain that is isorefractive with the solvent? Assume the flexible chain follows the Gaussian statistics of  $N$  segments.

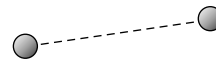


**Solution 2.29:** Two spheres are at  $\mathbf{r}_i$  and  $\mathbf{r}_j$ , separated by a distance between the two Gaussian chain ends. The scattering comes from the two spheres only.

Their structure factor is

$$\begin{aligned}
 S_1 &= \frac{1}{2} \sum_{i=1}^2 \sum_{j=1}^2 \langle \exp[i\mathbf{k} \cdot (\mathbf{r}_i - \mathbf{r}_j)] \rangle = 1 + \langle \exp[i\mathbf{k} \cdot (\mathbf{r}_1 - \mathbf{r}_2)] \rangle \\
 &= 1 + \int d(\mathbf{r}_1 - \mathbf{r}_2) (2\pi N b^2 / 3)^{-3/2} \exp\left(-\frac{3(\mathbf{r}_1 - \mathbf{r}_2)^2}{2N b^2}\right) \exp[i\mathbf{k} \cdot (\mathbf{r}_1 - \mathbf{r}_2)] \\
 &= 1 + \exp\left(-\frac{1}{6} N b^2 \mathbf{k}^2\right) = 1 + \exp(-R_g^2 \mathbf{k}^2)
 \end{aligned}$$

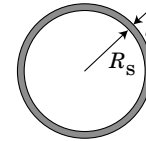
**Problem 2.30:** What is the scattering from a telechelic molecule in which two identical small spheres are attached to the end of a rodlike molecule of length  $L$  that is isorefractive with the solvent?



**Solution 2.30:** Two spheres are at  $\mathbf{r}_i$  and  $\mathbf{r}_j$  separated by  $L$ . The scattering comes from the two spheres only. Let the angle between  $\mathbf{k}$  and the rod be  $\theta$ .

$$S_1 = 1 + \langle \exp[i\mathbf{k} \cdot (\mathbf{r}_1 - \mathbf{r}_2)] \rangle = 1 + \frac{1}{2} \int_0^\pi \sin\theta d\theta \exp(ikL \cos\theta) = 1 + \frac{\sin kL}{kL}$$

**Problem 2.31:** What is the scattering from a spherical molecule of radius  $R_s$  uniformly coated with a layer of thickness  $l$ ? Assume that only the coated layer is visible, i.e., the interior of the sphere is isorefractive with the solvent, and  $l \ll R_s$ .



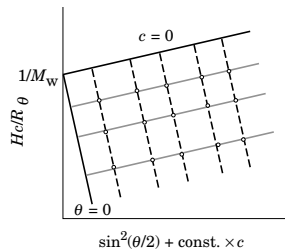
**Solution 2.31:** The single-scatterer structure factor is

$$\begin{aligned}
 S_1 &= N \langle \exp[i\mathbf{k} \cdot (\mathbf{r}_1 - \mathbf{r}_2)] \rangle = N \frac{1}{4\pi R_s^2 l} \int_{R_s}^{R_s+l} r^2 dr \int_0^\pi \sin\theta d\theta \int_0^{2\pi} d\phi \exp(ikr \cos\theta) \\
 &= N \frac{4\pi}{4\pi R_s^2 l} \int_{R_s}^{R_s+l} r^2 dr \frac{\sin kr}{kr} = N \frac{\sin kR_s}{kR_s}
 \end{aligned}$$

where  $N$  is the number of small molecules that coat the sphere surface.

**Problem 2.32:** Draw a sketch of the Zimm plot for a solution of a polymer with the same  $M_w$  and  $R_g$  but with  $A_2$  just the opposite in sign to the one shown in Figure 2.49.

**Solution 2.32:**



## 2.5 SIZE EXCLUSION CHROMATOGRAPHY AND CONFINEMENT

### 2.5.1 Separation System

**Size exclusion chromatography (SEC)** has been widely used since its introduction during the 1960s. It offers a simple yet unbiased method to characterize the molecular weight distribution of a polymer. Although it uses a flow system, the separation principle and the analysis are based on a static property of the polymer molecules in solution. We briefly look at the separation system here before learning the principle.

Figure 2.54 illustrates the separation system. A high-pressure liquid pump draws a solvent called a **mobile phase** from the reservoir and pumps it into a column at a constant flow rate. At one time, a small amount of a dilute solution of polymer dissolved in the same solvent is injected into the stream from a sample loop by changing the position of the injection valve. The column is packed with porous materials, typically polymeric beads with many tiny through holes (pores).

The polymer molecules are partitioned between the small confines of the **pore**, called the **stationary phase**, and the interstitial space between the beads (mobile phase). Polymer molecules with a dimension smaller than the pore size enter the pore more easily than larger polymer molecules do. As the injected polymer solution is transported along the column, low-molecular-weight components are frequently partitioned to the stationary phase, whereas high-molecular-weight components remain mostly in the mobile phase (see Fig. 2.55). Therefore, it takes a longer time for the low-molecular-weight components to reach the column outlet. The band of the polymer in the mobile phase is narrow when injected but spreads according to the molecular weight distribution as the solution moves along the column.

The liquid that comes off the column is called the **eluent**. A detector with a flow cell is placed downstream to measure the concentration (mass/volume) of the polymer in the eluent. A differential refractometer is most commonly used to measure

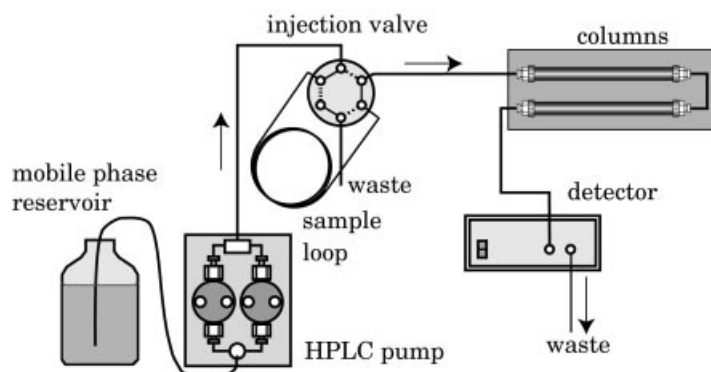


**Figure 2.54.** Schematic of the size exclusion chromatography system.

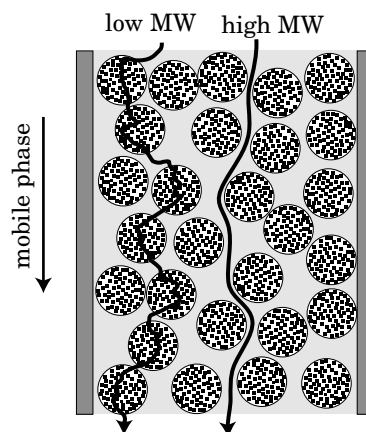


**Figure 2.55.** Transport of polymer molecules in the size exclusion column. High-molecular-weight (MW) components stay mostly in the mobile phase, whereas low-MW components are partitioned to the stationary phase more frequently.

the difference in the refractive index between the eluent and the pure solvent (Section 2.4.7). The difference is proportional to the concentration, with  $dn/dc$  being the proportionality constant. If the polymer has an ultraviolet absorption but the solvent does not, one can use an ultraviolet detector. The absorbance is proportional to the concentration by Beer's law.

Figure 2.56 shows the signal intensity of the detector plotted as a function of **retention time** ( $t_R$ ), the time measured from the injection of the polymer solution. The **retention volume** ( $V_R$ ), the cumulative volume of the fluid out of the column since the injection, can also be used for the abscissa. The curve is called a **retention curve** or a **chromatogram**. The height of a point on the curve above the baseline is proportional to the concentration at a given retention time. The signal maximizes at the peak retention time ( $t_p$ ). The integral of the curve is proportional to the total

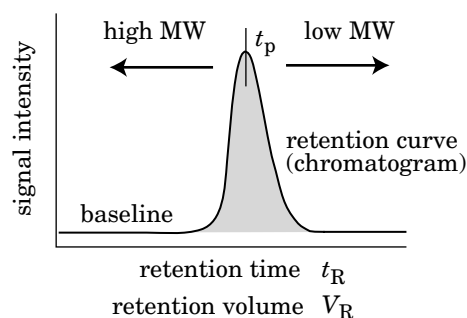


**Figure 2.56.** Typical SEC chromatogram. The signal intensity proportional to the eluent concentration is plotted.

amount of the polymer injected. The spread of the polymer band by the column is translated into a broadened chromatogram. Because high-molecular-weight components elute earlier, the time axis can be regarded as a reversed molecular weight axis.

SEC has other names. When the mobile phase is an organic solvent, SEC is also called **gel permeation chromatography (GPC)**. When it is aqueous, SEC is also called **gel filtration chromatography (GFC)** or aqueous GPC.

### 2.5.2 Plate Theory

**Plate theory** is useful to explain the band broadening during the transport of polymer molecules along the column. In the theory, the whole length of the column is divided into  $N_{pl}$  plates of an equal height. Each plate consists of the mobile phase and the stationary phase. Figure 2.57 explains what is supposed to occur in the plates. In each plate, the polymer molecules are partitioned between the two phases. The mobile phase moves to the next plate in a given time  $t_1$  (plate height/linear velocity of the mobile phase), whereas the stationary phase does not. The moved mobile phase establishes concentration equilibrium with the stationary phase in the next plate. Equilibration and transport of the mobile phase are repeated in all of the plates each time. As a result, a completely excluded polymer (too large to enter the pore) requires a time of  $t_1 N_{pl}$  to reach the outlet. A lower-molecular-weight polymer molecule needs a longer time to come out of the column.

When equilibrium is reached in the plate, the polymer concentration is  $c_S$  in the stationary phase and  $c_M$  in the mobile phase. Their ratio is called the **partition coefficient  $K$** :

$$K \equiv c_S/c_M \quad (2.124)$$

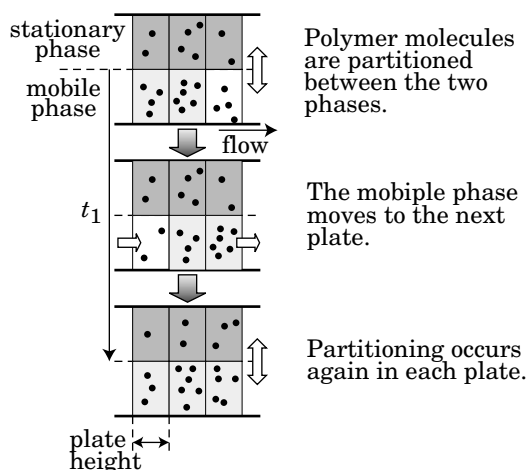


**Figure 2.57.** Plate theory in column chromatography.



When the concentration is sufficiently low ( $c_M \ll c^*$ , overlap concentration),  $K$  does not depend on  $c_M$  but depends on the ratio of the chain dimension to the pore size.

The **partition ratio**  $k'$  is defined as the ratio in the number of molecules between the two phases and given as

$$k' = KV_S/V_M \quad (2.125)$$

where  $V_S$  and  $V_M$  are the volumes of the two phases. The polymer molecules are partitioned with a probability of  $k'/(1+k')$  to the stationary phase and with a probability of  $1/(1+k')$  to the mobile phase. Partitioning in each occurs independently of the other plates and of the equilibration at other times. If the retention time of a particular polymer molecule is  $t_R = t_1(N_{pl} + N_{ex})$ , then this polymer molecule has been partitioned  $N_{ex}$  times to the stationary phase and  $N_{pl}$  times to the mobile phase before it reaches the outlet. Then,

$$k' = N_{ex}/N_{pl} \quad (2.126)$$

From Eqs. 2.125 and 2.126, we find that  $K$  depends linearly on  $t_R$  by

$$K = \frac{V_M}{V_S} \left( \frac{t_R}{t_1 N_{pl}} - 1 \right) \quad (2.127)$$

as seen in Figure 2.58, where  $t_1 N_{pl}$  is the retention time for a completely excluded component.

### 2.5.3 Partitioning of Polymer with a Pore

**2.5.3.1 Partition Coefficient** Figure 2.59 illustrates equilibrium of polymer molecules between the pore space (stationary phase) and the surrounding fluid

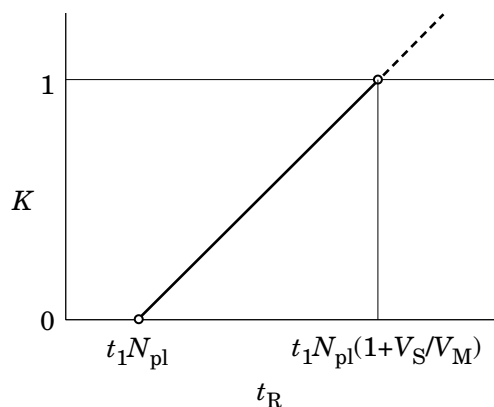


**Figure 2.58.** The partition coefficient  $K$  has a linear relationship with the retention time  $t_R$ . At  $t_R = t_1 N_{pl}$ ,  $K = 0$  (total exclusion).  $K$  does not exceed 1 in SEC unless there is an attractive interaction between the polymer and the pore surface.

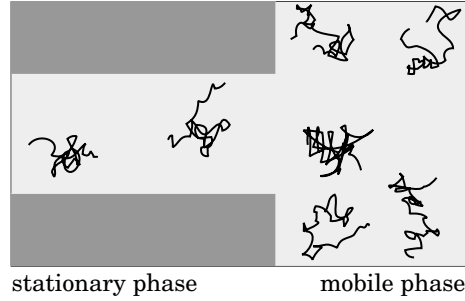


**Figure 2.59.** Polymer chains are partitioned between the stationary phase (pore space) and the mobile phase (surrounding fluid).

(mobile phase). The concentration equilibrium is reached when the chemical potential of the polymer molecule becomes equal between the two phases. At low concentrations, the solution is ideal. The chemical potential of the polymer molecule ( $\mu_M$ ) in the mobile phase of concentration ( $c_M$ ) is given by

$$\mu_M = \mu^\circ + k_B T \ln(c_M/c^\circ) \quad (2.128)$$

where  $\mu^\circ$  is the chemical potential in a reference state of concentration  $c^\circ$  in the ideal solution. When the polymer molecule is brought into the stationary phase, its entropy changes by  $\Delta S$  and its enthalpy by  $\Delta H$ . The entropy change is related to the decrease in the available space the centroid of the molecule can reach as well as the decrease in the total number of conformations. Because of these geometrical restrictions,  $\Delta S < 0$ . The enthalpy change is due to interactions of the polymer molecule with the pore surface and can be positive or negative. When the polymer chain enters the pore, surface–monomer contacts replace some of the monomer–solvent contacts, resulting in the enthalpy change. The chemical potential in the stationary phase ( $\mu_S$ ) of concentration ( $c_S$ ) is then given by

$$\mu_S = \mu^\circ + k_B T \ln(c_S/c^\circ) - T\Delta S + \Delta H \quad (2.129)$$

The concentration equilibrium is dictated by  $\mu_S = \mu_M$ :

$$k_B T \ln(c_S/c^\circ) - T\Delta S + \Delta H = k_B T \ln(c_M/c^\circ) \quad (2.130)$$

which gives the partition coefficient  $K = c_S/c_M$ :

$$K = \exp\left(\frac{\Delta S}{k_B} - \frac{\Delta H}{k_B T}\right) \quad (2.131)$$

Because of the specific nature in the three-way interactions between polymer, surface, and solvent, there is hardly a universal method that allows us to predict  $\Delta H$

for a given combination of the polymer, surface, and solvent. In contrast,  $\Delta S$  is universal because it is determined by the geometrical confinement of the polymer molecule by the pore. In ideal SEC, the stationary phase is designed to provide purely entropic effects for any combination of polymer and solvent as long as the solvent is good to the polymer. Then,  $\Delta H = 0$  and

$$K = \exp(\Delta S/k_B) \quad (2.132)$$

Because  $\Delta S < 0$ ,  $K < 1$ . With Eq. 2.127, we then find that  $t_R$  ranges between  $t_1 N_{pl}$  and  $t_1 N_{pl}(1 + V_S/V_M)$ .

In a different mode of chromatography,  $\Delta S$  is rather suppressed and the differences in  $\Delta H$  between different polymers are utilized to analyze the chemical composition of the polymer. If  $\Delta H > 0$ , the pore wall repels the polymer. Otherwise, it adsorbs the polymer.

Recall that a polymer chain is described by a thin thread in the crudest approximation. This geometrical object interacts with the pore, another geometrical object. The confinement effect is manifested in the partition coefficient and the change in the chain conformation. We can expect an interesting relationship between the chain and the geometry of the pore. However, the geometry in the porous medium used in SEC is far from simple. The pore is rather highly tortuous. Theories have been developed for some simple geometries such as a slit, a square tube, and a cylinder.

**2.5.3.2 Confinement of a Gaussian Chain** We learn here how a Gaussian chain changes upon confinement by various geometries such as a slit, a square tube, and a cylindrical tube. It is possible to obtain a formula for the partition coefficient in each of the three geometries.

We first recall that the Gaussian transition probability  $G(\mathbf{r}, \mathbf{r}')$  given by Eq. 1.34 can be factored into three independent components  $G_x$ ,  $G_y$ , and  $G_z$ , where  $G_z$  is given by

$$G_z(z, z') = \frac{1}{2\pi^{1/2}R_g} \exp\left[-\frac{(z - z')^2}{4R_g^2}\right] \quad (2.133)$$

for example, for chains with radius of gyration  $R_g$ . When the Gaussian chain is brought into a slit of width  $d$  extending in  $x$  and  $y$  directions (Fig. 2.60),  $G_x$  and  $G_y$  do not change because each component is independent. Only  $G_z$  experiences a change. Casassa<sup>27</sup> calculated  $G_z$  for a one-dimensional random walker starting at  $z'$  to reach  $z$  after necessary number of steps without touching the slit walls. The result is

$$G_{z,\text{slit}}(z, z') = \frac{2}{d} \sum_{k=1}^{\infty} \sin \frac{k\pi z}{d} \sin \frac{k\pi z'}{d} \exp[-(k\pi R_g/d)^2] \quad (2.134)$$

Figure 2.61 compares the two distribution functions for the chain end  $z$  when the other end is at  $z' = d/2$ .  $R_g = d/4$  was assumed.

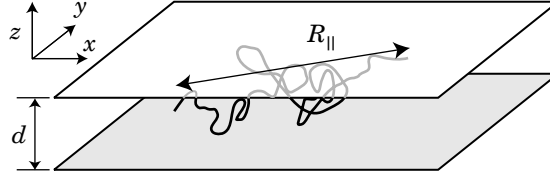


**Figure 2.60.** Polymer chain confined to a slit of width  $d$ . The chain has a dimension of  $R_{||}$  along the slit walls. Its dimension in  $z$  direction is bound to  $d$ .

The partition coefficient  $K_{\text{slit}}$  is then calculated as the average of  $G_z(z, z'; N)$  with respect to  $z$  and  $z'$ :

$$K_{\text{slit}} = d^{-1} \int_0^d dz \int_0^d dz' G_z(z, z') = \frac{8}{\pi^2} \sum_{k:\text{odd}} k^{-2} \exp[-(k\pi R_g/d)^2] \quad (2.135)$$

When  $R_g \gg d$ , the first term dominates:

$$K_{\text{slit}} \cong \exp[-(\pi R_g/d)^2] \quad (2.136)$$

It is now clear that  $K_{\text{slit}}$  decreases sharply as  $R_g$  increases and becomes comparable to  $d$ .

Because there is no confinement in the  $x$  and  $y$  directions,  $G_x$  and  $G_y$  do not change. The mean square end-to-end distance does not change its  $x$  and  $y$  components. Thus, the chain dimension  $R_{||}$  along the slit wall is given by

$$R_{||}^2 = \langle R_{Fx}^2 \rangle + \langle R_{Fy}^2 \rangle = \frac{2}{3} Nb^2 \quad (2.137)$$

Confinement by a square tube extending in the  $x$  direction and having a square cross section of length  $d$  changes each of  $G_y$  and  $G_z$  in the same way as the slit does

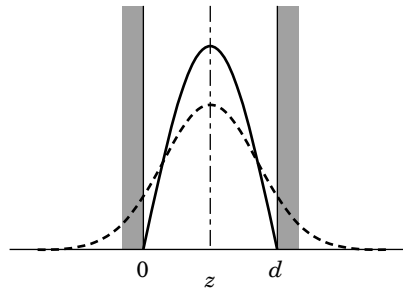


**Figure 2.61.** Density profile of the end of the Gaussian chain when the other end is at  $z = d/2$ . The density is compared for the confined chain (solid line) in a slit of walls at  $z = 0$  and  $z = d$  and the unconfined chain (dashed line).  $R_g = d/4$  was assumed.

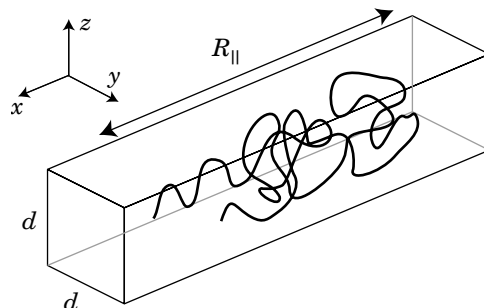


**Figure 2.62.** Polymer chain confined to a square tube of side  $d$ . The chain has a dimension of  $R_{\parallel}$  along the tube. Its dimensions in  $y$  and  $z$  directions are bound to  $d$ .

on  $G_z$  (Fig. 2.62). Confinement in one direction contributes to decreasing the partition coefficient by a factor of  $K_{\text{slit}}$ . The confinement in the  $y$  and  $z$  directions results in the partition coefficient of  $K_{\text{slit}}^2$ . The chain dimension along the  $x$  direction is unchanged from that of the unconfined chain:

$$R_{\parallel}^2 = \langle R_{\text{Fx}}^2 \rangle = \frac{1}{3}Nb^2 \quad (2.138)$$

The three relationships in Eqs. 2.136–2.138 apply to other, non-Gaussian ideal chains. When the ideal chain is sufficiently long, then Eqs. 2.134 and 2.135 also apply.

The partition coefficient for a cylindrical pore was obtained similarly.<sup>27</sup> Likewise, the partition coefficient was calculated for a rodlike molecule in some simple geometries.<sup>28</sup> Figure 2.63 compares the partitioning of a Gaussian chain and a rodlike molecule in a cylindrical pore of radius  $R_p$ .<sup>29</sup> The plot of  $K$  is given as a

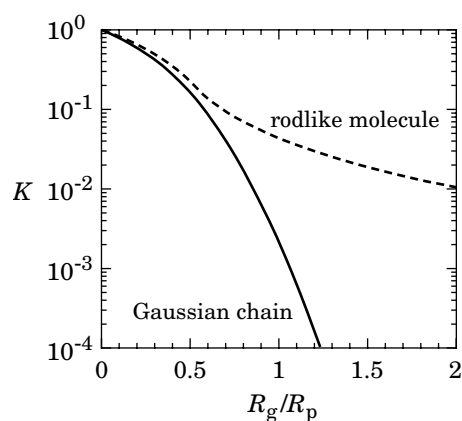


**Figure 2.63.** Partition coefficients  $K$  of a Gaussian chain and a rodlike molecule in a cylindrical pore of radius  $R_p$  as a function of  $R_g/R_p$ . (From Ref. 29.)

function of  $R_g/R_p$ . At  $R_g = R_p$ , only 1 of about 470 Gaussian chains finds itself in the pore. For the rodlike molecule ( $R_g = L/12^{1/2}$ ; at  $R_g = R_p$ , the rod length is  $3^{1/2} \times$  pore diameter), this odd is as large as 1 of 23 rods. The rod can align along the pore channel to fit in.

**2.5.3.3 Confinement of a Real Chain** The Gaussian chain is folded back into a dense packing of monomers when confined. In a real chain, overlay of monomers into the same space is prohibited. We can therefore expect that the real chain is more extended in the confined space compared with the free space. It is, however, all but impossible to treat the confinement of the real chain theoretically. We do not have a formula for the partition coefficient of the real chain even in simple confining geometries. Fortunately, it is possible to obtain an asymptotic functional relationship between  $\Delta S$  and the chain length  $N$  for sufficiently long chains in a simple geometrical consideration.

We consider a real chain consisting of  $N$  monomers of size  $b$  and confined to a cylindrical pore of diameter  $d$ . When the chain dimension  $R_g$  in the free solution is smaller than the pore size, the chain does not feel much of the effect of the pore wall. As  $R_g$  exceeds  $d$ , the chain must adopt a conformation extending along the pore because of the excluded volume effect. As  $R_g$  increases further, the confined chain will look like a train of spheres of diameter  $d$  (see Fig. 2.64). The excluded volume effect prohibits the spheres from overlapping with each other. Therefore, the spheres can be arranged only like a shish kebab. The partial chain within each sphere follows a conformation of a real chain in the absence of confinement. The number  $n_d$  of monomers in the sphere is then given by

$$d \cong b n_d^{3/5} \quad (2.139)$$

where  $n = 3/5$  was used (we will use the value in this section). The confined chain consists of  $N/n_d$  spheres. The length  $R_{||}$  of the chain in the tube is then given as

$$R_{||} \cong d(N/n_d) \cong dN(b/d)^{5/3} \cong d(R_g/d)^{5/3} \quad (2.140)$$

Unlike a Gaussian chain,  $R_{||}$  increases linearly with  $N$ . Note that  $R_g$  refers to the radius of gyration of unconfined chains.

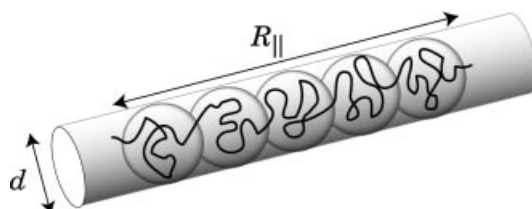


**Figure 2.64.** Real chain confined to a cylindrical pore of diameter  $d$ . The chain is regarded as a packed array of spheres of diameter  $d$  in one dimension. Within each sphere, the chain is three-dimensional.

Now we calculate the partition coefficient. The polymer chain consists of  $N/n_d$  spheres of size  $d$ . This sequence of self-avoiding spheres has the same end-to-end distance in the three-dimensional space as the chain of  $N$  monomers does (Problem 2.33). Therefore, grouping the monomers into spheres of  $n_d$  monomers does not introduce an artificial change in the statistical property of the chain. How the spheres are arranged in the three-dimensional space determines the overall conformation of the chain. We imagine a cubic lattice and place the spheres on the grid points separated by  $d$ . In the absence of the cylindrical pore, the number of possible grid points available to place the next sphere is five (six minus one, one being the preceding sphere; see Fig. 2.65 (a)). Thus the total number of the arrangement of the  $N/n_d$  spheres is roughly  $5^{N/n_d}$ . The condition that the spheres do not overlap decreases the total number, but the correction is small. Within the cylindrical pore, in contrast, there is only one possibility to place the next sphere, once the second sphere is placed (Fig. 2.65 (b)). There is only one possibility or two for the conformation of the whole sequence of spheres. The partition coefficient is calculated as the ratio of the possible numbers of arrangement:

$$K \cong \frac{1}{5^{N/n_d}} \quad (2.141)$$

Because  $K = \exp(\Delta S/k_B)$ , the entropy change  $\Delta S$  is expressed as

$$-\Delta S/k_B = -\ln K \cong N/n_d \cong N(b/d)^{5/3} \cong (R_g/d)^{5/3} \quad (2.142)$$

The decrease in the entropy,  $-\Delta S$ , grows linearly with  $N$ , i.e., a longer chain experiences a greater restriction on its conformation in the pore. It is interesting to see that the same power law,  $-\Delta S \sim N$ , also applies to the ideal chain if we replace  $5/3 = 1/\nu$  by 2. The proportionality to  $N$  is common between the ideal chain and the real chain. This result is not a coincidence. If we follow the same discussion as above to calculate  $K$  for the ideal chain, the number of arrangement for the spheres in the pore is  $2^{N/n_d}$ , as opposed to  $6^{N/n_d}$  in the free solution. The ratio leads to  $-\Delta S/k_B \cong N/n_d \cong (R_g/d)^2$ . The confinement of the Gaussian chain gives the same relationship: From  $K = K_{\text{slit}}^2$  and Eq. 2.136, we find  $-\Delta S/k_B \cong (R_g/d)^2$ .

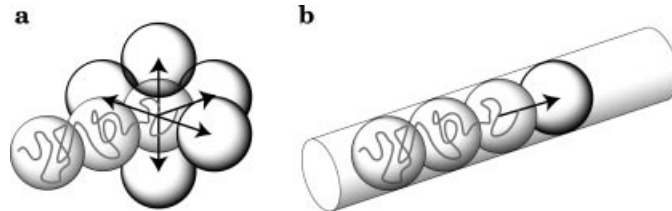


**Figure 2.65.** Conformation of a real chain. When the next sphere is attached to the growing end, there are five possible positions in the absence of the cylindrical pore (a), but only one is available within the pore (b).

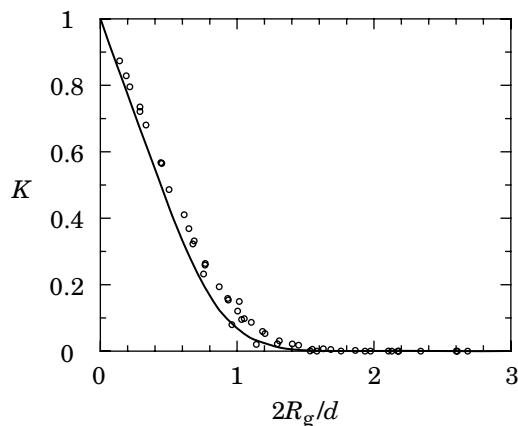


**Figure 2.66.** Partition coefficients  $K$  of a Gaussian chain (solid line) and a real chain (circles) with a radius of gyration  $R_g$  in a slit of width  $d$ . The data for the real chain were obtained in the computer simulation (From Ref. 5).

How about the confinement by the slit? The spheres are arranged in the two-dimensional space. The number of arrangements is now  $3^{N/n_d}$ . Then,  $-\Delta S$  follows the same scaling relationship as Eq. 2.142 except the numerical coefficient. Figure 2.66 compares the partition coefficients of the Gaussian chain (solid line) and the real chain (circles) with a radius of gyration  $R_g$  in a slit of width  $d$ . The coefficients for the real chain were obtained in lattice computer simulations.<sup>5</sup>

The linear dimension of the chain in the slit is different from the counterpart in the cylindrical pore. Because the confined chain follows the conformation of two-dimensional excluded-volume chain,

$$R_{||} \cong d(N/n_d)^{3/4} \cong d(R_g/d)^{5/4} \quad (2.143)$$

Here we used the fact that, in two dimensions, the self-avoiding random walk has an exponent of  $3/4$  in the relationship between  $R_F$  and  $N$  (Problem 1.13). We can also derive the above relationship by applying Flory's method that we used to derive the chain dimension in three dimensions (Problem 2.34).

As seen in the above examples, confinement lowers the number of dimensions available to a polymer chain. In the Gaussian chain, on the one hand, the confinement changes the confined components only. The root mean square end-to-end distance changes only by a numerical coefficient without changing the dependence of  $R_F$  on  $N$ . In the real chain, on the other hand, the decrease in the dimensionality changes qualitatively the relationship between  $N$  and  $R_{||}$  from that in the free solution. The confinement manifests the excluded volume effect more prominently.

#### 2.5.4 Calibration of SEC

We have learned in Section 2.5.2 that the retention time  $t_R$  of SEC increases linearly with  $K$ . We also learned in Section 2.5.3 that  $K \cong (1/5)^{N/n_d}$  for the partitioning of



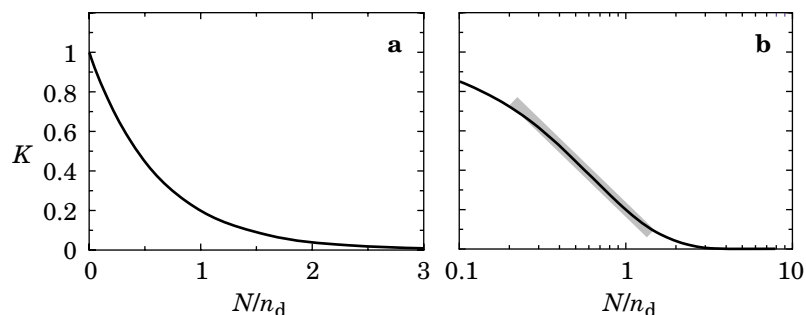


**Figure 2.67.** Sketch of the partition coefficients  $K$  of a real chain as a function of the number of blobs,  $N/n_d$ . In linear scale (a) and in semi-logarithmic scale (b) of  $N/n_d$ . The shaded region in (b) indicates a nearly straight portion of the plot.

the real chain with a cylindrical pore. The porous material used in SEC has a tortuous, interconnected pore structure. The pore resembles a cylindrical pore over a short distance.

Figure 2.67a is a plot of  $K = (1/5)^{N/n_d}$  as a function of  $N/n_d$ . The plot of  $K_0$  for the Gaussian chain with a cylindrical pore in Figure 2.63 is close to this plot when the abscissa is changed to  $(R_g/R_p)^{5/3} \sim N$  and the ordinate is in linear scale. Therefore, we can extend the use of  $K = (1/5)^{N/n_d}$ , originally derived for sufficiently long chains, to shorter chains. The same plot in panel a, when the abscissa is in a log scale (Fig. 2.67b), is nearly straight in the middle range of  $K$ . An SEC column packed with such porous materials will have a linear relationship between  $t_R$  and  $\log M$  in a certain range of the molecular weight  $M$ . The relationship is schematically depicted in Figure 2.68. The column is therefore able to resolve the molecular weight distribution in the logarithmic scale, but in a limited range. Above the upper threshold,  $t_R$  becomes insensitive to  $M$ . This limit is called the **exclusion limit**. Polymer chains with a molecular weight higher than the limit do not partition with the stationary phase and travel the column straight through to elute in  $t_1 N_{pl}$ . Below

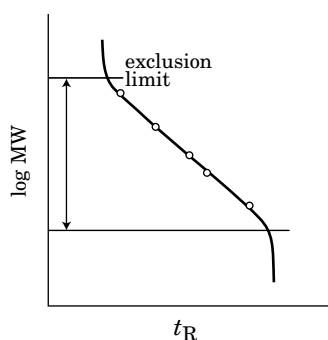


**Figure 2.68.** Calibration curve of a size-exclusion column. The column can analyze the molecular weight (MW) of the polymer only in the range indicated by the arrow.

the lower threshold,  $t_R$  becomes again insensitive to  $M$ . The pore size is too large to distinguish the polymer chain by its dimension.

The packing material with a greater pore size effectively increases  $n_d$  and shifts the range of molecular weight that the column can analyze to a greater molecular weight. The range can be broadened by mixing packing materials of different pore diameters at the expense of the resolution. A so-called linear column is prepared in this way. Another way is to connect columns of different pore diameters in series.

To relate the retention time to molecular weight for a given series of columns, we use molecular weight standards. They are commercially available. Manufacturers supply the data of  $M_w$ ,  $M_n$ , and  $M_p$ , where  $M_p$ , the peak molecular weight, is the molecular weight at the peak of the SEC retention curve. A calibrated column can convert the retention curve into the plot of the molecular weight distribution.

### 2.5.5 SEC With an On-Line Light-Scattering Detector

Since approximately 1990, light-scattering detectors have been increasingly used as an on-line detector in SEC, providing more detailed information on the polymer chain conformation in the solution state. The detector has a flow cell with a small cell volume and measures the scattering intensities at different angles. The advantage of this scheme for characterization of polymer in solution is obvious. As the column separates the polymer according to molecular weight, each fraction is led to the light-scattering detector for instantaneous measurement of the scattering intensities [ $I_{ex}(\theta)$ ], as illustrated in Figure 2.69. The concentration detector such as a refractive index detector and an ultraviolet absorption detector connected in series gives the estimate of the polymer concentration  $c$ . Then with the preinput data of  $dn/dc$ , a Zimm plot is prepared for each fraction. The plot is for one concentration only, but it is sufficiently low because of the band broadening (further dilution) by the SEC column of the already dilute injected solution.

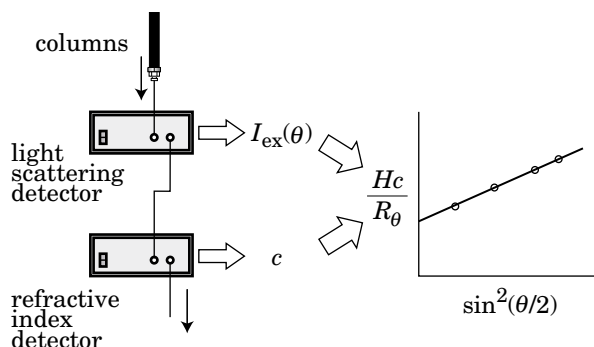


**Figure 2.69.** Use of an online light-scattering detector and a concentration detector in series allows a Zimm plot for every eluent. Thus, the molecular weight and radius of gyration can be estimated as a function of the retention time without using any standard.

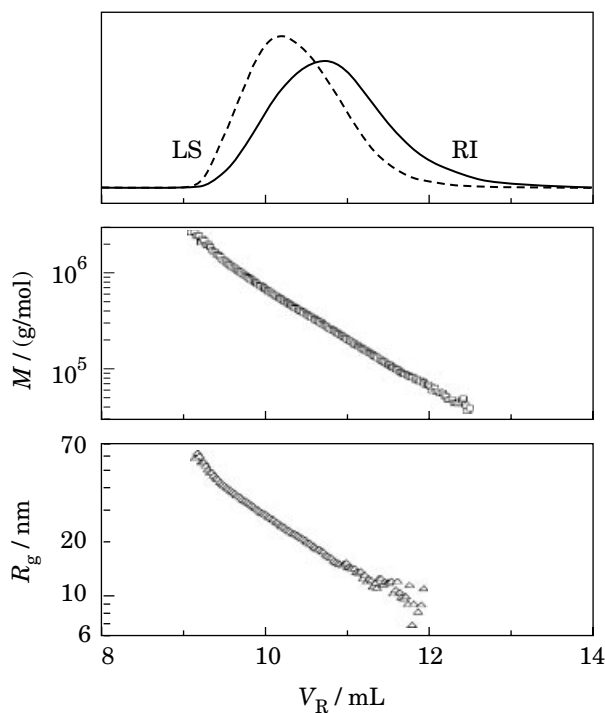


**Figure 2.70.** Typical examples of chromatograms. The solution is branched polyethylene in tetrahydrofuran. Top: light-scattering intensity  $I_{\text{ex}}$  (LS;  $90^\circ$ ) and refractive index difference  $\Delta n$  (RI). Middle: molecular weight  $M$ . Bottom: radius of gyration  $R_g$ , plotted as a function of the retention volume  $V_R$ . (From Ref. 9.)

Thus  $A_2Mc$  is negligible in Eq. 2.116. Because the measurement is instantaneous, injection of a broad-distribution polymer sample results in a plot of the molecular weight  $M$  and the radius of gyration  $R_g$  as a function of the retention time. Thus we can obtain a plot of  $R_g$  as a function of  $M$ . In fact, Figure 1.38 was obtained in this way.

This method eliminates the need to fractionate the polydisperse polymer on a preparative scale and run the tedious light-scattering measurements for each fraction. Figure 2.70 shows an example of SEC chromatograms for branched polyethylene.<sup>9</sup> Panel a shows the refractive index signal  $\Delta n$ , which is proportional concentration, and the light-scattering intensity  $I_{\text{ex}}$  at  $90^\circ$ . Because  $I_{\text{ex}} \propto cM$ , the peak of  $I_{\text{ex}}$  appears ahead of the peak in  $\Delta n$ . Panel b shows the molecular weight  $M$ , and panel c plots  $R_g$ . At both ends of the chromatogram, the concentration is low. The uncertainty in the estimates of  $M$  and  $R_g$  are larger at both ends.

Furthermore, an on-line viscosity detector can be connected in tandem to the concentration detector (and the light-scattering detector). As we will learn in Section 3.3, the solution viscosity gives an important piece of information on the state of polymer molecules in solution.

### 2.5.6 PROBLEMS

**Problem 2.33:** An excluded-volume chain of  $N$  monomers of size  $b$  has a dimension of  $R_F \cong bN^\nu$ . Grouping  $n_d$  monomers into one “big monomer” makes a chain of  $N/n_d$  big monomers with excluded volume. Within each big monomer, the chain is still an excluded-volume chain of monomer size  $b$ . Show that this coarse-grained chain has the same dimension as that of the original chain.

**Solution 2.33:** The size of the big monomer is  $bn_d^\nu$ . Therefore, the dimension of the coarse-grained chain is  $(bn_d^\nu)(N/n_d)^\nu = bN^\nu$ , identical to  $R_F$  of the original chain. The choice of  $n_d$  is arbitrary.

**Problem 2.34:** Flory’s method, we learned in Section 1.4 to find the dimension of the real chain, can be extended to the confined real chain. Find the relationship between the dimension of the chain along the slit wall or the tube wall,  $R_{||}$ , and the degree of polymerization  $N$  for the confinement by (1) a slit of width  $d$  and (2) a tube of diameter  $d$ .

**Solution 2.34 (1):** The volume for a polymer chain confined to the slit is  $R_{||}^2 d$ . Then, the monomer density is  $N/(R_{||}^2 d)$ . The interaction term in Eq. 1.63 is now  $b^3 N^2/(R_{||}^2 d)$ . The free energy  $A_{ch}$  of the chain with a dimension of  $R_{||}$  is Flory’s method given as

$$\frac{A_{ch}}{k_B T} \cong \frac{R_{||}^2}{Nb^2} + b^3 \frac{N^2}{R_{||}^2 d}$$

At its minimum,

$$\frac{\partial}{\partial R_{||}} \frac{A_{ch}}{k_B T} \cong \frac{2R_{||}}{Nb^2} - 2b^3 \frac{N^2}{R_{||}^3 d} = 0$$

Therefore,

$$R_{||} \cong b^{5/4} N^{3/4} / d^{1/4} = d(bN^{3/5}/d)^{5/4} = d(R_g/d)^{5/4}$$

which is identical to Eq. 2.143.

**Solution 2.34 (2):** In the tube, the volume for the polymer chain is  $R_{||} d^2$ . Then,

$$\frac{A_{ch}}{k_B T} \cong \frac{R_{||}^2}{Nb^2} + b^3 \frac{N^2}{R_{||} d^2}$$

At its minimum,

$$\frac{\partial}{\partial R_{||}} \frac{A_{ch}}{k_B T} \cong \frac{2R_{||}}{Nb^2} - b^3 \frac{N^2}{R_{||}^2 d^2} = 0$$

Therefore,

$$R_{\parallel} \cong b^{5/3}N/d^{2/3} = d(bN^{3/5}/d)^{5/3} = d(R_g/d)^{5/3}$$

which is identical to Eq. 2.140.

**Problem 2.35:** Repeat the preceding problem for the theta chains.

**Solution 2.35 (1):** The interaction term in Eq. 1.63 is  $b^6N^3/(R_{\parallel}^2d)^2$ . The free energy  $A_{\text{ch}}$  of the chain with a dimension of  $R_{\parallel}$  is given as

$$\frac{A_{\text{ch}}}{k_B T} \cong \frac{R_{\parallel}^2}{Nb^2} + b^6 \frac{N^3}{R_{\parallel}^4 d^2}$$

At its minimum,

$$\frac{\partial}{\partial R_{\parallel}} \frac{A_{\text{ch}}}{k_B T} \cong \frac{2R_{\parallel}}{Nb^2} - 4b^6 \frac{N^3}{R_{\parallel}^5 d^2} = 0$$

Therefore,

$$R_{\parallel} \cong b^{4/3}N^{2/3}/d^{1/3} = d(bN^{1/2}/d)^{4/3} = d(R_g/d)^{4/3}$$

**Solution 2.35 (2):** The volume is  $R_{\parallel}d^2$ . Then,

$$\frac{A_{\text{ch}}}{k_B T} \cong \frac{R_{\parallel}^2}{Nb^2} + b^6 \frac{N^3}{R_{\parallel}^2 d^4}$$

At its minimum,

$$\frac{\partial}{\partial R_{\parallel}} \frac{A_{\text{ch}}}{k_B T} \cong \frac{2R_{\parallel}}{Nb^2} - 2b^6 \frac{N^3}{R_{\parallel}^3 d^4} = 0$$

Therefore,

$$R_{\parallel} \cong b^2N/d = d(bN^{1/2}/d)^2 = d(R_g/d)^2$$

Note that these results for the theta chains are different from the chain dimensions of ideal chains in the slit and the tube. The confined ideal chains have the dimension of  $\sim N^{1/2}$  in both confining geometries. The difference between the ideal chain and the theta chain shows up because of the third virial coefficient  $A_3$ . Compensation of the excluded volume effect by the attractive polymer–polymer interaction allows the theta chain to have the same dimension as that of the ideal chain, but it is valid only in the three-dimensional free solution. In spaces of a reduced dimensionality, the same attractive interaction cannot mask the excluded volume.

## APPENDIX 2.A: REVIEW OF THERMODYNAMICS FOR COLLIGATIVE PROPERTIES IN NONIDEAL SOLUTIONS

### 2.A.1 Osmotic Pressure

We briefly review here thermodynamics of a nonideal binary solution. The osmotic pressure  $\Pi$  is the extra pressure needed to equilibrate the solution with the pure solvent at pressure  $p$  across a semipermeable membrane that passes solvent only. The equilibration is attained when the chemical potential  $\mu_S^*$  of the pure solvent becomes equal to the chemical potential  $\mu_S$  of the solvent molecule in solute volume fraction  $\phi$  at temperature  $T$ :

$$\mu_S^*(T, p) = \mu_S(T, p + \Pi, \phi) \quad (2.A.1)$$

We separate the right-hand side into two parts:

$$\mu_S(T, p + \Pi, \phi) = \mu_S^*(T, p + \Pi) + \Delta\mu_S \quad (2.A.2)$$

where  $\Delta\mu_S$  denotes the change in the chemical potential from  $\mu_S^*$ . Colligative properties make  $\Delta\mu_S$  negative. Because the volume of a liquid depends little on the pressure,

$$\mu_S^*(T, p + \Pi) = \mu_S^*(T, p) + \int_p^{p+\Pi} \frac{\partial \mu_S^*}{\partial p} dp = \mu_S^*(T, p) + v^* \Pi \quad (2.A.3)$$

with  $v^*$  being the volume of the solvent molecule in the liquid phase. From Eqs. 2.A.1 to 2.A.3, we find

$$\Pi = -\frac{\Delta\mu_S}{v^*} \quad (2.A.4)$$

### 2.A.2 Vapor Pressure Osmometry

The colligative property shows up also in the vapor pressure of the solution. The vapor pressure  $p$  of the solvent above the solution is lower than the vapor pressure  $p^*$  of pure solvent. The vapor phase is nearly ideal. Therefore, the chemical potential of the solvent molecule in the vapor phase is given by  $\mu^\circ(T) + k_B T \ln(p/p^\circ)$ , where  $\mu^\circ(T)$  is the chemical potential at a reference pressure  $p^\circ$ . The vapor–liquid equilibrium for pure solvent is dictated by

$$\mu^\circ(T) + k_B T \ln(p^*/p^\circ) = \mu_S^*(T, p^*) \quad (2.A.5)$$

For a solution with a polymer volume fraction at  $\phi$ , the equilibrium is given by

$$\mu^\circ(T) + k_B T \ln(p/p^\circ) = \mu_S(T, p, \phi) \quad (2.A.6)$$

From Eqs. 2.A.2, 2.A.5, and 2.A.6, we find

$$k_B T \ln(p/p^*) = \Delta\mu_S + \mu_S^*(T, p) - \mu_S^*(T, p^*) \quad (2.A.7)$$

Because  $\mu_S^*(T, p) = \mu_S^*(T, p^*) + v^*(p - p^*)$  and  $\Delta\mu_S = -v^*\Pi$ ,

$$\frac{\Pi v^*}{k_B T} = -\ln(p/p^*) + \frac{v^*(p - p^*)}{k_B T} \quad (2.A.8)$$

The second term on the right-hand side is much smaller compared with the first term. Thus,

$$\frac{\Pi v^*}{k_B T} = -\ln(p/p^*) \cong \frac{p^* - p}{p^*} \quad (2.A.9)$$

This equation gives the principle of **vapor pressure osmometry**: In place of measuring  $\Pi$  directly, we can measure the drop in the vapor pressure of the solvent above the solution to estimate  $\Pi$ .

## APPENDIX 2.B: ANOTHER APPROACH TO THERMODYNAMICS OF POLYMER SOLUTIONS

Once we have obtained the free energy or the chemical potential expressed as a function of  $\phi$ , we can forget that it was derived for a two-component incompressible fluid consisting of polymer and solvent. We can neglect the presence of solvent molecules and assume that polymer chains are suspended in “vacuum” at volume fraction  $\phi$ . The system is essentially a single-component nonideal gas whose free energy is given by Eq. 2.7.  $\Delta A_{\text{mix}}$  is then the free-energy change of “vaporization” of polymer molecules from their liquid state. The osmotic pressure  $\Pi$  can be obtained directly from  $\Delta A_{\text{mix}}$  (Problem 2.4). In this scenario, the interaction is present only between two monomers of polymer:  $\chi = -Z \varepsilon_{PP}/(2k_B T)$ .

The Gibbs free energy change  $\Delta G_{\text{mix}}$  is given by

$$\Delta G_{\text{mix}} = \Delta A_{\text{mix}} + \Pi \Delta V_{\text{mix}} \quad (2.B.1)$$

where  $\Delta V_{\text{mix}} = V(1 - \phi)$ . It can be shown that this  $\Delta G_{\text{mix}}$  is equal to  $n_P \Delta \mu_P$  (Problem 2.5). Note that this  $\Delta G_{\text{mix}}$  is different from the one we find in the mixing of  $n_P$  polymer chains and  $n_S$  solvent molecules at a constant total volume.

### APPENDIX 2.C: CORRELATION FUNCTION OF A GAUSSIAN CHAIN

The segment density autocorrelation function the Gaussian chain is calculated as follows.

$$\begin{aligned} \frac{N}{\rho} \langle \rho(\mathbf{r})\rho(0) \rangle &= \int_0^N dn \int_0^N dn' (2\pi|n - n'|b^2/3)^{-3/2} \exp\left(-\frac{3\mathbf{r}^2}{2|n - n'|b^2}\right) \\ &= 2 \int_0^N dn \int_0^n dn' (2\pi|n - n'|b^2/3)^{-3/2} \exp\left(-\frac{3\mathbf{r}^2}{2|n - n'|b^2}\right) \end{aligned} \quad (2.C.1)$$

We change the variable of integration from  $n'$  to  $m = n - n'$  and then exchange the order of the double integral:

$$\frac{N}{\rho} \langle \rho(\mathbf{r})\rho(0) \rangle = 2 \int_0^N dm (N - m) (2\pi m b^2/3)^{-3/2} \exp\left(-\frac{3\mathbf{r}^2}{2m b^2}\right) \quad (2.C.2)$$

We change the variable of integration further from  $m$  to  $x$  where  $x^2 = 3\mathbf{r}^2/(2b^2m)$ . With  $u \equiv 3\mathbf{r}^2/(2b^2N) = r^2/(4R_g^2)$  and  $m = Nu/x^2$ , Eq. 2.C.2 is transformed to

$$\frac{N}{\rho} \langle \rho(\mathbf{r})\rho(0) \rangle = \frac{6N}{\pi^{3/2}b^2r} \left[ \int_{u^{1/2}}^{\infty} \exp(-x^2) dx - u \int_{u^{1/2}}^{\infty} \frac{1}{x^2} \exp(-x^2) dx \right] \quad (2.C.3)$$

Using integration by parts, the integral in the second term is changed to

$$\int_{u^{1/2}}^{\infty} \frac{1}{x^2} \exp(-x^2) dx = u^{-1/2} \exp(-u) - 2 \int_{u^{1/2}}^{\infty} \exp(-x^2) dx \quad (2.C.4)$$

Then,

$$\frac{1}{\rho} \langle \rho(\mathbf{r})\rho(0) \rangle = \frac{6}{\pi^{3/2}b^2r} [(1 + 2u)\text{Erfc}(u^{1/2}) - u^{1/2}\exp(-u)] \quad (2.C.5)$$



---

# 3

---

## Dynamics of Dilute Polymer Solutions

### 3.1 DYNAMICS OF POLYMER SOLUTIONS

In the first two chapters, we learned about thermodynamics (free energy, osmotic pressure, chemical potential, phase diagram) of polymer solutions at equilibrium and static properties (radius of gyration, static structure factor, density correlation function) of dissolved polymer chains. This chapter is about dynamics of polymer solutions. Polymer solutions are not a dead world. Solvent molecules and polymer chains are constantly and vigorously moving to change their positions and shapes. Thermal energy causes these motions in a microscopic world.

Solution dynamics deals with the motion of molecules dissolved in a solvent. A typical mode of motion is center-of-mass diffusion. A nonuniform concentration distribution is leveled to a uniform distribution as the solution approaches the equilibrium state. Viscosity of the solution is another form of dynamics. Slowly moving solute molecules increase the viscosity more than fast moving molecules.

Center-of-mass diffusion and viscosity are universally observed in all fluids including pure solvents. What makes the polymer solution dynamics distinctly different from the dynamics of other solutions is the numerous degrees of freedom for the internal motion of each solute molecule. As we learned in Chapter 1, polymer chains can take many different conformations. They are incessantly switching from one to another, thereby changing the shape of the polymer chain. In small molecules, the internal motions such as vibration (changes in the bond lengths, bond angles, and dihedral angles) and rotation are observed at frequencies typically between 1 GHz and 100 THz. The motions are resonant. In contrast, the change in the conformation of the polymer chains occurs at much lower frequencies (radio, audio, and lower frequencies) in addition to the resonant vibrational motions at the high frequencies.

Solvent viscosity makes the motion overdamped and therefore relaxational. Different modes of motion are observed over an extended range at the low frequencies.

A small change in the thermodynamic properties of the solution, as represented by  $A_2$ , leads to a shift in the dynamics, typically the time scale of motion and dependence on the concentration and the molecular weight. It often happens that the shift in the dynamic properties is more pronounced compared with the shift in the static properties. Thus, how the time scale depends on the polymer concentration, the molecular weight, and the temperature gives us an important piece of information on the state of the polymer molecules, especially their interactions with the solvent molecules.

In Chapter 3, we will learn about the dynamics of an isolated polymer chain in the dilute solution limit and the first-order change in the dynamics with polymer concentration. We will also learn typical experimental methods to investigate the dynamics—dynamic light scattering and viscosity. The dynamics of polymer solutions above the overlap concentration will be discussed in Chapter 4, along with their thermodynamics.

## 3.2 DYNAMIC LIGHT SCATTERING AND DIFFUSION OF POLYMERS

### 3.2.1 Measurement System and Autocorrelation Function

**3.2.1.1 Measurement System** Motions of polymer molecules in solution can be conveniently studied by using **dynamic light scattering (DLS)**. It is also called **quasi-elastic light scattering (QELS)** and **photon correlation spectroscopy (PCS)**. Measurement at a single scattering angle gives information on the dimension of the polymer molecule in the solution with reasonable accuracy. Unlike its static version, DLS does not rely on the excess scattering. There is no need to calculate a small difference in the scattering intensity between the pure solvent and a dilute solution. The signal from the slowly moving polymer is unambiguously separated from the signal that originates from the rest of the solution. The principle of DLS has been utilized in some commercial particle-sizing systems for many years. The measurement and data analysis are automated. Users need only to prepare clean solutions by filtration. In recent years, DLS has been also used as an on-line detector in size exclusion chromatography (SEC). In this section, we will learn how the signal obtained in DLS is related to the dimension and motions of solute molecules and other dynamic modes.

As shown in Figure 3.1, a DLS system requires an **autocorrelator** on top of a regular SLS system. The light-scattering intensity from the polymer solution is not a constant. Figure 3.2a illustrates how the intensity ( $I$ ) varies with time ( $t$ ).  $I(t)$  fluctuates around its mean  $\langle I \rangle$ . It may appear completely random (white noise) and therefore meaningless, but it is not. Motions of the polymer molecules and the solvent molecules contribute to a change of  $I(t)$  with time. The noisy signal then

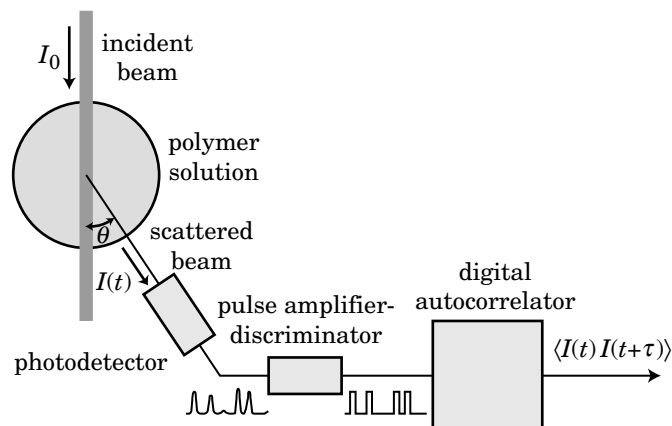


**Figure 3.1.** Dynamic light scattering measurement system. The pulse-amplifier discriminator converts the analog signal of the photodetector,  $I(t)$ , into a digital signal, which is further converted by the autocorrelator into the autocorrelation function of the signal.

carries the information on the motions and other fluctuations. The autocorrelator uncovers the embedded information.

**3.2.1.2 Autocorrelation Function** The autocorrelator calculates the average of the product of two scattering intensities  $I(t)$  and  $I(t + \tau)$  measured at the two times separated by  $\tau$ . Here  $\tau$  is called the **delay time**. The average  $\langle I(t)I(t + \tau) \rangle$  is a function of  $\tau$  and is called the **autocorrelation function** of  $I(t)$  or the intensity-intensity autocorrelation function. The autocorrelator converts  $I(t)$  into  $\langle I(t)I(t + \tau) \rangle$ .

What the autocorrelator calculates is the average of  $I(t)I(t + \tau)$  with respect to  $t$  over a long period  $T_A$ . We assume that the long-time average is equal to the ensemble average—the average with respect to the configuration of the system or, simply put, the average over all possible positions and shapes of the molecules in the solution:

$$\langle I(t)I(t + \tau) \rangle = \lim_{T_A \rightarrow \infty} \frac{1}{T_A} \int_0^{T_A} I(t)I(t + \tau) dt \quad (3.1)$$

This assumption, in general, is called **ergodicity**. It is one of the few hypotheses in statistical mechanics. We cannot prove it but believe it is correct. Note that, if the system is at equilibrium, the ensemble average does not change with time and therefore  $\langle I(t)I(t + \tau) \rangle = \langle I(0)I(\tau) \rangle$ .

The autocorrelation function of  $I(t)$  in panel a of Figure 3.2 is shown in panel b. When  $\tau = 0$ ,  $\langle I(t)I(t + \tau) \rangle = \langle I^2 \rangle$ . With an increasing  $\tau$ ,  $I(t + \tau)$  becomes more irrelevant to  $I(t)$ , and  $\langle I(t)I(t + \tau) \rangle$  decays to an asymptotic level called a **baseline**. The baseline level is  $\langle I \rangle^2$ ; when  $I(t + \tau)$  and  $I(t)$  are irrelevant,  $\langle I(t)I(t + \tau) \rangle = \langle I(t) \rangle \langle I(t + \tau) \rangle = \langle I \rangle^2$ .

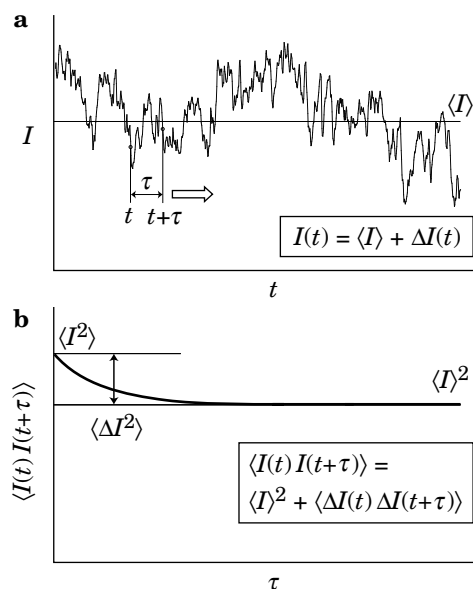


**Figure 3.2.** a: Light scattering intensity  $I(t)$  fluctuates around its mean  $\langle I \rangle$ . b: Autocorrelation function  $\langle I(t)I(t + \tau) \rangle$  is obtained as the long-time average of  $I(t)I(t + \tau)$  with respect to  $t$  for various delay times  $\tau$ . The autocorrelation function decays from  $\langle I^2 \rangle$  to  $\langle I \rangle^2$  over time. The amplitude of the decaying component is  $\langle \Delta I^2 \rangle$ .

**3.2.1.3 Photon Counting** The scattering intensity  $I(t)$  can be measured as an analog quantity  $I$  that varies continuously with time  $t$ . More often than not,  $I(t)$  is measured as pulses. Each pulse corresponds to a photon that reaches the photodetector. For this purpose, a photomultiplier or an avalanche photodiode is used in a photon-counting mode. A pulse amplifier–discriminator eliminates ghost pulses of a low height and converts each proper pulse into a pulse of a fixed height and width to be led to the autocorrelator (see Fig. 3.1). With the use of pinholes of different openings, the number of photons reaching the detector can be adjusted so that there are not too many photons entering the photodetector in each time window ( $\sim 1 \mu\text{s}$ ). The intensity is now expressed as the number of pulses in each time window. It is a nonnegative integer.

## 3.2.2 Autocorrelation Function

**3.2.2.1 Baseline Subtraction and Normalization** Because the scattering intensity  $I(t)$  fluctuates around its mean  $\langle I \rangle$ , it is convenient to separate its fluctuating component  $\Delta I(t)$  as

$$I(t) = \langle I \rangle + \Delta I(t) \quad (3.2)$$

By definition,  $\langle \Delta I(t) \rangle = 0$ . Then, the autocorrelation function is rewritten to

$$\langle I(t)I(t + \tau) \rangle = \langle I \rangle^2 + \langle \Delta I(t)\Delta I(t + \tau) \rangle \quad (3.3)$$

The autocorrelation of  $\Delta I(t)$  is lost to zero with an increasing  $\tau$ . When  $\tau \rightarrow \infty$ ,  $\langle \Delta I(t)\Delta I(t + \tau) \rangle = \langle \Delta I(t) \rangle \langle \Delta I(t + \tau) \rangle = 0$ . The decaying component in  $\langle I(t)I(t + \tau) \rangle$  is  $\langle \Delta I(t)\Delta I(t + \tau) \rangle$ . The initial height of the decaying component is  $\langle \Delta I^2 \rangle = \langle I^2 \rangle - \langle I \rangle^2$  (see Fig. 3.2).

Division of  $\langle I(t)I(t + \tau) \rangle$  by  $\langle I \rangle^2$  leads to

$$\begin{aligned} \langle I(t)I(t + \tau) \rangle / \langle I \rangle^2 &= 1 + \langle \Delta I(t)\Delta I(t + \tau) \rangle / \langle I^2 \rangle && \text{intensity autocorrelation} \\ &= 1 + f_c g_2(\tau) && \text{function} \end{aligned} \quad (3.4)$$

where  $f_c$  is called the **coherence factor**, defined as

$$f_c \equiv \langle \Delta I^2 \rangle / \langle I \rangle^2 \quad (3.5)$$

and the second factor is the baseline-subtracted, normalized intensity autocorrelation function:

$$g_2(\tau) \equiv \langle \Delta I(t)\Delta I(t + \tau) \rangle / \langle \Delta I^2 \rangle \quad (3.6)$$

The coherence factor depends, as the name suggests, on the coherence of the light falling on the photodetector. The beam has a finite cross section, and different parts of the beam may not have the same phase. If they have the same phase, the number of photons will be distributed with a Poisson distribution. The variance of  $I$  is then equal to the square of the mean, i.e.,  $f_c = 1$ . In general,  $0 < f_c < 1$ . Use of a smaller pinhole increases  $f_c$  at the expense of a weakening intensity. As shown in Figure 3.3a,  $g_2(\tau)$  is 1 at  $\tau = 0$  and decays to zero as  $\tau \rightarrow \infty$ .

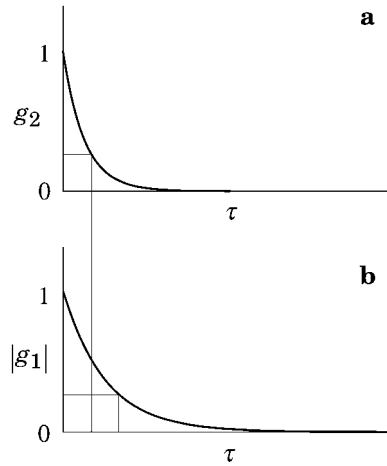


**Figure 3.3.** Baseline-subtracted, normalized intensity autocorrelation function  $g_2(t)$  (a) and the absolute value of the baseline-subtracted, normalized electric-field autocorrelation function,  $|g_1(t)|$  (b).

**3.2.2.2 Electric-Field Autocorrelation Function** We consider the autocorrelation function of the electric field  $\mathbf{E}_s(t)$  of the light scattered by solutes. As we have seen in Section 2.4,  $\mathbf{E}_s(t)$  is a complex quantity. We introduce another normalized autocorrelation function  $g_1(\tau)$ , which is defined as

$$g_1(\tau) \equiv \frac{\langle \mathbf{E}_s^*(t) \cdot \mathbf{E}_s(t + \tau) \rangle}{\langle \mathbf{E}_s^*(t) \cdot \mathbf{E}_s(t) \rangle} \quad (3.7)$$

It is known that  $g_2(\tau)$  is related to  $g_1(\tau)$  by<sup>21</sup>

$$g_2(\tau) = |g_1(\tau)|^2 \quad (3.8)$$

Figure 3.3 compares  $g_2(\tau)$  and  $|g_1(\tau)|$ . It takes twice as long for  $|g_1(\tau)|$  to decay to a given level as it takes for  $g_2(\tau)$ .

Sometimes,  $g_2(\tau)$  is defined as  $g_2(\tau) \equiv \langle I(t)I(t + \tau) \rangle / \langle I \rangle^2$ . This  $g_2$  decays to 1 as  $\tau \rightarrow \infty$ . Then,  $|g_1(\tau)|^2 = [g_2(\tau) - 1] / [g_2(0) - 1]$ .

### 3.2.3 Dynamic Structure Factor of Suspended Particles

**3.2.3.1 Autocorrelation of Scattered Field** We assume that the scattering volume contains  $n_p$  identical small particles and consider the autocorrelation function of  $\mathbf{E}_s(t)$  for the scattering by the volume. Examples include a suspension of colloidal particles. The autocorrelation of the scattering by a polymer solution will be discussed in Section 3.2.6.

In Section 2.4, we considered light scattering by a chain of beads. Equation 2.53, along with Eq. 2.52, was obtained without assuming that the beads were connected to form a chain molecule. The same equation can therefore be used for a system of  $n_p$  particles, each consisting of a single bead. A photon detected at  $\mathbf{r}$  and  $t$  was scattered some time ago by one of the particles at  $\mathbf{r}'_m (m = 1, 2, \dots, n_p)$  at  $t_0$ . The electric field  $\mathbf{E}_s$  of the photon propagating in the direction of  $\mathbf{k}_s$  is given as

$$\begin{aligned} \mathbf{E}_s(\mathbf{r}, t) &= \mathbf{E}_{\text{sm}} \exp[i(\mathbf{k}_s \cdot (\mathbf{r} - \mathbf{r}'_1) - \omega(t - t_0))] \sum_{m=1}^{n_p} \exp[i\mathbf{k} \cdot (\mathbf{r}'_1 - \mathbf{r}'_m)] \\ &= \mathbf{E}_{\text{sm}} \exp[i(\mathbf{k}_s \cdot \mathbf{r} - \mathbf{k}_i \cdot \mathbf{r}'_1) - i\omega(t - t_0)] \sum_{m=1}^{n_p} \exp(-i\mathbf{k} \cdot \mathbf{r}'_m) \end{aligned} \quad (3.9)$$

where the scattering event by particle 1 at  $\mathbf{r}'_1$  and  $t_0$  was selected as a reference point in space and time (Fig. 3.4). We take  $(\mathbf{r}, t)$  to be the position and time of detection.

Another photon detected at  $\mathbf{r}$  and  $t + \tau$  is scattered by the particles at  $\mathbf{r}_n (n = 1, 2, \dots, n_p)$  at  $t_0 + \tau$ . Motion of the particles makes  $\mathbf{r}'_m$  and  $\mathbf{r}_n$  in general different. The reference point has moved to  $\mathbf{r}_1$  as well, and the scattering occurs at  $t_0 + \tau$ . The incident light has changed its phase, since it hit particle 1 at  $\mathbf{r}'_1$  and  $t_0$ . We take into account the phase shift due to the change in the scattering by the reference. We find

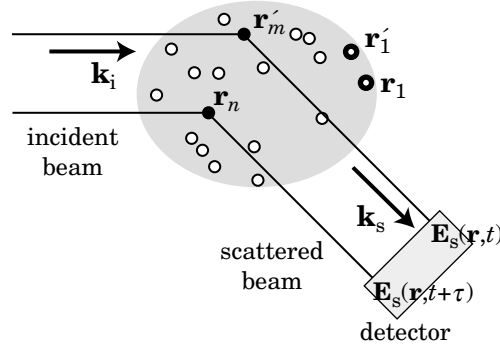


**Figure 3.4.** Scattering by the  $m$ th particle at  $t$  and by the  $n$ th particle at  $t + \tau$  can be correlated. The two photons reach the detector at different times separated by  $\tau$ .

the electric field of this second scattering is given as

$$\begin{aligned} \mathbf{E}_s(\mathbf{r}, t + \tau) &= \mathbf{E}_{\text{sm}} \exp[i(\mathbf{k}_i \cdot (\mathbf{r}_1 - \mathbf{r}'_1) - i\omega\tau)] \exp[i(\mathbf{k}_s \cdot \mathbf{r} - \mathbf{k}_i \cdot \mathbf{r}_1) \\ &\quad - i\omega(t - t_0 - \tau)] \sum_{n=1}^{n_p} \exp(-i\mathbf{k} \cdot \mathbf{r}_n) \\ &= \mathbf{E}_{\text{sm}} \exp[i(\mathbf{k}_s \cdot \mathbf{r} - \mathbf{k}_i \cdot \mathbf{r}'_1) - i\omega(t - t_0)] \sum_{n=1}^{n_p} \exp(-i\mathbf{k} \cdot \mathbf{r}_n) \end{aligned} \quad (3.10)$$

Then, the autocorrelation function of  $\mathbf{E}_s(\mathbf{r}, t)$  is

$$\mathbf{E}_s^*(\mathbf{r}, t) \cdot \mathbf{E}_s(\mathbf{r}, t + \tau) = |\mathbf{E}_{\text{sm}}|^2 \sum_{m,n=1}^{n_p} \exp[i\mathbf{k} \cdot (\mathbf{r}_m(t) - \mathbf{r}_n(t + \tau))] \quad (3.11)$$

where  $\mathbf{r}'_m$  was rewritten to  $\mathbf{r}_m(t)$  and  $\mathbf{r}_n$  to  $\mathbf{r}_n(t + \tau)$ . Strictly speaking,  $\mathbf{r}'_m = \mathbf{r}_m(t_0)$  and  $\mathbf{r}_n = \mathbf{r}_n(t_0 + \tau)$ , but we can replace  $t_0$  by  $t$  because the time difference between the scattering and the detection,  $t - t_0$ , is much smaller compared with  $\tau$ . The statistical average of Eq. 3.11 is

$$\begin{aligned} \langle \mathbf{E}_s^*(\mathbf{r}, t) \cdot \mathbf{E}_s(\mathbf{r}, t + \tau) \rangle &= |\mathbf{E}_{\text{sm}}|^2 \left\langle \sum_{m,n=1}^{n_p} \exp[i\mathbf{k} \cdot (\mathbf{r}_m(t) - \mathbf{r}_n(t + \tau))] \right\rangle \\ &= |\mathbf{E}_{\text{sm}}|^2 \left\langle \sum_{m,n=1}^{n_p} \exp[i\mathbf{k} \cdot (\mathbf{r}_m(0) - \mathbf{r}_n(\tau))] \right\rangle \end{aligned} \quad (3.12)$$

The last transformation is allowed because the system is stationary. The autocorrelation function for  $\tau = 0$  is

$$\langle \mathbf{E}_s^*(\mathbf{r}, t) \cdot \mathbf{E}_s(\mathbf{r}, t) \rangle = |\mathbf{E}_{\text{sm}}|^2 \left\langle \sum_{m,n=1}^{n_p} \exp[i\mathbf{k} \cdot (\mathbf{r}_m(0) - \mathbf{r}_n(0))] \right\rangle \quad (3.13)$$

**3.2.3.2 Dynamic Structure Factor** From Eq. 3.7, division of Eq. 3.12 by Eq. 3.13 gives

$$|g_1(\tau)| = \frac{\left\langle \sum_{m,n=1}^{n_p} \exp[i\mathbf{k} \cdot (\mathbf{r}_m(0) - \mathbf{r}_n(\tau))] \right\rangle}{\left\langle \sum_{m,n=1}^{n_p} \exp[i\mathbf{k} \cdot (\mathbf{r}_m(0) - \mathbf{r}_n(0))] \right\rangle}. \quad (3.14)$$

It is convenient to introduce **dynamic structure factor**  $S(\mathbf{k}, \tau)$ , defined as

$$S(\mathbf{k}, \tau) = \left\langle \frac{1}{n_p} \sum_{m,n=1}^{n_p} \exp[i\mathbf{k} \cdot (\mathbf{r}_m(0) - \mathbf{r}_n(\tau))] \right\rangle \quad \begin{array}{l} \text{dynamic structure factor} \\ \text{suspension of particles} \end{array} \quad (3.15)$$

Then,

$$|g_1(\tau)| = S(\mathbf{k}, \tau)/S(\mathbf{k}, 0) \quad \begin{array}{l} \text{normalized electric-field} \\ \text{autocorrelation function} \end{array} \quad (3.16)$$

As we have separated the static structure factor  $S(\mathbf{k})$  into  $S_1(\mathbf{k})$  and the rest (see Eq. 2.60), we can separate  $S(\mathbf{k}, \tau)$  into two parts:

$$S(\mathbf{k}, \tau) = S_1(\mathbf{k}, \tau) + \langle (n_p - 1) \exp[i\mathbf{k} \cdot (\mathbf{r}_1(0) - \mathbf{r}_2(\tau))] \rangle \quad (3.17)$$

with the single-particle dynamic structure factor defined as

$$S_1(\mathbf{k}, \tau) = \langle \exp[i\mathbf{k} \cdot (\mathbf{r}_1(0) - \mathbf{r}_1(\tau))] \rangle \quad \begin{array}{l} \text{single-particle} \\ \text{dynamic structure factor} \end{array} \quad (3.18)$$

It is apparent that the dynamic structure factor for  $\tau = 0$  is identical to the static structure factor:

$$S(\mathbf{k}, 0) = S(\mathbf{k}), \quad S_1(\mathbf{k}, 0) = 1 \quad (3.19)$$

for a system of particles suspended in a liquid.

**3.2.3.3 Transition Probability** The ensemble average in Eq. 3.15 is taken with respect to the positions of the particles at  $t = 0$  and  $t = \tau$ . Rewriting  $\mathbf{r}_m(0)$  to  $\mathbf{r}'_m$  and  $\mathbf{r}_n(\tau)$  to  $\mathbf{r}_n$ , it is expressed as

$$S(\mathbf{k}, \tau) = \frac{1}{n_p^2} \prod_{m=1}^{n_p} \int_V d\mathbf{r}'_m \prod_{n=1}^{n_p} \int_V d\mathbf{r}_n \sum_{i,j=1}^{n_p} \exp[i\mathbf{k} \cdot (\mathbf{r}'_i - \mathbf{r}_j)] \quad (3.20)$$

$$\times P(\mathbf{r}_1, \dots, \mathbf{r}_{n_p}; \mathbf{r}'_1, \dots, \mathbf{r}'_{n_p}; \tau) \rho(\mathbf{r}'_1, \dots, \mathbf{r}'_{n_p}; 0)$$

where  $\rho(\mathbf{r}'_1, \dots, \mathbf{r}'_{n_p}; 0)$  is the joint density distribution for the  $n_p$  particles at time 0, and  $P(\mathbf{r}_1, \dots, \mathbf{r}_{n_p}; \mathbf{r}'_1, \dots, \mathbf{r}'_{n_p}; \tau) d\mathbf{r}_1 \dots d\mathbf{r}_{n_p}$  is the joint probability for the particles to



move from  $\mathbf{r}'_1, \dots, \mathbf{r}'_{n_p}$  into a ( $n_p$ -dimensional) volume  $d\mathbf{r}_1 \dots d\mathbf{r}_{n_p}$  at  $\mathbf{r}_1, \dots, \mathbf{r}_{n_p}$  in time  $\tau$ . The **transition probability**  $P(\mathbf{r}_1, \dots, \mathbf{r}_{n_p}; \mathbf{r}'_1, \dots, \mathbf{r}'_{n_p}; \tau)$  satisfies the normalization condition:

$$\prod_{n=1}^{n_p} \int_V d\mathbf{r}_n P(\mathbf{r}_1, \dots, \mathbf{r}_{n_p}; \mathbf{r}'_1, \dots, \mathbf{r}'_{n_p}; \tau) = 1 \quad (3.21)$$

Integration of  $\rho(\mathbf{r}'_1, \dots, \mathbf{r}'_{n_p}; 0)$  gives the number of particles in volume  $V$ :

$$\prod_{m=1}^{n_p} \int_V d\mathbf{r}'_m \rho(\mathbf{r}'_1, \dots, \mathbf{r}'_{n_p}; 0) = n_p \quad (3.22)$$

In a homogeneous solution, the particles are uniformly distributed in  $V$  at  $t = 0$ , i.e.,  $\rho(\mathbf{r}'_1, \dots, \mathbf{r}'_{n_p}; 0) = n_p/V^{n_p}$ . The transition probability depends only on the displacement ( $\mathbf{r}_1 - \mathbf{r}'_1$ , etc) and is an even function of the displacement. Then,

$$S(\mathbf{k}, \tau) = \frac{1}{n_p} \prod_{n=1}^{n_p} \int_V d(\mathbf{r}_n - \mathbf{r}'_n) \sum_{i,j=1}^{n_p} \exp[i\mathbf{k} \cdot (\mathbf{r}_j - \mathbf{r}'_i)] P(\mathbf{r}_1 - \mathbf{r}'_1, \dots, \mathbf{r}_{n_p} - \mathbf{r}'_{n_p}; \tau) \quad (3.23)$$

where the sign in the exponential function has been changed. The even function  $P(\mathbf{r}_1 - \mathbf{r}'_1, \dots, \mathbf{r}_{n_p} - \mathbf{r}'_{n_p}; \tau)$  makes  $S(\mathbf{k}, \tau)$  a real function.

If each particle moves independently, the second term in Eq. 3.17 disappears:

$$S(\mathbf{k}, \tau) = S_1(\mathbf{k}, \tau) \quad (3.24)$$

Independent motions are typically observed at low concentrations. The single-particle ( $n_p = 1$ ) version of Eq. 3.20 is

$$S_1(\mathbf{k}, \tau) = \int_V d\mathbf{r}' \int_V d\mathbf{r} \exp[i\mathbf{k} \cdot (\mathbf{r} - \mathbf{r}')] P(\mathbf{r}, \mathbf{r}'; \tau) \rho(\mathbf{r}'; 0) \quad (3.25)$$

where  $P(\mathbf{r}, \mathbf{r}'; \tau)$  is the single-particle transition probability. If the solution is homogeneous at time 0, i.e.,  $\rho(\mathbf{r}'; 0) = 1/V$ , then

$$\boxed{S_1(\mathbf{k}, \tau) = \int_V d\mathbf{r} \exp[i\mathbf{k} \cdot (\mathbf{r} - \mathbf{r}')] P(\mathbf{r}, \mathbf{r}'; \tau)} \quad \begin{array}{l} \text{single-particle} \\ \text{dynamic structure factor} \end{array} \quad (3.26)$$

which is the single-particle version of Eq. 3.23. Equation 3.26 means that  $|g_1(\tau)| = S_1(\mathbf{k}, \tau)/S_1(\mathbf{k}, 0) = S_1(\mathbf{k}, \tau)$  is the Fourier-transform of the transition probability  $P(\mathbf{r}, \mathbf{r}'; \tau)$ .

Motion of the particles can be caused by an external flow and diffusion. In the flow, solvent molecules move together with the particles. Diffusion occurs regardless

of the presence of the external flow. We look closely at the diffusion phenomena of particles in a quiescent solution in the following subsection.

### 3.2.4 Diffusion of Particles

**3.2.4.1 Brownian Motion** When we place a blot of ink in still water, the colored region expands with time but the color fades, eventually filling the entire water in the container. The final state is a uniform concentration of the ink. Spreading of a substance throughout accessible volume is called **diffusion**. The phenomena is made possible by microscopic movement of water molecules.

Particles suspended in a liquid change their positions in the container by diffusion. If a particle is much larger compared with the solvent molecules, we can regard that particle to be suspended in a continuous medium of solvent. Figure 3.5 illustrates how the particle has traveled, starting at  $\mathbf{r}'$  at time  $t = 0$ , to reach  $\mathbf{r}$  at time  $t$ . The trajectory is random. The random motion of the particle is called a **Brownian motion**. It was discovered by Scottish botanist R. Brown when he was looking into an optical microscope to observe pollen on water. What he had thought was a motionless, dead world turned out to be filled with vigorous and perpetual movements. Later, it was found that a similar type of motion exists for suspensions in a liquid. Solvent molecules collide randomly with particles all the time to change the velocity of the particle, resulting in a random motion. The motions of the solvent molecules are activated by thermal energy;  $k_B T$  is sufficient to cause the Brownian motion.

The Brownian motion is stochastic. There is no knowing in advance where the particle will reach in a given time. What we can know is the transition probability  $P(\mathbf{r}, \mathbf{r}'; t)$  for the particle to move from  $\mathbf{r}'$  at  $t = 0$  to reach  $\mathbf{r}$  at time  $t$ .

Polymer molecules in solution also display Brownian motion. Because the polymer molecule is not a simple sphere, each polymer conformation has its own diffusion characteristics. For rigid molecules, the shape of the molecule, spherical or rodlike, for instance, makes a difference. For a linear flexible molecule, connectivity

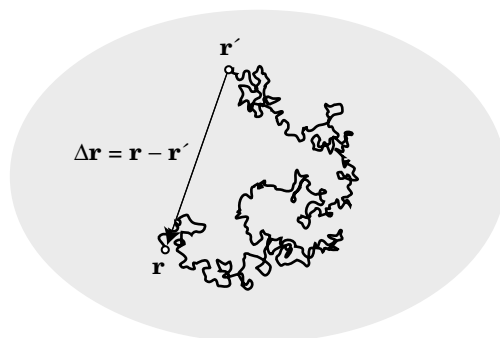


**Figure 3.5.** Trajectory of a Brownian particle. Starting at  $\mathbf{r}'$  at time zero, it moves to  $\mathbf{r}$  in time  $t$ . We cannot predict the displacement  $\Delta \mathbf{r} = \mathbf{r} - \mathbf{r}'$ .

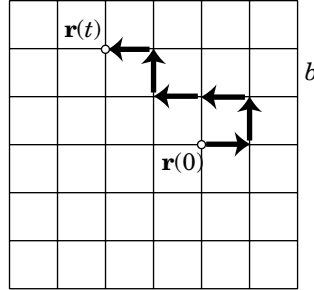


**Figure 3.6.** Random walk on a cubic lattice (two-dimensional rendering). In each step, the walker moves a distance of  $b$  randomly. Starting at  $\mathbf{r}(0)$ , the walker moves to  $\mathbf{r}(t)$  in  $N$  steps.

of monomers generates a specific pattern in its Brownian motion. Before we elaborate on the motion of the polymer molecule (Section 3.4), we look at the Brownian motion of a simple particle suspended in a continuous medium and obtain the transition probability.

**3.2.4.2 Diffusion Coefficient** We learned about random walks in Section 1.2 to describe an ideal chain. The random walk on the cubic lattice (Fig. 3.6) shares stochastic nature of the whereabouts with the Brownian motion of the particle in solution. We can apply the results obtained for the ideal chains to the motion of the random walker.

Let  $t_1$  be the time of each step and  $b$  the displacement. The **mean square displacement** of  $N$  steps in time  $t = Nt_1$ ,

$$\langle [\mathbf{r}(t) - \mathbf{r}(0)]^2 \rangle = Nb^2 \quad \text{mean square displacement} \quad (3.27)$$

is proportional to the total time  $t$ . The ratio of the mean square displacement to the time, divided by 6 for the three dimensions, gives, in general, the **diffusion coefficient**  $D$ :

$$D = \frac{\langle [\mathbf{r}(t) - \mathbf{r}(0)]^2 \rangle}{6t} \quad \text{diffusion coefficient} \quad (3.28)$$

For the random walker on the cubic lattice,

$$D = \frac{Nb^2}{6Nt_1} = \frac{b^2}{6t_1} \quad \text{random walk, 3D} \quad (3.29)$$

The last equality proves that the ratio is the same for the whole motion of  $N$  steps and for the single-step motion. To estimate  $D$ , we can use either an  $N$ -step motion or a single-step motion. The results should be identical as long as the step motions are mutually independent (Markoffian).

**3.2.4.3 Gaussian Transition Probability** We learned in Section 1.2 that the transition probability becomes Gaussian in the limit of small  $b$  and large  $N$ . The Gaussian probability given by Eq. 1.18 gives the transition probability  $P(\mathbf{r}, \mathbf{r}'; t)$  for the Brownian motion by replacing  $(2/3)Nb^2$  by  $4Dt$ :

$$P(\mathbf{r}, \mathbf{r}'; t) = (4\pi Dt)^{-3/2} \exp\left(-\frac{(\mathbf{r} - \mathbf{r}')^2}{4Dt}\right) \quad \text{Gaussian transition probability} \quad (3.30)$$

The motion of the particle whose transition probability is given by this equation is called diffusion or a Wiener process.

The probability is independent for each of  $x$ ,  $y$ , and  $z$  directions in the isotropic solution. In the  $x$  direction, for instance,

$$P_x(x, x'; t) = (4\pi Dt)^{-1/2} \exp\left(-\frac{(x - x')^2}{4Dt}\right) \quad (3.31)$$

and  $P(\mathbf{r}, \mathbf{r}'; t) = P_x(x, x'; t)P_y(y, y'; t)P_z(z, z'; t)$ .

The transition probability  $P_x(x, x'; t)$  is essentially a normal distribution of a random variable  $x - x'$  with a zero mean and a variance of  $2Dt$ . Therefore,

$$\langle x - x' \rangle = 0, \quad \langle (x - x')^2 \rangle = 2Dt \quad \text{1D diffusion} \quad (3.32)$$

These equations apply also to a particle that diffuses along a one-dimensional path. The mean square displacement  $\langle (x - x')^2 \rangle$  is proportional to  $t$ . Figure 3.7 shows how  $P_x$  broadens with time. The plots are given as a function of  $(x - x')/b$  for  $4Dt/b^2 = 0.1, 1$ , and  $10$ , where  $b$  is a unit length. Initially ( $t \rightarrow 0$ ), the particle is at  $x'$ , i.e.,  $P(x, x'; 0) = \delta(x - x')$ .

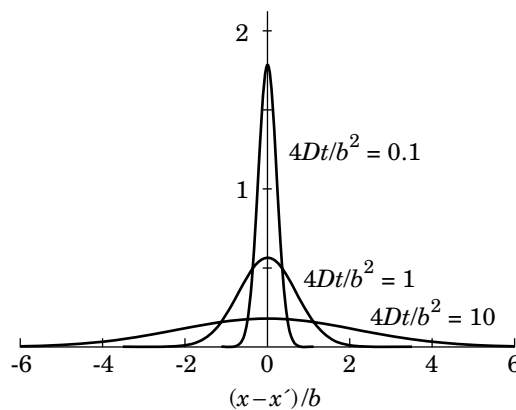


**Figure 3.7.** Broadening of the distribution with time for the position of a one-dimensional Brownian particle. Plots are for  $4Dt/b^2 = 0.1, 1$ , and  $10$ .

For the three-dimensional diffusion, the displacement  $\mathbf{r} - \mathbf{r}'$  satisfies

$$\langle \mathbf{r} - \mathbf{r}' \rangle = 0, \quad \langle (\mathbf{r} - \mathbf{r}')^2 \rangle = 6Dt \quad \text{3D diffusion} \quad (3.33)$$

because  $\langle (\mathbf{r} - \mathbf{r}')^2 \rangle = \langle (x - x')^2 \rangle + \langle (y - y')^2 \rangle + \langle (z - z')^2 \rangle = 3 \times 2Dt$ .

**3.2.4.4 Diffusion Equation** It is easy to find that  $P_x(x, x'; t)$  given by Eq. 3.31 satisfies the one-dimensional **diffusion equation**:

$$\frac{\partial P_x}{\partial t} = D \frac{\partial^2 P_x}{\partial x^2} \quad \text{1D diffusion equation} \quad (3.34)$$

The initial condition is  $P_x(x, x'; 0) = \delta(x - x')$ . Likewise,  $P(\mathbf{r}, \mathbf{r}'; t)$  given by Eq. 3.30 satisfies the three-dimensional diffusion equation:

$$\frac{\partial P}{\partial t} = D \nabla^2 P \quad \text{3D diffusion equation} \quad (3.35)$$

where  $\nabla^2 = \partial^2/\partial x^2 + \partial^2/\partial y^2 + \partial^2/\partial z^2$  is the Laplacian. It is also written as  $\partial^2/\partial \mathbf{r}^2$ . The initial condition is  $P(\mathbf{r}, \mathbf{r}'; 0) = \delta(\mathbf{r} - \mathbf{r}')$ .

**3.2.4.5 Concentration** The meaning of the transition probability  $P(\mathbf{r}, \mathbf{r}'; t)$  will be clearer when we look at the local concentration profile of the particles,  $c(\mathbf{r}, t)$ , at position  $\mathbf{r}$  and time  $t$ . It is the mass of the particles in a small volume around  $\mathbf{r}$ , divided by the volume. The volume contains sufficiently many particles. With  $P(\mathbf{r}, \mathbf{r}'; t)$ , we can write

$$c(\mathbf{r}, t) = \int P(\mathbf{r}, \mathbf{r}'; t) c(\mathbf{r}', 0) d\mathbf{r}' \quad (3.36)$$

The particles we find at  $\mathbf{r}$  and  $t$  have come from all different positions in the system. At time zero, the particles were at  $\mathbf{r}'$  with concentration profile  $c(\mathbf{r}', 0)$  (Fig. 3.8). They have migrated to  $\mathbf{r}$  with the probability of  $P(\mathbf{r}, \mathbf{r}'; t)$ . Integration of

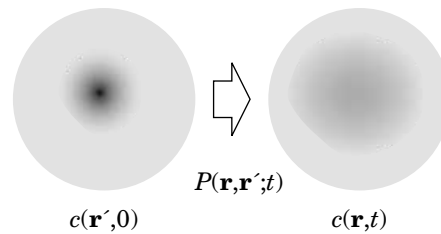


**Figure 3.8.** Transition probability  $P(\mathbf{r}, \mathbf{r}'; t)$  accounts for a change from the initial concentration profile  $c(\mathbf{r}', 0)$  to the final concentration profile  $c(\mathbf{r}, t)$ . The concentration is indicated by the gray level.

$c(\mathbf{r}', 0)P(\mathbf{r}, \mathbf{r}'; t)$  with respect to  $\mathbf{r}'$  gives the concentration profile  $c(\mathbf{r}, t)$  at time  $t$ . It is easy to show that  $c(\mathbf{r}, t)$  satisfies the same diffusion equation as Eq. 3.35:

$$\frac{\partial c}{\partial t} = D\nabla^2 c \quad (3.37)$$

The initial concentration profile is  $c(\mathbf{r}, 0)$ .

**3.2.4.6 Long-Time Diffusion Coefficient** In various experiments and computer simulations, the mean square displacement  $\langle(\mathbf{r} - \mathbf{r}')^2\rangle$  is often measured or calculated as a function of time  $t$ . If the double logarithmic plot of  $\langle(\mathbf{r} - \mathbf{r}')^2\rangle$  versus  $t$  has a slope of 1, we can say that the relevant motion is diffusional. It often happens that the proportionality is reached only after a sufficiently long time. It is therefore customary to define the diffusion coefficient in the long-time limit:

$$D = \lim_{t \rightarrow \infty} \frac{\langle(\mathbf{r} - \mathbf{r}')^2\rangle}{6t} \quad \text{long-time diffusion coefficient} \quad (3.38)$$

for dynamics in three dimensions. The denominator is  $2 \times (\text{dimensions}) \times t$ . This diffusion coefficient is called the **long-time diffusion coefficient**. The dynamics may have different diffusion coefficients in other time scales, or it may not be diffusional. The plot of  $\langle(\mathbf{r} - \mathbf{r}')^2\rangle$  versus  $t$  will tell the nature of the dynamics. We will see variations of dynamics in different time scales in Sections 3.4 and 4.3.

In Section 1.5, we learned that the mean square end-to-end distance  $\langle R_F^2 \rangle$  of a wormlike chain becomes proportional to the contour length as the chain becomes longer. The tendency for  $\langle(\mathbf{r} - \mathbf{r}')^2\rangle$  to become proportional to  $t$  in a long time is parallel to the tendency for  $\langle R_F^2 \rangle$  of the wormlike chain.

### 3.2.5 Diffusion and DLS

**3.2.5.1 Dynamic Structure Factor and Mean Square Displacement** Here we learn how  $|g_1(\tau)|$  obtained in DLS gives an estimate of the diffusion coefficient. We are concerned with dilute solutions here. Hence,  $|g_1(\tau)| = S_1(\mathbf{k}, \tau)$ .

In Eq. 3.26, we use the Taylor expansion at low scattering angles:  $\exp[\mathbf{i}\mathbf{k} \cdot (\mathbf{r} - \mathbf{r}')] = 1 + \mathbf{i}\mathbf{k} \cdot (\mathbf{r} - \mathbf{r}') - (1/2)[\mathbf{k} \cdot (\mathbf{r} - \mathbf{r}')]^2 + \dots$ . Then  $S_1(\mathbf{k}, \tau)$  is transformed to

$$S_1(\mathbf{k}, \tau) = 1 - \frac{1}{6} \mathbf{k}^2 \langle(\mathbf{r} - \mathbf{r}')^2\rangle + \dots \cong \exp\left[-\frac{1}{6} \mathbf{k}^2 \langle(\mathbf{r} - \mathbf{r}')^2\rangle\right] \quad (3.39)$$

where  $\langle(\mathbf{r} - \mathbf{r}')^2\rangle = 0$ , and  $\langle(x - x')^2\rangle = \langle(y - y')^2\rangle = \langle(z - z')^2\rangle = \langle(\mathbf{r} - \mathbf{r}')^2\rangle/3$ ,  $\langle(x - x')(y - y')\rangle = 0$ , and so forth were used. This  $|g_1(\tau)| = S_1(\mathbf{k}, \tau)$  is rewritten to

$$\langle(\mathbf{r} - \mathbf{r}')^2\rangle = -6 \ln |g_1(\tau)| / \mathbf{k}^2 \quad \text{small } k \quad (3.40)$$

If plots of  $\ln |g_1(\tau)| / \mathbf{k}^2$  vs.  $\tau$  measured at different angles overlap each other, then  $k$  is already sufficiently small. Typically,  $k \times (\text{size of the particle}) < 1$  qualifies as small  $k$ .

The mean square displacement in time  $\tau$  is evaluated by using Eq. 3.40. The slope in the plot is equal to  $6D$ . It is, however, more common to follow the approach described below.

**3.2.5.2 Dynamic Structure Factor of a Diffusing Particle** More often than not, the particles move according to the diffusion equation. The transition probability is given by Eq. 3.30. Then

$$\begin{aligned} S_1(\mathbf{k}, \tau) &= \int \exp[i\mathbf{k} \cdot (\mathbf{r} - \mathbf{r}')] (4\pi D\tau)^{-3/2} \exp\left(-\frac{(\mathbf{r} - \mathbf{r}')^2}{4D\tau}\right) d\mathbf{r} \\ &= \int (4\pi D\tau)^{-3/2} \exp\left(-\frac{(\mathbf{r} - \mathbf{r}' - i\mathbf{k} \cdot 2D\tau)^2}{4D\tau} - D\tau\mathbf{k}^2\right) d\mathbf{r} = \exp(-D\tau\mathbf{k}^2) \end{aligned} \quad (3.41)$$

Thus,  $|g_1(\tau)|$  is an exponentially decaying function with a decay constant of  $D\mathbf{k}^2$ . It is customary to first introduce the **decay rate**  $\Gamma$  of  $|g_1(\tau)|$  by

$$\boxed{|g_1(\tau)| = \exp(-\Gamma\tau)} \quad (3.42)$$

and then relate  $\Gamma$  to  $\mathbf{k}^2$  as

$$\boxed{\Gamma = D\mathbf{k}^2 \text{ decay rate for diffusion}} \quad (3.43)$$

for the diffusional motion. It is apparent that  $|g_1(\tau)|$  decays faster at a higher scattering angle.

The procedure to obtain the diffusion coefficient  $D$  is as follows. First, measure the autocorrelation function at different angles. Second, obtain  $\Gamma$  as the negative of the slope in the semi-logarithmic plot of  $|g_1(\tau)|$  as shown in Figure 3.9. Third, plot

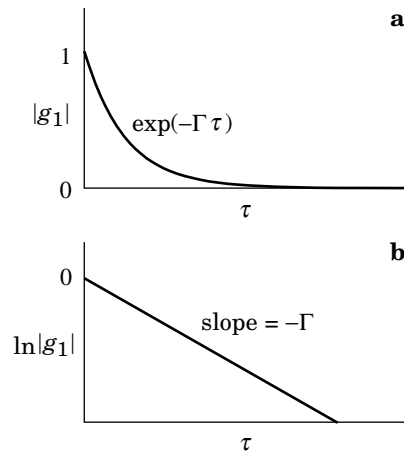


**Figure 3.9.** When  $|g_1(\tau)|$  decays in a single exponential (a), the plot of  $\ln|g_1(\tau)|$  is a straight line with a slope of  $-\Gamma$  (b).

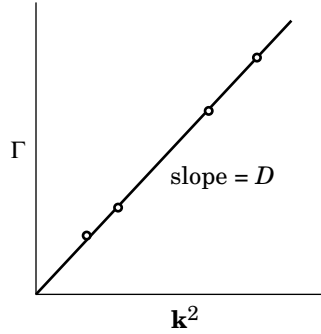


**Figure 3.10.** Decay rate  $\Gamma$  of  $|g_1(\tau)|$ , plotted as a function of  $\mathbf{k}^2$ . If the particles move by diffusion, the plot is on a straight line through the origin with a slope equal to the diffusion coefficient  $D$ .

$\Gamma$  as a function of  $\mathbf{k}^2$ . The plot should be approximated by a straight line through the origin (see Fig. 3.10). The slope of the line is  $D$ . We can show that conversely, if the measured  $\Gamma$  versus  $\mathbf{k}^2$  is on a straight line through the origin, then the dynamics is diffusional (Problem 3.3).

When the suspension is not spherical or, in general, is a particle with an internal structure such as a linear polymer chain, the decay rate deviates from the one given by Eq. 3.43 at higher scattering angles. The diffusion coefficient defined in the low  $\mathbf{k}$  limit refers to the overall displacement of the molecule, i.e., the motion for the center of mass.

### 3.2.6 Dynamic Structure Factor of a Polymer Solution

**3.2.6.1 Dynamic Structure Factor** The electric field of the light scattered by a volume that contains  $n_p$  chains ( $n_p \gg 1$ ), each consisting of  $N$  beads, can be written in the same way as Eq. 3.15. The dynamic structure factor is now given as

$$S(\mathbf{k}, \tau) = \frac{1}{N_p N} \sum_{m,n=1}^{N_p} \sum_{i,j=1}^N \langle \exp[i\mathbf{k} \cdot (\mathbf{r}_{mi}(0) - \mathbf{r}_{nj}(\tau))] \rangle \quad \begin{array}{l} \text{dynamic structure factor} \\ \text{polymer solution} \end{array} \quad (3.44)$$

which is decomposed into two parts:

$$S(\mathbf{k}, \tau) = S_1(\mathbf{k}, \tau) + \frac{n_p}{N} \sum_{i,j=1}^N \langle \exp[i\mathbf{k} \cdot (\mathbf{r}_{1i}(0) - \mathbf{r}_{2j}(\tau))] \rangle \quad (3.45)$$

where  $S_1(\mathbf{k}, \tau)$  is the single-chain dynamic structure factor:

$$S_1(\mathbf{k}, \tau) = \frac{1}{N} \sum_{i,j=1}^N \langle \exp[i\mathbf{k} \cdot (\mathbf{r}_{1i}(0) - \mathbf{r}_{1j}(\tau))] \rangle \quad \begin{array}{l} \text{single-chain} \\ \text{dynamic structure factor} \end{array} \quad (3.46)$$



At  $\tau = 0$ , the dynamic structure factors are identical to the static structure factors (Eqs. 2.59 and 2.60):

$$S(\mathbf{k}, 0) = S(\mathbf{k}), \quad S_1(\mathbf{k}, 0) = S_1(\mathbf{k}) \quad (3.47)$$

Thus,  $|g_1(\tau)| = S_1(\mathbf{k}, \tau)/S_1(\mathbf{k}, 0)$  when each polymer chain moves independently of other chains at low concentrations.

**3.2.6.2 Long-Time Behavior** In a short time scale,  $S_1(\mathbf{k}, \tau)$  exhibits a complicated pattern, reflecting complex motions of different parts of the polymer chain. Over a long time, however, the motion is simplified. It is dominated by the translation of the chain as a whole in the solution for any conformation. We can prove the dominance of the center-of-mass motion as follows.

In Eq. 3.46, the displacement  $\mathbf{r}_{1i}(0) - \mathbf{r}_{1j}(\tau)$  between bead  $i$  at time 0 and bead  $j$  at time  $\tau$  on chain 1 consists of three parts:

$$\mathbf{r}_{1i}(0) - \mathbf{r}_{1j}(\tau) = [\mathbf{r}_{1i}(0) - \mathbf{r}_{1G}(0)] + [\mathbf{r}_{1G}(0) - \mathbf{r}_{1G}(\tau)] + [\mathbf{r}_{1G}(\tau) - \mathbf{r}_{1j}(\tau)] \quad (3.48)$$

where  $\mathbf{r}_{1G}(0)$  and  $\mathbf{r}_{1G}(\tau)$  are the center of mass positions of the chain at time 0 and  $\tau$ , respectively. The three parts are represented by three vectors in Figure 3.11. Initially, the three parts are correlated. As  $\tau$  increases, the chain conformation becomes randomized, and the three vectors become more irrelevant to each other. For instance,  $\mathbf{r}_{1i}(0) - \mathbf{r}_{1G}(0)$  becomes uncorrelated to  $\mathbf{r}_{1G}(\tau) - \mathbf{r}_{1j}(\tau)$  regardless of  $i = j$  or not. Thus the statistical average of the square is

$$\begin{aligned} \langle [\mathbf{r}_{1i}(0) - \mathbf{r}_{1j}(\tau)]^2 \rangle &= \langle [\mathbf{r}_{1i}(0) - \mathbf{r}_{1G}(0)]^2 \rangle + \langle [\mathbf{r}_{1G}(0) - \mathbf{r}_{1G}(\tau)]^2 \rangle \\ &+ \langle [\mathbf{r}_{1G}(\tau) - \mathbf{r}_{1j}(\tau)]^2 \rangle \end{aligned} \quad (3.49)$$

The first and third terms are equal to  $R_g^2$  by definition. Only the second term grows with time because of diffusion of the chain as a whole. After a long time, the

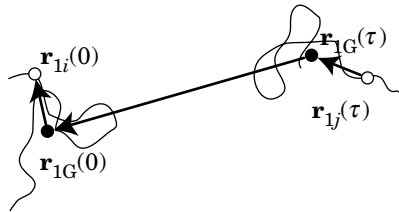


**Figure 3.11.** The polymer chain moves its center of mass and changes its orientation and internal arrangement. The displacement between monomers  $i$  and  $j$ ,  $\mathbf{r}_{1i}(0) - \mathbf{r}_{1j}(\tau)$ , is decomposed into three parts indicated by the arrows. Only the center-of-mass distance keeps growing with time.

second term becomes dominant. Thus,

$$-6 \ln |g_1(\tau)| / \mathbf{k}^2 = \langle [\mathbf{r}_{1i}(0) - \mathbf{r}_{1j}(\tau)]^2 \rangle \rightarrow \langle [\mathbf{r}_{1G}(0) - \mathbf{r}_{1G}(\tau)]^2 \rangle \quad (3.50)$$

and therefore  $|g_1(\tau)|$  gives the **center-of-mass diffusion coefficient**.

The above discussion applies only to a long time. In a short time,  $\ln |g_1(\tau)|$  may exhibit non- $\mathbf{k}^2$  behavior. In Section 3.4, we will learn in more details how  $S_1(\mathbf{k}, \tau)$  depends on  $\mathbf{k}$  and  $\tau$  for a bead-spring model.

### 3.2.7 Hydrodynamic Radius

**3.2.7.1 Stokes-Einstein Equation** To drag a particle suspended in a viscous medium at a constant velocity  $\mathbf{v}$ , a constant force of  $\mathbf{F} = \zeta \mathbf{v}$  must be applied to the particle (Fig. 3.12). The coefficient  $\zeta$  is called the friction coefficient. Einstein showed that the diffusion coefficient  $D$  of the particle in a quiescent solution at temperature  $T$  is related to  $\zeta$  by

$$D = \frac{k_B T}{\zeta} \quad \text{Nernst-Einstein equation} \quad (3.51)$$

This equation is the simplest form of the so-called fluctuation-dissipation theorem. The diffusion, which is a typical equilibrium phenomenon, is related to the friction, a typical energy dissipation phenomenon.

Stokes showed that the friction coefficient for a sphere of radius  $R_s$  is given by

$$\zeta = 6\pi\eta_s R_s \quad (3.52)$$

in a solvent of viscosity  $\eta_s$ . The viscosity of a fluid expresses how difficult it is to flow the fluid. We will learn the exact definition of viscosity in Section 3.3.1. Combining the above two equations gives the **Stokes-Einstein** equation:

$$D = \frac{k_B T}{6\pi\eta_s R_s} \quad \text{diffusion coefficient of a sphere} \quad (3.53)$$

The radius  $R_s$  is called the **Stokes radius**. The diffusion is faster at a higher temperature, in a less viscous solvent, and for a smaller particle.

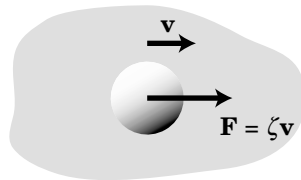


**Figure 3.12.** A particle moving at a constant velocity  $\mathbf{v}$  in a viscous liquid needs to be pulled by force  $\mathbf{F} = \zeta \mathbf{v}$ .

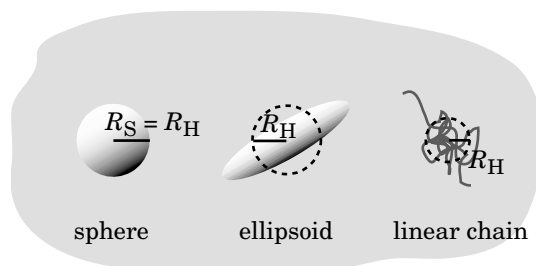


**Figure 3.13.** For the center-of-mass motion, an ellipsoid with a hydrodynamic radius  $R_H$  receives the same friction as a sphere of radius  $R_H$  does. Likewise, a linear chain with a hydrodynamic radius  $R_H$  diffuses with the same diffusion coefficient as the sphere of radius  $R_H$ .

We now extend the concept of the Stokes radius to nonspherical suspensions and molecules (Fig. 3.13). Once the center-of-mass diffusion coefficient  $D$  is measured for the suspension or the molecule, we can introduce the **hydrodynamic radius**  $R_H$  by

$$R_H = \frac{k_B T}{6\pi\eta_s D} \quad \text{hydrodynamic radius} \quad (3.54)$$

For the spherical suspension,  $R_H = R_S$ . We can regard  $R_H$  as another quantity to characterize the dimension of the molecule.

**3.2.7.2 Hydrodynamic Radius of a Polymer Chain** For a linear chain molecule,  $R_H$  is proportional to  $R_g$  and  $R_F$ . Therefore,  $R_H \propto N^\nu$ , where  $\nu = 1/2$  in the theta solvent and  $\nu \cong 0.59$  or  $3/5$  in the good solvent. We can prove the proportionality, as shown below.

When all of the  $N$  monomers in the polymer chain move, each monomer receives a friction from the solvent. The overall friction, however, is not proportional to  $N$  but rather is proportional to  $N^\nu$ . Because  $\nu < 1$ ,  $N^\nu < N$ . The friction of the chain molecule is smaller than the friction nonbonded, independently moving  $N$  monomers receive. It is explained as follows. The motion of one of the monomers accompanies motions of adjacent solvent molecules in the same direction, and their effect propagates to another monomer to facilitate its motion in the same direction in an otherwise stagnant solvent (Fig. 3.14). This interaction is called **hydrodynamic interaction**. It is different from the other interactions we have seen so far. It exists only when the particles move. Static properties such as the osmotic pressure are not affected by the hydrodynamic interactions. They only affect dynamic properties, such as diffusion, but do so strongly.

Oseen found that the magnitude of the hydrodynamic interaction between two particles at  $\mathbf{r}$  and  $\mathbf{r}'$  is proportional to  $|\mathbf{r} - \mathbf{r}'|^{-1}$ . The interaction decays only algebraically with a small exponent of  $-1$  and therefore is long ranged. In a chain molecule, all monomers affect all other monomers because they are close to each other.

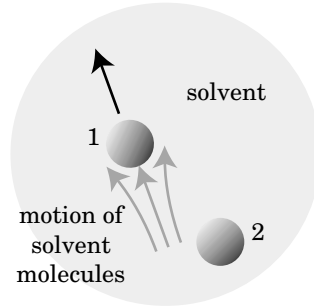


**Figure 3.14.** Movement of particle 1 generates the motion of solvent molecules, which eases the motion of particle 2 in the same direction. Thus, the hydrodynamic interaction reduces friction.

In Section 3.4.6, we will learn that  $1/R_H$  of the chain molecule is given as the average of the reciprocal of the distance between two monomers on the chain:

$$\frac{1}{R_H} = \left\langle \frac{1}{|\mathbf{r}_m - \mathbf{r}_n|} \right\rangle \quad \begin{array}{l} \text{hydrodynamic radius} \\ \text{of a polymer chain} \end{array} \quad (3.55)$$

The average is taken with respect to possible positions of the two monomers  $m$  and  $n$  ( $m \neq n$ ) and then with respect to  $m$  and  $n$  that run over all monomers of the chain.

Here we calculate  $R_H$  of a chain with a Gaussian conformation. Using the Gaussian distribution given by Eq. 1.34,  $\langle |\mathbf{r}_m - \mathbf{r}_n|^{-1} \rangle_{mn}$  for a given  $m$  and  $n$  is calculated as

$$\begin{aligned} \left\langle \frac{1}{|\mathbf{r}_m - \mathbf{r}_n|} \right\rangle_{mn} &= \int_0^\infty (2\pi|n-m|b^2/3)^{-3/2} \exp\left(-\frac{3r^2}{2|n-m|b^2}\right) 4\pi r^2 \frac{1}{r} dr \\ &= (2\pi|n-m|b^2/3)^{-3/2} 4\pi \cdot |n-m|b^2/3 = (6/\pi)^{1/2} b^{-1} |n-m|^{-1/2} \end{aligned} \quad (3.56)$$

The average of  $|n-m|^{-1/2}$  with respect to  $m$  and  $n$  is calculated as

$$N^{-2} \int_0^N dn \int_0^N dm |n-m|^{-1/2} = 2N^{-2} \int_0^N 2n^{1/2} dn = (8/3)N^{-1/2} \quad (3.57)$$

Thus,  $R_H$  is given by

$$\frac{1}{R_H} = \left(\frac{6}{\pi}\right)^{1/2} \frac{1}{b} \times \frac{8}{3} N^{-1/2} = 8 \left(\frac{2}{3\pi}\right)^{1/2} \frac{1}{bN^{1/2}} \quad (3.58)$$

$R_H$  is quite small compared with  $R_F$ :  $R_H/R_F = (3\pi/2)^{1/2}/8 \cong 0.271$ .  $R_H$  is smaller than  $R_g$ :  $R_H/R_g = (3/8)\pi^{1/2} \cong 0.665$ . Thus,  $R_H < R_g < R_F$  for a chain with a Gaussian conformation.

The real chain has  $R_H \cong bN^\nu$ , since  $\langle |\mathbf{r}_m - \mathbf{r}_n|^{-1} \rangle_{mn} \cong b^{-1}|n-m|^{-\nu}$ . More exact results for polymer chains in a good solvent were obtained in the renormalization

**Table 3.1** Various Measures of the Chain Dimension

Polymer Chain	$R_H/R_g$	$R_H/R_F$	$R_F/R_g$
Ideal/theta solvent*	0.665 $(=(3/8)\pi^{1/2})$	0.271 $(=(3\pi/2)^{1/2}/8)$	2.45 $(=6^{1/2})$
Real (good solvent)	0.640	0.255	2.51
Rod-like	$3^{1/2}/(\ln(L/b)-\gamma)^{**}$	$1/[2(\ln(L/b)-\gamma)]^{**}$	3.46 $(=12^{1/2})$

\*Chains with an ideal-chain conformation.

\*\*Depends on the rod length  $L$  and rod diameter  $b$ .  $\gamma \cong 0.3$ .

group theory and will be given in Section 3.4. The relationship,  $R_H < R_g < R_F$ , is the same as for the Gaussian chain.

Table 3.1 compares various measures of the dimension for chains with an ideal-chain conformation (or at the theta condition), excluded-volume chains, and rodlike molecules. The latter will be considered in Section 3.5.

Figure 3.15 shows examples of  $R_H$  measured by using DLS for different molecular weight fractions. Panel a was obtained for polystyrene in 2-fluorotoluene at

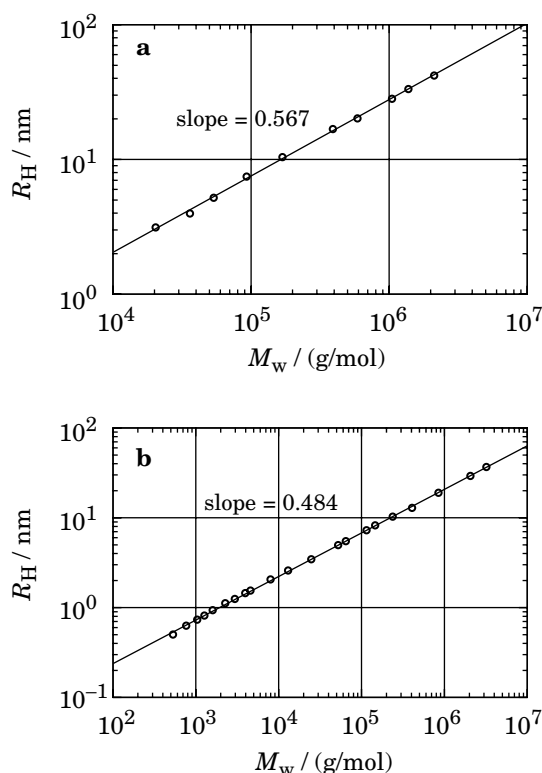


**Figure 3.15.** Hydrodynamic radius  $R_H$  of different molecular weights of a polymer. a: Polystyrene in 2-fluorotoluene at 42.6°C (good solvent). (From Ref. 30.) b: Poly( $\alpha$ -methyl styrene) in cyclohexane at 30.5°C (theta solvent). (From Ref. 31.)

42.6°C (good solvent),<sup>30</sup> and panel b was obtained for poly( $\alpha$ -methyl styrene) in cyclohexane at 30.5°C (theta condition).<sup>31</sup> In the two panels of the figure, the plots are on a straight line, in agreement with the predicted power relationship,  $R_H \propto N^{-\nu}$ . The exponents  $\nu$  obtained in the fitting are 0.567 and 0.484, slightly smaller than the values predicted for the two environments.

### 3.2.8 Particle Sizing

**3.2.8.1 Distribution of Particle Size** It is all but impossible that every solute molecule or particle has exactly the same hydrodynamic radius in a given solution. There is always a distribution in  $R_H$ , as illustrated in Figure 3.16. The peak position and width of the distribution vary from sample to sample. The distribution in  $R_H$  leads to a distribution in the diffusion coefficient and therefore a distribution in the decay rate  $\Gamma$  of  $|g_1(\tau)|$ . Then,  $|g_1(\tau)|$  is not a simple exponential decay.

A particle with  $\Gamma$  contributes to the measured  $|g_1(\tau)|$  with  $\exp(-\Gamma\tau)$ . Therefore, the measured  $|g_1(\tau)|$  is a superposition of  $\exp(-\Gamma\tau)$  with different values of  $\Gamma$ :

$$|g_1(\tau)| = \int G(\Gamma) \exp(-\Gamma\tau) d\Gamma \quad (3.59)$$

where  $G(\Gamma)$  represents the contribution of each  $\Gamma$  and is normalized, i.e.,  $\int G(\Gamma) d\Gamma = 1$ . The magnitude of the electric-field autocorrelation function is proportional to the scattering intensity ( $I \propto E^2$ ). After normalization to  $|g_1(\tau)|$ , each contribution from a different  $\Gamma$  is still weighted by the scattering intensity of particles that exhibit the decay rate of  $\Gamma$ . Thus,  $G(\Gamma)$  is the scattering intensity-weighted distribution.

**3.2.8.2 Inverse-Laplace Transform** The distribution makes  $|g_1(\tau)|$  deviate from a single exponential decay, as illustrated in Figure 3.17a. Conversely the analysis of the deviation allows estimation of  $G(\Gamma)$ . Mathematically,  $|g_1(\tau)|$  is the Laplace transform of  $G(\Gamma)$ , as Eq. 3.59 shows. Then, the procedure to estimate  $G(\Gamma)$  from

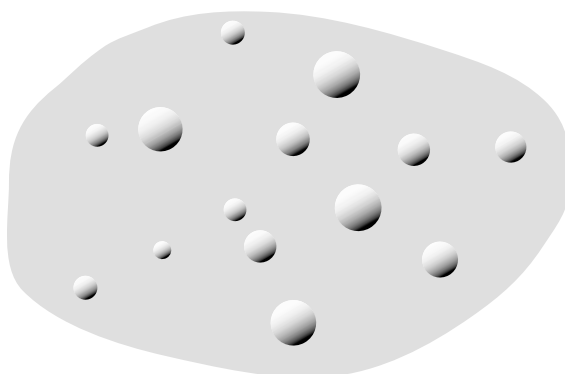


**Figure 3.16.** Suspension of particles with different diameters.

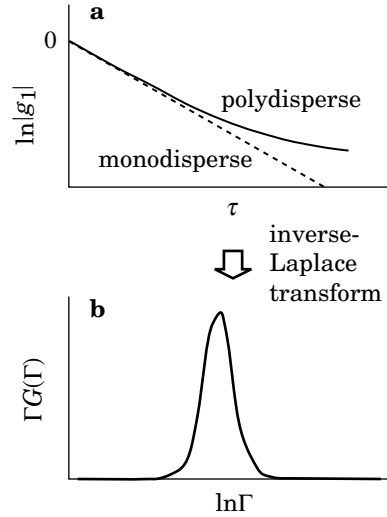


**Figure 3.17.** a: In a suspension of monodisperse particles, the plot of  $\ln|g_1|$  is a straight line (dashed line). Polydispersity of the particle size deviates  $\ln|g_1|$  (solid line) from the straight line. b: The inverse Laplace transform of  $|g_1(\tau)|$  gives the distribution of the decay rate  $\Gamma$ .

$|g_1(\tau)|$  is **inverse-Laplace transform**. There are computer program packages available for the procedure. Among others, CONTIN<sup>32</sup> has been most frequently used and implemented in commercial DLS measurement systems. The result of the transformation is displayed in  $\Gamma G(\Gamma)$  on a logarithmic scale of  $\Gamma$  (Fig. 3.17b). The following equation explains why  $\Gamma G(\Gamma)$  is plotted, not just  $G(\Gamma)$ :

$$|g_1(\tau)| = \int \Gamma G(\Gamma) \exp(-\Gamma \tau) d \ln \Gamma \quad (3.60)$$

The autocorrelator computes  $|g_1(\tau)|$  for a finite range of  $\tau$ , from  $\tau_{\min}$  to  $\tau_{\max}$ . Therefore,  $G(\Gamma)$  can be estimated only in a finite range of  $\Gamma$ . Usually, the lower and upper limits of the integral in Eq. 3.59 are  $1/\tau_{\max}$  and  $1/\tau_{\min}$ , respectively.

**3.2.8.3 Cumulant Expansion** The inverse-Laplace transform is a convenient analysis method when the distribution is broad, especially bimodal or trimodal. When the distribution is narrow and  $|g_1(\tau)|$  is close to a single exponential decay, a simpler analysis method, called a **cumulant expansion**, is more useful. In this method,  $\ln |g_1(\tau)|$  is approximated by a polynomial of  $\tau$ , typically of the second order. The first two coefficients represent the mean and the variance of  $\Gamma$ :

$$\ln |g_1(\tau)| = -\langle \Gamma \rangle \tau + \frac{1}{2} \langle \Delta \Gamma^2 \rangle \tau^2 - \frac{1}{6} \langle \Delta \Gamma^3 \rangle \tau^3 + \dots \quad \text{cumulant expansion} \quad (3.61)$$

where  $\Delta\Gamma = \Gamma - \langle\Gamma\rangle$  and the averages are weighted with  $G(\Gamma)$ :

$$\langle\Gamma\rangle = \int \Gamma G(\Gamma) d\Gamma, \quad \langle\Delta\Gamma^2\rangle = \int \Delta\Gamma^2 G(\Gamma) d\Gamma, \dots \quad (3.62)$$

Problem 3.8 proves this expansion. In the absence of distribution, i.e.,  $\Delta\Gamma = 0$ , the second- and higher-order terms disappear, and  $\ln |g_1(\tau)|$  is a straight line. Curve-fitting of the measured  $\ln |g_1(\tau)|$  by a polynomial gives an estimate of  $\langle\Gamma\rangle$  and  $\langle\Delta\Gamma^2\rangle$ . As found in Problem 3.10, the diffusion coefficient estimated from  $\langle\Gamma\rangle$  for a solution of a polydisperse polymer is a  $z$ -average diffusion coefficient. Often, we use a simple symbol of  $\Gamma$  for  $\langle\Gamma\rangle$ .

**3.2.8.4 Example** Figure 3.18 shows an example of  $g_2(\tau)$  ( $|g_1(\tau)|$  on the right axis) obtained by a commercial particle-sizing system (Beckman-Coulter, N4Plus) for a 6.9 g/L solution of a polystyrene standard ( $M_w = 1.7 \times 10^5$  g/mol) in toluene at 30°C ( $\lambda = 632.8$  nm). The scattering angles were 14.0, 20.5, 26.7, and 65.6°. On a logarithmic scale of the ordinate,  $g_2(\tau)$  [and  $|g_1(\tau)|$ ] is mostly straight at the four scattering angles, indicating a narrow distribution in  $G(\Gamma)$ . In the particle-sizing system, the distribution of  $\Gamma$  is converted to a distribution  $G_d$  of the apparent particle diameter  $d_{app}$  by  $d_{app} = k_B T / [3\pi\eta_s(\Gamma/k^2)]$ . In the small  $k$  limit and the low concentration limit,  $d_{app} = 2R_H$ . Figure 3.19 displays  $G_d(d_{app})$  on the logarithmic scale of  $d_{app}$ , obtained from the  $|g_1(\tau)|$  data in Figure 3.18. As expected, the CONTIN analysis returns a single peak. The peak position and width are the same within experimental errors for the measurements at the four angles, indicating that the decay

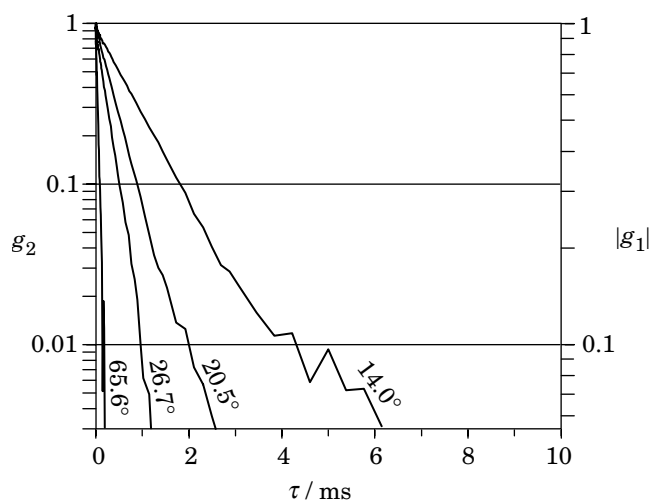


**Figure 3.18.** Example of autocorrelation functions  $g_2(\tau)$  and  $|g_1(\tau)|$  obtained in DLS measurements at four scattering angles for a dilute solution of polystyrene in toluene. The two autocorrelation functions differ in the ordinate scale only.



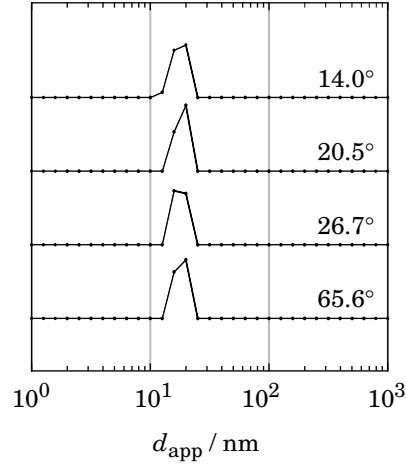


**Figure 3.19.** CONTIN analysis results for the autocorrelation functions shown in Fig. 3.18. The distribution of the apparent diameter  $d_{\text{app}}$  is plotted as a function of  $d_{\text{app}}$  in a logarithmic scale.

of  $g_2(\tau)$  is due to the center-of-mass diffusion of the polystyrene molecules and that the measurement was carried out in the range of a sufficiently small  $k$ . In fact,  $kR_H = 0.056$  at  $\theta = 26.7^\circ$ , for instance. Displaying  $G_d(d_{\text{app}})$  in place of  $G(\Gamma)$  or the distribution of the diffusion coefficient is handy when results from measurements in different solvents and/or at different temperatures need to be compared.

### 3.2.9 Diffusion From Equation of Motion

Here we look at the diffusion from another perspective. We will obtain the diffusional behavior, i.e.,  $\langle [\mathbf{r}(t) - \mathbf{r}(0)]^2 \rangle \propto t$ , from the equation of motion.

A particle suspended in a liquid receives a random force  $\mathbf{f}(t)$  when solvent molecules collide with the particle. We assume that the random force has the following statistical properties:

$$\langle \mathbf{f}(t) \rangle = 0 \quad (3.63)$$

$$\langle \mathbf{f}(t) \cdot \mathbf{f}(t') \rangle = A\delta(t - t') \quad (3.64)$$

where  $A$  is a constant yet to be determined. The random force is, on average, zero. It loses its memory instantaneously  $[\delta(t - t')]$ . The force at a given time has nothing to do with the force at the next moment. Figure 3.20 shows an example of such a force (white noise).

In a viscous solvent, the motion of the particle is overdamped. Then, the equation of motion of the particle has the friction term and the force term only:

$$\zeta \frac{d\mathbf{r}}{dt} = \mathbf{f}(t) \quad (3.65)$$

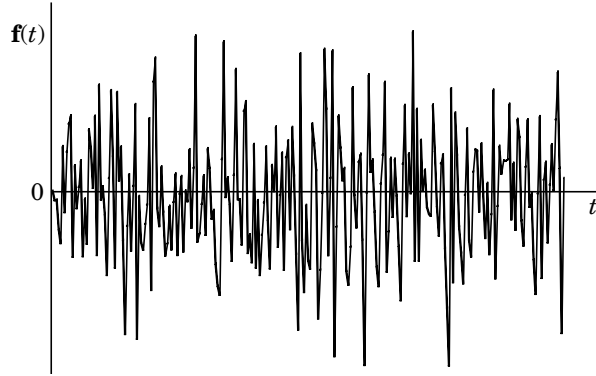


**Figure 3.20.** Example of a random force  $\mathbf{f}(t)$  (its  $x$  component) with zero mean and no memory.

The mean square displacement in time  $t$  is calculated from

$$\langle [\mathbf{r}(t) - \mathbf{r}(0)]^2 \rangle = \frac{1}{\zeta^2} \left\langle \int_0^t \mathbf{f}(t_1) dt_1 \cdot \int_0^t \mathbf{f}(t_2) dt_2 \right\rangle \quad (3.66)$$

We exchange the order of the integration and the averaging:

$$\langle [\mathbf{r}(t) - \mathbf{r}(0)]^2 \rangle = \frac{1}{\zeta^2} \int_0^t dt_1 \int_0^t dt_2 \langle \mathbf{f}(t_1) \cdot \mathbf{f}(t_2) \rangle \quad (3.67)$$

With Eq. 3.64,

$$\langle [\mathbf{r}(t) - \mathbf{r}(0)]^2 \rangle = \frac{1}{\zeta^2} \int_0^t dt_1 \int_0^t dt_2 A \delta(t_1 - t_2) = \frac{A}{\zeta^2} \int_0^t dt_1 = \frac{A}{\zeta^2} t \quad (3.68)$$

The mean square displacement is proportional to  $t$ . The particle makes a diffusional motion on all time scales. We also find that the average displacement is zero:

$$\langle \mathbf{r}(t) - \mathbf{r}(0) \rangle = \frac{1}{\zeta} \int_0^t dt \langle \mathbf{f}(t) \rangle = 0 \quad (3.69)$$

For the mean and variance of the displacement to be identical to those of the diffusion with diffusion coefficient  $D$ ,  $6D = A/\zeta^2$ . Thus,

$$A = 6D\zeta^2 = 6 \frac{k_B T}{\zeta} \zeta^2 = 6k_B T \zeta \quad (3.70)$$

Thus, the random force satisfies

$$\langle \mathbf{f}(t) \cdot \mathbf{f}(t') \rangle = 6k_B T \zeta \delta(t - t') \quad (3.71)$$

The magnitude of the random force is greater for a particle with a larger friction coefficient, typically a larger particle. This random force satisfies the requirement of the equipartition law: thermal energy per degree of freedom is  $k_B T/2$  (Problem 3.13).

### 3.2.10 Diffusion as Kinetics

**3.2.10.1 Fick's Law** Here, we look at the diffusion from a phenomenological point of view. The treatment in Sections 3.2.4 and 3.2.9 needs tracing each particle and therefore is microscopic.

We consider a container consisting of two parts that hold the solutions of the same solute at different concentrations (see Figure 3.21). The concentration is uniform in each part. As soon as the partition is quietly removed, the solute starts to move from the right compartment where the concentration is higher to the left compartment where it is lower. The distinct boundary becomes fuzzy. After a long time, the concentration becomes uniform throughout the container. The figure shows also a snapshot of the concentration profile during the equilibration process. There is a natural tendency for the system to become uniform as it maximizes its entropy toward the equilibrium. A spatial variation in the concentration  $c(\mathbf{r})$  promotes a transfer of the solute from the more concentrated region to the less concentrated region.

The rate of transfer is called a **flux** (also called a flow; but it is necessary to avoid confusion from the macroscopic flow of the fluid). The transfer occurs in the absence of the solvent flow as well as in the presence of the solvent flow. The flux is defined as the mass of the solute that moves across a unit area in a unit time. The direction of the flux is the same as that of the velocity  $\mathbf{v}(\mathbf{r})$  of the solute molecules. By definition, the flux  $\mathbf{j}(\mathbf{r})$  is related to  $\mathbf{v}(\mathbf{r})$  by

$$\mathbf{j}(\mathbf{r}) = c(\mathbf{r})\mathbf{v}(\mathbf{r}) \quad (3.72)$$

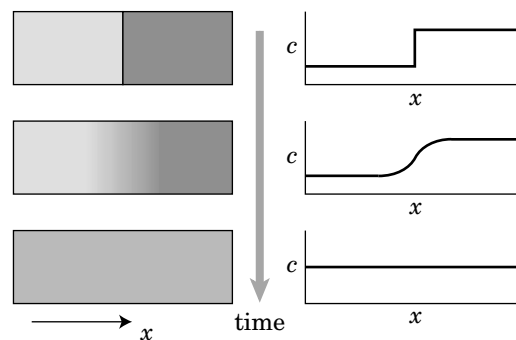


**Figure 3.21.** When the partition is removed, solute molecules move from the higher-concentration zone to the lower-concentration zone. The concentration profiles before the partition removal, during equilibration, and at equilibrium are shown on the right.

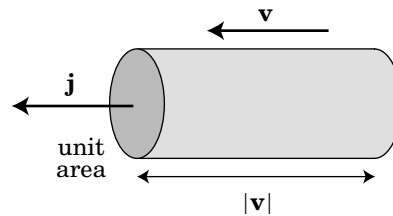


**Figure 3.22.** Flux  $\mathbf{j}$  is defined as the number of solute molecules that pass the cross section of a unit area in a unit time. The solute molecules in the cylinder of height  $|\mathbf{v}|$  pass the cross section in the next unit time.

Figure 3.22 will help us understand this relationship. The solute molecules in a cylinder that has a base of a unit area and a height of  $|\mathbf{v}|$  pass the base in the next unit time. The mass of solute molecules in the cylinder,  $c|\mathbf{v}|$ , is by definition equal to  $|\mathbf{j}|$ . In the following, we consider a quiescent solution.

The local concentration variation is represented by the **concentration gradient**  $\nabla c(\mathbf{r})$ . In one dimension, it is  $\partial c/\partial x$  (Fig. 3.23). When  $\nabla c$  is sufficiently small, the flux  $\mathbf{j}(\mathbf{r})$  is proportional to  $\nabla c(\mathbf{r})$  (Fick's law). In the absence of the concentration

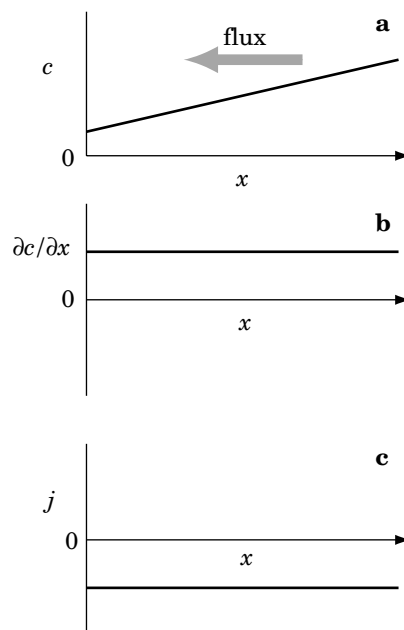


**Figure 3.23.** Concentration gradient causes a flux. The illustration is for one dimension. a: Profile of concentration  $c$ . b: Concentration gradient  $\partial c/\partial x$ . c: Flux  $j$ .

gradient, there is no flux. On reversal of the sign of  $\nabla c$ ,  $\mathbf{j}$  also changes its sign. We introduce the diffusion coefficient  $D$  as the proportionality constant in

$$\boxed{\mathbf{j} = -D\nabla c \quad \text{Fick's law}} \quad (3.73)$$

The minus sign is necessary to account for the transfer from the high- $c$  region to the low- $c$  region. In one dimension, the flux is negative when  $\partial c/\partial x > 0$  as indicated in the figure. We will soon find that the diffusion coefficient defined in this way is equivalent to the one we defined microscopically in Section 3.2.4. The diffusion that follows this equation is called a Fickian diffusion.

**3.2.10.2 Diffusion Equation** The other equation that relates  $\mathbf{j}$  and  $c$  is from the conservation of mass. We consider a small fixed volume  $V$  (Fig. 3.24). The rate of change in the total mass of the solute in the volume,  $V(\partial c/\partial t)$ , is equal to the negative of the integral of the surface-normal component of  $\mathbf{j}$  over the surface of the volume:

$$V \frac{\partial c}{\partial t} = - \int_{\text{surface}} \mathbf{j} \cdot d\mathbf{S} \quad (3.74)$$

Note that  $\mathbf{j} \cdot d\mathbf{S}$  accounts for the mass of the solute molecules that leave the volume through a small area  $d\mathbf{S}$ . The minus sign is needed because a positive  $\mathbf{j} \cdot d\mathbf{S}$  means an outflow. By Green's theorem, the surface integral is converted to the volume integral. In the limit of small  $V$ ,

$$\int_{\text{surface}} \mathbf{j} \cdot d\mathbf{S} = \int_V \nabla \cdot \mathbf{j} \, d\mathbf{r} = V \nabla \cdot \mathbf{j} \quad (3.75)$$

Combining the two equations, we obtain the law of mass conservation:

$$\boxed{\frac{\partial c}{\partial t} + \nabla \cdot \mathbf{j} = 0 \quad \text{mass conservation}} \quad (3.76)$$

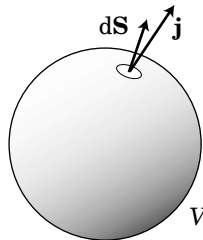


**Figure 3.24.** Flux  $\mathbf{j}$  and the surface normal  $d\mathbf{S}$  on a sphere of a small volume  $V$ .

With Fick's law, we can obtain the diffusion equation:

$$\boxed{\frac{\partial c}{\partial t} = -\nabla \cdot \mathbf{j} = D\nabla \cdot \nabla c = D\nabla^2 c} \quad (3.77)$$

which is identical to Eq. 3.37. The phenomenological definition of the diffusion coefficient is equivalent to the microscopic definition of the diffusion coefficient.

**3.2.10.3 Chemical Potential Gradient** With Eq. 3.72, Fick's law can be rewritten to

$$\mathbf{v}(\mathbf{r}) = -D\nabla \ln(c/c^\circ) \quad (3.78)$$

where  $c^\circ$  is a reference concentration. We recall that  $D = k_B T / \zeta$  (Eq. 3.51). In a solution of a uniform temperature, Eq. 3.78 is converted to

$$\zeta \mathbf{v}(\mathbf{r}) = -\nabla [k_B T \ln(c(\mathbf{r})/c^\circ)] \quad (3.79)$$

In the right-hand side,  $k_B T \ln(c/c^\circ)$  is the chemical potential in an ideal solution. This equation dictates a balance in the forces acting on the solute molecule at  $\mathbf{r}$ . The friction  $\zeta \mathbf{v}(\mathbf{r})$  is balanced by the chemical potential gradient, resulting in the velocity  $\mathbf{v}(\mathbf{r})$  of the solute molecule. The chemical potential gradient causes a transfer of matter from a higher potential to a lower potential, just as a force on the particle moves it.

### 3.2.11 Concentration Effect on Diffusion

**3.2.11.1 Self-Diffusion and Mutual Diffusion** When each suspension or solute molecule is moving independently, the diffusion is a single-particle phenomenon. The latter is observed in the dilute solution limit where there are no other solute molecules in the neighborhood. When other solute molecules are nearby, the diffusion is strongly affected by the other solute molecules. The second terms in Eqs. 3.17 and 3.45 are not negligible any more. What DLS measures is  $S(\mathbf{k}, \tau)$ , not  $S_1(\mathbf{k}, \tau)$ . Only when  $c \ll c^*$ ,  $S(\mathbf{k}, \tau)$  is equal to  $S_1(\mathbf{k}, \tau)$ . Otherwise, the apparent diffusion coefficient  $D$  estimated from the slope of  $|g_1(\tau)|$  depends on  $c$ . We will learn how the apparent  $D$  depends on  $c$ .

To have an intuitive understanding of the concentration effect, we consider a suspension of hard spheres. Suppose that a portion of the suspension acquires temporarily a higher concentration than the surrounding, as shown in Figure 3.25a. The particles in the locally concentrated region tend to move away from each other, resulting in the collision of black particles with white particles (Fig. 3.25b). Upon collision, the particles bounce back, although the motion is overdamped in a viscous environment (Fig. 3.25c). When we trace the motion of each black particle, the collision makes the square displacement smaller compared with the one in the absence of collisions. The effect of the local concentration fluctuation is, however,

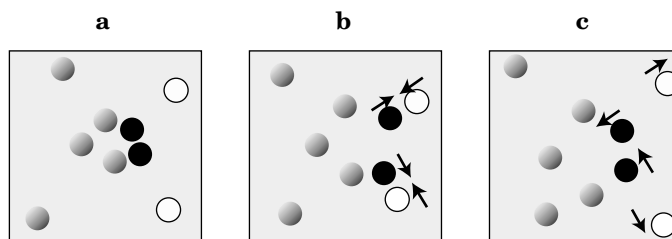


**Figure 3.25.** A temporary local congestion of spherical particles is dispersed by diffusion and collisions. Black spheres (in a) move to collide with white spheres (b) and bounce back (c). Propagation of the local concentration fluctuation (in a) is carried faster and farther by the white spheres (c).

transmitted farther by the white particles because of the collisions. When we trace the distance between the black particle and the white particle, the collision increases the distance more quickly compared with the counterpart in the absence of collisions.

The first concept, tracing each particle, is for the **self-diffusion**, and the second for the **mutual diffusion**. The **self-diffusion coefficient**  $D_s$  is defined for the motion of a given particle as

$$D_s = \lim_{t \rightarrow \infty} \frac{\langle [\mathbf{r}_1(t) - \mathbf{r}_1(0)]^2 \rangle}{6t} \quad \text{self-diffusion coefficient} \quad (3.80)$$

and the **mutual diffusion coefficient**  $D_m$  is defined for the motion of two particles as

$$D_m = \lim_{t \rightarrow \infty} \frac{\langle [\mathbf{r}_1(t) - \mathbf{r}_2(0)]^2 \rangle}{6t} \quad \text{mutual diffusion coefficient} \quad (3.81)$$

At sufficiently low concentrations, both  $D_s$  and  $D_m$  are equal to  $D_0$ , the diffusion coefficient of an isolated solute (Problem 3.14). With an increasing concentration,  $D_s$  tends to decrease but  $D_m$  tends to increase (Fig. 3.26). There are exceptions.

**3.2.11.2 Measurement of Self-Diffusion Coefficient** What is measured in DLS is  $D_m$ . DLS cannot measure  $D_s$  because it does not distinguish one solute from another. It is necessary to use other more specialized techniques such as **forced Rayleigh scattering (FRS)**, **fluorescence recovery after photo-bleaching (FRAP)**, and **pulsed-field gradient nuclear magnetic resonance (PFG-NMR)**.

The details of the instruments for the first two optical methods are explained, for instance, in Ref. 33. In short, FRS creates a temporary diffraction grating by intersecting two beams (write-beam) split from a strong, short-wavelength laser at a low angle. The polymer molecules must be labeled with a fluorescent dye. The grating is an alternate pattern of ground-state molecules and excited-state molecules. After the write-beam is turned off, a weak read beam is fired onto the grating to monitor

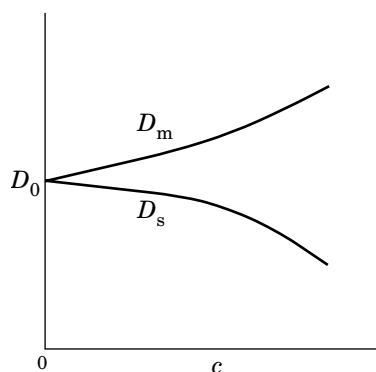


**Figure 3.26.** As the solute concentration  $c$  increases, the mutual diffusion coefficient  $D_m$  usually increases and the self-diffusion coefficient  $D_s$  decreases. In the low concentration limit,  $D_m$  and  $D_s$  are equal to  $D_0$ .

the decay in the intensity of the diffracted beam as the polymer chains diffuse to diminish the contrast. The decay rate gives an estimate of the self-diffusion coefficient. In FRAP, typically a circular spot beam bleaches the dyes attached to polymer chains. After the laser is turned off, the unbleached polymers sitting outside the spot diffuses into the circular domain to recover a uniform dye distribution. The build-up transient of the dye concentration in the circle gives an estimate of the self-diffusion coefficient. However, instruments that use these techniques are not commercially available.

In PFG-NMR, a pulsed gradient magnetic field is applied across a sample in phase to a spin-echo RF pulse sequence. The amplitude of the free induction decay is given by  $S_1(q, \tau)$  with  $q = \gamma\delta g$ , where  $\gamma$  is the magnetogyric ratio of the nucleus measured,  $\delta$  is the duration of the gradient field,  $g$  is the field gradient, and  $\tau$  is the separation between successive field pulses. By changing the field gradient, the scattering function is measured at different wave vectors, allowing the user to estimate  $D_s$ .

Although  $D_s$  cannot be measured in DLS, a closely related **tracer diffusion coefficient**  $D_t$  can be measured. In the tracer diffusion, the motion of a labeled solute called a **probe** or a **tracer** is traced selectively. A second solute called a **matrix** is added to the solution and its concentration is varied, whereas the concentration of the probe molecules is held low. The matrix must be invisible, and the probe must be visible. We can give a large contrast between the matrix and probe by choosing a pair of solvent and matrix that are nearly **isorefractive**, i.e., having the same refractive index. Then, the light scattering will look at the probe molecules only. For instance, we can follow the tracer diffusion of polystyrene in a matrix solution of poly(dimethyl siloxane) in tetrahydrofuran.

**3.2.11.3 Concentration Dependence of the Diffusion Coefficients** Now we consider the effect of the concentration on the diffusion coefficients quantitatively.



First, we consider the concentration effect on the self-diffusion coefficient. Other molecules tend to interrupt the otherwise free diffusion of a given solute molecule. In effect, the presence of other molecules increases the friction coefficient:

$$\zeta = \zeta_0(1 + \zeta_1 c + \dots) \quad (3.82)$$

where  $\zeta_0$  is the friction coefficient in the dilute solution limit, and  $\zeta_0 \zeta_1 (>0)$  is the first-order concentration coefficient. Then,

$$D_s = \frac{k_B T}{\zeta} = \frac{k_B T}{\zeta_0} (1 - \zeta_1 c + \dots) \quad (3.83)$$

The self-diffusion coefficient decreases linearly with  $c$  at low concentrations.

For the mutual diffusion coefficient, we start with generalizing Eq. 3.79 to an equation that applies to nonideal solutions:

$$\zeta \mathbf{v}(\mathbf{r}) = -\nabla \mu(\mathbf{r}) \quad (3.84)$$

In terms of flux,

$$\mathbf{j}(\mathbf{r}) = -\frac{c(\mathbf{r})}{\zeta} \nabla \mu(\mathbf{r}) \quad (3.85)$$

Now we use the virial expansion for  $\mu$  (Problem 2.9):

$$\mu = k_B T [\ln(c/c^\circ) + (2A_2 M - v_{sp})c + \dots] \quad (3.86)$$

Its gradient is given as

$$\nabla \mu = k_B T [c^{-1} + (2A_2 M - v_{sp}) + \dots] \nabla c \quad (3.87)$$

Then,

$$\mathbf{j} = -\frac{k_B T}{\zeta} (1 + (2A_2 M - v_{sp})c + \dots) \nabla c = -\frac{k_B T}{\zeta_0} [1 + (2A_2 M - \zeta_1 - v_{sp})c + \dots] \nabla c \quad (3.88)$$

where Eq. 3.82 was used for  $\zeta$ . Thus,  $D_m$  changes with  $c$  as

$$D_m = D_0(1 + k_D c + \dots) \quad \text{low concentrations} \quad (3.89)$$

with a linear coefficient  $k_D$  given by

$$k_D = 2A_2 M - \zeta_1 - v_{sp} \quad \text{linear coefficient} \quad (3.90)$$

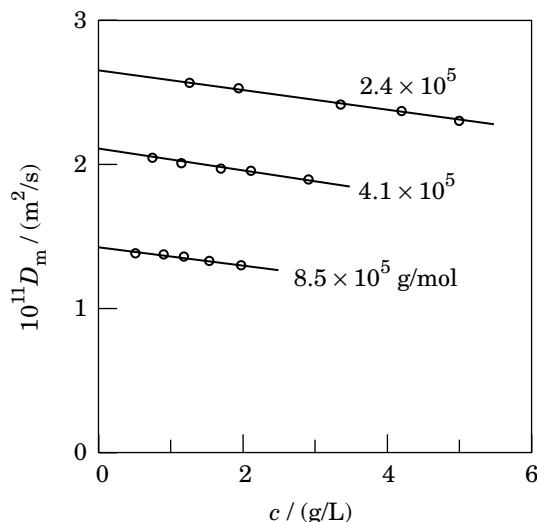


**Figure 3.27.** Mutual diffusion coefficient  $D_m$  of poly( $\alpha$ -methyl styrene) in a theta solvent at different concentrations in the dilute regime. The molecular weight of the polymer is indicated adjacent to each plot. (From Ref. 31.)

In a sufficiently good solvent,  $2A_2M > \zeta_1 + v_{sp}$  and therefore  $D_m$  increases with  $c$ . As the solvent quality becomes poorer,  $A_2$  decreases and therefore  $k_D$  becomes eventually negative.

Figure 3.27 shows an example of the concentration dependence of  $D_m$  in a theta solvent condition.<sup>31</sup> The light-scattering autocorrelation functions were measured for solutions of poly( $\alpha$ -methyl styrene) fractions of different molecular weights in the theta solvent of cyclohexane at 30.5°C. The first-order concentration coefficient is negative because  $A_2 = 0$  at this temperature and therefore  $k_D = -(\zeta_1 + v_{sp}) < 0$ .

So far, we have assumed that the solvent remains quiescent while the solute molecules move. There is, however, always a backflow of solvent molecules into the space originally occupied by the solute. This effect is to decrease  $D_m/D_0$  by  $v_{sp}c$ , where  $v_{sp}c$  is the fraction of the volume occupied by the polymer in solution. Then,

$$\boxed{k_D = 2A_2M - \zeta_1 - 2v_{sp}} \quad \text{with backflow correction} \quad (3.91)$$

### 3.2.12 Diffusion in a Nonuniform System

In some systems, the chemical potential depends explicitly on  $\mathbf{r}$ , not only through  $c(\mathbf{r})$ . An example is charged colloidal particles in an electric field. Here, we consider diffusion of particles in an external field such as an electric field. We limit the discussion to the low concentration limit.

When a stationary external field is applied, the chemical potential has an extra term  $U_E(\mathbf{r})$  due to the field:

$$\mu/k_B T = \ln(c/c^\circ) + U_E(\mathbf{r})/k_B T \quad (3.92)$$

Charged particles will experience  $U_E(\mathbf{r}) = (\text{charge}) \times (\text{electrostatic potential at } \mathbf{r})$ , for instance. The diffusion equation is rewritten to

$$\frac{\partial c}{\partial t} = D \nabla \cdot (\nabla c + c \nabla U_E/k_B T) \quad (3.93)$$

We can immediately obtain the equilibrium distribution  $c_{\text{eq}}(\mathbf{r})$  from  $\nabla c_{\text{eq}} + c_{\text{eq}} \nabla U_E/k_B T = 0$  as

$$c_{\text{eq}}(\mathbf{r}) = \text{const.} \times \exp(-U_E(\mathbf{r})/k_B T) \quad (3.94)$$

which is the Boltzmann distribution for particles with space-dependent energy of  $U_E(\mathbf{r})$ .

### 3.2.13 PROBLEM

**Problem 3.1:** We consider a walk on a cubic lattice. Its  $i$ th step motion  $\Delta \mathbf{r}_i$  in step time  $t_1$  satisfies

$$\langle \Delta \mathbf{r}_i \rangle = 0$$

$$\langle \Delta \mathbf{r}_i \cdot \Delta \mathbf{r}_j \rangle = \begin{cases} b^2 & (i = j) \\ pb^2 & (|i - j| = 1) \\ 0 & (\text{otherwise}) \end{cases}$$

where  $p < 1$  is a constant. What is the mean square displacement in  $N$  steps? Can we define the long-time diffusion coefficient? If yes, what is it?

**Solution 3.1:** The mean square displacement of  $N$  steps is

$$\begin{aligned} \langle \Delta \mathbf{r}^2 \rangle &= \sum_{i,j=1}^N \langle \Delta \mathbf{r}_i \cdot \Delta \mathbf{r}_j \rangle = \sum_{i=1}^N \langle \Delta \mathbf{r}_i^2 \rangle + \sum_{i=1}^{N-1} \langle \Delta \mathbf{r}_{i+1} \cdot \Delta \mathbf{r}_i \rangle + \sum_{i=2}^N \langle \Delta \mathbf{r}_{i-1} \cdot \Delta \mathbf{r}_i \rangle \\ &= Nb^2 + 2(N-1)pb^2 = b^2[(2p+1)N - 2p] \end{aligned}$$

For  $N \gg 1$ ,  $\langle \Delta \mathbf{r}^2 \rangle = b^2(2p+1)N$ . Therefore, the long-time diffusion coefficient  $D$  can be defined. It is

$$D = \frac{\langle \Delta \mathbf{r}^2 \rangle}{6Nt_1} = \frac{b^2(2p+1)}{6t_1}$$

**Problem 3.2:** Use the definition of  $S_1(\mathbf{k}, \tau)$  (Eq. 3.26) and the diffusion equation for  $P(\mathbf{r}, \mathbf{r}'; \tau)$  (Eq. 3.35) to show that  $S_1(\mathbf{k}, \tau) = S_1(\mathbf{k}, 0) \exp(-D\mathbf{k}^2\tau)$ .

**Solution 3.2:** From Eqs. 3.26 and 3.35,

$$\begin{aligned}\frac{\partial}{\partial \tau} S_1(\mathbf{k}, \tau) &= \int d\mathbf{r} \exp[i\mathbf{k} \cdot (\mathbf{r} - \mathbf{r}')] \frac{\partial}{\partial \tau} P(\mathbf{r}, \mathbf{r}'; \tau) \\ &= \int d\mathbf{r} \exp[i\mathbf{k} \cdot (\mathbf{r} - \mathbf{r}')] D \nabla^2 P(\mathbf{r}, \mathbf{r}'; \tau)\end{aligned}$$

Integral by parts yields

$$\begin{aligned}\frac{\partial}{\partial \tau} S_1(\mathbf{k}, \tau) &= D \int d\mathbf{r} P(\mathbf{r}, \mathbf{r}'; \tau) \nabla^2 \exp[i\mathbf{k} \cdot (\mathbf{r} - \mathbf{r}')] \\ &= D \int d\mathbf{r} P(\mathbf{r}, \mathbf{r}'; \tau) (-\mathbf{k}^2 \exp[i\mathbf{k} \cdot (\mathbf{r} - \mathbf{r}')] \\ &= -D\mathbf{k}^2 \int d\mathbf{r} P(\mathbf{r}, \mathbf{r}'; \tau) \exp[i\mathbf{k} \cdot (\mathbf{r} - \mathbf{r}')] = -D\mathbf{k}^2 S_1\end{aligned}$$

The solution of this differential equation is given as

$$S_1(\mathbf{k}, \tau) = S_1(\mathbf{k}, 0) \exp(-D\mathbf{k}^2 \tau)$$

**Problem 3.3:** Use Eq. 3.26 to show that

$$\langle (\mathbf{r} - \mathbf{r}')^2 \rangle = -\left. \frac{\partial^2}{\partial \mathbf{k}^2} S_1(\mathbf{k}, \tau) \right|_{\mathbf{k}=0}$$

without relying on the Taylor expansion.

**Solution 3.3:** By definition,

$$\langle (\mathbf{r} - \mathbf{r}')^2 \rangle = \int d\mathbf{r} (\mathbf{r} - \mathbf{r}')^2 P(\mathbf{r}, \mathbf{r}'; \tau)$$

Because

$$(\mathbf{r} - \mathbf{r}')^2 = -\left. \frac{\partial^2}{\partial \mathbf{k}^2} \exp[i\mathbf{k} \cdot (\mathbf{r} - \mathbf{r}')] \right|_{\mathbf{k}=0}$$

we obtain

$$\begin{aligned}\langle (\mathbf{r} - \mathbf{r}')^2 \rangle &= - \int d\mathbf{r} \left. \frac{\partial^2}{\partial \mathbf{k}^2} \exp[i\mathbf{k} \cdot (\mathbf{r} - \mathbf{r}')] \right|_{\mathbf{k}=0} P(\mathbf{r}, \mathbf{r}'; \tau) \\ &= -\frac{\partial^2}{\partial \mathbf{k}^2} \int d\mathbf{r} \exp[i\mathbf{k} \cdot (\mathbf{r} - \mathbf{r}')] P(\mathbf{r}, \mathbf{r}'; \tau) \Big|_{\mathbf{k}=0} \\ &= -\left. \frac{\partial^2}{\partial \mathbf{k}^2} S_1(\mathbf{k}, \tau) \right|_{\mathbf{k}=0}\end{aligned}$$

**Problem 3.4:** The viscosity of water is 0.893 cP at 25°C and 0.355 cP at 80°C. How much faster is the diffusion at 80°C compared with 25°C for a particle suspended in water?

**Solution 3.4:**

$$\frac{D_{80^\circ\text{C}}}{D_{25^\circ\text{C}}} = \frac{273.15 + 80}{273.15 + 25} \times \frac{0.893 \text{ cP}}{0.355 \text{ cP}} = 2.98$$

**Problem 3.5:** For the same number of monomers, which conformation has stronger hydrodynamic interactions, flexible or semirigid?

**Solution 3.5:** Flexible chain; For the same pair of monomers separated by a given distance along the chain contour, the spatial distance between them is shorter in the flexible chain than it is in the semirigid chain.

**Problem 3.6:** Use Eq. 3.55 to calculate  $R_{\text{H,star}}$  of a star polymer consisting of  $n_A$  arms that have a conformation of a Gaussian chain with  $N_1$  segments of length  $b$ . What is  $g_{\text{H}} \equiv (R_{\text{H,star}}/R_{\text{H,lin}})^2$ , where  $R_{\text{H,lin}}$  is for a linear chain of  $n_A N_1$  segments? Compare  $g_{\text{H}}$  with  $g_{\text{g}}$  defined as the ratio of the mean square radii of gyration for the same pair of polymers (Eq. 1.85).

**Solution 3.6:** We define  $\mathbf{r}_{im}$  and  $\mathbf{r}_{jn}$  in the same way as we did in Section 1.6.  $R_{\text{H,star}}^{-1} = \langle |\mathbf{r}_{im} - \mathbf{r}_{jn}|^{-1} \rangle$  is calculated separately for  $\mathbf{r}_{im}$  and  $\mathbf{r}_{jn}$  on the same arm and the pairs on different arms. For the pair on the same arm,

$$\left(\frac{\pi}{6}\right)^{1/2} b \left\langle \frac{1}{|\mathbf{r}_{im} - \mathbf{r}_{in}|} \right\rangle = \frac{1}{N_1^2} \int_0^{N_1} dn \int_0^{N_1} dm |n - m|^{-1/2} = \frac{8}{3} \frac{1}{N_1^{1/2}}$$

For pairs on different arms,

$$\left(\frac{\pi}{6}\right)^{1/2} b \left\langle \frac{1}{|\mathbf{r}_{im} - \mathbf{r}_{jn}|} \right\rangle = \frac{1}{N_1^2} \int_0^{N_1} dn \int_0^{N_1} dm (n + m)^{-1/2} = \frac{8}{3} (2^{1/2} - 1) \frac{1}{N_1^{1/2}}$$

The two types of pairing occur with probabilities of  $1/n_A$  and  $1 - 1/n_A$ , respectively. Then,  $R_{\text{H,star}}$  is given by

$$\begin{aligned} \frac{1}{R_{\text{H,star}}} &= \left(\frac{6}{\pi}\right)^{1/2} \frac{1}{b} \times \frac{8}{3} \frac{1}{N_1^{1/2}} \frac{(2^{1/2} - 1)(2^{1/2} + n_A)}{n_A} \\ &= 8 \left(\frac{2}{3\pi}\right)^{1/2} \frac{1}{bN_1^{1/2}} \frac{(2^{1/2} - 1)(2^{1/2} + n_A)}{n_A} \end{aligned}$$

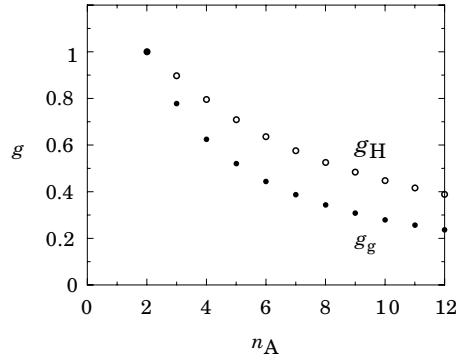
The  $R_{\text{H}}$  of a linear polymer with  $n_A N_1$  segments is

$$\frac{1}{R_{\text{H,lin}}} = 8 \left(\frac{2}{3\pi}\right)^{1/2} \frac{1}{b(n_A N_1)^{1/2}}$$

The ratio  $g_H$  is

$$g_H \equiv \left( \frac{R_{H,\text{star}}}{R_{H,\text{lin}}} \right)^2 = \frac{n_A}{[(2^{1/2} - 1)(2^{1/2} + n_A)]^2}$$

The following figure compares  $g_H$  with  $g_g$ :



**Problem 3.7:** What is the addition rule for  $R_g$  and  $R_H$  when an a block with  $R_{ga}$  and  $R_{Ha}$  and a b block with  $R_{gb}$  and  $R_{Hb}$  are joined to form an a–b diblock copolymer? Assume that the two blocks follow the same chain statistics.

**Solution 3.7:** The addition rule is

$$R_g^{1/\nu} = R_{ga}^{1/\nu} + R_{gb}^{1/\nu}, R_H^{1/\nu} = R_{Ha}^{1/\nu} + R_{Hb}^{1/\nu}$$

**Problem 3.8:** Derive Eq. 3.61 from Eq. 3.59.

**Solution 3.8:** From Eq. 3.59,

$$\begin{aligned} \frac{\partial}{\partial \tau} \ln |g_1(\tau)| &= -|g_1(\tau)|^{-1} \int \Gamma G(\Gamma) \exp(-\Gamma \tau) d\Gamma \\ \frac{\partial^2}{\partial \tau^2} \ln |g_1(\tau)| &= |g_1(\tau)|^{-1} \int \Gamma^2 G(\Gamma) \exp(-\Gamma \tau) d\Gamma \\ &\quad - \left( |g_1(\tau)|^{-1} \int \Gamma G(\Gamma) \exp(-\Gamma \tau) d\Gamma \right)^2 \\ \frac{\partial^3}{\partial \tau^3} \ln |g_1(\tau)| &= -|g_1(\tau)|^{-1} \int \Gamma^3 G(\Gamma) \exp(-\Gamma \tau) d\Gamma \\ &\quad + 3|g_1(\tau)|^{-2} \int \Gamma^2 G(\Gamma) \exp(-\Gamma \tau) d\Gamma \int \Gamma G(\Gamma) \exp(-\Gamma \tau) d\Gamma \\ &\quad - 2 \left( |g_1(\tau)|^{-1} \int \Gamma G(\Gamma) \exp(-\Gamma \tau) d\Gamma \right)^3 \end{aligned}$$

The derivatives at  $\tau = 0$  are

$$\begin{aligned}\frac{\partial}{\partial \tau} \ln |g_1(\tau)| \Big|_{\tau=0} &= - \int \Gamma G(\Gamma) d\Gamma = -\langle \Gamma \rangle \\ \frac{\partial^2}{\partial \tau^2} \ln |g_1(\tau)| \Big|_{\tau=0} &= \langle \Gamma^2 \rangle - \langle \Gamma \rangle^2 = \langle \Delta \Gamma^2 \rangle \\ \frac{\partial^3}{\partial \tau^3} \ln |g_1(\tau)| \Big|_{\tau=0} &= -\langle \Gamma^3 \rangle + 3\langle \Gamma^2 \rangle \langle \Gamma \rangle - 2\langle \Gamma \rangle^3 = -\langle \Delta \Gamma^3 \rangle\end{aligned}$$

Thus, the Taylor expansion of  $\ln |g_1(\tau)|$  at  $\tau = 0$  is expressed as

$$\ln |g_1(\tau)| = -\langle \Gamma \rangle \tau + \frac{1}{2} \langle \Delta \Gamma^2 \rangle \tau^2 - \frac{1}{6} \langle \Delta \Gamma^3 \rangle \tau^3 + \dots$$

**Problem 3.9:** Explain why  $|g_1(\tau)|$  deviates upward from the straight line for a polydisperse system?

**Solution 3.9:** In the final answer of Problem 3.8, the second-order term is always positive.

**Problem 3.10:** When the DLS measurement is carried out for a solution of a polymer with a molecular weight distribution, how is  $G(\Gamma)$  weighted? What average of diffusion coefficient does the initial slope of  $|g_1(\tau)|$  give? Component  $i$  of the polymer with molecular weight  $M_i$  is dissolved in the solution at concentration  $c_i$ .

**Solution 3.10:** The excess scattering intensity  $I_i$  by component  $i$  is proportional to  $c_i M_i$  (Eq. 2.118 with  $\mathbf{k} = 0$ ). Thus, the weight for the component in  $G(\Gamma)$  is  $c_i M_i$ , and

$$|g_1(\tau)| \propto \sum_i c_i M_i \exp(-D_i \mathbf{k}^2 \tau)$$

where  $D_i$  is the diffusion coefficient of component  $i$ . The initial decay rate is

$$-\frac{\partial}{\partial t} \ln |g_1(\tau)| \Big|_{\tau=0} = \frac{\sum_i c_i M_i D_i}{\sum_i c_i M_i} \mathbf{k}^2$$

The average of  $D$  is weighted by  $c_i M_i$ :

$$\langle D \rangle = \frac{\sum_i D_i c_i M_i}{\sum_i c_i M_i}$$

Because  $c_i M_i$  is proportional to the product of the weight fraction and  $M_i$ , the above average is a  $z$ -average.

**Problem 3.11:** DLS measurement is conducted for a dilute ternary solution of two different polymers a and b in a non-selective solvent. The two polymers are dissolved at concentrations  $c_a$  and  $c_b$ . The differential refractive index of polymer a in the solvent is  $dn/dc_a$  and that of polymer b is  $dn/dc_b$ . We assume that the two polymers are monodisperse with molecular weights  $M_a$  and  $M_b$ , and the decay rates in  $|g_1(\tau)|$  measured for a binary solution of polymer a (i.e., polymer a + the same solvent) and another binary solution of polymer b are  $\Gamma_a$  and  $\Gamma_b$ , respectively. Find the apparent distribution  $G(\Gamma)$  for the ternary solution. What is  $|g_1(\tau)|$  for the solution? Assume that the two polymers are molecularly dispersed in the ternary solution.

**Solution 3.11:**  $G(\Gamma) = G_a \delta(\Gamma - \Gamma_a) + G_b \delta(\Gamma - \Gamma_b)$ , where

$$G_a \propto \left( \frac{dn}{dc_a} \right)^2 c_a M_a, \quad G_b \propto \left( \frac{dn}{dc_b} \right)^2 c_b M_b$$

Then,

$$G(\Gamma) = \frac{\left( \frac{dn}{dc_a} \right)^2 c_a M_a \delta(\Gamma - \Gamma_a) + \left( \frac{dn}{dc_b} \right)^2 c_b M_b \delta(\Gamma - \Gamma_b)}{\left( \frac{dn}{dc_a} \right)^2 c_a M_a + \left( \frac{dn}{dc_b} \right)^2 c_b M_b}$$

and we obtain

$$|g_1(\tau)| = \frac{\left( \frac{dn}{dc_a} \right)^2 c_a M_a \exp(-\Gamma_a \tau) + \left( \frac{dn}{dc_b} \right)^2 c_b M_b \exp(-\Gamma_b \tau)}{\left( \frac{dn}{dc_a} \right)^2 c_a M_a + \left( \frac{dn}{dc_b} \right)^2 c_b M_b}$$

**Solution 3.12:** In principle, the particle-sizing system should be able to find the distribution of molecular weight  $M$  of a polymer in solution. Assume a narrow distribution of  $M$  around  $\bar{M}$  given by

$$M^2 f(M) d \ln M = (2\pi \bar{M}^2 \sigma^2)^{-1/2} \exp\left(-\frac{\Delta M^2}{2\bar{M}^2 \sigma^2}\right) d\Delta M$$

which is obtained from Eq. 1.102 with  $M = \bar{M} + \Delta M$  ( $|\Delta M/\bar{M}| \ll 1$ ). The diffusion coefficient  $D$  is related to  $M$  by  $D = D(M/\bar{M})^{-\nu}$  where  $D$  is the



value of  $D$  for  $M = \bar{M}$ . Let  $\Delta D = D - \langle D \rangle$ , where

$$\langle \dots \rangle \equiv \int \dots (2\pi\bar{M}^2\sigma^2)^{-1/2} \exp\left(-\frac{\Delta M^2}{2\bar{M}^2\sigma^2}\right) d\Delta M$$

What is  $\langle \Delta D^2 \rangle / \langle D \rangle^2$ ?

**Solution 3.12:** With  $M = \bar{M}(1 + \Delta M/\bar{M})$ ,  $D = \bar{D}(1 + \Delta M/\bar{M})^{-\nu} \cong \bar{D}(1 - \nu\Delta M/\bar{M})$ . Then,

$$\langle D \rangle = \int \bar{D}(1 - \nu\Delta M/\bar{M})(2\pi\bar{M}^2\sigma^2)^{-1/2} \exp\left(-\frac{\Delta M^2}{2\bar{M}^2\sigma^2}\right) d\Delta M = \bar{D}$$

Because  $\Delta D = -\bar{D}\nu\Delta M/\bar{M}$ ,

$$\langle \Delta D^2 \rangle = \bar{D}^2\nu^2 \int (\Delta M/\bar{M})^2 (2\pi\bar{M}^2\sigma^2)^{-1/2} \exp\left(-\frac{\Delta M^2}{2\bar{M}^2\sigma^2}\right) d\Delta M = \bar{D}^2\nu^2\sigma^2$$

Thus,

$$\langle \Delta D^2 \rangle / \langle D \rangle^2 = \nu^2\sigma^2$$

Because  $\sigma^2 = \ln \text{PDI}$  from Eq. 1.106,

$$\langle \Delta D^2 \rangle / \langle D \rangle^2 = \nu^2 \ln \text{PDI} = \begin{cases} \frac{1}{4} \ln \text{PDI} & (\text{theta solvent}) \\ \frac{9}{25} \ln \text{PDI} & (\text{good solvent}) \end{cases}$$

Note  $\langle \Delta D^2 \rangle / \langle D \rangle^2 = \langle \Delta \Gamma^2 \rangle / \langle \Gamma \rangle^2$ .

**Problem 3.13:** Show that, when a particle of mass  $m$  receives a random force  $\mathbf{f}(t)$  with  $\langle \mathbf{f}(t) \rangle = 0$  and  $\langle \mathbf{f}(t) \cdot \mathbf{f}(t') \rangle = 6k_B T \zeta \delta(t - t')$ , its average kinetic energy satisfies the equipartition law:  $m\langle \mathbf{v}^2 \rangle / 2 = (3/2)k_B T$  [ $k_B T / 2$  per degree of freedom,  $(3/2)k_B T$  for 3D].

**Solution 3.13:** The equation of motion of the particle (Langevin equation) is

$$\mathbf{f} = m \frac{d\mathbf{v}}{dt} + \zeta \mathbf{v}$$

Its solution is given as

$$\mathbf{v}(t) = m^{-1} \int_{-\infty}^t \mathbf{f}(t_1) \exp[(\zeta/m)(t_1 - t)] dt_1$$

Then,

$$\begin{aligned}
 \langle \mathbf{v}(t)^2 \rangle &= m^{-2} \int_{-\infty}^t dt_1 \int_{-\infty}^t dt_2 \langle \mathbf{f}(t_1) \cdot \mathbf{f}(t_2) \rangle \exp[(\zeta/m)(t_1 - t + t_2 - t)] \\
 &= 6k_B T \zeta m^{-2} \int_{-\infty}^t dt_1 \int_{-\infty}^t dt_2 \delta(t_1 - t_2) \exp[(\zeta/m)(t_1 - t + t_2 - t)] \\
 &= 6k_B T \zeta m^{-2} \int_{-\infty}^t dt_1 \exp[(2\zeta/m)(t_1 - t)] = \frac{3k_B T}{m}
 \end{aligned}$$

which leads to  $m\langle \mathbf{v}^2 \rangle / 2 = (3/2)k_B T$ .

**Problem 3.14:** Show that  $D_m$  defined by Eq. 3.81 becomes equal to  $D_0$  in the dilute solution limit.

**Solution 3.14:** In the dilute solution limit, displacement of particle 1 has nothing to do with particle 2. Thus,

$$\begin{aligned}
 \langle [\mathbf{r}_1(t) - \mathbf{r}_2(0)]^2 \rangle &= \langle [\mathbf{r}_1(t) - \mathbf{r}_1(0) + \mathbf{r}_1(0) - \mathbf{r}_2(0)]^2 \rangle \\
 &= \langle [\mathbf{r}_1(t) - \mathbf{r}_1(0)]^2 \rangle + \langle [\mathbf{r}_1(t) - \mathbf{r}_1(0)][\mathbf{r}_1(0) - \mathbf{r}_2(0)] \rangle + \langle [\mathbf{r}_1(0) - \mathbf{r}_2(0)]^2 \rangle \\
 &= \langle [\mathbf{r}_1(t) - \mathbf{r}_1(0)]^2 \rangle + 0 + \langle [\mathbf{r}_1(0) - \mathbf{r}_2(0)]^2 \rangle
 \end{aligned}$$

When  $t \rightarrow \infty$ , the first term is dominant.

**Problem 3.15:** What is the diffusion equation for a suspension of particles when there is a macroscopic flow  $\bar{\mathbf{v}}(\mathbf{r})$  in the fluid?

**Solution 3.15:** The flow adds a term to the flux  $\mathbf{j}$ :

$$\mathbf{j} = -D\nabla c + c\bar{\mathbf{v}}$$

With Eq. 3.76,

$$\frac{\partial c}{\partial t} = D\nabla^2 c - \nabla \cdot (c\bar{\mathbf{v}})$$

**Problem 3.16:** A linear flexible chain is tethered to the surface of a spherical molecule. The sphere-chain molecules are suspended in a solvent that is isorefractive with the chain portion but not with the sphere portion. The solvent is good to both the sphere and the chain. Answer the following questions regarding the static and dynamic light scattering of the solution.

- (1) Are the apparent  $R_g$  and  $A_2$  estimated in the Zimm plot different from those obtained for solutions of spherical molecules without a tethered chain? If yes, what is the difference?
- (2) How about  $D_0$  and  $k_D$  in the expression of the mutual diffusion coefficient  $D_m = D_0(1 + k_D c)$ ?

**Solution 3.16 (1):** Because the scattering comes only from the spheres,  $R_g$  is the same. Because  $A_{2,\text{sphere}} \ll A_{2,\text{linear}}$ ,  $A_2$  is greater when a chain is tethered.

**Solution 3.16 (2):**  $D_0$  is smaller. There is now extra friction.  $k_D$  is greater because of the greater  $A_2$ .

**Problem 3.17:** In the preceding problem, another solvent that gives  $(dn/dc)_{\text{sphere}} + (dn/dc)_{\text{chain}} = 0$  (the refractive index of the solvent is exactly the average of the refractive indices of the sphere and the chain) was used. The solvent is good to both the sphere and the chain. Answer the following questions.

- (1) Are the apparent  $R_g$  and  $A_2$  estimated in the Zimm plot different from those obtained for solutions of linear chains without a sphere tag? If yes, what is the difference?
- (2) How about  $D_0$  and  $k_D$ ?

**Solution 3.17 (1):**  $R_g$  is slightly larger because of the sphere tag.  $A_2$  is smaller.

**Solution 3.17 (2):**  $D_0$  is smaller.  $k_D$  is smaller.

### 3.3 VISCOSITY

#### 3.3.1 Viscosity of Solutions

**3.3.1.1 Viscosity of a Fluid** Solutions of a high-molecular-weight polymer, even at low concentrations, can flow only slowly. Addition of a small amount of the polymer to the fluid can make it **viscous**, thereby preventing unwanted turbulence in the flow.

Let us consider a fluid filling a space between two parallel plates, as illustrated in Figure 3.28. The bottom plate does not move, but the top plate slides in the  $y$  direction without changing the distance to the stationary plate. When the fluid adjacent to the plate sticks to the plate (nonslip boundary condition), the fluid moves in the same direction. Near the bottom plate, the fluid barely moves. However, with an increasing distance from the bottom plate, the fluid moves faster. As long as the flow is sufficiently slow, the fluid flows parallel to the plates. In other words, the velocity of the fluid has only an  $x$  component ( $v_x$ ). This flow mode is called a **laminar flow**. We can regard the fluid as a stack of sheets, each sliding against the sheet beneath it. The velocity of the sheet,  $v_x$ , changes linearly with  $y$ ,

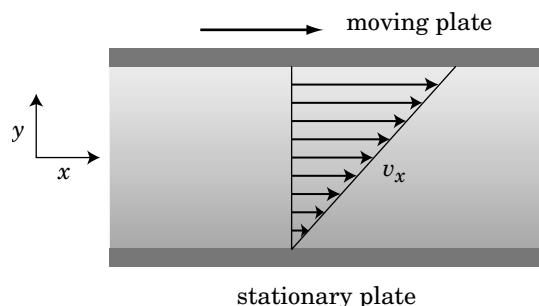


**Figure 3.28.** Fluid between a stationary bottom plate and a moving top plate. The velocity of the fluid is parallel to the plates and is proportional to the distance from the bottom plate, thereby generating a uniform velocity gradient.

the distance from the stationary plate. The gradient of  $v_x$  with respect to  $y$ ,  $\partial v_x / \partial y$ , is called the **velocity gradient**.

To move the top plate at a constant velocity, a constant force must be applied in the  $x$  direction. The same applies to any small volume of the fluid. We consider a small disk parallel to the plates at distance  $y$  from the bottom plate (see Fig. 3.29). The disk has a height of  $dy$ . The fluid on the lower base flows at  $v_x$ , and the fluid on the upper base flows at  $v_x + (\partial v_x / \partial y)dy$ . To make this velocity difference possible, a constant force needs to be exerted on the disk in the  $x$  direction. The force per area is called **shear stress** and has a dimension of the pressure. The shear stress  $\sigma_{yx}$  denotes the force per area in the  $x$  direction exerted across the plane normal to  $y$ . To be precise,  $\sigma$  is a tensor of the second rank. It is symmetric, that is,  $\sigma_{yx} = \sigma_{xy}$ , and so forth. The regular pressure is expressed as  $\sigma_{xx}$ ,  $\sigma_{yy}$ , and  $\sigma_{zz}$ . In the isotropic fluid,  $\sigma_{xx} = \sigma_{yy} = \sigma_{zz}$ , and it is called hydrostatic pressure.

We next examine the relationship between  $\sigma_{yx}$  and  $\partial v_x / \partial y$ . When  $\partial v_x / \partial y = 0$ ,  $\sigma_{yx} = 0$ . If there is no velocity gradient, then no force exists. When flow direction changes, both  $\sigma_{yx}$  and  $\partial v_x / \partial y$  change their signs. Therefore,  $\sigma_{yx}$  is proportional to  $\partial v_x / \partial y$  when  $\partial v_x / \partial y$  is sufficiently small (**Newtonian fluid**):

$$\eta \frac{\partial v_x}{\partial y} = \sigma_{yx} \quad (3.95)$$

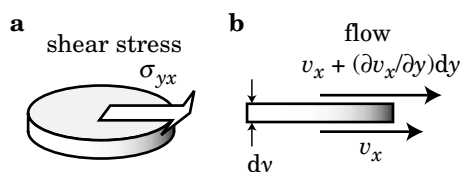


**Figure 3.29.** A small, thin disk parallel to the plates in Fig. 3.28. a: A shear stress  $\sigma_{yx}$  must be applied to the disk to have a different velocity between the upper base and the lower base. b: Side view.

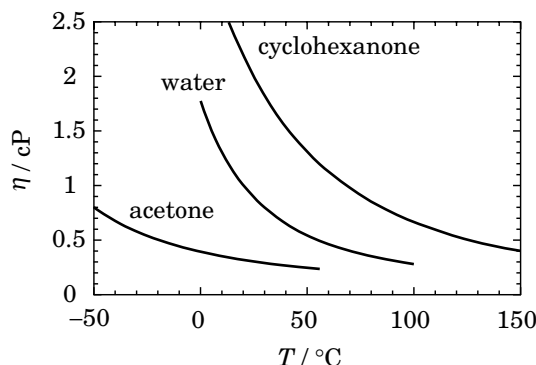


**Figure 3.30.** Viscosity  $\eta$  of water, acetone, and cyclohexanone at different temperatures.

The proportionality coefficient  $\eta$  is called the **viscosity**. Because  $\partial v_x / \partial y$  has a dimension of  $s^{-1}$  and  $\sigma_{yx}$  has a dimension of  $N/m^2$ , the unit of  $\eta$  is  $N \cdot s / m^2 = kg / (m \cdot s)$  in the SI unit. In the cgs system, the unit is  $g / (cm \cdot s)$ , which defines **poise**. Because most low-molecular-weight liquids have a viscosity of around 0.01 poise at room temperature, centipoise [cP; equal to 0.01 poise] is commonly used for the unit of viscosity. Note that  $1 \text{ cP} = 10^{-3} \text{ kg} / (m \cdot s)$ .

Equation 3.95 illustrates that, to realize the same velocity gradient, a fluid with a greater  $\eta$  needs a larger shear stress. A greater force is needed to move the top plate at the same velocity. The viscosity is a measure for the resistance of the fluid to flow. The viscosity of the fluid sensitively depends on the temperature. Figure 3.30 shows the dependence for water, acetone, and cyclohexanone. The temperature dependence of viscosity is listed in reference books<sup>34</sup> for most organic solvents.

**3.3.1.2 Viscosity of a Solution** Now we learn how to express the concentration dependence of the viscosity in solutions. When the concentration  $c$ , expressed in  $g/L$ , is sufficiently low, the viscosity  $\eta$  of the solution is not much different from the viscosity  $\eta_s$  of the pure solvent. The ratio of  $\eta$  to  $\eta_s$  is called the **relative viscosity**. Although the ratio is dimensionless, it is customary to use the symbol  $\eta_r$  for the relative viscosity. When  $c$  is low,

$$\eta_r \equiv \frac{\eta}{\eta_s} = 1 + [\eta]c + K_v c^2 + \dots \quad \text{relative viscosity} \quad (3.96)$$

Figure 3.31 illustrates how  $\eta_r$  changes with  $c$ . The linear coefficient  $[\eta]$  is called the **intrinsic viscosity**. It can be obtained as the slope in the plot of  $\eta_r$  as a function of  $c$  in the low concentration limit:

$$[\eta] \equiv \lim_{c \rightarrow 0} \frac{\eta_r - 1}{c} = \lim_{c \rightarrow 0} \frac{\eta - \eta_s}{c \eta_s} \quad \text{intrinsic viscosity} \quad (3.97)$$

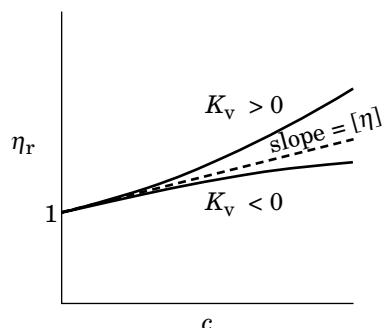


**Figure 3.31.** Relative viscosity  $\eta_r$  plotted as a function of  $c$ . The slope in the low  $c$  limit gives  $[\eta]$ . The plot deviates upward or downward, depending on the sign of  $K_v$ .

The dimension of  $[\eta]$  is (concentration) $^{-1}$ . As we will learn in Section 3.3.3, how  $[\eta]$  of the polymer solution depends on the molecular weight of the polymer gives a hint on the conformation of the polymer. The second-order coefficient  $K_v$  can be positive or negative.

Sometimes, the **specific viscosity**  $\eta_{sp}$ , defined as  $\eta_{sp} \equiv \eta_r - 1$ , is used:

$$\eta_{sp} \equiv \eta_r - 1 = \frac{\eta - \eta_s}{\eta_s} = [\eta]c + K_v c^2 + \dots \quad \text{specific viscosity} \quad (3.98)$$

The **reduced viscosity**  $\eta_{red}$  refers to the ratio of  $\eta_{sp}$  to  $c$ :

$$\eta_{red} \equiv \eta_{sp}/c = \frac{\eta - \eta_s}{\eta_s c} = [\eta] + K_v c + \dots \quad \text{reduced viscosity} \quad (3.99)$$

It has a dimension of (concentration) $^{-1}$ . Figure 3.32 illustrates how  $\eta_{red}$  changes with  $c$ .

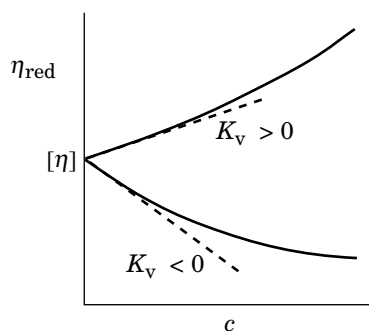


**Figure 3.32.** Reduced viscosity  $\eta_{red}$  plotted as a function of  $c$ . The intercept is  $[\eta]$ . The slope of the tangent at  $c = 0$  gives  $K_v$ .

The reciprocal of the intrinsic viscosity is often used to represent the overlap concentration of a given polymer:  $c^* = 1/[\eta]$  (Eq. 1.110). It means that we can expect the polymer solution at  $c^*$  to be about twice as viscous as the pure solvent.

### 3.3.2 Measurement of Viscosity

Automated viscometers are commercially available. To measure the viscosity of liquids in the centipoise range, it is, however, more common to use a capillary flow viscometer, unless the measurement is routinely conducted. This classical method is inexpensive, yet can measure the viscosity with a sufficient accuracy.

Figure 3.33 illustrates an **Ubbelohde viscometer**, an improved version of an Ostwald viscometer. The main part on the left has a straight section of capillary and a large cavity above the section. It is imperative that the capillary be straight and its cross section be uniform. Markers are inscribed above and below the cavity. A reservoir is on the bottom of the right side. A fluid is poured into the reservoir and drawn into the cavity by suction. The upper level of the fluid must be raised above the top marker, and the lower level of the fluid must be below the lower end of the capillary. The capillary must be filled with the fluid. The viscometer is held vertically. The suction is then released. As the fluid flows down, the upper level of the fluid passes the top mark and eventually the lower mark as well. The time between these two events, called an efflux time, is recorded. Measurement is carried out in a temperature-controlled bath.

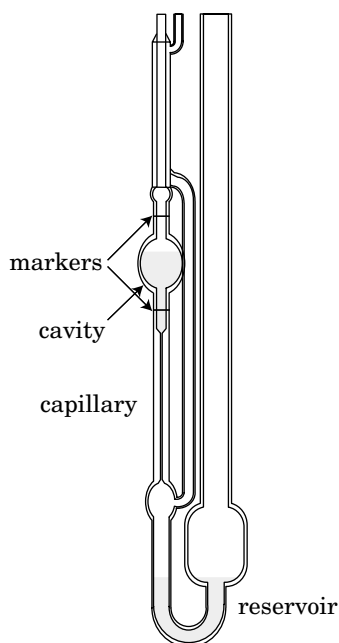


**Figure 3.33.** Ubbelohde viscometer. The efflux time between the time when the liquid level crosses the upper marker and the time when it crosses the lower marker is measured.

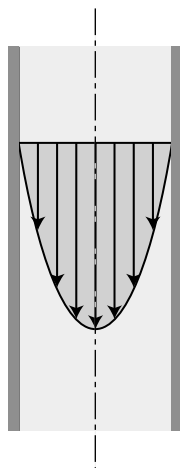


**Figure 3.34.** Cross section of the flow in the capillary. The flow velocity is parallel to the center line of the capillary. Velocity field is parabolic.

The measurement is based on the capillary flow. If the flow is slow and therefore laminar, the velocity profile in the capillary is of a parabolic cone. The velocity maximizes at the center line and declines to zero toward the wall (Fig. 3.34). The **Poiseuille law** holds for the viscosity of the fluid and the pressure drop  $\Delta P$  along the length  $l$  of the capillary (Fig. 3.35):

$$\eta = \frac{\pi r^4 t \Delta P}{8Vl} \quad \text{Poiseuille flow} \quad (3.100)$$

where  $r$  is the radius of the capillary and  $V$  is the volume of the fluid that flows in time  $t$ . In the viscometer in Figure 3.33,  $V$  is the volume of the cavity between the two markers.

The pressure difference can be generated by a liquid pump, but, in the capillary viscometer in the vertical position, it is the gravity that causes  $\Delta P$ , which is given by

$$\Delta P = \rho_{\text{liq}} g l \quad (3.101)$$

where  $\rho_{\text{liq}}$  is the density of the liquid, and  $g$  is the acceleration by the gravity. Equations 3.100 and 3.101 give the kinematic viscosity  $\nu_{\text{kin}}$  defined as  $\nu_{\text{kin}} \equiv \eta / \rho_{\text{liq}}$ :

$$\nu_{\text{kin}} \equiv \frac{\eta}{\rho_{\text{liq}}} = \frac{\pi r^4 g}{8V} t \quad (3.102)$$

Note that  $\pi r^4 g / (8V)$  is a constant for a given viscometer. The constant can be determined by using a fluid of a known kinematic viscosity. Once calibrated, the



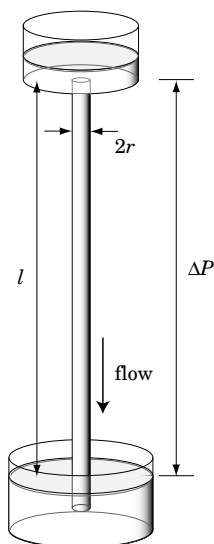


**Figure 3.35.** Flow in a vertical capillary. The pressure drop  $\Delta P$  over the length  $l$  of the capillary by the gravity causes the flow.

kinematic viscosity can be measured for any fluid from the measurement of the flow time. Together with the density, the viscosity of the fluid can be determined. Alternatively, we can use the formula of

$$\frac{\eta_1}{\eta_2} = \frac{\rho_1 t_1}{\rho_2 t_2} \quad (3.103)$$

to obtain the viscosity  $\eta_1$  of a solution (density  $\rho_1$ ) from the measurement of the efflux time  $t_1$ , if the efflux time  $t_2$  of a liquid with a known viscosity  $\eta_2$  and density  $\rho_2$  is measured for the same viscometer. The density of the solution at a given concentration can be estimated from the densities of the solvent and the polymer by assuming additiveness of the volume.

If the fluid is too viscous, the elution takes too long. If it is too fluid, the flow will be too fast, causing a nonlaminar flow. A given viscometer can be used for a finite range of viscosity. To allow for the viscosity measurement of fluids in a wide range of viscosity, Ubbelohde viscometers are available in different radii of the capillary.

### 3.3.3 Intrinsic Viscosity

The intrinsic viscosity  $[\eta]$  is a quantity characteristic of a polymer. It represents an increase in the solution viscosity when the concentration is raised to a certain level. As expected, a polymer molecule with a greater dimension has a larger  $[\eta]$ .

**Table 3.2 Mark-Houwink-Sakurada Exponents**

Conformation	$\alpha$
Linear flexible (theta solvent)	0.5
Linear flexible (good solvent)	0.7–0.8
Rigid	>1

Experimentally, it is expressed by **Mark-Houwink-Sakurada equation**:

$$[\eta] = K_M(M/(\text{g/mol}))^\alpha \quad \text{Mark-Houwink-Sakurada equation} \quad (3.104)$$

where  $K_M$  is a constant of the unit of L/g, and  $\alpha$  is called a **Mark-Houwink-Sakurada exponent**. Note that  $K_M$  and  $\alpha$  are different from polymer to polymer and can depend on the solvent as well.

The classical method to determine  $K_M$  and  $\alpha$  of a given polymer is as follows. First, prepare fractions of different molecular weights either by synthesis or by fractionation. Next, make dilute solutions of different concentrations for each fraction. Measure the viscosity of each solution, plot the reduced viscosity as a function of polymer concentration, and estimate  $[\eta]$  for each fraction. Plot  $[\eta]$  as a function of the molecular weight in a double logarithmic scale. This method has been extensively used to characterize polymer samples because the exponent  $\alpha$  provides a measure of the chain rigidity. Values of  $\alpha$  are listed in Table 3.2 for some typical shapes and conformations of the polymer. The value of  $\alpha$  is around 0.7–0.8 for flexible chains in the good solvent and exceeds 1 for rigid chains. In the theta solvent, the flexible chain has  $\alpha = 0.5$ .

Apparently,  $\alpha$  is greater for a more extended conformation. It is reasonable because a polymer molecule with a greater dimension for a given contour length will experience a greater friction to move in the solvent. We will obtain the formulas of  $[\eta]$  for linear flexible chains in the theta solvent and the good solvent in the next section.

SEC equipped with a viscosity detector and a light-scattering detector in tandem with a concentration detector (triple detector SEC) has been recently and increasingly used to obtain the Mark-Houwink-Sakurada plot. Figure 3.36 illustrates the scheme. The advantage is obvious. What is needed for the plot is only one polydisperse fraction of the polymer. As the polymer is separated by the SEC columns according to its dimension, the eluent containing the polymer is immediately led to the detectors in nearly simultaneous measurement of the solution viscosity, the concentration, the molecular weight, and the radius of gyration. Because the concentration is sufficiently low, the second- and higher-order terms are negligible in Eq. 3.96. Then, the ratio of the viscosity of the eluent to that of the pure solvent gives  $[\eta]$  with the information of the concentration to be obtained in the concentration detector. Figure 3.37 shows an example of such a measurement.<sup>35</sup> The samples were fractions of poly(vinyl *neo*-decanoate) prepared in radical polymerization and

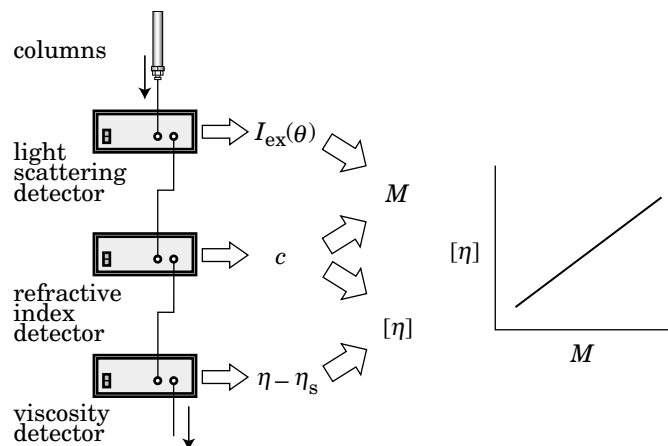


**Figure 3.36.** Size exclusion chromatography system with an on-line viscometer and a light-scattering detector allows to create the Mark-Houwink-Sakurada plot without fractionating the polymer somewhere else. The concentration is detected by a refractive index detector or an ultraviolet absorption detector.

pulsed laser polymerization. The mobile phase was tetrahydrofuran. The slope  $\alpha$  is 0.70 for most of the data, indicating a flexible chain conformation.

### 3.3.4 Flow Field

In Section 3.3.1, an example of flow fields was shown. We consider a flow  $\mathbf{v}$  at  $\mathbf{r}$  given as

$$\mathbf{v} = \kappa \mathbf{r} \tag{3.105}$$

where  $\kappa$  is the velocity gradient tensor defined as

$$\kappa_{\alpha\beta} = \frac{\partial v_\alpha}{\partial r_\beta} \quad (\alpha, \beta = x, y, z) \tag{3.106}$$

Here,  $r_x = x$ , for instance. In the example in Section 3.3.1, the flow field was a **shear flow** in the  $x$  direction (Fig. 3.38a). Then,  $\kappa_{xy} = \kappa$  is the only nonzero element in  $\kappa$ :

$$\kappa = \begin{bmatrix} 0 & \kappa & 0 \\ 0 & 0 & 0 \\ 0 & 0 & 0 \end{bmatrix} \quad \text{shear flow} \tag{3.107}$$

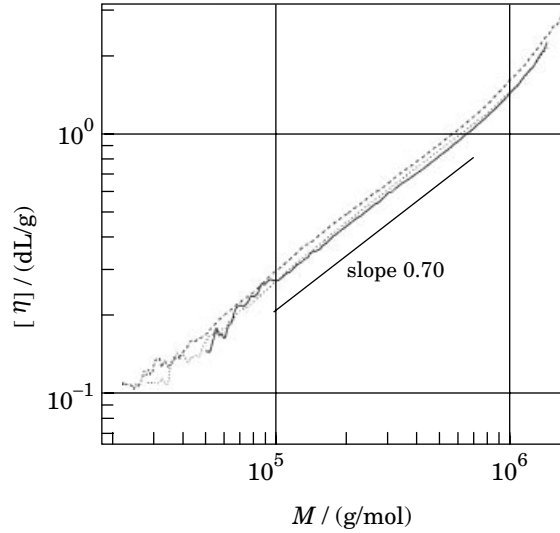


**Figure 3.37.** Example of the Mark-Houwink-Sakurada plot obtained in size exclusion chromatography. The sample is poly(vinyl *neo*-decanoate) in tetrahydrofuran. The data are along the slope of 0.70, indicating that the polymer is a flexible chain. (From Ref. 35.)

where the velocity gradient  $\kappa$  is also called a **shear rate**. The flow field generated by this  $\kappa$  is

$$\mathbf{v} = \begin{bmatrix} \kappa y \\ 0 \\ 0 \end{bmatrix} \quad \text{shear flow} \quad (3.108)$$

It is convenient to express  $[\eta]$  in terms of the shear stress. In the shear flow, the shear stress changes from  $\sigma_{yx} = \eta_s \kappa$  for the pure solvent to  $\sigma_{yx} + \Delta\sigma_{yx} = \eta \kappa$  for the solution of concentration  $c$  ( $c \ll c^*$ ). Then, from Eq. 3.97,

$$[\eta] = \frac{\Delta\sigma_{yx}}{\kappa c \eta_s} = \frac{\Delta\sigma_{xy}}{\kappa c \eta_s} \quad (3.109)$$

When  $\Delta\sigma_{yx}$  is calculated up to the linear term of  $\kappa$ , this equation gives  $\kappa$ -independent intrinsic viscosity. The latter is called a **zero-shear viscosity**.

Another flow field often used in theories and experiments is an **elongational flow** (Fig. 3.38b). Its  $\kappa$  is given by

$$\kappa = \begin{bmatrix} -\dot{\epsilon}/2 & 0 & 0 \\ 0 & -\dot{\epsilon}/2 & 0 \\ 0 & 0 & \dot{\epsilon} \end{bmatrix} \quad \text{elongational flow} \quad (3.110)$$

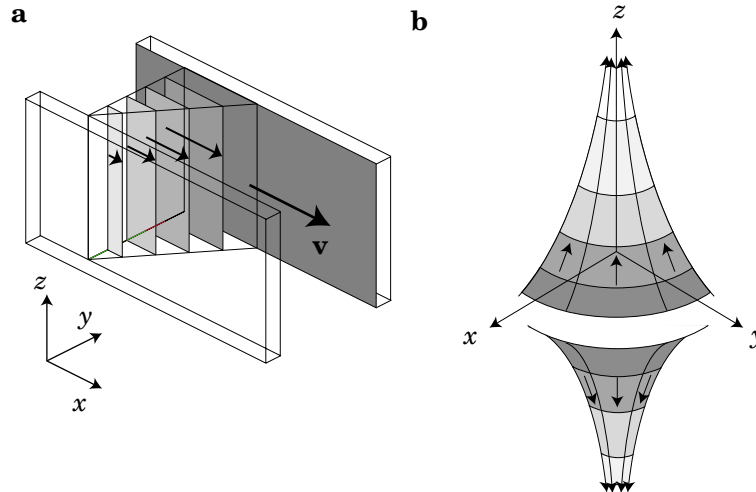


**Figure 3.38.** Typical flow fields. a: Shear flow. b: Elongational flow.

where  $\dot{\epsilon}$  is called the strain rate. The flow field generated by this  $\kappa$  is

$$\mathbf{v} = \begin{bmatrix} -(\dot{\epsilon}/2)x \\ -(\dot{\epsilon}/2)y \\ \dot{\epsilon}z \end{bmatrix} \text{ elongational flow} \quad (3.111)$$

The two velocity fields satisfy the incompressibility requirement:

$$\text{div } \mathbf{v} = 0 \quad (3.112)$$

### 3.3.5 PROBLEMS

**Problem 3.18:** It is not easy to place the viscometer in the perfectly vertical position. Evaluate the error in the estimate of  $\eta$  when the viscometer is at angle  $\theta \ll 1$  from the vertical.

**Solution 3.18:** The pressure difference  $\Delta P$  is smaller. It is now  $\rho_{\text{liq}} g l \cos \theta$ . Then, Eq. 3.102 changes to

$$v_{\text{kin}} = \frac{\pi r^4 g \cos \theta}{8V} t$$

When  $\theta \ll 1$ ,  $\cos \theta \cong 1 - \theta^2/2$ . The relative error in  $v_{\text{kin}}$  is  $\sim \theta^2/2$ .

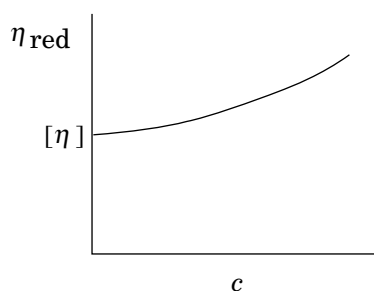
**Problem 3.19:** Measurement of the solution viscosity  $\eta$  at several different concentrations gives information on the state of the polymer chains in solution.

Answer the following questions for linear flexible polymer chains that show  $[\eta] \propto M^{0.8}$  when they are molecularly dispersed.

- (1) Suppose two polymer chains form an aggregate at low concentrations in a given solvent and behave as if they were a single chain of twice the molecular weight. How does this aggregate change  $[\eta]$ ?
- (2) Suppose the polymer chains are molecularly dispersed in the low concentration limit, but tend to form an aggregate of several chains with an increasing concentration. We assume that each aggregate behaves as if it were a single chain that has a molecular weight equal to the total molecular weight of the aggregate. Sketch a plot of  $\eta_{\text{red}}$  as a function of  $c$ .

**Solution 3.19:**

- (1) When molecularly dispersed, the intrinsic viscosity is  $[\eta]_{\text{true}} = K_M M_1^{0.8}$ , where  $M_1$  is the molecular weight of the polymer chain. When dimers (aggregates of two chains) are formed, the apparent intrinsic viscosity changes to  $[\eta]_{\text{app}} = K_M (2M_1)^{0.8} = 2^{0.8} K_M M_1^{0.8} \cong 1.74 \times [\eta]_{\text{true}}$ .
- (2) When  $n$ -mers are formed, the apparent intrinsic viscosity changes to  $[\eta]_{\text{app}} = K_M (nM_1)^{0.8} = n^{0.8} [\eta]_{\text{true}}$ . The reduced viscosity is therefore,  $\eta_{\text{red}} \cong n^{0.8} [\eta]_{\text{true}}$ . With an increasing  $c$ ,  $n$  increases. Then,  $\eta_{\text{red}}$  increases. The plot is similar to the curve for  $K_v > 0$  in Fig. 3.32.



**Problem 3.20:** A solution of a polydisperse polymer has component  $i$  dissolved at concentration  $c_i$ . The intrinsic viscosity of component  $i$  is given by  $[\eta]_i$ .

- (1) What is  $[\eta]$  of the polydisperse polymer?
- (2) Each component follows the Mark-Houwink-Sakurada equation:  $[\eta]_i = K_M M_i^\alpha$ . What is the molecular weight  $M_v$  estimated by assuming that the same equation applies to the polydisperse polymer, i.e.,  $[\eta] = K_M M_v^\sigma$ . What is the relationship of this  $M_v$  to  $M_n$  and  $M_w$ ?

**Solution 3.20 (1):** For the solution of the polydisperse polymer,

$$\eta = \eta_s \left( 1 + \sum_i c_i [\eta]_i + \dots \right)$$

which we equate to  $\eta = \eta_s(1 + c[\eta] + \dots)$ . Then,  $\sum_i c_i [\eta]_i = c[\eta] = [\eta] \sum_i c_i$

Thus,  $[\eta] = \frac{\sum_i c_i [\eta]_i}{\sum_i c_i}$

**Solution 3.20 (2):**  $K_M M_v^\alpha = \frac{\sum_i c_i K_M M_i^\alpha}{\sum_i c_i}$  Then,  $M_v = \left( \frac{\sum_i c_i M_i^\alpha}{\sum_i c_i} \right)^{1/\alpha}$

This  $M_v$  is another average molecular weight. For polymers with  $0 < \alpha < 1$ ,  $M_n < M_v < M_w$ .

### 3.4 NORMAL MODES

#### 3.4.1 Rouse Model

**3.4.1.1 Model for Chain Dynamics** In Sections 1.2 and 1.3, we learned about the conformation of the ideal chain and obtained the probability distribution of the conformation. The distribution tells how many chains in the system have a certain conformation at a given time. Each chain is moving and changing its conformation all the time. The probability distribution also gives the distribution of the period in which a given chain takes each conformation (ergodicity).

In this section, we learn how fast the conformation changes. To simplify the seemingly complicated motions of the monomers, we employ the bead-spring model of  $N$  beads with a spring force constant of  $k_{sp} = 3k_B T / b^2$ . Figure 3.39 illustrates how the beads move to change the lengths and the orientations of the springs, thereby reshaping the whole chain.

The **Rouse model**<sup>36</sup> is the simplest version of the bead-spring model that can treat the chain dynamics. The model assumes that the beads have no excluded volume (they are essentially a point) and that there are no hydrodynamic interactions

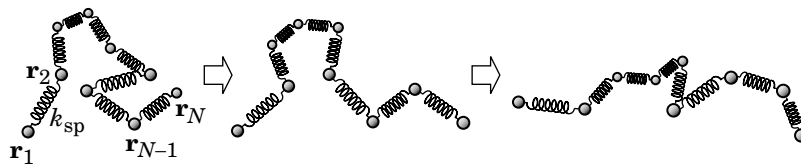


**Figure 3.39.** A polymer chain of a bead-spring model changes its conformation with time.

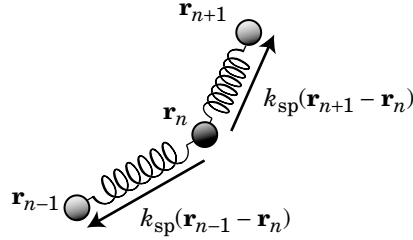


**Figure 3.40.** Spring force on the  $n$ th bead. It is pulled by the two springs.

between the beads. The model was subsequently refined to account for these effects. Unlike the later models, the Rouse model does not provide correct expressions for the center-of-mass diffusion coefficient or the relaxation time for the conformation change. We will learn the Rouse model here in detail, because the way a complicated motion of connected beads is simplified into different modes is noteworthy and used in the later models with modifications. Furthermore, the Rouse-like modes can be observed in solutions at high concentrations and in melts where the hydrodynamic interactions are shielded.

**3.4.1.2 Equation of Motion** The elastic forces on the  $n$ th bead ( $n = 2, 3, \dots, N - 1$ ) are exerted by the two springs that connect the adjacent beads, as illustrated in Figure 3.40. The spring between the  $(n - 1)$ th and the  $n$ th beads pulls the bead with the force of  $k(\mathbf{r}_{n-1} - \mathbf{r}_n)$ . Likewise, the other spring pulls the bead with  $k(\mathbf{r}_{n+1} - \mathbf{r}_n)$ . In addition, the  $n$ th bead receives a random force  $\mathbf{f}_n$  that changes with time  $t$  from nearby solvent molecules just as a single particle receives the random force (Fig. 3.20). Thus, the equation of motion for the  $n$ th bead is given as

$$\zeta \frac{d\mathbf{r}_n}{dt} = k_{sp}(\mathbf{r}_{n-1} - \mathbf{r}_n) + k_{sp}(\mathbf{r}_{n+1} - \mathbf{r}_n) + \mathbf{f}_n(t) \quad (n = 2, 3, \dots, N-1) \quad (3.113)$$

where  $\zeta$  is the friction coefficient of each bead in the solvent. The mass term (mass  $\times$  acceleration) is missing in this equation because the term is negligible on the time scales of our concern ( $\mu\text{s}$  to  $\text{s}$ ; the acceleration term is important at high frequencies such as vibrational motion). The motion of the bead is overdamped. A special care is necessary for the terminal beads ( $n = 1$  and  $N$ ). Their equations of motion are

$$\zeta \frac{d\mathbf{r}_1}{dt} = k_{sp}(\mathbf{r}_2 - \mathbf{r}_1) + \mathbf{f}_1(t), \quad \zeta \frac{d\mathbf{r}_N}{dt} = k_{sp}(\mathbf{r}_{N-1} - \mathbf{r}_N) + \mathbf{f}_N(t) \quad (3.114)$$

respectively. By introducing  $\mathbf{r}_0 = \mathbf{r}_1$  and  $\mathbf{r}_{N+1} = \mathbf{r}_N$ , the above two equations become a part of the general equation:

$$\zeta \frac{d\mathbf{r}_n}{dt} = k_{sp}(\mathbf{r}_{n-1} + \mathbf{r}_{n+1} - 2\mathbf{r}_n) + \mathbf{f}_n(t) \quad (n = 1, 2, \dots, N) \quad \text{bead-spring model} \quad (3.115)$$



The nature of the random force is the same as in Eqs. 3.63 and 3.71:

$$\langle \mathbf{f}_n(t) \rangle = 0 \quad (3.116)$$

$$\langle \mathbf{f}_n(t) \cdot \mathbf{f}_m(t') \rangle = 6\zeta k_B T \delta(t - t') \delta_{nm} \quad (3.117)$$

There is no relationship between the forces on difference beads ( $\delta_{nm} = 1$  only when  $n = m$ ). The random forces are needed to keep the chain in shape. Without the random forces, the beads would move until all of them collapse onto a single point and the elastic forces disappear.

### 3.4.2 Normal Coordinates

**3.4.2.1 Definition** We now need to solve the  $N$  equations in Eq. 3.115 simultaneously. The change in  $\mathbf{r}_n$  depends on  $\mathbf{r}_{n-1}$  and  $\mathbf{r}_{n+1}$ , and the change in  $\mathbf{r}_{n-1}$  depends on  $\mathbf{r}_{n-2}$  and  $\mathbf{r}_n$ , and so forth. Motions of different beads are related to each other. Solving these equations appears difficult, but use of the normal coordinates facilitates it. The  $i$ th **normal coordinate**  $\mathbf{q}_i(t)$  ( $i = 0, 1, \dots$ ) is defined as a linear combination of  $\mathbf{r}_n(t)$ :

$$\mathbf{q}_i(t) = \frac{1}{N} \sum_{n=1}^N \cos \frac{in\pi}{N} \mathbf{r}_n(t) \quad \text{normal coordinate} \quad (3.118)$$

The 0th **normal mode** is essentially the center-of-mass position,  $\mathbf{r}_G(t)$ , of the  $N$  beads:

$$\mathbf{q}_0(t) = \frac{1}{N} \sum_{n=1}^N \mathbf{r}_n(t) = \mathbf{r}_G(t) \quad (3.119)$$

Thus  $\mathbf{q}_0(t)$  represents the global motion of the bead-spring chain. All the other normal modes represent internal motions. The first and second modes are

$$\begin{aligned} \mathbf{q}_1(t) &= \frac{1}{N} \sum_{n=1}^N \cos \frac{n\pi}{N} \mathbf{r}_n(t) \\ &= \frac{1}{N} \left[ \cos \frac{\pi}{N} \mathbf{r}_1(t) + \cos \frac{2\pi}{N} \mathbf{r}_2(t) + \dots + \cos \pi \mathbf{r}_N(t) \right] \end{aligned} \quad (3.120)$$

$$\begin{aligned} \mathbf{q}_2(t) &= \frac{1}{N} \sum_{n=1}^N \cos \frac{2n\pi}{N} \mathbf{r}_n(t) \\ &= \frac{1}{N} \left[ \cos \frac{2\pi}{N} \mathbf{r}_1(t) + \cos \frac{4\pi}{N} \mathbf{r}_2(t) + \dots + \cos(2\pi) \mathbf{r}_N(t) \right] \end{aligned} \quad (3.121)$$

The superposition coefficient  $\cos(in\pi/N)$  is plotted in Figure 3.41 as a function of  $n$  for  $N = 100$  and  $i = 1, 2, \dots, 8$ . To be precise,  $\cos(in\pi/N)$  is given for integral

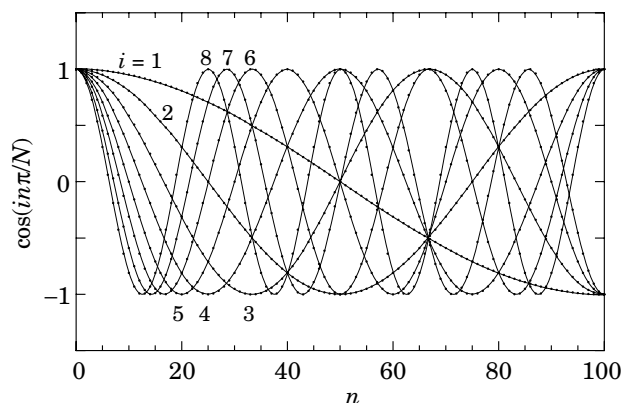


**Figure 3.41.** Coefficient  $\cos(in\pi/N)$  plotted as a function of  $n$  for  $N = 100$ . Curves for  $i = 1$  to 8 are shown.

values of  $n$  only (small dots on the curves). Figure 3.42 illustrates the sign of  $\cos(in\pi/N)$  along the contour of the Rouse chain for  $i = 0$  to 6. The zeroth mode is the mean of all  $\mathbf{r}_n$ . In the first mode, the superposition coefficient changes its sign at the midpoint along the chain contour. In the second mode, the coefficient is positive in the first and last quadrants, and negative in the two middle quadrants. As  $i$  increases, the sign alteration becomes more frequent. It is possible to give meanings to these normal modes.

The meaning of the first mode, for instance, may become clearer by considering another superposition coefficient:  $+2$  for positive  $\cos(in\pi/N)$  and  $-2$  for negative  $\cos(in\pi/N)$ . Then,  $\mathbf{q}_1$  is the vector that connects the centroid of the beads in the first half of the chain and the centroid of the beads in the second half of the chain (see Fig. 3.43a). As the chain makes an overall tumbling motion,  $\mathbf{q}_1$  changes its

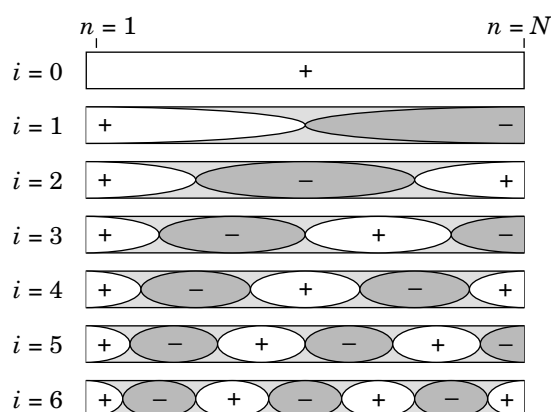


**Figure 3.42.** Sign of the coefficient  $\cos(in\pi/N)$  for  $i = 0$  to 6.

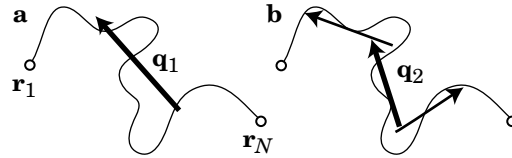


**Figure 3.43.** Schematic of the first normal mode  $\mathbf{q}_1$  (a) and the second normal mode  $\mathbf{q}_2$  (b) for a chain conformation given.

orientation. Therefore, we can associate the change in  $\mathbf{q}_1$  with rotation of the chain as a whole, although  $\mathbf{q}_1$  changes its length by rearrangement of the beads and thus  $\mathbf{q}_1$  can change its sign without overall rotation. With the actual coefficient,  $\cos(in\pi/N)$ , which changes gradually from 1 to  $-1$ ,  $\mathbf{q}_1$  still carries the characteristics that it represents the overall chain orientation.

The next mode  $\mathbf{q}_2$  can be viewed as the sum of the two vectors, one drawn from the second quadrant to the first quadrant and the other one drawn from the third quadrant to the fourth quadrant (Fig. 3.43b). Thus  $\mathbf{q}_2$  is more sensitive to the local details of the conformation compared with  $\mathbf{q}_1$ . As we move to  $\mathbf{q}_3, \mathbf{q}_4, \dots$ , the mode becomes increasingly sensitive to the local details and less sensitive to the overall conformation. The last mode  $\mathbf{q}_N$ , defined as

$$\mathbf{q}_N(t) = \frac{1}{N} \sum_{n=1}^N \cos(n\pi) \mathbf{r}_n(t) = \frac{1}{N} [-\mathbf{r}_1(t) + \mathbf{r}_2(t) - \dots + (-1)^N \mathbf{r}_N(t)] \quad (3.122)$$

represents the displacement of even-numbered beads relative to the odd-numbered beads divided by  $N$ .

An example of  $\mathbf{q}_1, \mathbf{q}_2, \dots$  is shown in Figure 3.44 for a realistic conformation in two dimensions ( $N = 32$ ). We can see that the magnitude of the normal mode tends

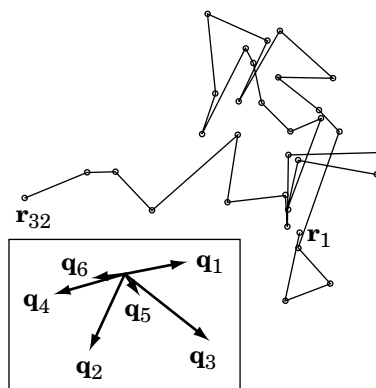


**Figure 3.44.** Example of a bead-spring model in two dimensions.  $N = 32$ . The first six normal modes  $\mathbf{q}_1$  through  $\mathbf{q}_6$  are shown in the inset by vectors (zoomed by a factor of two for easy observation).

to decrease with an increasing mode number  $i$ . We expect that  $\mathbf{q}_i(t)$  of a higher mode number to change more quickly with time because the mode picks up more localized motions, which do not have to wait for the whole chain to rearrange.

**3.4.2.2 Inverse Transformation** The normal coordinate is given as a linear combination of the bead positions. Conversely, we can express  $\mathbf{r}_n$  as a linear combination of  $\mathbf{q}_i$  ( $i = 1, 2, \dots, N$ ). From Eq. 3.118, we find

$$\begin{aligned}
& 2 \sum_{i=1}^{N-1} \cos \frac{in\pi}{N} \mathbf{q}_i + \mathbf{q}_0 + (-1)^n \mathbf{q}_N \\
&= \frac{1}{N} \sum_{m=1}^N \mathbf{r}_m \left( \sum_{i=1}^{N-1} 2 \cos \frac{im\pi}{N} \cos \frac{in\pi}{N} + 1 + (-1)^{m+n} \right) \\
&= \frac{1}{N} \sum_{m=1}^N \mathbf{r}_m \left[ \left( \sum_{i=1}^{N-1} \cos \frac{i(m+n)\pi}{N} + \frac{1}{2} + \frac{1}{2}(-1)^{m+n} \right) \right. \\
&\quad \left. + \left( \sum_{i=1}^{N-1} \cos \frac{i(m-n)\pi}{N} + \frac{1}{2} + \frac{1}{2}(-1)^{m-n} \right) \right]
\end{aligned} \tag{3.123}$$

Use of the identity

$$\sum_{i=1}^{N-1} \cos \frac{ik\pi}{N} + \frac{1}{2} + \frac{1}{2}(-1)^k = \begin{cases} N & (k = 0, \pm 2N, \pm 4N, \dots) \\ 0 & (\text{otherwise}) \end{cases} \tag{3.124}$$

leads Eq. 3.123 to

$$\boxed{\mathbf{r}_n(t) = 2 \sum_{i=1}^{N-1} \cos \frac{in\pi}{N} \mathbf{q}_i(t) + \mathbf{q}_0(t) + (-1)^n \mathbf{q}_N(t) \quad (n = 1, 2, \dots, N-1)} \tag{3.125}$$

Note that the superposition coefficient for  $i = 0$  and  $N$  is a half of the others. For  $n = N$ ,  $\mathbf{r}_N(t)$  is a half of the one given by this equation. We need to treat  $\mathbf{r}_N$  separately, because the superposition coefficient,  $\cos(in\pi/N)$  in Eq. 3.118 is not symmetric. Fortunately, the effect of the separate treatment is negligible when  $N \gg 1$ . In the following, we neglect this effect.

### 3.4.3 Equation of Motion for the Normal Coordinates in the Rouse Model

**3.4.3.1 Equation of Motion** The equation of motion for  $\mathbf{q}_i$  is obtained from Eqs. 3.115 and 3.118 as

$$\begin{aligned}
\zeta \frac{d\mathbf{q}_i}{dt} &= \frac{1}{N} \sum_{n=1}^N \cos \frac{in\pi}{N} \zeta \frac{d\mathbf{r}_n}{dt} = \frac{1}{N} \sum_{n=1}^N \cos \frac{in\pi}{N} \mathbf{f}_n \\
&\quad + k_{sp} \frac{1}{N} \sum_{n=1}^N \cos \frac{in\pi}{N} (\mathbf{r}_{n-1} + \mathbf{r}_{n+1} - 2\mathbf{r}_n)
\end{aligned} \tag{3.126}$$

In the second term,

$$\begin{aligned}
 \sum_{n=1}^N \cos \frac{in\pi}{N} (\mathbf{r}_{n-1} + \mathbf{r}_{n+1} - 2\mathbf{r}_n) &= \sum_{n=0}^{N-1} \cos \frac{i(n+1)\pi}{N} \mathbf{r}_n \\
 + \sum_{n=2}^{N+1} \cos \frac{i(n-1)\pi}{N} \mathbf{r}_n - 2 \sum_{n=1}^N \cos \frac{in\pi}{N} \mathbf{r}_n & \quad (3.127) \\
 \cong \sum_{n=1}^N \left( \cos \frac{i(n+1)\pi}{N} + \cos \frac{i(n-1)\pi}{N} - 2 \cos \frac{in\pi}{N} \right) \mathbf{r}_n
 \end{aligned}$$

Since

$$\begin{aligned}
 \cos \frac{i(n+1)\pi}{N} + \cos \frac{i(n-1)\pi}{N} - 2 \cos \frac{in\pi}{N} & \\
 = 2 \cos \frac{in\pi}{N} \left( \cos \frac{i\pi}{N} - 1 \right) \cong - \left( \frac{i\pi}{N} \right)^2 \cos \frac{in\pi}{N} & \quad (3.128)
 \end{aligned}$$

Eq. 3.126 is rewritten to

$$\zeta \frac{d\mathbf{q}_i}{dt} = -k_{\text{sp}} \left( \frac{i\pi}{N} \right)^2 \mathbf{q}_i + \frac{1}{N} \sum_{n=1}^N \cos \frac{in\pi}{N} \mathbf{f}_n \quad (3.129)$$

For later convenience, we introduce the friction coefficient  $\zeta_i$  for the  $i$ th mode by

$$\zeta_i = \begin{cases} N\zeta & (i = 0) \\ 2N\zeta & (i \neq 0) \end{cases} \quad \text{Rouse model} \quad (3.130)$$

and rewrite Eq. 3.129 to

$$\boxed{\zeta_i \frac{d\mathbf{q}_i}{dt} = -k_i \mathbf{q}_i + \mathbf{g}_i \quad (i = 0, 1, 2, \dots) \quad \text{normal coordinate}} \quad (3.131)$$

Because  $k_{\text{sp}} = 3k_{\text{B}}T/b^2$ , the force constant  $k_i$  of the  $i$ th mode is given as

$$k_i = k_{\text{sp}} \frac{\zeta_i}{\zeta} \left( \frac{i\pi}{N} \right)^2 = \frac{6\pi^2 k_{\text{B}}T}{Nb^2} i^2 \quad \text{Rouse model} \quad (3.132)$$

The random force  $\mathbf{g}_i$  for the  $i$ th mode is defined as

$$\mathbf{g}_i(t) = \frac{\zeta_i}{\zeta} \frac{1}{N} \sum_{n=1}^N \cos \frac{in\pi}{N} \mathbf{f}_n(t) \quad (3.133)$$

It is now apparent that the equation of motion for  $\mathbf{q}_i$  does not depend on other  $\mathbf{q}_j$  ( $j \neq i$ ). Each mode is independent (decoupled). With the relaxation time  $\tau_i$  defined as

$$\tau_i \equiv \zeta_i/k_i \quad (3.134)$$

Eq. 3.131 is further rewritten to

$$\boxed{\frac{d\mathbf{q}_i}{dt} = -\frac{1}{\tau_i} \mathbf{q}_i + \frac{1}{\zeta_i} \mathbf{g}_i \quad (i = 0, 1, \dots) \quad \text{normal coordinate}} \quad (3.135)$$

For the 0th mode,  $1/\tau_0 = 0$ . Other  $\tau_i$  are finite:

$$\boxed{\tau_i = \frac{\zeta N^2 b^2}{3\pi^2 k_B T} \frac{1}{i^2} \quad (i = 1, 2, \dots) \quad \text{Rouse model}} \quad (3.136)$$

The relaxation time of the normal mode decreases with  $i$  as  $\tau_i = \tau_1/i^2$  in the Rouse model. The higher-order mode relaxes more quickly.

**3.4.3.2 Correlation of Random Force** Statistical properties of the random force  $\mathbf{g}_i$  are similar to the counterparts of  $\mathbf{f}_n$ :

$$\langle \mathbf{g}_i(t) \rangle = 0 \quad (3.137)$$

$$\langle \mathbf{g}_i(t) \cdot \mathbf{g}_j(t') \rangle = 6\zeta_i k_B T \delta(t - t') \delta_{ij} \quad (3.138)$$

The first part is obvious. The second part can be proved as follows:

$$\begin{aligned} \langle \mathbf{g}_i(t) \cdot \mathbf{g}_j(t') \rangle &= \left( \frac{\zeta_i}{\zeta} \right)^2 \frac{1}{N^2} \sum_{n=1}^N \cos \frac{in\pi}{N} \sum_{m=1}^N \cos \frac{jm\pi}{N} \langle \mathbf{f}_n(t) \cdot \mathbf{f}_m(t') \rangle \\ &= \left( \frac{\zeta_i}{\zeta} \right)^2 \frac{1}{N^2} \sum_{n=1}^N \cos \frac{in\pi}{N} \cos \frac{jn\pi}{N} 6\zeta k_B T \delta(t - t') \\ &\equiv \left( \frac{\zeta_i}{\zeta} \right)^2 6\zeta k_B T \delta(t - t') \frac{1}{N^2} \int_0^N \cos \frac{in\pi}{N} \cos \frac{jn\pi}{N} dn \end{aligned} \quad (3.139)$$

Because

$$\frac{1}{N^2} \int_0^N \cos \frac{in\pi}{N} \cos \frac{jn\pi}{N} dn = \begin{cases} 1/N & (i = j = 0) \\ 1/(2N) & (i = j \neq 0) \\ 0 & (i \neq j) \end{cases} = \frac{\zeta}{\zeta_i} \delta_{ij} \quad (3.140)$$

we obtain Eq. 3.138.

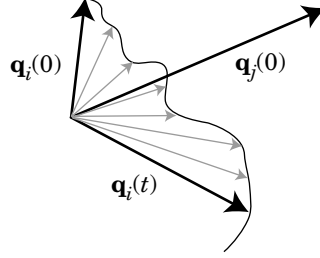


**Figure 3.45.** Correlation between  $\mathbf{q}_i(t)$  and  $\mathbf{q}_i(0)$ .  $\mathbf{q}_i(t)$  changes with time.

**3.4.3.3 Formal Solution** Equation 3.135 is solved as

$$\mathbf{q}_i(t) = \zeta_i^{-1} \int_{-\infty}^t \mathbf{g}_i(t_1) \exp[(t_1 - t)/\tau_i] dt_1 \quad (i = 0, 1, \dots) \quad (3.141)$$

This equation includes  $i = 0$ :

$$\mathbf{q}_0(t) = \zeta_0^{-1} \int_{-\infty}^t \mathbf{g}_0(t_1) dt_1 \quad (3.142)$$

Because  $\langle \mathbf{g}_i(t) \rangle = 0$ , we find the statistical average of  $\mathbf{g}_i(t)$  is zero for all modes:

$$\langle \mathbf{q}_i(t) \rangle = 0 \quad (i = 0, 1, \dots) \quad (3.143)$$

The average of  $\mathbf{q}_i(t) \cdot \mathbf{q}_i(0)$  is not zero, as we will see in the next subsection.

Before we look at the correlation of the end-to-end vector and the center-of-mass diffusion for the Rouse model, we derive general formulas for them by using Eqs. 3.135 and 3.138 only. These equations are also valid in the modified versions of the Rouse model. The assumptions specific to the Rouse model, such as  $k_{sp} = 3k_B T/b^2$  and the neglect of the hydrodynamic interactions, show up only in the expressions for the parameters  $\zeta_i$ ,  $k_i$ , and  $\tau_i$ .

### 3.4.4 Results of the Normal Coordinates

**3.4.4.1 Correlation of  $\mathbf{q}_i(t)$**  Although the average is always zero (Eq. 3.143), each  $\mathbf{q}_i(t)$  is in general nonzero and changes with time (Fig. 3.45). Here, we consider how  $\mathbf{q}_i(t)$  is related to  $\mathbf{q}_j(0)$  ( $i, j \neq 0$ ). When  $i = j$ ,  $\langle \mathbf{q}_i(t) \cdot \mathbf{q}_i(0) \rangle$  is the autocorrelation. When  $i \neq j$ ,  $\langle \mathbf{q}_i(t) \cdot \mathbf{q}_j(0) \rangle$  is the cross-correlation. Because different modes are irrelevant to each other, the cross-correlation is zero. We use Eq. 3.141 to

calculate the correlation:

$$\begin{aligned}
 \langle \mathbf{q}_i(t) \cdot \mathbf{q}_j(0) \rangle &= \int_{-\infty}^t dt_1 \exp[-(t - t_1)/\tau_i] \int_{-\infty}^0 dt_2 \exp(t_2/\tau_j) \frac{1}{\zeta_i \zeta_j} \langle \mathbf{g}_i(t_1) \cdot \mathbf{g}_j(t_2) \rangle \\
 &= \int_{-\infty}^t dt_1 \exp[-(t - t_1)/\tau_i] \int_{-\infty}^0 dt_2 \exp(t_2/\tau_j) \frac{1}{\zeta_i \zeta_j} 6\zeta_i \delta_{ij} k_B T \delta(t_1 - t_2) \\
 &= 6\delta_{ij} k_B T \frac{1}{\zeta_i} \int_{-\infty}^0 dt_2 \exp[-(t - 2t_2)/\tau_i] = \frac{6\delta_{ij} k_B T}{\zeta_i} \frac{\tau_i}{2} \exp(-t/\tau_i)
 \end{aligned} \tag{3.144}$$

for  $i, j = 1, 2, \dots$  Thus

$$\langle \mathbf{q}_i(t) \cdot \mathbf{q}_j(0) \rangle = \begin{cases} 3 \frac{k_B T}{k_i} \exp(-t/\tau_i) & (i = j \neq 0) \\ 0 & (i \neq j) \end{cases} \quad \begin{array}{l} \text{correlation of} \\ \text{normal coordinates} \end{array} \tag{3.145}$$

In the second case ( $i \neq j$ ), either  $i$  or  $j$  can be zero; The internal motion is decoupled from the center-of-mass motion. Equation 3.145 indicates that the autocorrelation of  $\mathbf{q}_i(t)$  is lost exponentially with a relaxation time of  $\tau_i$ .

We can obtain the mean square amplitude of  $\mathbf{q}_i(t)$  by setting  $t$  to 0 in the above equation:

$$\langle \mathbf{q}_i^2 \rangle = \frac{3k_B T}{k_i} \quad (i = 1, 2, \dots) \quad \text{fluctuations of normal coordinate} \tag{3.146}$$

The higher-order mode has a smaller amplitude, as we will see in the Rouse and other models.

**3.4.4.2 End-to-End Vector** In place of  $\mathbf{r}_N(t) - \mathbf{r}_1(t)$ , we calculate  $\mathbf{r}_{N-1}(t) - \mathbf{r}_1(t)$  as the end-to-end vector  $\mathbf{R}(t)$  of the Rouse chain; the difference is negligible when  $N \gg 1$ . From Eq. 3.125,  $\mathbf{R}(t)$  is expressed by  $\mathbf{q}_i$  as

$$\begin{aligned}
 \mathbf{R}(t) &= 2 \sum_{i=1}^{N-1} \left( \cos \frac{i(N-1)\pi}{N} - \cos \frac{i\pi}{N} \right) \mathbf{q}_i(t) \\
 &+ ((-1)^{N-1} + 1) \mathbf{q}_N(t) \cong -4 \sum_{i:\text{odd}} \mathbf{q}_i(t)
 \end{aligned} \tag{3.147}$$

where  $\cos(i\pi/N) \cong 1$  and  $\cos[i(N-1)\pi/N] \cong (-1)^i$  for  $N \gg 1$  were used. Note that  $\mathbf{R}(t)$  is dominated by  $\mathbf{q}_i$  with a small  $i$ . As the chain conformation changes,  $\mathbf{R}(t)$  changes as well (Fig. 3.46). Its autocorrelation is calculated as

$$\langle \mathbf{R}(t) \cdot \mathbf{R}(0) \rangle \cong 16 \sum_{i:\text{odd}} \langle \mathbf{q}_i(t) \cdot \mathbf{q}_i(0) \rangle = 16 \sum_{i:\text{odd}} \langle \mathbf{q}_i^2 \rangle \exp(-t/\tau_i) \quad \text{end-to-end-vector} \tag{3.148}$$



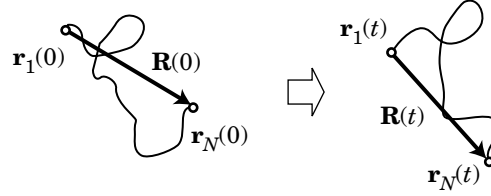


**Figure 3.46.** End-to-end vector  $\mathbf{R}(t)$  changes as the chain conformation changes.

The autocorrelation function of  $\mathbf{R}(t)$  is dominated by the first normal mode, as we will see in the Rouse and other models. Thus,  $\mathbf{R}(t)$  loses its memory approximately with a relaxation time of  $\tau_1$ :

$$\langle \mathbf{R}(t) \cdot \mathbf{R}(0) \rangle \cong \langle \mathbf{R}^2 \rangle \exp(-t/\tau_1) \quad \text{end-to-end vector} \quad (3.149)$$

Experimentally,  $\langle \mathbf{R}(t) \cdot \mathbf{R}(0) \rangle$  can be measured in dielectric relaxation spectroscopy for a polymer molecule that has a nonzero permanent dipole moment along the chain backbone. Other normal modes can also be observed.

**3.4.4.3 Center-of-Mass Motion** From Eqs. 3.119 and 3.142, the center-of-mass displacement in time  $t$  is calculated as

$$\mathbf{r}_G(t) - \mathbf{r}_G(0) = \mathbf{q}_0(t) - \mathbf{q}_0(0) = \frac{1}{\zeta_0} \int_0^t \mathbf{g}_0(t_1) dt_1 \quad (3.150)$$

The mean-square displacement is then calculated as

$$\begin{aligned} \langle [\mathbf{r}_G(t) - \mathbf{r}_G(0)]^2 \rangle &= \frac{1}{\zeta_0^2} \int_0^t dt_1 \int_0^t dt_2 \langle \mathbf{g}_0(t_1) \cdot \mathbf{g}_0(t_2) \rangle \\ &= \frac{1}{\zeta_0^2} \int_0^t dt_1 \int_0^t dt_2 6\zeta_0 k_B T \delta(t_1 - t_2) = \frac{6k_B T}{\zeta_0} \int_0^t dt_1 = 6 \frac{k_B T}{\zeta_0} t \end{aligned} \quad (3.151)$$

It is proportional to  $t$ . The center of mass of the bead-spring chain makes a diffusional motion on all time scales. From this equation, we obtain the center-of-mass diffusion coefficient  $D_G$ :

$$D_G = \frac{k_B T}{\zeta_0} \quad \text{center-of-mass diffusion} \quad (3.152)$$

The centroid motion of the bead-spring chain is identical to the motion of a particle that receives a friction of  $\zeta_0$ . The latter is also evident in Eq. 3.131 with  $i = 0$ .

**3.4.4.4 Evolution of  $\mathbf{q}_i(t)$**  In Section 3.4.4.1, we found that the autocorrelation of  $\mathbf{q}_i(t)$  with  $\mathbf{q}_i(0)$  is lost over time. We find here the transition probability for  $\mathbf{q}_i(t)$

from  $\mathbf{q}_i(0)$ . From Eq. 3.141,

$$\mathbf{q}_i(t) = \mathbf{q}_i(0) \exp(-t/\tau_i) + \zeta_i^{-1} \int_0^t \mathbf{g}_i(t_1) \exp[(t_1 - t)/\tau_i] dt_1 \quad (3.153)$$

Because  $\langle \mathbf{g}_i(t) \rangle = 0$ , the average of  $\mathbf{q}_i(t)$  for a given  $\mathbf{q}_i(0)$  decays with a time constant  $\tau_i$ :

$$\langle \mathbf{q}_i(t) \rangle_0 = \mathbf{q}_i(0) \exp(-t/\tau_i) \quad (3.154)$$

where subscript “0” denotes the average for a given  $\mathbf{q}_i(0)$ .

Now we find the variance. It is calculated as follows.

$$\begin{aligned} \langle [\mathbf{q}_i(t) - \mathbf{q}_i(0) \exp(-t/\tau_i)]^2 \rangle &= \zeta_i^{-2} \int_0^t \int_0^t dt_1 dt_2 \langle \mathbf{g}_i(t_1) \cdot \mathbf{g}_i(t_2) \rangle \exp[(t_1 + t_2 - 2t)/\tau_i] \\ &= \zeta_i^{-2} \int_0^t dt_1 \int_0^t dt_2 6\zeta_i k_B T \delta(t_1 - t_2) \exp[(t_1 + t_2 - 2t)/\tau_i] \\ &= 6\zeta_i^{-1} k_B T \int_0^t \exp[2(t_1 - t)/\tau_i] dt_1 = (3\zeta_i^{-1} k_B T \tau_i) [1 - \exp(-2t/\tau_i)] \quad (3.155) \\ &= (3k_B T/k_i) [1 - \exp(-2t/\tau_i)] \end{aligned}$$

At  $t = 0$ ,  $\langle \mathbf{q}_i(t) \rangle_0 = \mathbf{q}_i(0)$  and the variance is zero. At  $t \rightarrow \infty$ ,  $\langle \mathbf{q}_i(t) \rangle_0 = 0$  and the variance becomes equal to the square magnitude of  $\mathbf{q}_i(t)$  (see Eq. 3.146).

We have calculated the average and variance of  $\mathbf{q}_i(t)$  for a given  $\mathbf{q}_i(0)$ . It can be shown that  $\mathbf{q}_i(t)$  follows a normal distribution. Then, the transition probability  $P[\mathbf{q}_i, \mathbf{q}_i(0); t]$  for  $\mathbf{q}_i$  is given as

$$\begin{aligned} P(\mathbf{q}_i, \mathbf{q}_i(0); t) &= [(6\pi k_B T/k_i) (1 - \exp(-2t/\tau_i))]^{-3/2} \\ &\quad \times \exp \left[ -\frac{[\mathbf{q}_i - \mathbf{q}_i(0) \exp(-t/\tau_i)]^2}{(6k_B T/k_i) (1 - \exp(-2t/\tau_i))} \right] \quad (3.156) \end{aligned}$$

The probability distribution is shown for a few values of  $t/\tau_i$  in Figure 3.47. The initial sharp peak at  $\mathbf{q}_i = \mathbf{q}_i(0)$  gives way to a broader peak at  $\mathbf{q}_i = 0$ .

### 3.4.5 Results for the Rouse Model

**3.4.5.1 Correlation of the Normal Modes** Now we apply the general formulas obtained in the preceding subsection to the Rouse model. First, we study the correlation of  $\mathbf{q}_i(t)$ . It decays exponentially with a relaxation time  $\tau_i$ , given by Eq. 3.136. Figure 3.48 compares  $\langle \mathbf{q}_i(t) \cdot \mathbf{q}_i(0) \rangle$  for  $i = 1$  through 6. Each  $\langle \mathbf{q}_i(t) \cdot \mathbf{q}_i(0) \rangle$  is normalized by  $\langle \mathbf{q}_i^2 \rangle$ , the square magnitude of the first mode. The decay of  $\langle \mathbf{q}_1(t) \cdot \mathbf{q}_1(0) \rangle$  is

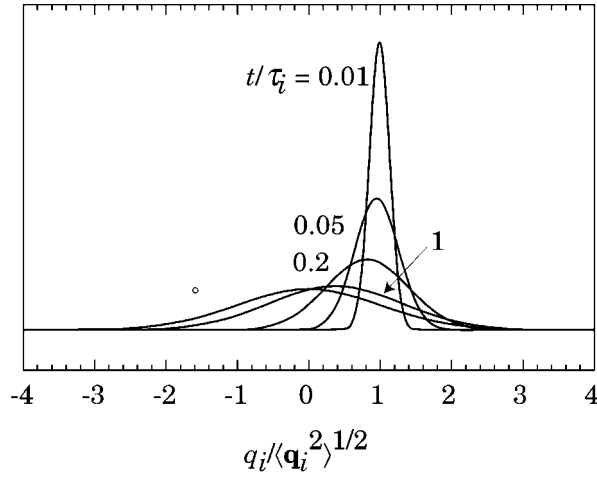


**Figure 3.47.** Transition probability  $q_i$  (one of the  $x$ ,  $y$ , and  $z$  components of  $\mathbf{q}_i$ ) for a given  $q_i(0)$ , plotted at  $t/\tau_i = 0.01, 0.05, 0.2, 1$  and  $\infty$ . This example has  $q_i(0) = \langle \mathbf{q}_i^2 \rangle^{1/2}$ .

the slowest. The second normal mode loses its memory four times as fast ( $\tau_2 = \tau_1/4$ ) and the third mode nine times as fast ( $\tau_3 = \tau_1/9$ ).

From Eqs. 3.132 and 3.146, the fluctuations of the normal coordinates are obtained as

$$\langle \mathbf{q}_i^2 \rangle = \frac{Nb^2}{2\pi^2} \frac{1}{i^2} \quad \text{Rouse model} \quad (3.157)$$

The decrease in the fluctuation for a higher-order mode is manifested in the declining intercept of the curves in the figure.

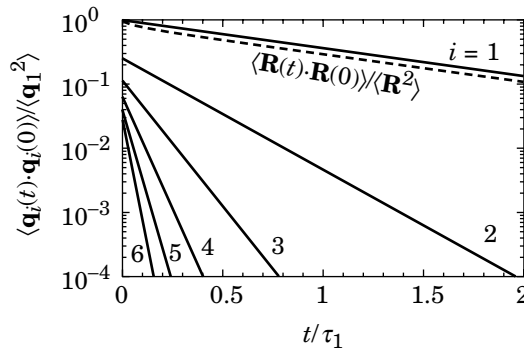


**Figure 3.48.** Autocorrelation function of  $\mathbf{q}_i(t)$  for  $i = 1$  to  $6$ , normalized by  $\langle \mathbf{q}_i^2 \rangle$ . The dashed line represents the autocorrelation of  $\mathbf{R}(t)$ , normalized by  $\langle \mathbf{R}^2 \rangle$ .

**3.4.5.2 Correlation of the End-to-End Vector** With Eqs. 3.148 and 3.157, the autocorrelation of the end-to-end vector is given as

$$\langle \mathbf{R}(t) \cdot \mathbf{R}(0) \rangle \cong \frac{8Nb^2}{\pi} \sum_{i:\text{odd}} \frac{1}{i^2} \exp(-t/\tau_i) \quad (3.158)$$

In the summation, the second term ( $i = 3$ ) has already only 1/9 of the intensity compared with the first term ( $i = 1$ ). The other terms are even smaller. The first term dominates in the summation. We can then replace  $\exp(-t/\tau_i)$  with  $\exp(-t/\tau_1)$ . Because  $\sum_{i:\text{odd}} i^{-2} = \pi^2/8$ ,

$$\langle \mathbf{R}(t) \cdot \mathbf{R}(0) \rangle \cong Nb^2 \exp(-t/\tau_1) \quad (3.159)$$

In Figure 3.48, the exact decay in  $\langle \mathbf{R}(t) \cdot \mathbf{R}(0) \rangle / \langle \mathbf{R}^2 \rangle$  is plotted as a dashed line. Except for short times,  $\langle \mathbf{R}(t) \cdot \mathbf{R}(0) \rangle$  and  $\langle \mathbf{q}_1(t) \cdot \mathbf{q}_1(0) \rangle$  have the same decay rate.

**3.4.5.3 Diffusion Coefficient** From Eqs. 3.130 and 3.152, the center-of-mass diffusion coefficient  $D_G$  of the Rouse model is given as

$$D_G \cong \frac{k_B T}{N\zeta} \quad \text{Rouse model} \quad (3.160)$$

which is equal to the diffusion coefficient of  $N$  connected beads, each of which move with a friction coefficient  $\zeta$  independently of the other beads.

**3.4.5.4 Molecular Weight Dependence** Because the Rouse model describes the static conformation of a polymer chain in the theta condition, we expect that the model can also describe the dynamics. However, this expectation is wrong.

In the Rouse model, the relaxation time  $\tau_1$  of the first mode is proportional to  $N^2$  (Eq. 3.136). The experimentally observed exponent for a polymer chain in a theta solvent is 3/2. The discrepancy also exists in the molecular weight dependence of  $D_G$ . Experimentally, we observe  $D_G \sim M^{-1/2}$  (Section 3.2.7) in the theta solvent. In the Rouse model (Eq. 3.160),  $D_G \sim N^{-1}$ . The model fails to give the correct exponent. The shortcoming of the model is ascribed to the neglect of hydrodynamic interactions. In the following subsection, we take into account the hydrodynamic interactions. In Section 4.3, we will see an example in which the Rouse model can describe the motion of polymer chains correctly.

### 3.4.6 Zimm Model

**3.4.6.1 Hydrodynamic Interactions** B. Zimm<sup>37</sup> improved the Rouse model by taking into account hydrodynamic interactions between beads. He successfully obtained the expressions for the diffusion coefficient and the relaxation times that agree with experimental results.

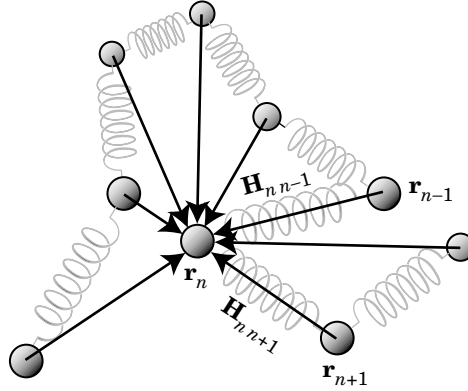


**Figure 3.49.** Motion of the  $n$ th bead is affected by the motion of all the other beads through the hydrodynamic interaction.

In the absence of the hydrodynamic interactions, the motion of the  $m$ th bead does not affect other beads except through the spring force. With the hydrodynamic interactions present, the velocity of one of the beads affects all the other beads through the flow of solvent (Fig. 3.49). Alternatively, the equation of motion for  $\mathbf{r}_n$  is written as

$$\frac{d\mathbf{r}_n}{dt} = \sum_{m=1}^N \mathbf{H}_{nm} [k_{\text{sp}}(\mathbf{r}_{m-1} + \mathbf{r}_{m+1} - 2\mathbf{r}_m) + \mathbf{f}_m] \quad (n = 1, 2, \dots, N) \quad (3.161)$$

where  $\mathbf{H}_{nm}$  is a second-rank tensor that represents how the velocity of the  $m$ th bead affects the velocity of the  $n$ th bead through the solvent between them. In the absence of the hydrodynamic interactions,  $\mathbf{H}_{nm} = (\mathbf{I}/\zeta)\delta_{nm}$ , where  $\mathbf{I}$  is a unit tensor ( $I_{\alpha\beta} = \delta_{\alpha\beta}$  with  $\alpha, \beta = x, y, z$ ). Then, Eq. 3.161 reduces to Eq. 3.115.

Usually, an **Oseen tensor** is used for  $\mathbf{H}_{nm}$ . Its magnitude is reciprocally proportional to  $|\mathbf{r}_n - \mathbf{r}_m|$  and is therefore a function of the chain conformation that changes with time according to Eq. 3.161. Zimm decoupled  $\mathbf{H}_{nm}$  from the rest of the equation and replaced it with its average at equilibrium (preaveraging approximation):

$$\frac{d\mathbf{r}_n}{dt} = \sum_{m=1}^N \langle \mathbf{H}_{nm} \rangle [k_{\text{sp}}(\mathbf{r}_{m-1} + \mathbf{r}_{m+1} - 2\mathbf{r}_m) + \mathbf{f}_m] \quad (n = 1, 2, \dots, N) \quad (3.162)$$

With the Oseen tensor,

$$\langle \mathbf{H}_{nm} \rangle = \frac{\mathbf{I}}{6\pi\eta_s} \left\langle \frac{1}{|\mathbf{r}_n - \mathbf{r}_m|} \right\rangle_{nm} \quad (3.163)$$

where the statistical average is taken with respect to given  $n$  and  $m$ .

The right-hand side depends on the chain conformation. We separately consider a polymer chain in the theta solvent and a polymer chain in the good solvent.

**3.4.6.2 Zimm Model in the Theta Solvent** For a polymer chain in the theta solvent, the Gaussian chain model conveniently gives us an analytical expression of Eq. 3.163. With Eq. 3.56,

$$\langle \mathbf{H}_{nm} \rangle = H_{nm} \mathbf{I} = \frac{\mathbf{I}}{(6\pi^3)^{1/2} \eta_s b |n - m|^{1/2}} \quad (3.164)$$

Because of  $|n - m|^{1/2}$  in the denominator,  $H_{nm}$  decays only slowly with an increasing  $|n - m|$ , that is, a distance between the two beads along the chain contour.

Equation 3.164 is not correct for  $n = m$ . It diverges as  $n$  and  $m$  approach each other. Upon integration with respect to  $n$  and  $m$ , however, the singularity is removed. We do not treat  $H_{nm}$  separately here. There is no need for that. The sum of the hydrodynamic interactions from other beads far exceeds the friction a given bead would receive in the absence of the hydrodynamic interactions. We will discuss this problem later when we derive the center-of-mass diffusion coefficient.

To convert Eq. 3.162 into equations of motion for the normal coordinate  $\mathbf{q}_i$ , we first express  $\mathbf{r}_{m-1} + \mathbf{r}_{m+1} - 2\mathbf{r}_m$  and  $\mathbf{f}_m$  by the normal coordinates  $\mathbf{q}_i$  and  $\mathbf{g}_i$ . From Eq. 3.125,

$$\begin{aligned} \mathbf{r}_{m-1} + \mathbf{r}_{m+1} - 2\mathbf{r}_m &= 2 \sum_{j=1}^{N-1} \mathbf{q}_j \left( \cos \frac{j(m-1)\pi}{N} + \cos \frac{j(m+1)\pi}{N} - 2\cos \frac{jm\pi}{N} \right) \\ &+ 4(-1)^{m-1} \mathbf{q}_N \cong -2 \sum_{j=0}^N \mathbf{q}_j \left( \frac{j\pi}{N} \right)^2 \cos \frac{jm\pi}{N} \end{aligned} \quad (3.165)$$

For  $\mathbf{g}_i$ , we use the same definition as Eq. 3.133 with  $\zeta_i/\zeta$  given by Eq. 3.130. It does not mean that  $\zeta_i$  is the same in the Rouse model and the Zimm model. We just use the same formula in the Zimm model to express the random force in the normal coordinates. As Eq. 3.125 is an inverse transform of Eq. 3.118, the following gives an inverse transform of Eq. 3.133 (Problem 3.21):

$$\mathbf{f}_m = \frac{1}{N} \sum_{j=0}^N \mathbf{g}_j \cos \frac{jm\pi}{N} - \frac{(-1)^m}{2N} \mathbf{q}_N \cong \frac{1}{N} \sum_{j=0}^N \mathbf{g}_j \cos \frac{jm\pi}{N} \quad (3.166)$$

With Eqs. 3.118, 3.165, and 3.166, Eq. 3.162 is transformed into

$$\frac{d\mathbf{q}_i}{dt} = N \sum_{j=0}^N h_{ij} \left( -2k_{sp} \left( \frac{j\pi}{N} \right)^2 \mathbf{q}_j + \frac{1}{N} \mathbf{g}_j \right) \quad (3.167)$$

where

$$h_{ij} = \frac{1}{N^2} \sum_{m=1}^N \sum_{n=1}^N H_{nm} \cos \frac{in\pi}{N} \cos \frac{jm\pi}{N} \quad (3.168)$$

In Eq. 3.167, all of the equations appear to be coupled with each other. Fortunately, they can be decoupled. It can be shown (Problem 3.22) that, when  $N \gg 1$ ,  $h_{ij}$  is approximated by

$$h_{ij} \cong \frac{1}{2(3\pi^3 i N)^{1/2} \eta_s b} \delta_{ij} \quad (\text{except } i = j = 0) \quad (3.169)$$

Then, we obtain

$$\zeta_i \frac{d\mathbf{q}_i}{dt} = -k_i \mathbf{q}_i + \mathbf{g}_i \quad (i = 0, 1, \dots, N) \quad \text{Zimm, theta} \quad (3.170)$$

Formally, the normal modes of the Zimm model follow the same differential equations as those of the Rouse model (Eq. 3.131).

The spring force constant for the  $i$ th mode

$$k_i = 2Nk_{\text{sp}} \left( \frac{i\pi}{N} \right)^2 = \frac{6\pi^2 k_B T}{Nb^2} i^2 \quad \text{Zimm, theta} \quad (3.171)$$

is identical to the counterpart in the Rouse model (Eq. 3.132) because the hydrodynamic interaction does not alter the equilibrium chain conformation. In the normal coordinate, the two modes are different only in the friction coefficient. Now it is

$$\zeta_i = h_{ii}^{-1} = 2(3\pi^3 i N)^{1/2} \eta_s b \quad (i = 1, 2, \dots, N) \quad \text{Zimm, theta} \quad (3.172)$$

A special care is needed for  $\zeta_0$  (Problem 3.23)

$$\zeta_0 = h_{00}^{-1} = \frac{3}{8}(6\pi^3 N)^{1/2} \eta_s b \quad \text{Zimm, theta} \quad (3.173)$$

Because Eq. 3.170 is identical to Eq. 3.131, we can use the general formulas in Section 3.4.4 to obtain  $D_G$  and  $\tau_i$  for the Zimm model in the theta solvent. The center-of-mass diffusion coefficient is obtained from Eqs. 3.152 and 3.173 as

$$D_G = \frac{8}{3(6\pi^3)^{1/2}} \frac{k_B T}{\eta_s b N^{1/2}} = \frac{8}{3(6\pi^3)^{1/2}} \frac{k_B T}{\eta_s R_F} \quad \text{Zimm, theta} \quad (3.174)$$

Its molecular weight dependence is  $D_G \sim N^{-1/2}$ . Thus, the hydrodynamic interactions increase the diffusivity of the chain, especially for a long chain, compared with a group of  $N$  independently moving beads (Rouse model). The friction on a

bead from the surrounding fluid is therefore much smaller than the sum of the hydrodynamic interactions the bead receives from the other beads. This result justifies our neglect of  $H_{mm}$  in deriving Eq. 3.164.

The relaxation time  $\tau_i$  of the  $i$ th mode is calculated from Eqs. 3.171 and 3.172 as

$$\tau_i = \frac{\zeta_i}{k_i} = \frac{1}{(3\pi)^{1/2}} \frac{\eta_s b^3 N^{3/2}}{k_B T} i^{-3/2} = \frac{1}{(3\pi)^{1/2}} \frac{\eta_s R_F^3}{k_B T} i^{-3/2} \quad \text{Zimm, theta} \quad (3.175)$$

The Zimm model successfully describes the experimentally observed dependence:  $D_G \sim M^{-1/2}$ ,  $\tau_1 \sim M^{3/2}$ , and  $\tau_i/\tau_1 \sim i^{-3/2}$ .

**3.4.6.3 Hydrodynamic Radius** By definition of  $h_{00}$  (Eq. 3.168), we can express  $D_G$  as

$$\begin{aligned} D_G &= k_B T h_{00} = k_B T \frac{1}{N^2} \int_0^N dn \int_0^N dm H_{nm} \\ &= k_B T \frac{1}{N^2} \int_0^N dn \int_0^N dm \frac{1}{6\pi\eta_s} \left\langle \frac{1}{|\mathbf{r}_n - \mathbf{r}_m|} \right\rangle_{nm} = \frac{k_B T}{6\pi\eta_s} \left\langle \frac{1}{|\mathbf{r}_n - \mathbf{r}_m|} \right\rangle \end{aligned} \quad (3.176)$$

where Eq. 3.163 was used. In the last line,  $\langle \dots \rangle$  implies a twofold statistical average: The first average is with respect to the positions of given beads  $n$  and  $m$ , and the second averaging scans  $n$  and  $m$ . Thus, from the definition of  $R_H$  (Eq. 3.54), it is given in the preaveraging approximation by

$$\frac{1}{R_H} = \left\langle \frac{1}{|\mathbf{r}_n - \mathbf{r}_m|} \right\rangle \quad \text{hydrodynamic radius, polymer chain} \quad (3.177)$$

Equation 3.55 was obtained in this way.

**3.4.6.4 Zimm Model in the Good Solvent** The Zimm model we used for the theta chains needs a small modification when we apply it to the chains in the good solvent. We must give up the numerical coefficients but can still obtain the exponents that agree with experimental results.

First, we work on  $h_{ij}$ . In place of  $|n - m|^{-1/2}$  in the preaveraged hydrodynamic interaction between the  $n$ th and  $m$ th beads, we now have  $|n - m|^{-\nu}$  with  $\nu \cong 3/5$  or 0.59. We can show that  $h_{ij}$  is still diagonal, that is,  $h_{ij} = 0$  for  $i \neq j$ , and the friction coefficient  $\zeta_i = h_{ii}^{-1}$  of the  $i$ th mode changes to (Problem 3.24)

$$\zeta_i \cong \eta_s b N^\nu i^{1-\nu} \quad (i = 1, 2, \dots) \quad (3.178)$$

$$\zeta_0 \cong \eta_s b N^\nu \quad (3.179)$$

Second, the force constant  $k_i$  needs some change because the Gaussian chain does not describe the conformation of the real chain. It can be obtained from



**Table 3.3 Models for Dynamics**

Model	Chain Statistics	Hydrodynamic Interactions	$D_G$	$\tau_i$	$[\eta]$
Rouse	ideal	absent	$M^{-1}$	$M^2/i^2$	$M^1$
Zimm	ideal	present	$M^{-1/2}$	$M^{3/2}/i^{3/2}$	$M^{1/2}$
Zimm	real	present	$M^{-\nu}$	$M^{3\nu}/i^{3\nu}$	$M^{3\nu-1}$
Kirkwood*	rod	present	$(\ln M - a)/M$	$M^3/[(\ln M - a) i(i + 1)]$	$M^2/(\ln M - a)$

\* $a$  represents a constant.

Eq. 3.146. Appendix 3.A.1 shows how to evaluate  $\langle \mathbf{q}_i^2 \rangle$  for the real chain. With Eq. 3.A.5,

$$k_i \cong \frac{k_B T}{b^2 N^{2\nu}} i^{2\nu+1} \quad (3.180)$$

With these modified  $\zeta_i$  and  $k_i$ ,  $\mathbf{q}_i$  follows the same equation as in the Zimm model in the theta solvent.

The center-of-mass diffusion coefficient is obtained from Eqs. 3.152 and 3.179 as

$$D_G \cong \frac{k_B T}{\eta_s b N^\nu} \cong \frac{k_B T}{\eta_s R_F} \quad (3.181)$$

The relaxation time  $\tau_i$  is calculated as

$$\tau_i = \frac{\zeta_i}{k_i} \cong \frac{\eta_s b^3 N^{3\nu}}{k_B T} i^{-3\nu} \cong \frac{\eta_s R_F^3}{k_B T} i^{-3\nu} \quad (3.182)$$

The Zimm model for the good solvent successfully describes the experimentally observed dependence:  $D_G \sim M^{-\nu}$ ,  $\tau_1 \sim M^{3\nu}$ , and  $\tau_i/\tau_1 \sim i^{-3\nu}$ .

According to a more elaborate calculation based on the renormalization group theory,<sup>38</sup>

$$D_G \cong 0.0829 \frac{k_B T}{\eta_s R_g} \quad \text{Zimm, good solvent} \quad (3.183)$$

Results for  $D_G$ ,  $\tau_1$ ,  $\tau_i/\tau_1$  are summarized in Table 3.3. The table also shows the results for the rodlike molecule (Section 3.5) and the  $M$  dependence of  $[\eta]$  (Section 3.4.7).

### 3.4.7 Intrinsic Viscosity

**3.4.7.1 Extra Stress by Polymers** Adding a polymer to a solvent increases its viscosity. Figure 3.50 illustrates a polymer chain in a shear flow. For the portion of

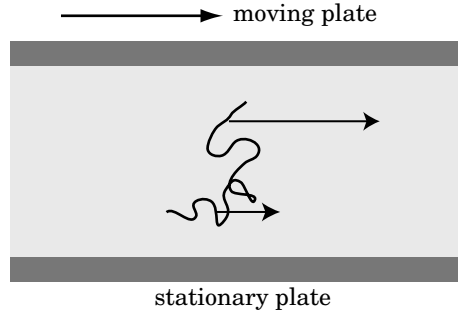


**Figure 3.50.** Portions of a polymer chain in shear flow experience different velocities depending on the distance from the stationary plate.

the chain closer to the moving plate to move faster compared with the other portion of the chain closer to the stationary plate, extra stress needs to be applied. In another word, flow becomes more difficult because of the polymer chain.

To estimate the intrinsic viscosity in the bead-spring model, we need to find how much the stress tensor in the flowing fluid changes when a unit amount of the polymer is added. At low concentrations, the increase in the stress tensor  $\sigma_{\alpha\beta}$  ( $\alpha, \beta = x, y, z$ ) due to the presence of bead-spring chains is given as

$$\Delta\sigma_{\alpha\beta} = \frac{cN_A}{M} \sum_{n=1}^N \left\langle \frac{\partial U}{\partial r_{n\alpha}} r_{n\beta} \right\rangle \quad (3.184)$$

where  $cN_A/M$  represents the number of the polymer chains in unit volume and  $U$  is the internal energy of the bead-spring model. As illustrated in Figure 3.51, an extra stress needs to be applied across the plane separating the  $n$ th bead from the  $n-1$ th bead in order to move the two beads with  $\mathbf{v}(\mathbf{r}_n)$  and  $\mathbf{v}(\mathbf{r}_{n-1})$ , respectively.

In the Rouse model, there is no excluded volume effect. In the Zimm model for the theta solvent, the chain conformation is the same as that of the Rouse model. For these two models,  $U$  is given by a sum of the elastic energy of the springs (Eq. 1.51), and therefore

$$\frac{\partial U}{\partial \mathbf{r}_n} = -k_{\text{sp}}(\mathbf{r}_{n-1} + \mathbf{r}_{n+1} - 2\mathbf{r}_n) \quad (3.185)$$

which is equal to the negative of the spring force in Eq. 3.115. Then, Eq. 3.184 leads to

$$\Delta\sigma_{\alpha\beta} = \frac{cN_A}{M} k_{\text{sp}} \sum_{n=1}^N \langle -(\mathbf{r}_{n-1} + \mathbf{r}_{n+1} - 2\mathbf{r}_n)_\alpha r_{n\beta} \rangle \quad (3.186)$$

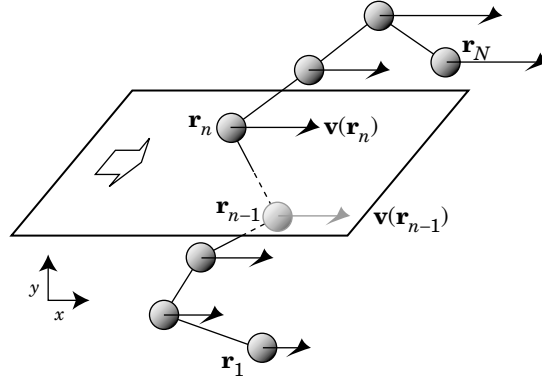


**Figure 3.51.** The  $xz$  plane separating the  $n - 1$ th bead from the  $n$ th bead receives a stress in  $y$  direction when the bead-spring chain is in a shear flow.

where  $\mathbf{r}_\alpha$  is the  $\alpha$  component of  $\mathbf{r}$  ( $\mathbf{r}_x = r_x = x$ , for instance). We now use Eqs. 3.125 and 3.165 to express the right-hand side in normal coordinates. Because  $\mathbf{q}_i$  and  $\mathbf{q}_j$  are irrelevant if  $i \neq j$ ,

$$\langle -(\mathbf{r}_{n-1} + \mathbf{r}_{n+1} - 2\mathbf{r}_n)_\alpha r_{n\beta} \rangle = 4 \sum_{i=1}^N \left( \frac{i\pi}{N} \right)^2 \cos^2 \frac{in\pi}{N} \langle q_{i\alpha} q_{i\beta} \rangle \quad (3.187)$$

Then, Eq. 3.186 is rewritten to

$$\Delta\sigma_{\alpha\beta} = \frac{cN_A}{M} k_{\text{sp}} 4 \sum_{i=1}^N \left( \frac{i\pi}{N} \right)^2 \langle q_{i\alpha} q_{i\beta} \rangle \sum_{n=1}^N \cos^2 \frac{in\pi}{N} \cong \frac{cN_A}{M} k_{\text{sp}} 2N \sum_{i=1}^N \left( \frac{i\pi}{N} \right)^2 \langle q_{i\alpha} q_{i\beta} \rangle \quad (3.188)$$

With Eq. 3.132 and 3.171, this equation is further rewritten to

$$\Delta\sigma_{\alpha\beta} = \frac{cN_A}{M} \sum_{i=1}^N k_i \langle q_{i\alpha} q_{i\beta} \rangle \quad (3.189)$$

It is now apparent that  $\Delta\sigma_{\alpha\beta} = \Delta\sigma_{\beta\alpha}$ , as required. Although the last equation was derived for the ideal chain conformations, it is also valid for real chains with an excluded volume.

**3.4.7.2 Intrinsic Viscosity of Polymers** In the absence of flow, the solution is isotropic. Each component ( $x$ ,  $y$ ,  $z$ ) of  $\mathbf{q}_i$  is independent. Then,  $\langle q_{i\alpha} q_{i\beta} \rangle = \langle q_{i\alpha} \rangle \langle q_{i\beta} \rangle = 0$ . Polymers do not add a stress. Our next job is to find how the flow changes  $\langle q_{i\alpha} q_{i\beta} \rangle$ .

In the presence of flow, the bead at  $\mathbf{r}_n$  has an additional velocity  $\kappa \mathbf{r}_n$ , as we learned in Section 3.3.4. The equation of motion for the  $n$ th bead, given by

Eq. 3.161, changes to

$$\frac{d\mathbf{r}_n}{dt} = \sum_{m=1}^N \mathbf{H}_{nm} [k_{sp}(\mathbf{r}_{m-1} + \mathbf{r}_{m+1} - 2\mathbf{r}_m) + \mathbf{f}_m] + \kappa \mathbf{r}_n \quad (n = 1, 2, \dots, N) \quad (3.190)$$

Note that  $\kappa \mathbf{r}_n$  is a linear function of  $\mathbf{r}_n$ . With the preaveraging approximation for  $\mathbf{H}_{nm}$  and conversion to the normal coordinates, it is straightforward to see the equation of motion for the  $i$ th normal mode acquire an additional term:

$$\frac{d\mathbf{q}_i}{dt} = -\frac{k_i}{\zeta_i} \mathbf{q}_i + \frac{1}{\zeta_i} \mathbf{g}_i + \kappa \mathbf{q}_i \quad (i = 0, 1, \dots) \quad (3.191)$$

Although we have used the Zimm model here, this equation is apparently valid for the Rouse model as well. The off-diagonal elements of the tensor  $\kappa$  couple different components ( $x$ ,  $y$ , and  $z$ ) of  $\mathbf{q}_i$ , as we will see below, but  $\mathbf{q}_i$  of different  $i$  are still independent of each other.

Now we consider a steady shear flow:  $\partial v_x / \partial y = \kappa_{xy} = \kappa$ , other elements are zero, as given by Eq. 3.107. This tensor couples  $q_{ix}$  and  $q_{iy}$ :

$$\begin{aligned} \frac{d}{dt} \langle q_{ix} q_{iy} \rangle &= \left\langle q_{ix} \left( -\frac{k_i}{\zeta_i} q_{iy} + \frac{1}{\zeta_i} g_{iy} + (\kappa \mathbf{q}_i)_y \right) + q_{iy} \left( -\frac{k_i}{\zeta_i} q_{ix} + \frac{1}{\zeta_i} g_{ix} + (\kappa \mathbf{q}_i)_x \right) \right\rangle \\ &= -2 \frac{k_i}{\zeta_i} \langle q_{ix} q_{iy} \rangle + \kappa \langle q_{iy}^2 \rangle \end{aligned} \quad (3.192)$$

where  $\langle q_{ix} g_{iy} + q_{iy} g_{ix} \rangle = \langle q_{ix} \rangle \langle g_{iy} \rangle + \langle q_{iy} \rangle \langle g_{ix} \rangle = 0$  and  $(\kappa \mathbf{q}_i)_y = 0$ ,  $(\kappa \mathbf{q}_i)_x = \kappa q_{iy}$  were used. The stationary solution ( $d\langle q_{ix} q_{iy} \rangle / dt = 0$ ) of Eq. 3.192 is

$$\langle q_{ix} q_{iy} \rangle = \frac{\kappa \zeta_i}{2k_i} \langle q_{iy}^2 \rangle \quad (3.193)$$

When the flow is sufficiently slow, the solution is nearly isotropic. Then,  $\langle q_{iy}^2 \rangle = \langle \mathbf{q}_i^2 \rangle / 3 = k_B T / k_i$  from Eq. 3.146, and we have

$$\langle q_{ix} q_{iy} \rangle = \frac{\kappa k_B T \zeta_i}{2k_i^2} \quad (3.194)$$

Then, from Eq. 3.189,

$$\Delta \sigma_{xy} = \frac{\kappa c N_A k_B T}{2M} \sum_{i=1}^N \tau_i \quad (3.195)$$

Finally, we obtain a general expression for the intrinsic viscosity. With Eq. 3.109,

$$\boxed{[\eta] \cong \frac{N_A k_B T}{2M \eta_s} \sum_{i=1}^N \tau_i \quad \text{intrinsic viscosity bead-spring model}} \quad (3.196)$$

The explicit expressions for  $[\eta]$  for the three cases of the bead-spring model are:

1. Rouse model. With Eq. 3.136,

$$[\eta] \cong \frac{N_A N^2 b^2 \zeta}{M \eta_s} \frac{1}{6\pi^2} \sum_{i=1}^N i^{-2} \cong \frac{N_A N^2 b^2 \zeta}{36M \eta_s} \sim M \quad (3.197)$$

where the upper limit in the summation was replaced by  $\infty$  and  $\sum_i i^{-2} = \pi^2/6$  was used.

2. Zimm model, theta solvent. With Eq. 3.175,

$$[\eta] \cong \frac{N_A (bN^{1/2})^3}{2(3\pi)^{1/2} M} \sum_{i=1}^N i^{-3/2} \cong 0.425 \times \frac{N_A R_F^3}{M} \sim M^{1/2} \quad (3.198)$$

where  $\sum_i i^{-3/2} \cong 2.612$  was used.

3. Zimm model, good solvent. With Eq. 3.182,

$$[\eta] \cong \frac{N_A (bN^\nu)^3}{M} \sum_{i=1}^N i^{-3\nu} \sim M^{3\nu-1} \quad (3.199)$$

The exponent is 0.8 for  $\nu = 3/5$  and 0.77 for  $\nu = 0.59$  (see Table 3.3). These values agree with experimental results (Fig. 3.37).

**3.4.7.3 Universal Calibration Curve in SEC** In the Zimm model (theta and good solvents), the intrinsic viscosity is essentially the ratio of the “volume” of the polymer chain,  $R_F^3$ , to the mass of each polymer chain,  $M/N_A$ . The solvent viscosity and the temperature do not show up explicitly in the final expression. Thus we can define **hydrodynamic volume**  $V_{hd}$  by

$$V_{hd} \equiv [\eta]M/N_A \quad \text{hydrodynamic volume} \quad (3.200)$$

There is a consensus that the retention time  $t_R$  in SEC is determined by  $V_{hd}$  for a given polymer fraction. The plot of  $[\eta]M/N_A$  vs.  $t_R$  obtained for different polymers but with the same column fall on a single master curve. In fact, the data for the theta condition and the data for rigid-chain polymers are also on the master curve obtained for flexible chains in good solvents. The curve is called a **universal calibration curve**. An example is shown in Figure 3.52.<sup>39</sup> The existence of the curve proves that the hydrodynamic volume governs the partitioning in the SEC column.

### 3.4.8 Dynamic Structure Factor

**3.4.8.1 General Formula** We consider in this subsection the dynamic structure factor of a bead-spring model. For now we do not distinguish the three cases of the model.

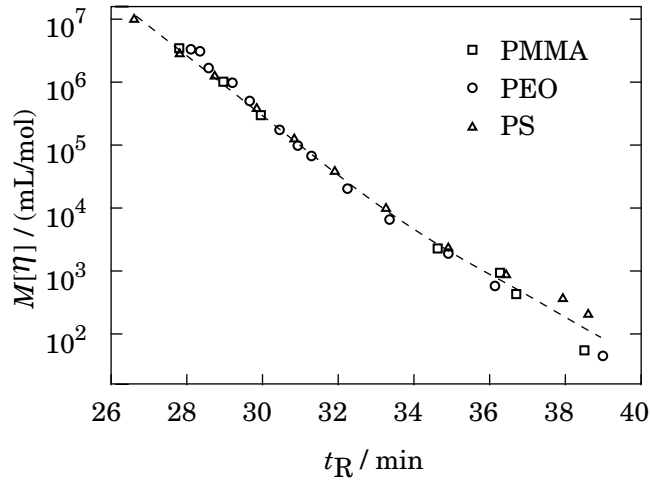


**Figure 3.52.** Universal calibration curve of SEC. The plots of  $M[\eta]$  obtained for poly(methyl methacrylate), poly(ethylene oxide), and polystyrene are on a master curve. The mobile phase was dimethylacetamide. (From Ref. 39.)

We define  $\mathbf{r}_{mn}(t) \equiv \mathbf{r}_n(t) - \mathbf{r}_m(0)$ , the displacement of the  $n$ th bead at time  $t$  with respect to the  $m$ th bead at time 0 (Fig. 3.53). Using Eq. 3.125, we find that  $\mathbf{r}_{mn}(t)$  is given as

$$\begin{aligned} \mathbf{r}_{mn}(t) = & [\mathbf{q}_0(t) - \mathbf{q}_0(0)] + 2 \sum_{i=1}^{N-1} \left[ \cos \frac{in\pi}{N} \mathbf{q}_i(t) - \cos \frac{im\pi}{N} \mathbf{q}_i(0) \right] \\ & + [(-1)^n \mathbf{q}_N(t) - (-1)^m \mathbf{q}_N(0)] \end{aligned} \quad (3.201)$$

Because different modes are uncorrelated, the average of  $\exp[i\mathbf{k} \cdot \mathbf{r}_{mn}(t)]$  for a given  $m$  and  $n$  is

$$\begin{aligned} \langle \exp[i\mathbf{k} \cdot \mathbf{r}_{mn}(t)] \rangle_{mn} = & \langle \exp[i\mathbf{k} \cdot (\mathbf{q}_0(t) - \mathbf{q}_0(0))] \rangle \\ & \times \prod_{i=1}^N \left\langle \exp \left[ 2i\mathbf{k} \cdot \left( \cos \frac{in\pi}{N} \mathbf{q}_i(t) - \cos \frac{im\pi}{N} \mathbf{q}_i(0) \right) \right] \right\rangle \end{aligned} \quad (3.202)$$

The last factor for  $i = N$  was incorporated into the product. The first factor represents the center-of-mass diffusion:

$$\langle \exp[i\mathbf{k} \cdot (\mathbf{q}_0(t) - \mathbf{q}_0(0))] \rangle = \exp(-D_G t \mathbf{k}^2) \quad (3.203)$$

Using Eq. 3.B.7 in Appendix 3.B [ $\sigma^2 = (3k_B T/k_i)/3 = k_B T/k_i$ ; note Eq. 3.B.3;  $\tau = \tau_i$ ;  $A = 2\cos(in\pi/N)$ ;  $B = 2\cos(im\pi/N)$ ], the  $i$ th factor in the  $N$ -fold product

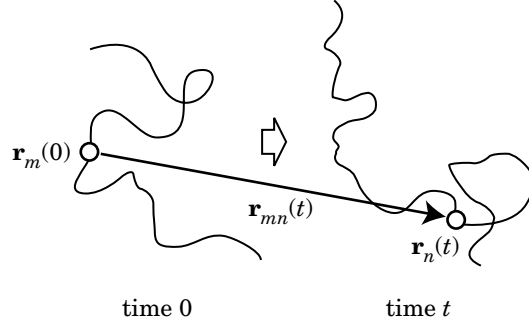


**Figure 3.53.**  $\mathbf{r}_{mn}(t)$  is the distance of the  $n$ th bead at time  $t$  from the  $m$ th bead at time 0.

is transformed to

$$\begin{aligned} & \left\langle \exp \left[ \mathbf{k} \cdot \left( 2 \cos \frac{in\pi}{N} \mathbf{q}_i(t) - 2 \cos \frac{im\pi}{N} \mathbf{q}_i(0) \right) \right] \right\rangle \\ &= \exp \left[ -\frac{2k_B T}{k_i} \mathbf{k}^2 \left( \cos^2 \frac{in\pi}{N} + \cos^2 \frac{im\pi}{N} - 2 \cos \frac{in\pi}{N} \cos \frac{im\pi}{N} \exp(-t/\tau_i) \right) \right] \end{aligned} \quad (3.204)$$

Thus,

$$\begin{aligned} & \langle \exp[i\mathbf{k} \cdot \mathbf{r}_{mn}(t)] \rangle_{mn} \\ &= \exp \left[ -D_G t \mathbf{k}^2 - 2\mathbf{k}^2 \sum_{i=1}^N \frac{k_B T}{k_i} \right. \\ & \quad \left. \times \left( \cos^2 \frac{in\pi}{N} + \cos^2 \frac{im\pi}{N} - 2 \cos \frac{in\pi}{N} \cos \frac{im\pi}{N} \exp(-t/\tau_i) \right) \right] \end{aligned} \quad (3.205)$$

At  $t = 0$ ,

$$\langle \exp[i\mathbf{k} \cdot \mathbf{r}_{mn}(0)] \rangle_{mn} = \exp \left[ -2\mathbf{k}^2 \sum_{i=1}^N \frac{k_B T}{k_i} \left( \cos \frac{in\pi}{N} - \cos \frac{im\pi}{N} \right)^2 \right] \quad (3.206)$$

Combined,

$$\begin{aligned} & \langle \exp[i\mathbf{k} \cdot \mathbf{r}_{mn}(t)] \rangle_{mn} = \langle \exp[i\mathbf{k} \cdot \mathbf{r}_{mn}(0)] \rangle_{mn} \\ & \quad \times \exp \left[ -D_G t \mathbf{k}^2 - 4\mathbf{k}^2 \sum_{i=1}^N \frac{k_B T}{k_i} \cos \frac{in\pi}{N} \cos \frac{im\pi}{N} [1 - \exp(-t/\tau_i)] \right] \end{aligned} \quad (3.207)$$

The dynamic structure factor of the chain is the average of the above equation with respect of  $m$  and  $n$ :

$$S_1(\mathbf{k}, t) = \exp(-D_G t \mathbf{k}^2) N^{-1} \sum_{m,n=1}^N \langle \exp[i\mathbf{k} \cdot \mathbf{r}_{mn}(0)] \rangle_{mn} \exp \left[ -4\mathbf{k}^2 \sum_{i=1}^N \frac{k_B T}{k_i} \right. \\ \left. \times \cos \frac{in\pi}{N} \cos \frac{im\pi}{N} [1 - \exp(-t/\tau_i)] \right] \quad \begin{array}{l} \text{dynamic structure factor} \\ \text{bead-spring model} \end{array} \quad (3.208)$$

The long-time behavior is simple. At  $t \gg \tau_1$ ,  $1 - \exp(-t/\tau_1) \cong 1$ , and therefore the time-dependent factor is  $\exp(-D_G \mathbf{k}^2 t)$  only. Then,  $S_1(\mathbf{k}, t)$  decays with a decay rate of  $D_G \mathbf{k}^2$ , indicating center-of-mass diffusion of the whole chain. This feature is common to all of the three models.

The short-time behavior for  $t \ll \tau_N$  is different:

$$S_1(\mathbf{k}, t) = \exp(-D_G t \mathbf{k}^2) N^{-1} \\ \times \sum_{m,n=1}^N \langle \exp[i\mathbf{k} \cdot \mathbf{r}_{mn}(0)] \rangle_{mn} \exp \left[ -4\mathbf{k}^2 t \sum_{i=1}^N \frac{k_B T}{\zeta_i} \cos \frac{in\pi}{N} \cos \frac{im\pi}{N} \right] \quad (3.209)$$

The slope of  $\ln S_1(\mathbf{k}, t)$  at  $t = 0$  is

$$\left. \frac{\partial}{\partial t} \ln S_1(\mathbf{k}, t) \right|_{t=0} = -D_G \mathbf{k}^2 - \frac{4\mathbf{k}^2 \sum_{m,n=1}^N \langle \exp[i\mathbf{k} \cdot \mathbf{r}_{mn}(0)] \rangle_{mn} \sum_{i=1}^N \frac{k_B T}{\zeta_i} \cos \frac{in\pi}{N} \cos \frac{im\pi}{N}}{\sum_{m,n=1}^N \langle \exp[i\mathbf{k} \cdot \mathbf{r}_{mn}(0)] \rangle_{mn}} \quad (3.210)$$

The initial slope may not follow  $\sim \mathbf{k}^2$  dependence and is different from model to model.

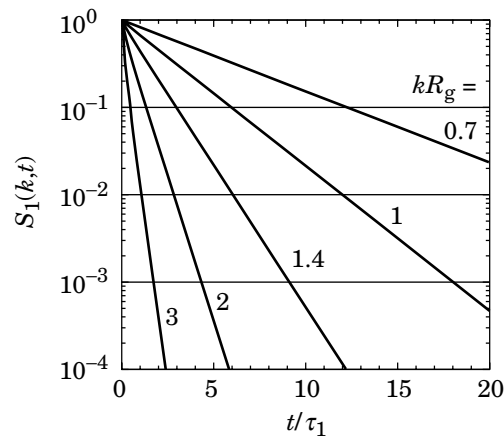


**Figure 3.54.** Dynamic structure factor  $S_1(\mathbf{k}, t)$  is plotted as a function of  $t/\tau_1$  for various values of  $kR_g$ . Calculation was done by using the Zimm model for the theta solvent.



Figure 3.54 shows how  $S_1(\mathbf{k}, t)$  changes with time  $t$  in the Zimm model for the theta condition. For  $kR_g = 0.7$ ,  $\ln S_1(\mathbf{k}, t)$  is almost straight over the entire range of time;  $S_1(\mathbf{k}, t)$  decays with a constant rate of  $D_G \mathbf{k}^2$ . With an increasing  $kR_g$ , the plot deviates from the straight line. The tangential to the curve is steep at near  $t = 0$ . At long times,  $S_1(\mathbf{k}, t)$  decays with  $D_G \mathbf{k}^2$ . Note that a small change in  $kR_g$  results in a large difference in the decay characteristics of  $S_1(\mathbf{k}, t)$ .

The plots are similar in the Rouse model except that it takes a longer time (in terms of  $t/\tau_1$ ) for  $S_1(\mathbf{k}, t)$  to decay to a given level.

In the following, we examine the initial slope of  $\ln S_1(\mathbf{k}, t)$  in the three models for the bead-spring chain.

**3.4.8.2 Initial Slope in the Rouse Model** In the Rouse model,  $\langle \exp[i\mathbf{k} \cdot \mathbf{r}_{mn}(0)] \rangle_{mn} = \exp(-b^2 \mathbf{k}^2 |n - m|/6)$  (Eq. 2.77). The denominator of Eq. 3.210 is equal to  $N^2 f_D(kR_g)$ , where the Debye function  $f_D(x)$  is defined by Eq. 2.79. The numerator is calculated as shown in Appendix 3.C. From Eq. 3.C.3,

$$\text{numerator} \cong 4\mathbf{k}^2 N^2 \sum_{i=1}^N \frac{k_B T}{\zeta_i} \frac{k^2 R_g^2}{(k^2 R_g^2)^2 + (i\pi)^2} \quad (3.211)$$

The sum is calculated as follows:

$$\begin{aligned} \sum_{i=1}^N \frac{k_B T}{\zeta_i} \frac{k^2 R_g^2}{(k^2 R_g^2)^2 + (i\pi)^2} &\cong \frac{k_B T}{2N\zeta} \frac{1}{\pi} \sum_{i=1}^{\infty} \frac{k^2 R_g^2 / \pi}{(k^2 R_g^2 / \pi)^2 + i^2} \\ &= \frac{k_B T}{2N\zeta} \frac{1}{\pi} \frac{\pi}{2} (\coth k^2 R_g^2 - (k^2 R_g^2)^{-1}) = \frac{1}{4} D_G (\coth k^2 R_g^2 - (k^2 R_g^2)^{-1}) \end{aligned} \quad (3.212)$$

where Eq. A4.1 was used. Thus,

$$\left. \frac{\partial}{\partial t} \ln S_1(\mathbf{k}, t) \right|_{t=0} = -D_G \mathbf{k}^2 \left( 1 + \frac{\coth k^2 R_g^2 - (k^2 R_g^2)^{-1}}{f_D(kR_g)} \right) \quad (3.213)$$

Because  $\coth x - x^{-1} \cong x/3$  and  $f_D(x) \cong 1$  when  $x \ll 1$ , the initial slope of  $\ln S_1(\mathbf{k}, t)$  is  $-D_G \mathbf{k}^2$  at small  $\mathbf{k}$ , the same as the long-time behavior. At large  $\mathbf{k}$ , the slope is  $-(1/2)D_G \mathbf{k}^2 (kR_g)^2$ , since  $\coth x - x^{-1} \cong 1$  and  $f_D(x) \cong 2/x^2$  when  $x \gg 1$ . The initial slope shows a crossover from  $\sim -k^2$  to  $\sim -k^4$  with an increasing  $kR_g$ .

**3.4.8.3 Initial Slope in the Zimm Model, Theta Solvent** Equation 3.211 is valid also in the Zimm model for the theta solvent because the equation depends on the chain conformation only. However, Eqs. 3.212 and 3.213 are different. We evaluate the sum in Eq. 3.211 for small  $\mathbf{k}$  and large  $\mathbf{k}$  separately. For small  $\mathbf{k}$ ,

$$\begin{aligned} \sum_{i=1}^N \frac{k_B T}{\zeta_i} \frac{k^2 R_g^2}{(k^2 R_g^2)^2 + (i\pi)^2} &\cong \frac{3 \cdot 2^{1/2}}{16} D_G \frac{1}{\pi} \sum_{i=1}^N \frac{k^2 R_g^2 / \pi}{i^{1/2} [(k^2 R_g^2 / \pi)^2 + i^2]} \\ &\leq \frac{3 \cdot 2^{1/2}}{16} D_G \frac{1}{\pi} \sum_{i=1}^{\infty} \frac{k^2 R_g^2 / \pi}{(k^2 R_g^2 / \pi)^2 + i^2} = \frac{3}{16 \cdot 2^{1/2}} D_G (\coth k^2 R_g^2 - (k^2 R_g^2)^{-1}) \end{aligned} \quad (3.214)$$

where Eqs. 3.172, 3.174 and A4.1 were used. Then, the second term in Eq. 3.210 is negligible, just as in the Rouse model. The initial slope of  $\ln S_1(\mathbf{k}, t)$  is  $-D_G \mathbf{k}^2$  at small  $\mathbf{k}$ .

For large  $\mathbf{k}$ , the sum is evaluated as follows:

$$\begin{aligned} \sum_{i=1}^N \frac{k_B T}{\zeta_i} \frac{k^2 R_g^2}{(k^2 R_g^2)^2 + (i\pi)^2} &\cong \frac{3 \cdot 2^{1/2}}{16} D_G \frac{1}{\pi} \int_0^\infty \frac{k^2 R_g^2 / \pi}{i^{1/2} [(k^2 R_g^2 / \pi)^2 + i^2]} di \\ &= \frac{3 \cdot 2^{1/2}}{16} D_G \frac{1}{\pi} \frac{\pi}{2^{1/2} k R_g / \pi^{1/2}} = \frac{D_G}{k R_g} \frac{3 \pi^{1/2}}{16} \end{aligned} \quad (3.215)$$

where Eq. A4.2 was used. Thus,

$$\left. \frac{\partial}{\partial t} \ln S_1(\mathbf{k}, t) \right|_{t=0} = -D_G \mathbf{k}^2 \left( 1 + \frac{3 \pi^{1/2} / 4}{k R_g f_D(k R_g)} \right) \quad k R_g \gg 1 \quad (3.216)$$

The initial slope of  $\ln S_1(\mathbf{k}, t)$  is  $-(3 \pi^{1/2} / 8) D_G \mathbf{k}^2 k R_g$  at large  $\mathbf{k}$ .

**3.4.8.4 Initial Slope in the Zimm Model, Good Solvent** We cannot use Eq. 3.211 because the conformation is not Gaussian. We need to start with Eq. 3.210. For small  $\mathbf{k}$ ,  $\langle \exp[i\mathbf{k} \cdot \mathbf{r}_{mn}(0)] \rangle_{mn} \cong 1$ . Therefore, the second term of Eq. 3.210 is

$$\frac{4\mathbf{k}^2}{N^2} k_B T \sum_{i=1}^N \frac{1}{\zeta_i} \left( \sum_{n=1}^N \cos \frac{in\pi}{N} \right)^2 \cong 0 \quad (3.217)$$

because of Eq. 3.124. Thus, the initial slope of  $\ln S_1(\mathbf{k}, t)$  is  $-D_G \mathbf{k}^2$  at small  $\mathbf{k}$ .

For large  $\mathbf{k}$ , the denominator of the second term of Eq. 3.210 is estimated as

$$\begin{aligned} \sum_{m,n=1}^N \langle \exp[i\mathbf{k} \cdot \mathbf{r}_{mn}(0)] \rangle_{mn} &\cong \int_0^N dn \int_0^n dm \exp(-b^2 \mathbf{k}^2 (n-m)^{2\nu}) \\ &\cong \int_0^N dm (N-m) \exp(-b^2 \mathbf{k}^2 m^{2\nu}) \\ &\cong N (bk)^{-1/\nu} \int_0^\infty \exp(-x^2) x^{1/\nu-1} dx \cong N (bk)^{-1/\nu} \end{aligned} \quad (3.218)$$

where the variable of integration was changed to  $x = bkm^\nu$ . For the numerator, we first evaluate the sum with respect to  $i$ :

$$\sum_{i=1}^N \frac{k_B T}{\zeta_i} \cos \frac{in\pi}{N} \cos \frac{im\pi}{N} \cong \frac{k_B T}{\eta_s b N^\nu} \sum_{i=1}^N \frac{1}{i^{1-\nu}} \left[ \cos \frac{i(n-m)\pi}{N} + \cos \frac{i(n+m)\pi}{N} \right]$$

$$\begin{aligned} &\cong D_G \left[ \delta_{mm} \sum_{i=1}^N i^{v-1} + (1 - \delta_{mm}) \int_0^\infty x^{v-1} \cos \frac{(n-m)\pi}{N} x dx \right. \\ &\quad \left. + \int_0^\infty x^{v-1} \cos \frac{(n+m)\pi}{N} x dx \right] \\ &\cong D_G N^v \left[ \delta_{mm} + (1 - \delta_{mm}) \frac{1}{|n-m|^v} + \frac{1}{|n+m|^v} \right] \end{aligned} \quad (3.219)$$

where Eq. A3.2 was used. Then, the numerator is dominated by the sum of  $|n-m|^{-v}$  and therefore estimated as

$$\begin{aligned} &k^2 \sum_{m,n=1}^N \langle \exp[i\mathbf{k} \cdot \mathbf{r}_{mn}(0)] \rangle_{mn} \frac{D_G N^v}{|n-m|^v} \\ &\cong k^2 D_G N^v \int_0^N dn \int_0^n dm \exp(-b^2 \mathbf{k}^2 |n-m|^{2v}) \frac{1}{|n-m|^v} \\ &\cong k^2 D_G N^v N (bk)^{1-1/v} \int_0^\infty \exp(-x^2) x^{1/v-2} dx \cong k^2 D_G N^v N (bk)^{1-1/v} \end{aligned} \quad (3.220)$$

Thus, the slope is approximated as

$$\left. \frac{\partial}{\partial t} \ln S_1(\mathbf{k}, t) \right|_{t=0} \cong -D_G \mathbf{k}^2 (1 + N^v kb) \cong -D_G \mathbf{k}^2 (1 + kR_g) \quad kR_g \gg 1 \quad (3.221)$$

The initial slope of  $\ln S_1(\mathbf{k}, t)$  is  $\sim -D_G \mathbf{k}^2 kR_g$  at large  $\mathbf{k}$ .

The initial decay rate of  $S_1(\mathbf{k}, t)$ , the negative of the initial slope of  $\ln S_1(\mathbf{k}, t)$ , is summarized in Table 3.4. The table includes the result for rodlike molecules (Section 3.5).

**3.4.8.5 Initial Slope: Experiments** The initial slope of  $\ln S_1(\mathbf{k}, t)$  is usually measured in DLS. At low concentrations,  $|g_1(t)| \propto S_1(\mathbf{k}, t)$ . Therefore, the initial

**Table 3.4 Initial Decay Rate of  $|g_1(t)|$**

Model	Long Time	Short Time	
		Small $\mathbf{k}$	Large $\mathbf{k}$
Rouse	$D_G \mathbf{k}^2$	$D_G \mathbf{k}^2$	$(1/2) D_G \mathbf{k}^2 (kR_g)^2$
Zimm, theta solvent	$D_G \mathbf{k}^2$	$D_G \mathbf{k}^2$	$(3\pi^{1/2}/8) D_G \mathbf{k}^2 (kR_g)$
Zimm, good solvent	$D_G \mathbf{k}^2$	$D_G \mathbf{k}^2$	$\sim D_G \mathbf{k}^2 (kR_g)$
Kirkwood (rod)	$D_G \mathbf{k}^2$	$D_G \mathbf{k}^2$	$(3/2) D_G \mathbf{k}^2$

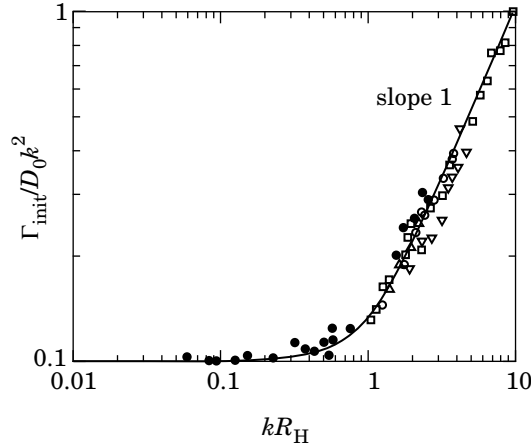


**Figure 3.55.** Initial decay rate  $\Gamma_{\text{init}}$  of  $|g_1(t)|$ , reduced by its low- $k$  asymptote  $D_0\mathbf{k}^2$ , is plotted as a function of  $kR_H$ . The data obtained for polystyrene in various solvents are on a theoretical curve (solid line) obtained for the Zimm model in the theta solvent. (From Ref. 40.)

decay rate  $\Gamma_{\text{init}}$  of  $|g_1(t)|$  defined as

$$\Gamma_{\text{init}} = -\lim_{t \rightarrow 0} \frac{\ln|g_1(t)|}{t} \quad (3.222)$$

is equal to the negative of the initial slope of  $\ln S_1(\mathbf{k}, t)$ .

Figure 3.55 shows  $\Gamma_{\text{init}}$  obtained in DLS for dilute solutions of polystyrene in various solvents that range from a good solvent to a near-theta solvent.<sup>40</sup> In the ordinate,  $\Gamma_{\text{init}}$  is reduced by  $D_0\mathbf{k}^2$ , the rate at low angles. The abscissa is the dimensionless  $kR_H$ . The solid line in the figure was calculated by using Eq. 3.210 for the Zimm model in the theta solvent. The data obtained in good solvents and theta solvents lie on the theoretical curve. At  $kR_H \ll 1$ ,  $\Gamma_{\text{init}} = D_0\mathbf{k}^2$ . At  $kR_H \gg 1$ , the master curve has a slope of 1, in agreement with Eqs. 3.216 and 3.221.

### 3.4.9 Motion of Monomers

**3.4.9.1 General Formula** In the preceding subsections, we considered the center-of-mass motion and also obtained a general formula for the statistical average of the Fourier transform of  $\mathbf{r}_{mn}(t) = \mathbf{r}_n(t) - \mathbf{r}_n(0)$ . In this subsection, we look at the motion of the beads (monomers) in different time scales. We first obtain expressions for  $\langle [\mathbf{r}_{mn}(t)]^2 \rangle_{mn}$ , the statistical average of the  $[\mathbf{r}_{mn}(t)]^2$  for given  $m$  and  $n$ , and consider how the average changes with time in the short time. We will then examine how the mean square displacement of the beads  $\langle [\mathbf{r}_m(t)]^2 \rangle$  changes with time for each model. The displacement of the beads is different from that of the center of mass. In the long time scale ( $t \gg \tau_1$ ), they should be identical, but, in the short time scale, the beads can move more quickly than the center of mass. In this subsection, we consider primarily the Rouse chain and the Zimm model in the theta solvent.

For that purpose, we apply the formula

$$\langle [\mathbf{r}_{mn}(t)]^2 \rangle_{mn} = -\frac{\partial^2}{\partial \mathbf{k}^2} \langle \exp[i\mathbf{k} \cdot \mathbf{r}_{mn}(t)] \rangle_{mn} \Big|_{\mathbf{k}=0} \quad (3.223)$$

to Eq. 3.207 and obtain

$$\begin{aligned} \langle [\mathbf{r}_{mn}(t)]^2 \rangle_{mn} - \langle [\mathbf{r}_{mn}(0)]^2 \rangle_{mn} &= 6D_G t + 24 \sum_{i=1}^N \frac{k_B T}{k_i} \\ &\times \cos \frac{in\pi}{N} \cos \frac{im\pi}{N} [1 - \exp(-t/\tau_i)] \end{aligned} \quad (3.224)$$

where the mean square distance between the two beads is

$$\langle [\mathbf{r}_{mn}(0)]^2 \rangle_{mn} = b^2 |m - n| \quad (3.225)$$

for the ideal-chain conformation. We can use Eq. 3.125 to derive Eq. 3.224 directly (Problem 3.26).

In the short time scale ( $t \ll \tau_N$ ),  $1 - \exp(-t/\tau_i) \cong t/\tau_i$  and therefore Eq. 3.224 reduces to

$$\langle [\mathbf{r}_{mn}(t)]^2 \rangle_{mn} - \langle [\mathbf{r}_{mn}(0)]^2 \rangle_{mn} \cong 6t \left[ D_G + 4 \sum_{i=1}^N \frac{k_B T}{\zeta_i} \cos \frac{in\pi}{N} \cos \frac{im\pi}{N} \right] \text{ short time} \quad (3.226)$$

In the long time scale ( $t \gg \tau_1$ ),  $1 - \exp(-t/\tau_i) \cong 1$  and therefore Eq. 3.224 reduces to

$$\langle [\mathbf{r}_{mn}(t)]^2 \rangle_{mn} - \langle [\mathbf{r}_{mn}(0)]^2 \rangle_{mn} = 6D_G t + 24 \sum_{i=1}^N \frac{k_B T}{k_i} \cos \frac{in\pi}{N} \cos \frac{im\pi}{N} \text{ long time} \quad (3.227)$$

In the long time scale, the first term dominates, and  $\langle [\mathbf{r}_{mn}(t)]^2 \rangle_{mn}$  becomes indistinguishable from the center-of-mass diffusion, as expected. The mean square displacement increases linearly with  $t$  in the two asymptotes. The motion of the monomers is diffusional in the two asymptotes but with different diffusion coefficients. Then, the motion cannot be diffusional in the intermediate time range.

**3.4.9.2 Mean Square Displacement: Short-Time Behavior Between a Pair of Monomers** Before considering the mean square displacement of the same beads (monomers) in Section 3.4.9.3, we look at the evolution of  $\langle [\mathbf{r}_{mn}(t)]^2 \rangle_{mn}$  for a pair of beads in the short time scale. Because  $\zeta_i$  is different between the Rouse model and the Zimm model for the theta solvent, we treat them separately.

In the Rouse model,  $k_B T / \zeta_i = D_G / 2$ , and the second term in Eq. 3.226 is calculated as

$$4 \sum_{i=1}^N \frac{k_B T}{\zeta_i} \cos \frac{in\pi}{N} \cos \frac{im\pi}{N} = D_G \sum_{i=1}^N \left[ \cos \frac{i(n-m)\pi}{N} + \cos \frac{i(n+m)\pi}{N} \right] \cong D_G N \delta_{nm} \quad (3.228)$$

where Eq. 3.124 was used. Thus, the overall short-time behavior is given as

$$\langle [\mathbf{r}_{mn}(t)]^2 \rangle_{mn} \cong b^2 |n - m| + 6D_G t (1 + N\delta_{nm}) \quad \begin{array}{l} \text{Rouse model} \\ \text{short time} \end{array} \quad (3.229)$$

There is a distinct difference between a different pair ( $m \neq n$ ) and the same pair ( $m = n$ ; self-diffusion of each bead). For the same pair,  $\langle [\mathbf{r}_{mn}(t)]^2 \rangle_{mn} = 6D_G(N + 1)t \cong 6(k_B T / \zeta)t$ . It means that each bead moves freely with its own friction coefficient as if the other beads were absent or not connected. For a pair of different beads, the short-time mean square displacement increases as  $6D_G t$ , the same as the center of mass diffusion. Different beads are uncorrelated.

In the Zimm model (theta solvent),  $k_B T / \zeta_i = (3 \cdot 2^{1/2} / 16) D_G / i^{1/2}$  from Eqs. 3.172 and 3.174. Therefore, the second term in Eq. 3.226 is calculated as

$$4 \sum_{i=1}^N \frac{k_B T}{\zeta_i} \cos \frac{in\pi}{N} \cos \frac{im\pi}{N} = \frac{3}{4 \cdot 2^{1/2}} D_G \sum_{i=1}^N \frac{1}{i^{1/2}} \left[ \cos \frac{i(n-m)\pi}{N} + \cos \frac{i(n+m)\pi}{N} \right] \quad (3.230)$$

When  $n = m$ ,  $\cos(2in\pi/N)$  is a rapidly changing function of  $i$ . The sum will be much smaller compared with the first term,  $\sum i^{-1/2} \cong 2N^{1/2}$ . Thus,

$$\langle [\mathbf{r}_{mn}(t)]^2 \rangle_{nn} \cong 6D_G t \left( 1 + \frac{3}{2^{3/2}} N^{1/2} \right) \quad (3.231)$$

When  $n \neq m$ , the sum is dominated with the first term because  $\cos[i(n+m)\pi/N]$  changes between positive and negative more rapidly compared with  $\cos[i(n-m)\pi/N]$ . From Eq. A3.3 in Appendix A3, we have

$$\langle [\mathbf{r}_{mn}(t)]^2 \rangle_{mn} \cong b^2 |n - m| + 6D_G t \left( 1 + \frac{3}{8} (N/|n - m|)^{1/2} \right) \quad \begin{array}{l} \text{Zimm, theta} \\ \text{short time} \end{array} \quad (3.232)$$

The hydrodynamic interactions allow the distance between a nearby pair of beads to grow more rapidly compared with a distant pair. For the latter, the short-time mean square displacement increases as in the Rouse model.

**3.4.9.3 Mean Square Displacement of Monomers** Now we trace the motion of the same bead ( $m = n$ ) in all time scales. From Eq. 3.224, the displacement of each

monomer,  $\langle [\mathbf{r}_{nm}(t)]^2 \rangle_{nm}$ , is given as

$$\langle [\mathbf{r}_{nm}(t)]^2 \rangle_{nm} = 6D_G t + 24 \sum_{i=1}^N \frac{k_B T}{k_i} \cos^2 \frac{in\pi}{N} [1 - \exp(-t/\tau_i)] \quad (3.233)$$

where  $\mathbf{r}_{nm}(t) = \mathbf{r}_n(t) - \mathbf{r}_n(0)$  is the displacement of the  $n$ th bead. We denote the average of  $\langle [\mathbf{r}_{nm}(t)]^2 \rangle_{nm}$  with respect to  $n$  by  $\langle [\mathbf{r}_m(t)]^2 \rangle$  without subscript and calculate it for the short, long, and intermediate time ranges. The average of  $\cos^2(in\pi/N)$  with respect to  $n$  is  $1/2$ . Thus,

$$\langle [\mathbf{r}_m(t)]^2 \rangle \cong 6D_G t + 12 \sum_{i=1}^N \frac{k_B T}{k_i} [1 - \exp(-t/\tau_i)] \quad (3.234)$$

In the short time ( $t \ll \tau_N$ ),

$$\langle [\mathbf{r}_m(t)]^2 \rangle \cong 6t \left[ D_G + 2 \sum_{i=1}^N \frac{k_B T}{\zeta_i} \right] \quad \text{short time} \quad (3.235)$$

In the long time ( $t \gg \tau_1$ ),

$$\langle [\mathbf{r}_m(t)]^2 \rangle \cong 6D_G t + 12 \sum_{i=1}^N \frac{k_B T}{k_i} \quad \text{long time} \quad (3.236)$$

In the intermediate time range, we need to deal with  $1 - \exp(-t/\tau_i)$  as it is.

In the following, we consider  $\langle [\mathbf{r}_{nm}(t)]^2 \rangle$  for the Rouse model and the Zimm model in the theta solvent separately. We will also briefly consider  $\langle [\mathbf{r}_{nm}(t)]^2 \rangle$  for the Zimm model in the good solvent.

1. In the Rouse model,  $\zeta_i = 2N\zeta$  for  $i \neq 0$ . Then, the second term in the bracket of Eq. 3.235 is

$$2 \sum_{i=1}^N \frac{k_B T}{\zeta_i} = \frac{k_B T}{\zeta} \quad (3.237)$$

which is much greater compared with  $D_G = k_B T / N\zeta$ . Thus, in the short time, monomers move with a diffusion coefficient of  $k_B T / \zeta$  as if there were not connected by springs:

$$\langle [\mathbf{r}_{nm}(t)]^2 \rangle \cong 6 \frac{k_B T}{\zeta} t = 6ND_G t \quad \begin{array}{l} \text{Rouse model} \\ \text{short time} \end{array} \quad (3.238)$$

as we have seen in Eq. 3.229.

For the long-time behavior, use of  $k_i = 6\pi^2 k_B T i^2 / Nb^2$  (Eq. 3.132) yields

$$12 \sum_{i=1}^N \frac{k_B T}{k_i} = \frac{2Nb^2}{\pi^2} \sum_{i=1}^N \frac{1}{i^2} \cong \frac{2Nb^2}{\pi^2} \sum_{i=1}^{\infty} \frac{1}{i^2} = \frac{2Nb^2}{\pi^2} \frac{\pi^2}{6} = \frac{1}{3} Nb^2 \quad (3.239)$$

Then, Eq. 3.236 is

$$\langle [\mathbf{r}_m(t)]^2 \rangle \cong 6D_G t + \frac{1}{3} N b^2 \quad \begin{array}{l} \text{Rouse model} \\ \text{long time} \end{array} \quad (3.240)$$

For the intermediate time range, we use  $\tau_i = \tau_1/i^2$  to calculate Eq. 3.234 as follows:

$$\langle [\mathbf{r}_m(t)]^2 \rangle \cong 6D_G t + \frac{2N b^2}{\pi^2} \sum_{i=1}^N \frac{1}{i^2} [1 - \exp(-i^2 t/\tau_1)] \quad (3.241)$$

We approximate the sum by an integral. Integral by parts yields

$$\sum_{i=1}^N \frac{1}{i^2} [1 - \exp(-i^2 t/\tau_1)] \cong \int_0^\infty \frac{1}{i^2} [1 - \exp(-i^2 t/\tau_1)] di = (\pi t/\tau_1)^{1/2} \quad (3.242)$$

Thus,

$$\langle [\mathbf{r}_m(t)]^2 \rangle \cong 6D_G t + (2N b^2/\pi^2)(\pi t/\tau_1)^{1/2} \quad \begin{array}{l} \text{Rouse model} \\ \text{intermediate time} \end{array} \quad (3.243)$$

Figure 3.56 illustrates how  $\langle [\mathbf{r}_m(t)]^2 \rangle$  changes with time  $t$ . The boundaries of the three time regimes can also be obtained as an interaction between two lines that correspond to the relevant sections and their extrapolates (Problem 3.27). The diffusion characteristics show a crossover from the single-bead diffusion to the  $N$ -bead

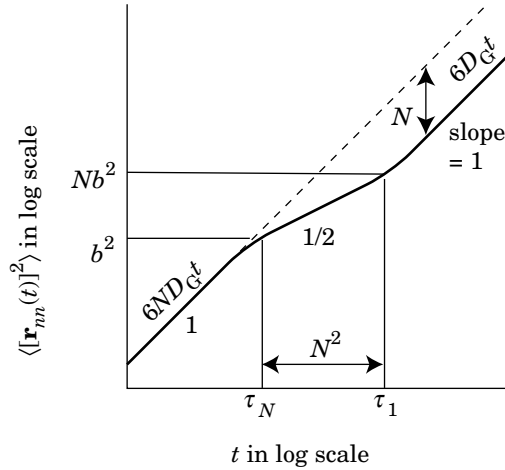


**Figure 3.56.** Mean square displacement of the beads on the Rouse chain,  $\langle [\mathbf{r}_m(t)]^2 \rangle$ , is plotted as a function of time  $t$ . The plot has three distinct regions. In  $t \ll \tau_N$  and  $t \gg \tau_1$ , the dynamics is diffusional with diffusion coefficients  $ND_G$  and  $D_G$ , respectively. In the time range between them,  $\langle [\mathbf{r}_m(t)]^2 \rangle \sim t^{1/2}$ .



diffusion. The latter is slower by a factor of  $N$ . Between the two diffusional asymptotes, the mean square displacement of the monomers on the Rouse chain increases in a power of  $t^{1/2}$ . The range of time that exhibits the power is roughly between  $\tau_N$  and  $\tau_1$ . The mean square displacement is  $b^2$  and  $Nb^2$  at the two boundaries of the range.

2. In the Zimm model for the theta solvent,  $k_B T / \zeta_i = (3 \cdot 2^{1/2} / 16) D_G / i^{1/2}$ . The second term of Eq. 3.235 is calculated as

$$2 \sum_{i=1}^N \frac{k_B T}{\zeta_i} = \frac{3 \cdot 2^{1/2}}{8} D_G \sum_{i=1}^N i^{-1/2} \cong \frac{3 \cdot 2^{1/2}}{4} D_G N^{1/2} \quad (3.244)$$

where the sum was approximated by the integral. This term is much greater compared with the first term,  $D_G$ . Thus, in the short time, monomers move with a diffusion coefficient of  $(3/4)(2N)^{1/2} D_G$ . From Eq. 3.174, we find this diffusion coefficient is equal to  $4(3/\pi)^{1/2} k_B T / (6\pi\eta_s b) \cong 3.9 \times k_B T / (6\pi\eta_s b)$ . Thus, the monomers move as if there were not connected by springs and with a diffusion coefficient about four times as large as that of a sphere of radius  $b$ :

$$\langle [\mathbf{r}_m(t)]^2 \rangle \cong 9(N/2)^{1/2} D_G t = 6 \cdot 4(3/\pi)^{1/2} \frac{k_B T}{6\pi\eta_s b} t \quad \begin{array}{l} \text{Zimm, theta} \\ \text{short time} \end{array} \quad (3.245)$$

The expression for  $\langle [\mathbf{r}_m(t)]^2 \rangle$  in the long time is the same as that of the Rouse model, because  $k_i$  is common between the two models. Thus, Eq. 3.240 holds as it does for the Zimm model in the theta solvent. Note, however, that  $D_G$  is different between the two models.

For the intermediate time range, we use  $\tau_i = \tau_1 / i^{3/2}$  to evaluate Eq. 3.234 as follows:

$$\langle [\mathbf{r}_m(t)]^2 \rangle \cong 6D_G t + \frac{2Nb^2}{\pi^2} \sum_{i=1}^N \frac{1}{i^2} [1 - \exp(-i^{3/2}t/\tau_1)] \quad (3.246)$$

We approximate the sum by an integral. Integral by parts yields

$$\sum_{i=1}^N \frac{1}{i^2} [1 - \exp(-i^{3/2}t/\tau_1)] \cong \int_0^\infty \frac{1}{i^2} [1 - \exp(-i^{3/2}t/\tau_1)] di = \Gamma_{1/3}(t/\tau_1)^{2/3} \quad (3.247)$$

where  $\Gamma_{1/3} = \Gamma(1/3) \cong 2.679$  (see Eq. A3.6). Thus,

$$\langle [\mathbf{r}_m(t)]^2 \rangle \cong 6D_G t + (2\Gamma_{1/3}/\pi^2) Nb^2 (t/\tau_1)^{2/3} \quad \begin{array}{l} \text{Zimm, theta} \\ \text{intermediate time} \end{array} \quad (3.248)$$

Figure 3.57 illustrates how  $\langle [\mathbf{r}_m(t)]^2 \rangle$  changes with time  $t$  in the Zimm model. The monomer motion is diffusional in the two asymptotes. Between them,  $\langle [\mathbf{r}_m(t)]^2 \rangle \sim t^{2/3}$ .

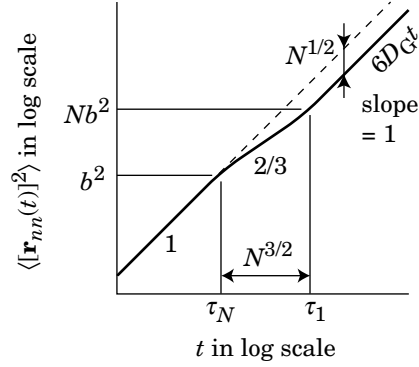


**Figure 3.57.** Mean square displacement of the beads on the chain for the Zimm model in the theta solvent,  $\langle [\mathbf{r}_{mn}(t)]^2 \rangle$

3. In the Zimm model for the good solvent, our discussion is limited to power relationships. For the short-time behavior, we note  $k_B T / \zeta_i \cong i^{\nu-1} D_G$ . Then, in Eq. 3.235,

$$\sum_{i=1}^N \frac{k_B T}{\zeta_i} \cong D_G \sum_{i=1}^N i^{\nu-1} \cong D_G N^\nu \quad (3.249)$$

which is much greater than  $D_G$ . Therefore, the short-time behavior is given as

$$\langle [\mathbf{r}_{mn}(t)]^2 \rangle \cong N^\nu D_G t \cong \frac{k_B T}{\eta_s b} t \quad \begin{array}{l} \text{Zimm, good} \\ \text{short time} \end{array} \quad (3.250)$$

The bead moves as if it were not connected with other beads.

The expression for the long-time behavior is almost the same as that for the other two models, namely,

$$\langle [\mathbf{r}_{mn}(t)]^2 \rangle \cong 6D_G t + N^{2\nu} b^2 \quad \begin{array}{l} \text{Zimm, good} \\ \text{long time} \end{array} \quad (3.251)$$

For the intermediate time range, we evaluate the following:

$$\langle [\mathbf{r}_{mn}(t)]^2 \rangle \cong 6D_G t + N^{2\nu} b^2 \sum_{i=1}^N \frac{1}{i^{2\nu+1}} [1 - \exp(-i^{3\nu} t / \tau_1)] \quad (3.252)$$

By replacing the sum with an integral and using integral by parts, we obtain

$$\langle [\mathbf{r}_{mn}(t)]^2 \rangle \cong 6D_G t + N^{2\nu} b^2 (t/\tau_1)^{2/3} \quad \begin{array}{l} \text{Zimm, good} \\ \text{intermediate} \end{array} \quad (3.253)$$

The exponent 2/3 is the same as the one we obtained for the theta solvent condition.

**3.4.10 PROBLEMS**

**Problem 3.21:** Show the inverse transform of Eq. 3.133:

$$\mathbf{f}_n = \frac{1}{N} \sum_{j=0}^N \mathbf{g}_j \cos \frac{jn\pi}{N} - \frac{(-1)^n}{2N} \mathbf{g}_N$$

**Solution 3.21:** We rewrite Eq. 3.133 to

$$\frac{\zeta}{\zeta_i} \mathbf{g}_i(t) = \frac{1}{N} \sum_{n=1}^N \cos \frac{in\pi}{N} \mathbf{f}_n(t)$$

This conversion has the same structure as Eq. 3.118 with  $(\zeta/\zeta_i)\mathbf{g}_i$  replacing  $\mathbf{q}_i$ . Then, we can apply the inverse transform, Eq. 3.125, as it is:

$$\mathbf{f}_n(t) = 2 \sum_{i=1}^{N-1} \cos \frac{in\pi}{N} \frac{\zeta}{\zeta_i} \mathbf{g}_i(t) + \frac{\zeta}{\zeta_0} \mathbf{g}_0(t) + (-1)^n \frac{\zeta}{\zeta_N} \mathbf{g}_N(t)$$

Because  $\zeta_0 = N\zeta$  and  $\zeta_i = 2N\zeta$  ( $i \geq 1$ )

$$\begin{aligned} \mathbf{f}_n(t) &= \frac{1}{N} \sum_{i=1}^{N-1} \cos \frac{in\pi}{N} \mathbf{g}_i(t) + \frac{1}{N} \mathbf{g}_0(t) + (-1)^n \frac{1}{2N} \mathbf{g}_N(t) \\ &= \frac{1}{N} \sum_{j=0}^N \mathbf{g}_j \cos \frac{jn\pi}{N} - \frac{(-1)^n}{2N} \mathbf{g}_N \end{aligned}$$

**Problem 3.22:** Show that, in the Zimm model for the theta solvent,

$$h_{ij} \cong \frac{1}{2(3\pi^3 i N)^{1/2} \eta_s b} \delta_{ij} \quad (\text{except } i = j = 0)$$

**Solution 3.22:** From Eqs. 3.164 and 3.168,

$$h_{ij} = \frac{1}{N^2} \frac{1}{(6\pi^3)^{1/2} \eta_s b} \int_0^N \int_0^N \mathrm{d}n \int_0^N \mathrm{d}m |n - m|^{-1/2} \cos \frac{in\pi}{N} \cos \frac{jm\pi}{N}$$

The integral with respect to  $m$  is calculated as

$$\begin{aligned} & \int_0^N \mathrm{d}m |n - m|^{-1/2} \cos \frac{jm\pi}{N} \\ &= \int_{n-N}^n \mathrm{d}(n - m) |n - m|^{-1/2} \left( \cos \frac{jn\pi}{N} \cos \frac{j(n - m)\pi}{N} + \sin \frac{jn\pi}{N} \sin \frac{j(n - m)\pi}{N} \right) \end{aligned}$$

$$\begin{aligned}
&\cong \cos \frac{jn\pi}{N} \int_{-\infty}^{\infty} d(n-m) |n-m|^{-1/2} \cos \frac{j(n-m)\pi}{N} \\
&\quad + \sin \frac{jn\pi}{N} \int_{-\infty}^{\infty} d(n-m) |n-m|^{-1/2} \sin \frac{j(n-m)\pi}{N} \\
&\cong 2 \cos \frac{jn\pi}{N} \int_0^{\infty} d(n-m) |n-m|^{-1/2} \cos \frac{j(n-m)\pi}{N} = 2 \cos \frac{jn\pi}{N} \left( \frac{N}{2j} \right)^{1/2}
\end{aligned}$$

where the lower and upper limits of the integral are set to  $-\infty$  and  $\infty$ , because frequent alterations of the sign in  $\cos[j(n-m)\pi/N]$  and  $\sin[j(n-m)\pi/N]$  at large values of  $|n-m|$  make its contribution much smaller compared with the contribution from small values of  $|n-m|$ . Equation A3.3 was used in the last equality. Then,

$$\begin{aligned}
h_{ij} &= \frac{1}{N} \frac{1}{(6\pi^3)^{1/2} \eta_s b} \left( \frac{N}{2j} \right)^{1/2} \frac{1}{N} \int_0^N 2 \cos \frac{in\pi}{N} \cos \frac{jn\pi}{N} dn \\
&= \frac{1}{N} \frac{1}{(6\pi^3)^{1/2} \eta_s b} \left( \frac{N}{2j} \right)^{1/2} \delta_{ij} = \frac{1}{2(3\pi^3 Ni)^{1/2} \eta_s b} \delta_{ij}
\end{aligned}$$

**Problem 3.23:** Show that, in the Zimm model for the theta solvent,

$$h_{00} = \frac{8}{3} \frac{1}{(6\pi^3 N)^{1/2} \eta_s b}$$

**Solution 3.23:** From Eqs. 3.164 and 3.168,

$$h_{00} = \frac{1}{N^2} \frac{1}{(6\pi^3)^{1/2} \eta_s b} \int_0^N dn \int_0^N dm |n-m|^{-1/2}$$

The integral is calculated as

$$\int_0^N dn \int_0^N dm |n-m|^{-1/2} = 2 \int_0^N dn \int_0^n dm (n-m)^{-1/2} = 2 \int_0^N dn 2n^{1/2} = \frac{8}{3} N^{3/2}$$

**Problem 3.24:** Show that, in the Zimm model for the good solvent,

$$\begin{aligned}
h_{ij} &\cong \frac{1}{N^\nu i^{1-\nu} \eta_s b} \delta_{ij} \quad (\text{except } i = j = 0) \\
h_{00} &= \frac{1}{\eta_s b N^\nu}
\end{aligned}$$

**Solution 3.24:**

$$h_{ij} \cong \frac{1}{N^2} \frac{1}{\eta_s b} \int_0^N dn \int_0^N dm |n - m|^{-\nu} \cos \frac{in\pi}{N} \cos \frac{jm\pi}{N}$$

The integral with respect to  $m$  is calculated as

$$\begin{aligned} & \int_0^N dm |n - m|^{-\nu} \cos \frac{jm\pi}{N} \\ &= \int_{n-N}^n d(n - m) |n - m|^{-\nu} \left( \cos \frac{jn\pi}{N} \cos \frac{j(n - m)\pi}{N} \right. \\ & \quad \left. + \sin \frac{jn\pi}{N} \sin \frac{j(n - m)\pi}{N} \right) \cong \cos \frac{jn\pi}{N} \int_{-\infty}^{\infty} d(n - m) |n - m|^{-\nu} \cos \frac{j(n - m)\pi}{N} \\ & \quad + \sin \frac{jn\pi}{N} \int_{-\infty}^{\infty} d(n - m) |n - m|^{-1/2} \sin \frac{j(n - m)\pi}{N} \\ & \cong 2 \cos \frac{jn\pi}{N} \int_0^{\infty} d(n - m) |n - m|^{-\nu} \cos \frac{j(n - m)\pi}{N} \\ &= 2 \cos \frac{jn\pi}{N} \times \frac{\Gamma(1 - \nu)}{(j\pi/N)^{1-\nu}} \cos \frac{(1 - \nu)\pi}{2} \cong \cos \frac{jn\pi}{N} \left( \frac{N}{j} \right)^{1-\nu} \end{aligned}$$

where the lower and upper limits of the integral are set to  $-\infty$  and  $\infty$ , because frequent alterations of the sign in  $\cos[j(n - m)\pi/N]$  and  $\sin[j(n - m)\pi/N]$  at large values of  $|n - m|$  make its contribution much smaller compared with the contribution from small values of  $|n - m|$ . Equation A3.2 was used in the last equality. Then,

$$\begin{aligned} h_{ij} &\cong \frac{1}{N} \frac{1}{\eta_s b} \left( \frac{N}{j} \right)^{1-\nu} \frac{1}{N} \int_0^N dn \cos \frac{in\pi}{N} \cos \frac{jn\pi}{N} \\ &\cong \frac{1}{N} \frac{1}{\eta_s b} \left( \frac{N}{j} \right)^{1-\nu} \delta_{ij} = \frac{1}{N^{\nu} i^{1-\nu} \eta_s b} \delta_{ij} \end{aligned}$$

For  $h_{00}$ ,

$$h_{00} \cong \frac{1}{N^2} \frac{1}{\eta_s b} \int_0^N dn \int_0^N dm |n - m|^{-\nu}$$

The integral is calculated as

$$\begin{aligned} \int_0^N dn \int_0^N dm |n - m|^{-\nu} &= 2 \int_0^N dn \int_0^n dm (n - m)^{-\nu} \\ &= \frac{2}{1 - \nu} \int_0^N dn n^{1-\nu} = \frac{2}{1 - \nu} \frac{1}{2 - \nu} N^{2-\nu} \end{aligned}$$

**Problem 3.25:** Estimate  $D_G$  and  $\tau_1$  for a polymer chain with  $R_F = 100$  nm in a solvent of  $\eta_s = 1.0$  cP at  $25^\circ\text{C}$  using the Zimm model for the theta solvent.

**Solution 3.25:**

$$\begin{aligned} D_G &= \frac{8}{3(6\pi^3)^{1/2}} \frac{k_B T}{\eta_s R_F} = \frac{8}{3(6\pi^3)^{1/2}} \times \frac{1.38 \times 10^{-23} \text{ J/K} \times 298.15 \text{ K}}{1.0 \times 10^{-3} \text{ kg/(m}\cdot\text{s)} \times 10^{-7} \text{ m}} \\ &= 8.0 \times 10^{-12} \text{ m}^2/\text{s} \\ \tau_1 &= \frac{1}{(3\pi)^{1/2}} \frac{\eta_s R_F^3}{k_B T} = \frac{1}{(3\pi)^{1/2}} \times \frac{1.0 \times 10^{-3} \text{ kg/(m}\cdot\text{s)} \times (10^{-7} \text{ m})^3}{1.38 \times 10^{-23} \text{ J/K} \times 298.15 \text{ K}} = 79 \mu\text{s} \end{aligned}$$

**Problem 3.26:** Use Eq. 3.125 to derive Eq. 3.224 directly.

**Solution 3.26:** From Eq. 3.125,

$$\begin{aligned} \langle [\mathbf{r}_{mn}(t)]^2 \rangle_{mn} &= \langle [\mathbf{q}_0(t) - \mathbf{q}_0(0)]^2 \rangle \\ &+ 4 \sum_{i=1}^N \left\langle \cos^2 \frac{i\pi}{N} [\mathbf{q}_i(t)]^2 + \cos^2 \frac{i\pi}{N} [\mathbf{q}_i(0)]^2 - 2 \cos \frac{i\pi}{N} \cos \frac{i\pi}{N} \mathbf{q}_i(t) \cdot \mathbf{q}_i(0) \right\rangle \end{aligned}$$

where term of  $\mathbf{q}_N$  was incorporated into the sum. The first term is the center-of-mass diffusion. Here, we use Eqs. 3.145, 3.146, and 3.151. Then, the above equation is rewritten to

$$\begin{aligned} \langle [\mathbf{r}_{mn}(t)]^2 \rangle_{mn} &= 6D_G t + 12 \sum_{i=1}^N \frac{k_B T}{k_i} \\ &\times \left[ \cos^2 \frac{i\pi}{N} + \cos^2 \frac{i\pi}{N} - 2 \cos \frac{i\pi}{N} \cos \frac{i\pi}{N} \exp(-t/\tau_i) \right] \end{aligned}$$

At  $t = 0$ ,

$$\langle [\mathbf{r}_{mn}(0)]^2 \rangle_{mn} = 12 \sum_{i=1}^N \frac{k_B T}{k_i} \left( \cos \frac{i\pi}{N} - \cos \frac{i\pi}{N} \right)^2$$

Thus, the evolution of  $\langle [\mathbf{r}_{mn}(t)]^2 \rangle_{mn}$  from its value at  $t = 0$  is given as

$$\begin{aligned} \langle [\mathbf{r}_{mn}(t)]^2 \rangle_{mn} - \langle [\mathbf{r}_{mn}(0)]^2 \rangle_{mn} &= 6D_G t + 24 \sum_{i=1}^N \frac{k_B T}{k_i} \\ &\times \cos \frac{i\pi}{N} \cos \frac{i\pi}{N} [1 - \exp(-t/\tau_i)] \end{aligned}$$

**Problem 3.27:** Where are the intersections between two adjacent time ranges in Figure 3.56?

**Solution 3.27:** Around  $\tau_N$ : the time  $t$  at the intersection between Eqs. 3.238 and 3.243 is obtained from

$$6ND_Gt = 6D_Gt + (2Nb^2/\pi^2)(\pi t/\tau_1)^{1/2}$$

Because  $N \gg 1$ , it is rewritten to  $3D_Gt = (b^2/\pi^2)(\pi t/\tau_1)^{1/2}$ , which leads to

$$t = \frac{b^4}{9\pi^3 D_G^2 \tau_1} = \frac{b^4}{9\pi^3} \frac{(N\zeta)^2}{(k_B T)^2} \frac{3\pi^2 k_B T}{\zeta N^2 b^2} = \frac{1}{3\pi} \frac{b^2 \zeta}{k_B T} = \pi \tau_N$$

Thus we find that the first section extends to  $\sim \tau_N$ .

Around  $\tau_1$ : the time  $t$  at the intersection between Eqs. 3.240 and 3.243 is obtained from

$$6D_Gt + (2Nb^2/\pi^2)(\pi t/\tau_1)^{1/2} = 6D_Gt + \frac{1}{3} Nb^2$$

which is converted to

$$t = \frac{\pi^3}{36} \tau_1 \cong 0.86\tau_1$$

The boundary between the second and third sections is around  $\tau_1$ .

**Problem 3.28:** Where are the intersections between two adjacent time ranges in Figure 3.57?

**Solution 3.28:** Around  $\tau_N$ : the time  $t$  at the intersection between Eqs. 3.245 and 3.248 is obtained from

$$9(N/2)^{1/2} D_G t = 6D_G t + (2\Gamma_{1/3}/\pi^2) N b^2 (t/\tau_1)^{2/3}$$

Because  $N \gg 1$ , the first term on the right-hand side is negligible. Then,

$$t = \left( \frac{2^{3/2} \Gamma_{1/3}}{9\pi^2} \right)^3 \frac{b^6 N^{3/2}}{D_G^3 \tau_1^2} = \frac{\eta_s b^3}{k_B T} \frac{(\Gamma_{1/3})^3}{8(3\pi)^{1/2}} = \frac{(\Gamma_{1/3})^3}{8} \tau_N \cong 2.4\tau_N$$

Thus we find that the first section extends to  $\sim \tau_N$ .

Around  $\tau_1$ : the time  $t$  at the intersection between Eqs. 3.240 and 3.248 is obtained from

$$6D_G t + (2\Gamma_{1/3}/\pi^2) N b^2 (t/\tau_1)^{2/3} = 6D_G t + \frac{1}{3} N b^2$$

which is converted to

$$t = \left( \frac{\pi^2}{6\Gamma_{1/3}} \right)^{3/2} \tau_1 \cong 0.48\tau_1$$

The boundary between the second and third sections is around  $\tau_1$ .

### 3.5 DYNAMICS OF RODLIKE MOLECULES

#### 3.5.1 Diffusion Coefficients

Dynamics of rodlike molecules is quite different from that of linear flexible chains. The rodlike molecule exhibits a well-defined rotational motion in addition to the center-of-mass motion (Fig. 3.58). The latter has two components: parallel to the rod axis and perpendicular to the rod axis. The expressions for the **translational diffusion coefficients**  $D_{\parallel}$  and  $D_{\perp}$  in the directions parallel and perpendicular to the rod axis and the **rotational diffusion coefficient**  $D_r$  were obtained by Kirkwood<sup>41</sup> for a model that consists of  $N$  beads in a straight line.

The diffusion along the rod axis is one-dimensional, and the diffusion in the direction perpendicular to the axis is two-dimensional, because the degree of freedom is 1 and 2 in the two directions, respectively. The three-dimensional diffusion coefficient  $D_G$  of the center of mass is the isotropic mean of  $D_{\parallel}$  and  $D_{\perp}$ , that is,  $D_G = (D_{\parallel} + 2D_{\perp})/3$ . It is expressed as

$$D_G = \frac{k_B T [\ln(L/b) - \gamma]}{3\pi\eta_s L} \quad \text{rodlike molecule} \quad (3.254)$$

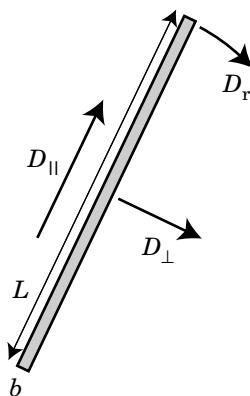


**Figure 3.58.** Rodlike molecule of length  $L$  and diameter  $b$ . The center-of-mass translation has two components, parallel and perpendicular to the rod axis, with the diffusion coefficients  $D_{\parallel}$  and  $D_{\perp}$ . The rod can also rotate around the center with diffusion coefficient  $D_r$ .



where  $L$  is the rod length,  $b$  is the rod diameter ( $b \ll L$ ), and  $\gamma$  is a constant. In the numerator,  $\ln(L/b)$  is the result of hydrodynamic interactions between different parts of the rod; without its correction,  $D_G \sim 1/L$  and thus  $D_G$  would be equal to the diffusion coefficient of  $N$  connected, independent beads (Problem 3.29). The constant  $\gamma$ , a result of the end effect, is around 0.3. The diffusion coefficients  $D_{\parallel}$  and  $D_{\perp}$  are

$$D_{\parallel} = \frac{3}{2}D_G, \quad D_{\perp} = \frac{3}{4}D_G \quad (3.255)$$

The diffusion is faster in the parallel direction than it is in the perpendicular direction. The difference is rather small;  $D_{\parallel}$  is only twice as large as  $D_{\perp}$ .

From Eq. 3.254, we find that the hydrodynamic radius  $R_H$  of the rodlike molecule is given as

$$R_H = \frac{L/2}{\ln(L/b) - \gamma} \quad (3.256)$$

Because the denominator depends only weakly on  $L$ ,  $R_H$  increases nearly linearly with molecular weight. The dependence is much stronger compared with a linear flexible chain.

The rotational diffusion coefficient  $D_r$  was obtained as

$$D_r = \frac{3k_B T [\ln(L/b) - \gamma]}{\pi \eta_s L^3} \quad \text{rodlike molecule} \quad (3.257)$$

and is related to  $D_G$  by  $D_r = 9D_G/L^2$ . Note that  $D_r$  has a dimension of  $s^{-1}$ . The rotational diffusion coefficient has an extremely steep dependence on the molecular weight. A rod twice as long can rotate only at the rate of 1/8 of the shorter rod.

### 3.5.2 Rotational Diffusion

**3.5.2.1 Pure Rotational Diffusion** Here we consider the rotational motion of the rodlike molecule in details. We do not pay attention to the center-of-mass position. Let us define by  $\mathbf{u}(t)$  the unit vector along the rod axis at time  $t$  and place the rodlike molecule in the spherical polar coordinate system (Fig. 3.59). The orientation vector  $\mathbf{u}(t)$  is represented by the polar angle  $\theta$  and the azimuthal angle  $\varphi$ . We define the probability density  $\psi(\theta, \varphi; t)$  for the distribution of  $\mathbf{u}(t)$  in the same way as the concentration represents the population of solute molecules per volume. The probability to find  $\mathbf{u}(t)$  between  $\theta$  and  $\theta + d\theta$  and between  $\varphi$  and  $\varphi + d\varphi$  is  $\psi(\theta, \varphi; t) \sin\theta d\theta d\varphi$ .

The rotational part of the motion is described by the **rotational diffusion equation** for  $\psi(\theta, \varphi; t)$ :

$$\frac{\partial \psi}{\partial t} = D_r \left( \frac{1}{\sin\theta} \frac{\partial}{\partial \theta} \sin\theta \frac{\partial}{\partial \theta} + \frac{1}{\sin^2\theta} \frac{\partial^2}{\partial \varphi^2} \right) \psi \quad (3.258)$$

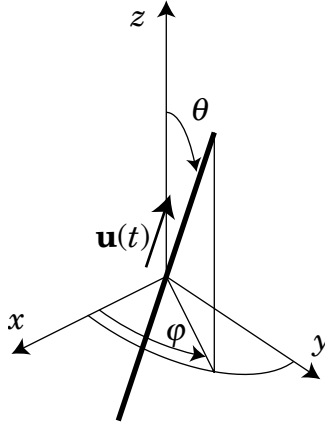


**Figure 3.59.** Rodlike molecule in the spherical polar coordinate system. The orientation of the rod,  $\mathbf{u}$ , is expressed by  $\theta$  and  $\varphi$ .

where the operator in the parenthesis is the orientational part of the Laplacian  $\nabla^2$  in the polar coordinate system. The solution of the diffusion equation is, in general, given as

$$\psi(\theta, \varphi; t) = \sum_{l=0}^{\infty} \sum_{m=-l}^l a_{lm}(t) Y_l^m(\theta, \varphi) \quad (3.259)$$

where  $Y_l^m(\theta, \varphi)$  is the spherical harmonic function ( $l = 0, 1, 2, \dots; m = -l, -l + 1, \dots, l$ ) and  $a_{lm}(t)$  is the expansion coefficient. The same diffusion equation applies to the transition probability  $P(\theta, \varphi; \theta', \varphi'; t)$  from  $(\theta', \varphi')$  to  $(\theta, \varphi)$ .

In some systems,  $\psi(\theta, \varphi; t)$  does not depend on  $\varphi$ . For instance, when we consider how the probability density  $\psi(\mathbf{u}; t)$  evolves for a rod with  $\mathbf{u}(0)$  parallel to the polar axis, the distribution is a function of  $\theta$  and  $t$  only. Another example is a rodlike molecule that has a permanent dipole moment along the axis in an electric field. The natural choice of the polar axis is the direction of the electric field. When  $\psi$  depends on  $\theta$  and  $t$  only, the rotational diffusion equation is simplified to

$$\frac{\partial \psi}{\partial t} = D_r \frac{1}{\sin \theta} \frac{\partial}{\partial \theta} \sin \theta \frac{\partial \psi}{\partial \theta} \quad \text{rotational diffusion, uniaxial} \quad (3.260)$$

Then,  $\psi(\theta, \varphi; t)$  is expanded in  $Y_l^0(\theta, \varphi) \propto P_l(\cos \theta)$  only:

$$\psi(\theta; t) = \sum_{l=0}^{\infty} a_l(t) P_l(\cos \theta) \quad (3.261)$$

where  $P_l(x)$  is the  $l$ th Legendre polynomial ( $l = 0, 1, 2, \dots$ ). The first few functions are  $P_0(x) = 1$ ,  $P_1(x) = x$ ,  $P_2(x) = (3x^2 - 1)/2$ .

We apply Eq. 3.260 to consider how fast the correlation of the rod orientation is lost. We place the polar axis in the direction of  $\mathbf{u}(0)$  and consider how  $\langle \mathbf{u}(t) \cdot \mathbf{u}(0) \rangle = \langle \cos\theta \rangle = \langle P_l(\cos\theta) \rangle$  changes with time. The statistical average is calculated with a weight of  $\sin\theta$ . From Eq. 3.260,

$$\begin{aligned} \frac{d\langle \cos\theta \rangle}{dt} &= \frac{d}{dt} \int_0^\pi \cos\theta \psi \sin\theta d\theta = D_r \int_0^\pi \sin\theta \cos\theta \frac{1}{\sin\theta} \frac{\partial}{\partial \theta} \sin\theta \frac{\partial \psi}{\partial \theta} d\theta \\ &= -2D_r \int_0^\pi \cos\theta \psi \sin\theta d\theta = -2D_r \langle \cos\theta \rangle \end{aligned} \quad (3.262)$$

where integration by parts was used twice. Likewise, we can show that (Problem 3.20)

$$\frac{d\langle P_l(\cos\theta) \rangle}{dt} = -l(l+1)D_r \langle P_l(\cos\theta) \rangle \quad (3.263)$$

Note that, at  $t = 0$ ,  $\langle P_l(\cos\theta) \rangle = \langle P_l(1) \rangle = 1$ . Then,  $\langle P_l(\cos\theta) \rangle$  relaxes with time according to

$$\langle P_l(\cos\theta) \rangle = \exp(-t/\tau_l) \quad (3.264)$$

with a relaxation time  $\tau_l = [l(l+1)D_r]^{-1}$ . The  $l$ th orientational correlation is lost with  $\tau_l$ .

Rotational motion of the rodlike molecule can be viewed as the motion of its end point on the surface of a sphere with the rod as its diameter (Fig. 3.60). Over a short period of time ( $D_r t \ll 1$ ),  $\theta \ll 1$  and therefore  $\langle P_l(\cos\theta) \rangle = \langle \cos\theta \rangle \cong \langle 1 - \theta^2/2 \rangle = 1 - \langle \theta^2 \rangle/2$ . The right-hand side of Eq. 3.264 is  $\cong 1 - t/\tau_1 = 1 - 2D_r t$ . Thus,  $\langle \theta^2 \rangle = 4D_r t$ . The end point makes a two-dimensional diffusion. Over a longer period of

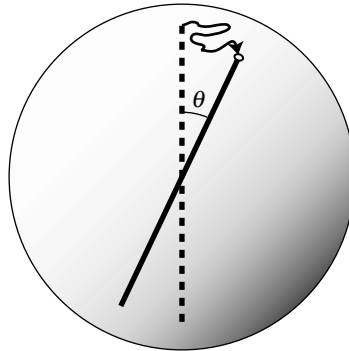


**Figure 3.60.** Rotational motion a rodlike molecule can be regarded as the motion of its end point on the sphere surface.

time, however, the mean square displacement loses a meaning in the rotational diffusion.

**3.5.2.2 Translation-Rotational Diffusion** We consider both the center-of-mass translation and the rotation now. The transition probability  $P(\mathbf{r}_G, \mathbf{u}; \mathbf{r}'_G, \mathbf{u}'; t)$  from  $(\mathbf{r}'_G, \mathbf{u}')$  at time 0 to  $(\mathbf{r}_G, \mathbf{u})$  at time  $t$  follows the diffusion equation:

$$\frac{\partial P}{\partial t} = D_t \nabla_{\mathbf{u}}^2 P + \frac{\partial}{\partial \mathbf{r}_G} \cdot [D_{\parallel} \mathbf{u} \mathbf{u} + D_{\perp} (\mathbf{I} - \mathbf{u} \mathbf{u})] \cdot \frac{\partial P}{\partial \mathbf{r}_G} \quad (3.265)$$

where  $\nabla_{\mathbf{u}}^2$  represents the differential operator in Eq. 3.258. The diffusivity is now anisotropic. The centroid diffusion constant  $D = D_{\parallel} \mathbf{u} \mathbf{u} + D_{\perp} (\mathbf{I} - \mathbf{u} \mathbf{u})$  is not a simple scalar but a tensor of the second rank. Note that, in the polar spherical coordinate system,

$$\mathbf{u} \mathbf{u} = \begin{bmatrix} 1 & 0 & 0 \\ 0 & 0 & 0 \\ 0 & 0 & 0 \end{bmatrix}, \quad \mathbf{I} - \mathbf{u} \mathbf{u} = \begin{bmatrix} 0 & 0 & 0 \\ 0 & 1 & 0 \\ 0 & 0 & 1 \end{bmatrix} \quad (3.266)$$

Therefore,  $D = D_{\parallel}$  in the direction of  $\mathbf{u}$ , and  $D = D_{\perp}$  in the direction perpendicular to  $\mathbf{u}$ . Upon integrating with respect to  $\mathbf{r}_G$ , Eq. 3.265 reduces to Eq. 3.258.

### 3.5.3 Dynamic Structure Factor

We consider the dynamic structure factor of a rodlike molecule. The long-time behavior is rather trivial. The orientational distribution will be averaged, and the center-of-mass diffusion alone will survive. Then,

$$S_1(\mathbf{k}, t)/S_1(\mathbf{k}, 0) \cong \exp(-D_G \mathbf{k}^2 t) \quad \text{long time} \quad (3.267)$$

The short-time behavior in the small  $\mathbf{k}$  limit is also given by this equation. To consider the short-time behavior for large  $\mathbf{k}$ , we first rewrite Eq. 3.46 into

$$S_1(\mathbf{k}, t) = \frac{1}{N} \sum_{m,n=1}^N \langle \exp[i\mathbf{k} \cdot (\mathbf{r}_m(t) - \mathbf{r}_n(0))] \rangle \quad (3.268)$$

where monomers  $m$  and  $n$  are distributed uniformly along the rod. For the short-time behavior, we can write

$$\mathbf{r}_m(t) - \mathbf{r}_n(0) = x_{mn}(0) \mathbf{u} + \mathbf{u} \Delta x + \Delta \mathbf{v} + r_m \Delta \mathbf{u} \quad (3.269)$$

where  $\mathbf{u}$  is the rod orientation at time zero,  $x_{mn}(0)$  is the distance between the two monomers at time zero. The center-of-mass displacement in time  $t$  is  $\Delta x$  along the

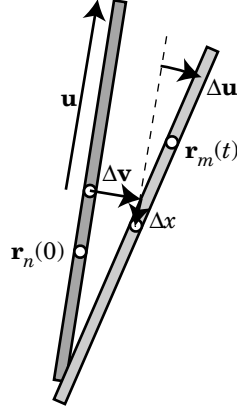


**Figure 3.61.** Short time motion of the rodlike molecule consists of the center-of-mass translation ( $\Delta x$  and  $\Delta v$  in the directions parallel and perpendicular to the rod axis) and rotation  $\Delta u$ .

rod axis and  $\Delta v$  in the perpendicular direction. Rotation in time  $t$  is  $\Delta u$ , and  $r_m$  is the distance of the  $m$ th bead from the center (see Fig. 3.61).

The center-of-mass motions in the two directions and the rotational motion are mutually independent. For a given  $\mathbf{u}$ ,

$$\begin{aligned} \langle \exp(i\mathbf{k} \cdot [\mathbf{r}_m(t) - \mathbf{r}_n(0)]) \rangle_{\mathbf{u}} &= \langle \exp[i\mathbf{k} \cdot \mathbf{u} x_{mm}(0)] \rangle_{\mathbf{u}} \langle \exp(i\mathbf{k} \cdot \mathbf{u} \Delta x) \rangle_{\mathbf{u}} \\ &\times \langle \exp(i\mathbf{k} \cdot \Delta \mathbf{v}) \rangle_{\mathbf{u}} \langle \exp(i\mathbf{k} \cdot \Delta \mathbf{u} r_m) \rangle_{\mathbf{u}} \end{aligned} \quad (3.270)$$

We calculate each term separately. When  $\mathbf{k}$  is large,  $\exp(i\mathbf{k} \cdot \mathbf{u} \Delta x)$  is a rapidly varying function. Its average is contributed mostly from small  $\Delta x$ . Then, we can regard that the random variable  $\Delta x$  is distributed with a normal distribution that has a zero mean and a variance of  $2D_{\parallel}t$ . Thus

$$\begin{aligned} \langle \exp(i\mathbf{k} \cdot \mathbf{u} \Delta x) \rangle_{\mathbf{u}} &= \int_{-\infty}^{\infty} \exp(ik_{\parallel} \Delta x) (4\pi D_{\parallel}t)^{-1/2} \exp\left(-\frac{\Delta x^2}{4D_{\parallel}t}\right) d\Delta x \\ &= \exp(-D_{\parallel} k_{\parallel}^2 t) \end{aligned} \quad (3.271)$$

where  $k_{\parallel} = \mathbf{k} \cdot \mathbf{u}$  is the parallel component of  $\mathbf{k}$ . Likewise, the random variable  $\Delta \mathbf{v}$  is distributed with a two-dimensional normal distribution that has a zero mean and a variance of  $4D_{\perp}t$ . Thus

$$\langle \exp(i\mathbf{k} \cdot \Delta \mathbf{v}) \rangle_{\mathbf{u}} = \int_{-\infty}^{\infty} \exp(i\mathbf{k} \cdot \Delta \mathbf{v}) (4\pi D_{\perp}t)^{-1} \exp\left(-\frac{\Delta \mathbf{v}^2}{4D_{\perp}t}\right) d\Delta \mathbf{v} = \exp(-D_{\perp} k_{\perp}^2 t) \quad (3.272)$$

where  $k_{\perp}^2 = \mathbf{k}^2 - (\mathbf{k} \cdot \mathbf{u})^2$  is the square of the perpendicular component of  $\mathbf{k}$ . Likewise,  $\Delta \mathbf{u}$  is distributed with a two-dimensional normal distribution that has a zero mean and a variance of  $4D_r t$ . Thus

$$\begin{aligned} \langle \exp(i\mathbf{k} \cdot \Delta \mathbf{u} r_m) \rangle_{\mathbf{u}} &= \int_{-\infty}^{\infty} \exp(i\mathbf{k} \cdot \Delta \mathbf{u} r_m) (4\pi D_r t)^{-1} \exp\left(-\frac{\Delta \mathbf{u}^2}{4D_r t}\right) d\Delta \mathbf{u} \\ &= \exp(-D_r k_{\perp}^2 t r_m^2) \end{aligned} \quad (3.273)$$

All combined,

$$\langle \exp(i\mathbf{k} \cdot [\mathbf{r}_m(t) - \mathbf{r}_n(0)]) \rangle_{\mathbf{u}} = \langle \exp[i\mathbf{k} \cdot \mathbf{u} x_{mm}(0)] \rangle_{\mathbf{u}} \exp(-D_{\parallel} k_{\parallel}^2 t - (D_{\perp} + D_r r_m^2) k_{\perp}^2 t) \quad (3.274)$$

Averaging with respect to  $r_m$  cannot be done analytically. We evaluate the initial slope of  $\ln S_1(\mathbf{k}, t)$ . It is equal to the initial slope of  $\langle \exp(i\mathbf{k} \cdot [\mathbf{r}_m(t) - \mathbf{r}_n(0)]) \rangle_{\mathbf{u}}$ :

$$\left. \frac{\partial}{\partial t} \langle \exp(i\mathbf{k} \cdot [\mathbf{r}_m(t) - \mathbf{r}_n(0)]) \rangle_{\mathbf{u}} \right|_{t=0} = -D_{\parallel} k_{\parallel}^2 - (D_{\perp} + D_r r_m^2) k_{\perp}^2 \quad (3.275)$$

for given  $\mathbf{u}$  and  $r_m$ . Now we take the average with respect to  $\mathbf{u}$  and  $r_m$ . First,  $r_m$  is uniformly distributed in  $[-L/2, L/2]$ . Therefore, the average of  $r_m^2$  is  $L^2/12$ . The average of  $k_{\parallel}^2$  with respect to  $\mathbf{u}$  is calculated as

$$\langle k_{\parallel}^2 \rangle = \int_0^{\pi} k^2 \cos^2 \theta \sin \theta \, d\theta \int_0^{\pi} \sin \theta \, d\theta = \frac{1}{3} k^2 \quad (3.276)$$

Then,  $\langle k_{\perp}^2 \rangle = (2/3)k^2$ . Thus the average of Eq. 3.275 is

$$\left. \frac{\partial}{\partial t} \ln S_1(\mathbf{k}, t) \right|_{t=0} = -\left[ \frac{1}{3} D_{\parallel} + \frac{2}{3} D_{\perp} + \frac{1}{18} D_r L^2 \right] k^2 = -\left[ D_G + \frac{1}{18} D_r L^2 \right] k^2 \quad (3.277)$$

With  $D_r = 9D_G/L^2$ ,

$$\left. \frac{\partial}{\partial t} \ln S_1(\mathbf{k}, t) \right|_{t=0} = -\frac{3}{2} D_G k^2 \quad (3.278)$$

Rotational motion makes the initial decay slightly faster at large  $\mathbf{k}$ .

Unlike the linear flexible chains, the initial decay rate at large  $\mathbf{k}$  is proportional to  $\mathbf{k}^2$  (Table 3.4). The difference is ascribed to the comparable diffusion coefficients (including  $L^2 D_r = 9D_G$ ) in the five modes of motion in the rodlike molecule. In the normal modes of a linear flexible chain, in contrast, higher-order modes have a significantly shorter relaxation time compared with the first mode.

### 3.5.4 Intrinsic Viscosity

In Section 3.3.3, we learned that the Mark-Houwink-Sakurada exponent greater than 1 indicates a stiffness in the chain conformation. Here, we consider the intrinsic viscosity of the rodlike molecule. However, calculation of the excess stress is tedious. We look at the result only. To the linear order of  $\kappa$ , the excess stress  $\Delta\sigma_{\alpha\beta}$  is given as

$$\Delta\sigma_{\alpha\beta} = \frac{N_A c}{M} \frac{2}{15} \frac{k_B T}{D_r} (\kappa_{\alpha\beta} + \kappa_{\beta\alpha}) \quad (3.279)$$

In the shear flow given by Eq. 3.107,

$$\Delta\sigma_{xy} = \frac{N_A c}{M} \frac{2}{15} \frac{k_B T}{D_r} \kappa \quad (3.280)$$

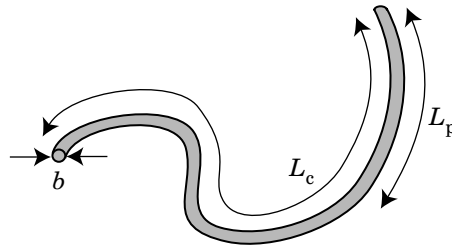
Then with Eq. 3.109, the intrinsic viscosity calculated from the zero-shear viscosity is given as

$$[\eta] = \frac{N_A}{M} \frac{2}{15} \frac{k_B T}{D_r \eta_s} = \frac{2\pi}{45} \frac{N_A}{M} \frac{L^3}{\ln(L/b) - \gamma} \quad (3.281)$$

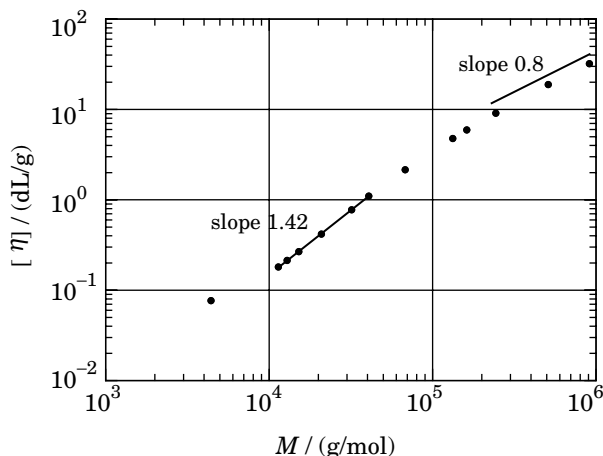
The molecular weight dependent factor in  $[\eta]$  is  $(L^3/M)(\ln(L/b) - \gamma)^{-1}$ . The dependence is weaker than  $M^2$  because of the  $\ln M$  term in the denominator (Table 3.3).

### 3.5.5 Dynamics of Wormlike Chains

A wormlike chain is specified by the persistence length  $L_c$  and the contour length  $L_p$ . However, it does not have a thickness. We need to give it a diameter  $b$  for the chain to have a finite diffusion coefficient. The model is called a wormlike cylinder (Fig. 3.62). The expressions for the center-of-mass diffusion coefficient and the intrinsic viscosity were derived by Yamakawa et al.<sup>42</sup> in the rigid-rod asymptote and the flexible-chain asymptote in a series of  $b/L_c$  and  $L_c/L_p$ .



**Figure 3.62.** Wormlike cylinder has a finite thickness  $b$  in addition to the nature of the wormlike chain.



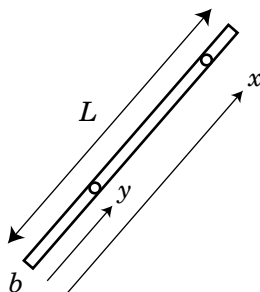
**Figure 3.63.** Intrinsic viscosity  $[\eta]$  of a semirigid polymer, plotted as a function of the molecular weight  $M$ . The sample is poly(*n*-hexyl isocyanate) in toluene at 25°C. The molecular weight dependence of  $[\eta]$  shows a cross-over from  $\sim M^{1.42}$  to  $\sim M^{0.8}$  with an increasing  $M$ . (From Ref. 43.)

Figure 3.63 shows the intrinsic viscosity of poly(*n*-hexyl isocyanate) in toluene at 25°C.<sup>43</sup> The polymer is semirigid with  $L_p \cong 37$  nm and  $b \cong 1.6$  nm. The slope of the tangent decreases from 1.4 to 0.8 with an increasing  $M$ . The locally rigid chain follows the viscosity law of the flexible chain when the molecular weight is sufficiently high.

### 3.5.6 PROBLEMS

**Problem 3.29:** Use the general formula, Eq. 3.55, to calculate the hydrodynamic radius of a rodlike molecule with length  $L$  and diameter  $b$ . The average between two beads at  $x$  and  $y$  on the rod measured from one of the ends is calculated only for  $|x - y| > b$ .

**Solution 3.29:**





$$\begin{aligned}
\frac{1}{R_H} &= \left\langle \frac{1}{|x-y|} \right\rangle = \frac{2}{(L-b)^2} \int_b^L dx \int_0^{x-b} dy \frac{1}{x-y} \\
&= \frac{2}{(L-b)^2} \int_b^L dx (\ln x - \ln b) = \frac{2}{(L-b)^2} L (\ln(L/b) - 1 + b/L) \\
&\cong \frac{2}{L} [\ln(L/b) - 1 + (2b/L)\ln(L/b)]
\end{aligned}$$

This rough method gives the same result as Eq. 3.256 to the leading order.

**Problem 3.30:** The Legendre polynomial  $P_l(z)$  satisfies the following differential equation:

$$(1-z^2) \frac{d^2 P_l(z)}{dz^2} - 2z \frac{dP_l(z)}{dz} + l(l+1)P_l(z) = 0$$

Prove Eq. 3.263.

**Solution 3.30:** Using the integral by parts leads to

$$\begin{aligned}
\frac{d\langle P_l(\cos\theta) \rangle}{dt} &= \frac{d}{dt} \int_0^\pi P_l(\cos\theta) \psi \sin\theta d\theta = D_r \int_0^\pi P_l(\cos\theta) \frac{\partial}{\partial \theta} \sin\theta \frac{\partial \psi}{\partial \theta} d\theta \\
&= D_r \int_0^\pi P_l'(\cos\theta) \sin^2\theta \frac{\partial \psi}{\partial \theta} d\theta \\
&= D_r \int_0^\pi [\sin^2\theta P_l''(\cos\theta) - 2\cos\theta P_l'(\cos\theta)] \psi \sin\theta d\theta
\end{aligned}$$

where  $P_l'(z)$  and  $P_l''(z)$  denote the first- and second-order derivatives of  $P_l(z)$ . Use of the above differential equation converts this equation into

$$\frac{d\langle P_l(\cos\theta) \rangle}{dt} = -l(l+1) D_r \int_0^\pi P_l(\cos\theta) \psi \sin\theta d\theta = -l(l+1) D_r \langle P_l(\cos\theta) \rangle$$

### APPENDIX 3.A: EVALUATION OF $\langle \mathbf{q}_i^2 \rangle_{\text{eq}}$

The amplitude of  $\mathbf{q}_i$  at equilibrium can be directly evaluated from its definition by Eq. 3.118. Because it is an equilibrium property, it has nothing to do with the hydrodynamic interactions. It depends only on the chain statistics as shown below. Here, we use the integral form of Eq. 3.118, that is,

$$\mathbf{q}_i = \frac{1}{N} \int_0^N dn \mathbf{r}_n \cos \frac{in\pi}{N} \quad (3.A.1)$$

to calculate  $\langle \mathbf{q}_i^2 \rangle$ :

$$\begin{aligned} \langle \mathbf{q}_i^2 \rangle &= \frac{1}{N^2} \int_0^N \mathbf{d}n \int_0^N \mathbf{d}m \langle \mathbf{r}_n \cdot \mathbf{r}_m \rangle \cos \frac{in\pi}{N} \cos \frac{im\pi}{N} \\ &= \frac{1}{(i\pi)^2} \int_0^N \mathbf{d}n \int_0^N \mathbf{d}m \frac{\partial^2}{\partial n \partial m} \langle \mathbf{r}_n \cdot \mathbf{r}_m \rangle \sin \frac{in\pi}{N} \sin \frac{im\pi}{N} \quad (3.A.2) \\ &= -\frac{1}{2(i\pi)^2} \int_0^N \mathbf{d}n \int_0^N \mathbf{d}m \frac{\partial^2}{\partial n \partial m} \langle (\mathbf{r}_n - \mathbf{r}_m)^2 \rangle \sin \frac{in\pi}{N} \sin \frac{im\pi}{N} \end{aligned}$$

where integration by parts was used, and the last equality is due to the identity:  $\langle \partial^2 / \partial n \partial m \rangle \langle \mathbf{r}_n \cdot \mathbf{r}_m \rangle = -(1/2) \langle \partial^2 / \partial n \partial m \rangle \langle (\mathbf{r}_n - \mathbf{r}_m)^2 \rangle$ . Now we use  $\langle (\mathbf{r}_n - \mathbf{r}_m)^2 \rangle = b^2 |n - m|^{2\nu}$ . Then,

$$\begin{aligned} \langle \mathbf{q}_i^2 \rangle &= \nu(2\nu - 1) \frac{b^2}{(i\pi)^2} \int_0^N \mathbf{d}n \int_0^N \mathbf{d}m |n - m|^{2\nu-2} \sin \frac{in\pi}{N} \sin \frac{im\pi}{N} \\ &= \nu \left( \nu - \frac{1}{2} \right) \frac{b^2}{(i\pi)^2} \int_0^N \mathbf{d}n \int_0^N \mathbf{d}m |n - m|^{2\nu-2} \left[ \cos \frac{i(n-m)\pi}{N} - \cos \frac{i(n+m)\pi}{N} \right] \quad (3.A.3) \end{aligned}$$

Here, we change the variables of integration from  $n$  and  $m$  to  $u = n - m$  and  $v = n + m$ . Then,

$$\begin{aligned} \langle \mathbf{q}_i^2 \rangle &= \nu \left( \nu - \frac{1}{2} \right) \frac{b^2}{2(i\pi)^2} \left[ \int_{-N}^0 \mathbf{d}u \int_{-u}^{2N+u} \mathbf{d}v (-u)^{2\nu-2} \left( \cos \frac{iu\pi}{N} - \cos \frac{iv\pi}{N} \right) \right. \\ &\quad \left. + \int_0^N \mathbf{d}u \int_u^{2N-u} \mathbf{d}v u^{2\nu-2} \left( \cos \frac{iu\pi}{N} - \cos \frac{iv\pi}{N} \right) \right] \\ &= \nu(2\nu - 1) \frac{Nb^2}{(i\pi)^2} \left[ \int_0^N \mathbf{d}u u^{2\nu-2} \cos \frac{iu\pi}{N} + \frac{2\nu}{i\pi} \int_0^N \mathbf{d}u u^{2\nu-2} \sin \frac{iu\pi}{N} \right] \quad (3.A.4) \end{aligned}$$

When  $N \gg 1$ , the upper limit of the integral can be replaced by  $\infty$ . Then, with Eqs. A3.2 and A3.4,

$$\begin{aligned} \langle \mathbf{q}_i^2 \rangle &= \nu(2\nu - 1) \frac{Nb^2}{(i\pi)^2} \left[ \int_0^\infty \mathbf{d}u u^{2\nu-2} \cos \frac{iu\pi}{N} + \frac{2\nu}{i\pi} \int_0^\infty \mathbf{d}u u^{2\nu-2} \sin \frac{iu\pi}{N} \right] \\ &= \nu(2\nu - 1) \frac{Nb^2}{(i\pi)^2} \frac{\Gamma(2\nu - 1)}{(i\pi/N)^{2\nu-1}} \left[ \cos \frac{(2\nu - 1)\pi}{2} + \frac{2\nu}{i\pi} \sin \frac{(2\nu - 1)\pi}{2} \right] \\ &\cong \frac{b^2 N^{2\nu}}{i^{2\nu+1}} \quad (3.A.5) \end{aligned}$$

Because of the approximations we used,  $\langle \mathbf{q}_i^2 \rangle$  vanishes when  $\nu = 1/2$ . The exponents are correct, however, in the final result.

**APPENDIX 3.B: EVALUATION OF  $\langle \exp[i\mathbf{k} \cdot (A\mathbf{q} - B\mathbf{p})] \rangle$** 

We obtain a formula for the statistical average of  $\exp[i\mathbf{k} \cdot (A\mathbf{q} - B\mathbf{p})]$ , where  $A$  and  $B$  are constants, and three-dimensional Gaussian random variables  $\mathbf{p}$  and  $\mathbf{q}$  are distributed with  $f_{\mathbf{p}}(\mathbf{p})$  and  $f_{\mathbf{Q}}(\mathbf{q}; \mathbf{p})$ , respectively:

$$f_{\mathbf{p}}(\mathbf{p}) = (2\pi\sigma^2)^{-3/2} \exp(-\mathbf{p}^2/2\sigma^2) \quad (3.B.1)$$

$$f_{\mathbf{Q}}(\mathbf{q}; \mathbf{p}) = (2\pi\sigma_Q^2)^{-3/2} \exp[-(\mathbf{q} - \mathbf{p} \exp(-t/\tau))^2/2\sigma_Q^2] \quad (3.B.2)$$

with

$$\sigma^2 = \langle \mathbf{p}^2 \rangle / 3 \quad (3.B.3)$$

and

$$\sigma_Q^2 \equiv \sigma^2(1 - \exp(-2t/\tau)) \quad (3.B.4)$$

At  $t = 0$ ,  $f_{\mathbf{Q}}(\mathbf{q}; \mathbf{p}) = \delta(\mathbf{q} - \mathbf{p})$ . At  $t \rightarrow \infty$ ,  $\mathbf{q}$  becomes independent of  $\mathbf{p}$ . The average is expressed as

$$\langle \exp[i\mathbf{k} \cdot (A\mathbf{q} - B\mathbf{p})] \rangle = \int f_{\mathbf{p}}(\mathbf{p}) d\mathbf{p} \int f_{\mathbf{Q}}(\mathbf{q}; \mathbf{p}) d\mathbf{q} \exp[i\mathbf{k} \cdot (A\mathbf{q} - B\mathbf{p})] \quad (3.B.5)$$

First, the integration with respect to  $\mathbf{q}$  is calculated as

$$\begin{aligned} \int d\mathbf{q} f_{\mathbf{Q}}(\mathbf{q}; \mathbf{p}) \exp(iA\mathbf{k} \cdot \mathbf{q}) &= (2\pi\sigma_Q^2)^{-3/2} \\ &\times \int d\mathbf{q} \exp\left[-(\mathbf{q} - \mathbf{p} \exp(-t/\tau) - i\sigma_Q^2 A\mathbf{k})^2/2\sigma_Q^2 + iA\mathbf{k} \cdot \mathbf{p} \exp(-t/\tau) \right. \\ &\quad \left. - \frac{1}{2}\sigma_Q^2 A^2 \mathbf{k}^2\right] \\ &= \exp\left[iA\mathbf{k} \cdot \mathbf{p} \exp(-t/\tau) - \frac{1}{2}\sigma_Q^2 A^2 \mathbf{k}^2\right] \end{aligned} \quad (3.B.6)$$

Then, the overall average is given as

$$\begin{aligned} \langle \exp[i\mathbf{k} \cdot (A\mathbf{q} - B\mathbf{p})] \rangle &= \exp\left[-\frac{1}{2}\sigma_Q^2 A^2 \mathbf{k}^2\right] (2\pi\sigma^2)^{-3/2} \\ &\times \int d\mathbf{p} \exp\left[-[\mathbf{p} + i\mathbf{k}\sigma^2(B - A \exp(-t/\tau))]^2/2\sigma^2 \right. \\ &\quad \left. - \frac{1}{2}\sigma^2 \mathbf{k}^2 (B - A \exp(-t/\tau))^2\right] \\ &= \exp\left[-\frac{1}{2}\mathbf{k}^2 \sigma^2 (A^2 + B^2 - 2AB \exp(-t/\tau))\right] \end{aligned} \quad (3.B.7)$$

### APPENDIX 3.C: INITIAL SLOPE OF $S_1(\mathbf{k}, t)$

We evaluate  $A \equiv$  numerator in Eq. 3.210 for the ideal-chain conformation,  $\langle \exp[i\mathbf{k} \cdot \mathbf{r}_{mn}(0)] \rangle_{mn} = \exp(-b^2\mathbf{k}^2|n-m|/6)$ .

$$\begin{aligned}
A &\equiv \sum_{m,n=1}^N \exp\left(-\frac{b^2\mathbf{k}^2}{6}|n-m|\right) \sum_{i=1}^N \frac{k_B T}{\zeta_i} \cos \frac{in\pi}{N} \cos \frac{im\pi}{N} \\
&\equiv \int_0^N dn \int_0^N dm \exp\left(-\frac{b^2\mathbf{k}^2}{6}|n-m|\right) \sum_{i=1}^N \frac{k_B T}{\zeta_i} \cos \frac{in\pi}{N} \cos \frac{im\pi}{N} \\
&= \int_0^N dn \exp(-b^2\mathbf{k}^2 n/6) \int_0^n dm \exp(b^2\mathbf{k}^2 m/6) \sum_{i=1}^N \frac{k_B T}{\zeta_i} \\
&\quad \times \left( \cos \frac{i(n-m)\pi}{N} + \cos \frac{i(n+m)\pi}{N} \right) \\
&= \operatorname{Re} \sum_{i=1}^N \frac{k_B T}{\zeta_i} \int_0^N dn \exp(-b^2\mathbf{k}^2 n/6) \int_0^n dm \exp(b^2\mathbf{k}^2 m/6) \\
&\quad \times (\exp(ii(n-m)\pi/N) + \exp(ii(n+m)\pi/N)) \\
&= \operatorname{Re} \sum_{i=1}^N \frac{k_B T}{\zeta_i} \int_0^N dn \exp(-b^2\mathbf{k}^2 n/6 + iin\pi/N) \int_0^n dm \\
&\quad \times (\exp[(b^2\mathbf{k}^2/6 - ii\pi/N)m] + \exp[(b^2\mathbf{k}^2/6 + ii\pi/N)m]) \quad (3.C.1)
\end{aligned}$$

After integration with respect to  $m$ ,

$$\begin{aligned}
A &= \operatorname{Re} \sum_{i=1}^N \frac{k_B T}{\zeta_i} \int_0^N dn \left[ \frac{1 - \exp[-(b^2\mathbf{k}^2/6 - ii\pi/N)n]}{b^2\mathbf{k}^2/6 - ii\pi/N} \right. \\
&\quad \left. + \frac{\exp(i2in\pi/N) - \exp[-(b^2\mathbf{k}^2/6 - ii\pi/N)n]}{b^2\mathbf{k}^2/6 + ii\pi/N} \right] \\
&= \operatorname{Re} \sum_{i=1}^N \frac{k_B T}{\zeta_i} \frac{1}{b^2\mathbf{k}^2/6 - ii\pi/N} \left\{ N - \frac{1 - (-1)^i \exp(-Nb^2\mathbf{k}^2/6)}{b^2\mathbf{k}^2/6 - ii\pi/N} \right. \\
&\quad \left. - \frac{1 - (-1)^i \exp(-Nb^2\mathbf{k}^2/6)}{b^2\mathbf{k}^2/6 + ii\pi/N} \right\} \quad (3.C.2) \\
&= \sum_{i=1}^N \frac{k_B T}{\zeta_i} \frac{b^2\mathbf{k}^2/6}{(b^2\mathbf{k}^2/6)^2 + (i\pi/N)^2} \left[ N - \frac{(b^2\mathbf{k}^2/3)[1 - (-1)^i \exp(-Nb^2\mathbf{k}^2/6)]}{(b^2\mathbf{k}^2/6)^2 + (i\pi/N)^2} \right]
\end{aligned}$$

The second term in the square bracket is negligible compared with  $N$  in both the small  $\mathbf{k}$  and large  $\mathbf{k}$  limits. Therefore,

$$A \cong N \sum_{i=1}^N \frac{k_B T}{\zeta_i} \frac{b^2 \mathbf{k}^2 / 6}{(b^2 \mathbf{k}^2 / 6)^2 + (i\pi/N)^2} = N^2 \sum_{i=1}^N \frac{k_B T}{\zeta_i} \frac{k^2 R_g^2}{(k^2 R_g^2)^2 + (i\pi)^2} \quad (3.C.3)$$

---

# 4

---

## Thermodynamics and Dynamics of Semidilute Solutions

### 4.1 SEMIDILUTE POLYMER SOLUTIONS

So far we have paid attention mostly to dilute solutions,  $c < c^*$ , in which polymer chains are more or less separated from each other. Chapter 2 focused on thermodynamics, and Chapter 3 focused on dynamics. These solutions were mostly ideal. We also learned how the concentration  $c$  might change the thermodynamics and dynamics, as represented by the osmotic pressure and the diffusion coefficient, from those in the ideally dilute solutions.

This chapter is about semidilute solutions,  $c > c^*$ . We learn both thermodynamics and dynamics. The properties of semidilute solutions are drastically different from those of dilute solutions. With a mere tenfold increase in the concentration, the osmotic pressure can easily increase by a factor of several hundred. In the ideal solution, in contrast, the osmotic pressure is proportional to  $c$ . Furthermore, the overall chain motion is slow in semidilute solutions because the chains are entangled: semidilute solutions of a high-molecular-weight polymer can barely flow. The solutions are highly viscous and may even behave like elastic rubber.

The osmotic pressure and the time scale of motion depend heavily on concentration and molecular weight. The dependence is universal for a certain class of solutions; each class, however, exhibits a characteristic dependence. For many years, we had not had a good understanding of those characteristics until the blob concept, the scaling theory, and the reptation model were introduced in 1970s.<sup>44,45</sup> With simple ideas and simple mathematics, these concepts elegantly explained the observed complicated dependence.

Semidilute solution,  $c > c^*$ , is unique to polymer solutions. Because  $c^*$  is low, the semidilute regime extends to a low concentration (in terms of g/L). As we have

seen in Section 1.8, polystyrene of  $M = 3 \times 10^5$  g/mol has  $c^* \cong 13$  g/L. The upper limit of the semidilute range is sometimes denoted by  $c^{**}$ . Above  $c^{**}$ , the monomers are congested and the solution is sometimes called concentrated (it is not a well-defined term). In semidilute solutions, monomers are not congested, but polymer chains have many other chains overlapping them. The chains as a whole are congested, and the interactions between the chains are therefore strong. With a further increase in  $c$ , the overlaps become more serious. In contrast, in solutions of a low-molecular-weight nonionic compound, the low concentration (in g/L) promises weak interactions between the solute molecules.

The semidilute regime is often specified by  $c^* \ll c < c^{**}$ . With  $c^*$  at around 10 g/L for polystyrene of  $M_w = 6 \times 10^5$  g/mol, for instance, and  $c^{**}$  at around 300 g/L, the double inequality may appear to impose a severe restriction on the accessibility by an ordinary polymer. In practice, however, solutions several times as concentrated as  $c^*$  already qualify as semidilute solutions. With ambiguity in the definition of  $c^*$  (Eqs. 1.108–1.110), it does not make sense to ask how high the concentration should be for the solution to be semidilute. As we will see in many experimental results, there is an easy way to find whether or not the concentration is sufficiently high.

In Section 4.2, we will learn about the thermodynamics of semidilute solutions. We will consider linear flexible chains only. The mean-field theory explained in Section 2.2 is assumed to be effective in a whole range of concentrations. The theory, however, fails to explain various experimental results. The failure can be ascribed to the stronger interactions between chain molecules consisting of covalently bonded monomers compared with the mean-field interactions that do not distinguish bonded monomers from nonbonded monomers. Fortunately, the blob model and the scaling theory explain the thermodynamics that characterize semidilute solutions.

Section 4.3 focuses on dynamics. We will first examine the overall concentration fluctuations of highly entangled chains. We will then look at the motions of each chain through the maze of other chains.

In this chapter, we attach the subscript “0” to denote the value of the relevant quantity in the dilute solution limit. For instance,  $R_{g0}$  is the root-mean-square radius of gyration,  $R_g$ , in solutions at sufficiently low concentrations. It may appear strange that the chain size changes with concentration, but, as we will learn in Section 4.2.2, the chain size diminishes because the excluded volume that swells the chains at low concentrations becomes negligible at higher concentrations.

## 4.2 THERMODYNAMICS OF SEMIDILUTE POLYMER SOLUTIONS

### 4.2.1 Blob Model

**4.2.1.1 Blobs in Semidilute Solutions** In the semidilute solutions, the chains are congested and highly overlapping with other chains, as shown in Figure 4.1a.

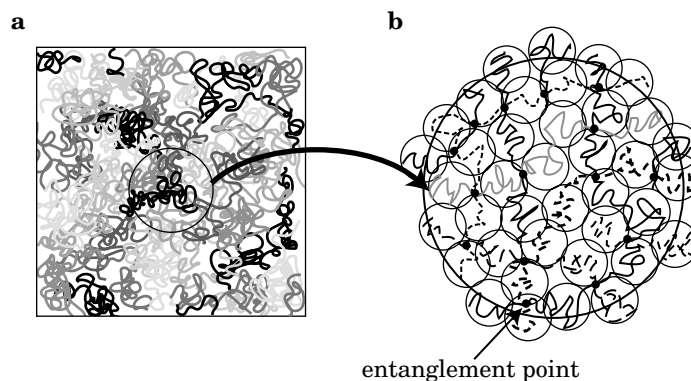


**Figure 4.1.** a: Highly entangled polymer chains in a semidilute polymer solution. b: When zoomed in, the entangled chains can be regarded as consisting of blobs.

Different gray levels are used to distinguish the chains. When zoomed in, the solution would look like Figure 4.1b. The intersections between different chains, indicated by small filled circles, are called **entanglement points**. Between two neighboring entanglement points on the same chain, the chain claims its own territory; there is only a small chance for monomers of other chains to sneak in. We can superimpose a sphere called a **blob** onto this sovereign. The same monopolized territory applies to the other parts of the chain and to other chains as well. In this way, we can fill up the entire solution with blobs.

The blob concept, which was introduced in the 1970s, solved then mysterious problems elegantly.<sup>44</sup> The **blob model** is extremely useful and robust in predicting various static and dynamic properties of the semidilute solutions of polymers. Although limited to power relationships, the blob model allows us to find how these properties depend on the concentration and the molecular weight. In this section, we will first find the blob size in the semidilute solution of polymer chains of a given length at a given concentration. We will then use the blob model to obtain various thermodynamic quantities of the semidilute solution.

**4.2.1.2 Size of the Blob** Let us first estimate the size of the blob  $\xi$  (Fig. 4.2). Each polymer chain consists of  $N$  monomers of size  $b$ . The polymer is monodisperse. For convenience, we use the monomer density  $\rho$  defined in Section 2.4.5.2. It is the number of monomers in a unit volume and related to the mass concentration  $c$  by

$$\frac{\rho}{N} = \frac{cN_A}{M} \quad (4.1)$$

where  $M$  is the molecular weight of the polymer. The two sides express the number of polymer chains in a unit volume.



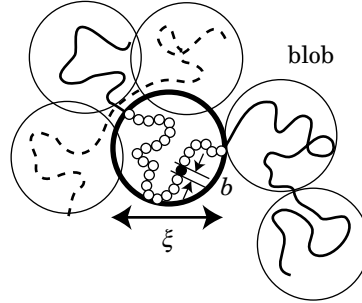


**Figure 4.2.** A blob of size  $\xi$  has  $g_N$  monomers of size  $b$  from the same chain.

At the overlap concentration (defined in Section 1.8), the  $N$  monomers in a volume of  $R_{g0}^3$  give the overall monomer density  $\rho^*$ :

$$\rho^* = Nc^*N_A/M \cong NR_{g0}^{-3} \cong b^{-3}N^{1-3\nu} \quad \text{or} \quad \rho^* \cong b^{-3}N^{-4/5} \quad (4.2)$$

where  $R_{g0} \cong bN^\nu$  was used. The second equality is for  $\nu = 3/5$  in the good solvent. In what follows, we often display the power relationships for a general  $\nu$  and  $\nu = 3/5$  side by side. If necessary, we can also derive a relevant power relationship for semidilute solutions in the theta condition by setting  $\nu = 1/2$  (see Section 4.2.2.6).

The blob size  $\xi$  is equal to  $R_{g0}$  at  $\rho^*$ . As the solution becomes more concentrated, the chains become more heavily overlapped with each other. When there are more entanglement points, the blob must decrease its size (Fig. 4.3).

We make two assumptions to estimate the blob size in the semidilute solution at monomer density  $\rho$ :

- (1) Within each blob, the partial chain takes a conformation of the isolated parent chain. Let  $g_N$  monomers be in each blob. Then,

$$bg_N^\nu \cong \xi \quad \text{or} \quad bg_N^{3/5} \cong \xi \quad (4.3)$$

- (2) The blobs occupy the whole volume of the solution without voids. Therefore, the density of monomers in the blob mirrors the density in the whole solution:

$$\rho \cong g_N/\xi^3 \quad (4.4)$$

Combining the two equations, we obtain

$$\xi \cong b^{-1/(3\nu-1)}\rho^{-\nu/(3\nu-1)} \quad \text{or} \quad \xi \cong b^{-5/4}\rho^{-3/4} \quad (4.5)$$

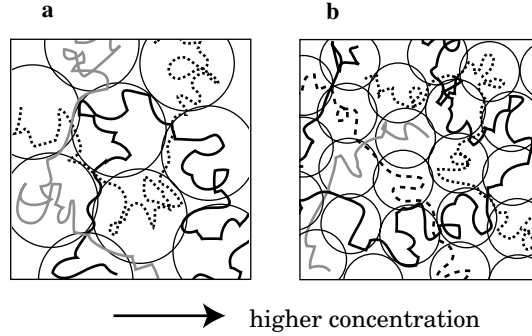


**Figure 4.3.** As the concentration increases, the blob size decreases from the one shown in panel a to the one in panel b.

The negative exponent on  $\rho$  tells that the blobs become smaller with an increasing  $\rho$ . Note also that  $\xi$  does not depend on  $N$  explicitly. It is determined by the monomer density or the mass concentration only, once the polymer is given.

The blob size relative to  $R_{g0}$  is calculated from  $\xi^{1-3\nu} \cong b\rho^\nu \cong (\rho/\rho^*)^\nu b(NR_{g0}^{-3})^\nu \cong (\rho/\rho^*)^\nu R_{g0}^{1-3\nu}$  as

$$\xi \cong R_{g0}(\rho/\rho^*)^{-\nu/(3\nu-1)} \quad \text{or} \quad \xi \cong R_{g0}(\rho/\rho^*)^{-3/4} \quad \text{blob size} \quad (4.6)$$

Apparently Eq. 4.6 holds only for  $\rho > \rho^*$ . Below the overlap concentration, the chains are isolated. The blob contains the whole chain and therefore  $\xi \cong R_{g0}$ . Figure 4.4 illustrates how the blob size decreases with an increasing concentration for three different chain lengths specified by their radii of gyration in the dilute solution limit,  $R_{g0}(1)$ ,  $R_{g0}(2)$ , and  $R_{g0}(3)$ . In a solution of polymer chains with  $R_{g0}(2)$ ,  $\xi \cong R_{g0}(2)$  at low concentrations. As  $\rho$  exceeds its overlap concentration  $\rho^*(2)$ ,  $\xi$  approaches a straight line with a slope of  $-3/4$ . In a solution of the longer chains [ $R_{g0}(1)$ ], the crossover from a constant at  $R_{g0}$  to a slope of  $-3/4$  occurs at a lower concentration because its  $\rho^*$  is smaller [ $\rho^*(1)$ ]. The straight line they approach at  $\rho > \rho^*$  is identical to the straight line that the chains with  $R_{g0}(2)$  approach. The curve for the shorter chains [ $R_{g0}(3)$ ] merges with the same straight line at a higher concentration  $\rho^*(3)$ . Note that  $\xi$  is independent of  $N$  in Eq. 4.5.

Once  $\xi$  is obtained,  $g_N$  is evaluated as follows:

$$g_N \cong \rho\xi^3 \cong (b^3\rho)^{-1/(3\nu-1)} \cong N(\rho/\rho^*)^{-1/(3\nu-1)} \quad \text{or} \quad g_N \cong (b^3\rho)^{-5/4} \cong N(\rho/\rho^*)^{-5/4} \quad (4.7)$$

where Eqs. 4.2, 4.4, and 4.5 were used. At the overlap concentration,  $g_N \cong N$  as required. In the blob model, the polymer chain of  $N$  monomers is replaced by a chain of  $N/g_N \cong (\rho/\rho^*)^{1/(3\nu-1)} \cong (\rho/\rho^*)^{5/4}$  blobs, each consisting of  $g_N$  monomers. The number of blobs constituting the polymer chain increases as their size decreases. Note that both  $\xi$  and  $g_N$  decrease with an increasing  $\rho$ , but in different exponents.

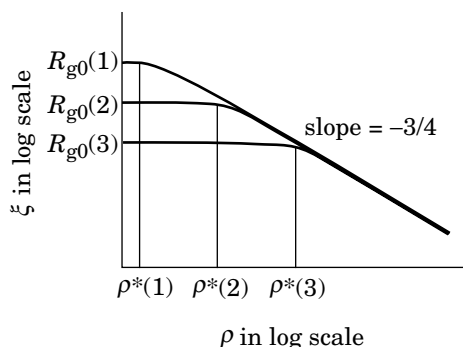


**Figure 4.4.** Blob size  $\xi$  plotted as a function of monomer density  $\rho$  in a double logarithmic scale for three different chain lengths. Their radii of gyration in the dilute solution limit are  $R_{g0}(1)$ ,  $R_{g0}(2)$ , and  $R_{g0}(3)$ . Their overlap concentrations are  $\rho^*(1)$ ,  $\rho^*(2)$ , and  $\rho^*(3)$ . In the semidilute solutions,  $\xi \sim \rho^{-3/4}$ .

The blob is a conceptual object. Unlike  $R_{g0}$ , we cannot measure the size of the blob. Later, we will derive the identity, *blob size = correlation length*. The latter can be conveniently measured in static and dynamic light scattering.

It is now apparent that there is an upper limit for the concentration range in which the blob model is effective. With an increasing  $\rho$ ,  $\xi$  decreases, but it cannot be smaller than  $b$ , the monomer size. The upper limit of  $\rho$ , which we denote by  $\rho^{**}$ , is determined from the condition of  $\xi \cong b$ . Using Eq. 4.5,  $\rho^{**}$  is evaluated as

$$\rho^{**} \cong b^{-3} \quad (4.8)$$

Unlike  $\rho^*$ , the upper limit is independent of  $N$ . It is considered that, in real polymer solutions, the volume fraction of the polymer at  $\rho^{**}$  is around 0.2–0.3.

With Eq. 4.2, we find

$$\rho^{**}/\rho^* \cong N^{3\nu-1} \quad \text{or} \quad \rho^{**}/\rho^* \cong N^{4/5} \quad (4.9)$$

Thus, the lower limit and the upper limit of the semidilute regime are widely separated, especially when  $N \gg 1$ . As expected,  $g_N \cong 1$  at the upper limit.

**4.2.1.3 Osmotic Pressure** The osmotic pressure counts the number of independently moving units per volume of the solution. It is one of the colligative properties of the solution. At low concentrations, the whole chain moves as a unit. The center-of-mass displacement is synonymous to a change in the position of the whole chain (in the small wave vector limit). The dilute polymer solution is an ideal solution of  $\rho/N = cN_A/M$  solute molecules in a unit volume. The osmotic pressure  $\Pi_{\text{ideal}}$  of the solution is therefore

$$\Pi_{\text{ideal}} = \frac{cN_A}{M} k_B T = \frac{\rho}{N} k_B T \quad (4.10)$$

In the semidilute solution, monomers in a given blob are moving independently of the monomers in the other blobs, at least in a short time scale. Entanglement makes rearrangement of monomers within a blob by far easier and faster compared with the rearrangement of the blobs. The monomers in the blob move more or less together (correlated motion), just as the whole chain moves together at low concentrations. Now in the semidilute solution, the blob is a moving unit. Therefore, the osmotic pressure of the semidilute solution is given as  $k_B T \times$  (the number of blobs in a unit volume):

$$\Pi \cong \xi^{-3} k_B T \quad (4.11)$$

With Eq. 4.5, we obtain

$$\boxed{\Pi/k_B T \cong (b\rho^\nu)^{3/(3\nu-1)} \quad \text{or} \quad \Pi/k_B T \cong b^{15/4} \rho^{9/4} \quad \text{osmotic pressure}} \quad (4.12)$$

In the semidilute solution,  $\Pi$  does not depend explicitly on  $N$ . It is determined by  $\rho$  only. Compared at the same mass concentration, solutions of a polymer have the same  $\Pi$  regardless of the molecular weight of the polymer. It means that a small volume that contains 1,000 chains of 1,000 monomers is thermodynamically equivalent to the volume that contains 100 chains of 10,000 monomers or 10 chains of 100,000 monomers, as long as the concentration is in the semidilute range. The dependence of  $\Pi/(\rho k_B T)$  on  $\rho$  is depicted in Figure 4.5 for three different chain lengths. At low concentrations, the solution of the shorter chain claims a higher osmotic pressure because the unit volume of the solution has more moving units. When  $\rho \ll \rho^*$ ,  $\Pi/(\rho k_B T)$  is constant at  $1/N$ . A departure from this ideal-solution behavior occurs at around  $\rho^*$ . Thus the departure occurs at a lower concentration for the longer chains. In the semidilute solution, the plots of  $\Pi/(\rho k_B T)$  for different values of  $N$  should overlap with each other and follow a common straight line with

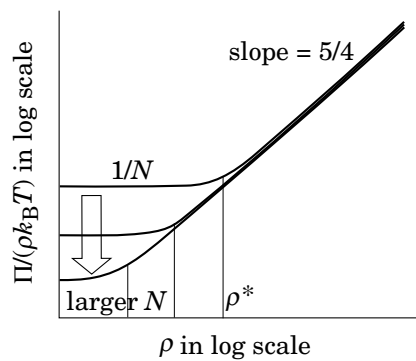


**Figure 4.5.** Osmotic pressure  $\Pi$  reduced by  $\rho k_B T$  is plotted as a function of monomer density  $\rho$  in a double logarithmic scale for three different chain lengths. At low concentrations,  $\Pi/(\rho k_B T) = N^{-1}$ . In the semidilute solutions,  $\Pi/(\rho k_B T) \sim \rho^{5/4}$ . The cross over occurs at around  $\rho^*$ .

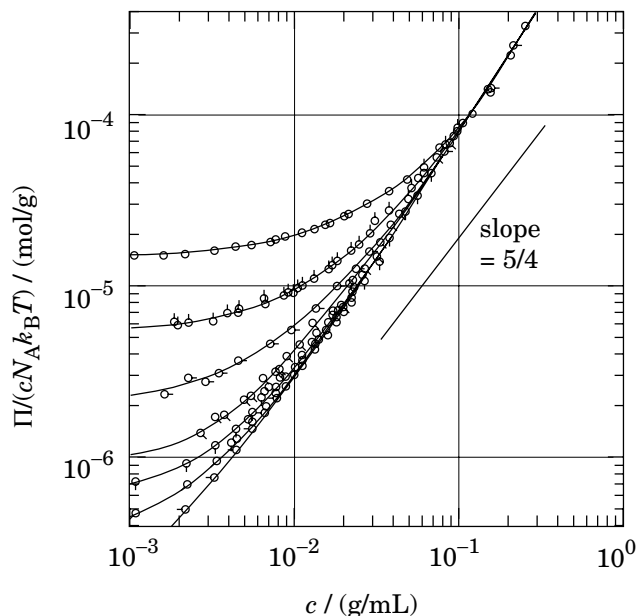


**Figure 4.6.** Osmotic pressure  $\Pi$  of poly( $\alpha$ -methyl styrene) in toluene at 25°C, reduced by  $cN_A k_B T$ , plotted as a function of mass concentration  $c$  of the polymer. Data were obtained, from top to bottom, for various molecular weights from  $7 \times 10^4$  to  $7.47 \times 10^6$  g/mol. The solid line has a slope of 5/4. (From Ref. 46.)

a slope of 5/4. The shorter chains need a higher concentration for its osmotic pressure to approach the straight line.

Experimental results support the presence of the asymptotic straight line. Figure 4.6 shows the osmotic pressure, reduced by  $cN_A k_B T$ , for different molecular weights of poly( $\alpha$ -methyl styrene) in toluene, measured at 25°C.<sup>46</sup> The vapor pressure osmometry, explained in Appendix 2.A, was used for the measurements. The nearly flat line at low concentrations is seen only for the lowest-molecular-weight fraction. At high concentrations, data obtained for fractions of different molecular weights approach a single straight line with a slope of 1.5, slightly greater than 5/4, the predicted exponent in the blob model. We will discuss this difference in Section 4.2.2.1.

The ratio of  $\Pi$  of the semidilute solution to  $\Pi_{\text{ideal}}$  of the ideal solution compared at the same concentration is

$$\boxed{\Pi/\Pi_{\text{ideal}} \cong (\rho/\rho^*)^{1/(3\nu-1)} \quad \text{or} \quad \Pi/\Pi_{\text{ideal}} \cong (\rho/\rho^*)^{5/4}} \quad (4.13)$$

where Eq. 4.2 was used. In the semidilute solution,  $\rho/\rho^*$  can be large. Then the osmotic pressure is much greater than the one we would expect for the ideal solution of the same concentration. When equilibrated with a pure solvent through a semipermeable membrane that passes solvent molecules only, the semidilute solution will suck in a large amount of solvent.

**4.2.1.4 Chemical Potential** We find here how the excess chemical potential  $\delta\mu$  depends on  $\rho$ , where  $\delta\mu$  is the difference of the chemical potential  $\mu$  from the chemical potential in the ideal solution of the same concentration. We note that  $\delta\mu$  is calculated from the nonideal part of the free energy. In the semidilute solution, it is approximately given by  $\Pi V$ , where  $\Pi$  is given by Eq. 4.12. Because  $\rho V/N$  is the number of polymer chains in volume  $V$ ,  $\delta\mu$  is obtained as

$$\delta\mu \cong \left( \frac{\partial(\Pi V)}{\partial(\rho V/N)} \right)_V = N \left( \frac{\partial\Pi}{\partial\rho} \right)_V \cong Nk_B T b^{3/(3\nu-1)} \rho^{1/(3\nu-1)} \quad (4.14)$$

We can rewrite  $\delta\mu$  into a dimensionless quantity:

$$\boxed{\delta\mu/k_B T \cong (\rho/\rho^*)^{1/(3\nu-1)} \quad \text{or} \quad \delta\mu/k_B T \cong (\rho/\rho^*)^{5/4} \quad \text{excess chemical potential}} \quad (4.15)$$

The right-hand side is identical to that of Eq. 4.13, as expected.

The following equation can be used for the overall chemical potential  $\mu$ . It is an approximate formula valid from dilute to semidilute solutions:

$$(\mu - \mu^\circ)/k_B T \cong \ln \phi + a_\mu (\phi/\phi^*)^{1/(3\nu-1)} \quad \text{or} \quad \ln \phi + a_\mu (\phi/\phi^*)^{5/4} \quad (4.16)$$

with  $\mu^\circ$  is the chemical potential at an appropriate reference state, and  $a_\mu$  is a constant independent of  $N$ . Equation 4.16 uses the volume fraction  $\phi$  and the overlap volume fraction  $\phi^*$ , but we can use  $\rho$  and  $\rho^*$  or  $c$  and  $c^*$  as well.

Figure 4.7 depicts  $\mu/k_B T$  for three different chain lengths. At low concentrations, the solution is ideal. As  $\rho$  exceeds  $\rho^*$ ,  $\mu$  deviates upward. The deviation occurs at a lower concentration for the longer chain, and the deviation is more serious, compared with the shorter chain at the same  $\rho$ .

As we have seen in this subsection, the blob model does not give an estimate of the missing numerical coefficient. Often, our interest is to find the power relationship only, however. Then, the blob model is a powerful tool.

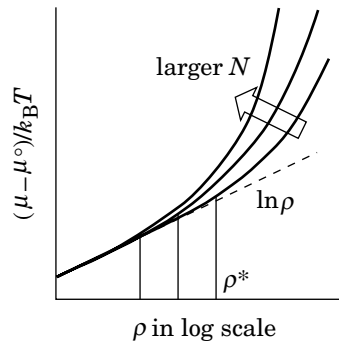


**Figure 4.7.** Chemical potential  $\mu$ , plotted as a function of monomer density  $\rho$  for three different chain lengths.

## 4.2.2 Scaling Theory and Semidilute Solutions

**4.2.2.1 Scaling Theory** In the preceding subsection, we employed a blob model to derive power relationships for various thermodynamic quantities that characterize the semidilute solutions. The simple assumption produced useful results that agree with those obtained in experiments. We can derive the same results without assuming a blob. We will use the **scaling theory** here for that purpose.

The scaling theory has been successfully used to explain critical phenomena. The latter are about an often drastic change in physical quantities as the system approaches the order-disorder transition point. Well-known examples include ferromagnet–paramagnet phase transition in magnets and nematic–isotropic phase transition in liquid crystals. The demixing transition near the UCST and LCST in a blend of two liquids also belongs to the order-disorder transition. The system changes from the disordered phase to the ordered phase as the temperature  $T$  approaches the critical temperature  $T_c$ . Deep in the disordered phase, the system is uniform and structureless. As  $T$  approaches  $T_c$ , fluctuations grow in the local magnetization, the local alignment of the liquid crystalline molecules, or the local composition of the two-component liquid. Increasingly larger domains develop with a partially ordered structure. At  $T = T_c$ , the domain size becomes infinite, and the whole system separates into macroscopically ordered phase. In the demixing of two liquids, the system separates into two macroscopic domains. It is known that at near  $T_c$  the domain size grows in a power of the temperature difference  $|T - T_c|$ .

The scaling theory has been successfully applied to polymer systems by drawing analogy between  $T - T_c \rightarrow 0$  and  $N^{-1} \rightarrow 0$ . Increasing the chain length is equivalent to approaching  $T_c$ . Together with the blob model, the theory has been particularly instrumental in elucidating the thermodynamics and dynamics of the semidilute polymer solutions. Since its initiation by de Gennes in the 1970s, applications of this theory have proliferated.<sup>44</sup> The scaling theory has become a common language in polymer science. To apply the scaling theory to our own polymer systems, we do not need to know the details of the mathematics behind the theory; however, we can still obtain illuminating results from the application, as we will see below.

Let us first consider the osmotic pressure  $\Pi$ . The virial expansion of  $\Pi$  reduced by  $\Pi_{\text{ideal}}$  needs to be a power series of the dimensionless concentration of the polymer chains,  $\rho R_{g0}^3/N$ :

$$\frac{\Pi}{k_B T} = \frac{\rho}{N} [1 + \text{const.} \times (\rho R_{g0}^3/N) + \text{const.} \times (\rho R_{g0}^3/N)^2 + \dots] \quad (4.17)$$

Note that  $\rho R_{g0}^3/N$  is equal to the reduced concentration  $\rho/\rho^* = \phi/\phi^* = c/c^*$ . In general, the factor in the square bracket of Eq. 4.17 is a universal function of  $\rho R_{g0}^3/N$  defined for  $\rho R_{g0}^3/N \geq 0$ . By “universal,” we mean that the functional form is independent of  $N$  or  $b$  except through  $\rho R_{g0}^3/N$ . Therefore, different polymer–solvent combinations share a common function, as long as the solvent is good to the polymer or the polymer chain follows the same statistics. The universal

function is called a **scaling function**. We express it by  $f_{\Pi}$ :

$$\frac{\Pi}{k_{\text{B}}T} = \frac{\rho}{N} f_{\Pi}(\rho R_{\text{g}0}^3/N) \quad (4.18)$$

Note that a dimensionless quantity  $\Pi/(k_{\text{B}}T)$  is equated to another dimensionless quantity  $f_{\Pi}(x)$  with  $x = \rho R_{\text{g}0}^3/N$ .

As  $x \rightarrow 0$ ,  $f_{\Pi}(x)$  approaches unity, that is, the solution is ideal in the dilute-solution limit. The scaling theory assumes that  $f_{\Pi}(x)$  for large  $x$  asymptotically approaches a power of  $x$  with a **scaling exponent**  $m$  yet to be determined. Thus,

$$f_{\Pi}(x) \begin{cases} = 1 & (x \rightarrow 0) \\ \cong x^m & (x \gg 1) \end{cases} \quad (4.19)$$

In the semidilute solution ( $x \gg 1$ ),

$$\frac{\Pi}{k_{\text{B}}T} \cong \frac{\rho}{N} (\rho R_{\text{g}0}^3/N)^m \cong b^{3m} \rho^{1+m} N^{m(3\nu-1)-1} \quad (4.20)$$

In a solution of highly overlapped chains, the thermodynamic properties do not explicitly depend on  $N$  but on  $\rho$  only, as the result of the blob model indicates. From the condition that  $\Pi/k_{\text{B}}T$  be independent of  $N$ , we determine  $m$  as  $m = 1/(3\nu - 1)$  or  $m = 5/4$ , and Eq. 4.20 becomes identical to Eq. 4.12. Without assuming the blobs, we derived an expression for  $\Pi$  that is identical to the one we obtained earlier in the blob model. This identity is already a proof for the blob model.

It is apparent in Eq. 4.20 that only a power of  $x$  for  $f_{\Pi}(x)$  can make  $\Pi$  independent of  $N$ . Although we assumed the power dependence, it is rather a prerequisite for the independence of  $N$ .

As in the blob model, the scaling theory does not provide an estimate of the numerical coefficient missing in Eq. 4.19. The theory tells only that  $f_{\Pi}(x) \sim x^{5/4}$  when  $x \gg 1$ . If needed, we can find the exact relationship in experiments or computer simulations with the help of the scaling prediction. Often, the renormalization group theory can provide the missing coefficient.

It is natural to expect that  $f_{\Pi}(x)$  shows a smooth crossover from 1 at  $x \ll 1$  to  $x^{5/4}$  at  $x \gg 1$ . The scaling function can be displayed by plotting  $\Pi/\Pi_{\text{ideal}} = \Pi M/(cRT)$  as a function of  $\rho/\rho^* = c/c^*$ . This type of plot is called a **scaling plot**. The three curves in Figure 4.5 can be superimposed on top of the other by rescaling the abscissa and the ordinate and therefore by translating the three curves vertically and horizontally, as shown in Figure 4.8. The overlapped curve is called a **master curve**.

The scaling function obtained in the renormalization group theory by Ohta and Oono<sup>47</sup> has the same power relationship at  $\rho \gg \rho^*$  as that of Eq. 4.19. They proposed an interpolation formula:

$$\Pi/\Pi_{\text{ideal}} = 1 + \frac{1}{2}X \exp \left\{ \frac{1}{4} [X^{-1} + (1 - X^{-2}) \ln(1 + X)] \right\} \quad (4.21)$$



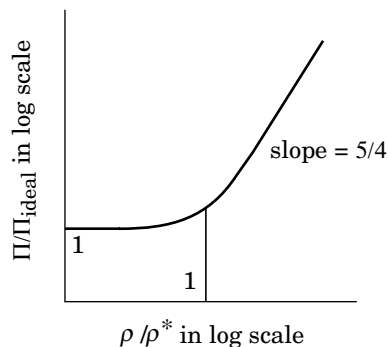


**Figure 4.8.** Scaling plot for the osmotic pressure. The reduced osmotic pressure  $\Pi/\Pi_{\text{ideal}}$  is plotted as a function of the reduced concentration  $\rho/\rho^*$  in a double logarithmic scale. The scaling function changes smoothly from unity at  $\rho/\rho^* \ll 1$  to a slope of  $5/4$  at  $\rho/\rho^* \gg 1$ .

where  $X = (16/9)A_2Mc$ . The latter is another way to scale the concentration into a reduced quantity. We can use  $X = 3.49 \times c/c^*$  as well.

A master curve was obtained for the data shown in Figure 4.6 by rescaling both the abscissa and the ordinate for each set of the data. The definition of  $c^*$  by Eq. 1.108 was employed. In Figure 4.9, data obtained for different molecular weights of the polymer lie on a master curve.<sup>46</sup> At sufficiently high concentrations,

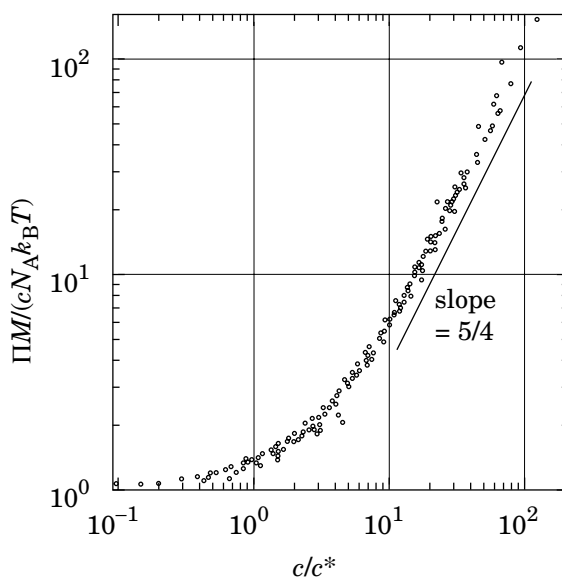


**Figure 4.9.** Scaling plot for the osmotic pressure for the data shown in Figure 4.6. The reduced osmotic pressure  $\Pi M / (c N_A k_B T)$  is plotted as a function of the reduced concentration  $c/c^*$ . The solid line has a slope of  $5/4$ . (From Ref. 46.)

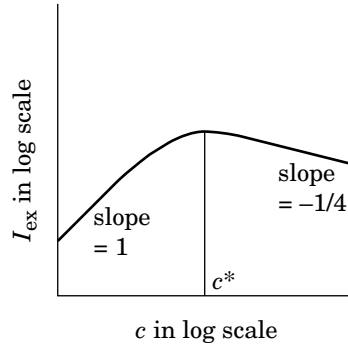


**Figure 4.10.** Excess scattering intensity  $I_{\text{ex}}$  of a polymer solution peaks at around  $c^*$ . In the dilute solution,  $I_{\text{ex}} \sim c$ . In the semidilute solution,  $I_{\text{ex}} \sim c^{-1/4}$ .

the curve runs along a straight line with a slope of  $5/4$ . Compared with Figure 4.6, the agreement with the scaling prediction is better because in the scaling plot the data obtained for the higher-molecular-weight fractions dominate the range of  $c/c^* \gg 1$ . In Figure 4.6, in contrast, the asymptotic curve is drawn for the data at large values of  $c$  obtained for low-molecular-weight fractions. Whether the master curve is obtained from the experimental results and whether the same exponent as the theoretical prediction is obtained gives a final word to the soundness of the blob model and the assumption that  $\Pi$  is independent of  $N$  in the semidilute solution.

**4.2.2.2 Osmotic Compressibility** In Section 2.4, we learned that the molecular weight and concentration-dependent factor in the excess scattering intensity  $I_{\text{ex}}$  of the polymer solution is  $c/(\partial\Pi/\partial c)$ . The denominator is the osmotic compressibility. See Eqs. 2.104–2.107. At low concentrations,  $\partial\Pi/\partial c = N_A k_B T/M$ , and therefore  $I_{\text{ex}} \sim c$ . In the semidilute solution,  $\partial\Pi/\partial c \sim c^{5/4}$ , and therefore  $I_{\text{ex}} \sim c^{-1/4}$ . Figure 4.10 shows a sketch for  $I_{\text{ex}}$ . The intensity peaks at around  $c^*$ . There is a crossover from  $c$  to  $c^{-1/4}$  as  $c$  exceeds  $c^*$ .

Conversely,  $I_{\text{ex}}$  should provide an estimate of  $\partial\Pi/\partial c$ . Another master curve should be obtained when  $(M/N_A k_B T)(\partial\Pi/\partial c)$ , estimated in light-scattering experiments, is plotted as a function of  $c/c^*$  (Problem 4.2). Furthermore, the master curve in the double logarithmic plot should asymptotically run along a straight line with a slope of  $5/4$  at  $c/c^* \gg 1$ . These properties were verified in experiments. Figure 4.11 compiles data obtained for different molecular weights of polystyrene in toluene and methyl ethyl ketone.<sup>48</sup> The reduced osmotic compressibility  $(M/N_A k_B T)(\partial\Pi/\partial c)$  is plotted as a function of  $(16/9)A_2 M c$ . It is easy to draw a master curve that runs in the middle of the scattered experimental data. The master curve approaches unity in the low concentration limit and adopts a slope of  $5/4$  in the semidilute regime, in agreement with the scaling prediction.

**4.2.2.3 Correlation Length and Monomer Density Correlation Function** We now apply the scaling theory to the correlation length  $\xi$  of local monomer density

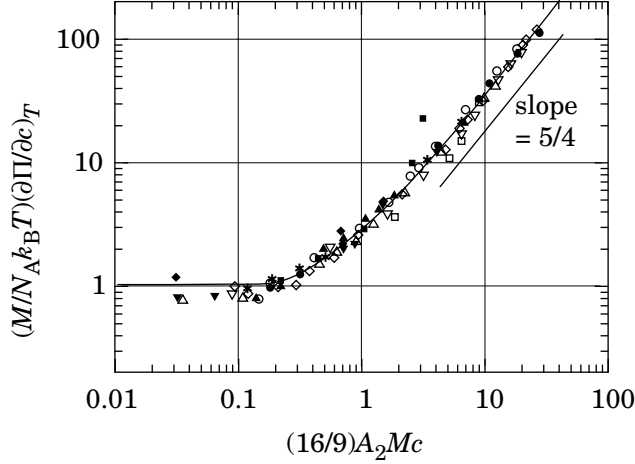


**Figure 4.11.** Reduced osmotic compressibility,  $(M/N_A k_B T)(\partial\Pi/\partial c)_T$ , plotted as a function of  $(16/9)A_2Mc$  in a double logarithmic scale, obtained in the static light-scattering experiments for solutions of polystyrene of various molecular weights in toluene and methyl ethyl ketone. (From Ref. 48.)

fluctuations in solution. The symbol is the same as the one we used for the blob size. In fact, we will find here that *correlation length*  $\cong$  *blob size*.

A homogeneous solution of polymer is not exactly uniform to the length scale of the monomer size. Connectivity of monomers gives rise to a nonuniform distribution of monomer density in the neighborhood of a given monomer. At low concentrations, the chains are well separated. The local density is higher in the neighborhood of a given monomer than it is away from the polymer chain, as we learned in Section 2.4.6. The nonuniform local density distribution persists in the semidilute solution as well. Figure 4.12a depicts polymer chains in the semidilute polymer solution. Figure 4.12b shows the monomer density profile along the solid line in panel a. The density fluctuates but not completely randomly. When  $\rho$  is above the average at one spot, the tendency persists for some distance  $\xi$ . This distance is called a correlation length.

We learned in Section 2.4.6 that  $\xi \cong R_{g0}$  at low concentrations. As the chains overlap in the semidilute solution, the correlation in the density fluctuations over the distance of  $R_{g0}$  is quickly lost, and the correlation length becomes shorter. We introduce another scaling function  $f_\xi(x)$  and write

$$\xi = R_{g0} f_\xi(x) \quad \text{with} \quad f_\xi(x) \begin{cases} = 1 & (x \rightarrow 0) \\ \cong x^u & (x \gg 1) \end{cases} \quad (4.22)$$

where  $x = \rho/\rho^*$ . We expect the scaling exponent  $u$  to be negative. In terms of  $b$ ,  $N$ , and  $\rho$ ,  $\xi$  is expressed as

$$\xi \cong b^{1+3u} N^{\nu+u(3\nu-1)} \rho^u \quad (4.23)$$

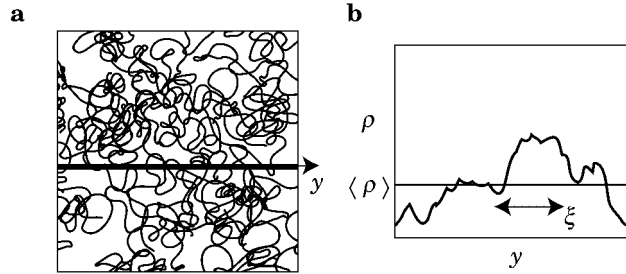


**Figure 4.12.** a: Polymer chains in semidilute solution. b: The density profile along the straight line in panel a.

Again, we impose that  $\xi$  be independent of  $N$  when  $\rho/\rho^* \gg 1$ . The condition is given as  $\nu + u(3\nu - 1) = 0$ , i.e.,  $u = -\nu/(3\nu - 1)$  or  $u = -3/4$ . Thus, we find the correlation length decreases with an increasing concentration in a power law with an exponent of  $-3/4$ . The dependence is exactly the same as the one given by Eq. 4.6 for the blob size. Thus, the blob is essentially a sphere with a diameter equal to the correlation length. It indicates that the monomers within a blob move cooperatively and motions of monomers in different blobs are not correlated with each other.

The scaling plot for  $\xi/R_{g0}$  is shown schematically in Figure 4.13. It was prepared by translating the three curves in Figure 4.4 vertically and horizontally.

The correlation length of the polymer solution can be estimated in the static light scattering. Here, we use the **Ornstein-Zernike correlation function**  $g_{oz}(\mathbf{r})$  to find  $\xi$  experimentally. This correlation function is often used for the correlation  $\langle \Delta\rho(\mathbf{r})\Delta\rho(0) \rangle / \rho$  of the density fluctuation  $\Delta\rho(\mathbf{r}) = \rho(\mathbf{r}) - \langle \rho \rangle$  in the semidilute polymer solution. The function is expressed as

$$g_{oz}(r) = \frac{A}{4\pi\xi^2 r} \exp(-r/\xi) \quad \text{Ornstein-Zernike correlation function} \quad (4.24)$$

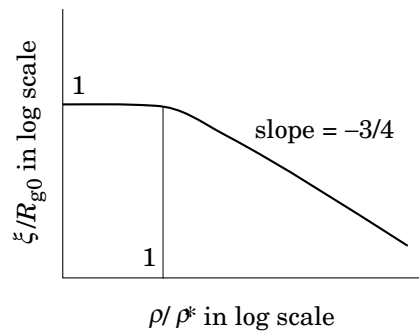


**Figure 4.13.** Scaling plot for the correlation length  $\xi$ . The reduced correlation length  $\xi/R_{g0}$  is plotted as a function of the reduced concentration  $\rho/\rho^*$  in a double logarithmic scale.

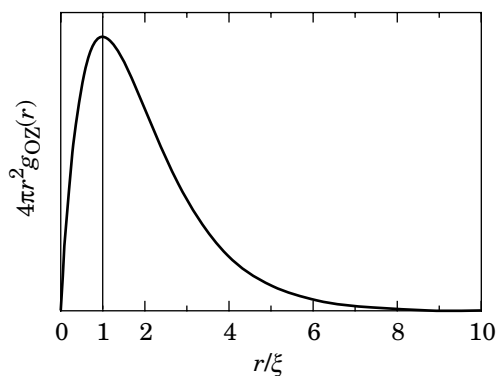


**Figure 4.14.** Ornstein-Zernike monomer density autocorrelation function  $g_{OZ}(r)$ . The other monomers are most likely found at  $r = \xi$ .

where  $r = |\mathbf{r}|$ , and  $A$  is a constant to be determined later. It has a singularity at  $r = 0$ , but it disappears on integration. Figure 4.14 shows a plot of  $4\pi r^2 g_{OZ}(r)$ . The excess probability of finding other monomers at the distance between  $r$  and  $r + dr$  from a given monomer is given by  $4\pi r^2 g_{OZ}(r) dr$ . The plot peaks at  $r = \xi$ . The other monomers are most likely found at  $r = \xi$ .

The static structure factor  $S(\mathbf{k})$  for this correlation function is simple:

$$S(\mathbf{k}) = \int \exp(i\mathbf{k} \cdot \mathbf{r}) g_{OZ}(\mathbf{r}) d\mathbf{r} = \frac{A}{1 + \xi^2 \mathbf{k}^2} \quad (4.25)$$

The reciprocal of  $S(\mathbf{k})$  is plotted as a function of  $\mathbf{k}^2$  in Figure 4.15. The plot is a straight line with a slope of  $\xi^2$ . Because  $S(\mathbf{k})$  is proportional to the excess scattering intensity at  $\mathbf{k}$ , we can use this plot to find  $\xi$  in the scattering experiments.

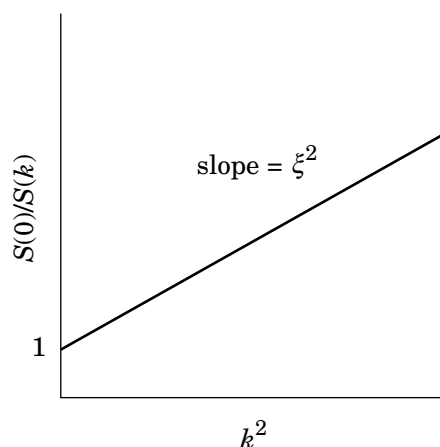


**Figure 4.15.** The reciprocal of the static structure factor  $S(k)$  plotted as a function of  $k^2$ . The slope of the plot is equal to the square of the correlation length  $\xi$ .

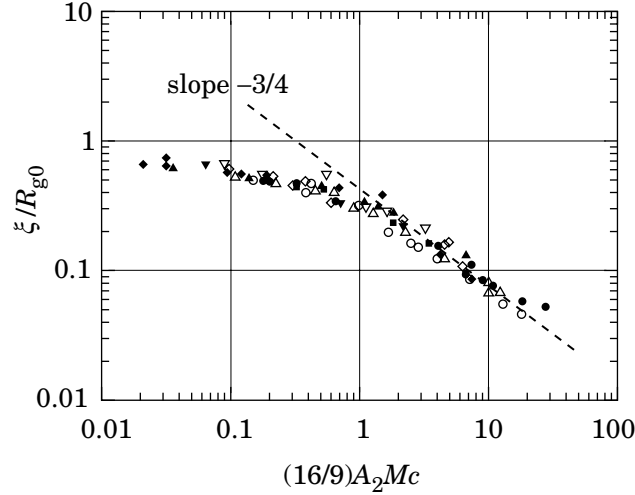


**Figure 4.16.** Scaling plot for the correlation length  $\xi$  evaluated in static light-scattering measurements for solutions of polystyrene in toluene and methyl ethyl ketone. The reduced correlation length  $\xi/R_{g0}$  is plotted as a function of  $(16/9)A_2Mc$  in a double logarithmic scale. The dashed line has a slope of  $-3/4$ . (From Ref. 48.)

The constant  $A$  in  $g_{OZ}(\mathbf{r})$  is determined as follows.  $V^{-1}\psi_{cc}(\mathbf{k})$  is the Fourier transform of  $\langle\Delta c(\mathbf{r})\Delta c(0)\rangle$  (see Eq. 2.105), as  $\rho S(\mathbf{k})$  is the Fourier transform of  $\langle\Delta\rho(\mathbf{r})\Delta\rho(0)\rangle$  (see Eq. 2.64; a constant term that results in the forward scattering is eliminated here). Together with  $c(\mathbf{r}) \propto \rho(\mathbf{r})$ , we find

$$\frac{S(0)}{\psi_{cc}(0)} = \frac{\rho}{c^2V} \quad (4.26)$$

Then,

$$A = S(0) = \frac{\rho k_B T}{c} \frac{\partial c}{\partial \Pi} = N \frac{N_A k_B T}{M} \frac{\partial c}{\partial \Pi} \quad (4.27)$$

where Eqs. 2.106 and 2.107 were used.

The correlation length  $\xi$  estimated in static light-scattering experiments is plotted in Figure 4.16 in the scaling plot.<sup>48</sup> The reduced concentration is  $(16/9)A_2Mc$ . Data obtained for polystyrene fractions of different molecular weights in toluene and methyl ethyl ketone fall on a single master curve. At  $(16/9)A_2Mc \gg 1$ , the data lie along a straight line with a slope of  $-3/4$ , in agreement with the scaling prediction. Note that the low concentration limit of  $\xi/R_{g0}$  is not unity but  $3^{-1/2}$  because the single-chain structure factor is  $S_1(\mathbf{k}) = N/(1 + \mathbf{k}^2 R_{g0}^2/3)$ , that is,  $\xi = R_{g0}/3^{1/2}$  at low concentrations (Eq. 2.75).

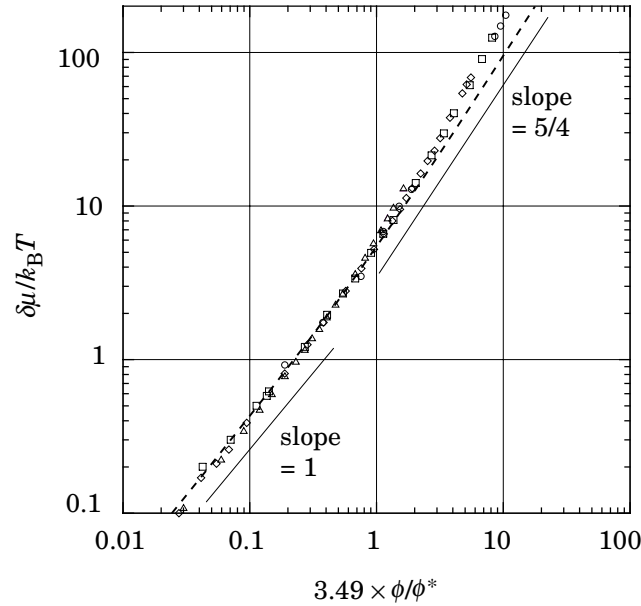


**Figure 4.17.** Scaling plot for the excess chemical potential  $\delta\mu$  plotted as function of the reduced concentration,  $3.49 \times \phi/\phi^*$ . Data were obtained in lattice Monte Carlo simulation for self-avoiding walks of  $N = 25, 100, 200,$  and  $300$  on a cubic lattice. The dashed line is by the Ohta-Oono formula. (From Ref. 5.)

**4.2.2.4 Chemical Potential** The excess chemical potential  $\delta\mu(c)$  at concentration  $c$  can be obtained from the reduced osmotic pressure  $\Pi(c)/\Pi_{\text{ideal}}(c)$  as (Problem 4.4)

$$\frac{\delta\mu(c)}{k_B T} = \frac{\Pi(c)}{\Pi_{\text{ideal}}(c)} - 1 + \int_0^c x^{-1} [\Pi(x)/\Pi_{\text{ideal}}(x) - 1] dx \quad (4.28)$$

Another expression of the concentration such as  $\rho$  or  $\phi$  can be used in place of  $c$ .

It can be shown that  $\delta\mu$  is a function of  $c/c^*$  (Problem 4.5). At  $c \ll c^*$ , the virial expansion of  $\Pi(c)$ ,  $\Pi(c)/\Pi_{\text{ideal}}(c) = 1 + A_2 M c + \dots$ , gives  $\delta\mu \sim c$ . At  $c \gg c^*$ ,  $\Pi(c)/\Pi_{\text{ideal}}(c) \sim c^{5/4}$ ; therefore,  $\delta\mu \sim c^{5/4}$  as well. Data for  $\delta\mu/k_B T$  obtained for different chain lengths should be on a master curve when plotted as a function of  $c/c^*$ . Figure 4.17 shows  $\delta\mu/k_B T$  evaluated in the Monte Carlo simulation on a cubic lattice for self-avoiding walks of  $N = 25, 100, 200,$  and  $300$ .<sup>5</sup> As we see, the data are on a master curve. At  $\phi \ll \phi^*$ , the master curve runs along a straight line with a slope of 1. At  $\phi \gg \phi^*$ , the master curve runs along a straight line, but the slope is slightly greater than 5/4, the value predicted in the scaling theory. The dashed line was calculated by using Eq. 4.21 with a slight modification<sup>50</sup> (0.3089 in place of 1/4) and Eq. 4.28.

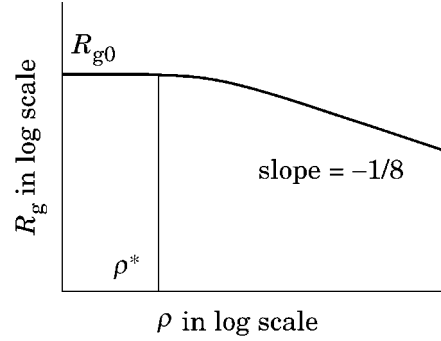


**Figure 4.18.** The polymer chain contracts with an increasing concentration because of shielding of excluded volume. The radius of gyration  $R_g$  decreases in a power of monomer density  $\rho$  with an exponent of  $-1/8$ .

**4.2.2.5 Chain Contraction** Over a length greater than  $\xi$ , monomer concentration is nearly uncorrelated. A monomer on a given polymer chain will not interact with other monomers on the same chain but in different blobs. In other words, a blob will not feel the presence of other blobs that belong to the same chain. The excluded volume is predominantly between blobs belonging to different chains. Thus, the excluded volume effect that swells the polymer chain at low concentrations is absent over the length beyond  $\xi$ . This **shielding of the excluded volume** changes the chain statistics drastically.

In the semidilute solution, blobs do not feel the excluded volume by the other blobs. Therefore, a chain of blobs takes a conformation of an ideal chain consisting of  $N/g_N$  blobs of size  $\xi$ . Its radius of gyration  $R_g$  in the semidilute solution at monomer density  $\rho$  is estimated as

$$R_g^2 \cong (N/g_N)\xi^2 \cong R_{g0}^2(\rho/\rho^*)^{-(2\nu-1)/(3\nu-1)} \quad \text{or} \quad (\rho/\rho^*)^{-1/4} \quad (4.29)$$

where Eqs. 4.6 and 4.7 were used. The polymer chain is swollen in the dilute solution because of the excluded volume, but shrinks in the semidilute solution. The contraction factor for  $R_g$  is

$$R_g/R_{g0} \cong (\rho/\rho^*)^{-(\nu-1/2)/(3\nu-1)} \quad \text{or} \quad (\rho/\rho^*)^{-1/8} \quad (4.30)$$

The same contraction factor applies to  $R_F$ . Figure 4.18 illustrates the contraction in the scaling plot.

In terms of  $b$ ,  $N$ , and  $\rho$ ,  $R_g^2$  is expressed as

$$R_g^2 \cong (b\rho^{1-2\nu})^{1/(3\nu-1)}N \quad \text{or} \quad (b\rho^{-1/5})^{5/4}N \quad (4.31)$$

In the semidilute solution,  $R_g \sim N^{1/2}$ , the same as the ideal chain. The chain keeps contracting with an increasing  $\rho$  by effectively decreasing the monomer size of the



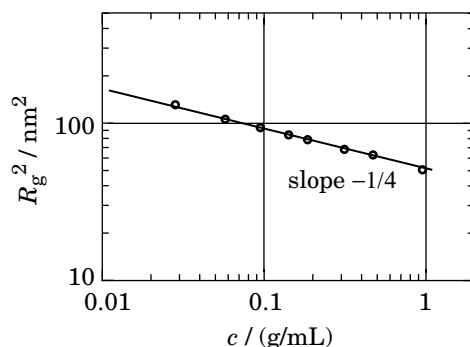


**Figure 4.19.** Reduced mean square radius of gyration,  $R_g^2$ , of polystyrene in carbon disulfide, plotted as a function of the polymer concentration  $c$ . Data were obtained in small-angle neutron scattering. The straight line has a slope of  $-1/4$ . (From Ref. 49.)

ideal chain while holding the relationship of  $R_g \sim N^{1/2}$ . At  $\rho = \rho^{**}$ ,  $\rho \cong b^{-3}$ , and  $R_g \cong bN^{1/2}$ , the same as  $R_g$  of the ideal chain of monomer size  $b$ .

The chain contraction was verified in small-angle neutron-scattering experiments.<sup>49</sup> A mixture of hydrogenated polystyrene (h-PS) and deuterated polystyrene (d-PS) with an equal degree of polymerization (at around 1,100) was dissolved in carbon disulfide. The concentration of d-PS was changed in a wide range, whereas the concentration of h-PS was held low. Thus, the radius of gyration of each h-PS in a matrix of d-PS in the semidilute solution could be measured. Figure 4.19 shows  $R_g^2$  as a function of polymer concentration  $c$ . The data are on a straight line with a slope of  $-1/4$ , in agreement with the scaling theory. The same power dependence is observed in the range of concentrations that exceeds  $c^{**}$ .

Lattice computer simulation also verified the scaling relationship.<sup>5</sup> Figure 4.20 shows the scaling plot for four different chain lengths of self-avoiding walks on the cubic lattice. The data plotted as a function of reduced concentration  $\phi/\phi^*$  are on a single master plot given by

$$R_g/R_{g0} = [1 + 0.96403(\phi/\phi^*) + 0.34890(\phi/\phi^*)^2]^{-1/16} \quad (4.32)$$

This equation has an asymptote identical to Eq. 4.30, but the scaling exponent of  $-1/8$  is not reached in the range shown. Apparently, longer chains are needed to observe the exponent.

**4.2.2.6 Theta Condition** We can apply all of the relationships that we obtained in the preceding section and the present section to semidilute solutions of a polymer in the theta condition by setting  $\nu = 1/2$ . We list the relationships in Table 4.1 together with the results for the good solvent.

At the upper limit of the semidilute regime, there will be little distinction between the good solvent and the theta solvent, as the excluded volume is shielded

**TABLE 4.1** Properties of Semidilute Solutions<sup>†</sup>

	General	With $\nu = 3/5$	With $\nu = 1/2$
$\Pi/k_B T$	$(b\rho^*)^{3/(3\nu-1)}$	$b^{15/4}\rho^{9/4}$	$b^6\rho^3$
$\Pi/\Pi_{\text{ideal}}$	$(\rho/\rho^*)^{1/(3\nu-1)}$	$(\rho/\rho^*)^{5/4}$	$(\rho/\rho^*)^2$
$\delta\mu/k_B T$	$(\rho/\rho^*)^{1/(3\nu-1)}$	$(\rho/\rho^*)^{5/4}$	$(\rho/\rho^*)^2$
$\xi/R_{g0}$	$(\rho/\rho^*)^{-\nu/(3\nu-1)}$	$(\rho/\rho^*)^{-3/4}$	$(\rho/\rho^*)^{-1}$
$R_g/R_{g0}$	$(\rho/\rho^*)^{-(\nu-1/2)/(3\nu-1)}$	$(\rho/\rho^*)^{-1/8}$	$(\rho/\rho^*)^0$
$D_{\text{coop}}/D_0$	$(\rho/\rho^*)^{\nu/(3\nu-1)}$	$(\rho/\rho^*)^{3/4}$	$(\rho/\rho^*)^1$

<sup>†</sup> $\rho/\rho^*$  can be replaced with  $c/c^*$  or  $\phi/\phi^*$ .

to the length of the monomer size. All thermodynamic quantities will be the same between the two solvent conditions. Note that the semidilute range is narrower in the theta solvent compared with the good solvent. The solution in the theta solvent becomes nearly identical to the solution in the good solvent by changing its thermodynamics more quickly with an increasing concentration. For instance, the dependence of  $\xi$  on the concentration is steeper compared with the good solvent condition. Figure 4.21 compares  $\xi/b$  in the good solvent and in the theta solvent. We can draw a similar sketch for other thermodynamic quantities. In the theta solvent, the chain dimension is unchanged from that in the dilute solution limit, as required.

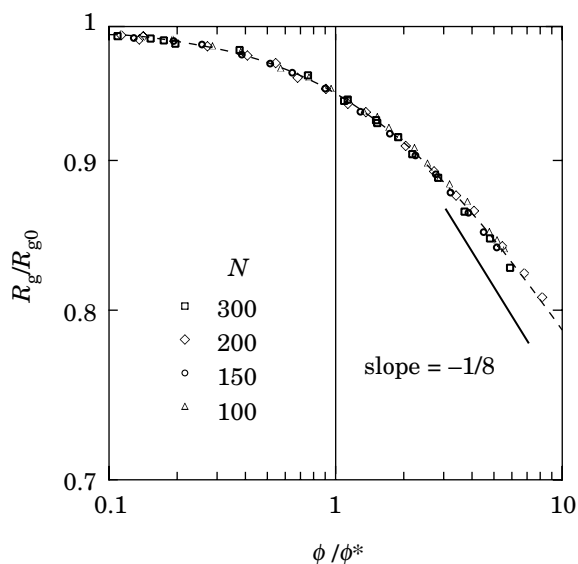


**Figure 4.20.** Scaling plot for  $R_g/R_{g0}$  plotted as a function of the reduced concentration  $\phi/\phi^*$ . The data were obtained in the lattice Monte Carlo simulation for self-avoiding walks. The dashed line represents the best fit by a curve that is identical to the scaling prediction at  $\phi/\phi^* \gg 1$ . (From Ref. 5.)

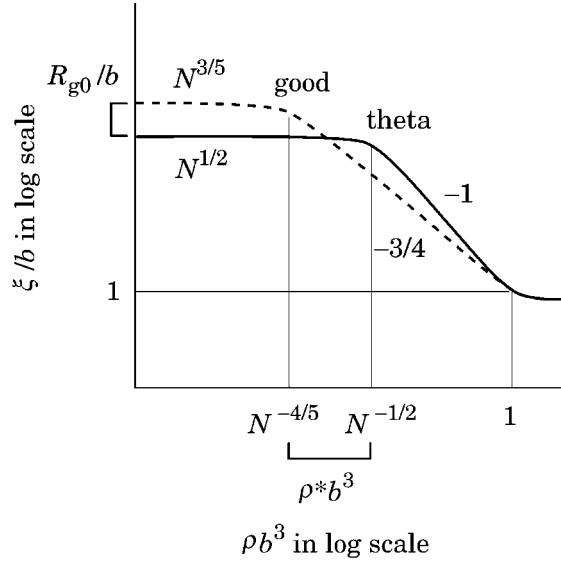


**Figure 4.21.** Comparison of the correlation length  $\xi$  in the good solvent (dashed line) and in the theta solvent (solid line). As the monomer density reaches  $\rho^{**}$  ( $b^3\rho^{**} \cong 1$ ), the distinction between the two solvent conditions nearly disappears.

### 4.2.3 Partitioning with a Pore

**4.2.3.1 General Formula** Another phenomenon that exhibits a marked departure from the dilute solution is partitioning of polymer solutions with a small pore. The partitioning rule (size-exclusion principle), which was discussed in Section 2.5, applies to dilute solutions only, in which each polymer chain interacts with the pore independently of other chains. As soon as the chain feels the presence of nearby chains, the rule changes. Here, we apply the results of the scaling theory to consider the change. For simplicity, we adopt  $\nu = 3/5$  here.

A solution that contains a polymer at a volume fraction  $\phi_E$  is in contact with a pore of diameter  $d$ . The pore walls are neutral to the polymer, that is, the pore does not have an attractive or repulsive interaction other than the excluded volume (polymers cannot intersect the pore wall). At equilibrium, the polymer volume fraction is  $\phi_1$  in the pore. We allow  $\phi_1$  and  $\phi_E$  to be anywhere from dilute to semidilute regimes. Except near the pore–exterior boundary,  $\phi_1$  is uniform along the pore (Fig. 4.22).

We adopt Eq. 4.16 for the chemical potential  $\mu_E$  of the chain exterior to the pore:

$$\mu_E/k_B T = \mu^\circ/k_B T + \ln \phi_E + a_\mu (\phi_E/\phi^*)^{5/4} \quad (4.33)$$

Within the pore, the polymer chain has an extra term due to confinement (see Eq. 2.142):

$$\mu_1/k_B T = \mu^\circ/k_B T + \ln \phi_1 + a_\mu (\phi_1/\phi^*)^{5/4} + a_c (R_{g0}/d)^{5/3} \quad (4.34)$$

where  $a_c$  is another numerical coefficient.

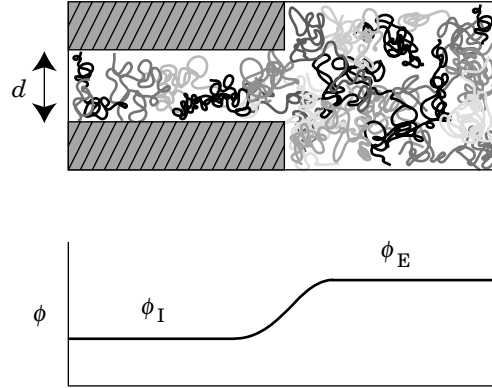


**Figure 4.22.** Partitioning of a semidilute polymer solution with a pore. The concentration profile is shown in the bottom panel.

We neglect the effect of chain contraction at high concentrations. Although the chain contraction decreases the confinement entropy, its effect is usually small (Problem 4.9). Therefore, we also use the confinement entropy of a single chain in the low concentration limit,  $k_B a_c (R_{g0}/d)^{5/3}$ , for the semidilute solution.

Equating the above two chemical potentials for equilibrium, we obtain

$$\ln \phi_I + a_\mu (\phi_I/\phi^*)^{5/4} + a_c (R_{g0}/d)^{5/3} = \ln \phi_E + a_\mu (\phi_E/\phi^*)^{5/4} \quad (4.35)$$

We evaluate the partition coefficient  $K = \phi_I/\phi_E$  in the two concentration regimes.

**4.2.3.2 Partitioning at Low Concentrations** In the low concentration limit ( $\phi_I/\phi^* < \phi_E/\phi^* \ll 1$ ), the interaction terms can be dropped. We obtain the partition coefficient  $K_0$  as  $\ln K_0 \cong -(R_{g0}/d)^{5/3}$  (Eq. 2.142).

With an increasing  $\phi_E$ , the interaction term becomes nonnegligible, which occurs first for  $\mu_E$  because  $\phi_I < \phi_E$ . Then, Eq. 4.35 is simplified to

$$\ln \phi_I + a_c (R_{g0}/d)^{5/3} = \ln \phi_E + a_\mu (\phi_E/\phi^*)^{5/4} \quad (4.36)$$

The right-hand side should be rather expressed by the virial expansion of  $\mu$ :

$$\ln \phi_I + a_c (R_{g0}/d)^{5/3} = \ln \phi_E + a_2 (\phi_E/\phi^*) \quad (4.37)$$

with  $a_2/\phi^*$  being the second virial coefficient when the excess chemical potential is expanded with respect to  $\phi$ . The partition coefficient is then evaluated as

$$\boxed{\ln K = \ln K_0 + a_2 (\phi_E/\phi^*) \quad (\phi_E \ll \phi^*)} \quad (4.38)$$

The increase in  $\phi_E$  results in an increase in  $K$  because  $a_2 > 0$  in the good solvent. The concentration increases more rapidly in the pore than it does in the surrounding solution. The positive second virial coefficient is the driving force to increase  $K$ .

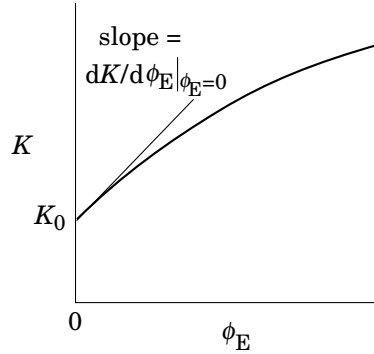


**Figure 4.23.** The tangential to the curve of  $K$  at  $\phi = 0$  has a positive slope in the good solvent.

The plot of  $K$  versus  $\phi$  has a positive slope at  $\phi = 0$ , as depicted in Figure 4.23. From Eq. 4.38, we find  $dK/d\phi_E = a_2 K/\phi^*$  at  $\phi_E = 0$ . Size exclusion chromatography (SEC) is based on the partitioning of a polymer chain with a small pore. Our naive expectation is that each polymer chain is partitioned between the pore and the surrounding solution independently of interactions of other chains. Equation 4.38 demonstrates, however, that the partition coefficient increases strongly with concentration. In terms of mass concentration  $c_E$  in the exterior solution, Eq. 4.38 is written as

$$\ln K = \ln K_0 + 2A_2 M c_E \cong \ln K_0 + 4c_E/c^* \quad (c_E \ll c) \quad (4.39)$$

where  $a_2 \phi_E/\phi^*$  was replaced with  $2A_2 M c_E$  (Problem 2.9), and  $(16/9)A_2 M c = 3.49 \times c/c^*$  was used. For instance, if  $K_0 = 0.1$  and  $c^* = 5$  g/L, then  $K \cong 0.22$  at  $c/c^* = 1$  g/L. This is why an extremely low concentration is mandated for polymer solutions to be injected into the column in SEC. An overloading (injection of a solution more concentrated than  $c^*/10$ ) significantly alters the chromatogram.

We can generalize the partitioning to solutions in solvents other than good solvents. With a decreasing  $A_2$  (or  $a_2$ ), the driving force weakens, and, when  $A_2 = 0$ ,  $dK/d\phi_E = 0$  at  $\phi_E = 0$ . The partition coefficient will remain unchanged over a wide range of concentrations before it starts to increase, helped by  $A_3 > 0$ . When  $A_2 < 0$ ,  $K$  will initially decrease, followed by an upturn at higher concentrations, as illustrated in Figure 4.24. Note that, in the low concentration limit, the chain with  $A_2 > 0$  has the smallest  $K_0$  because its dimension is the greatest.

**4.2.3.3 Partitioning at High Concentrations** Now we consider the partitioning of the semidilute solution,  $\phi_E/\phi^* > \phi_I/\phi^* \gg 1$ . The entropy-of-mixing terms are now negligible compared with the other terms. Equation 4.35 is then simplified to

$$(\phi_I/\phi^*)^{5/4} + (a_c/a_\mu)(R_{g0}/d)^{5/3} = (\phi_E/\phi^*)^{5/4} \quad (4.40)$$

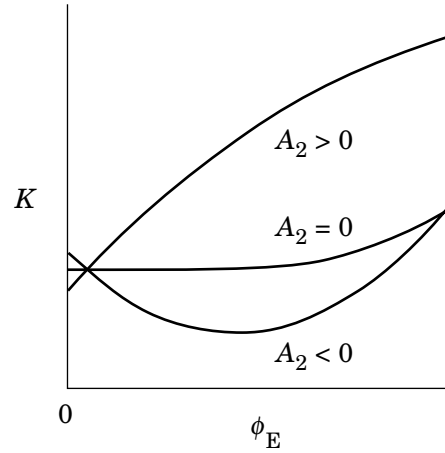


**Figure 4.24.** The concentration dependence of the partition coefficient  $K$  is sensitive to the sign of the second virial coefficient  $A_2$ .

which leads to

$$K = [1 - (a_c/a_\mu)(R_{g0}/d)^{5/3}(\phi_E/\phi^*)^{-5/4}]^{4/5} \quad (4.41)$$

Recall that the correlation length  $\xi$  is given by  $\xi/R_{g0} \cong (\phi_E/\phi^*)^{-3/4}$  (Eq. 4.6). Then,

$$\ln K \cong -(\xi/d)^{5/3} \quad (\phi_E \gg \phi^*) \quad (4.42)$$

With an increasing  $\phi_E$ ,  $\xi$  decreases, and  $K$  approaches unity.

Comparison of Eqs. 2.142 and 4.42 demonstrates that the partitioning of the semidilute solution is determined by the ratio of the correlation length  $\xi$  (blob size) to the pore size in the same way as the partitioning of the dilute solution is governed by the ratio of the chain dimension  $R_{g0}$  to the pore size. Figure 4.25 illustrates the partitioning in two concentration regimes. We expect a smooth change from  $R_{g0}$  to  $\xi$  as the concentration increases.

Because  $\xi$  becomes progressively smaller with an increasing concentration, even long polymer chains, strongly excluded at low concentrations, can fill up the pore space at high concentrations. The limiting scenario is polymer melt. It will fill the pore space unless the pore surface is strongly repulsive, although it may take a long time. Eventually  $K$  will approach unity. The crossover behavior is called a **weak-to-strong penetration transition**.<sup>44</sup> The transition occurs at around  $\phi^*$ , but a longer chain that has a smaller  $K_0$  requires a higher concentration (Fig. 4.26).

#### 4.2.4 PROBLEMS

**Problem 4.1:** The sequence of blobs that enclose monomers of a given polymer chain has a contour length  $L_b \cong \xi N/g_N$ . How does  $L_b$  depend on  $\rho/\rho^*$ ? Also

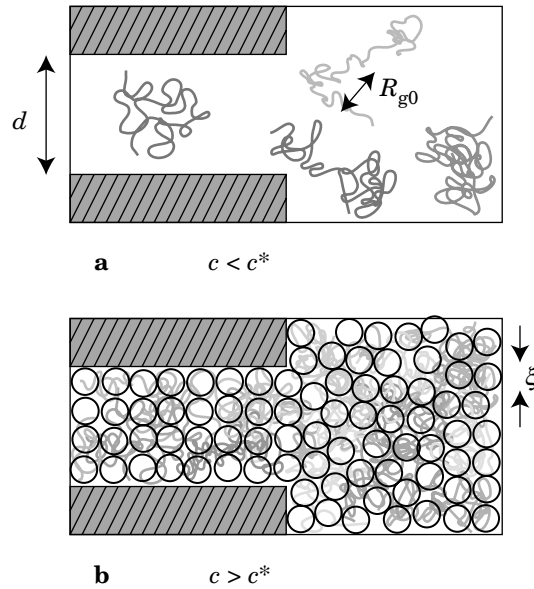


**Figure 4.25.** a: Partitioning of a dilute polymer solution is governed by the ratio of  $R_{g0}$  to the pore diameter  $d$ . b: Partitioning of a semidilute polymer solution is governed by  $\xi/d$ .

show that  $L_b < Nb$ , where  $Nb$  is the contour length of the polymer chain. Use  $\nu = 3/5$ .

**Solution 4.1:**

$$L_b \cong \xi(N/g_N) \cong R_{g0}(\rho/\rho^*)^{-3/4}(\rho/\rho^*)^{5/4} = R_{g0}(\rho/\rho^*)^{1/2}$$

$$\frac{L_b}{Nb} \cong \frac{(bN^{3/5})\rho^{1/2}(b^{3/2}N^{2/5})}{Nb} = (b^3\rho)^{1/2} < 1$$

because the concentration is still low, that is,  $b^3\rho \ll 1$ .

**Problem 4.2:** Show that

$$\frac{M}{N_A k_B T} \frac{\partial \Pi}{\partial c} = f_{II}(x) + x f'_{II}(x)$$

where  $x = c/c^*$ .

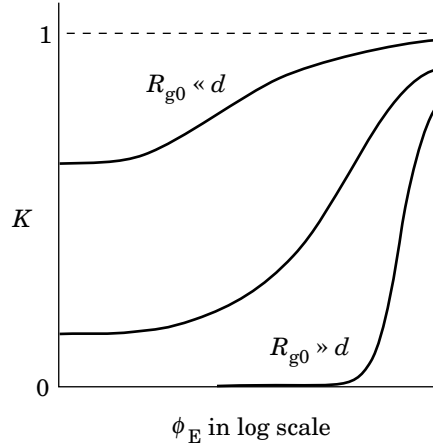


**Figure 4.26.** Weak-to-strong penetration transition. The partition coefficient  $K$  is plotted as a function of the volume fraction of the polymer in the exterior solution. The transition requires a higher concentration with an increasing chain length.

**Solution 4.2:**

$$\begin{aligned} \frac{M}{N_A k_B T} \frac{\partial \Pi}{\partial c} &= \frac{\partial}{\partial c} \left( c \frac{M \Pi}{c N_A k_B T} \right) = \frac{M \Pi}{c N_A k_B T} + c \frac{\partial}{\partial c} \frac{M \Pi}{c N_A k_B T} \\ &= f_{\Pi}(x) + x \frac{d}{dx} f_{\Pi}(x) \end{aligned}$$

**Problem 4.3:** Verify that Eq. 4.27 gives  $A = N$  in the dilute solution limit as required.

**Solution 4.3:** At low concentrations,  $\partial \Pi / \partial c = N_A k_B T / M$ . Then,  $A = N(N_A k_B T / M) \partial c / \partial \Pi = N$ .

**Problem 4.4:** In the lattice chain model, the osmotic pressure is given as (Problem 2.4)

$$\Pi = \frac{\phi^2}{v_{\text{site}}} \frac{\partial}{\partial \phi} \frac{1}{\phi} \frac{\Delta A_{\text{mix}}}{n_{\text{site}}}$$

Use Eq. 2.26 to show that

$$\frac{\Delta \mu_{\text{rep}}(\phi)}{k_B T} = \ln(\phi) + P(\phi) - 1 + \int_0^{\phi} x^{-1} [P(x) - 1] dx$$

where  $P(\phi) \equiv \Pi(\phi) / \Pi_{\text{ideal}}(\phi)$ .



**Solution 4.4:** From the given expression for  $\Pi/k_B T$ ,

$$\frac{\Delta A_{\text{mix}}}{n_{\text{site}}} = v_{\text{site}} \phi \int \frac{\Pi}{\phi^2} d\phi$$

Then, with Eq. 2.26,

$$\begin{aligned} \frac{\Delta \mu_{\text{rep}}(\phi)}{k_B T} &= \frac{N}{n_{\text{site}}} \frac{\partial}{\partial \phi} \frac{\phi n_{\text{site}} v_{\text{site}}}{k_B T} \int \frac{\Pi}{\phi^2} d\phi = \frac{\partial}{\partial \phi} \phi \int \frac{1}{\phi} \frac{\Pi}{\Pi_{\text{ideal}}} d\phi \\ &= \frac{\partial}{\partial \phi} \phi \int \frac{1}{\phi} P(\phi) d\phi = \ln \phi + P(\phi) + \int \frac{P(\phi) - 1}{\phi} d\phi \end{aligned}$$

We add a constant  $-1$  to make the nonideal part of  $\Delta \mu_{\text{rep}}$  disappear at  $\phi = 0$ :

$$\frac{\Delta \mu_{\text{rep}}(\phi)}{k_B T} = \ln \phi + P(\phi) - 1 + \int \frac{P(\phi) - 1}{\phi} d\phi$$

**Problem 4.5:** Show that  $\delta \mu(c)/k_B T$  given by Eq. 4.28 is a function of  $c/c^*$ .

**Solution 4.5:** Let  $\Pi(c)/\Pi_{\text{ideal}}(c) \equiv P(c/c^*)$ . Then, the integral  $I$  in Eq. 4.28 is expressed as

$$I \equiv \int_0^c x^{-1} [\Pi(x)/\Pi_{\text{ideal}}(x) - 1] dx = \int_0^c x^{-1} [P(x/c^*) - 1] dx$$

We change the variable of integration to  $y \equiv x/c^*$ . Then,

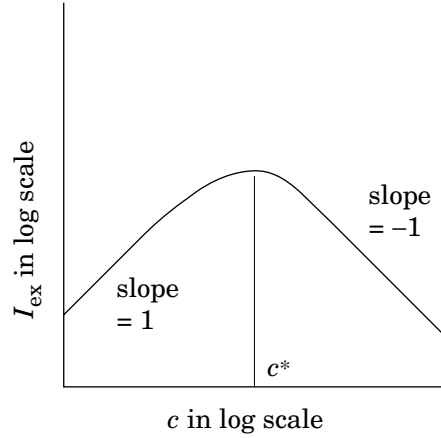
$$I = \int_0^{c/c^*} [P(y) - 1] \frac{dy}{y}$$

Thus,

$$\frac{\delta \mu(c)}{k_B T} = P(c/c^*) - 1 + \int_0^{c/c^*} [P(y) - 1] \frac{dy}{y}$$

**Problem 4.6:** Draw a sketch for the excess light scattering intensity  $I_{\text{ex}}$  of a polymer solution in the theta solvent as a function of concentration  $c$  of the polymer in a double logarithmic plot. Indicate the slope of the plot at each of  $c/c^* \ll 1$  and  $c/c^* \gg 1$ .

**Solution 4.6:** At low concentrations,  $I_{\text{ex}} \sim c$ . At  $c/c^* \gg 1$ ,  $\partial\Pi/\partial c \sim c^2$  in the theta solvent. Then,  $I_{\text{ex}} \sim c^{-1}$ . The sketch is given below.



**Problem 4.7:** We can apply Flory's method to evaluate the chain contraction in the semidilute solution. In Flory's expression for the free energy of a polymer chain  $A_{\text{ch}}$  in Eq. 1.63, the binary monomer–monomer interaction was limited to a pair on the same polymer chain. In the semidilute solution of monomer density  $\rho$ , the partner of the interaction is mostly the monomers on the other chains. We can approximate this change by introducing the probability  $(N/R^3)/(N/R^3 + \rho)$ . A monomer on a given polymer chain interacts with other monomers on the same chain with this probability. Then, Eq. 1.63 is changed to

$$\frac{A_{\text{ch}}}{k_{\text{B}}T} \cong \frac{R^2}{Nb^2} + b^3 \frac{N^2}{R^3} \frac{N/R^3}{N/R^3 + \rho}$$

In the semidilute solution, this equation is simplified to

$$\frac{A_{\text{ch}}}{k_{\text{B}}T} \cong \frac{R^2}{Nb^2} + b^3 \frac{N^3}{R^6} \frac{1}{\rho}$$

Show that minimization of  $A_{\text{ch}}$  leads to the same contraction factor as the one predicted in the scaling theory.

**Solution 4.7:** From  $(\partial/\partial R)(A_{\text{ch}}/k_{\text{B}}T) = 0$ ,

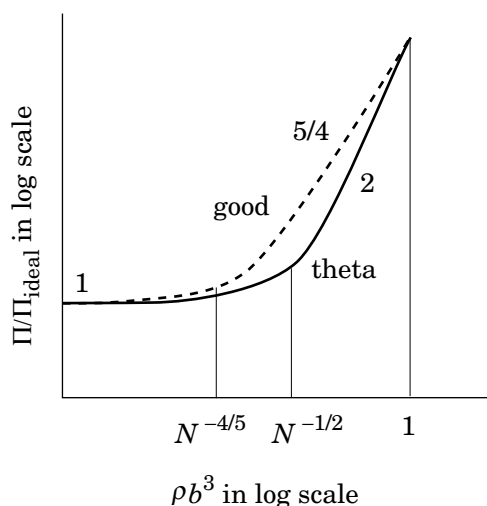
$$\frac{2R}{Nb^2} - 6b^3 \frac{N^3}{R^7} \frac{1}{\rho} \cong 0$$

which is rewritten to

$$R \cong b^{5/8} N^{1/2} \rho^{-1/8}$$

**Problem 4.8:** Compare the osmotic compressibility of a given polymer in the good solvent and in the theta solvent by drawing a sketch of  $\Pi/\Pi_{\text{ideal}}$  as a function of  $b^3\rho$  in a double logarithmic scale.

**Solution 4.8:**



**Problem 4.9:** Estimate the effect of the chain contraction on the partition coefficient of the semidilute solution with a pore of diameter  $d$ .

**Solution 4.9:** When we allow  $R_g$  to change with concentration,

$$\ln K \cong -(a_c/a_\mu)(R_g/d)^{5/3}(\phi_E/\phi^*)^{-5/4}$$

With  $R_g/d$  given by

$$R_g/d = (R_g/R_{g0})(R_{g0}/d) \cong (\phi_E/\phi^*)^{-1/8}(R_{g0}/d)$$

we have

$$\begin{aligned} \ln K &\cong -[(R_{g0}/d)(\phi_E/\phi^*)^{-1/8}]^{5/3}(\phi_E/\phi^*)^{-5/4} \\ &= -(R_{g0}/d)^{5/3}(\phi_E/\phi^*)^{-35/24} \end{aligned}$$

The exponent is  $-35/24 \cong -1.46$ , as opposed to  $-5/4 \cong -1.25$  in Eq. 4.41.

**Problem 4.10:** Discuss the partitioning of polymer chains in semidilute solution in the theta condition with a pore of diameter  $d$ . Can the partitioning of the semidilute solution be treated as the partitioning of independent blobs?

**Solution 4.10:** In the theta condition, Eq. 4.40 is rewritten to

$$(\phi_l/\phi^*)^2 + (a_c/a_\mu)(R_{g0}/d)^2 = (\phi_E/\phi^*)^2$$

which leads to

$$\ln K = -(a_c/a_\mu)(R_{g0}/d)^2(\phi_E/\phi^*)^{-2}$$

Because  $\xi/R_{g0} \cong (\phi_E/\phi^*)^{-1}$ ,

$$\ln K \cong -(\xi/d)^2$$

This equation demonstrates that the partitioning of the semidilute solution is equivalent to the partitioning of independent blobs in the theta condition. Compare the last equation with Eq. 2.136.

## 4.3 DYNAMICS OF SEMIDILUTE SOLUTIONS

### 4.3.1 Cooperative Diffusion

In Section 3.2, we learned that dynamic light scattering (DLS) measures the mutual diffusion coefficient  $D_m$  and that it increases with an increasing polymer concentration in the good solvent. We extend it here to the semidilute solution. Figure 4.27

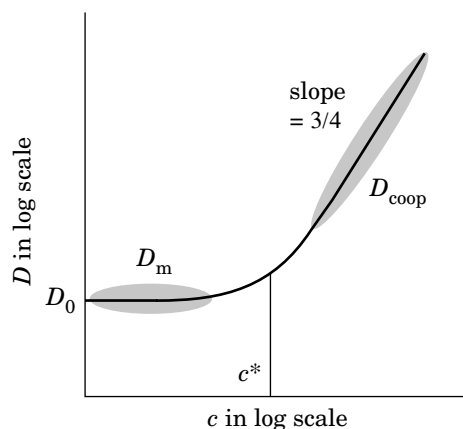


**Figure 4.27.** Diffusion coefficient measured in DLS for various concentrations of a polymer in a good solvent is schematically shown as a function of polymer concentration  $c$ . In the low concentration limit, it is  $D_0$ , the diffusion coefficient of an isolated chain. With an increasing concentration, the mutual diffusion coefficient  $D_m$  increases linearly, followed by a sharp upturn to a crossover to the cooperative diffusion coefficient  $D_{coop}$  in the semidilute solution. The latter increases in a power law with an exponent close to  $3/4$ .

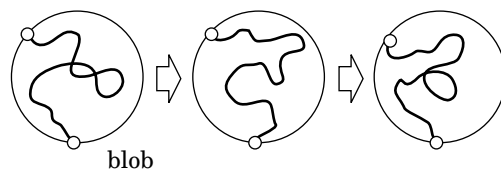


**Figure 4.28.** Monomer density fluctuation within a blob. The monomers can rearrange internally without changing the connection to the outside world.

shows schematically how the diffusion coefficient measured in DLS changes with the polymer concentration  $c$  in a wide range of concentrations.

The diffusion coefficient  $D_0$  in the dilute solution limit gives the hydrodynamic radius  $R_H$  of the isolated polymer chain in solution. The mutual diffusion coefficient  $D_m$  increases linearly with concentration in the dilute regime,  $c \ll c^*$ , as we have seen in Section 3.2.11. The increase is mostly ascribed to repulsive interactions between polymer chains that are manifested in the positive second virial coefficient. With a further increase in  $c$ ,  $D_m$  deviates upward from the linear relationship. As  $c$  exceeds  $c^*$  and the solution enters the semidilute regime, the diffusion coefficient starts to follow a straight line in a double logarithmic scale. The mutual diffusion observed by DLS in the semidilute solution is called the **cooperative diffusion**, since it represents cooperative motion of monomers within a blob. As Figure 4.28 illustrates, the partial chain within a blob is constantly rearranging itself without a need to move the two anchoring points. The dynamics follows a diffusion equation. As we will find below, the **cooperative diffusion coefficient** ( $D_{\text{coop}}$ ) is related to the blob size  $\xi$  (=correlation length) by

$$D_{\text{coop}} = \frac{k_B T}{6\pi\eta_s \xi} \quad \text{cooperative diffusion coefficient} \quad (4.43)$$

As  $\xi$  decreases with an increasing concentration, the cooperative diffusion becomes faster. Because  $\xi \sim c^{-\nu/(3\nu-1)}$ ,  $D_{\text{coop}}$  increases as  $D_{\text{coop}} \sim \xi^{-1} \sim c^{\nu/(3\nu-1)}$ . In the good solvent,  $D_{\text{coop}} \sim c^{3/4}$ . In the theta solvent,  $D_{\text{coop}} \sim c$ . These dependences are included in Table 4.1. Note that  $D_{\text{coop}}$  is independent of the molecular weight of the polymer.

We can use Eq. 4.43 to estimate the correlation length  $\xi$  of a given semidilute solution from the measurement of  $D_{\text{coop}}$  in DLS. The correlation length estimated in this way is often called the **dynamic correlation length**. Figure 4.29 shows an example for semidilute solutions of polystyrene with different molecular weights in various good solvents.<sup>51</sup> The data are on a straight line with a slope close to  $-3/4$ .

The difference in the expression of the diffusion coefficient between the single-chain diffusion (Eq. 3.54) and the cooperative diffusion is only  $R_H$  and  $\xi$ . The motional unit of size  $R_H$  gives way to the blob size  $\xi$  as the concentration exceeds  $c^*$ .

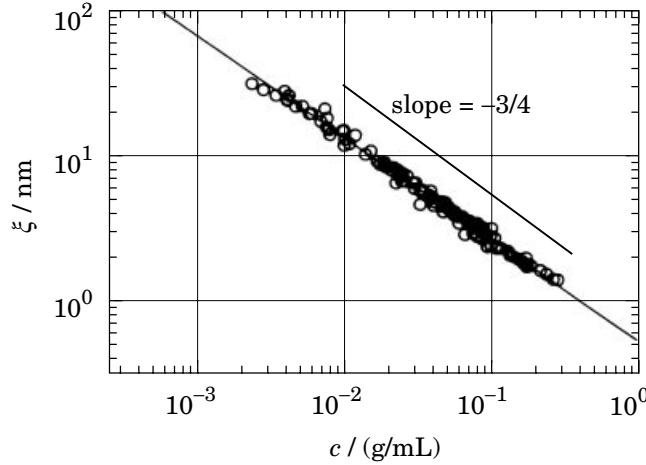


**Figure 4.29.** Correlation length  $\xi$  estimated from the cooperative diffusion coefficient. Data were obtained for polystyrene of different molecular weights in various good solvents. (From Ref. 51.)

The reason why  $D_{\text{coop}}$  is given by Eq. 4.43 is as follows. In Section 3.2.7, we learned that the hydrodynamic radius  $R_{\text{H}}$  of a linear chain polymer is given as the reciprocal of the average of  $r^{-1}$ , where  $r$  is the distance between two monomers on the chain. We used the definition to estimate  $R_{\text{H}}$  for a chain with a Gaussian chain conformation. We can use the same formula to calculate  $D_{\text{coop}}$  for the cooperative dynamic mode of the blob. It is given by

$$D_{\text{coop}} = \frac{k_{\text{B}}T}{6\pi\eta_{\text{s}}} \left\langle \frac{1}{r} \right\rangle \quad (4.44)$$

where  $r$  is the distance between two monomers that move cooperatively. The distance  $r$  is distributed with the Ornstein–Zernike correlation function. From Eq. 4.24,

$$\left\langle \frac{1}{r} \right\rangle = \frac{\int_0^{\infty} 4\pi r^2 \frac{1}{r} g_{\text{OZ}}(r) dr}{\int_0^{\infty} 4\pi r^2 g_{\text{OZ}}(r) dr} = \frac{1}{\xi} \quad (4.45)$$

Thus we obtain Eq. 4.43.

The decay rate  $\Gamma$  in the autocorrelation function  $|g_1(\tau)|$  for this cooperative mode is proportional to  $\mathbf{k}^2$ . It means that the monomer density fluctuation within the blob is diffusional. There is a good reason for this dynamic mode to be called the cooperative diffusion.

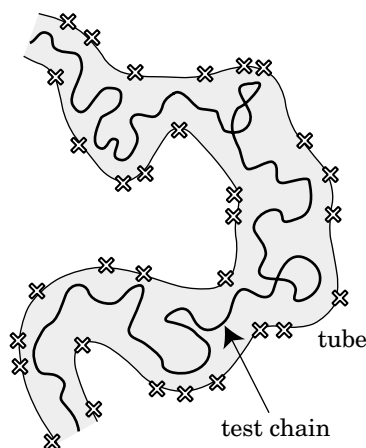


**Figure 4.30.** The test chain is trapped in a tube (indicated by the gray area) created by neighboring chains. The crossings represent the intersection of the neighboring chains with the curved surface on which the test chain lies.

### 4.3.2 Tube Model and Reptation Theory

**4.3.2.1 Tube and Primitive Chain** In the preceding subsection, we paid attention to the short-time motion of monomers within a blob. The motion does not involve translation of the polymer chain as a whole. Here we look at the overall motion of the chain over a distance longer than the blob size.

Polymer melts and semidilute and concentrated solutions of polymer are highly viscous. Even at a concentration of 1 wt %, solutions of polymer with a molecular weight greater than several million g/mol can flow only slowly. Their behaviors are even elastic like rubber at accessible time and frequency ranges. These exquisite properties had eluded researchers for decades until the **tube model** and the **reptation theory** elegantly solved the mystery. The tube model and the reptation theory were introduced by de Gennes.<sup>44</sup> They were refined and applied to the viscoelasticity of semidilute solutions of polymers and polymer melts in the late 1970s by Doi and Edwards.<sup>45</sup> Until then, there had been no molecular theory to explain these phenomena. We will learn the tube model and the reptation theory here.

We pick up a single chain, called a **test chain**, out of many chains in the solution. The test chain is highly entangled with neighboring chains. We can imagine a **tube-like** region surrounded by these neighboring chains around the test chain, as illustrated in Figure 4.30. These neighboring chains prohibit the test chain from moving beyond them, effectively confining the test chain into a tubelike region. Although the contour of the test chain is winding in three dimensions, we draw a two-dimensional illustration in which the test chain is constrained to the tube, as shown in the figure. We can regard the illustration as being drawn on the surface, curved along the test chain's contour and then pulled flat. The crosses in the figure represent intersections of the neighboring chains with the surface. Within the tube,

the test chain is winding. The tube diameter varies along the test tube's contour and also in time.

The tube model assumes the followings:

- (1) Over a short period of time, the test chain wiggles within the tube just as the monomers in the blob move cooperatively without moving out of the blob (Section 4.3.1).
- (2) Beyond that time scale, the test chain can move only along the tube. The test chain cannot move beyond the constraints imposed by the tube.
- (3) The head portion of the test chain can explore the next direction freely. As the head moves out of the existing tube, a new section is added to the tube. At the same time, the tail vacates a portion of the existing tube. Overall, there is little change in the length of the tube with time.

Later we will find that the test chain that follows the above assumptions makes a diffusional motion in the solution at sufficiently long times, although it is slow. The freedom allowed for the ends of the test chain makes the diffusion possible.

We learned in Section 4.2.2 that the polymer chain in the semidilute solution takes a conformation of an ideal chain. We therefore can use a random-walk model to construct the test chain. Let the random walk consist of  $N$  independent steps of step length  $b$ . Then, the contour length of the test chain is  $Nb$ , and the mean square end-to-end distance is  $Nb^2$ .

It is convenient to define a **primitive chain**. It is the centerline of the tube. The test chain wiggles around the primitive chain (Fig. 4.31). The motion of the primitive chain is nothing more than a coarse-grained view for the motion of the test chain it represents. Wiggling motion in the short time scale is averaged to form the primitive chain.

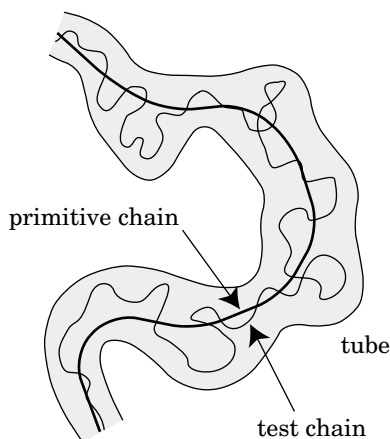


**Figure 4.31.** The primitive chain lies along the centerline of the tube. The test chain winds around the primitive chain.



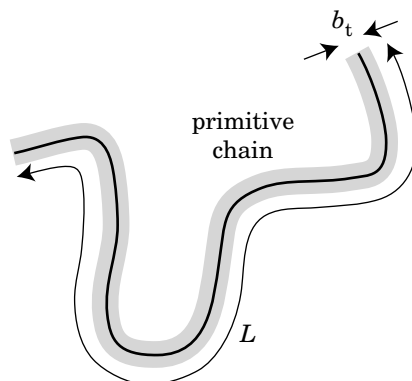


**Figure 4.32.** The primitive chain is regarded as an ideal chain of a step length of  $b_t$  and a contour length of  $L$ . The primitive chain and the test chain share the end-to-end distance.

According to the three assumptions of the tube model given earlier, the primitive chain moves only along its contour. Its motion is like a snake slithering on earth. This motion is called **reptation**. The end of the primitive chain can explore its next direction, but the rest follows its own existing path.

The primitive chain shares some of the statistical properties with the parent test chain. Both are ideal. Their end-to-end distance is the same. The conformation of the primitive chain is a coarse-grained version of the conformation of the test chain. When we apply the random-walk model to the primitive chain, its step length is equal to the tube diameter  $b_t$  (Fig. 4.32). Because the tube encases the test chain,  $b_t > b$ . We can appreciate the coarse-grained nature of the primitive chain in this inequality. The contour length  $L$  of the primitive chain is shorter than that of the test chain. We can estimate  $L$  as follows. For the primitive chain to have a contour length of  $L$ , the random walk must have  $L/b_t$  steps. We equate the mean square end-to-end distance of the test chain and that of the primitive chain:  $b_t^2(L/b_t) \cong b^2N$ . Then,

$$L \cong b^2N/b_t \quad (4.46)$$

For now, we proceed without knowing how to assess  $b_t$ . Just as the blob size,  $b_t$  will depend on the monomer density but not on the chain length; the density of crosses in Figure 4.30 is determined by the monomer density not by the chain length. Later, we will find the dependence.

**4.3.2.2 Tube Renewal** We illustrate in Figure 4.33 how the primitive chain changes its shape by continuously renewing its head or tail. The tube moves together with the primitive chain.

The primitive chain in panel a slides along its own contour. The advancing end emerges from the existing tube and finds a new path, just as a random walker moves another step forward, as shown in panel b. A new section is added

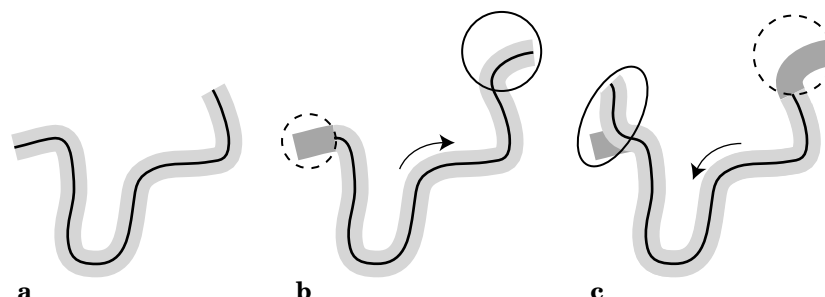


**Figure 4.33.** The tube changes its shape and position when the primitive chain slides along its contour. When the primitive chain moves from the one shown in panel a to the one shown in panel b, the advancing end adds a new portion to the existing tube (shown as a solid circle) and the receding end discards the other end of the old tube (shown as a dashed circle). When the primitive chain reverses its direction (panel c), the advancing end does not need to go back into the old tube. A new section is added at the advancing end, and an old section is depleted from the other end.

immediately to the growing end of the tube. At the same time, the receding end of the primitive chain vacates a portion of the existing tube, effectively annihilating the end of the tube. When the primitive chain reverses its course and goes back along its contour, as shown in panel c, the advancing end, formerly the receding end, does not need to move back into the old tube. The new advancing end can freely choose another path. Thus, a new section is always added to the tube while the other end is destroyed. The motion of the primitive chain is made possible by the motion of the test chain. As the test chain moves out of the existing tube while wiggling around, the new section of the tube is created. Along with the creation and annihilation of the tube sections, the primitive chain itself grows at one end and declines at the other end.

As the primitive chain moves back and forth along its own contour, the chain constantly renews the end portions of the tube. In each reversal of the course, the primitive chain adds a new section and loses a part of the memory regarding the constraint it had earlier. In Figure 4.34, panel a depicts the tube and the primitive chain when they have still some memory of the old tube. Eventually, none of the trace will be left of the old tube, as shown in panel b. The complete renewal can occur even when the centroid of the primitive chain is at the same position as the one when we started tracking the motion of the primitive chain. More likely, though, the primitive chain moves over a distance of its end-to-end distance. So does the test chain. In other words, the tube renewal occurs each time the centroid of the primitive chain moves the distance of  $bN^{1/2}$ .

**4.3.2.3 Disengagement** The tube renewal is made possible by reptation of the primitive chain along its own contour. To estimate the time necessary for the tube renewal, we need to know the nature of the reptation motion. The motion is a one-dimensional diffusion along a curve in three dimensions. Whether the primitive

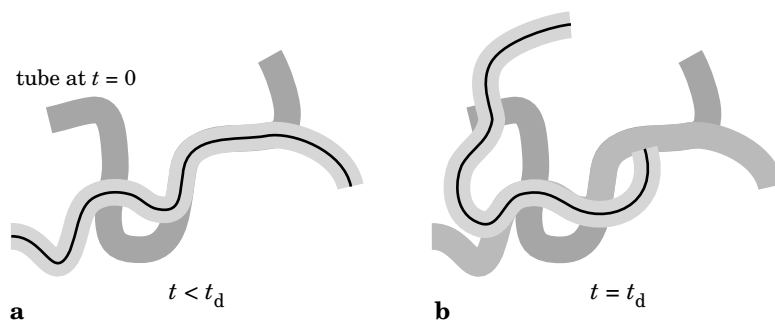


**Figure 4.34.** Tube renewal. a: The tube at a certain time (light gray) shares a part with the old tube that enclosed the test chain at  $t = 0$  (dark gray). b: The tube renewal continues, and finally the tube (light gray) shares no part with the old tube. The time needed to reach the latter state is called the disengagement time ( $t_d$ ).

chain moves back or forth is stochastic, reflecting the random motion of the test chain.

In the semidilute solution, the hydrodynamic interactions are shielded over the distance beyond the correlation length, just as the excluded volume is shielded. We can therefore approximate the dynamics of the test chain by a Rouse model, although the motion is constrained to the space within the tube. In the Rouse model, the chain as a whole receives the friction of  $N\zeta$ , where  $\zeta$  is the friction coefficient per bead. When the motion is limited to the curvilinear path of the primitive chain, the friction is the same. Because the test chain makes a Rouse motion within the tube, only the motion along the tube survives over time, leading to the translation of the primitive chain along its own contour. The one-dimensional diffusion coefficient  $D_c$  for the motion of the primitive chain is called the **curvilinear diffusion coefficient**. It is therefore equal to  $D_G$  of the Rouse chain (Eq. 3.160) and given by

$$D_c \cong \frac{k_B T}{N\zeta} \quad (4.47)$$

When the primitive chain slides along the tube with  $D_c$ , the **disengagement time**  $t_d$ , the time needed for the primitive chain to renew its encasing tube, is given as

$$t_d \cong \frac{L^2}{D_c} \quad (4.48)$$

In  $t_d$ , the primitive chain escapes the existing tube. With Eqs. 4.46 and 4.47,  $t_d$  is rewritten to

$$t_d \cong \frac{b^4 N^3 \zeta}{b_c^2 k_B T} \quad \text{disengagement time} \quad (4.49)$$

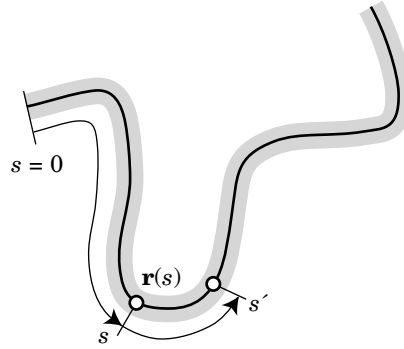


**Figure 4.35.** Two points,  $s$  and  $s'$ , on the primitive chain. Their mean square distance in the three-dimensional space is  $b_l |s - s'|$ .

The disengagement time is proportional to  $N^3$ . A slight increase in  $N$  leads to a large increase in  $t_d$ . The overall dynamics of the chains becomes a lot slower.

Let us compare  $t_d$  and  $\tau_1$ , the relaxation time of the first normal mode of the Rouse chain in the absence of entanglement. With  $\tau_1 \cong \zeta N^2 b^2 / k_B T$  (Eq. 3.136), we obtain

$$t_d / \tau_1 \cong N b^2 / b_l^2 \cong L / b_l \quad (4.50)$$

which is equal to the number of steps for the primitive chain in the random walk model. The chain is sufficiently long, and therefore  $L / b_l \gg 1$ . Thus,  $t_d \gg \tau_1$ .

**4.3.2.4 Center-of-Mass Motion of the Primitive Chain** First, we consider the motion of a point on the primitive chain when it makes one-dimensional diffusion. In Figure 4.35, we represent the contour of the primitive chain at a given time by  $\mathbf{r}(s)$ , where  $s$  is the distance along the chain measured from one of the chain ends, as we did for the wormlike chain in Section 1.5. Because  $\mathbf{r}(s)$  is described by the ideal chain model, the mean square distance measured in the three-dimensional space between two points  $s$  and  $s'$  on the primitive chain is given by (step length)<sup>2</sup>  $\times$  (number of steps). The step length is  $b_l$ . The contour between  $s$  and  $s'$  that registers the curvilinear length of  $|s - s'|$  has  $|s - s'| / b_l$  steps. Thus,

$$\langle [\mathbf{r}(s) - \mathbf{r}(s')]^2 \rangle \cong b_l |s - s'| \quad (4.51)$$

Now we move the primitive chain. The chain reptates along the tube with a diffusion coefficient  $D_c$ . The point at  $s = s(0)$  moves with the same diffusion coefficient  $D_c$ . We record the slithering motion of the point by the curvilinear distance measured from the end of the primitive chain at  $t = 0$  (gray line), as shown in Figure 4.36. Let the point on the primitive chain slide to  $s(t)$  in time  $t$ . Then, the one-dimensional displacement  $s(t) - s(0)$  along the contour of the primitive chain

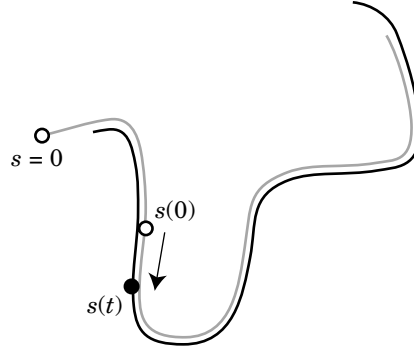


**Figure 4.36.** The primitive chain slides along its own contour. The point  $s(0)$  moves to  $s(t)$ , but it is still on the contour of the chain at  $t = 0$ , drawn in light gray. The distance  $s$  is measured from the end of the primitive chain at  $t = 0$ .

is given as

$$[s(t) - s(0)]^2 \cong D_c t \quad (4.52)$$

When  $t < t_d$ , most of the points on the primitive chain stay on its contour at  $t = 0$ . The two points  $s$  and  $s'$  in Eq. 4.51 can be  $s(0)$  and  $s(t)$ , respectively. Thus,

$$\langle [\mathbf{r}(s(t)) - \mathbf{r}(s(0))]^2 \rangle \cong b_l |s(t) - s(0)| \cong b_l (D_c t)^{1/2} \quad (4.53)$$

The mean square displacement in the three-dimensional space for a point on the primitive chain is proportional to  $t^{1/2}$ . Figure 4.37 illustrates the difference between the two distances. Recall that the mean square displacement is proportional to  $t$  in regular, unrestricted diffusion in solution. The exponent  $1/2$  in Eq. 4.53 is due to the one-dimensional random walk on a path created by another random walker in the three-dimensional space.

The  $t^{1/2}$  dependence is limited to  $t < t_d$ . As the primitive chain escapes the presently trapping tube in  $t_d$ , it may change the dependence in the time scale of  $t > t_d$ . Now we pay attention to the overall movement of the primitive chain in that time scale. The overall movement consists of step motions. In each step time, the end of the primitive chain moves a distance of  $b_l$  to find a new direction. The rest of the chain follows the existing contour. The step time  $t_1$  is the time needed for the one-dimensional diffusion to move a distance of  $b_l$  with the diffusion coefficient  $D_c$ , that is,  $D_c t_1 \cong b_l^2$ . Thus,

$$t_1 \cong b_l^2 / D_c \quad (4.54)$$

The step displacement for the centroid of the primitive chain in time  $t_1$  is evaluated as follows. The contour of the primitive chain at  $t = 0$  is given as  $\{\mathbf{r}(s); 0 \leq s \leq L\}$ . The contour at  $t = t_1$  is built on the contour at  $t = 0$ . We can use the contour

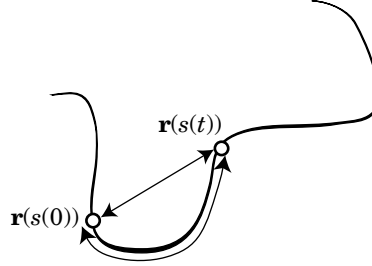


**Figure 4.37.** The mean square distance between  $\mathbf{r}(s(t))$  and  $\mathbf{r}(s(0))$  in the three-dimensional space is around  $(D_c t)^{1/2}$ . The mean square distance between the two points measured along the contour of the primitive chain is around  $D_c t$ .

$\mathbf{r}(s)$  at  $t = 0$  to describe the contour at  $t = t_1$  as  $\{\mathbf{r}(s); b_t \leq s \leq L + b_t\}$ . In the latter,  $\{\mathbf{r}(s); L \leq s \leq L + b_t\}$  represents the newly created portion and  $\{\mathbf{r}(s); 0 \leq s \leq b_t\}$  is the discarded portion. The rest is the same as the contour at  $t = 0$  (Fig. 4.38). The center-of-mass positions  $\mathbf{r}_G(0)$  and  $\mathbf{r}_G(t_1)$  of the primitive chain at  $t = 0$  and  $t = t_1$  are respectively given as

$$\mathbf{r}_G(0) = L^{-1} \int_0^L \mathbf{r}(s) ds, \quad \mathbf{r}_G(t_1) = L^{-1} \int_{b_t}^{L+b_t} \mathbf{r}(s) ds \quad (4.55)$$

Then,

$$\mathbf{r}_G(t_1) - \mathbf{r}_G(0) = L^{-1} \int_0^{b_t} [\mathbf{r}(L+s) - \mathbf{r}(s)] ds \quad (4.56)$$

Its mean square is

$$\langle [\mathbf{r}_G(t_1) - \mathbf{r}_G(0)]^2 \rangle = L^{-2} \int_0^{b_t} \int_0^{b_t} \langle [\mathbf{r}(L+s) - \mathbf{r}(s)] \cdot [\mathbf{r}(L+s') - \mathbf{r}(s')] \rangle ds ds' \quad (4.57)$$

Because  $b_t \ll L$ ,  $\mathbf{r}(L+s) - \mathbf{r}(s) \cong \mathbf{r}(L) - \mathbf{r}(0)$  for  $0 < s < b_t$ . Thus, the mean square displacement in one step is

$$\begin{aligned} \langle [\mathbf{r}_G(t_1) - \mathbf{r}_G(0)]^2 \rangle &\cong L^{-2} \int_0^{b_t} \int_0^{b_t} \langle [\mathbf{r}(L) - \mathbf{r}(0)]^2 \rangle ds ds' \\ &\cong L^{-2} \int_0^{b_t} \int_0^{b_t} Nb^2 ds ds' = Nb^2 b_t^2 / L^2 \end{aligned} \quad (4.58)$$

The primitive chain repeats this step motion to move its center of mass. Each step is independent because the chain end is free to choose its next direction. The displacement in the second step,  $\mathbf{r}_G(2t_1) - \mathbf{r}_G(t_1)$ , is uncorrelated with the displacement

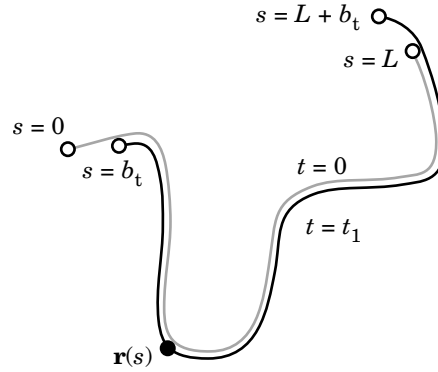


**Figure 4.38.** The primitive chain at  $t = t_1$  is on the contour of the chain at  $t = 0$  and its extension. The chain at  $t_1$  occupies the portion from  $s = b_t$  to  $s = L + b_t$  measured from one end of the primitive chain at  $t = 0$ .

in the first step,  $\mathbf{r}_G(t_1) - \mathbf{r}_G(0)$ . Thus, the ratio of the mean square displacement to the step time gives the center-of-mass diffusion coefficient  $D_G$  of the primitive chain in solution:

$$D_G \cong \frac{\langle [\mathbf{r}_G(t_1) - \mathbf{r}_G(0)]^2 \rangle}{t_1} \cong \frac{Nb^2 b_t^2 D_c}{L^2 b_t^2} = D_c \frac{Nb^2}{L^2} \quad (4.59)$$

With Eqs. 4.46 and 4.47,

$$D_G \cong \frac{k_B T b_t^2}{N^2 \zeta b^2} \quad \text{diffusion coefficient} \\ \text{reptation theory} \quad (4.60)$$

Note that this  $D_G$  is also the center-of-mass diffusion coefficient for the test chain.  $D_G$  decreases as  $\sim N^{-2}$  with an increasing chain length. The absolute value of the exponent is much greater compared with the center-of-mass diffusion coefficient of linear chain polymer in dilute solutions in which  $D_G \sim N^{-1}$  for the Rouse chain and  $\sim N^{-1/2}$  for the Zimm model in the theta condition.

How much does the primitive chain move its center of mass in  $t_d$  with this diffusion coefficient? From Eqs. 4.49 and 4.60, it is easy to find that

$$D_G t_d \cong Nb^2 \quad (4.61)$$

As the primitive chain renews the existing tube, its center of mass moves a distance equal to its end-to-end distance, a reasonable result.

**4.3.2.5 Estimation of the Tube Diameter** So far, we have been using the tube diameter  $b_t$  as a given quantity. We expect that the tube will become thinner as the concentration increases and therefore the other chains impose crossings nearer to

the test chain. As  $D_G \sim b_t^2$ , we expect  $D_G$  to decrease with an increasing concentration. To find the dependence, we simply apply the scaling theory to  $D_G$  and assume

$$D_G = D_{G0} f_G(\rho R_{g0}^3/N) \quad (4.62)$$

where the scaling function  $f_G(x)$  satisfies

$$f_G(x) \begin{cases} = 1 & (x \rightarrow 0) \\ \cong x^m & (x \gg 1) \end{cases} \quad (4.63)$$

with a scaling exponent  $m$ . Because  $D_{G0} \cong k_B T / (\eta_s R_{g0})$ ,  $D_G$  at  $\rho R_{g0}^3/N \gg 1$  is

$$D_G = \frac{k_B T}{\eta_s R_{g0}} (\rho R_{g0}^3/N)^m \cong \frac{k_B T}{\eta_s} \rho^m b^{3m-1} N^{\nu(3m-1)-m} \quad (4.64)$$

where  $R_{g0} \cong bN^\nu$  was used. The requirement that this  $D_G$  have the same  $N$  dependence as Eq. 4.60 leads to  $\nu(3m-1)-m = -2$ ; that is,  $m = (\nu-2)/(3\nu-1)$ . The exponent  $m$  is  $-7/4$  for  $\nu = 3/5$ . Thus,  $D_G$  decreases with  $c$  in the good solvent as

$$\boxed{D_G/D_{G0} \cong (c/c^*)^{-7/4} \quad \text{good solvent}} \quad (4.65)$$

If we use  $\nu = 0.59$ ,  $m = -1.83$ . In the theta solvent,  $m = -3$ . The decrease is steeper:

$$\boxed{D_G/D_{G0} \cong (c/c^*)^{-3} \quad \text{theta solvent}} \quad (4.66)$$

The comparison of Eqs. 4.60 and 4.64 with  $m = -7/4$  allows us to estimate  $b_t$  for the good solvent condition. It is obtained as

$$b_t \cong (\zeta/\eta_s)^{1/2} b^{-17/8} \rho^{-7/8} \quad (4.67)$$

With an increasing  $\rho$ ,  $b_t$  decreases in a power with an exponent of  $-7/8$ . As required,  $b_t$  is independent of  $N$ .

**4.3.2.6 Measurement of the Center-of-Mass Diffusion Coefficient** The center-of-mass diffusion coefficient  $D_G$  we obtained here is the self-diffusion coefficient  $D_s$ . DLS cannot measure the self-diffusion coefficient. It is necessary to use more specialized techniques such as FRS, FRAP, and PFG-NMR, described in Section 3.2.11. Figures 4.39 and 4.40 show examples of FRS studies of  $D_s$  for dye-labeled polystyrene in benzene.<sup>52</sup>

Figure 4.39 shows a plot of  $D_s$  as a function of the molecular weight  $M$  of the polymer at two concentrations, 0.1 and 0.2 g/g (mass fraction of the polymer in solution), in the semidilute regime. The data at each concentration are apparently on a straight line with a slope of  $-2$ , in agreement with the prediction given by



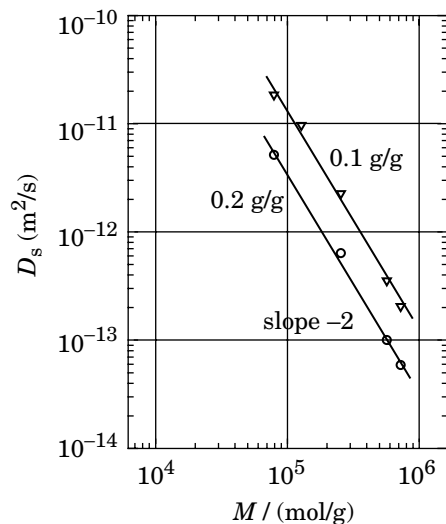


**Figure 4.39.** Self-diffusion coefficient  $D_s$  of dye-labeled polystyrene in benzene at different concentrations, plotted as a function of the molecular weight  $M$  of the polymer. The lines have a slope of  $-2$ . (From Ref. 52.)

Eq. 4.60. The concentration dependence of  $D_s$  is shown in Figures 4.40. There is a gradual decrease in  $D_s$  with an increasing concentration. The data obtained for the semidilute solutions are on straight lines with a slope of  $-7/4$ , in agreement with Eq. 4.65.

We can use DLS to measure the tracer diffusion coefficient  $D_t$  in a ternary solution of two polymers and a solvent. The concentration of the matrix polymer is changed widely from dilute to semidilute, whereas the concentration of the probe polymer is held low. It is necessary to choose a solvent that is isorefractive with the matrix polymer and at the same time is nonselective to the two polymers. Then, DLS will selectively detect the light scattering from the probe polymer. For  $D_t$  to simulate  $D_G$ , the interaction between the matrix polymer and probe polymer must be identical to the interaction between the matrix polymers. We hope that a pair of miscible polymers such as polystyrene probe and poly(vinyl methyl ether) matrix will satisfy this requirement. Figure 4.41 shows an example for the pair.<sup>53</sup> The common solvent is *o*-fluorotoluene. The figure shows a plot of  $D_t$  as a function of  $M_{PS}$ , the molecular weight of polystyrene, for different concentrations of the matrix polymer (molecular weight =  $1.3 \times 10^6$  g/mol). In the absence of the matrix,  $D_t \sim M_{PS}^{-0.56}$ , indicating self-diffusion of isolated polystyrene chains in a good solvent. With an increasing matrix concentration, the slope becomes steeper. In the semidilute solutions, the slope is around  $-2$ , in agreement with Eq. 4.60 assuming  $D_t \cong D_G$ .

**4.3.2.7 Constraint Release** The reptation theory assumes that the environment is frozen while the test chain moves. This assumption is questionable. The other

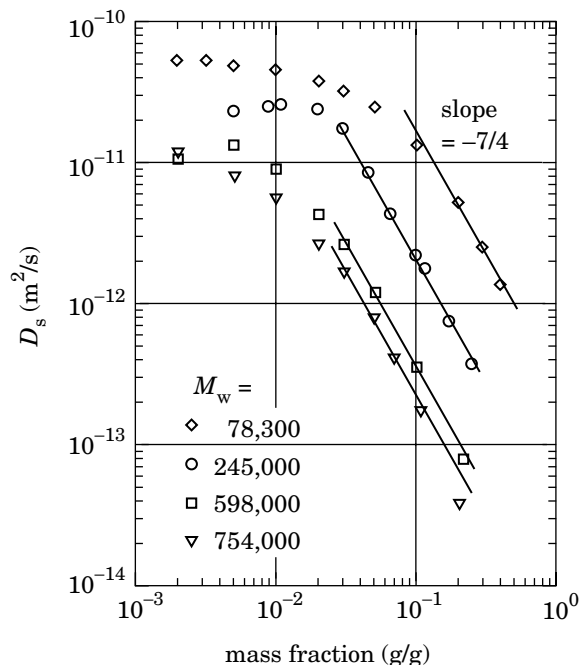


**Figure 4.40.** Self-diffusion coefficient  $D_s$  of dye-labeled polystyrene of different molecular weights  $M_w$  in benzene, plotted as a function of the polymer mass fraction. The lines have a slope of  $-7/4$ . (From Ref. 52.)

chains surrounding the test chain are moving in the same way in the same time scale as the test chain moves. Some entanglement points will come loose. New entanglement points will be created, as shown in Figure 4.30, while the test chain tries to get out of the existing tube. Annihilation and creation of the entanglement points will allow the tube to be renewed by another mechanism—**constraint release**. In the latter, the motion of the test chain is not limited to the one along the tube. The test chain can also move laterally.

**4.3.2.8 Diffusion of Polymer Chains in a Fixed Network** Although the tube model and the reptation model were originally developed to explain the diffusion of polymer chains in concentrated solutions and melts, we can use it more naturally for the motion of polymer chains in a fixed network, for instance, a cross-linked network of polymer swollen in a good solvent. In the fixed network, the constraint release is absent. Therefore, we should be able to observe the reptation without being compromised.

The cross-linked network of polymer is called a **gel**. In the absence of the cross-linking, the swollen gel would form a solution. A probe polymer is added to the gel matrix, and the motion of the probe chains is traced by using DLS. The solvent needs to be isorefractive with the gel matrix to allow one to selectively detect the

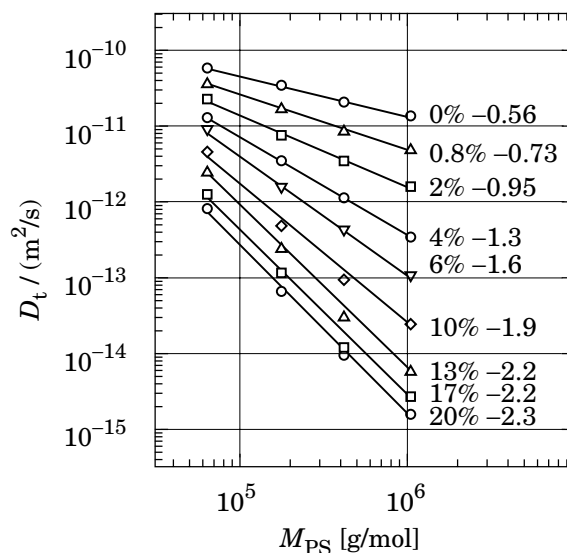


**Figure 4.41.** Tracer diffusion coefficient  $D_t$  of polystyrene in solutions of matrix polymer, poly(vinyl methyl ether), in *o*-fluorotoluene at various concentrations of the matrix polymer, plotted as a function of molecular weight  $M_{PS}$  of polystyrene. The solvent is isorefractive with the matrix polymer. The concentration of the matrix polymer and the slope obtained in the best fitting by a power law (straight line) are indicated adjacent to each plot. (From Ref. 53.)

scattering by the probe chains. Figure 4.42 shows an example for the tracer diffusion coefficient  $D_t$  of the probe chains.<sup>54</sup> The matrix is cross-linked poly(vinyl methyl ether) swollen in toluene. The probe is linear polystyrene of different molecular weights. For sufficiently high molecular weights  $M_{PS}$  of polystyrene,  $D_t$  decreases in a power law of  $M_{PS}^{-2.8}$ , steeper than the theoretically predicted  $M_{PS}^{-2}$ . Other experimental techniques can also be used, for instance, FRS, FRAP, and PFG-NMR.

**4.3.2.9 Motion of the Monomers** Here, we consider the mean square displacement of monomers on the entangled chains. Over a long time,  $t > t_d$ , the mean square displacement of the monomer,  $\langle [\mathbf{r}_n(t) - \mathbf{r}_n(0)]^2 \rangle$ , becomes identical to the mean square displacement of the centroid of the primitive chain. Our interest is the short-time behavior in  $t < t_d$ . We expect that the monomers have a greater mobility in short time scales as in the bead-spring chain, which was discussed in Section 3.4.

We focus our attention primarily on the time range of  $t > t_e$ , where  $t_e$  is the time for the mean square displacement of a monomer on the test chain to reach  $b_1^2$ . At  $t < t_e$ , the test chain wiggles within the tube without feeling the presence of the geometrical constraint imposed by neighboring chains. At  $t > t_e$ , the motion of the test chain is the same as that of the primitive chain.

In Sections 4.3.2.3 and 4.3.2.4, we assumed that the primitive chain follows a simple one-dimensional diffusion along its contour. This view is correct only for

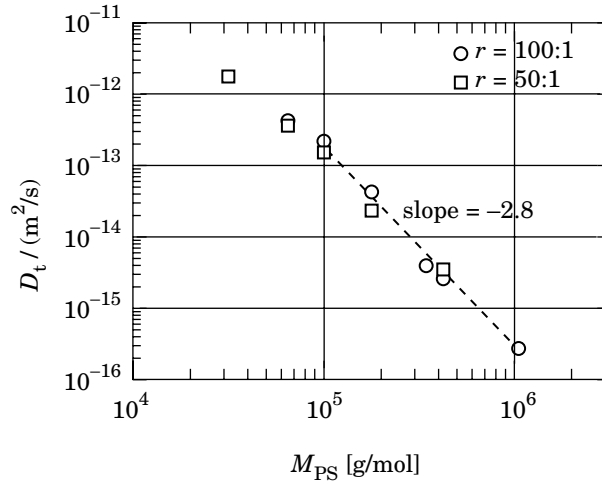


**Figure 4.42.** Tracer diffusion coefficient  $D_t$  of polystyrene in a cross-linked matrix of poly(vinyl methyl ether) in toluene, plotted as a function of molecular weight  $M_{PS}$  of polystyrene. The concentration of the matrix gel was 0.235 g/mL. The monomer to cross-linker ratio,  $r$ , was 100 and 50. The dashed line has a slope of  $-2.8$ . (From Ref. 54.)

sufficiently long time scales,  $t > \tau_1$ , the relaxation time of the first normal mode (but  $t < t_d$ ). In short time scales,  $t < \tau_1$ , the motion of the primitive chain is not a simple diffusion along its contour.

The test chain would follow the dynamics of the unrestricted Rouse chain if the entanglements were absent, as would the primitive chain at  $t > t_e$ . In Section 3.4.9, we considered the mean square displacement of monomers on the Rouse chain. We found that the dynamics is diffusional at  $t < \tau_N$  and  $\tau_1 < t$ , where  $\tau_N$  is the relaxation time of the  $N$ th normal mode but not in between. When the motion of the Rouse chain is restricted to the tube, the mean square displacement of monomers along the tube,  $\langle [s(t) - s(0)]^2 \rangle$ , will follow the same time dependence as the mean square displacement of the unrestricted Rouse chain in three dimensions. Thus, from Eqs. 3.240 and 3.243,

$$\langle [s(t) - s(0)]^2 \rangle \cong \begin{cases} Nb^2(t/\tau_1)^{1/2} & (t_e < t < \tau_1) \\ D_c t & (\tau_1 < t) \end{cases} \quad (4.68)$$

where  $D_c = k_B/N\zeta$  gives the center-of-mass diffusion coefficient of the Rouse chain in the absence of the entanglements.

We can map Eq. 4.68 onto the one-dimensional reptation dynamics, as we mapped a simple one-dimensional diffusion in Section 4.3.2.4. With Eq. 4.51 and  $s = s(0)$  and  $s' = s(t)$ , we have

$$\langle [\mathbf{r}_n(t) - \mathbf{r}_n(0)]^2 \rangle \cong \begin{cases} N^{1/2} b b_0 (t/\tau_1)^{1/4} & (t_e < t < \tau_1) \\ b_1 (D_c t)^{1/2} & (\tau_1 < t < t_d) \end{cases} \quad (4.69)$$

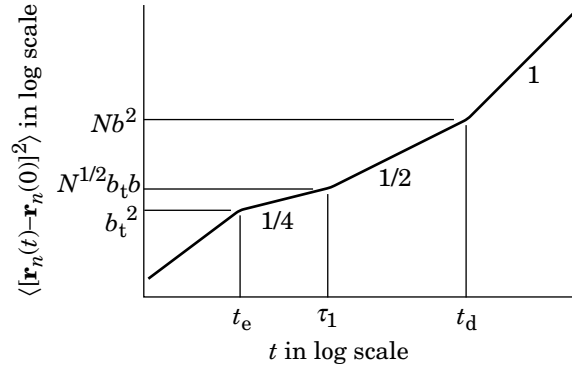


**Figure 4.43.** Mean square displacement of monomers on entangled chains,  $\langle [\mathbf{r}_n(t) - \mathbf{r}_n(0)]^2 \rangle$  plotted as a function of time  $t$ . The plot has four sections with distinct slopes. They are indicated adjacent to the plot. The boundaries of the four sections are specified by their values of  $t$  and  $\langle [\mathbf{r}_n(t) - \mathbf{r}_n(0)]^2 \rangle$ .

In the time scale of  $t > t_d$ , the effect of finding the new direction by the chain ends becomes dominant, and the mean square displacement of monomers will become equal to that of the center of mass. In the time scale of  $t < t_e$ , the motion of the monomers is complicated. At sufficiently short times ( $t < \tau_N$ ), the monomers will make a diffusional motion without feeling the presence of other monomers, as we have seen for both the Rouse chain and the Zimm model. We can at least say that the dependence of  $\langle [\mathbf{r}_n(t) - \mathbf{r}_n(0)]^2 \rangle$  on  $t$  is sharper at  $t < t_e$ .

Thus, we have the mean square displacement of monomers on the test chain for  $t > t_e$  as

$$\langle [\mathbf{r}_n(t) - \mathbf{r}_n(0)]^2 \rangle \cong \begin{cases} N^{1/2} b b_t (t/\tau_1)^{1/4} & (t_e < t < \tau_1) \\ b_t (D_c t)^{1/2} & (\tau_1 < t < t_d) \\ D_G t & (t_d < t) \end{cases} \quad \begin{array}{l} \text{monomer diffusion} \\ \text{by reptation} \end{array} \quad (4.70)$$

Figure 4.43 illustrates the different regimes in the plot of  $\langle [\mathbf{r}_n(t) - \mathbf{r}_n(0)]^2 \rangle$ . The boundary of each section is shown both for the time and the mean square displacement.

Presence of a section in which  $\langle [\mathbf{r}_n(t) - \mathbf{r}_n(0)]^2 \rangle \sim t^{1/2}$  is due to the reptation dynamics. Presence of a section in which  $\langle [\mathbf{r}_n(t) - \mathbf{r}_n(0)]^2 \rangle \sim t^{1/4}$  is due to the Rouse dynamics added on top of the reptation.

### 4.3.3 Problems

**Problem 4.11:** Estimate the tube diameter  $b_t$  for solutions in the theta condition.

**Solution 4.11:** Comparison of Eqs. 4.60 and 4.64 with  $m = -3$  leads to

$$b_t \cong (\zeta/\eta_s)^{1/2} b^{-4} \rho^{-3/2}$$

## REFERENCES

1. M. Doi, *Introduction to Polymer Physics*, Oxford Univ. Press: Clarendon, 1996.
2. J. des Cloizeaux, G. Jannink, *Polymers in Solution: Their Modelling and Structure*, Oxford Univ. Press: Clarendon (1990).
3. P. J. Flory, *Principles of Polymer Chemistry*, Cornell University Press, Ithaca (1953).
4. S. Trainoff, P. J. Wyatt, in *International GPC Symposium '98*. R. Nielson, Ed. Waters: Milford (1999).
5. Y. Wang, I. Teraoka, *Macromolecules* **33**, 3478 (2000).
6. P. Cifra, T. Bleha, *Macromol Theory Simul* **8**, 603 (1999).
7. M. M. Green, N. C. Peterson, T. Sato, A. Teramoto, R. Cook, *Science* **268**, 1860 (1995).
8. H. Murakami, T. Norisuye, H. Fujita, *Macromolecules* **13**, 345 (1980).
9. P. M. Cotts, Z. Guan, E. McCord, S. McLain, *Macromolecules* **33**, 6945 (2000).
10. S. Matsuyama, H. Nakahara, K. Takeuchi, R. Nagahata, S. Kinugasa, I. Teraoka, *Polym J* **32**, 249 (2000).
11. J. Brandrup, E. H. Immergut, E. A. Grulke, Ed. *Polymer Handbook* (4th Ed), Wiley: New York (1999).
12. M. L. Huggins, *Ann. NY Acad Sci* **43**, 1 (1942).
13. E. A. Guggenheim, *Mixtures*, Oxford University Press: London, 1952.
14. J. P. Cotton, *J Phys Lett* **41**, L-231 (1980).
15. A. R. Shultz, P. J. Flory, *J Am Chem Soc* **74**, 4760 (1952).
16. C. Strazielle, H. Benoit, *Macromolecules* **8**, 203 (1975).
17. A. Z. Panagiotopoulos, V. Wong, M. A. Floriano, *Macromolecules* **31**, 912 (1998).
18. P. Grassberger, R. Hegger, *J Chem Phys* **102**, 6881 (1995).
19. X. Wang, X. Qiu, C. Wu. *Macromolecules* **31**, 2972 (1998).
20. Y. Wang, Private communications.
21. B. Chu, *Laser Light Scattering: Basic Principles and Practice* (2nd ed.), Academic Press: San Diego, 1991.
22. K. S. Schmitz, *An Introduction to Dynamic Light Scattering by Macromolecules*, Academic Press: San Diego, 1990.
23. M.-P. Nieh, A. A. Goodwin, J. R. Stewart, B. M. Novak, D. A. Hoagland, *Macromolecules* **31**, 3151 (1998).
24. Waters, Inc.
25. Wyatt Technology Corporation.
26. D. Pötschke, M. Ballauff, P. Lindner, M. Fischer, F. Vögtle, *Macromolecules* **32**, 4079 (1999).
27. E. F. Casassa, *J Polym Sci Polym Lett Ed.* **5**, 773 (1967); E. F. Casassa, Y. Tagami, *Macromolecules* **2**, 14 (1969),
28. J. C. Giddings, E. Kucera, C. P. Russell, M. N. Myers, *J Phys Chem* **72**, 4397 (1968).
29. I. Teraoka, *Progr. Polym Sci* **21**, 89 (1996).
30. M. T. Bishop, K. H. Langley, F. E. Karasz, *Macromolecules* **22**, 1220 (1989).
31. I. Suda, Y. Tominaga, M. Osa, T. Yoshizaki, H. Yamakawa, *Macromolecules* **33**, 9322 (2000).
32. S. W. Provencher, *Macromol Chem* **180**, 201 (1979).

33. K. H. Langley, I. Teraoka, in *Methods in the Physics of Porous Media*. P.-Z. Wong, Ed. Academic Press: San Diego (1999).
34. D. S. Viswanath, G. Natarajan, *Data Book on the Viscosity of Liquids*, Hemisphere, New York (1989).
35. R. Balic, R. G. Gilbert, M. D. Zammit, T. P. Davis, C. M. Miller, *Macromolecules* **30**, 3775 (1997).
36. P. E. Rouse, *J Chem Phys* **21**, 1272 (1953).
37. B. H. Zimm, *J Chem Phys* **24**, 269 (1956).
38. Y. Oono, M. Kohmoto, *J Chem Phys* **78**, 520 (1983).
39. C. Kuo, T. Provder, R. A. Sanayei, K. F. O'Driscoll in *International GPC Symposium '94*. R. Nielson, Ed. Waters, Milford (1994).
40. D. W. Schaefer, C. C. Han, in *Dynamic Light Scattering*. Ed. R. Pecora, Plenum, NY (1985).
41. J. G. Kirkwood, P. L. Auer, *J Chem Phys* **19**, 281 (1951).
42. H. Yamakawa, *Helical Wormlike Chains in Polymer Solutions*, Springer, Berlin (1997).
43. T. Itou, H. Chikiri, A. Teramoto, S. M. Aharoni, *Polym J* **20**, 143 (1988).
44. P.-G. de Gennes, *Scaling Concepts in Polymer Physics*, Cornell Univ. Press: Ithaca (1979).
45. M. Doi, S. F. Edwards, *The Theory of Polymer Dynamics*, Oxford Univ. Press: Clarendon (1986).
46. I. Noda, N. Kato, T. Kitano, M. Nagasawa, *Macromolecules* **14**, 668 (1981).
47. T. Ohta, Y. Oono, *Phys Lett* **89A**, 460 (1982).
48. P. Wiltzius, H. R. Haller, D. S. Cannell, D. W. Schaefer, *Phys Rev Lett* **51**, 1183 (1983).
49. M. Daoud, J. P. Cotton, B. Farnoux, G. Jannink, G. Sarma, H. Benoit, R. Duplessix, C. Picot, P.-G. de Gennes. *Macromolecules* **8**, 804 (1975).
50. Y. Oono, *Adv Chem Phys* **61**, 301 (1985).
51. W. Brown, T. Nicolai, in *Dynamic Light Scattering: The Method and Some Applications*. Ed. W. Brown, Oxford Univ. Press: Clarendon (1993).
52. L. Léger, H. Hervet, F. Rondelez, *Macromolecules* **14**, 1732 (1981).
53. L. M. Wheeler, T. P. Lodge, *Macromolecules* **22**, 3399 (1989).
54. N. A. Rotstein, T. P. Lodge, *Macromolecules* **25**, 1316 (1992).

## FURTHER READINGS

There are several textbooks and research monographs on polymer solutions. Some of the contents partly overlap with the scope of this textbook. The following books are recommended to readers interested in further studies:

1. P.-G. de Gennes, *Scaling Concepts in Polymer Physics*, Cornell Univ. Press: Ithaca (1979).

This is a good introduction to the scaling theory by the pioneer of the theory. The scaling concept is used for polymer solutions, polymer blends, melts, and gels.

2. M. Doi, S. F. Edwards, *The Theory of Polymer Dynamics*, Oxford Univ. Press: Clarendon (1986).

Detailed explanations on theoretical tools are given. Emphasis is on viscoelastic properties. The book contains a few chapters on dilute, semidilute, and concentrated solutions of rodlike molecules. The following is a simplified version: M. Doi, *Introduction to Polymer Physics*, Oxford Univ. Press: Clarendon, 1996.

3. G. Strobl, *The Physics of Polymers* (2nd ed), Springer: Berlin (1997).

This book deals with polymer physics in general, including solid states of polymers. It offers a succinct account of solution properties.

4. H. Yamakawa, *Helical Wormlike Chains in Polymer Solutions*, Springer: Berlin (1997).

This book offers a detailed explanation on conformation and dynamics of wormlike chains and helical wormlike chains by an expert of the model.

5. H. Morawetz, *Macromolecules in Solution* (2nd ed), Wiley: New York (1975).

This book is a historical standard of polymer solution textbook. It is now available from Krieger.

6. P. J. Flory, *Principles of Polymer Chemistry*, Cornell University Press: Ithaca, 1953.

This book is another historical standard of polymer in general.

7. A. Y. Grosberg, A. R. Khokhlov, *Statistical Physics of Macromolecules*, AIP Press: Woodbury, 1994.

This book offers a detailed account of the scaling theory. It contains many applications.

8. J. des Cloizeaux, G. Jannink, *Polymers in Solution: Their Modelling and Structure*, Oxford Univ. Press: Clarendon (1990).

This book offers a detailed account of the renormalization group theory. The book contains an excellent review of many experimental data on the thermodynamic properties of polymer solutions.

9. H. Fujita, *Polymer Solutions*, Elsevier: Amsterdam (1990).

This book offers a formal introduction to polymer solution theory. It contains many experimental data.

There are several books on light scattering:

1. K. S. Schmitz, *An Introduction to Dynamic Light Scattering by Macromolecules*, Academic Press: San Diego, 1990.
2. B. Chu, *Laser Light Scattering: Basic Principles and Practice* (2nd ed.), Academic Press: San Diego, 1991.
3. W. Brown ed. *Dynamic Light Scattering: The Method and Some Applications*, Oxford Univ. Press: Clarendon, 1993.



## APPENDIX

Some of the mathematics used in this textbook are detailed here.

### A1 DELTA FUNCTION

A delta function [ $\delta(x)$ ] has an infinite value at  $x = 0$  and is zero everywhere else. It is impossible to draw a plot of  $\delta(x)$ , but it may be convenient to regard it as a positive spike at  $x = 0$ . The integral of  $\delta(x)$  over a finite interval that contains  $x = 0$  is 1:

$$\int_{0^-}^{0^+} \delta(x) dx = \int_{-\infty}^{\infty} \delta(x) dx = 1 \quad (\text{A1.1})$$

where  $0^-$  is infinitesimally smaller than 0, and  $0^+$  is infinitesimally greater than 0. On integration of the product of  $\delta(x)$  and an arbitrary function  $f(x)$ , we obtain

$$\int_{-\infty}^{\infty} \delta(x) f(x) dx = f(0) \quad (\text{A1.2})$$

The following formula is useful:

$$\int_{-\infty}^{\infty} \delta(x-a) f(x) dx = f(a) \quad (\text{A1.3})$$

In three dimensions, we write

$$\delta(\mathbf{r}) \equiv \delta(x)\delta(y)\delta(z) \quad (\text{A1.4})$$

It is easy to find

$$\int_{-\infty}^{\infty} \delta(\mathbf{r}) d\mathbf{r} = 1 \quad (\text{A1.5})$$

where  $d\mathbf{r} = dx dy dz$  and the range of integration can be any volume that contains  $\mathbf{r} = 0$ . We can evaluate an arbitrary function  $f(\mathbf{r})$  at  $\mathbf{r} = \mathbf{a}$ :

$$\int_{-\infty}^{\infty} \delta(\mathbf{r}-\mathbf{a}) f(\mathbf{r}) d\mathbf{r} = f(\mathbf{a}) \quad (\text{A1.6})$$

There are several ways to define  $\delta(x)$  by an equation. One of them is

$$\delta(x) \equiv \frac{1}{2\pi} \int_{-\infty}^{\infty} \exp(ikx) dk \quad (\text{A1.7})$$

In three dimensions,

$$\delta(\mathbf{r}) \equiv \frac{1}{(2\pi)^3} \int_{-\infty}^{\infty} \exp(i\mathbf{k} \cdot \mathbf{r}) d\mathbf{k} \quad (\text{A1.8})$$

## A2 FOURIER TRANSFORM

For an arbitrary function  $f(x)$  of a space variable  $x$ , its Fourier transform  $\hat{f}(k)$  is defined by

$$\hat{f}(k) \equiv \int_{-\infty}^{\infty} f(x) \exp(ikx) dx \quad (\text{A2.1})$$

The variable  $k$  is called a wave vector also for one dimension. To see what information of  $f(x)$  is carried into  $\hat{f}(k)$ , let us consider a sinusoidal wave with wave vector  $k_1$  and amplitude  $A_1$ :

$$f(x) = A_1 \cos k_1 x = (A_1/2)[\exp(ik_1 x) + \exp(-ik_1 x)] \quad (\text{A2.2})$$

Then, from the definition,

$$\begin{aligned} \hat{f}(k) &\equiv \frac{A_1}{2} \int_{-\infty}^{\infty} [\exp(ik_1 x) + \exp(-ik_1 x)] \exp(ikx) dx \\ &= \frac{A_1}{2} \int_{-\infty}^{\infty} [\exp(i(k + k_1)x) + \exp(i(k - k_1)x)] dx \\ &= \pi A_1 [\delta(k + k_1) + \delta(k - k_1)] \end{aligned} \quad (\text{A2.3})$$

which means that  $\hat{f}(k)$  is nonzero only at  $k = \pm k_1$ . The integral of  $\hat{f}(k)$  in a range including  $k = k_1$  or  $k = -k_1$  but not both of them gives  $\pi A_1$  that is proportional to the amplitude of the wave.  $\hat{f}(k)$  indicates which wave-vector components are contained in  $f(x)$ .

Let us integrate  $\hat{f}(k) \exp(-ikx)$  with respect to  $k$ :

$$\begin{aligned} \int_{-\infty}^{\infty} \hat{f}(k) \exp(-ikx) dk &= \int_{-\infty}^{\infty} \exp(-ikx) dk \int_{-\infty}^{\infty} f(x') \exp(ikx') dx' \\ &= \int_{-\infty}^{\infty} f(x') dx' \int_{-\infty}^{\infty} \exp[ik(x' - x)] dk \quad (\text{A2.4}) \\ &= \int_{-\infty}^{\infty} f(x') dx' 2\pi \delta(x' - x) = 2\pi f(x) \end{aligned}$$

Thus, we can recover  $f(x)$  from  $\hat{f}(k)$  by

$$\boxed{f(x) = \frac{1}{2\pi} \int_{-\infty}^{\infty} \hat{f}(k) \exp(-ikx) dk} \quad (\text{A2.5})$$

This operation is called the inverse Fourier transform.

In three dimensions, the Fourier transform of a spatial function  $f(\mathbf{r})$  is defined by

$$\hat{f}(\mathbf{k}) \equiv \int_{-\infty}^{\infty} f(\mathbf{r}) \exp(i\mathbf{k} \cdot \mathbf{r}) d\mathbf{r} \quad (\text{A2.6})$$

The inverse transform is given by

$$f(\mathbf{r}) \equiv \frac{1}{(2\pi)^3} \int_{-\infty}^{\infty} \hat{f}(\mathbf{k}) \exp(-i\mathbf{k} \cdot \mathbf{r}) d\mathbf{k} \quad (\text{A2.7})$$

We often need to calculate a three-dimensional Fourier transform of  $f(r)$  that depends only on the radial distance  $r$ . For this purpose, we use a spherical polar coordinate for  $\mathbf{r}$  with the polar axis running along  $\mathbf{k}$ . Then, the transform proceeds as follows.

$$\begin{aligned} \int f(r) \exp(i\mathbf{k} \cdot \mathbf{r}) d\mathbf{r} &= 2\pi \int_0^{\infty} r^2 f(r) dr \int_0^{\pi} \sin \theta \exp(ikr \cos \theta) d\theta \quad (\text{A2.8}) \\ &= \frac{4\pi}{k} \int_0^{\infty} r f(r) \sin kr dr = \frac{4\pi}{k} \text{Im} \int_0^{\infty} r f(r) \exp(ikr) dr \end{aligned}$$

**A3 INTEGRALS****Gaussian integral:**

$$\int_0^{\infty} x^{2n} \exp(-\alpha x^2) dx = \frac{(2n-1)!!}{2^{n+1}} \left( \frac{\pi}{\alpha^{2n+1}} \right)^{1/2} \quad (\text{A3.1})$$

**Fourier cosine integral:**

$$\int_0^{\infty} x^{\alpha-1} \cos bx dx = \frac{\Gamma(\alpha)}{b^\alpha} \cos \frac{\alpha\pi}{2} \quad (0 < \alpha < 1, b > 0) \quad (\text{A3.2})$$

When  $\alpha = 1/2$ ,  $\Gamma(1/2) = \pi^{1/2}$ . Thus,

$$\int_0^{\infty} x^{-1/2} \cos bx dx = \left( \frac{\pi}{2b} \right)^{1/2} \quad (\text{A3.3})$$

**Fourier sine integral:**

$$\int_0^{\infty} x^{\alpha-1} \sin bx dx = \frac{\Gamma(\alpha)}{b^\alpha} \sin \frac{\alpha\pi}{2} \quad (0 < \alpha < 1, b > 0) \quad (\text{A3.4})$$

For  $\alpha = 1/2$ ,

$$\int_0^{\infty} x^{-1/2} \sin bx dx = \left( \frac{\pi}{2b} \right)^{1/2} \quad (\text{A3.5})$$

**Gamma function:**

$$\int_0^{\infty} x^{\alpha-1} \exp(-x) dx = \Gamma(\alpha) \quad (\alpha > 0) \quad (\text{A3.6})$$

For integral values of  $\alpha$ ,  $\Gamma(\alpha) = (\alpha - 1)!$ .

**Miscellaneous integral:**

$$\int_0^{\infty} \frac{dx}{x^4 + b^4} = \frac{2^{1/2}\pi}{4b^3} \quad (\text{A3.7})$$

**A4 SERIES**

$$\sum_{n=1}^{\infty} \frac{a}{n^2 + a^2} = -\frac{1}{2a} + \frac{\pi}{2} \coth a\pi \quad (\text{A4.1})$$

$$\begin{aligned} \sum_{n=1}^{\infty} \frac{a}{n^{1/2}(n^2 + a^2)} &\cong \int_0^{\infty} \frac{a}{x^{1/2}(x^2 + a^2)} dx - \int_0^{1/2} \frac{a}{x^{1/2}(x^2 + a^2)} dx \\ &\cong 2a \int_0^{\infty} \frac{dy}{y^4 + a^2} - \frac{1}{a} \int_0^{1/2} \frac{dx}{x^{1/2}} = \frac{\pi}{(2a)^{1/2}} - \frac{2^{1/2}}{a} \cong \frac{\pi}{(2a)^{1/2}} \end{aligned} \quad (a \gg 1) \quad (\text{A4.2})$$